SPACE SCIENCES SERIES OF ISSI

The Outer Planets and their Moons

T. Encrenaz, R. Kallenbach,
T.C. Owen and C. Sotin (Eds.)

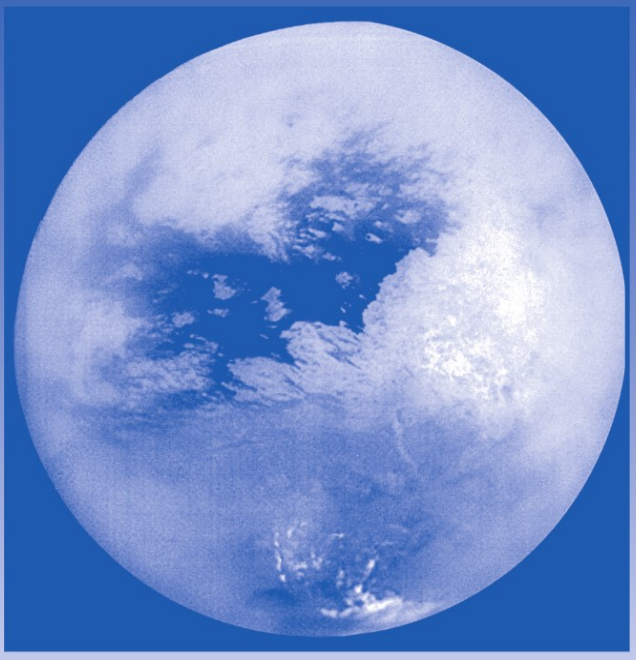

Springer

INTERNATIONAL SPACE SCIENCE INSTITUTE

THE OUTER PLANETS AND THEIR MOONS

Cover illustration:

A mosaic of nine processed images recently acquired during Cassini's first very close flyby of Saturn's moon Titan on 26 October, 2004, constitutes the most detailed full-disc view of the mysterious moon prior to December 2004. Courtesy of NASA/JPL/Space Science Institute.

Space Sciences Series of ISSI

Volume 19

The International Space Science Institute is organized as a foundation under Swiss law. It is funded through recurrent contributions from the European Space Agency, the Swiss Confederation, the Swiss National Science Foundation, and the University of Bern. For more information, see the homepage at http://www.issi.unibe.ch/.

THE OUTER PLANETS AND THEIR MOONS

Comparative Studies of the Outer Planets prior to the Exploration of the Saturn System by Cassini-Huygens

Volume Resulting from an ISSI Workshop
12–16 January 2004, Bern, Switzerland

Edited by

T. ENCRENAZ
Laboratoire d'Etudes Spatiales et Instrumentales en Astrophysique, Observatoire de Paris, F-92195 Meudon Cedex, France

R. KALLENBACH
International Space Science Institute, CH-3012 Bern, Switzerland

T. C. OWEN
University of Hawaii at Manoa, Honolulu, HI 96822, USA

C. SOTIN
Laboratoire de Planétologie et Géodynamique, F-44322 Nantes Cedex 3, France

Reprinted from *Space Science Reviews*, Volume 116, Nos. 1–2, 2005

Springer

INTERNATIONAL SPACE SCIENCE INSTITUTE
Space Sciences Series of ISSI

A.C.I.P. Catalogue record for this book is available from the Library of Congress

ISBN: 1-4020-3362-1

Published by Springer
P.O. Box 990, 3300 AZ Dordrecht, The Netherlands

Sold and distributed in North, Central and South America
by Springer,
101 Philip Drive, Norwell, MA 02061, U.S.A.

In all other countries, sold and distributed
by Springer,
P.O. Box 322, 3300 AH Dordrecht, The Netherlands

Printed on acid-free paper

Printed in the Netherlands

TABLE OF CONTENTS

FORMATION AND EVOLUTION OF THE GIANT PLANETS

NEUTRAL ATMOSPHERES OF THE GIANT PLANETS AND THEIR SATELLITES

AURORAE AND MAGNETOSPHERES

SATELLITES AND RINGS

EPILOGUE

The Outer Planets and their Moons Comparative Studies of the Outer Planets prior to the Exploration of the Saturn System by Cassini-Huygens
ISSI Workshop, 12–16 January 2004, Bern, Switzerland

Group Photograph

1. Brigitte Fasler
2. Silvia Wenger
3. Saliba Saliba
4. Tobias Owen
5. Maarten Roos-Serote
6. Darrell Strobel
7. Reta Beebe
8. Norbert Krupp
9. Christophe Sotin
10. Thérèse Encrenaz
11. Reinald Kallenbach
12. Emmanuell Lellouch
13. Jing Li
14. Sushil Atreya
15. Steve Miller
16. Roger Bonnet
17. Jonathan Lunine
18. Angioletta Coradini
19. Alberto Adriani
20. Torrence Johnson
21. Willy Benz
22. Margaret Kivelson
23. Dale Cruikshank
24. François Raulin
25. Daniel Gautier
26. Stuart Weidenschilling
27. Jack Lissauer
28. Régis Courtin
29. Daniel Prieur
30. Dave Jewitt
31. Isabelle Baraffe
32. Olivier Mousis
34. Yann Alibert
35. Michel Blanc
36. Christoph Mordasini
37. Philippe Zarka

PREFACE

The workshop organized by ISSI on the study of the outer planets came exactly one year after it was decided by a group of scientists and by its Science Committee meeting in Beatenberg near Bern in January 2003, that ISSI should broaden its range of subjects, in particular through introducing comparative planetology in its program of workshops and teams. This is a remarkable performance that reflects ISSI's rapid reaction to the advice of its users, i.e. the scientific community. Therefore the book is the first of the ISSI series to address the topic of comparing the planets and their satellites in the Solar System beyond the orbit of Jupiter. The book comes also at a very crucial moment, while the NASA-ESA Cassini-Huygens mission starts the exploration of Saturn and of its system of rings and satellites, including the biggest of them, Titan, with the European Huygens probe.

From the very beginning, ISSI has emphasized the importance of its role in offering to the scientific community a service in the organization of interdisciplinary and truly international meetings, providing a strongly needed cross-fertilization approach between various scientific disciplines. It will be easily recognized through the various chapters of the book that, indeed, the workshop responded exactly to this requirement. The objects that are present in the outer Solar System are so varied, that only can they be properly analyzed, and their properties properly understood, by assembling the best experts in the world in as divers disciplines as the formation of planetary systems, atmospheric and magnetospheric physics and ... biology!

Certainly, the topic addressed here is progressing very fast as the new data from the Galileo and the Cassini-Huygens missions are arriving. The field is therefore moving and the book has no other ambition than to provide a reference of the state of knowledge acquired as of now by these space missions and from their interpretation by an international group of experts. It is offering a tool that the scientists involved in these missions might find useful for the continuation of their work. I am pleased that it comes at such a critical time and that it should remain such a reference, until the work it will inspire opens new avenues in the field which will probably require another workshop in a few years from nowĚ

Preparing a workshop like this one, publishing its proceedings in less than a year, relies on the dedication and on the work of many people, from the scientists involved in establishing the program to those who have written their contributions and those who have taken a substantial portion of their scientific time to read and referee them. Acknowledgements are warmly addressed to all of them on behalf of R. Kallenbach and me. The experts who have reviewed the articles of the book have agreed to be identified:

Fran Bagenal	University of Colorado, Boulder, CO, USA
Reta Beebe	New Mexico State University, Las Cruces, NM, USA
Peter Bodenheimer	UCO/Lick Observatory, University of California, Santa Cruz, CA, USA
Alan Boss	Carnegie Institution of Washington, Washington DC, USA
Barney J. Conrath	Cornell University, Smithsburg, MD, USA
Régis Courtin	Observatoire de Paris, Meudon, France
Stan Cowley	University of Leicester, Leicester, United Kingdom
Pascale Ehrenfreund	Leiden Observatory, Leiden, The Netherlands
Kathryn Fishbaugh	International Space Science Institute, Bern, Switzerland
Marina Galand	Boston University, Boston, MA, USA
Daniel Gautier	Observatoire de Paris, Meudon, France
Tristan Guillot	Observatoire de la Côte d'Azur, Nice, France
Jim Head	Brown University, Providence, RI, USA
Satoshi Inaba	Tokyo Institute of Technology, Tokyo, Japan
Andy Ingersoll	Caltech, Pasadena, USA
Konstantin Kabin	University of Michigan, Ann Arbor, USA
Margaret Kivelson	University of California, Los Angeles, USA
Helmut Lammer	Austrian Academy of Sciences, Graz, Austria
Emmanuel Lellouch	Observatoire de Paris, Meudon, France
Alessandro Morbidelli	Observatoire de la Côte d'Azur, Nice, France
John D. Richardson	Massachusetts Institute of Technology, Cambridge, MA, USA
Dave Stevenson	Caltech, Pasadena, USA
Darrell F. Strobel	The John Hopkins University, Baltimore, MD, USA
Caroline Terquem	Institut d'Astrophysique de Paris, Paris, France
Rudolf Treumann	Max-Planck-Institute of Extraterrestrial Physics, Garching, Germany
Ah-San Wong	University of Michigan, Ann Arbor, USA
Günter Wuchterl	Max-Planck-Institute of Extraterrestrial Physics, Garching, Germany

Certainly, it is also a pleasure to acknowledge the support and the continuous assistance of the ISSI staff without which no such achievement would be possible.

I am particularly pleased to congratulate one of the authors of this volume, Michel Blanc of the Observatoire Midi Pyrénées, for having received the Jean Dominique Cassini Medal and the 2004 Honorary Membership of the European Geosciences Union. Since the early 1990's, Michel Blanc has obtained important new results on planetary magnetospheres, in particular on plasma transport and radiation belts in the highly axisymetric environment of Saturn. He has played an outstanding role in the preparation of the Cassini/Huygens mission as an Interdisciplinary Scientist. The topic of his medal lecture carried the title 'A Journey to Saturn through Solar System Magnetospheres.'

As this is the second edition of the volume, we meanwhile know that with Margaret Kivelson we also have the holder of the 2005 Hannes Alfvén medal of the European Geosciences Union among the authors. The reprint of this book gives me the chance to direct my cordial congratulations to Margaret Kivelson.

November 2004 and July 2005

Roger-Maurice Bonnet, ISSI Executive Director

A COMPARATIVE STUDY OF THE OUTER PLANETS BEFORE THE EXPLORATION OF SATURN BY CASSINI/HUYGENS: INTRODUCTION

T. ENCRENAZ[1], R. KALLENBACH[2], T.C. OWEN[3] and C. SOTIN[4]
[1]*DESPA, Observatoire de Paris, F-92195 Meudon Cedex, France*
[2]*International Space Science Institute, CH-3012 Bern, Switzerland*
[3]*University of Hawaii at Manoa, Honolulu, HI 96822, USA*
[4]*Laboratoire de Planétologie et Géodynamique, F-44322 Nantes Cedex 3, France*

Received: 15 November 2004; Accepted in final form: 30 November 2004

This volume, number 19 in the "Space Sciences Series of ISSI," presents the proceedings of the workshop on "A comparative study of the outer planets before the exploration of Saturn by Cassini-Huygens" which was held at ISSI in Bern on January 12–16, 2004. The purpose of this workshop was to bring together representatives of several scientific communities, such as planetary scientists, astronomers, space physicists, chemists and astrobiologists, to review our knowledge on four major themes: (1) the study of the formation and evolution processes of the outer planets and their satellites, beginning with the formation of compounds and planetesimals in the solar nebula, and the subsequent evolution of the interiors of the outer planets, (2) a comparative study of the atmospheres of the outer planets and Titan, (3) the study of the planetary magnetospheres and their interactions with the solar wind, and (4) the formation and properties of satellites and rings, including their interiors, surfaces, and their interaction with the solar wind and the magnetospheres of the outer planets.

At present, the study of the outer planets is particularly motivated by the fact that the Saturn system is being investigated by the Cassini-Huygens mission which will last until 2008 and possibly beyond. Ground-based and space observations of the giant planets over the past decade give evidence that each system has unique characteristics. Jupiter has been extensively studied over the past ten years by the Galileo mission, which, for instance, has measured a global enrichment of heavy elements as compared to hydrogen, with respect to the solar values, showing evidence for a solar composition of the icy planetesimals which formed Jupiter; Galileo has also revealed the unexpected internal dynamics of the Jovian satellites. Comparisons among the giant planets' satellites have provided clues to our understanding of the major processes driving the evolution of Earth-like planets. Jupiter has also been explored at the time of the Cassini flyby, while all four giant planets have been studied by HST, ISO and ground-based observations.

The following key questions were addressed at the workshop: What will we explore on Saturn and Titan with Cassini-Huygens, and what do we expect to find? Which coordinated ground-based observations should be made to complement and

Space Science Reviews 116: 1–7, 2005.
DOI: 10.1007/s11214-005-1944-4

extend those observations? What can we expect from future large ground-based and Earth-orbit observatories? What are the concepts of future space missions, orbiters or probes exploring the outer planets?

The program of the workshop was set up by four conveners, Thérèse Encrenaz (Observatoire de Paris, Meudon, France), Reinald Kallenbach (ISSI, Bern, Switzerland), Tobias Owen (University of Hawaii, USA) and Christophe Sotin (Université de Nantes, France), who invited experts to give reviews in four areas: (1) formation of the outer planets, (2) neutral atmospheres of the giant planets and their satellites, (3) aurorae and magnetospheres, and (4) satellites and rings. In addition, a keynote lecture on the Cassini-Huygens mission was given by J.-P. Lebreton as an introduction. Most of these reviews, with the addition of a few others, have been collected in the present book. The following introduction to the four workshop themes have benefitted from the input of the authors of these reviews.

1. Formation and Evolution of the Giant Planets

In the first section, "Formation and evolution of the giant planets," J. Lissauer gives an overview of the giant planets' formation, while S. Weidenschilling studies more specifically the accretion mechanism of planetary cores. I. Baraffe presents theoretical models of the giant planets' internal structure, with special emphasis to the extrasolar giant planets. W. Benz and Y. Alibert review the models of exo-giant planets' formation and, in particular, the constraints related to the timescale of the mechanisms involved. D. Gautier and F. Hersant present a model in which volatiles are trapped by clathration.

The discussions associated to this first section can be tentatively summarized as follows. The is a general agreement on the following points: (1) the nucleation model seems to be generally accepted for the giant planets of the solar system; this model is supported, in particular, by the enrichment in heavy elements observed in Jupiter, it is also supported by the carbon enrichment observed in the other giant planets, and by the deuterium enrichment observed in Uranus and Neptune; (2) in the case of exo-giant planets, the high-metallicity correlation seems to be also in favor of the nucleation formation scenario; (3) theoretical models show that the giant and the exo-giant planets can migrate over substantial distances during their formation.

There are many remaining open questions, however. What were the timescales of the three different phases of the nucleation model: runaway solid accretion, solid and gas accretion, and (for Jupiter and Saturn only) runaway gas accretion? Did the giant planets migrate, and how? In which form (ices or clathrates) were the volatiles trapped? How can we explain the low temperature trapping of the planetesimals which formed Jupiter? What were the sizes of the central cores of the giant planets, and what can we expect for exo-giant planets?

What would be the key measurements for the future? A crucial parameter is the determination of elemental and isotopic abundance ratios in all giant planets, as was done by the GCMS experiment aboard the Galileo probe in the case of Jupiter. The CIRS infrared spectrometer aboard the Cassini orbiter is expected to better constrain some of these ratios but the ultimate answer will come from descent probes, in Saturn but also in Uranus and Neptune. We note that in the case of Uranus and Neptune whose cloud structure is expected to extend at deep tropospheric levels (down to 100 bars or more), a probe could measure at least the abundance ratios of carbon and the rare gases. To better constrain the internal structure of the giant planets, we need an accurate measurement of their gravitational moments. Here again, Cassini will hopefully provide some measurements on Saturn's gravity field.

2. Neutral Atmospheres of the Giant Planets and their Satellites

Comparative studies of the giant planets' neutral atmospheres are given by T. Encrenaz for the chemical composition, S.K. Atreya and A.S. Wong for the cloud structure, R.F. Beebe for the dynamics and D.F. Strobel for the photochemical processes. An overview on the formation and evolution of Titan's atmosphere is presented by A. Coustenis, while the behavior of Titan's haze is studied by M. Roos-Serote. A comparative analysis of the nature of aerosols in the giant planets and Titan is presented by R. Courtin. Finally, E. Lellouch summarizes our knowledge of Io's atmosphere and surface-atmosphere interactions.

There is a general agreement within the community about the abundance ratios in Jupiter and, in the three other giant planets, about the C/H and D/H ratios. As mentioned above, these results strongly favor the nucleation model of the giant planets. The main cloud composition and structure in the giant planets seems to be globally understood, on the basis of thermochemical models; however, it was measured only in the case of Jupiter, from the Galileo probe in-situ measurements. The wind profiles are well determined (but not so well understood) for all giant planets. The atmospheric composition of Titan and Io is now well known. The stability of Io's atmosphere can be understood as a balance between sources (SO_2 sublimation, volcanic output) and losses (SO_2 condensation, photolysis and escape).

What are the open questions raised by these results? First, as mentioned above, we need to determine the abundance ratios of Saturn, Uranus and Neptune. Were these planets also made of solar composition icy planenesimals, as seems to be Jupiter? In addition, the O/H ratios measured in Jupiter's and Saturn's tropospheres appear to be smaller than the solar value. This anomaly, in the case of Jupiter, was attributed to local meteorological effects. Is it the case of Saturn too, and what are the mechanisms which drive the general circulations of the giant planets? Another challenging question is related to the observed differences between Uranus and Neptune. Why is there no internal energy in Uranus? Why is the eddy dffusion

coefficient much smaller on Uranus than on Neptune? Why are CO and HCN much more abundant in Neptune's stratosphere than in Uranus'? What is the origin of HCN in Neptune, and of CO in both planets? More generally, what is the nature of the oxygen source in the four giant planets and Titan? Finally, what are the elemental abundances in Titan's atmosphere? What is the physical and chemical nature of its surface? What is the source of the atmospheric methane?

Many questions related to Saturn and Titan will be addressed by the Cassini mission. Hopefully, the Huygens probe will provide in-situ masurements of Titan's atmospheric and surface composition. The orbiter instruments will give information on Saturn's atmospheric composition, cloud structure, photochemistry and general circulation. The Herschel submillimeter Earth-orbiting observatory, to be launched in 2007, will hopefully allow us to better understand the nature of the external oxygen source in the giant planets and Titan. Their atmospheric composition will be studied with further detail by HST, NGST, the ground-based submillimeter array Alma and large ground-based optical telescopes. The JIMO space mission, in orbit around Jupiter, will hopefully provide constraints on the composition of Jupiter's deep troposphere and on Io's atmosphere. The next step of space exploration will have to be, as mentioned above, a multiprobe mission toward the giant planets. Concerning theoretical work, future modelling will be necessary to understand the general circulations of the giant planets (Uranus in particular) and Titan. Phochemical models will have to be developed to model the stratospheric composition and evolution of the giant planets in the presence of an external oxygen source.

3. Aurorae and Magnetospheres

The exploration of the Saturn system by Cassini/Huygens offers the opportunity to study many types of interactions between planetary bodies and space plasma. Saturn itself has an intrinsic magnetic field and forms a corotation-dominated magnetosphere inside the solar wind. Unmagnetized Titan with its dense atmosphere forms an induced magnetosphere inside the plasma of the Kronian magnetosphere or at times inside the solar wind. The surfaces and exospheres of the icy satellites such as Dione or Rhea interact directly by microscopic processes with the plasma of the Kronian magnetosphere. M. Blanc, R. Kallenbach, and N.V. Erkaev classify the various types of solar system magnetospheres in order to motivate comparative studies based on Cassini/Huygens results. M. Kivelson describes in detail the large-scale current systems of the terrestrial and Jovian magnetospheres in order to make predictions for Saturn. S. Miller, A. Aylward, and M. Millward review the physics of giant planet ionospheres and thermospheres. N. Krupp summarizes the results from previous space missions to Saturn with emphasis on energetic particle measurements. P. Zarka and W.S. Kurth explain the various processes of radio emission from the giant planets.

Any intrinsic magnetosphere is almost naturally compared to the two best studied magnetospheres, namely those of Earth and Jupiter. As pointed out by M. Kivelson, the surface current of the terrestrial magnetopause (Chapman-Ferraro current) and that of the terrestrial magnetotail, closing through a current sheet in the center of the tail region, have analogues at Jupiter and presumably also at Saturn. However, the large-scale current systems driving the aurorae are very different for Jupiter and Earth. At Jupiter they are mainly driven by the fast planetary rotation, while at Earth they are mainly driven by solar wind energy released through reconnection of the interplanetary with the terrestrial magnetic field. Saturn is intermediate between Earth and Jupiter. It is a fast rotator but the aurorae are driven by the solar wind. The latter prediction by M. Kivelson in this volume has already been confirmed by tracing a CME-driven interplanetary shock from the Sun to Saturn by planetary auroral storms. These coordinated observations involved data of the space missions Cassini, Galileo, HST, POLAR, ACE, WIND, IMAGE, and SOHO (Prangé, R., *et al.*: 2004, 'A CME-driven interplanetary shock traced from the Sun to Saturn by planetary auroral storms', *Nature*, in press).

The aurorae are also a central topic of the reviews by S. Miller and co-authors. They study the ion-neutral coupling in the giant planets' exospheres in regions where H_3^+ ions are a dominant species. The key question is why the exospheric temperatures are several hundred degrees higher than can be produced by the effects of solar EUV heating alone. Solar EUV radiation accounts for an energy input of 2.4 TW at Jupiter and 0.5 TW at Saturn. Energetic particles precipitating in auroral regions of Jupiter could dissipate 10-100 TW by ion-neutral coupling. The amount of energy input from the solar wind through energetic particles into Saturn's ionosphere remains to be determined by Cassini. For both Jupiter and Saturn, it remains to be explored how the energy is distributed from the auroral regions all over the planet.

A remote diagnostic of aurorae is the detection of radio waves. As reported by P. Zarka and W.S. Kurth, the main auroral radio emissions at Jupiter originate from flux tubes which are magnetically connected to regions where the plasma corotation breaks down, Cassini needs to test the hypothesis that Saturn's kilometric radiation (SKR) mainly arises from upward currents at the boundaries between open and closed field lines. Temporal and spatial correlations suggest that SKR may also be related to variations in the solar wind pressure, to Kelvin-Helmholtz instabilities at the magnetopause, or to interplanetary shocks as observed at Jupiter during the Cassini flyby.

At Jupiter, correlations of HST ultraviolet images with radio wave emissions, driven by energetic electrons through the cyclotron maser instability, gave evidence for a special class of aurorae. They occur at the ionospheric footpoints of magnetic flux tubes that connect to the wakes of the Jovian satellites Io, Europa, and Ganymede. There may be analogues to these satellite-ionosphere interactions at Saturn. Towards the end of its tour around Saturn, Cassini will explore the high latitudes where the magnetic flux tubes connecting to Dione enter Saturn's iono-

sphere. The pick-up, transport, and acceleration processes that generate energetic particles will be studied near the satellites and rings of Saturn, but in particular near Titan.

To date, however, no radio emissions indicating the cyclotron maser instability have been observed in or near Titan's wake. Instead, the radio emissions indicate lightning. Lightning in Titan's atmosphere could be very important for the chemical evolution of organic molecules at low temperatures. Cassini/RPWS measurements will be co-ordinated with Huygens/HASI data and HST observations. In Saturn's atmosphere, the 'imaging' of electric discharge emissions serves to monitor the storm activity which depends on the variation of the ring shadows and the ion-neutral coupling in the thermosphere and ionosphere.

4. Rings and Satellites

T.V. Johnson, D.P. Cruikshank, D.C. Jewitt, and B. Sicardy summarize the knowledge on the satellite and ring systems of the four giant planets and the Kuiper belt and Oort cloud objects. F. Raulin discusses the conditions on Europa and Titan with respect to the possibility of formation of any pre-biotic matter on the satellite surfaces or under-ice oceans.

The properties of the satellites and trans-Neptunian objects give clues on the formation scenario of the solar system: (i) Solar nebula models (Hueso, R. and Guillot, T.: 2003, 'Evolution of the protosolar nebula and formation of the giant planets', *Space Sci. Rev.* **106**, 105–120; Lissauer, J., this volume) seem to be supported by the fact that most satellites and trans-Neptunian objects are formed from a mixture of rock and ice, where water ice dominates out to Uranus' orbit as outlined by T.V. Johnson. (ii) Models on outward migration (Levison, H.F. and Morbidelli, A.: 2003, 'The formation of the Kuiper belt by the outward transport of bodies during Neptune's migration', *Nature* **426**, 419–421) are supported by the fact that Kuiper belt objects must have grown in a denser environment of the protoplanetary disk, i.e. closer to the Sun than their present location, to reach the observed sizes (see D.P. Cruikshank, this volume). (iii) D. Jewitt argues that direct gravitational collapse of the giant planets within about 1000 years seems unlikely because on such a short time scale the solid irregular satellites could not have formed to be available for capture. Core accretion near Jupiter's or Saturn's orbits and outward migration with subsequent collisional capture of irregular satellites is suggested as a possible scenario for the formation of the Uranus and Neptune systems. (iv) Giant planet ring dynamics, composition, size distributions of grains and larger bodies, and the associated formation time scales and lifetimes provide important insights on formation scenarios of proto-planetary disks (see Sicardy, this volume). For instance, spiral density waves are believed to be important collective modes in proto-planetary disks. They are in fact observed in Saturn's rings and can be used to probe the physical propoerties of the disk.

Among the outstanding questions that will be investigated during the Cassini tour around Saturn and the Huygens descent to Titan are:

1. What is the 'relation' between the rings and the satellites? How was the Saturn system including its satellites formed (e.g., Magni, G. and Coradini, A.: 2004, 'Formation of Jupiter by nucleated instability', *Planet. Space Sci.* **52**, 343–360)?
2. What is the internal structure of the satellites of Saturn?
3. Why is Enceladus – although it is rather small and its present orbit's eccentricity suggests insufficient tidal heating – differentiated? Which are the internal heat sources – for instance radioactive decay – of the satellites of Saturn?
4. Which are and were the impactor populations causing the cratering of Saturn's satellites? Is there clear evidence for cryovolcanism?
5. How large is and was the meteoroid flux at Saturn's orbit? How important is this meteoroid flux for the ring erosion and for the source processes of the plasma in the Kronian magnetosphere?
6. Do the rings contain organic material and, if yes, where could it come from?
7. How much of macromolecular carbon-bearing material condensed and accreted in the outer parts of the solar nebula is pre-solar in origin? Most icy bodies in the outer Solar System show colors or low surface albedos that indicate the presence of complex organic material of the kind typically found in comets.
8. And last but not least: Are there liquid layers at the surface and/or in the deep interior of Titan and can this environment offer conditions for the development of life?

The volume is concluded by the article of F. Raulin on exo-astrobiological aspects of Europa and Titan. After Mars, Europa, with its potential subsurface ocean, is usually thought to be better suited for the search of any form of extraterrestrial life than Titan. On the surface of Titan, the emergence of life is not very likely because of the almost certain lack of liquid water and because of the low temperatures. However, it will be interesting to explore how far pre-biotic chemistry can develop under these conditions.

It is our pleasure to thank all those who have contributed to this volume and to the workshop in general. We are grateful to all authors for their contributions, and to the reviewers for their reports. We also want to express our thanks to the directorate and staff of ISSI, for their support in making the workshop happen and in getting the book finalized.

I. FORMATION AND EVOLUTION OF THE GIANT PLANETS

FORMATION OF THE OUTER PLANETS

JACK J. LISSAUER
NASA Ames Research Center, Space Science Division, MS 245-3, Moffett Field, CA 94035, USA

Received: 15 April 2004; Accepted in final form: 19 August 2004

Abstract. Models of the origins of gas giant planets and 'ice' giant planets are discussed and related to formation theories of both smaller objects (terrestrial planets) and larger bodies (stars). The most detailed models of planetary formation are based upon observations of our own Solar System, of young stars and their environments, and of extrasolar planets. Stars form from the collapse, and sometimes fragmentation, of molecular cloud cores. Terrestrial planets are formed within disks around young stars via the accumulation of small dust grains into larger and larger bodies until the planetary orbits become well enough separated that the configuration is stable for the lifetime of the system. Uranus and Neptune almost certainly formed via a bottom-up (terrestrial planet-like) mechanism; such a mechanism is also the most likely origin scenario for Saturn and Jupiter.

Keywords: planet formation, giant planets, solar nebula

1. Introduction

There is convincing observational evidence that stars form by gravitationally-induced compression of relatively dense regions within molecular clouds (Lada *et al.*, 1993; André *et al.*, 2000). The nearly planar and almost circular orbits of the planets in our Solar System argue strongly for planetary formation within flattened circumstellar disks. Observations by Goodman *et al.* (1993) indicate that typical star-forming dense cores inside dark molecular clouds have specific angular momentum $> 10^{21}$ cm^2 s^{-1}. When these clouds undergo gravitational collapse, this angular momentum leads to the formation of pressure-supported protostars surrounded by rotationally-supported disks. Such disks are analogous to the primordial solar nebula that was initially conceived by Kant and Laplace to explain the observed properties of our Solar System (e.g., Cassen *et al.*, 1985). Observational evidence for the presence of disks of Solar System dimensions around pre-main sequence stars has increased substantially in recent years (McCaughrean *et al.*, 2000). The existence of disks on scales of a few tens of astronomical units is inferred from the power-law spectral energy distribution in the infrared over more than two orders of magnitude in wavelength (Chiang and Goldreich, 2000). Observations of infrared excesses in the spectra of young stars suggest that the lifetimes of protoplanetary disks span the range of 10^6 – 10^7 years (Strom *et al.*, 1993; Alencar and Batalha, 2002).

Dust within a protoplanetary disk initially agglomerates via sticking/local electromagnetic forces. The later phases of solid body growth are dominated by pair-

Space Science Reviews 116: 11–24, 2005.
DOI: 10.1007/s11214-005-1945-3

wise collisions of bodies that also influence one another's trajectories gravitationally. Terrestrial planets continue to grow by pairwise accretion of solid bodies until the spacing of planetary orbits becomes large enough that the configuration is stable to gravitational interactions among the planets for the lifetime of the system (Safronov, 1969; Wetherill, 1990; Lissauer, 1993; 1995; Chambers, 2001; Laskar, 2000). The largest uncertainty in our understanding of solid planet formation is the agglomeration from cm-sized pebbles to km-sized bodies that are referred to as planetesimals. Collective gravitational instabilities (Safronov, 1969; Goldreich and Ward, 1973) might be important, although turbulence could prevent protoplanetary dust layers from becoming thin enough to be gravitationally unstable (Weidenschilling and Cuzzi, 1993). Recent calculations suggest that high metallicity disks may form planetesimals via gravitational instabilities, but that dust in disks with lower solids contents may not be able to overcome turbulence and settle into a subdisk that is dense enough to undergo gravitational instability (Youdin and Shu, 2002). Planetesimal formation is a very active research area (Goodman and Pindor, 2000; Ward, 2000), and results may have implications for our estimates of the abundance of both terrestrial and giant planets within our galaxy.

Our understanding, such as it is, of planet formation comes from a widely diverse range of observations, laboratory studies and theoretical models. Detailed observations obtained from the ground and from space are now available for the planets and many smaller bodies (moons, asteroids and comets) within our Solar System. Studies of the composition, minerals and physical structure have been used to deduce conditions within the protoplanetary disk (Hewins, Jones and Scott, 1996). Data on the now more numerous known extrasolar planets are less detailed and more biased, yet still very important. Observations of young stars and their surrounding disks provide clues to planet formation now taking place within our galaxy. Laboratory experiments on the behavior of hydrogen and helium at high pressures have been combined with gravitational measures of the mass distribution within giant planets deduced from the trajectories of passing spacecraft and moons to constrain the internal structure and composition of the largest planets in our Solar System.

Theorists have attempted to assemble all of these pieces of information together into a coherent model of planetary growth. But note that planets and planetary systems are an extremely heterogeneous lot, the 'initial conditions' for star and planet formation vary greatly within our galaxy (Mac Low and Klessen, 2004), and at least some aspects of the process of planet formation are extremely sensitive to small changes in initial conditions (Chambers *et al.*, 2002).

The remainder of this chapter concentrates on the formation of bodies much larger than Earth yet substantially smaller than the Sun. Observations of giant planets in our Solar System and beyond are summarized in Section 2. Formation models are reviewed in Section 3, and conclusions are given in Section 4.

2. Observations

About 90% of Jupiter's mass is H and He, and these two light elements make up ∼75% of Saturn. The two largest planets in our Solar System are generally referred to as *gas giants* even though these elements aren't gases at the high pressures that most of the material in Jupiter and Saturn is subjected to. Analogously, Uranus and Neptune are frequently referred to as *ice giants* even though the astrophysical ices such as H_2O, CH_4, H_2S and NH_3 that models suggest make up the majority of their mass (Hubbard *et al.*, 1995) are in fluid rather than solid form. Note that whereas H and He *must* make up the bulk of Jupiter and Saturn because no other elements can have such low densities at plausible temperatures, it is possible that Uranus and Neptune are primarily composed of a mixture of 'rock' and H/He (Hubbard *et al.*, 1995).

The large amounts of H and He contained in Jupiter and Saturn imply that these planets must have formed within $\sim 10^7$ yrs of the collapse of the Solar System's natal cloud, before the gas in the protoplanetary disk was swept away. Any formation theory of the giant planets should account for these time scales. In addition, formation theories should explain the elemental and isotopic composition of these planets and variations therein from planet to planet, the presence and/or absence of internal heat fluxes, axial tilts, etc.

Lithium and heavier elements constitute $< 2\%$ of the mass of a solar composition mixture. The *atmospheric* abundances of volatile gases heavier than helium* are ∼3 times solar in Jupiter (Young, 2003), a bit more enriched in Saturn, and substantially more for Uranus and Neptune. The *bulk* enhancements in heavy elements relative to the solar value are roughly 5, 15, and 300 times for Jupiter, Saturn and Uranus/Neptune, respectively. Thus, all four giant planets accreted solid material substantially more effectively than gas from the surrounding nebula. Moreover, the total mass in heavy elements varies by only a factor of a few between the four planets, while the mass of H and He varies by about two orders of magnitude between Jupiter and Uranus/Neptune.

The extrasolar planet discoveries of the past decade have vastly expanded our database by increasing the number of planets known by more than an order of magnitude (Mayor *et al.*, 2004). The distribution of known extrasolar planets is highly biased towards those planets that are most easily detectable using the Doppler radial velocity technique. The extrasolar planetary systems that have been found are quite different from our Solar System; however, it is not yet known whether our planetary system is the norm, quite atypical or somewhere in between.

Nonetheless, the following unbiased statistical information can be distilled from available exoplanet data: Approximately 1% of sunlike stars (chromospherically-

* One notable exception to this trend is neon, which is substantially depleted relative to solar abundance. However, the paucity of neon in Jupiter's atmosphere is believed to be the result of gravitationally-induced settling of neon (together with some of the helium) towards the center of Jupiter within the past 1 – 2 Gyr, and thus is not taken to be a clue to the planet's formation.

quiet late F, G and early K dwarf stars without close binary star companions that are located in our region of the Milky Way galaxy) have planets more massive than Saturn within 0.1 AU. Roughly 7% of sunlike stars have planets more massive than Jupiter within 2 AU. Some of these planets have very eccentric orbits. Within about 5 AU of sunlike stars, Jupiter-mass planets are more common than planets of several Jupiter masses, and substellar companions that are more than ten times as massive as Jupiter are rare (Mayor *et al.*, 2004; Marcy *et al.*, 2004). Stars with higher metallicity are more likely to host detectable planets than are metal-poor stars (Santos *et al.*, 2003; Fischer and Valenti, 2003). The distribution of planets is more clustered than it would be if detectable planets were randomly assigned to stars, i.e., stars with one detectable planet are more likely to host more detectable planets. At least a few percent of sunlike stars have very Jupiter-like companions ($0.5 - 2$ M_J, 4 AU $< a <$ 10 AU, but $>$ 20% lack such companions (Marcy *et al.*, 2004). The one extrasolar giant planet with a well-measured mass and radius, HD 209458b (which was discovered using the Doppler technique and subsequently observed to transit across the disk of its star), is predominantly hydrogen (Charbonneau *et al.*, 2000; Burrows *et al.*, 2003), as are Jupiter and Saturn.

Transit observations have also yielded an important negative result: Hubble Space Telescope photometry of a large number of stars in the globular cluster 47 Tucanae failed to detect any transiting inner giant planets, even though $\sim$17 such transiting objects would be expected if the frequency of such planets in this low metallicity cluster was the same as that for sunlike stars in the solar neighborhood (Gilliland *et al.*, 2000). However, it appears likely that a $\sim$3 M_J planet is orbiting $\sim$20 AU from the pulsar PSR B1620-26 – white dwarf binary system, which is located in the globular cluster Messier 4. This system has been taken to be evidence for ancient planet formation in a low metallicity (5% solar) protoplanetary disk within the globular cluster by Sigurdsson (1993) and Sigurdsson *et al.* (2003). Sigurdsson's formation scenario requires a fairly complex stellar exchange to account for the planet in its current orbit. There is a much more likely explanation for the planet orbiting PSR B1620-26, which requires neither planetary formation in a low metallicity disk nor stellar exchange. This system has two post-main sequence stars sufficiently close to have undergone disk-producing mass transfer during the white dwarf's distended red giant phase, which occurred within the past 10^9 years (Sigurdsson *et al.*, 2003). Such a metals-enriched disk could have been an excellent location for the giant planet to form, and growth within such a disk (whether near its observed location or closer to the stars) would fit well with both planet formation theories and the observed strong correlation of planetary detections with stellar (and presumably protostellar disk) metallicity. Sigurdsson (1993) noted the possibility that the planet formed in a post-main sequence disk, but he discounted this scenario because he relied on the planetary growth timescales given by Nakano (1987), whose model requires an implausibly long 4×10^9 years to form Neptune.

3. Formation Models

The observation that the mass function of young objects in star-forming regions extends down through the brown dwarf mass range to below the deuterium burning limit (Zapatero *et al.*, 2000), together with the lack of any convincing theoretical reason to believe that the collapse process that leads to stars cannot also produce substellar objects (Wuchterl and Tscharnuter, 2003), strongly implies that most isolated (or distant companion) brown dwarfs* and isolated high planetary mass objects formed via the same collapse process as do stars.

By similar reasoning, the 'brown dwarf desert', a profound dip in the mass function of companions orbiting within several AU of sunlike stars (Mayor *et al.*, 2004; Marcy *et al.*, 2004), strongly suggests that the vast majority of extrasolar giant planets formed via a mechanism different from that of stars. Moreover, the relationship between bulk composition and mass within our Solar System, wherein bodies up to the mass of Earth consist almost entirely of condensable (under reasonable protoplanetary disk conditions) material, and the fraction of highly volatile gas increases with mass through Uranus/Neptune, to Saturn and finally Jupiter (which is still enriched in condensables at least threefold compared to the Sun), argues for a unified formation scenario for all of the planets and smaller bodies within our Solar System. The continuum of observed extrasolar planetary properties, which stretches to systems not very dissimilar to our own, suggests that extrasolar planets formed as did the planets within our Solar System.

Models for the formation of gas giant planets were reviewed by Wuchterl *et al.* (2000). Star-like direct quasi-spherical collapse is not considered viable, both because of the observed brown dwarf desert mentioned above and theoretical arguments against the formation of Jupiter-mass objects via fragmentation (Bodenheimer *et al.*, 2000a). The theory of giant planet formation that is favored by most researchers is the *core instability model*, in which the planet's initial growth resembles that of a terrestrial planet, but it becomes sufficiently massive (several $M_\oplus$) that it is able to accumulate substantial amounts of gas from the surrounding protoplanetary disk. The only other hypothesis receiving significant attention is the *gas instability model*, in which the giant planet forms directly from the contraction of a clump that was produced via a gravitational instability in the protoplanetary disk.

* Following Lissauer (2004), the following definitions are used throughout this chapter:

- *Planet*: negligible fusion (< 13 M_J) + orbits star(s) or stellar remnant(s).
- *Star*: self-sustaining fusion is sufficient for thermal pressure to balance gravity.
- *Stellar remnant*: dead star - 'no' more fusion (i.e., thermal pressure sustained against radiative losses by energy produced from fusion is no longer sufficient to balance gravitational contraction).
- *Brown dwarf*: substellar object with substantial deuterium fusion (more than half of the object's original inventory of deuterium is ultimately destroyed by fusion).

Numerical calculations on gravitationally unstable disks by Adams and Benz (1992) and recent work by Boss (2000) and Mayer *et al.* (2002) have revived interest in the gas instability model. Although there are uncertainties in the processes of gaseous giant protoplanet formation, the disk instabilities are a dynamical effect and the planets would form very rapidly on time scales of at most a few tens of orbits. Boss (1998) suggested that ice and rock cores *should* be able to form inside Jupiter after the occurrence of gravitational instability, but more detailed calculations, including realistic (fractal) models of grain growth and the affects of fluid motions within the planet are needed to test this claim. Furthermore, the masses of the condensations in most calculations of this process tend to be 5–10 M_J, although Boss (2001) finds condensations of mass $\sim$1 M_J. Nevertheless these models suggest that under appropriate conditions in the disk, fragmentation into objects of $\sim$10 M_J is likely to occur on a time scale short compared with the disk dispersal time of a few million years (Haisch *et al.*, 2001; Lada, 2003; Chen and Kamp, 2004; Metchev *et al.*, 2004), thus avoiding one of the main problems with the core accretion mechanism. Numerical simulations show that sufficiently unstable disks can, indeed, produce clumps comparable in mass to giant planets (Mayer *et al.*, 2002). In contrast, simulations performed with the same code, but different initial conditions, demonstrate that mildly unstable disks can redistribute mass via spiral density waves. Moreover, Laughlin and Bodenheimer (1994) showed that the unstable disk develops spiral arms that saturate at low amplitude and result in angular momentum transport and accretion of disk material onto the star, rather than fragmentation into subcondensations. Computational limitations to date have precluded simulations that begin with stable disks and allow the disk to become unstable via cooling or growth by accretion on astrophysically realistic timescales. Whether disks which are prone to fragmentation are a likely result of gravitational collapse of a molecular cloud core has still to be determined. An even more serious difficulty is that the gas instability hypothesis only accounts for massive stellar-composition planets, requiring a separate process to account for the smaller bodies in our Solar System and the heavy element enhancements in Jupiter and Saturn. The existence of intermediate objects like Uranus and Neptune is particularly difficult to account for in such a scenario.

The core-instability model relies on a combination of planetesimal accretion and gravitational accumulation of gas. In this theory, the core of the giant planet forms first by accretion of planetesimals, while only a small amount of gas is accreted. Core accretion rates depend upon the surface mass density of solids in the disk and physical assumptions regarding gas drag, etc. (Lissauer, 1987; Inaba *et al.*, 2003). The escape velocity from a planetary embryo with $M > 0.1$ $M_\oplus$ is larger than the sound speed in the gaseous protoplanetary disk. Such a growing planetary core first attains a quasi-static atmosphere that undergoes Kelvin-Helmholtz contraction as the energy released by the planetesimal and gas accretion is radiated away at the photosphere. The contraction timescale is determined by the efficiency of radiative transfer, which is relatively low in some regions of the

envelope. Spherically symmetric (1-D) quasi-hydrostatic models show that the minimum contraction timescale is a rapidly decreasing function of the core's mass. The gas accretion rate, which is initially very slow, accelerates with time and becomes comparable to the planetesimal bombardment rate after the core has grown to $\sim$10 $M_\oplus$. Once the gaseous component of the growing planet exceeds the solid component, gas accretion becomes very rapid, and leads to a runaway accretion of gas.

The composition of the atmospheres of a giant planet is largely determined by how much heavy material was mixed with the lightweight material in the planet's envelopes. Once the core mass exceeds $\sim$0.01 $M_\oplus$, the temperature becomes high enough for water to evaporate into the protoplanet's envelope. As the envelope becomes more massive, late-accreting planetesimals sublimate before they can reach the core, thereby enhancing the heavy element content of the envelopes considerably.

The fact that Uranus and Neptune contain much less H_2 and He than Jupiter and Saturn suggests that Uranus and Neptune never quite reached runaway gas accretion conditions, possibly due to a slower accretion of planetesimals (Pollack *et al.*, 1996). The rate at which accretion of solids takes place depends upon the surface density of condensates and the orbital frequency, both of which decrease with heliocentric distance. Alternatively/additionally, Uranus and Neptune may have avoided gas runaway as a result of the removal of gas from the outer regions of the disk via photoevaporation (Hollenbach *et al.*, 2000). Additional theoretical difficulties for forming planets at Uranus/Neptune distances have been addressed by Lissauer *et al.* (1995) and Thommes *et al.* (2003). New models are being proposed to address these problems by considering the possibility of rapid runaway accretion of a very small number of planetary embryos beyond 10 AU. In the model presented by Weidenschilling *et al.* (2004), an embryo is scattered from the Jupiter-Saturn region into a massive disk of small planetesimals. In the model presented by Goldreich *et al.* (2004), planetesimals between growing embryos are ground down to very small sizes and are forced into low inclination, nearly circular orbits by frequent mutual collisions. Planetary embryos can accrete rapidly in such a dynamically cold disks as those in the models of Weidenschilling et al. and Goldreich et al. Alternatively, Thommes *et al.* (2003) propose that Uranus and Neptune formed closer to the Sun, and were subsequently scattered out to their current distances by gravitational perturbations of Jupiter and Saturn.

During the runaway planetesimal accretion epoch, the protoplanet's mass increases rapidly. The internal temperature and thermal pressure increase as well, preventing substantial amounts of nebular gas from falling onto the protoplanet. When the planetesimal accretion rate decreases, gas falls onto the protoplanet more rapidly. The protoplanet accumulates gas at a gradually increasing rate until its gas mass is comparable to its heavy element mass. The key factor limiting gas accumulation during this phase of growth is the protoplanet's ability to radiate away energy and contract (Figure 1). The rate of gas accretion then accelerates more rapidly,

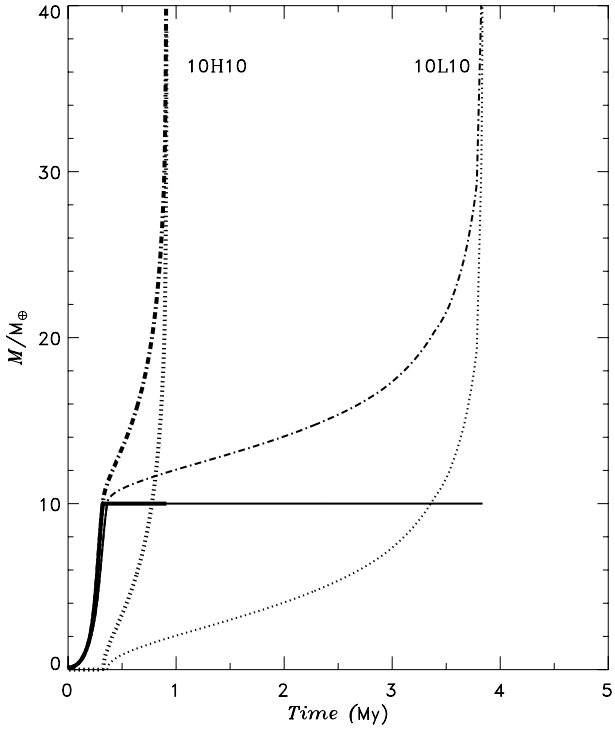

Figure 1. Evolution of a giant protoplanet for two values of the atmospheric opacity. The planet's mass is plotted as a function of time. The solid line denotes the mass of the core (which for these models has been limited to 10 $M_\oplus$), the dotted line denotes the mass of the envelope, and the dash-dotted line denotes the total mass. Both models are computed at 5.2 AU from a 1 $M_\odot$ star in a disk with planetesimal surface density = 10 g/cm^2. The thick curves, labeled 10L10, denote models using opacity values that correspond to an atmospheric abundance of grains equal to 2% that of typical interstellar matter. The thin curves, labeled 10H10, denote models computed with full interstellar grain opacity. Calculations by Podolak (2003) suggest that the grain abundance in a giant protoplanet's atmosphere is likely to be lower than that in interstellar matter. (Courtesy: O. Hubickyj; details will be presented in Hubickyj, Bodenheimer, and Lissauer, 2005.)

and a gas runaway occurs. The gas runaway continues as long as there is gas in the vicinity of the protoplanet's orbit. The protoplanet may cut off its own supply of gas by gravitationally clearing a gap within the disk (Lin and Papaloizou, 1979), as the moonlet Pan does within Saturn's rings (Showalter, 1991). D'Angelo *et al.* (2002, 2003) are using a 3-D adaptive mesh refinement code to follow the flow of gas onto an accreting giant planet. Models such as this will eventually allow the determination of final planetary mass as a function of the time-varying properties (density, temperature, viscosity, longevity, etc.) of the surrounding disk. Such a self-regulated growth limit provides a possible explanation to the observed mass distribution of extrasolar giant planets. Alternatively, the planet may accumulate all of the gas that remains in its region of the protoplanetary disk.

A major uncertainty associated with the emergence of planets is their orbital migration as a consequence of the same type of gravitational torque between the disk and the planet that may allow planets to clear gaps around themselves (Goldreich and Tremaine, 2000; Ward, 1986; Bate *et al.*, 2003). Planetary orbits can migrate towards (or in some circumstances away from) their star as a consequence of angular momentum exchange between the protoplanetary disk and the planet. Calculations indicate that the torque exerted by the planet on the outer disk is usually stronger than that on the inner disk. Planets that are more massive than Mars may be able to migrate substantial distances prior to the dispersal of the gaseous disk. Thus, it is quite possible that giant planets may form several AU from their star and then migrate inwards to the locations at which most extrasolar planets have been observed. Disk-induced migration is considered to be the most likely explanation for the 'giant vulcan' planets with periods of less than a week, because *in situ* formation of such objects is quite unlikely (Bodenheimer *et al.*, 2000b). Livio and Pringle (2003) find no basis to suggest that planetary migration is sensitive to disk metallicity, and conclude that higher metallicity probably results in a higher likelihood of planet formation. The difficulty with the migration models is that they predict that planets should migrate *too rapidly*, especially in the Earth to Neptune mass range that planetary cores grow through in the core accretion scenario. Moreover, as migration rates should increase as a planet approaches a star, most planets that migrate significant distances should be swallowed up by their star. However, a planet may end up in very close 51 Peg-like orbits if stellar tides can counteract the migration or if the disk has a large inner hole (Lin *et al.*, 1996; Lin *et al.*, 2000). Resolution of this rapid migration dilemma may require the complete and nonlinear analysis of the disk response to the protoplanet in the corotation regions. See Ward and Hahn (2000), Masset and Papaloizou (2003), and Thommes and Lissauer (2003) for more detailed discussions of planetary migration.

Many of the known extrasolar giant planets move on quite eccentric ($0.2 < e < 0.7$) orbits. These eccentric orbits may be the result of stochastic gravitational scatterings among massive planets (which have subsequently merged or been ejected to interstellar space, Rasio and Ford, 1996; Weidenschilling and Marzari, 1996; Levison *et al.*, 1998; Ford *et al.*, 2001), by perturbations of a binary companion (Holman *et al.*, 1997), or by past stellar companions if the now single stars were once members of unstable multiple star systems (Laughlin and Adams, 1998). However, as neither scattering nor migration offer a simple explanation for those planets with nearly circular orbits and periods from a few weeks to a few years, the possibility of giant planet formation quite close to stars should not be dismissed (Bodenheimer *et al.*, 2000b).

4. Conclusions: Summary of Giant Planet Formation Models

The smoothness of the distribution of masses of young M stars, free-floating brown dwarfs, and even free-floating objects somewhat below the deuterium burning limit, argues strongly that these bodies formed in the same manner, via collapse, in some cases augmented by fragmentation. In contrast, the mass gap in nearby companions to sunlike stars (the brown dwarf desert) is convincing evidence that at least most known giant planets formed in a different manner.

Various models for giant planet formation have been proposed. According to the prevailing core instability model, giant planets begin their growth by the accumulation of small solid bodies, as do terrestrial planets. However, unlike terrestrial planets, the growing giant planet cores become massive enough that they are able to accumulate substantial amounts of gas before the protoplanetary disk dissipates. The primary questions regarding the core instability model is whether planets with small cores can accrete very massive gaseous envelopes within the lifetimes of gaseous protoplanetary disks.

The main alternative giant planet formation model is the disk instability model, in which gaseous planets form directly via gravitational instabilities within protoplanetary disks. Formation of giant planets via gas instability has never been demonstrated for realistic disk conditions. Moreover, this model has difficulty explaining the supersolar abundances of heavy elements in Jupiter and Saturn, and it does not explain the origin of planets like Uranus and Neptune. Nonetheless, it is possible that some giant planets form via disk instability.

Most models for extrasolar giant planets suggest that they formed as Jupiter and Saturn are believed to have (in nearly circular orbits, far enough from the star that ice could condense), and subsequently migrated to their current positions, although some models suggest *in situ* formation. Issues involving the ultimate sizes and spacings of gas giant planets are complex and poorly understood (Lissauer, 1995), and provide a major source of uncertainty for modeling the potential diversity of planetary systems. Gas giant planet formation may or may not be common, because the majority of protoplanetary disks could be depleted before solid planetary cores can grow large enough to gravitationally trap substantial quantities of gas. Additionally, an unknown fraction of giant planets migrate into their star and are consumed, or are ejected into interstellar space via perturbations of neighboring giant planets, so even if giant planet formation is common, these planets may be scarce.

Acknowledgements

This work was supported by NASA's Solar System Origins Program under RTOP 188-07-1L.

References

Adams, F.C. and Benz, W.: 1992, 'Gravitational instabilties in circumstellar disks and the formation of binary companions', in H.A. McAlister and W.I. Hartkopf (eds.), *Complementary approaches to double and multiple star research*, ASP Conf. Ser. **32**, IAU Colloquium 135, pp. 185–194.

Alencar, S.H.P. and Batalha, C.: 2002, 'Variability of Southern T Tauri Stars. II. The Spectral Variability of the Classical T Tauri Star TW Hydrae', *Astrophys. J.* **571**, 378–393.

André, P., Ward-Thompson, D., and Barsony, M.: 2000, 'From Prestellar Cores to Protostars: the Initial Conditions of Star Formation', in V. Mannings, A. P. Boss, and S. Russells (eds.), *Protostars and Planets IV*, Univ. Arizona Press, Tucson, pp. 59–96.

Bate, M.R., Lubow, S.H., Ogilvie, G.I., and Miller, K.A.: 2003, 'Three-dimensional calculations of high- and low-mass planets embedded in protoplanetary discs', *Mon. Not. Roy. Astron. Soc.* **341**, 213–229.

Bodenheimer, P., Burkert, A., Klein, R.I., Boss, A.P.: 2000a, 'Multiple Fragmentation of Protostars', in V. Mannings, A.P. Boss, and S. Russells (eds.), *Protostars and Planets IV*, Univ. Arizona Press, Tucson, pp. 675–701.

Bodenheimer, P., Hubickyj, O., and Lissauer, J.J.: 2000b, 'Models of the in Situ Formation of Detected Extrasolar Giant Planets', *Icarus* **143**, 2–14.

Boss, A.P.: 1998, 'Evolution of the solar nebula. IV. Giant gaseous protoplanet formation', *Astrophys. J.* **503**, 923–937.

Boss, A.P.: 2000, 'Possible rapid gas giant planet formation in the solar nebula and other protoplanetary disks', *Astrophys. J.* **536**, L101–L104.

Boss, A.P.: 2001, 'Gas Giant Protoplanet Formation: Disk Instability Models with Thermodynamics and Radiative Transfer', *Astrophys. J.* **563**, 367–373.

Burrows, A., Sudarsky, D., Hubbard, W.B.: 2003, 'A Theory for the Radius of the Transiting Giant Planet HD 209458b', *Astrophys. J.* **594**, 545–551.

Cassen, P., Shu, F.H., and Terebey, S.: 1985, 'Protostellar disks and star formation', in D.C. Black and M.S. Matthews (eds.), *Protostars and Planets II*, Univ. Arizona Press, Tucson, pp. 448–483.

Chambers, J.E.: 2001, 'Making More Terrestrial Planets', *Icarus* **152**, 205–224.

Chambers, J.E., Quintana, E.V., Duncan, M.J., and Lissauer, J.J.: 2002, 'Symplectic Integrator Algorithms for Modeling Planetary Accretion in Binary Star Systems', *Astron. J.* **123**, 2884–2894.

Charbonneau, D., Brown, T.M., Latham, D.W., and Mayor, M.: 2000, *Astrophys. J.* **529**, L45–L48.

Chen, C.H. and Kamp, I.: 2004, 'Are giant planets forming around HR 4796A?', *Astrophys. J.* **602**, 985–992.

Chiang, E. and Goldreich, P.: 1997, 'Spectral Energy Distributions of T Tauri Stars with Passive Circumstellar Disks', *Astrophys. J.* **490**, 368–376.

D'Angelo, G., Henning, T., and Kley, W.: 2002, 'Nested-grid calculations of disk-planet interaction', *Astron. Astrophys.* **385**, 647–670.

D'Angelo, G., Kley, W., and Henning, T.: 2003, 'Orbital Migration and Mass Accretion of Protoplanets in Three-dimensional Global Computations with Nested Grids' *Astrophys. J.* **586**, 540–561.

Fischer, D.A. and Valenti, J.A.: 2003, 'Metallicities of stars with extrasolar planets', in D. Deming and S. Seager (eds.), *Scientific Frontiers in Research on Extrasolar Planets*, ASP Conference Series **294**, ASP, San Francisco, ISBN: 1-58381-141-9, pp. 117–128.

Ford, E.B., Havlickova, M., and Rasio, F.A.: 2001, 'Dynamical instabilities in extrasolar planetary systems containing two giant planets', *Icarus* **150**, 303–313.

Gilliland, R.L., *et al.*: 2000, 'A lack of planets in 47 Tucanae from a Hubble Space Telescope search', *Astrophys. J.* **545**, L47–L51.

Goldreich, P., Lithwick, Y., and Sari, R.: 2004, 'Planet Formation by Coagulation: A Focus on Uranus and Neptune', *Ann. Rev. Astron. Astrophys.* **42**, in press.

Goldreich, P. and Tremaine, S.: 1980, 'Disk-satellite interactions', *Astrophys. J.* **241**, 425–441.
Goldreich, P. and Ward, W.R.: 1973, 'The Formation of Planetesimals', *Astrophys. J.* **183**, 1051–1062.
Goodman, A.A., Benson, P.J., Fuller, G.A., and Myers, P.C.: 1993, 'Dense cores in dark clouds. VIII - Velocity gradients', *Astrophys. J.* **406**, 528–547.
Goodman, J. and Pindor, B.: 2000, 'Secular instability and planetesimal formation in the dust layer', *Icarus* **148**, 537–549.
Haisch, K.E., Jr., Lada, E.A., and Lada, C.J.: 2001, 'Disk frequencies and lifetimes in young clusters', *Astrophys. J.* **553**, L153–L156.
Inaba, S., Wetherill, G.W., and Ikoma, M.: 2003, 'Formation of gas giant planets: core accretion models with fragmentation and planetary envelope', *Icarus* **166**, 46–62.
Hewins, R., Jones, R., and Scott, E. (eds.): 1996, *Chondrules and the Protoplanetary Disk*, Cambridge Univ. Press.
Hollenbach, D., Yorke, H.W., and Johnstone, D.: 2000, 'Disk dispersal around young stars', in V. Mannings, A.P. Boss, and S. Russell (eds.), *Protostars and Planets IV*, Univ. Arizona Press, Tucson, pp. 401–428.
Holman, M.J., Touma, J., and Tremaine, S.: 1997, 'Chaotic variations in the eccentricity of the planet orbiting 16 CYG B.', *Nature* **386**, 254–256.
Hubbard, W.B., Podolak, M., and Stevenson, D.J.: 1995, 'The interior of Neptune', in D.P. Cruikshank (ed.), *Neptune and Triton*, Univ. Arizona Press, Tucson, pp. 109–138.
Hubickyj, O., Bodenheimer, P., and Lissauer, J.J.: 2005, in preparation.
Lada, E.A., Strom, K.M., and Myers, P.C.: 1993, 'Environments of star formation – Relationship between molecular clouds, dense cores and young stars', in E.H. Levy and J.I. Lunine (ed.), *Protostars and Planets III*, Univ. Arizona Press, Tucson, pp. 245–277.
Lada, E.A.: 2003, 'Evolution of circumstellar disks in young stellar clusters', Am. Astron. Soc. Meeting 202, abstract # 24.06.
Laskar, J.: 2000, 'On the spacing of planetary systems', *Phys. Rev. Lett.* **84**, 3240–3243.
Laughlin, G., and Bodenheimer, P.: 1994, 'Nonaxisymmetric evolution in protostellar disks', *Astrophys. J.* **436**, 335–354.
Laughlin, G. and Adams, F.C.: 1998, 'The modification of planetary orbits in dense open clusters', *Astrophys. J.* **508**, L171–L174.
Levison, H.F., Lissauer, J.J., and Duncan, M.J.: 1998, 'Modeling the diversity of outer planetary systems', *Astron. J.* **116**, 1998–2014.
Lin, D.N.C., Bodenheimer, P., and Richardson, D.C.: 1996, 'Orbital migration of the planetary companion of 51 Pegasi to its present location', *Nature* **380**, 606–607.
Lin, D.N.C. and Papaloizou, J.C.B.: 1979, 'Tidal torques on accretion discs in binary systems with extreme mass ratios', *Mon. Not. Royal Astron. Soc.* **186**, 799–812.
Lin, D.N.C., Papaloizou, J.C.B., Terquem, C., Bryden, G., and Ida, S.: 2000, 'Orbital evolution and planet-star tidal interaction', in V. Mannings, A. P. Boss, and S. Russell (eds.), *Protostars and Planets IV*, Univ. Arizona Press, Tucosn, pp. 1111–1134.
Lissauer, J.J.: 1987, 'Timescales for planetary accretion and the structure of the protoplanetary disk', *Icarus* **69**, 249–265.
Lissauer, J.J.: 1993, 'Planet formation', *Ann. Rev. Astron. Astrophys.* **31**, 129–174.
Lissauer, J.J.: 1995, 'Urey prize lecture: On the diversity of plausible planetary systems', *Icarus* **114**, 217–236.
Lissauer, J.J.: 2004, 'Formation of giant planets and brown dwarfs', in J.-P. Beaulieu, A. Lecavelier des Etangs, and C. Terquem (eds.), *Extrasolar Planets, Today and Tomorrow*, ASP Conf. Ser. 3xx, Astron. Soc. of the Pacific, San Francisco, in press.
Lissauer, J.J., Pollack, J.B., Wetherill, G.W., and Stevenson, D.J.: 1995, 'Formation of the Neptune System', in D. Cruikshank (ed.), *Neptune and Triton*, Univ. Arizona Press, Tucson, pp. 37–108.

Livio, M. and Pringle, J.E.: 2003, 'Metallicity, planetary formation and migration', *Mon. Not. Roy. Astron. Soc.* **346**, L42–L44.

Mac Low, M. and Klessen, R.S.: 2004, 'Control of star formation by supersonic turbulence', *Rev. Modern Phys.* **76**, 125–194.

Marcy, G.W., Butler, R.P., Fischer, D.A., and Vogt, S.S.: 2004, in J.-P. Beaulieu, A. Lecavelier des Etangs, and C. Terquem (eds.), *Extrasolar Planets, Today and Tomorrow*, ASP Conf. Ser. 3xx, Astron. Soc. of the Pacific, San Francisco, in press.

Masset, F.S., and Papaloizou, J.C.B.: 2003, 'Runaway migration and the formation of hot Jupiters', *Astrophys. J.* **588**, 494–508.

Mayer, L., Quinn, T., Wadsley, J., and Stadel, J.: 2002, 'Formation of giant planets by fragmentation of protoplanetary disks', *Science* **298**, 1756–1759.

Mayor, M., *et al.*: 2004, in J.-P. Beaulieu, A. Lecavelier des Etangs, and C. Terquem (eds.), *Extrasolar Planets, Today and Tomorrow*, ASP Conf. Ser. 3xx, Astron. Soc. of the Pacific, San Francisco, in press.

McCaughrean, M.J., Stepelfeldt, K.R., and Close, L.M.: 2000, 'High-resolution optical and near-infrared imaging of young circumstellar disks', in V. Mannings, A.P. Boss, and S. Russell (eds.), *Protostars and Planets IV*, Univ. Arizona Press, Tucson, pp. 485–507.

Metchev, S.A., Hillenbrand, L.A., and Meyer, M.R.: 2004, 'Ten micron observations of nearby young stars', *Astrophys. J.* **600**, 435–450.

Nakano, T.: 1987, 'Formation of planets around stars of various masses. I – Formulationand a star of one solar mass', *Mon. Not. Roy. Astron. Soc.* **224**, 107–130.

Podolak, M.: 2003, 'The contribution of small grains to the opacity of protoplanetary atmospheres', *Icarus* **165**, 428–437.

Pollack, J.B., Hubickyj, O., Bodenheimer, P., Lissauer, J.J., Podolak, M., and Greenzweig, Y.: 1996, 'Formation of the giant planets by concurrent accretion of solids and gas', *Icarus* **124**, 62–85.

Rasio, F.A. and Ford, E.B.: 1996, 'Dynamical instabilities and the formation of extrasolar planetary systems', *Science* **274**, 954–956.

Safronov, V.S.: 1969, *Evolution of the protoplanetary cloud and formation of the Earth and planets*, in Russian, Nauka Press, Moscow, 1972 English translation: NASA TTF-677.

Santos, N.C., Israelian, G., Mayor, M., Rebolo, R., and Udry, S.: 2003, 'Statistical properties of exoplanets. II. Metallicity, orbital parameters, and space velocities', *Astron. Astrophys.* **398**, 363–376.

Showalter, M.R.: 1991, 'Visual detection of 1981S13, Saturn's eighteenth satellite, and its role in the Encke gap', *Nature* **351**, 709–713.

Sigurdsson, S.: 1993, 'Genesis of a planet in Messier 4', *Astrophys. J.* **415**, L43–L46.

Sigurdsson, S, Richer, H.B., Hansen, B.M., Stairs, I.H., and Thorsett, S.E.,: 2003, 'A young white dwarf companion to pulsar B1620-26: Evidence for early planet formation', *Science* **301**, 193–196.

Strom, S.E., Edwards, S., and Skrutskie, M.F.: 1993, 'Evolutionary time scales for circumstellar disks associated with intermediate- and solar-type stars', in E.H. Levy, and J.I. Lunine (eds.), *Protostars and Planets III*, Univ. Arizona Press, Tucson, pp. 837–866.

Thommes, E.W. and Lissauer, J.J.: 2003, in *Proc. Astrophysics of Life Conf.*, Cambridge Univ. Press, in press.

Thommes, E.W., Duncan, M.J., and Levison, H.F.: 2003, 'Oligarchic growth of giant planets', *Icarus* **161**, 431–455.

Ward, W.R.: 1986, 'Density waves in the solar nebula – differential Lindblad torque', *Icarus* **67**, 164–180.

Ward, W.R.: 2000, 'On planetesimal formation: the role of collective particle behavior', in R.M. Canup, and K. Righter (eds.), *Origin of the Earth and Moon*, Univ. Arizona Press, Tucson, pp. 75–84.

Ward, W.R. and Hahn, J.M.: 2000, 'Disk-planet interactions and the formation of planetary systems', in V. Mannings, A.P. Boss, and S. Russell (eds.), *Protostars and Planets IV*, Univ. Arizona Press, Tucson, pp. 1135–1155.

Weidenschilling, S.J. and Cuzzi, J.N.: 1993, 'Formation of planetesimals in the solar nebula', in E.H. Levy and J.I. Lunine (eds.), *Protostars and Planets III*, Univ. Arizona Press, Tucson, pp. 1031–1060.

Weidenschilling, S.J. and Marzari, F.: 1996, 'Gravitational scattering as a possible origin for giant planets at small stellar distances', *Nature* **384**, 619–621.

Weidenschilling, S.J., Marzari, F., Davis, D.R.,: 2004, 'Accretion of the Outer Planets: Oligarchy or Monarchy?', *Lunar and Planetary Institute Conference Abstracts* **35**, 1174.

Wetherill, G.W.: 1990, 'Formation of the Earth', *Ann. Rev. Earth Plan. Sci.* **18**, 205–256.

Wuchterl, G. and Tscharnuter, W.M.: 2003, 'From clouds to stars. Protostellar collapse and the evolution to the pre-main sequence I. Equations and evolution in the Hertzsprung-Russell diagram', *Astron. Astrophys.* **398**, 1081–1090.

Wuchterl, G., Guillot, T., and Lissauer, J.J.: 2000, 'Giant planet formation', in V. Mannings, A. P. Boss, and S. Russell (eds.), *Protostars and Planets IV*, Univ. Arizona Press, Tucson, pp. 1081–1109.

Youdin, A.N. and Shu, F.H.: 2002, 'Planetesimal formation by gravitational instability', *Astrophys. J.* **580**, 494–505.

Young, R.E.: 2003, 'The Galileo probe: how it has changed our understanding of Jupiter', *New Astron. Rev.* **47**, 1–51.

Zapatero Osorio, M.R., Béjar, V.J.S., Martín, E.L., Rebolo, R., Barrado y Navascués, D., Bailer-Jones, C.A.L., and Mundt, R.: 2000, 'Discovery of young, isolated planetary mass objects in the C9-Orionis star cluster', *Science* **290**, 103–107.

Address for Offprints: Jack J. Lissauer, NASA Ames Research Center, Space Science Division, MS 245-3, Moffett Field, CA 94035, USA; `jlissauer@ringside.arc.nasa.gov`

FORMATION AND COMPOSITION OF PLANETESIMALS

Trapping Volatiles by Clathration

DANIEL GAUTIER[1] and FRANCK HERSANT[2]
[1] *Laboratoire d'Etudes et d'Instrumentation en Astrophysique (LESIA), Observatoire de Paris, F-92195 Meudon Cedex, France*
[2] *Institut für Theoretische Astrophysik, Tiergartenstraße 15, D-69121 Heidelberg, Germany*

Received: 19 July 2004; Accepted in final form: 28 October 2004

Abstract. The composition of planetesimals depends upon the epoch and the location of their formation in the solar nebula. Meteorites produced in the hot inner nebula contain refractory compounds. Volatiles were present in icy planetesimals and cometesimals produced in the cold outer nebula. However, the mechanism responsible for their trapping is still controversial. We argue for a general scenario valid in all regions of the turbulent nebula where water condensed as a crystalline ice (Hersant *et al.*, 2004). Volatiles were trapped in the form of clathrate hydrates in the continuously cooling nebula. The epoch of clathration of a given species depends upon the temperature and the pressure required for the stability of the clathrate hydrate. The efficiency of the mechanism depends upon the local amount of ice available. This scenario is the only one so far which proposes a quantitative interpretation of the non detection of N_2 in several comets of the Oort cloud (Iro *et al.*, 2003). It may explain the large variation of the CO abundance observed in comets and predicts an Ar/O ratio much less than the upper limit of 0.1 times the solar ratio estimated on C/2001 A2 (Weaver *et al.*, 2002). Under the assumption that the amount of water ice present at 5 AU was higher than the value corresponding to the solar O/H ratio by a factor 2.2 at least, the clathration scenario reproduces the quasi uniform enrichment with respect to solar of the Ar, Kr, Xe, C, N and S elements measured in Jupiter by the Galileo probe. The interpretation of the non-uniform enrichment in C, N and S in Saturn requires that ice was less abundant at 10 AU than at 5 AU so that CO and N_2 were not clathrated in the feeding zone of the planet while CH_4, NH_3 and H_2S were. As a result, the $^{14}N/^{15}N$ ratio in Saturn should be intermediate between that in Jupiter and the terrestrial ratio. Ar and Kr should be solar while Xe should be enriched by a factor 17. The enrichments in C, N and S in Uranus and Neptune suggest that available ice was able to form clathrates of CH_4, CO and the NH_3 hydrate, but not the clathrate of N_2. The enrichment of oxygen by a factor 440 in Neptune inferred by Lodders and Fegley (1994) from the detection of CO in the troposphere of the planet is higher by at least a factor 2.5 than the lower limit of O/H required for the clathration of CO and CH_4 and for the hydration of NH_3. If CO detected by Encrenaz *et al.* (2004) in Uranus originates from the interior of the planet, the O/H ratio in the envelope must be around of order of 260 times the solar ratio, then also consistent with the trapping of detected volatiles by clathration. It is predicted that Ar and Kr are solar in the two planets while Xe would be enriched by a factor 30 to 70. Observational tests of the validity of the clathration scenario are proposed.

Keywords: planet formation; composition of planetesimals; clathrates

Space Science Reviews 116: 25–52, 2005.
DOI: 10.1007/s11214-005-1946-2

1. Introduction

Disks observed around young stars are composed of gases and grains. It is believed that the primitive Solar Nebula exhibited a similar structure and evolution. Although it is relatively simple, in principle, to model from hot temperature chemistry the composition in refractory material of grains embedded in the nebula, it is less obvious to explain the presence of a number of volatiles, difficult to condense, in giant planets and comets. Moreover, it was currently assumed in the ancient literature that elements which formed volatiles were in solar abundance throughout the nebula. However, as early as 1978, Gulkis *et al.* suggested that sulfur is substantially oversolar in the tropospheres of Uranus and Neptune. Observations made in the eighties subsequently revealed that the four giant planets are enriched in carbon with respect to the solar abundance (Gautier and Owen, 1989). Recently, the Galileo probe performing in situ measurements in the troposphere of Jupiter found that C, N, S, Ar, Kr and Xe were all enriched by a factor 2 to 4 (Owen *et al.*, 1999; Mahaffy *et al.*, 2000). This uniform enrichment was unexpected. Moreover, Cochran *et al.* (2000) and Cochran (2002) observed that N_2 is strongly depleted with respect to CO in three comets originating from the Oort cloud.

In this report, we attempt to explain all these results by a unique mechanism which is the trapping of volatiles in crystalline water ice in the form of clathrate hydrates, in the cooling solar nebula. The quantitative interpretation requires the use of an evolutionary model of the nebula consistent with observations of disks around young stars and with Solar System data.

Observational constraints used for the adopted model are described in Section 2. The characteristics of the model are summarized in Section 3. In Section 4, the radial distributions of gases and grains present in the early nebula are discussed. Various scenarios for trapping volatiles are presented in Section 5, and reasons for exploring in details the clathration scenario for interpreting enrichments in giant planets and comets are given. An interpretation of the unexpected strong depletion of N_2 with respect to CO observed in comets is described in Section 6. Section 7 is devoted to the interpretation of the enrichments measured in Jupiter, Saturn, Uranus and Neptune, and to predictions about the enrichments of noble gases in the three last planets. In Section 8, we present a global interpretation of the enrichments, and we show that they depend upon the amount of ices available in the regions of formation of the considered objects. Tests of the clathration scenario are proposed in Section 9.

2. Observational Constraints on Models

Many models of the solar nebula have been elaborated. Unfortunately, these models are not always compared to solar system data and observations of disks around young stars.

2.1. Constraints from Circumstellar Disks

The evolutionary character of accretion disks around young stars is now well established (Hartmann, 2000; Calvet *et al.*, 2000). The luminosity and the inferred accretion rate decrease with time. In spite of a substantial scatter of measurements, the trend seems to be real and the decrease of the accretion rate may be reproduced by a power law of time, as that initially proposed by Makalkin and Dorofeyeva (1991) from numerical models. This implies a decrease with time of the radial temperature, as modeled for instance by Hersant *et al.* (2001). The lifetime of observed disks does not exceed 10 My (Calvet *et al.*, 2000) in agreement with the assumption that the accretion flow is turbulent. This assumption also provides a satisfying interpretation of the amount of energy dissipation required to explain observed luminosities (Pringle, 1981). In addition, as detailed below, there is evidence that microscopic grains persist or are replenished in disks for several millions of years (Clampin *et al.*, 2003).

2.2. Constraints from Solar System Data

An obvious constraint is that the angular momentum must have been transported throughout the nebula, since the momentum of the solar system today is mainly due to Jupiter. It is currently admitted that this transport was made by turbulence. Turbulent motions enhance transport properties and accelerate the evolution of the temperature and density in the disk (Pringle, 1981).

A second constraint on the temperature model of the early inner nebula is provided from the composition of meteorites. The temperature must have been between 400 K and 1400 K in the 1-5 AU heliocentric range during the so-called T Tauri epoch, as discussed in details by Bell *et al.* (2000). High temperatures as well as low temperatures are inferred from calculations of condensation of various elements present in meteorites.

The D/H ratio radial distribution in water, or in other trace species present in Solar System objects, provides powerful constraints on the structure of nebula models. Observations reveal that a gradient of D/H does occur between meteorites formed in the inner nebula and comets formed in the outer nebula (for a review, see Robert *et al.*, 2000). The D/H ratio in water and in HCN in comets is much higher than the protosolar value, namely the D/H ratio in hydrogen of the nebula. The protosolar D/H ratio derived by Geiss and Gloeckler (1998) from solar wind measurements of ^{3}He/^{4}He is $(2.1 \pm 0.5) \times 10^{-5}$. In H_2O in comets, it is equal to about 15 times the protosolar value. This must result from the isotopic enrichment acquired in ices in the presolar cloud through ion-molecules reactions. A modest decrease of the D/H value subsequently occurred in the nebula due to isotopic exchange with hydrogen as soon as ices vaporized (Drouart *et al.*, 1999; Mousis *et al.*, 2000; Hersant *et al.*, 2001). On the other hand, the D/H ratio in OH in chondrules of LL3 meteorites is about 4 times higher than the protosolar value (Robert *et al.*, 2000). High temperatures present in the early nebula imply that D

in OH was initially completely reequilibrated with D in H_2 in the inner nebula. When the nebula subsequently cooled, only a modest enrichment with respect to the protosolar value may have occurred around 3 AU from the Sun (by a factor less than 1.5). The only way to interpret the D/H measurements in LL3 is then to take into account the turbulent mixing of the matter of the inner nebula with that of the outer nebula, as made by Drouart *et al.* (1999) and Hersant *et al.* (2001). These authors have integrated the equation of transport of the enrichment factor throughout the nebula which depends upon the physical characteristics of the nebula. As in most of nebula models, they follow the prescription of Shakura and Sunyaev (1973) in which the turbulent viscosity is defined as the product of a dimensionless coefficient α multiplied by the local speed of sound and by the half-thickness of the disk. Constraining calculations to fit D/H values in LL3 meteorites and comets then imposes a limited range of values of α. In turn, the ranges of temperature and density distributions throughout the nebula are constrained to be consistent with deuterium observations.

3. An Example of Evolutionary Turbulent Model

The two-dimensional evolutionary model of Hersant *et al.* (2001) satisfies all spatial and temporal constraints mentioned above. The characteristic time of mixing in the nebula in this model is of order of 20,000 y. The Prandtl number has been taken equal to 0.7. The angular momentum is assumed to have been transported outwards to Neptune in 250,000 y. The structure of this model is represented on Figure 1 at $t = 100,000$ y and $t = 650,000$ y. It is defined by the values of α, of the initial accretion rate and of the initial radius indicated on the figure caption. Isodensity contours and isothermal contours are shown. It can be seen that the radial extent of the nebula increases with time while its thickness decreases with time. The whole nebula cools with time. However, at 5 AU, water has not yet begun to condense at $t = 0.65$ My.

This α model of Hersant *et al.* (2001) is not complete for several reasons. It assumes that the heating comes uniquely from the turbulent viscosity, so that the slant heating from the early Sun central is not taken into account. Indeed, D'Alessio *et al.* (1998) showed that the Sun must have heated the envelope of the nebula at large heliocentric distances, which must have resulted to some increase of the temperature in the ecliptic plane where planets formed. However, observations of circumstellar disks indicate that the heating by the central star does not preclude the dramatic decline of the luminosity and of the accretion rate (by three orders of magnitude in a few My). In our approach, this is the main cause, through the cooling of the radial temperature distribution, of the trapping of volatiles studied in the present work. Moreover, the persistence of the dust opacity for several millions of years in circumstellar disks, revealed by images from Hubble and by millimeter ground based observations(see Section 4.4) suggests that the radial heating of the

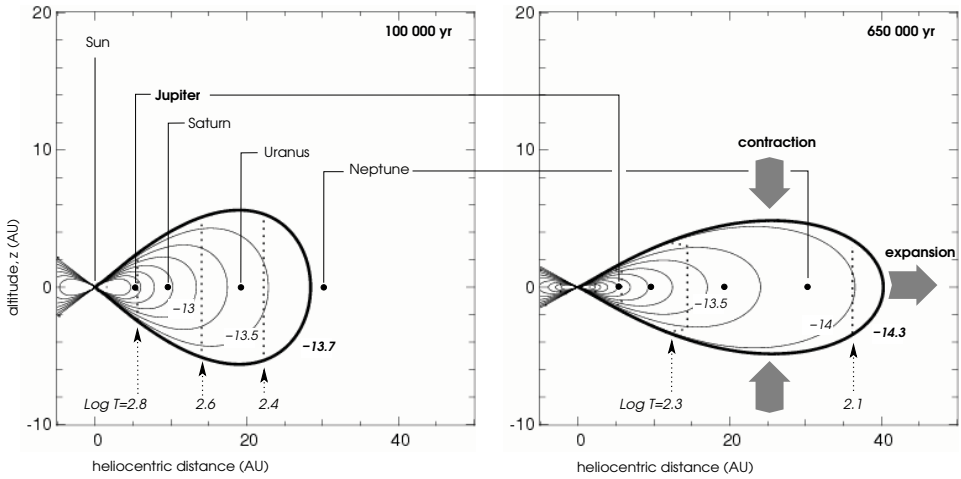

Figure 1. 2-D representation of the nebula model of Hersant *et al.* (2001) at $t = 0.1$ My and $t = 0.65$ My after the formation of the Sun. Contours in continuous line correspond to isodensities indicated by the logarithm of the value in g.cm^{-3}; dashed lines correspond to isotherms given in logarithm of the temperature in K. The vertical ordinate indicates the thickness of the disk, in AU, the horizontal ordinate indicates the heliocentric distance, in AU. The model is calculated for $\alpha = 9 \times 10^{-3}$, an initial accretion rate of 5×10^{-6} solar mass per year, and a initial radius of 17 AU. Locations of giant planets today are indicated by dots. (Courtesy of Jean-Marc Huré.)

nebula by the Sun did not occur during the life time of the nebula, and in any case at epochs where Jupiter, Saturn and comets formed. We also believe that neglecting the self gravity (Huré, 2000) is acceptable at distances of interest, namely in the part of the nebula interior to the present location of Neptune. Finally, we did not make any attempt to take into account a possible migration of the giant planets. This problem is discussed by Alibert *et al.* (2004). In spite of these restrictive assumptions, the model of Hersant *et al.* (2001) permits up to plausibly reproduce, under the assumption that volatiles were trapped by clathration, the enrichment in volatiles with respect to solar values measured in giant planets, and the nitrogen deficiency in comets of the Oort cloud.It provides interpretations for the gradient of D/H in water between meteorites and comets, and for the enrichment in deuterium in Uranus and Neptune with respect to the value in Jupiter and Saturn. Finally, it is consistent with suspected differences in the composition of grains between the inner and the outer nebula.

4. Origin of Planetesimals: Gases and Grains in the Early Nebula

Modeling the chemistry of the presolar cloud is complex. The medium is tenuous, ionized and at very low temperature. However, we know that elements were in

solar abundance. On the other hand, the cloud contained dust material which was presumably a mixture of many different condensates with quite different compositions (Pollack *et al.*, 1994). The fate of gases and grains entering the disk depended upon the temperature-density structure of the nebula and of its evolution.

4.1. The Inner Nebula

Recent models of the chemistry of the inner nebula consider two sources of material. Quite close to the Sun, very high temperatures (6000 K) dissociated the falling matter in elements, especially in free H, C, N, O, Mg, Fe, Si, and S atoms (Finocchi *et al.*, 1997). Atoms subsequently formed molecules or chemically combined to produce dust in the cooling nebula. Alternatively, the interstellar dust may have survived to its fall from the presolar cloud farther than about 1 AU from the Sun. When moving inwards to hot regions, it was destroyed and also produced gases. This question has been extensively discussed by a number of authors (see, for instance, Prinn and Fegley, 1989; Gail, 1998), but is far to be completely solved.

The case of CNO compounds is especially important because of their large cosmic abundance. According to chemical models of the nebula, N atoms formed N_2 molecules near the Sun. C atoms combined to OH and free O atoms and produced a substantial amount of CO. Moreover, CH_4 and more complex organics were produced between the present positions of Venus and Mars (Finocchi *et al.*, 1997). Part of C and N may also have been in the form of organics originating from the presolar cloud, as like-kerogen compounds which do not vaporize at temperatures lower than 625 K. Sulfur atoms formed H_2S at high temperatures, a part of which was subsequently converted into solid FeS and/or SiS, MgS and CaS (Fegley, 2000; Pasek *et al.*, 2004). Oxygen formed water vapor or combined to minerals to produce H_2O-bearing components.

Solid phase materials produced grains and subsequently planetesimals. Meteorites found today are presumably relics of planetesimals which formed telluric planets, and possibly the cores of giant planets. Their composition does not permit us however to interpret that of envelopes of these planets.

4.2. The Outer Nebula

The situation is completely different in the cold outer nebula where the chemistry between neutral components is kinetically inhibited. Falling interstellar ices may vaporize, depending on the local temperature, the shock heating and the gas drag. If they did, they condensed again as soon as the local temperature was lower than that of their condensation. For this reason, it is currently argued that the composition of icy grains and thus of comets must be similar to that of the presolar cloud. However, molecular nitrogen expected to be the main carrier of nitrogen in the ISM, is missing in several comets, as discussed in Section 5. Argon has not been detected either: its upper limit compared to oxygen is as low as 0.1 times the solar Ar/O ratio (Weaver *et al.*, 2002). Nitrogen is mainly in the form of NH_3 in the

envelope of comets, and carbon in the form of CO (although CH_4 is as abundant as CO in a few comets, Gibb *et al.*, 2003).

However, C and N are also contained in solid organics. The most abundant sulfured compound is H_2S, although CS_2, SO_2, and OCS were also found in a significant abundance in comet Hale-Bopp (Bockelée-Morvan *et al.*, 2000). The total amount of sulfur contained in the four sulfured compounds corresponds to an approximatively solar S/O ratio.

The D/H ratio in water, and in HCN, in comets is strongly enriched with respect to the protosolar value, which implies an interstellar origin for water ices, but does not rule out that HDO and HCN in gaseous phase partially reequilibrated with H_2 in the early nebula (Hersant *et al.*, 2001).

It is important to note that *most of the mass of the gaseous nebula is located in its outer part* (in current nebula models). In other words, the mass of a gas for which the mixing ratio is assumed to be constant with heliocentric distance is mainly in the outer nebula.

4.3. Mixing of Matter Between the Two Regions

As mentioned in Section 2.1, the main evidence of mixing of matter between the inner and the outer nebula comes measurements of D/H in OH in LL3 meteorites. Accordingly, gaseous components should have been mixed throughout the nebula, unless a source (efficient chemical conversion from another species) or a sink (condensation or conversion to another gaseous or solid component) occurs somewhere. In this last case, the determination of the radial distribution of the species throughout the whole nebula requires the integration, with respect to space and time (since chemical reactions strongly depend upon time), of the equation of transport with diffusion. Such a complex exercise is frequently omitted in the literature. The inwards accretion of water from the outer nebula is especially important since it can result in a large amount of water ice in the region of formation of Jupiter. Implications of this statement are developed in Section 5.

4.4. The Story of Grains in the Nebula

Theoretical calculations of the agglomeration of grains in the nebula suggest that planetesimals grew fast, in a few ten thousand years (Weidenschilling, 1997), so that microscopic grains should rapidly disappear. However, observations of disks around T Tauri or Herbig Ae stars lead to different conclusions. Millimeter measurements of the continuum opacity, mainly due to grains, provide evidence for the persistence of small size grains for millions of years. They suggest massive dust disks of millimeter-size grains (Beckwith *et al.*, 2000; Natta *et al.*, 2000; Haisch *et al.*, 2001) which disappear not earlier than a few 10^6 or 10^7 y. Moreover, pictures made by the Hubble Space Telescope reveal that relatively ancient circumstellar disks are dusty. A beautiful example is the disk observed around HD 141569 A, a 5-million-year-old-star (Clampin *et al.*, 2003). The disk which extends up to

400 AU from the star, is full of small size grains. Clampin *et al.* (2003) suggested a distribution of grain sizes which obeys a power law, with radii extrema of 0.4 and 10 μm. We do not negate that grains must have rapidly agglomerated and grown up, but *we argue that disk observations provide evidence that small size grains are replenished in the disk for millions of years, either by collisions between large size planetesimals, or from an unidentified source*. The catastrophic disruption of planetesimals by collisions has been investigated by a number of authors (see, for instance, Benz, 2000). Michel *et al.* (2003) found evidence for disruption of fragmented parent parent bodies which formed a number of asteroid families In the following section, we will show that microscopic grains of water ice play a major role in the envisaged scenarios for trapping volatiles.

5. Trapping Volatiles in Planetesimals and Cometesimals

Processes responsible for trapping volatiles in planetesimals are controversial. One enigma is the unexpected low value of the upper limit of the N_2/CO ratio inferred in three comets of the Oort cloud (Cochran *et al.*, 2000; Cochran, 2002). Another puzzling result was found by the mass spectrometer aboard the Galileo entry probe in Jupiter. The six following elements were measured enriched by a factor 2 to 4 with respect to the solar abundance of Anders and Grevesse (1989): Ar, Kr, Xe, C, N, and S (Atreya *et al.*, 1999; Mahaffy *et al.*, 2000).

A self-consistent scenario for the formation of the four giant planets has been described by Pollack *et al.* (1996). Although certainly subject to revisions, this scenario is considered as the most plausible so far. According to Pollack *et al.* (1996), Jupiter and Saturn were formed in three phases, while Uranus and Neptune did not reach the third phase. During phase 1, a core of order of 10 Earth masses ($M_\oplus$) is accreted from a swarm of planetesimals in about 0.5 My. These planetesimals were presumably mainly composed of rocks. Phase 2, which is strongly model dependent, took 7 My in the baseline model of Pollack *et al.* (1996), and was characterized by a slow accretion of icy planetesimals and of some hydrogen. Phase 3, which was extremely fast (10,000 to 20,000 y, Magni and Coradini, 2004), corresponded to the collapse of all hydrogen and solid matter located within the radius of Hill. Assuming that the core was not eroded since its formation, the collapse formed most of the present envelope of Jupiter.

In the framework of this theory, three mechanisms for trapping volatiles in the feeding zone of the planet, can be a priori envisaged: (i) condensation of gases in the cooling nebula, (ii) adsorption of volatiles on amorphous water ice, (iii) trapping of volatiles in the form of clathrate hydrates.

5.1. CONDENSATION

The uniform enrichment found in Jupiter could result from the condensation of volatiles and their incorporation in planetesimals during phase 2. Argon condenses at about 20 K in nebula pressure conditions. According to the nominal model of nebula of Hersant *et al.* (2001), this temperature was reached at 5 AU at about 4.6 My after the formation of the Sun (Iro *et al.*, 2003; Hersant *et al.*, 2004), which may have occurred during phase 2 in the nominal model of Pollack *et al.* (1996). However, the condensation process is in conflict with the strong depletion of N_2 with respect to CO in several Oort cloud comets. These gases exhibit quite close temperatures of condensation, so that both should be present in comets in near solar proportions. It is currently assumed that C was mainly in the form of CO, and N in the form of N_2 in the solar nebula, so that the N_2/CO ratio should be of order of 0.16. However, the upper limit of N_2/CO ratio does not exceed 10^{-4} to 5.5×10^{-4} in comets deVico, Hale-Bopp, and 153P/Ikeya-Zhang (Cochran *et al.*, 2000; Cochran, 2002).

5.2. TRAPPING VOLATILES IN AMORPHOUS ICE

On the basis of laboratory measurements conducted at very low temperatures, it was argued that volatiles were trapped in amorphous ice (Owen and Bar-Nun, 1995; Notesco *et al.*, 2003). This scenario likely occurred in the tenuous presolar cloud. However, thermophysical conditions occurring in the dense solar nebula are very different from those in the ISM. Water ices falling from the presolar cloud onto the nebula discoid vaporized outwards to about 30 AU from the Sun (Chick and Cassen, 1997), either because the local temperature was higher than the condensation temperature, or because of the heating shock or because of the gas drag (Lunine *et al.*, 1991; Chick and Cassen, 1997). When they condensed again in the cooling nebula, ice was necessarily crystalline (Kouchi *et al.*, 1994). Since the temperature continued to decrease, all water vapor initially available was rapidly consumed so that only a tiny amount of amorphous ice, if any, could have been produced at very low temperature and pressure, very late in the story in the nebula. The trapping of volatiles by amorphous ice thus does not seem to have occurred in the region of formation of giant planets. Interestingly enough, water ice has been detected to be mainly crystalline in the cold part of the disk surrounding the young star HD 142527 (Malfait *et al.*, 1999). Moreover, crystalline ice has also been detected in comet Hale-Bopp with the long wavelength spectrometer aboard the Infrared Space Observatory (ISO) by Lellouch *et al.* (1998). However, it might be objected that ice may have been converted from an amorphous to a cubic crystalline form either at the surface of the core or in the coma when the temperature reached temperatures higher than $125 - 130$ K (Schmitt *et al.*, 1998). On the other hand, Kawakita *et al.* (2004), observing comet C/2002 T7 (Linear) in the near infrared range argue that the absence on the observed spectrum of the 1.65 micron feature of crystalline ice implies that ice is amorphous. But Schmitt (2004,

private communication) objects that Kawakita *et al.* (2004) used optical constants of ice at 40 K for which the 1.65 μm band is very strong while it is substantially weaker at 140 K (Schmitt *et al.*, 1998). The blackbody temperature of the comet during the observations of Kawakita *et al.* (2004) was 149 K.

The main objection to trapping volatiles in amorphous ice comes again from the observed N_2/CO ratio in comets. Owen and Bar-Nun (1995) predicted that, if volatiles were trapped in amorphous ice, icy planetesimals produced in the Uranus-Neptune region would have N_2/CO of about 0.06, which is higher by at least two orders of magnitude than the upper limits obtained by Cochran *et al.* (2000) and Cochran (2002) from observations mentioned above.

However, comets formed substantially farther than the present position of Neptune and could contain amorphous ice which originated from the presolar cloud and never evaporated. Future space missions towards periodic comets currently assumed to have been formed in the Kuiper-Edgeworth Belt could then detect a N_2 abundance moderately depleted with respect to that of CO, and consistent with the predictions of Owen and Bar-Nun (1995).

5.3. Trapping Volatiles in the Form of Clathrate Hydrates

Clathrate hydrates are water ice compounds in which water molecules form a lattice of cages where gaseous molecular species can be trapped (Van der Waals and Platteuw, 1959; Sloan, 1998). Clathrates of type I are X - 5.75 H_2O, where X is the guest molecule; clathrates of type II are X - 5.66 H_2O. CH_4, CO, Xe, and H_2S are of type I. N_2, Ar, and Kr are of type II. Applications to astrophysics have been detailed by Lunine and Stevenson (1985), and updated by Iro *et al.* (2003). Clathrate hydrates are stable only in a domain of temperatures and pressures located below the so-called curves of stability in the space ($T - P$). Such curves are represented on Figure 2 for species relevant to the enrichments of elements observed in Jupiter. Since carbon in gaseous phase is in the nebula in the form of CO and CH_4, and nitrogen in the form of N_2 or NH_3, we have plotted the curves of stability of these four species (Hersant *et al.*, 2004), assuming CO/CH_4 and N_2/NH_3 both equal to ten. C/H and N/H ratios in the nebula are assumed to be solar, which implies that the presence of C and N in organics is not considered. H_2S/H_2 is assumed to be equal to 1/2 the solar S/H ratio, namely neglecting CS_2, SO_2, and OCS found in a substantial abundance, as previously mentioned, in the comet Hale-Bopp (Bockelée-Morvan *et al.*, 2000). The conversion of H_2S to FeS and/or to other bearing sulfur compounds which may have occurred in the hot inner nebula (Lodders, 2003; Pasek *et al.*, 2004), is also ignored. Ar, Kr, and Xe are solar. All elemental abundances are from Anders and Grevesse (1989).

Adiabats of the nebula corresponding to the nominal model of Hersant *et al.* (2001) are shown on Figure 2 at 5, 10, and 15 AU. Clathrate hydrates of a given species are formed when the adiabat intercepts the curve of stability of the species. The key point of the analysis, initially proposed by Gautier *et al.* (2001), is that *it*

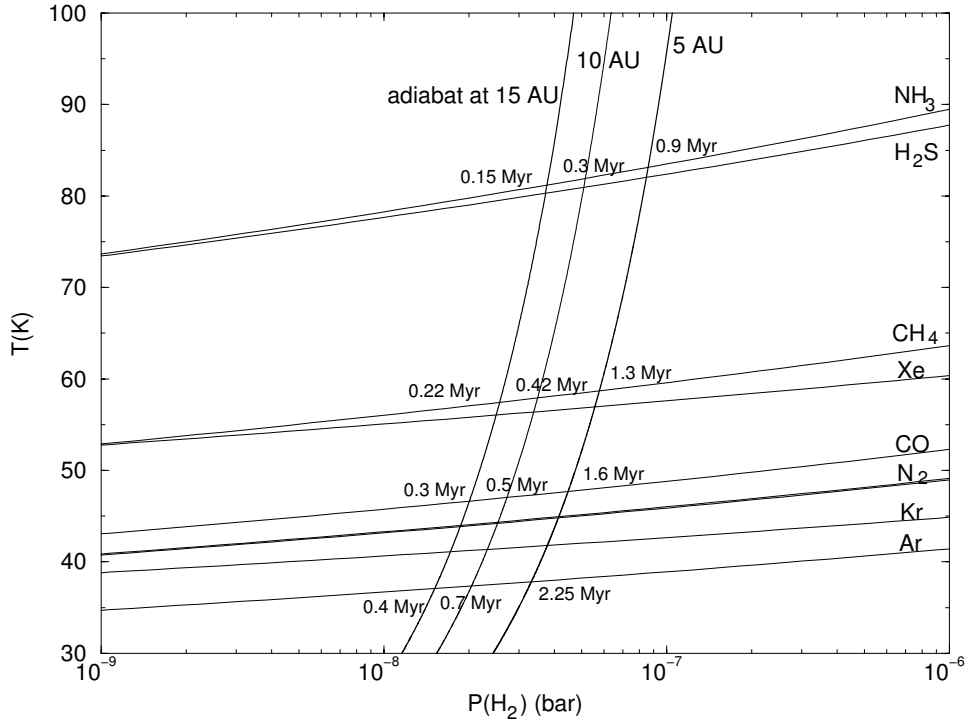

Figure 2. Curves of stability $T = f(P)$, where T is the temperature, and P the pressure of hydrogen in the nebula, of the clathrate hydrates of H_2S, CH_4, Xe, CO, N_2, Xe, Kr, and Ar together with the nebula adiabats of the nominal model of Hersant *et al.* (2001). The curve of condensation of the NH_3. H_2O hydrate is also shown. Calculations are made for mixing ratios of the considered species, with all elements in solar abundance. The CO/CH_4 and N_2/NH_3 ratios are both equal to ten. All sulfur is supposed to be in the form of H_2S (see text for discussions). The clathrate hydrate of a given species is stable in the domain located between the corresponding curve of stability. Considered volatiles are indicated on the right side of the figure. Epochs when they were trapped in the form of clathrate hydrates correspond, as indicated, to the intersection of adiabats with curves of stability. (Adapted from Hersant *et al.*, 2004.)

is assumed that solid clathrates agglomerated and formed grains which grew up rapidly: as soon as grains are of meter size, they decoupled from gas and orbit around the sun, or possibly migrated towards the central part of the nebula as a result of gas drag. In the case of giant planets, they orbited around the planetary core within the feeding zone of each planet. They are trapped in vortices by turbulence (see Section 8). Their surface density then remains constant while the surface density of untrapped gases continues to decrease with time. In the following, we will examine the consequences of adopting this scenario to the composition of comets and to that of giant planets.

6. Trapping Volatiles by Clathration in Cometary Grains

Figure 2 shows how volatiles were progressively trapped in the form of clathrate hydrates in the cooling nebula. The clathration (for the considered species) occurs relatively early in the 10-15 AU heliocentric range, where presumably comets of the Oort cloud formed. At 15 AU, all considered species might have been trapped at epochs between 0.15 My and 0.4 My after the formation of the Sun (in the adopted model of nebula). Water condensed at $T = 150$ K, which occurred at $t = 70,000$ y at 15 AU (Hersant *et al.*, 2001). Its surface density remained subsequently constant with time. The first chronological clathration is that of H_2S which occurred at $t = 150,000$ y (NH_3-H_2O is a simple hydrate). The surface density of H_2S decreases up to $t = 150,000$ y. The H_2S/H_2O ratio is then equal to the ratio of the surface density of water at $t = 70,000$ y to the surface density of H_2S at $t = 150,000$ y. Iro *et al.* (2003) then derived by this procedure a value of 1.4% for this ratio, which is compatible with measured values ranging, on a sample of 11 comets, from 0.12 to 1.5% (Biver *et al.*, 2002). Predictions for the cometary abundance can similarly be done for all species shown on Figure 2.

However, an interesting part of the scenario is that forming clathrate hydrates consumes a substantial amount of water (5.75 or 5.66 molecules of H_2O for one guest molecule in clathrates of Type I, 5.66 molecules of H_2O in clathrates of type II). CH_4, CO and N_2 being the most abundant species, they consume most of available water, in this chronological order. It then may happen that not enough water is available to trap N_2, or even a part of CO. Iro *et al.* (2003) have calculated that the amount of trapped CO increases with the abundance of available water ice, which may explain the large variability of CO in comets. They also showed that no N_2 can be trapped if the amount of water is less than about 2.8 times the solar O/H ratio per number (or 2.2, depending upon the CO/CH_4 ratio, Hersant *et al.*, 2004). This explains why N_2 is dramatically underabundant in comets Hale-Bopp, DeVico and Ikeya-Zhang. Figure 3 shows the N_2/CO ratio which would be obtained from the H_2O/H_2 ratio mentioned above, and that corresponding to a H_2O/H_2 ratio of 1.3 solar (O/H) ratio (which is the nebula abundance when oxygen has been used to form CO). The value predicted by this last model is clearly lower than the upper limits of N_2/CO in the three comets mentioned above. Actually, as shown on Figure 3, only the N_2^+/CO^+ ratio can be measured from ground based experiments. However, calculations predict that this ratio does not differ from the N_2/CO ratio by more than 10% (Cochran *et al.*, 2000). As mentioned in Section 4.4, argon has not been detected either and the upper limit of Ar/O is less than 0.1 time the solar Ar/O ratio (Weaver *et al.*, 2002). This is consistent with the depletion of N_2 since argon would have been clathrated at lower temperature than N_2, and thus at later epochs when crystalline ice required for clathration was missing.

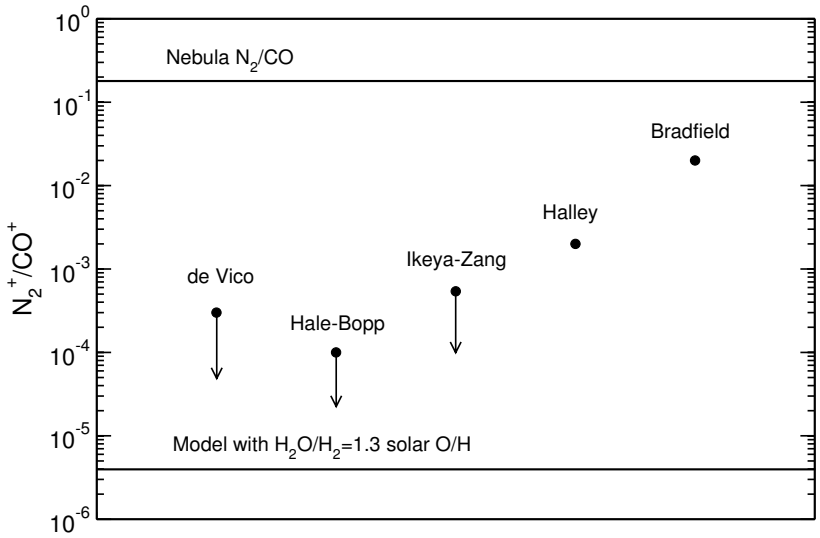

Figure 3. N_2^+/CO^+, equivalent to N_2/CO (Cochran *et al.*, 2000) in several comets. Values for comets Halley and Bradfield are from Wyckoff *et al.* (1991) for Comet Halley, and Lutz *et al.* (1993) for comet Bradfield ; The upper limits for Comet deVico and Comet Hale-Bopp are from Cochran *et al.* (2000) and the upper limit for Comet Ikeya-Zhang is from Cochran (2002). Calculated values of N_2/CO are from Iro *et al.* (2003). (Adapted from Iro *et al.*, 2003.)

7. Enrichment in Volatiles in Giant Planets by Clathration

7.1. Enrichment in Jupiter

The uniform enrichment in Ar, Kr, Xe, C, N, and O observed in Jupiter can be explained if all volatiles indicated on Figure 2, including Ar, were trapped in the form of clathrate hydrates, during phase 2 of the formation of Jupiter. For the considered model of nebula, at 5 AU, H_2O condensed at about 0.4 My, H_2S was clathrated at 0.5 My, and Ar at 2.25 My. As mentioned earlier, once formed the mass of each clathrate hydrate remained constant with time within the feeding zone of the planet, while the pressure of H_2 and other non condensable gases continued to decrease until the feeding zone collapsed onto the core of the planet. Therefore, the mixing ratio of the considered trapped volatile increased with time uniquely because the density of H_2 decreased. The abundance of any species brought to Jupiter corresponds to the mixing ratio acquired at the time of the hydrogen collapse. It is simply calculated from the ratio of the surface density of the considered species at the epoch of its clathration over the surface density of hydrogen at the time of the collapse. Determining this time is made by fitting the calculated enrichment of a given element to that measured in Jupiter: noble gases are more appropriate since

TABLE I
Enrichments of volatiles in the four giant planets[1].

species	Jupiter		Saturn		Uranus-Neptune	
	Observed	Calculated	Observed	Calculated	Observed	Calculated
Ar	2.5 ± 0.5[a]	2.46		1		1
Kr	2.7 ± 0.5[b]	2.70*		1		1
Xe	2.5 ± 0.7[b]	3.50		17.3		35 to 70
C	2.9 ± 0.5[b]	3.04	2.85 ± 0.95[c]	2.47	45 ± 15[e]	45 ± 15*
N	3.6 ± 0.8[b]	2.96	2.0 ± 0.5[d]	2.0		3 to 5
S	2.5 ± 0.15[b]	2.55	12.5 ± 1.5[d]	12.5*	20 ± 10[f]	25 to 50

[1] All enrichments are with respect to the solar abundance of Anders and Grevesse (1989).
[a] Mahaffy *et al.* (2000); [b] Atreya *et al.* (1999); [c] Kerola *et al.* (1997); [d] Briggs and Sackett (1989);
[e] Gautier *et al.* (1995); [f] de Pater *et al.* (1991);
* Element used for calibration

they do not combine with any other species. Calculations shown on Figure 3 and given in Table I, were "calibrated" on Kr by Hersant *et al.* (2004).

The corresponding epoch for the collapse is 5.8 My after the formation of the Sun. In turn, this determines the width of the feeding zone permitting us to reproduce the mass of hydrogen in the envelope of Jupiter today. This also permits the calculation of the enrichment for the other elements. Thermochemical models of Jupiter (Fegley and Lodders, 1994) show that, in the upper troposphere, practically all C is in the form of CH_4 and all N is in the form of NH_3, whatever the initial abundances of CO, CH_4, N_2 and NH_3 which fell onto Jupiter. C and N enrichments with respect to the solar abundance plotted on Figure 3 are then derived from measurements of CH_4 and NH_3, respectively. Calculations made for CO/CH_4=10, and N_2/NH_3=10, result in C and N enrichments compatible with observations. The fit of the N enrichment is in agreement with the conclusions of Owen *et al.* (2001) who argue, from the value of $^{14}N/^{15}N$ measured in Jupiter, that nitrogen accreted by the planet was initially mainly in the form of N_2. The case of S is not so satisfying. Adopting a solar H_2S/H_2 results in too high a S enrichment. In order to fit the observed S enrichment, Hersant *et al.* (2004) concluded that H_2S/H_2 in the nebula at 5 AU was equal, at the time of the clathration of H_2S, to only 0.57 times the solar abundance. This might imply that S was initially partitioned between various bearing-sulfur compounds, as those detected in comets (CS_2, OCS, SO_2). Moreover, H_2S was also presumably converted to solid elements, as troilite FeS in the hot inner nebula (see Section 4.1). Calculating the variation of the radial distribution of H_2S throughout the nebula would require the integration of the equation of transport with turbulent diffusion, taking into account the appropriate

sulfur chemistry. However, it is easy to predict that, once the chemistry is inhibited because the temperature is too low, the radial distribution of gaseous H_2S is only governed by the diffusive mixing and becomes a plateau. In other words, after some time the H_2S/H_2 ratio does not vary with the heliocentric distance, as long as it does not condense or is not trapped. On this basis, Hersant *et al.* (2004) assumed that the abundance of H_2S prior to clathration had the same value at 5 AU as in the regions of formation of Saturn, Uranus and Neptune. Note that Guillot (2004, private communication) suggests that sulfur could be partly trapped in deep clouds of Jupiter so that the Calileo measurement of S/H would be less than the value in the bulk of the planet.

The question of noble gases enrichment is linked to a proper estimate of the solar abundance. The problem is that solar data compilations are frequently revised by an amount which in some cases substantially exceeds uncertainties announced in previous tables. The most recent updating has been published by Lodders (2003). It appears that the solar abundance of argon is not very different from that of Anders and Grevesse (1989). To the contrary, those of Kr and Xe are higher by 70%, which reduces the value of enrichments of these elements given in Table II. However, the solar abundance of Ar is derived from solar wind measurements while those of Kr and Xe are calculated from a nucleosynthesis modeling of s-process, which might be subject to revisions. Therefore, at this point we still evaluate the enrichments from the solar values of Anders and Grevesse (1989), which makes easier comparisons with enrichments quoted by other authors.

The enrichment in C and N implies that all CO, CH_4, N_2, and NH_3 contained in the feeding zone during phase 2 have been clathrated. This requires an abundance of water in the nebula at 5 AU, at the time of condensation, at least equal to 2.2 times the solar O/H ratio (see Table II and discussion Section 8). This is a lower limit since some cages of C and N clathrates may have not been occupied by guest molecules. Unfortunately, the O/H ratio in the deep envelope of Jupiter is not yet known.

7.2. Enrichment in Saturn

Noble gases can be detected in Saturn only by *in situ* measurements made aboard an atmospheric probe. Remote measurements of equilibrium species concern only CH_4 and NH_3 from which are deduced the C and N enrichments (Figure 4). In addition, an indirect determination of the abundance of H_2S was obtained by matching the microwave spectrum of Saturn at centimeter wavelengths. The spectrum can be explained by depleting the NH_3 abundance in the upper troposphere below the saturation level, assuming that NH_3 combines with H_2S to form clouds of NH_4HS.

Hersant *et al.* (2004) calibrated enrichments by fitting the measured S enrichment. Assuming that H_2S/H_2 at 10 AU in the nebula was equal to the value at 5 AU, namely 0.57 times the solar value, this requires that the hydrodynamic collapse occurred 11 My after the formation of the Sun. Should all CO and all CH_4 have been

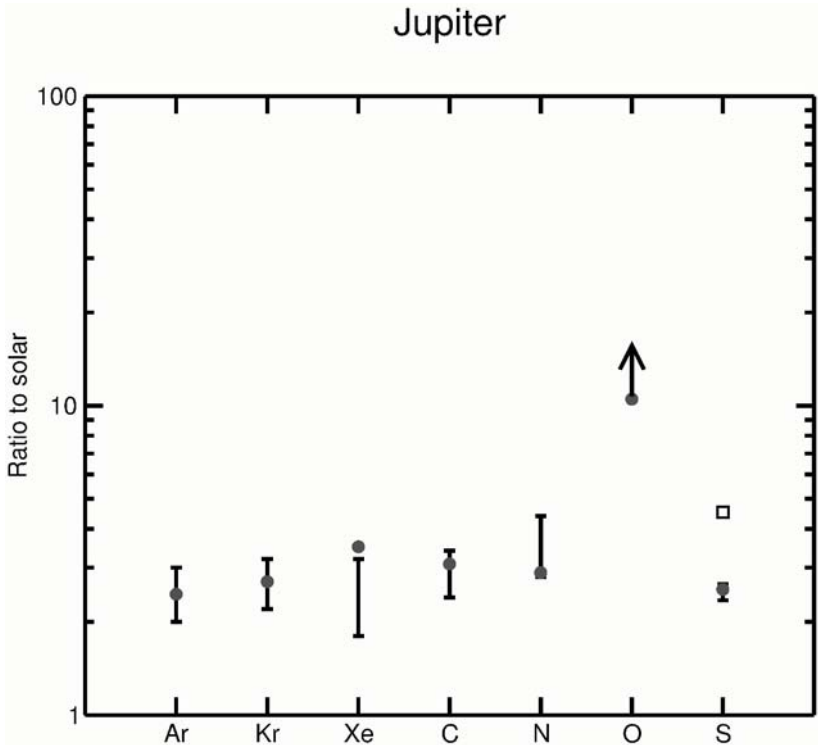

Figure 4. Enrichment in volatiles in Jupiter. Measured values are indicated with their uncertainties. Dots correspond to calculations (see text for the procedure). The square indicates the sulfur enrichment in Jupiter calculated for a solar H_2S/H_2 ratio in the nebula. The vertical arrow corresponds to the lower limit of the calculated oxygen enrichment (see Table II). (Adapted from Hersant *et al.*, 2004.)

trapped as clathrate hydrates in the feeding zones of Saturn, the C/H ratio today (CO having been converted into CH_4 in the deep atmosphere of Saturn) would be equal to 15.1 times the solar C/H ratio, in conflict with observations. Fitting the carbon enrichment carbon enrichment measured by Kerola *et al.* (1997), which is rather low, then requires that CO was never trapped (or only in a tiny amount) in the form of clathrate hydrates. Its mixing ratio to H_2 remained constant during the whole phase 2 of the evolution of the feeding zone. It collapsed with hydrogen during phase 3, and, since it was much more abundant than CH_4 in the nebula, it contributed by about one solar value to the C/H observed today. The carbon enrichment with respect to solar in Saturn's envelope thus results only from the trapping of CH_4 in the form of clathrate hydrate. This is consistent with the low value of the CO/CH_4 ratio in Titan ($\sim 10^{-3}$), if planetesimals which formed the satellite were in fact produced in the feeding zone of Saturn (Mousis *et al.*, 2002).

However, should the C/H ratio in Saturn been revised up by future measurements (as those to be made from the Cassini spacecraft), that would imply that some CO has also been clathrated in the feeding zone of the planet.

Similarly, if N_2 had been trapped as well as NH_3, the N enrichment in the deep troposphere would have been equal to 14.8, in conflict with microwave observations. Fitting the observed N/H requires that N_2 was never clathrated and collapsed with hydrogen during phase 3. It contributed to about one solar value to N/H in Saturn since N_2 was substantially more abundant than NH_3 in the nebula. The observed enrichment in Saturn with respect to solar thus results in fact from the condensation of the NH_3 - H_2O hydrate in the feeding zone of the planet during Phase 2 of the formation. Consequences of this scenario on the $^{14}N/^{15}N$ ratio are discussed in Section 9. If the non trapping of CO and N_2 resulted from the lack of ices, and that all cages of clathrates were occupied by guest molecules, the O/H in Saturn could be as low as 6 times the solar O/H ratio. A partial occupancy of cages would increase of course the required O/H value.

Interestingly enough, the non clathration of CO and N_2 also implies that Ar and Kr were never trapped as clathrate hydrates since they would have been trapped at lower temperatures than CO and N_2, namely at an epoch where all water ice were already used for clathration. Accordingly, their mixing ratio with respect to H_2 remained solar during all the evolution of the feeding zone, and their abundance must be still solar today (Figure 2). To the contrary, Xe, which was clathrated at temperatures close to that of CH_4, is predicted to be enriched by a factor 17 (see Table I).

7.3. Enrichment in Uranus and Neptune

The calculation of enrichments in Uranus and Neptune is more uncertain than that in Jupiter and Saturn because the weak amount of the mass of hydrogen with respect to the total mass of the planets implies that the first two planets never reached phase 3 of the scenario of Pollack *et al.* (1996). They must have been completed later that the epoch where gas of the nebula was dissipated. Therefore, the enrichments must be calculated in two steps. First, enrichments of considered species Y_i are calculated with respect to the abundance of another minor species X for which the abundance with respect to H_2 has been measured. Enrichments are equal to the ratio of the surface density of Y_i at the time of its clathration to that of X. In a second step, the enrichments with respect to H_2 are calculated from the observed mixing ratio of X.

The CH_4/H_2 mixing ratio has been measured in Uranus and Neptune (Gautier *et al.*, 1995). In addition, the H_2S/H_2 ratio was inferred from the fit of the microwave spectrum of both planets. As in Jupiter and Saturn, all nitrogen is in the form of NH_3 in the troposphere (Fegley and Prinn, 1986). Gulkis *et al.* (1978), followed by a number of authors have assumed that NH_3 reacted with H_2S to form NH_4SH around the 30 bar pressure level, which, considering the solar abundance of S and

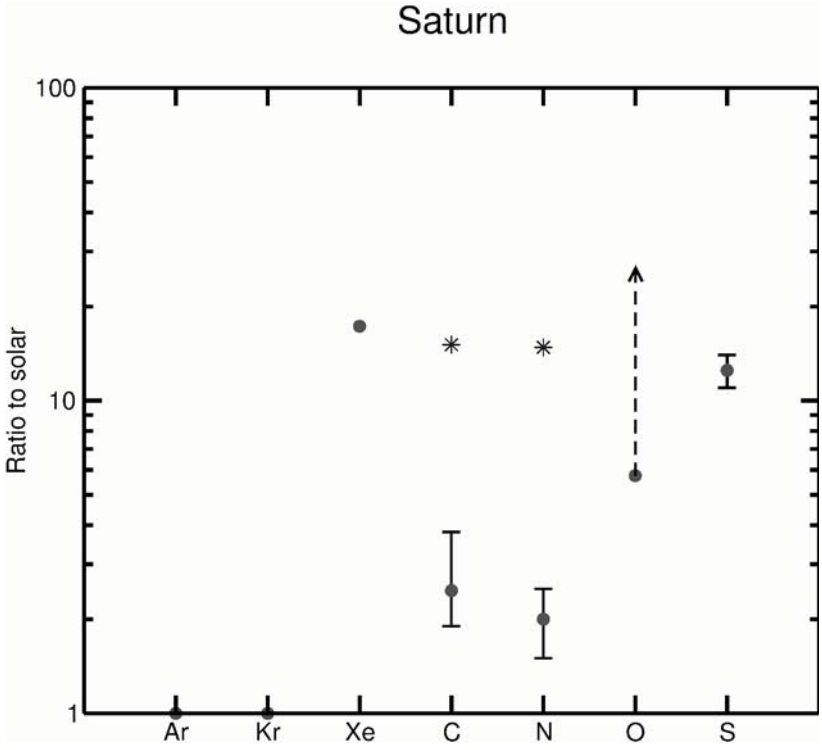

Figure 5. Enrichments of volatiles in Saturn. Measured values of C, N and S are indicated with their uncertainties. Dots correspond to calculations when only CH_4 for C and only NH_3 for N are trapped (see text). Asterisks represent the enrichments in C and N if all CO and all N_2 respectively had been trapped in the feeding zone of the planet. Ar and Kr are shown not enriched while the calculated Xe enrichment is substantially enhanced because it is assumed to have been clathrated. The dash vertical line with an arrow represents the calculated lower limit of the oxygen enrichment in the Saturn envelope. (From Hersant *et al.*, 2004.)

N, requires that S/H in Uranus and Neptune must be strongly oversolar (from 10 to 30, according to de Pater *et al.*, 1991). On the other hand, the NH_3/H_2 ratio in the deep troposphere, currently assumed to be solar in the literature, is in fact quite uncertain. It does not seem to be significantly oversolar, however.

Hersant *et al.* (2004) have chosen to "calibrate" enrichments with respect to CH_4 which is between 30 and 60 times the solar abundance, for both Uranus and Neptune (Gautier *et al.*, 1995). The large measured carbon enrichment implies that both CO and CH_4 were trapped in the form of clathrate hydrate in the feeding zones of these planets.

Calculations of N and S enrichments made by Hersant *et al.* (2004) are shown on Figure 6. Since the C enrichment is uncertain, they have chosen to calibrate on the lower value, the nominal value, and the upper value, respectively, of the mea-

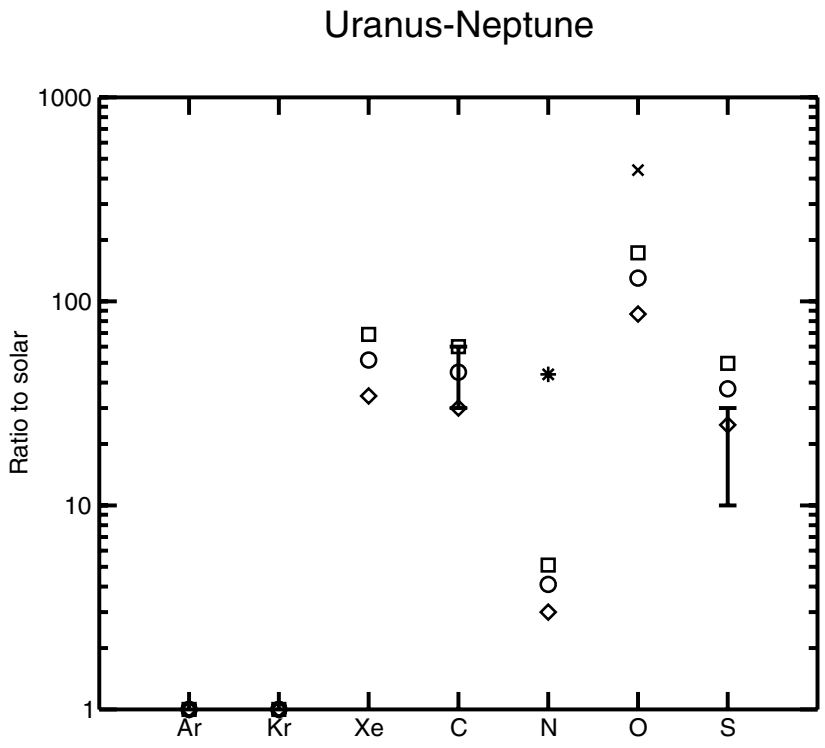

Figure 6. Enrichments of volatiles in Uranus and Neptune. Measured values are those of C (Gautier *et al.*, 1995) and of S (de Pater *et al.*, 1991). The too uncertain N/H enrichment is not shown (see text). The lower limit of C is indicated by a diamond, the central value by an empty circle, the upper limit by a square. Calculations of the enrichments in N, Xe, O and S are made for these three values. Elements are assumed to be solar, except S which is assumed to be equal (in the form of H_2S) to the value at 5 and 10 AU. It is assumed that CO/CH_4 was equal to 10 in the nebula and that both CO and CH_4 were trapped as clathrate hydrates. The star indicates the calculated high N enrichment when N_2 is supposed have been trapped. The diamond, the circle and the square correspond to the case where N_2 was never clathrated, so that the enrichment results only from the condensation of the NH_3 hydrate (assuming $N_2/NH_3 = 10$) The lower limit, the central value and the upper limit of the Xe, S and N enrichments, and of the minimum oxygen enrichment are indicated by the same symbols. The cross (x) is the oxygen enrichment inferred by Lodders and Fegley (1994) from the value of CO measured in the upper troposphere of Neptune (see Table II). Ar and Kr are shown not enriched. (From Hersant *et al.*, 2004.)

sured C enrichment. Symbols on the figure indicate how the assumed calibration from C results on calculated enrichments for N and S. Should all N_2 present in the feeding zone have been clathrated, the calculated enrichment would have been as high as 44, which would depress the calculated spectrum of Uranus and Neptune at 20 cm wavelength. If N_2 was not clathrated, the enrichment in nitrogen at deep atmospheric levels deep is between 3 and 5. The S enrichment of 25 calculated

TABLE II

Oxygen enrichment in the four Giant planets and required concentration of ice in the feeding zone of the planets (adapted from Hersant *et al.*, 2004).

Planet	O/H enrichment inferred in water	Calculated O/H enrichment	$H_2O/H_2\|_{FZ}/H_2O/H_2\|_{neb}$ [c]
Jupiter	$0.2 - 9$[a]	> 10.53	> 2.2
Saturn		> 5.76	> 0.4
Uranus	< 260[b]	$> 90 - 175$	$> 0.4 - 1.9$
Neptune	440[b]	$> 90 - 175$	$> 0.4 - 1.9$

[a] Bézard *et al.* (2002); [b] Lodders and Fegley (1994);
[c] $H_2O/H_2|_{FZ}$ is the water mixing ratio in the feeding zone of the planet while $H_2O/H_2|_{neb}$ is the average water mixing ratio in the nebula, namely 1.06×10^{-3} (Hersant *et al.*, 2004). $H_2O/H_2|_{FZ}/H_2O/H_2|_{neb}$ is thus the local enhancement of the water mixing ratio in the feeding zone of the planet.

from the lower value of CH_4/H_2 is compatible with the S enrichment inferred by de Pater *et al.* (1991). Calculations also agree with the lower limit of a S/N ratio of 5 times solar estimated by the same authors. The theory of the trapping of volatiles by clathration then provides for the first time a physical explanation of the high sulfur enrichment in Uranus and Neptune previously only assumed by modelers.

Predictions concerning noble gases are the same as for Saturn. Ar and Kr must have a solar abundance while Xe is expected to be oversolar by a factor from 35 to 70 (Table I).

8. Trapping Volatiles by Clathration in the Solar Nebula: A Universal Scenario?

Trapping volatiles by clathration in the nebula appears to be an efficient mechanism for interpreting the composition of giant planets, and to some extent, of comets. *The local abundance of water ice in the nebula is the key parameter which permits us to reproduce the pattern of the enrichments of volatiles measured in the envelope of giant planets*. Volatiles present in the nebula in the region of formation of planets may be or may not be trapped, depending of the amount of ice available for clathration. Results of the analysis made by Hersant et al. (2004) are summarized in Table II.

As described in Section 7, all volatiles enriched in Jupiter must have been trapped as clathrate hydrates in the feeding zone of the planet. CO, CH_4, N_2, NH_3 are the components which consumed most of available water ice. The minimum

total water abundance required for clathration, is indicated in column 4 of Table II, expressed in terms of vaporized water at the time of condensation with respect to the H_2O/H_2 ratio in the nebula. The number 2.2 for Jupiter indicates that at 5 AU, the amount of water must have been higher than the so-called solar abundance of water which is between 1.16 times the solar O/H ratio when all carbon is in the form of CO and 2.0 times the solar O/H ratio when all carbon is in the form of CH_4 (Iro *et al.*, 2003, neglecting other chemical combinations of oxygen). In Table II, the nebula water abundance is calculated for $CO/CH_4 = 10$. Contrary to the Jupiter case, the minimum value of O/H in the region of Saturn is 0.4 times the nebula water abundance. The minimum value is more uncertain for Uranus and Neptune because it depends on the measured CH_4/H_2 ratio.

The minimum abundance of oxygen, present in form of water in the upper troposphere of Giant planets, is expressed in column 3, in units of solar O/H ratio. The value of H_2O/H_2 in the deep atmosphere of Giant planets is not known so far, even in Jupiter since the Galileo probe did not penetrate deep enough in the atypical dry sounded region. However, we dispose of an indirect estimate of the water abundance derived from the measurements of CO (which has been found in excess with respect to the CO/CH_4 value at the equilibrium in the upper troposphere. Lodders and Fegley (1994) have demonstrated that the presence of CO at observable levels requires a large enhancement of water in the deep atmosphere. The value of 440 times the solar O/H ratio they derived for Neptune from the millimeter detection of CO (column 2 of Table II) is much higher than the minimum value required for clathration (90 to 175). Recently, Encrenaz *et al.* (2004) have detected CO on near infrared spectra of Uranus. They were not able to decide whether the origin of CO is external or internal. If CO originates from the interior of the planet, its value is close to the upper limit previously derived from millimeter measurements. The analysis of Lodders and Fegley (1994) then results in a firm enrichment of 260 in Uranus, consistent with the trapping of volatiles by clathration. Bézard *et al.* (2002) applied the approach of Lodders and Fegley (1994), using an updated chemistry, to interpret their measurement of CO in Jupiter. They derived a maximum value of 9 times the solar O/H ratio, while Hersant *et al.* (2004) have calculated a lower limit for clathration of 10.5 times solar O/H (column 3). Considering the uncertainties on the theory of dynamics of the deep troposphere (Smith *et al.*, 1996), we feel that this difference does not firmly rule out the clathration scenario for Jupiter. Note that the number for Saturn in column 3 is a lower limit for the oxygen enrichment. The actual value in Saturn could be much higher if a number of cages of the clathrate were not occupied by guest molecules.

As concerns comets, the clathration theory permitted Iro *et al.* (2003) to interpret the large depletion of N_2 with respect to CO in several comets of Oort, as well as the non detection of Ar, and the variability of CO from a comet to another. The amount of trapped CO clearly depends upon the amount of available water ice. The lack of laboratory data precludes us to investigate in more details whether the composition of comets could be fully interpreted by the clathration theory. In fact,

it is plausible that a number of volatiles cannot be clathrated for physical reasons, as the too high or too small size of the considered molecule (Sloan, 1998) and thus were incorporated in cometary grains by condensation.

The theory of the trapping of volatiles developed in the present report implies that the distribution of the density of ice varies with heliocentric distance, and probably with time. Such variations have been predicted by number of authors. It has been proposed, for instance, that large vortices – similar to the Great Red Spot of Jupiter – could locally concentrate icy grains by a large factor (Barge and Sommeria, 1995; Tanga *et al.*, 1996; Bracco *et al.*, 1999). Another approach considers that concentration of icy grains could result from small scale distributions of turbulent eddies (Squires and Eaton, 1991; Cuzzi *et al.*, 2001; Hersant, 2002). This challenging problem will certainly be extensively studied in the future.

9. Possible Tests of the Clathration Scenario

9.1. Ground-based Observations of Comets and of Saturn

Although a limited number of tests can be done from the ground, they could be precious. The first obvious research consists in continuing to search for crystalline ice on comets. High spectral resolution observations for detecting simultaneously CO^+ and N_2^+ must be continued.

The comparison of the scenario of formation of Jupiter with that of Saturn suggests that the values of $^{14}N/^{15}N$ in the two planets could be different. Fouchet *et al.* (2000) discovered from infrared observations of Jupiter made from the Infrared Space Observatory ISO that the $^{14}N/^{15}N$ ratio is substantially higher in this planet than the terrestrial ratio of 270. Subsequently, Owen *et al.* (2001) derived from measurements made with the *Galileo* Probe Mass Spectrometer a value of $^{14}N/^{15}N$ in Jupiter of order of 435, a result quite close to the value 448 recently obtained by Abbas *et al.* (2004) from far infrared observations made from the Cassini spacecraft during its encounter with Jupiter. Fouchet *et al.* (2004) derived a similar value from the same data. Owen *et al.* (2001) concluded that nitrogen was incorporated into Jupiter as N_2, and that nitrogen on the Earth has a different origin, possibly resulting from the outgassing of a bearing-N organic compound. The clathration scenario also implies that most of nitrogen came into Jupiter as N_2. On the other hand, we have seen, Section 7, that half of nitrogen in Saturn, in which N/H is enhanced by a factor 2, came as N_2, and half came as NH_3. Therefore, since NH_3 must have been fractionated with respect to N_2 in the presolar cloud, its $^{14}N/^{15}N$ ratio should be lower than that in N_2. If for instance, it is equal to the terrestrial value, the $^{14}N/^{15}N$ in Saturn should be of order of 350. In principle, $^{15}NH_3$ can be detected from ground based observations of Saturn at 10 microns (Fouchet, 2004, private communication). However, it is not guaranteed that the observations will be precise enough to firmly detect a difference with the Jupiter value, for which the

lower limit obtained by both Owen *et al.* (2001) and Abbas *et al.* (2004) is 385, and that of Fouchet *et al.* (2004) is 365.

9.2. Ground-based Observations of Circumstellar Disks

A key point of the clathration theory is that temperatures as low as 35 K must have occurred in the solar nebula at the location of Jupiter, namely at 5 AU (or farther if Jupiter initially migrated, Alibert *et al.*, 2004). The IRAM interferometer permits the determination of disks temperatures as low as 35 K and of the surface density at distances of 100 AU from the central star (Dutrey *et al.*, 1998). The US-European ALMA project will permit us to reduce this distance to 10 AU before the end of the decade. The expected progress in sensibility will also permit the observation of hundred of new young stars and to improve the determination of the variation of luminosity of disks as a function of the age of star. Images from Hubble are expected to reveal new data on the physical characteristics and the evolution of dust in disks.

9.3. Observations from Space Missions

9.3.1. *Results Expected from the Huygens Probe in Titan*

The GCMS instrument aboard the Huygens probe of the Cassini mission will measure the isotopic composition of Titan's atmosphere. According to the scenario for the origin of Titan developed by Mousis *et al.* (2002), the nitrogen present in the atmosphere of Titan today originates uniquely from NH_3 which outgassed from planetesimals produced in the solar nebula and which subsequently formed the satellite and its atmosphere. NH_3 was subsequently converted to N_2 by photolysis or shock chemistry. In such a case, the $^{14}N/^{15}N$ measured in N_2 in Titan might reveal the initial value in NH_3 in the nebula. As a matter of fact, this is questionable because $^{14}N/^{15}N$ measured in HCN has been surprisingly found equal to 60 (Marten *et al.*, 2002). Assuming that the ratio in HCN is the same as in N_2, which is probably not true, and that the ratio in the early atmosphere of Titan was equal to the terrestrial value, which may be or may not be true, it is currently stated that this low $^{14}N/^{15}N$ ratio results from a strong differential atmospheric escape of ^{14}N with respect to ^{15}N (Lunine *et al.*, 1999; Lammer *et al.*, 2000). However, we agree with Owen (2000) that the cause of this isotopic anomaly is still mysterious.

A less ambiguous test should come from the GCMS measurements of abundance of noble gases: Mousis *et al.* (2002) predict the Xe/Ar and Xe/Kr ratios should be substantially oversolar if Xe was trapped as a clathrate hydrate(but not Ar and Kr) in planetesimals which formed Titan. Within the clathration scenario, the Xe/Ar and Xe/Kr ratios would be strongly oversolar, and the CO/CH_4 ratio would less than unity by a very large factor, as observed.

9.3.2. *Tests from Possible Future Missions*

Jupiter: Test from the water enhancement

The clathration scenario implies that water was trapped in abundance in Jupiter (10.5 times the solar O/H ratio, at least) while the trapping of volatiles by amorphous ice would require a water enhancement by a factor 3 to 4. Determining the O/H ratio in Jupiter could then permit us to discriminate between the two scenarios. This may require to send a new probe into Jupiter since the Galileo probe penetrated in an atypical dry region. However, Bolton *et al.* (2001) have proposed a dedicated spacecraft permitting the retrieval of the water abundance in the deep troposphere of Jupiter from remote sensing radiometric measurements of the Jupiter emission at decimeter wavelengths, during a close flyby of the planet.

Saturn, Uranus, and Neptune: Tests from noble gases abundance

Figures 4, 5, and 6 show that while Ar, Kr and Xe are enhanced in Jupiter, only Xe is enriched in Saturn, Uranus and Neptune. There is no way to remotely detect noble gases in giant planets. Therefore we need a family of probes into the three outer giant planets.

Comets: the Argon test and the N_2/CO test

The clathration scenario predicts that only comets formed in a rich icy environment will trap Ar in solar proportion with respect to H_2O (Iro *et al.*, 2003). Comets which do not trap substantially N_2 will not trap Ar either. It is highly desirable that appropriate ultraviolet space observatories continue to search argon on bright comets, in order to estimate their Ar/O ratio. CO, CO^+, and N_2^+ should be simultaneously observed from the ground.

Acknowledgements

We acknowledge Jean-Marc Huré for kindly providing us with the representation of the solar nebula model shown on Figure 1. We also thank Emmanuel Lellouch for suggesting us that determining the $^{14}N/^{15}N$ ratio on Saturn could provide a test of the validity of the clathration scenario, and Bernard Schmitt for clarifying the question of the temperature dependence of amorphous and crystalline ice. We thank Dominique Bockelée-Morvan for very helpful comments on the manuscript. Referees comments of Tristan Guillot and Dave Stevenson were appreciated. One of us (D.G.) benefited from stimulating discussions with Toby Owen. F.H. acknowledges support from an ESA research fellowship.

References

Abbas, M.M., *et al.*: 2004, 'The nitrogen isotopic ratio in Jupiter's atmosphere from observations by the composite infrared spectrometer on the Cassini spacecraft', *Astrophys. J.* **602**, 1063–1074.

Alibert, Y., Mordasini, C., Mousis, O., and Benz, W.: 2004, 'Formation of giant planets – an attempt in matching observational constraints', this volume.

Anders, E. and Grevesse, N.: 1989, 'Abundances of the elements – meteoritic and solar', *Geochim. Cosmochim. Acta* **53**, 197–214.

Atreya, S.K., Wong, M.H., Owen, T.C., Mahaffy, P.R., Niemann, H.B., de Pater, I., Drossart, P., and Encrenaz, T.: 1999, 'A comparison of the atmospheres of Jupiter and Saturn: deep atmospheric composition, cloud structure, vertical mixing, and origin', *Planet. Space Sci.* **47**, 1243–1262.

Barge, P. and Sommeria, J.: 1995, 'Did planet formation begin inside persistent gaseous vortices?', *Astron. Astrophys.* **295**, L1–L4.

Beckwith, S.V.W., Henning, T., and Nakagawa, Y.: 2000, 'Dust properties and assembly of large particles in protoplanetary disks', in V. Mannings, A.P. Boss, and S.B. Russell (eds.), *Protostars and Planets IV*, The University of Arizona Press, Tucson, Arizona, 533.

Bell, K.R., Cassen, P.M., Wasson, J.T., and Woolum, D.S.: 2000, 'The Fu Orionis phenomenon and solar nebula material', in V. Mannings, A.P. Boss, and S.B. Russell (eds.), *Protostars and Planets IV*, The University of Arizona Press, Tucson, Arizona, 896.

Benz, W.: 2000, 'Low velocity collisions and the growth of planetesimals', *Space Sci. Rev.* **92**, 279–294.

Bézard, B., Lellouch, E., Strobel, D., Maillard, J., and Drossart, P.: 2002, 'Carbon monoxide on Jupiter: evidence for both internal and external sources', *Icarus* **159**, 95–111.

Biver, N., Bockelée-Morvan, D., Crovisier, J., Colom, P., Henry, F., Moreno, R., Paubert, G., Despois, D., and Lis, C.: 2002, 'Chemical composition diversity among 24 comets observed at radio wavelengths', *Earth, Moon and Planets* **90**, 323–333.

Bockelée-Morvan, D., *et al.*: 2000, 'New molecules found in comet C/1995 O1 (Hale-Bopp). Investigating the link between cometary and interstellar material', *Astron. Astrophys.* **353**, 1101–1114.

Bolton, S.J., *et al.*: 2001, 'Jupiter: Atmospheric Sounding and Sensing of the Interior (JASSI)', *Forum on Innovative Approaches to Outer Planetary Exploration 2001–2020*, 12.

Bracco, A., Chavanis, P.H., Provenzale, A., and Spiegel, E.A.: 1999, 'Particle aggregation in a turbulent Keplerian flow', *Phys. Fluids* **11**, 2280.

Briggs, F.H. and Sackett, P.D.: 1989, 'Radio observations of Saturn as a probe of its atmosphere and cloud structure', *Icarus* **80**, 77.

Calvet, N., Hartmann, L., and Strom, S.E.: 2000, 'Evolution of disk accretion', in V. Mannings, A.P. Boss, and S.B. Russell (eds.), *Protostars and Planets IV*, The University of Arizona Press, Tucson, Arizona, 377.

Chick, K.M. and Cassen, P.: 1997, 'Thermal processing of interstellar dust grains in the primitive solar environment', *Astrophys. J.* **477**, 398–409.

Clampin, M., *et al.*: 2003, 'Hubble Space Telescope ACS coronagraphic imaging of the circumstellar disk around HD 141569A', *Astron. J.* **126**, 385–392.

Cochran, A.L., Cochran, W.D., and Barker, E.S.: 2000, 'N_2^+ and CO^+ in comets 122P/1995 S1 (deVico) and C/1995 O1 (Hale-Bopp)', *Icarus* **146**, 583–593.

Cochran, A.L.: 2002, 'A search for N_2^+ in spectra of comet C/2002 C1 (Ikeya-Zhang)', *Astrophys. J.* **576**, L165–L168.

Cuzzi, J.N., Hogan, R.C., Paque, J.M., and Dobrovolskis, A.R.: 2001, 'Size-selective concentration of chondrules and other small particles in protoplanetary nebula turbulence', *Astrophys. J.* **546**, 496–508.

D'Alessio, P., Canto, J., Calvet, N., and Lizano, S.: 1998, 'Accretion disks around young objects. I. The detailed vertical structure', *Astrophys. J.* **500**, 411–427.

de Pater, I., Romani, P.N., and Atreya, S.K.: 1991, 'Possible microwave absorption by H_2S gas in Uranus' and Neptune's atmospheres', *Icarus* **91**, 220–233.

Drouart, A., Dubrulle, B., Gautier, D., and Robert, F.: 1999, 'Structure and transport in the solar nebula from constraints on deuterium enrichment and Giant planets formation', *Icarus* **140**, 129–155.

Dutrey, A., Guilloteau, S., Prato, L., Simon, M., Duvert, G., Schuster, K., and Menard, F.: 1998, 'CO study of the GM Aurigae Keplerian disk', *Astron. Astrophys.* **338**, L63–L66.

Encrenaz, Th., Lellouch, E., Drossart, P., Feuchtgruber, H., Orton, G.S., Atreya, S.K.: 2004, 'First detection of carbon monoxide in the atmosphere of Uranus', *The Messenger* **115**, 35–36.

Fegley, B.J.: 2000, 'Kinetics of gas-grain reactions in the solar nebula', *Space Sci. Rev.* **92**, 177–200.

Fegley, B. and Prinn, R.G.: 1986, 'Chemical models of the deep atmosphere of Uranus', *Astrophys. J.* **307**, 852–865.

Fegley, B.J. and Lodders, K.: 1994, 'Chemical models of the deep atmospheres of Jupiter and Saturn', *Icarus* **110**, 117–154.

Finocchi, F., Gail, H.-P., and Duschl, W.J.: 1997, 'Chemical reactions in protoplanetary accretion disks. II. Carbon dust oxidation', *Astron. Astrophys.* **325**, 1264–1279.

Fouchet, T., Lellouch, E., Bézard, B., Encrenaz, T., Drossart, P., Feuchtgruber, H., and de Graauw, T.: 2000, 'ISO-SWS observations of Jupiter: measurement of the ammonia tropospheric profile and of the $^{15}N/^{14}N$ isotopic ratio', *Icarus* **143**, 223–243.

Fouchet, T., Irwin, P.G.J., Parrish, P., Calcutt, S.B., Taylor, F.W., Nixon, C.A., and Owen, T.: 2004, 'Search for spatial variation in the jovian $^{14}N/^{15}N$ ratio from Cassini/CIRS observations', *Icarus*, in press.

Gail, H.-P.: 1998, 'Chemical reactions in protoplanetary accretion disks. IV. Multicomponent dust mixture', *Astron. Astrophys.* **332**, 1099–1122.

Gautier, D. and Owen, T.: 1989, 'The composition of outer planet atmospheres', in S.K. Atreya, J.B. Pollack, M.S. Matthews (eds.), *Origin and Evolution of Planetary and Satellite Atmospheres*, The University of Arizona Press, Tucson, Arizona, pp. 487–512.

Gautier, D., Conrath, B.J., Owen, T., de Pater, I., and Atreya, S.K.: 1995, 'The troposphere of Neptune, in D.P. Cruikshank (ed.), *Neptune and Triton*, The University of Arizona Press, Tucson, Arizona, pp. 547–611.

Gautier, D., Hersant, F., Mousis, O., and Lunine, J.I.: 2001, 'Enrichments in volatiles in Jupiter: a new interpretation of the Galileo measurements', *Astrophys. J.* **550**, L227–L230.

Geiss, J. and Gloeckler, G.: 1998, 'Abundances of deuterium and helium-3 in the protosolar cloud', *Space Sci. Rev.* **84**, 239–250.

Gibb, E.L., Mumma, M.J., dello Russo, N., Disanti, M.A., and Magee-Sauer, K.: 2003, 'Methane in Oort cloud comets', *Icarus* **165**, 391–406.

Gulkis, S., Janssen, M.A., and Olsen, E.T.: 1978, 'Evidence for the depletion of ammonia in the Uranus atmosphere', *Icarus* **34**, 10–19.

Haisch, K.E., Jr., Lada, E.A., and Lada, C.J.: 2001, 'Disk frequencies and lifetimes in young clusters', *Astrophys. J.* **553**, L153–L156.

Hartmann, L.: 2000, 'Observational constraints on transport (and mixing) in pre-main sequence disks', *Space Sci. Rev.* **92**, 55–68.

Hersant, F.: 2002, *Turbulence dans la nébuleuse solaire primitive et formation du système solaire externe*, Thèse de l'Université Paris 7.

Hersant, F., Gautier, D., and Huré, J.-M.: 2001, 'A two-dimensional model for the primordial nebula constrained by D/H measurements in the solar system: implications for the formation of Giant planets', *Astrophys. J.* **554**, 391–407.

Hersant, F., Gautier, D., and Lunine, J.I.: 2004, 'Enrichment in volatiles in the Giant planets of the solar system', *Planet. Space Sci.*, in press.

Huré, J.-M.: 2000, 'On the transition to self-gravity in low mass AGN and YSO accretion discs', *Astron. Astrophys.* **358**, 378–394.

Iro, N., Gautier, D., Hersant, F., Bockelée-Morvan, D., and Lunine, J.I.: 2003, 'An interpretation of the nitrogen deficiency in comets', *Icarus* **161**, 511–532.

Kawakita, H., Watanabe, J., Ootsubo, T., Nakamura, R., Fuse, T., Takato, N., Sasaki, S., and Sasaki, T.: 2004, 'Evidence of icy grains in comet C/2002 T7 (LINEAR) at 3.52 AU', *Astrophys. J.* **601**, L191–L194.

Kerola, D.X., Larson, H.P., and Tomasko, M.G.: 1997, 'Analysis of the near-IR spectrum of Saturn: a comprehensive radiative transfer model of its middle and upper troposphere', *Icarus* **127**, 190–212.

Kouchi, A., Yamamoto, T., Kozasa, T., Kuroda, T., and Greenberg, J.M.: 1994, 'Conditions for condensation and preservation of amorphous ice and crystallinity of astrophysical ices', *Astron. Astrophys.* **290**, 1009–1018.

Lammer, H., Stumptner, W., Molina-Cuberos, G.J., Bauer, S.J., and Owen, T.: 2000, 'Nitrogen isotope fractionation and its consequence for Titan's atmospheric evolution', *Planet. Space Sci.* **48**, 529–543.

Lellouch, E., Crovisier, J., Lim, T., Bockelée-Morvan, D., Leech, K., Hanner, M.S., Altieri, B., Schmitt, B., Trotta, F., and Keller, H.U.: 1998, 'Evidence for water ice and estimate of dust production rate in comet Hale-Bopp at 2.9 AU from the Sun', *Astron. Astrophys.* **339**, L9–L12.

Lodders, K. and Fegley, B.: 1994, 'The origin of carbon monoxide in Neptune's atmosphere', *Icarus* **112**, 368–375.

Lodders, K.: 2003, 'Solar system abundances and condensation temperatures of the elements', *Astrophys. J.* **591**, 1220–1247.

Lunine, J.I. and Stevenson, D.J.: 1985, 'Thermodynamics of clathrate hydrate at low and high pressures with application to the outer solar system', *Astrophys. J. Suppl.* **58**, 493–531.

Lunine, J.I., Engel, S., Rizk, B., and Horanyi, M.: 1991, 'Sublimation and reformation of icy grains in the primitive solar nebula', *Icarus* **94**, 333–344.

Lunine, J.I., Yung, Y.L., and Lorenz, R.D.: 1999, 'On the volatile inventory of Titan from isotopic abundances in nitrogen and methane', *Planet. Space Sci.* **47**, 1291–1303.

Lutz, B.L., Womack, M., and Wagner, R.M.: 1993, 'Ion abundances and implications for photochemistry in Comets Halley (1986 III) and Bradfield (1987 XXIX)', *Astrophys. J.* **407**, 402–411.

Magni, G. and Coradini, A.: 2004, 'Formation of Jupiter by nucleated instability', *Planet. Space Sci.* **52**, 343–360.

Mahaffy, P.R., Niemann, H.B., Alpert, A., Atreya, S.K., Demick, J., Donahue, T.M., Harpold, D.N., and Owen, T.C.: 2000, 'Noble gas abundance and isotope ratios in the atmosphere of Jupiter from the Galileo Probe Mass Spectrometer', *J. Geophys. Res.* **105**, 15061–15072.

Makalkin, A. and Dorofeyeva, V.: 1991, 'Temperatures in the protoplanetary disk: models, constraints, and consequences for the planets', *Isvestiya, Earth Phys.* **27**, 650.

Malfait, K., Waelkens, C., Bouwman, J., de Koter, A., and Waters, L.B.F.M.: 1999, 'The ISO spectrum of the young star HD 142527', *Astron. Astrophys.* **345**, 181–186.

Marten, A., Hidayat, T., Biraud, Y., and Moreno, R.: 2002, 'New millimeter heterodyne observations of Titan: vertical distributions of nitriles HCN, HC_3N, CH_3CN, and the isotopic ratio $^{15}N/^{14}N$ in its atmosphere', *Icarus* **158**, 532–544.

Michel, P., Benz, W., and Richardson, D.C.: 2003, 'Disruption of fragmented parent bodies as the origin of asteroid families', *Nature* **421**, 608–611.

Mousis, O., Gautier, D., Bockelée-Morvan, D., Robert, F., Dubrulle, B., and Drouart, A.: 2000, 'Constraints on the formation of comets from D/H ratios measured in H_2O and HCN', *Icarus* **148**, 513–525.

Mousis, O., Gautier, D., and Bockelée-Morvan, D.: 2002, 'An evolutionary turbulent model of Saturn's subnebula: implications for the origin of the atmosphere of Titan', *Icarus* **156**, 162–175.

Natta, A., Grinin, V., and Mannings, V.: 2000, 'Properties and evolution of disks around pre-main-sequence stars of intermediate', in V. Mannings, A.P. Boss, and S.B. Russell (eds.), *Protostars and Planets IV*, The University of Arizona Press, Tucson, Arizona, 559.

Notesco, G., Bar-Nun, A., and Owen, T.: 2003, 'Gas trapping in water ice at very low deposition rates and implications for comets', *Icarus* **162**, 183–189.

Owen, T. and Bar-Nun, A.: 1995, 'Comets, impacts and atmospheres', *Icarus* **116**, 215–226.

Owen, T., Mahaffy, P., Niemann, H.B., Atreya, S., Donahue, T., Bar-Nun, A., and de Pater, I.: 1999, 'A low-temperature origin for the planetesimals that formed Jupiter', *Nature* **402**, 269–270.

Owen, T.C.: 2000, 'On the origin of Titan's atmosphere', *Planet. Space Sci.* **48**, 747–752.

Owen, T., Mahaffy, P.R., Niemann, P.R., Atreya, S., and Wong, M.: 2001, 'Protosolar nitrogen', *Astrophys. J.* **553**, L77–L79.

Pasek, M., Milsom, D., Ciesla, F., Sharp, C., Lauretta, D., and Lunine, J.I.: 2004, 'Sulfur chemistry in the solar nebula', submitted to *Icarus*.

Pollack, J.B., Hollenbach, D., Beckwith, S., Simonelli, D.P., Roush, T., and Fong, W.: 1994, 'Composition and radiative properties of grains in molecular clouds and accretion disks', *Astrophys. J.* **421**, 615–639.

Pollack, J.B., Hubickyj, O., Bodenheimer, P., Lissauer, J.J., Podolak, M., and Greenzweig, Y.: 1996, 'Formation of the Giant planets by concurrent accretion of solids and gas', *Icarus* **124**, 62–85.

Pringle, J.E.: 1981, 'Accretion discs in astrophysics', *Ann. Rev. Astron. Astrophys.* **19**, 137–162.

Prinn, R.G. and Fegley, B. Jr,: 1989, 'Solar nebula chemistry: origin of planetary, satellite and cometary volatiles', in S.K. Atreya, J.B. Pollack and M.S. Matthews (eds.), *Origin and evolution of planetary and satellites atmospheres*, The University Arizona Press, Tucson, pp. 78–136.

Robert, F., Gautier, D., and Dubrulle, B.: 2000, 'The solar system D/H ratio: observations and theories', *Space Sci. Rev.* **92**, 201–224.

Schmitt, B., Quirico, E., Trotta, F., and Grundy, W.M.: 1998, 'Optical properties of ices from UV to infrared', in B. Schmitt, C. de Bergh, and M. Festou (eds.), *Solar System Ices*, Kluwer Academic Publishers, Dortrecht (Netherlands), pp. 199–240.

Shakura, N.I. and Sunyaev, R.A.: 1973, 'Black holes in binary systems, observational appearance', *Astron. Astrophys.* **24**, 337–355.

Sloan, E.D.; Jr.: 1998, *Clathrate Hydrates of Natural Gases*, Marcel Dekker Inc., New York.

Smith, M.D., Conrath, B.J., and Gautier, D.: 1996, 'Dynamical influence on the isotopic enrichment of CH_3D in the Outer planets', *Icarus* **124**, 598–607.

Squires, K.D. and Eaton, J.K.: 1991, 'Preferential concentration of particles by turbulence', *Phys. Fluids* **3**, 1169–1178.

Tanga, P., Babiano, A., Dubrulle, B., and Provenzale, A.: 1996, 'Forming planetesimals in vortices', *Icarus* **121**, 158–170.

Van der Waals, J.H. and Platteuw, J.C.: 1959, 'Clathrate solutions', in *Advances in Chemical Physics*, Volume 2, Interscience Publishers Inc., New York, pp. 1–57.

Weaver, H.A., Feldman, P.D., Combi, M.R., Krasnopolsky, V., Lisse, C.M., and Shemansky, D.E.: 2002, 'A search for argon and O VI in three comets using the far ultraviolet spectroscopic explorer', *Astrophys. J.* **576**, L95–L98.

Weidenschilling, S.J.: 1997, 'The origin of comets in the solar nebula: a unified model', *Icarus* **127**, 290–306.

Wyckoff, S., Tegler, S.C., and Engel, L.: 1991, 'Nitrogen abundance in comet Halley', *Astrophys. J.* **367**, 641–648.

Address for Offprints: Daniel Gautier, Laboratoire d'Etudes et d'Instrumentation en Astrophysique (LESIA), Observatoire de Paris, 2 place Jules Janssen, F-92195 Meudon Cedex, France;
Daniel.Gautier@obspm.fr

FORMATION OF THE CORES OF THE OUTER PLANETS

S. J. WEIDENSCHILLING
Planetary Science Institute, 1700 E. Fort Lowell Road, Suite 106, Tucson, AZ 85719, USA

Received: 29 June 2004; Accepted in final form: 22 September 2004

Abstract. The formation of the giant planets seems to be best explained by accretion of planetesimals to form massive cores, which in the case of Jupiter and Saturn were able to capture nebular gas. However, the timescale for accretion of such cores has been a problem. Accretion in the outer solar system differs qualitatively from planetary growth in the terrestrial region, as the larger embryo masses and lower orbital velocities make bodies more subject to gravitational scattering. The planetesimal swarm in the outer nebula may be seeded by earlier-formed large bodies scattered from the region near the nebular "snow line." Such a seed body can experience rapid runaway growth undisturbed by competitors; the style of growth is not oligarchy, but monarchy.

Keywords: Accretion, giant planets, planetesimals

1. Introduction

The four giant planets are naturally classified into two groups: the gas giants Jupiter and Saturn, and the ice giants Uranus and Neptune. The gas giants consist mostly of hydrogen and helium, yet these planets are significantly enriched in heavier elements (metal, silicates, and ices) by about an order of magnitude relative to solar composition. For Jupiter, uncertainties in the equation of state of hydrogen allow ambiguity in the location of the heavy elements; they may be concentrated in a central core, or distributed throughout its interior. However, Saturn is required to have a core of about 10 $M_\oplus$ (Wuchterl *et al.*, 2000). Uranus and Neptune contain about 10% by mass of H and He, which is only a small fraction (< 1%) of their solar complement relative to their heavy elements. They may be regarded in some sense as "nearly naked cores."

The formation of these planets poses problems for theorists. The most widely accepted model for the formation of the gas giants is "core-accretion." In this scenario, planetesimals accreted by collisions, building up massive protoplanetary embryos. Such an embryo could capture a massive H-He atmosphere from the surrounding solar nebula. The mass of this atmosphere increased with the embryo (core) mass, and when the core attained a critical mass, estimated to be about $10M_\oplus$, the gaseous envelope underwent a hydrodynamic collapse, capturing gas from the nebula until the supply near its orbit was exhausted. This description is rather simplified; for a more complete explanation see Pollack *et al.* (1996).

Space Science Reviews 116: 53–66, 2005.
DOI: 10.1007/s11214-005-1947-1

Core-accretion seems to provide a natural explanation for the heavy element contents of the gas giants. However, the details of the model pose some severe problems, particularly the timescale for the growth of the cores. At least for Jupiter and Saturn, the critical mass had to be reached within the lifetime of the solar nebula, generally believed to be $\sim 10^7$ y (Podosek and Cassen, 1994). Standard accretion models have difficulty forming an embryo of $\sim 10 M_\oplus$ at Jupiter's distance on such a timescale in a minimum-mass solar nebula. As accretion rates scale with the surface density of the planetsimal swarm, most theorists have assumed that the nebula was more massive (Kokubo and Ida, 2002; Thommes *et al.*, 2003). This approach can at least marginally account for the formation of a core at Jupiter's distance in the requisite time. At larger heliocentric distances, the growth of an embryo is slower due to the lower surface density of the planetesimal swarm and the longer orbital period. Standard accretion models have great difficulty accounting for Saturn's core (Thommes *et al.*, 2003; Inaba *et al.*, 2003), and the problem becomes worse at larger distances.

The ice giants contain relatively small amounts of H-He, and might in principle have completed their accretion after the dissipation of the solar nebula, easing the constraint on accretion time. However, such a scenario does not solve the problem. It is necessary in any case that these planets form within the age of the solar system. The analytic model of Safronov (1969) predicted accretion times for Uranus and Neptune of order 10^{10} and 10^{11} y, respectively. Levison and Stewart (2001) performed N-body orbital integrations of systems of several hundred sub-Earth-mass embryos beyond the orbit of Saturn. They found that these bodies failed to accrete into giant planets. Instead, their mutual perturbations (with those of Jupiter and Saturn) stirred up the swarm to high eccentricities. Collisions were rare, and many of the bodies were ejected from the system, leaving insufficient mass to make Uranus and Neptune.

The well-known difficulties with accreting the ice giants in situ led Thommes *et al.* (1999; 2002) to suggest that they actually formed much closer to the Sun than their present distances. They postulated that multiple cores accreted in the Jupiter-Saturn region. Two cores were able to accrete gas from the nebula. The resulting increase in their masses allowed them to scatter the others into larger orbits; these were circularized by gravitational interactions with the swarm of planetesimals in the outer solar system. This seems to be a promising scenario, but it is not without problems: the introduction of such massive bodies would stir the outer swarm significantly, while the formation of the Kuiper Belt seems to require the planetesimal disk to be dynamically cold after the formation of Neptune (Levison and Morbidelli, 2003).

Boss (2000) has suggested an entirely different mechanism for the formation of the giant planets. His models of circumstellar disk evolution suggest that gravitationally bound clumps of gas, with masses comparable to that of Jupiter, could form within an accretion disk. If these clumps can survive long enough to collapse to higher density, they could produce gas giant planets on short dynamical

timescales of a few hundred orbital periods. As Jupiter and Saturn are not of solar composition, it is necessary to assume that they accreted more heavy elements in the form of planetesimals and/or lost H-He after their formation. In the context of this model, Boss *et al.* (2002) suggested that the ice giants formed by a variant of this mechanism. Their present compositions imply that if they started with solar abundances, their original content of hydrogen and helium had to be almost totally removed. Boss *et al.* proposed that dust grains coagulated and settled to the centers of the gaseous condensations. The gas was then removed by photoevaporation due to a nearby OB star in the cluster in which the Sun formed. This removal would have to occur before the gaseous protoplanets collapsed to become gas giant planets. Jupiter and Saturn were shielded from the stellar radiation by the solar nebula, and so retained their gaseous envelopes until they collapsed to planetary size. Due to their larger distances, Uranus and Neptune were less shielded, and lost their envelopes. Boss *et al.* estimated that dust grains within the gaseous protoplanets would grow to cm size and settle to the centers in only a few thousand years, so the gas giants would have rock/ice cores, while the ice giants comprise such cores minus their gaseous envelopes. This model solves the timescale problem, but has another serious flaw. The pre-collapse condensations would have rotation periods comparable to their orbital periods. As the particles are coupled to the gas by drag, with response times that are short compared with their settling times, they would give up their angular momentum to the gas as they settled toward the center. The gas giants would retain the angular momentum of their envelopes, and rotate rapidly after their collapse (their cores might be spun up by magnetic coupling to the gas), but one would expect the ice giant planets to have rotation periods of the order of a century.

For this reason, we do not give further consideration to the disk instability model. In the following sections, we examine implications and requirements for the core-accretion model. We consider the effects of varying the configuration of the solar nebula, particularly relaxation of the usual assumption that it had the "minimum mass." We then analyze the process of a core's growth by accretion of planetesimals, and show that the nature of this process in the outer solar system is qualitatively different from that in the region of terrestrial planets. We present results of numerical simulations that suggest that core-accretion model may be more viable than has been generally assumed.

2. The Solar Nebula

The so-called "minimum mass solar nebula" is constructed by augmenting the current masses of the planets with enough H-He to restore them to solar composition, and spreading each resulting mass through some region about its orbit. For reasonable assumptions as to the size of the corresponding source regions, this procedure gives a mass of a few per cent of the solar mass, and a surface density that

varies with heliocentric distance a as $a^{-3/2}$ (Weidenschilling, 1977). This power law index has become the standard, although some theorists have been willing to consider shallower or steeper slopes. It should be emphasized that the mass derived in this manner is an absolute lower limit. There is good reason to believe that the nebular mass was a few times larger: the formation of planetesimals from dust was probably not perfectly efficient (Weidenschilling, 1997), and in the outer solar system, a significant amount of mass was ejected to form the Oort comet cloud. This ejection was accompanied by redistribution of angular momentum among the outer planets; as a result, Jupiter moved inward while the other giant planets migrated outward. About $50M_\oplus$ of residual planetesimals were ejected, and as a result Neptune moved from ~21 to 30 AU (Malhotra *et al.*, 2000; Levison and Morbidelli, 2003). This evolution implies that the nebular surface density in the range $\sim 10 - 20$ AU was significantly higher than estimates based on the present planetary masses and orbits. The slope of the surface density was almost certainly shallower than $a^{-3/2}$, and may have been more like a^{-1}. The total heavy element content of the giant planets is $\sim 60 - 100M_\oplus$ (Wuchterl *et al.*, 2000); adding the $50M_\oplus$ ejected and adding the complement of H-He implies that the minimum mass was $\sim 0.02 - 0.03M_\odot$.

This nebula configuration would have important consequences for accretion in the outer solar system. The surface density of solid matter, σ, in the Earth's region is fairly well constrained at ~8 g cm^{-2}, as no process has been identified that could produce significant depletion during accretion of the terrestrial planets. Using this value at 1 AU as a fulcrum, we can show the corresponding values in the outer nebula for $a^{-3/2}$ and a^{-1} variations (Figure 1). The latter is more massive ($\sim 0.05M_\odot$ inside 30 AU for a^{-1}, vs. $0.02M_\odot$ for $a^{-3/2}$), but for reasonable assumptions for its temperature it is gravitationally stable as defined by the Toomre Q parameter. The difference in surface density between the two is more than a factor of 2 at 5 AU, and more than 5 times at 30 AU. Note that the surface density of solids has a discontinuity at the "snow line," here assumed to be at 5 AU, where condensation of water ice increases by about a factor of 4.

3. Runaway Growth and Oligarchy

It is now generally accepted that the growth of planetesimals by accretion proceeds by runaway, that is, the largest body becomes dominant. If the starting condition consists of equal-mass bodies, stochastic collisions produce a spectrum of sizes. The larger bodies are exposed to the same background population of smaller bodies. Each gains mass at a rate proportional to its cross section, which is its geometrical area augmented by its gravitational effect on approaching bodies. This cross-section is equal to $\pi R^2 \left(1 + V_e^2/V^2\right)$, where $V_e = \sqrt{2GM/R}$ is the escape velocity from the target body, and V is the approach velocity of the smaller bodies. If $V < V_e$, the cross section, and hence the rate of mass gain, is proportional to

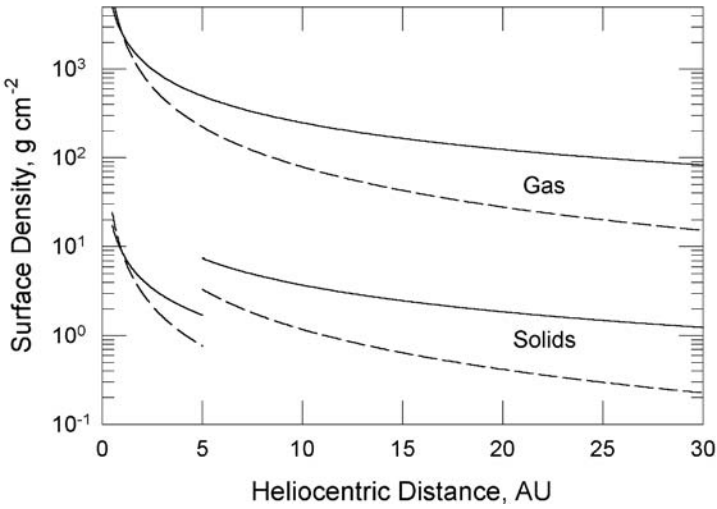

Figure 1. Surface density of gas and condensed solids in the solar nebula for two assumptions as to the gradient of surface density with heliocentric distance, a. The solid line is for surface density proportional to a^{-1}, while the dashed line shows the "standard" $a^{-3/2}$ gradient. In both models, the surface density is fixed at 8 g cm^{-2} of metal + silicate at 1 AU; the condensation of water ice causes the jump in the abundance of solids at 5 AU.

R^4; in an interval dt, d$M/M \sim R$. If two bodies have different values of M and R, the larger one grows more rapidly, in both absolute and relative terms, and the mass ratio of the largest to next largest increases (Wetherill and Stewart, 1989). This runaway by the largest body begins when the mass difference between it and the second largest becomes statistically significant, i.e., greater than the mean mass of the accreted bodies.

Runaway growth proceeds until the swarm parameters are changed, i.e., the small bodies are stirred up so that the approach velocity becomes comparable to V_e, or the supply of planetesimals is exhausted. Because the embryo and the accreted small bodies are orbiting the Sun, only planetesimals whose orbits bring them close enough to the embryo can collide with it. If the embryo is in a circular orbit, then the restricted three-body problem sets a limit (an energy barrier in a frame rotating with the embryo) due to the constancy of the Jacobi parameter; only orbits initially within a critical distance can collide with it after multiple synodic encounters. This distance is $2\sqrt{3}$ times the Hill radius R_H, where

$$R_H = \left(\frac{M}{3M_\odot}\right)^{1/3} a \, . \tag{1}$$

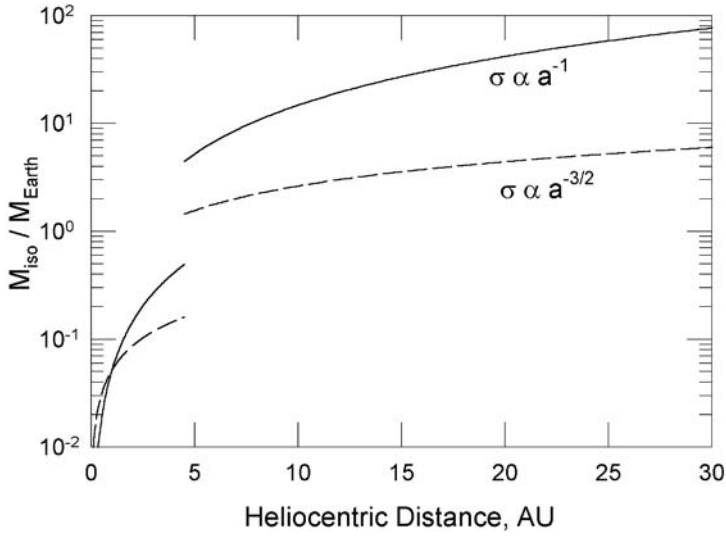

Figure 2. Isolation mass vs. heliocentric distance for the two nebular models shown in Figure 1.

As the embryo gains mass, $R_{\rm H}$ increases, but only as $M^{1/3}$. If the local surface density of the planetesimal swarm is σ, the available mass is $8\pi\sqrt{3}\sigma a R_{\rm H}$. Equating this to M gives the "isolation mass" at which accretion ceases,

$$M_{\rm iso} = \frac{\left(8\pi\sqrt{3}\sigma a^2\right)^{3/2}}{(3M_\odot)^{1/2}} = 2.1\times10^{-3}\left(\frac{a}{1\ \rm AU}\right)^3\left(\frac{\sigma}{1\ \rm g\,cm^{-2}}\right)^{3/2} M_\oplus \qquad (2)$$

(Lissauer and Stewart, 1993). Although the conditions of the restricted three-body problem are not strictly met (there may be collisions among the small bodies, effects of gas drag, perturbations by other embryos, etc.), in practice, $M_{\rm iso}$ is a reasonable estimate of the mass attained by an embryo during runaway growth. $M_{\rm iso}$ increases with a, unless σ decreases at least as steeply as a^{-2}. Figure 2 shows $M_{\rm iso}$ vs. heliocentric distance for the nominal nebular models of Figure 1. The dependence on σ produces a significant increase of $M_{\rm iso}$ by about a factor of 8 at the snow line. At larger distances, the difference between the $a^{-3/2}$ and a^{-1} nebular models becomes quite large.

4. Gravitational Scattering and Migration of Embryos

In the terrestrial planet region, runaway growth leads to an outcome that Kokubo and Ida (1998) called "oligarchy." At any given heliocentric distance, runaway produces a dominant embryo of mass $\sim M_{\rm iso}$, but its influence is limited. It can collide with planetesimals within a few $R_{\rm H}$ of its orbit, and its gravitational perturbations stir the swarm to a few times that distance, so the process of runaway growth

repeats more or less independently at intervals of $\sim 5 - 10 R_{\rm H}$. In the inner solar system, this spacing is much less than the heliocentric distance, and so σ varies by only a small amount. The outcome is similar in each case, producing a series of embryos of comparable mass with fairly uniform orbital spacing. The embryos are close enough for their perturbations to stir the remaining small planetesimals and decrease their gravitational cross-sections, so their growth slows significantly when about half the mass of the swarm has been incorporated into the embryos. From Equation (2), a surface density of 8 g cm^{-2} at 1 AU yields embryos $\sim 0.05 M_\oplus$. In order to produce the terrestrial planets, $\sim$50 such bodies must coalesce into a few planets and sweep up the remaining small planetesimals on a timescale of $\sim 10^7 - 10^8$ y (Chambers *et al.*, 1996; Chambers and Wetherill, 1998).

Kokubo and Ida (2000) developed empirical scaling laws for masses, spacing, and growth times for oligarchic growth of embryos, based on N-body integrations of planetesimals in the terrestrial region. Although they expressed reservations as to the application of this scaling to the outer solar system, these relations were used by Kokubo and Ida (2002) and Thommes *et al.* (2003) to estimate outcomes of oligarchic growth of the outer planets. Kokubo and Ida calculated that the solar nebula had to be at least 5 times the minimum mass in order to form gas giant planets within its $\sim 10^7$ y lifetime. Thommes *et al.* made similar estimates, and supplemented their calculations with N-body numerical simulations, starting with protoplanetary embryos with masses $\sim 0.1 - 0.5 M_\oplus$ spaced $\sim 10 R_{\rm H}$ apart in a swarm of planetesimals. They found that the oligarchs rarely collided, and they stirred the swarm up so that the accretion of small bodies was slow. Protoplanetary cores large enough to accrete gas could form inside $\sim$10 AU within 10^7 y only if the nebula had $\sim$10 times the minimum mass, while no bodies a large as $M_\oplus$ accreted at $\sim$20 AU. In summary, the standard model of oligarchic growth fails to produce the observed outer planets, unless unreasonably large mass and/or lifetime is assumed for the solar nebula.

Oligarchic growth is basically the result of localized runaway growth, i.e., the onset of runaway and its outcome are determined solely by the local parameters of the planetesimal swarm. This assumption is not correct in the outer nebula, due to the increased mobility of bodies at larger heliocentric distances. A planetesimal that has an encounter with an embryo without a collision has its orbit changed by gravitational scattering. In a close encounter, the change in the planetesimal's heliocentric velocity can be comparable to the embryo's escape velocity. In the outer nebula embryo masses ($\sim M_{\rm iso}$) are larger, producing larger velocity impulses, and the Kepler velocity $V_{\rm K}$ is smaller, so that a given velocity change yields a larger change in orbital elements. Using the value of $M_{\rm iso}$ from Equation (2), one can show that the ratio of the embryo's escape velocity $V_{\rm e}$(iso) to the local Kepler velocity is

$$\frac{V_{\rm e;iso}}{V_{\rm K}} \sim 0.036 \left(\frac{\rho}{1 {\rm g\,cm^{-3}}} \right)^{1/6} \left(\frac{\sigma}{1 {\rm g\,cm^{-2}}} \right)^{1/2} \left(\frac{a}{1 \text{ AU}} \right)^{3/2} \tag{3}$$

where ρ is the density of the embryo. At 1 AU, for $\sigma = 8$ g cm^{-2}, $V_{e;iso}/V_K \sim 0.12$, and the velocity impulse due to a close encounter can only change a planetesimal's semimajor axis by a modest amount. For nebular surface density proportional to a^{-1}, with water condensed at 5 AU, $\sigma = 7$ g cm^{-2}, and $V_{e;iso}/V_K \sim 1.0$. For $\sigma \propto a^{-1}$, $V_{e;iso}/V_K \propto a$. Thus, everywhere beyond the snow line, an embryo has the potential ability to scatter planetesimals over large distances, or to eject them from the nebula completely.

The migration of planetesimals by scattering can cause significant qualitative differences in the outcomes of accretion in the outer nebula compared with the terrestrial region. We have modeled the evolution of a swarm of small planetesimals accreting in the outer nebula, using the PSI multi-zone accretion code (Weidenschilling *et al.*, 1997). This code has unique features that allow it to treat small bodies as a statistical continuum, while large bodies above some threshold size are treated as individuals. The continuum is divided into a series of radial zones; their populations can interact by both collisions and gravitational stirring when their eccentricities are high enough for their orbits to overlap. Their gravitational interactions are adapted from the model of Stewart and Ida (2000) for stirring and dynamical friction. Viscous stirring tends to increase eccentricities and inclinations, while dynamical friction tends to produce equipartition of energy, damping random velocities of the larger bodies. The large discrete bodies interact with the continuum according to the Stewart-Ida equations, but gravitational interactions among them are modeled as a series of scattering events due to stochastic close encounters. This hybrid approach allows a large dynamic range of sizes, unattainable with N-body integrations, while allowing discontinuous jumps in orbital elements, which are not allowed in a purely continuum model.

5. Numerical Simulation: Monarchical Growth

We show an example of a simulation of accretion in the heliocentric range 4 – 30 AU, with nebular surface density proportional to a^{-1}. At $t = 0$, all solid matter is in the form of planetesimals of 1 km diameter; collisions are assumed to result in coagulation (no fragmentation). Aerodynamic drag is included, although this is a minor effect due to the low gas density; collisions are more effective at damping the small bodies. Bodies larger than 10^{24} g (diameter $\sim 10^3$ km) are treated as discrete objects, subject to mutual scattering. Figure 3 shows the masses and semimajor axes of these bodies, with horizontal bars indicating the range between their perihelia and aphelia. The initial growth is oligarchic, producing a number of sub-Earth sized bodies ($\sim 10^{27}$ g) between 4 and 7 AU by 10^5 y. By 2×10^5 y, two smaller bodies, $\sim 10^{25}$ and 10^{26} g, have been scattered outward to about 9 and 11 AU; their orbits are circularized by dynamical friction due to the swarm of small planetesimals in the continuum. These bodies are relatively isolated, and much more massive than the background population in their vicinity. The low velocities

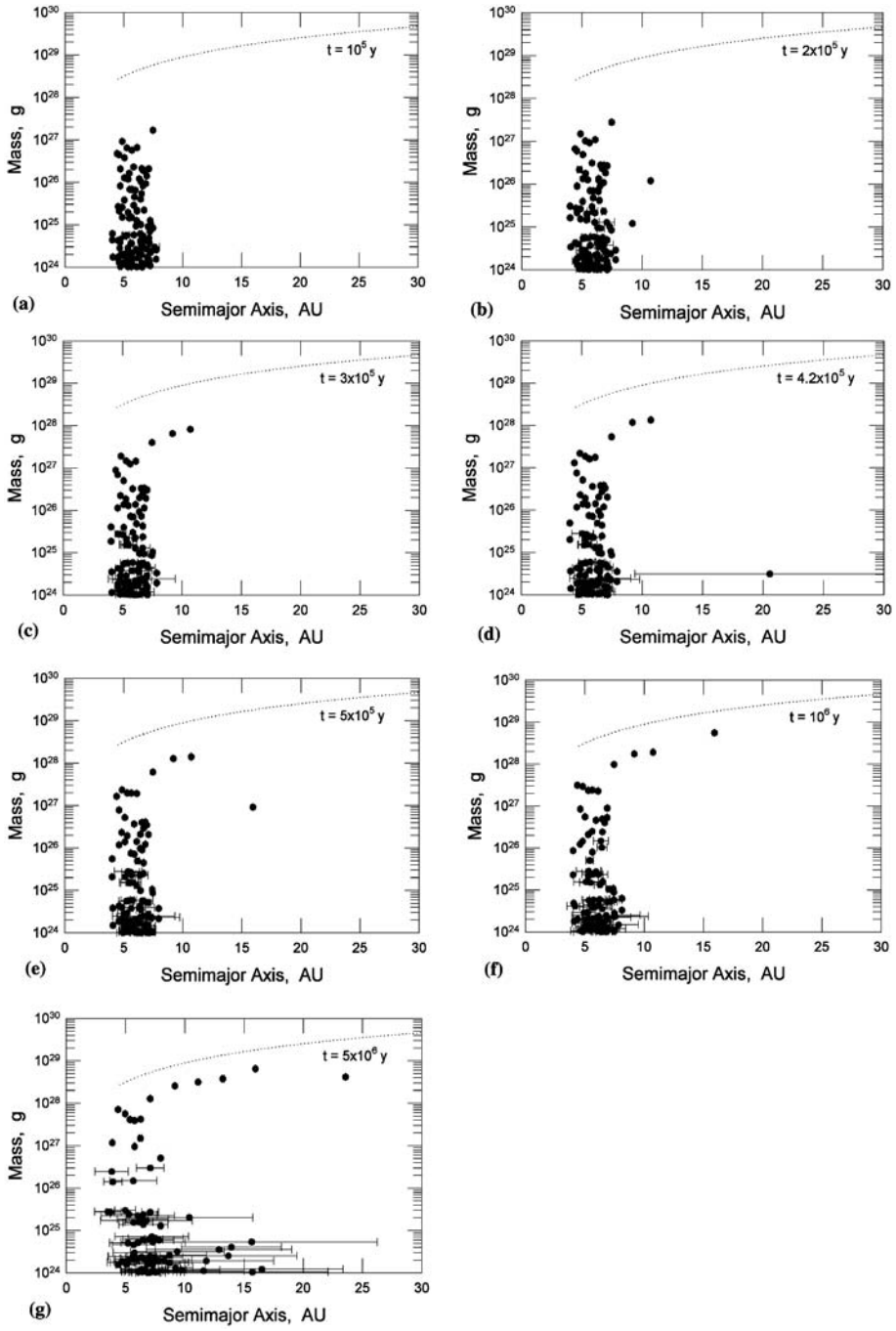

Figure 3. Results of one accretion simulation, with the nebular surface density proportional to a^{-1}. At $t = 0$, all solids were present as km-sized planetesimals ($m \sim 10^{15}$ g) between 5 and 30 AU; the total swarm mass is $\sim 230 M_\oplus$. The plots show masses vs. semimajor axes for the discrete bodies ($M > 10^{24}$ g); the horizontal bars show their perihelia and aphelia. The dotted curve shows $M_{\rm iso}$.

result in large gravitational cross-sections and rapid accretion; by 3×10^5 y, these bodies have grown larger than $M_\oplus$. A more extreme scattering event occurs at 4.2×10^5 y, when a body of mass $\sim 3 \times 10^{24}$ g is scattered into an eccentric orbit with semimajor axis ~20 AU and eccentricity ~0.5. Some 10^4 y later, dynamical friction damps its eccentricity such that it decouples from the large bodies inside 11 AU. Its orbit becomes circularized at ~16 AU. Because the growth rate decreases with increasing heliocentric distance, the size distribution at that location has not evolved very far; the scattered embryo is about 10^5 times the mass of the next largest body in that region, and about 10^8 times the mean mass. This large mass ratio allows the embryo to undergo extreme runaway growth, and by 6×10^5 y, it reaches $\sim 8 M_\oplus$. Somewhat later, similar scattering events trigger runaway growth of embryos at ~13 and 23 AU. By 5×10^6 y, there are six bodies with masses in the range $2 - 10 M_\oplus$ between 7 and 23 AU.

Unlike the case of oligarchic growth, the large bodies do not begin runaway growth by emerging from the local population by stochastic coagulation, but are placed among that population with an overwhelming advantage in mass, which allows the most extreme form of runaway growth. We refer to this style of growth as "monarchy." The most rapid growth occurs when the small bodies approach the embryo by keplerian shear rather than random motions due to their eccentricities. This condition also guarantees that the swarm is highly flattened, i.e., its thickness is less than the embryo's Hill radius. If we assume that the random velocities in the swarm are of the order of the escape velocity of the median-mass bodies of mass m, and radius r, then

$$V_{\mathrm{e;med}} = \left(\frac{2Gm}{r} \right)^{1/2} , \tag{4}$$

and the shear velocity is

$$\Omega R_{\mathrm{H}} = V_{\mathrm{K}} \left(\frac{M}{3M_\odot} \right)^{1/3} , \tag{5}$$

where Ω is the local Kepler frequency, then shear dominates if

$$\frac{M}{m} > \left(\frac{9M_\odot}{4\pi V_{\mathrm{K}}^3} \right) \left(\frac{8\pi G}{3} \right)^{3/2} \rho^{1/2} \sim 2.3 \times 10^4 \left(\frac{\rho}{1\,\mathrm{g\,cm^{-3}}} \right)^{1/2} \left(\frac{a}{1\ \mathrm{AU}} \right)^{3/2} \tag{6}$$

This condition requires $M/m \sim 10^6$ at 10 AU; i.e., the scattered embryo must be ~100 times the diameter of the local population. Thus, extreme runaway can be triggered by introducing a 100-km body into a km-sized population, or a 1000-km body if the median size is 10 km. The seed mass needed to trigger extreme runaway is somewhat uncertain. The minimum mass of discrete bodies in the simulation was 10^{24} g, in order to limit their number. One would expect smaller bodies to be more numerous, and they might be scattered more frequently, although they would also be more subject to collisional damping and gas drag. The critical mass

ratio may be less than implied by Equation (6). Tests of the code with artificially introduced seeds at 15 AU show extreme runaway growth when $M/m \sim 10^4$. However, this occurs under ideal conditions, with the seed placed in a circular orbit with negligible inclination in a dynamically cold swarm.

Once this style of growth begins, the embryo's mass gain is very rapid. Unlike the case of oligarchic growth, the "monarch" has no rivals. It is the only effective perturber; therefore, the conditions of the restricted three-body problem are fulfilled almost ideally. In the case of a continuous size distribution, inclinations are typically about half the value of eccentricities. However, stirring by a single dominant body raises inclinations of the small planetesimals much less effectively than eccentricities (Greenzweig and Lissauer, 1992), so the swarm remains highly flattened; typically the small bodies have inclination/eccentricity $i/e \sim 0.01 - 0.1$ during the core's growth. Although the eccentricities of the small bodies are increased, conservation of the Jacobi parameter implies that their velocities relative to the embryo remain constant in successive synodic encounters. Thus, approach velocities remain lower than in oligarchic growth where the small planetesimals are subject to perturbations of other embryos that randomize their orbits. We can crudely estimate the embryo's growth time as follows: The synodic period of a small body encountering the embryo is $\sim 2\pi a/\Omega R_{\rm H}$, and the approach velocity is $V_{\rm rel} \sim \Omega R_{\rm H}$. For a highly flattened swarm, the effective collision radius is $R_{\rm eff} \sim R(V_{\rm e}/V_{\rm rel})$, where R is the physical radius of the embryo. The collision probability for a planetesimal entering the Hill sphere is $\sim R_{\rm eff}/R_{\rm H}$. For this expression to be valid, $R_{\rm eff}$ must exceed the thickness of the swarm. Estimating the swarm thickness as $\sim V_{\rm e;med}/\Omega$, this implies $(R/R_{\rm H})(V_{\rm e}/V_{\rm e;med}) > 1$, or $R/r_{\rm med} > R_{\rm H}/R$. From Equation (1) one can show that $R_{\rm H}/R \sim 133\left(\rho/1\,{\rm g\,cm^{-3}}\right)^{-1/3}(a/1{\rm AU})$, so the collision probability is maximized if $R/r_{\rm med} > 10^2\, a({\rm AU})$. This requires a "seed" embryo of $\sim$1000 km in a km-sized swarm population at 10 AU, a more stringent requirement than dominance of keplerian shear from Equation (6). If the growing embryo becomes surrounded by a gaseous envelope, the larger value of R will relax this condition to some degree (such rapid growth would result in significant heating, with vaporization of water ice and probable formation of an extended steam atmosphere). If this condition is met, the rate of mass gain is ${\rm d}m/{\rm d}t \sim 2\sigma V_{\rm rel} R_{\rm eff} = 2\sigma R V_{\rm e}$. The e-folding timescale for the embryo to increase its mass is

$$t_{\rm grow} = \left(\frac{M}{{\rm d}M/{\rm d}t}\right) \sim \frac{M}{2\sigma R V_{\rm e}} \sim 10\left(\frac{\rho}{1\,{\rm g\,cm^{-3}}}\right)^{1/2}\left(\frac{R}{1\,{\rm km}}\right)\left(\frac{1\,{\rm g\,cm^{-2}}}{\sigma}\right)\ y. \quad (7)$$

Somewhat surprisingly, this expression does not depend on heliocentric distance (except indirectly, with σ). If $\sigma = 1$ g cm^{-2}, then $t_{\rm grow}$ increases from $\sim 10^4$ y for $R = 1000$ km to $\sim 10^5$ y for an Earth-sized body ($R = 10^4$ km). Thus, if the assumed conditions are met, it is possible in principle for the core of a giant planet to grow in only a few times 10^5 y. For less extreme mass ratios of seed to swarm population, runaway growth will still proceed, but on longer timescales.

6. Summary and Conclusions

We have shown that, contrary to previous conclusions, massive planetary cores can accrete in situ in the outer solar system on timescales shorter than the lifetime of the solar nebula. The process begins with conventional "oligarchic" growth of multiple embryos just outside the nebular snow line. These scatter a smaller embryo into an orbit with large semimajor axis and eccentricity, with perihelion near the oligarchs. Dynamical friction due to gravitational interactions with the small planetesimals in the outer nebula damps its eccentricity (and inclination), decoupling its orbit from the oligarchs. Due to the slower growth rate in the outer nebula, the scattered "seed" is much larger than the indigenous population. Once its orbit becomes circularized, it undergoes rapid runaway growth until it approaches the isolation mass. This growth in dynamical isolation produces a local "monarch," rather than a series of "oligarchs." This process can be repeated in other regions of the nebula as more seeds are scattered into appropriate orbits. The introduction of a seed body avoids one problem with in situ formation models such as that of Bryden *et al.* (2000), which assumes without explanation that a single body grows while its neighbors remain small.

Several conditions must be met in order for this scenario to be effective. First, the surface density outside the snow line must be sufficient to produce a first generation of oligarchs large enough ($\sim M_\oplus$) to be effective scatterers. Numerical tests indicate that a surface density of solids $\sim$7 g cm^{-2} at 5 AU is sufficient. Second, the scattered bodies must be much larger than the local population at the distance where they are "seeded." In practice, the median size must be $<$10 km for a Ceres-sized (1000 km) seed body to initiate rapid runaway growth. Finally, the local population has to be dynamically cold, with low eccentricities and inclinations. In addition to small median size, this condition requires that the swarm not be stirred up by an earlier-formed embryo in a nearby orbit; this limits the number of cores that can be formed by this process. The process of monarchical growth differs from the model of Thommes *et al.* (2002), in which the cores that became Uranus and Neptune reached their full sizes in the Jupiter-Saturn region, and then were scattered outward. Zharkov and Kozenko (1990) proposed a variant of this model, in which massive embryos ($\sim 5M_\oplus$) were scattered outward by Jupiter and Saturn, completing their growth at the present distances of Uranus and Neptune. In the present model, the masses of the scattered seeds are much less than those of the final planets, so their compositions are dominated by indigenous material that condensed in the outer region of the nebula beyond 10 AU. The seeds can be circularized without stirring up the planetesimal swarm, which is more compatible with models for the formation of the Kuiper Belt that require a dynamically cold disk to exist after the formation of Neptune (Levison and Morbidelli, 2003). Another consequence of this mode of growth is the acquisition of prograde spin angular momentum of the accreting core (Ohtsuki and Ida, 1998), which is consistent with

the rotation periods of Uranus and Neptune (their obliquities would require another source, such as late impacts of large bodies).

Although monarchical growth may allow the formation of Uranus and Neptune on a reasonable timescale, some problems remain. The fate of the oligarchic embryos that must accrete near the snow line is unclear. Perhaps they would eventually merge to form Jupiter's core, although it remains to be seen if they could do this before the dissipation of the nebula. Jupiter's core might have formed at a larger distance, and migrated inward by tidal interaction with the nebula, in which case the oligarchs may have been accreted and/or ejected by Jupiter after it reached its final mass. As $M_{\rm iso}$ increases with heliocentric distance for plausible nebular models, it seems that the formation of large cores should be easier for the outermost planets and we might expect them to become gas giants. It is not clear how Uranus and Neptune could have attained their present masses without accreting massive gaseous envelopes, unless the outer solar nebula dissipated on a short timescale.

Additional simulations with different starting conditions, or simply different sequences of random numbers, yield different outcomes. Often there are fewer monarchical planetary cores than the example shown here, and some produce none at all. It has become accepted that the terrestrial planets formed by collisions of oligarchic embryos, with the numbers and orbital parameters of the final systems depending on unpredictable stochastic events (Chambers and Wetherill, 1998). As the scattering events that can plant seeds in the outer solar nebula are similarly chaotic, it may be that the numbers of giant planets, and the times and places of their formation, were also the results of random events.

Acknowledgements

This research was supported by NASA's Planetary Geology and Geophysics program.

References

Boss, A.P.: 2000, 'Possible rapid gas giant planet formation in the solar nebula and other protoplanetary disks', *Astrophys. J.* **536**, L101–L104.

Boss, A.P., Wetherill, G.W., and Haghighipour, N.: 2002, 'Rapid formation of ice giant planets', *Icarus* **156**, 291–295.

Bryden, G., Lin, D.N.C., and Ida, S.: 2000, 'Protoplanetary formation I: Neptune', *Astrophys. J.* **544**, 481–495.

Chambers, J.E., Wetherill, G.W., and Boss, A.P.: 1996, 'The stability of multi-planet systems', *Icarus* **119**, 261–268.

Chambers, J.E. and Wetherill, G.W.: 1998, 'Making the terrestrial planets: N-body integrations of planetary embryos in three dimensions', *Icarus* **136**, 304–327.

Greenzweig, Y. and Lissauer, J.J.: 1992, 'Accretion rates of protoplanets II. Gaussian distributions of planetesimal velocities', *Icarus* **100**, 440–463.

Inaba, S., Wetherill, G.W., and Ikoma, M.: 2003, 'Formation of gas giant planets: Core accretion models with fragmentation and planetary envelope', *Icarus* **166**, 46–62.

Kokubo, E. and Ida, S.: 1998, 'Oligarchic growth of protoplanets', *Icarus* **131**, 171–178.

Kokubo, E., and Ida, S.: 2000, 'Formation of protoplanets from planetesimals in the solar nebula', *Icarus* **143**, 15–27.

Kokubo, E. and Ida, S.: 2002, 'Formation of Protoplanet Systems and Diversity of Planetary Systems', *Astrophys. J.* **581**, 666–680.

Levison, H.F. and Stewart, G.R.: 2001, 'Remarks on modeling the formation of Uranus and Neptune', *Icarus* **153**, 224–228.

Levison, H.F. and Morbidelli, A.: 2003, 'The formation of the Kuiper belt by the outward transport of bodies during Neptune's migration', *Nature* **426**, 419–421.

Lissauer, J.J. and Stewart, G.R.: 1993, 'Growth of planets from planetesimals', in E.H. Levy and J.I. Lunine (eds.), *Protostars and Planets III*, University of Arizona Press, Tucson, pp. 1061–1088.

Malhotra, R., Duncan, M. J., and Levison, H. F.: 2000, 'Dynamics of the Kuiper belt', in V. Mannings, A.P. Boss, S.S. Russell (eds.), *Protostars and Planets IV*, University of Arizona Press, Tucson, pp. 1231–1254.

Ohtsuki, K. and Ida, S.: 1998, 'Planetary rotation by accretion of planetesimals with nonuniform spatial distribution formed by the planet's gravitational perturbation', *Icarus* **131**, 393–420.

Podosek, F.A. and Cassen, P.: 1994, 'Theoretical, observational, and isotopic estimates of the lifetime of the solar nebula', *Meteoritics* **29**, 6–25.

Pollack, J.B., Hubickyj, O., Bodenheimer, P., Lissauer, J.J., Podolak, M., and Greenzweig, Y.: 1996, 'Formation of the giant planets by concurrent accretion of solids and gas', *Icarus* **124**, 62–85.

Safronov, V.S.: 1969, 'Evolution of the protoplanetary cloud and formation of the Earth and planets', *Nauka*, Moscow, (Transl. 1972, NASA TT F-677).

Stewart, G.R. and Ida, S.: 2000, 'Velocity evolution of planetesimals: Unified analytical formulas and comparisons with N-Body simulations', *Icarus* **143**, 28–44.

Thommes, E.W., Duncan, M.J., and Levison, H.F.: 1999, 'The formation of Uranus and Neptune in the Jupiter-Saturn region of the Solar System', *Nature* **402**, 635–638.

Thommes, E.W., Duncan, M.J., and Levison, H.F.: 2002, 'The formation of Uranus and Neptune among Jupiter and Saturn', *Astron. J.* **123**, 2862–2883.

Thommes, E.W., Duncan, M.J., and Levison, H.F.: 2003, 'Oligarchic growth of giant planets', *Icarus* **161**, 431–455.

Weidenschilling, S.J.: 1977, 'The distribution of mass in the planetary system and solar nebula', *Astrophys. Space Sci.* **51**, 153–158.

Weidenschilling, S.J.: 1997, 'The origin of comets in the solar nebula: A unified model', *Icarus* **127**, 290–306.

Weidenschilling, S.J., Spaute, D., Davis, D.R., Marzari, F., and Ohtsuki, K.: 1997, 'Accretional evolution of a planetesimal swarm 2. The terrestrial zone', *Icarus* **128**, 429–455.

Wetherill, G.W. and Stewart, G.R.: 1989, 'Accumulation of a swarm of small planetesimals', *Icarus* **77**, 330–357.

Wuchterl, G., Guillot, T., and Lissauer, J.J.: 2000, 'Giant planet formation', in V. Mannings, A.P. Boss, S.S. Russell (eds.), *Protostars and Planets IV*, University of Arizona Press, Tucson, pp. 1081–1109.

Zharkov, V.N. and Kozenko, A.V.: 1990, 'On the role of Jupiter in the formation of the giant planets', *Sov. Astron. Lett.* **16**, 73–74.

Address for Offprints: Stuart J. Weidenschilling, Planetary Science Institute, 1700 E. Fort Lowell Road, Suite 106, Tucson, AZ 85719, USA; `sjw@psi.edu`

STRUCTURE AND EVOLUTION OF GIANT PLANETS

ISABELLE BARAFFE
Ecole Normale Supérieure, 69364 Lyon Cedex 07, France

Received: 3 May 2004; Accepted in final form: 10 August 2004

Abstract. The understanding of the structure and evolution of our solar system giant planets has significantly advanced within the past years. Important progress is due not only to direct observations and in situ measurements, but also to high pressure laboratory experiments which test the properties of hydrogen under the same conditions of pressure and density as in the interior of giant planets. The modelling of giant planets has also improved due to theoretical and observational activities devoted to another type of objects, the brown dwarfs, closely related to giant planets in terms of atmospheric and thermodynamic properties. Since the best constraints are now available for Jupiter and Saturn, this review summarizes the latest improvements regarding the description of the interior and atmosphere of these two giant planets. We will also extend the discussion to extrasolar giant planets.

Keywords: Jupiter, Saturn, interiors, planets, exoplanets, brown dwarfs

1. Inner Structure of Jupiter and Saturn

Extensive works on the structure of our giant planets have been conducted by several teams within the past years and are mainly based on the so-called three-layer model (Chabrier *et al.*, 1992; Guillot *et al.*, 1995; 1995; Hubbard *et al.*, 1999). In the framework of this model, the interior consists of (i) a central rocky and/or icy core of mass $M_{\rm core}$, (ii) an inner ionized hydrogen envelope, characterised by a helium abundance $Y_{\rm ion}$ (He may also be ionized in the deep envelope depending on the size of the core) and heavy element abundance $Z_{\rm ion}$, (iii) an atomic helium and molecular hydrogen envelope and outer atmosphere, characterised by abundances $Y_{\rm mol}$ and $Z_{\rm mol}$.

Details on the structure of Jupiter and Saturn can be found in Guillot *et al.* (1995). Jupiter has an equilibrium radius $R_{\rm eq} = 7.149 \times 10^9$ cm and an effective temperature $T_{\rm eff} = 125$ K. 91% of its total mass is characterised by pressures greater than 1 Mbar, which covers a critical and uncertain regime in terms of the equation of state of hydrogen, as described below. Comparatively, Saturn, which has about $\approx 30\%$ of the mass of Jupiter, has an equilibrium radius $R_{\rm eq} = 6.02 \times 10^9$ cm and $T_{\rm eff} = 95$ K. 67% of its mass is characterised by pressures greater than 1 Mbar and is thus less sensitive than Jupiter to the equation of state uncertainties.

The main properties of H/He mixture under the interior conditions of giant planets are briefly described below. Details can be found in the reviews by Chabrier and Baraffe (2000) and Hubbard *et al.* (2002), and references therein. Ions are strongly

Space Science Reviews 116: 67–76, 2005.
DOI: 10.1007/s11214-005-1948-0

correlated, characterised by a plasma coupling parameter $\Gamma = (Ze)^2/akT > 1$, where a is the mean inter-ionic distance. Electrons are partially degenerate, with the Fermi energy close to or larger than the thermal energy, and are characterised by a degeneracy parameter $\theta = kT/kT_F \approx 0.05 - 1$. Moreover, the electron average binding energy can be of the order of the Fermi energy $Ze^2/a_0 \approx \epsilon_F$, with a_0 the electronic Bohr radius, so that pressure-ionisation takes place along the internal profile. Another complexity which may characterise giant planets is the existence of a phase separation of the H/He mixture (Salpeter, 1973; Stevenson and Salpeter, 1977), where He becomes insoluble in H and forms He-rich droplets which sink toward the central regions under the action of gravity. Such sedimentation process provides an additional source of energy which slows down the cooling of a planet during its evolution. Finally, at pressures ≈ 1 Mbar, H dissociates from molecular H_2 to metallic H^+ and whether this transition is continuous or is described by a first order transition, the so-called Plasma Phase Transition as suggested by Saumon and Chabrier (1992), is still an open question. To summarize, the equation of state (EOS) characterising the interior properties of giant planets thus requires a detailed description of strongly correlated, polarisable, partially degenerate classical and quantum plasmas, plus an accurate treatment of pressure partial ionization, a severe challenge for dense matter physicists. Most of the recent interior models for Jupiter and Saturn use the Saumon *et al.* (1995) EOS, which is also used for the description of low mass objects such as brown dwarfs and very low mass stars. Indeed, the conditions of pressure and temperature of these objects are similar to those found in giant planets (see Chabrier and Baraffe, 2000, for a review).

Along with theoretical developments, important efforts have been recently devoted to shock compression experiments. The possibility to test in laboratory the properties of dense hydrogen up to Mbar pressures provides a fantastic opportunity to improve our understanding of the complex processes described above. An excellent summary of the most recent experiments and their comparison with theoretical hugoniots computed from current EOS can be found in the paper by Saumon and Guillot (2004). The work of Saumon and Guillot (2004) stresses the current disagreement between different experimental data and shows how the current uncertainty on the hydrogen EOS affects the inferred structures of Jupiter and Saturn.

2. Model Construction

Several constraints are available for the elaboration of interior models for Jupiter and Saturn. Knowing the mass and the radius, the first constraints enabling the derivation of the planet density profile are provided by the knowledge of the gravitational moments, essentially J_2 and J_4, measured during spacecraft flybys of both planets. Another important constraint is provided by the estimate of the temperature at the 1 bar level, $T_{1bar} = 165 - 170$ K as measured by Galileo for Jupiter, and

TABLE I

Interior properties of Jupiter and Saturn based on current uncertainties on the hydrogen equation of state (Saumon and Guillot, 2004). $M_{\rm core}$ is the mass of the rocky/icy core; $M_{\rm Z}$ the mass of heavy elements in the envelope; $M_{\rm Z}^{\rm tot} = M_{\rm core} + M_{\rm Z}$ the total mass of heavy elements; $Z/Z_\odot$ is the ratio of heavy elements in the planet to that in the Sun.

	Jupiter	Saturn
$M_{\rm core}$	$0 - 11 M_\oplus$	$9 - 22 M_\oplus$
$M_{\rm Z}$	$1 - 39 M_\oplus$	$1 - 8 M_\oplus$
$M_{\rm Z}^{\rm tot}$	$8 - 39 M_\oplus$	$13 - 28 M_\oplus$
$Z/Z_\odot$	$1 - 6$	$6 - 14$

$T_{\rm 1bar} = 135 - 145$ K for Saturn according to the Pioneer and Voyager spacecrafts (see Guillot, 1999, for details and references). Estimate of the atmospheric helium mixing ratio provides another important constraint, with a value $Y = 0.23$ for Jupiter, according to Galileo. For Saturn, the value of $Y = 0.06$ obtained from Voyager is controversial and could be significantly larger, up to $Y \approx 0.2$ as suggested by Conrath and Gautier (2000). Note that less helium is found in Jupiter than in the protosolar nebula for which $Y_{\rm proto} = 0.275$ (Bahcall *et al.*, 1995) and which is also representative of the amount of helium present when the planet formed. Such a lower abundance of helium may be explained by the phase separation of helium in hydrogen and the subsequent formation of He-rich droplets falling to deeper levels. This is also expected to happen in Saturn and a better in situ determination of the He abundance in this planet is highly desirable to confirm this suggestion.

Assuming that all heavy elements are homogeneously mixed in the envelope, the two remaining free parameters are the mass of the central core $M_{\rm core}$ and the mass of heavy elements in the hydrogen-helium envelope $M_{\rm Z}$. Results based on the most recent work (Saumon and Guillot, 2004) are displayed in Table I. This work takes into account the uncertainties on the EOS of hydrogen, according to the different experimental results (see Figs. 4 and 5 of Saumon and Guillot, 2004). More details on the physical assumptions used in the model construction can be found in Guillot (1999) and Guillot *et al.* (1994).

The main uncertainties appearing in Table I are essentially due to the uncertainties on the EOS (see Fig. 9 and Fig. 11 in Saumon and Guillot, 2004). Interestingly enough, a model of Jupiter with no solid core ($M_{\rm core} = 0$) is within the errorbars. However, this solution is definitely excluded for Saturn. These results are important in terms of formation scenarios of these planets in the solar nebula. With the perspective of the Cassini mission to Saturn, it is worth stressing that another important source of uncertainty in the models of this planet results from the large uncertainty on the current value of its gravitational moment J_4. As shown

by Guillot (1999), 1 σ variation on J_4 yields a variation of 10 $M_\oplus$ on $M_{\rm core}$. A better determination of the temperature at the 1 bar level would also improve the quality of the interior models, since a variation of $T_{\rm 1bar}$ from 145 K to 135 K yields a central core larger by 4 $M_\oplus$.

3. Atmospheric Properties

Significant progress were made within the past decade on the modelling of cool atmospheres ($T_{\rm eff} < 2000$ K), which are no longer a major source of uncertainty in cooling theories of Jupiter and Saturn. This field largely improved due to recent developments in the field of low mass stars and brown dwarfs. Indeed, the coolest brown dwarfs referred to as methane dwarfs ($T_{\rm eff} \lesssim 1200$ K), can reach effective temperatures similar to that of our solar system giant planets. There are two major sources of opacities in cool atmospheres, namely molecules (H_2O, TiO, H_2, CH_4, etc...) and dust ($MgSiO_3$, NH_3, see Chabrier and Baraffe, 2000, and references therein). The recent discovery of a new class of substellar objects, the so-called L-dwarfs (1200 K $\lesssim T_{\rm eff} \lesssim$ 2000 K), which show peculiar spectral and photometric properties reflecting the presence of atmospheric dust, allowed substantial progress in this field. One of the main difficulties remaining in the modelling of such atmospheres is the description of the different processes affecting dust formation, such as gravitational settling, convection, grain growth and coagulation (see Allard *et al.*, 2001; Sudarsky *et al.*, 2003, and references therein). Another interesting property of such atmospheres is the significant absorption due to alkali metals, such as K, Na, Cs. Indeed, strong absorption features in the optical spectrum of methane dwarfs were only recently recognised to be due to alkali metals (Burrows *et al.*, 2000). Theoretical efforts are now devoted to the modelling of absorption profiles perturbed by He and molecular H, a complex fundamental problem in physics (Allard *et al.*, 2003). Since this discovery, it is now clear that alkali metal absorption cannot be ignored anymore in the modelling of brown dwarf and giant planet atmospheres. An important consequence of this discovery is the significant increase of the mean opacity in Jupiter's atmosphere, at the kbar pressure level with temperatures ranging from $\approx 1200\,{\rm K} - 1500\,{\rm K}$, and the subsequent suppression of the deep radiative layer found previously in the interior of Jupiter by Guillot *et al.* (1994).

4. Evolutionary Models

Evolutionary models taking into account the uncertainties on the EOS (Saumon and Guillot, 2004) can reach Jupiter's effective temperature and radius in 4.6 $\pm$ 1 Gyr. The properties of Saturn are reached in $\approx$ 2 Gyr, indicating that the models evolve too rapidly. An additional source of energy is thus required, which could

be provided by the sedimentation of He-rich droplets (Salpeter, 1973). However, evolutionary models taking into account a phase separation based on existing H/He phase diagrams (Stevenson, 1975; Hubbard and DeWitt, 1985; Pfaffenzeller *et al.*, 1995) cannot provide the time delay required to fit Saturn at its age (Fortney and Hubbard, 2003). We stress that this recent result does not question the existence of the phase separation in Saturn, which seems to be the most natural explanation for such time delay, but rather indicates the crudeness of current theoretical description of this process. Important progress is expected in the forthcoming years with the elaboration of a new method, based on first principles, devoted to an accurate calculation of the H/He phase diagram (Winisdoerffer *et al.*, 2004).

In parallel, a better observational determination of the atmospheric He abundance of Saturn is crucial, in order to constrain the sedimentation model. Note also that evolutionary models based on the Voyager value $Y = 0.06$ cannot reproduce the observed properties of Saturn, which require a value $Y > 0.10$ (Hubbard *et al.*, 1999). Although the existence of a phase separation in Saturn affecting its cooling timescale seems to be the favored explanation, whether this process is important in terms of cooling age for Jupiter is still an open question. The sedimentation process may be needed to explain the low atmospheric abundance of He in this planet. However, because of remaining uncertainties on the EOS and atmosphere models, it is not possible to say whether a phase separation, which would yield a time delay, or, on the other hand, processes such as core erosion, which would accelerate the evolution, had a significant impact on Jupiter's cooling history. The recent models by Saumon and Guillot (2004) can indeed reach Jupiter's properties in an age younger or older than the solar system age, depending on the EOS used. Figure 1 also illustrates the uncertainties due to the atmosphere models by comparing the evolution of a non-irradiated 1 $M_{\rm Jup}$ based on two sets of models using the same EOS, but with different atmospheric input physics. In particular, the two sets of models (Burrows *et al.*, 1997; Baraffe *et al.*, 2003) use different molecular line lists for the main absorbers, such as H_2O and CH_4, and different absorption profiles for the alkali metals (see the details in Burrows *et al.*, 1997, and in Allard *et al.*, 2001, for the models of Baraffe *et al.*, 2003). Such a comparison shows that an effective temperature of $\approx$ 100K, characteristic of Jupiter, is reached in 3.6 Gyr by the Baraffe *et al.* (2003) models and in 5.6 Gyr by the Burrows *et al.* (1997) models.

5. Extension to Exoplanets

As mentioned in the previous section, important improvements in the physics describing the atmosphere of our giant planets are due to recent developments in the field of brown dwarfs. In the same vein, since the general theory for Jupiter and Saturn, in terms of EOS and atmosphere, also applies to extra-solar giant planets (EGPs), the increasing number of newly discovered EGPs provides other observa-

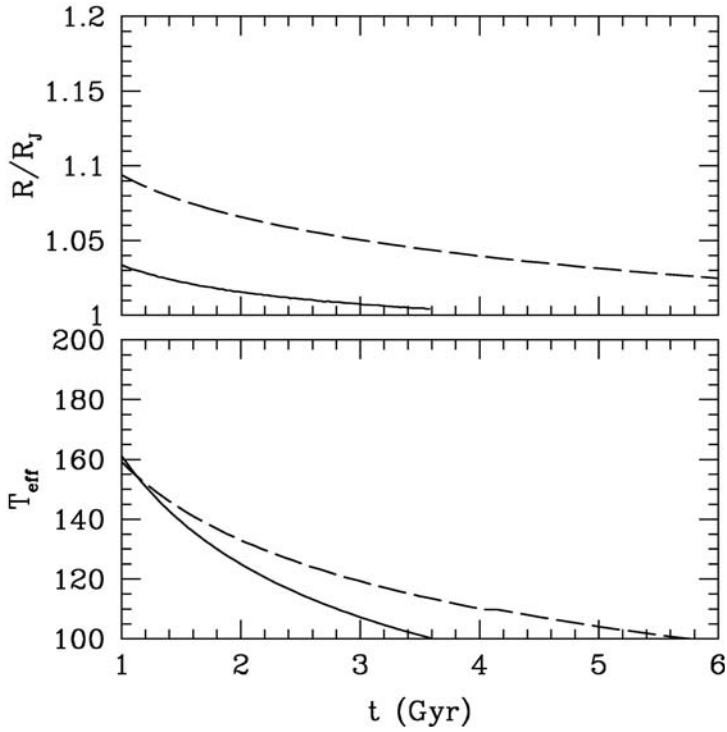

Figure 1. Evolution of a non-irradiated 1 $M_{\rm Jup}$ object taking into account the uncertainties on the treatment of atmospheric opacities and dust formation. Solid lines are the models from Baraffe *et al.* (2003) and dashed lines correspond to the models from Burrows *et al.* (1997). The two sets of models do not include a rocky core.

tional constraints on this theory. Since no direct detection of the light emitted by an EGP is yet available, direct constraints on the atmospheric properties of EGPs are unfortunately postponed to the future. However, good constraints on their structure and cooling properties are provided by transits. Indeed, with additional constraints from radial velocity observations, the mass m and radius of the planet can be estimated. The first transit ever discovered is HD209458b, at an orbital separation from its parent star $a = 0.046$AU (Charbonneau *et al.* , 2000) with $m = 0.69 \pm 0.02 M_{\rm Jup}$ and radius $1.42^{+0.10}_{-0.13}\, R_{\rm Jup}$ (Cody and Sasselov , 2002). The other known transit is OGLE-TR-56b, with $a = 0.023$AU (Konacki *et al.*, 2003), $m \simeq 1.45 \pm 0.23\, M_{\rm Jup}$, and radius $1.23 \pm 0.15\, R_{\rm Jup}$ (Torres *et al.*, 2003).

Because of the very small orbital separation, such planets are strongly irradiated by their parent star. Irradiation effects must then be included, affecting significantly not only the emitted spectrum of the planet, but also its structure and evolution. Evolutionary models based on consistent coupling between the irradiated atmospheric structure and the internal, partially radiative structure have been elaborated recently by Baraffe *et al.* (2003). Such a consistent treatment successfully reproduces the observed parameters of the transit planet OGLE-TR-56b (Chabrier *et*

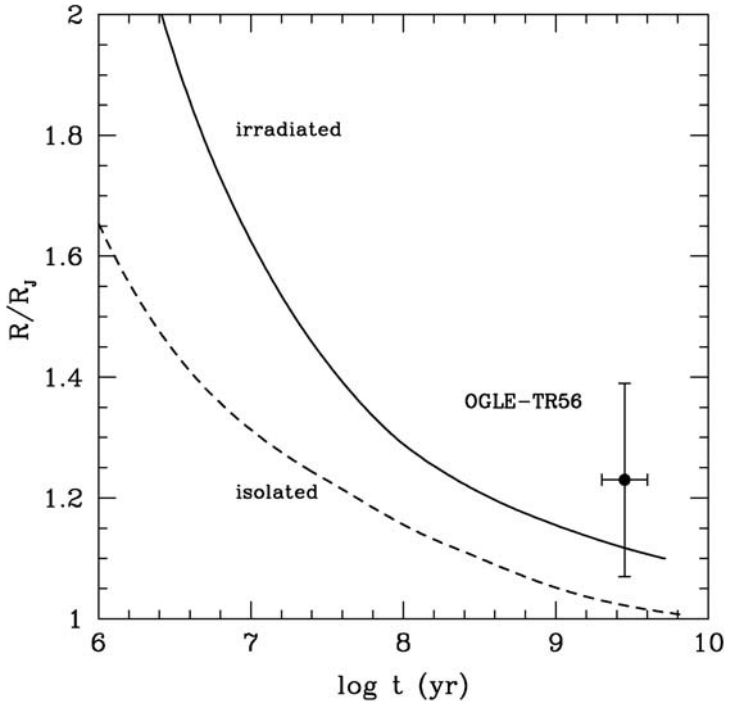

Figure 2. Evolution of the radius, in units of Jupiter radii, of a planet with mass m=1.5 $M_{\rm Jup}$ orbiting a G2 star at $a = 0.023$ AU (solid lines). This case corresponds to OGLE-TR-56b. The dashed curve displays the evolution in the non-irradiated case, corresponding to a planet far away from its parent star ($a >> 1$ AU). Note that the surface temperature of the irradiated planet, according to the models of Chabrier *et al.* 2004, is $\approx$ 2400K.

al., 2004). This success of the theory is illustrated in Figure 2, which compares the evolution of the radius of a 1.5 $M_{\rm Jup}$ giant planet, with and without irradiation, with the observed values for OGLE-TR-56b. The recent work by Burrows *et al.* (2004) also confirmed the results of Chabrier *et al.* (2004) and the success of current theory.

However, no consistent model can adequately reproduce the observationally determined radius of the transit planet HD209458b, as illustrated in Figure 3. Several suggestions have been proposed to explain the large observed radius for its mass and extensive discussions can be found in Baraffe *et al.* (2003) and Chabrier *et al.* (2004). In particular, Guillot and Showman (2002) suggested a kinetic heating mechanism related to atmospheric circulation and Bodenheimer *et al.* (2001) suggested a tidal heating caused by a possible unseen companion.

Also, because the mass of this transit planet is substantially lower than OGLE-TR-56b, this led to the suggestion that we may miss an important part of fundamental physics in the description of sub-jovian ($m < 1\ M_{\rm Jup}$) planets. At this level, it is premature to answer such a question, and more observed transits are required,

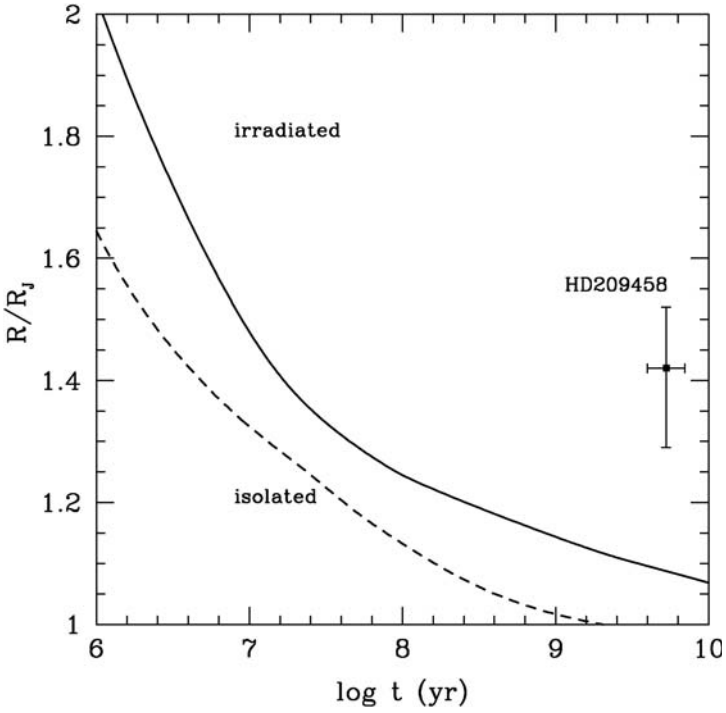

Figure 3. Evolution of the radius, in units of Jupiter radii, of a planet with mass m=0.69 $M_{\rm Jup}$ orbiting a G2 star at $a = 0.046$ AU (solid lines). This case corresponds to HD209458b. The dash-dotted curve displays the evolution in the non-irradiated case.

along with the development of improved models and better observed constraints for Saturn.

6. Conclusion

In the perspective of future in situ explorations of our giant planets, it is now crucial to obtain better observational constraints for Saturn, namely the gravitational moments J_4 and J_6 and atmospheric abundances of helium and heavy elements. Improved heavy element abundances in Jupiter are also highly desirable. Interesting constraints on the structure of Jupiter could also be provided by seismology. All these efforts will considerably reduce the range of acceptable models and could provide interesting constraints on the properties of H/He at high pressure. Important progress is also expected in the future from high pressure experiments (e.g, the laser project "Laser Mega Joule"), which will simulate physical conditions in the interior of giant planets. As also emphasized in this paper, efforts devoted to the analysis of giant planets have strong links with another active field of research devoted to very low mass stars, brown dwarfs and exo-planets. With the

combined efforts of different communities, namely planetology, stellar and plasma physics, and space science research, a wealth of exciting results on the structure and evolution of giant planets is expected in the near future.

Acknowledgements

I am extremely grateful to Didier Saumon and Tristan Guillot, who made available their most recent results before publication, as well as other material required for the elaboration of this review. I also thank Gilles Chabrier for valuable advice and discussions.

References

Allard F., Hauschildt P.H., Alexander D.R., Tamanai A., and Schweitzer, A.: 2001, *Astrophys. J.* **556**, 357–372.

Allard, N., Allard, F., Hauschildt, P.H., Kielkopf, J.F., and Machin, L.: 2003, *Astron. Astrophys.* **411**, L473–L476.

Bahcall, J.N., Pinsonneault, M.H., and Wasserburg, G.J.: 1995, *Rev. Mod. Phys.* **67**, 781–808.

Baraffe, I., Chabrier G., Barman, T., Allard F., and Hauschildt P.H.: 2003, *Astron. Astrophys.* **402**, 701–712.

Bodenheimer,P., Lin, D.N., and Mardling, R.A.: 2001, *Astrophys. J.* **548**, 466–472.

Burrows, A., Marley, M., Hubbard, W.B., Lunine, J.I., Guillot, T., Saumon, D., Freedman, R., Sudarsky, D., and Sharp, C.: 1997, *Astrophys. J.* **491**, 856–875.

Burrows, A., Marley, M., and Sharp, C.M.: 2000, *Astrophys. J.* **531**, 438–446.

Burrows, A., Hubeny, I., Hubbard, W.B., Sudarsky, D., and Fortney, J.J.: 2004, *Astrophys. J.* **610**, L53–L56.

Chabrier, G. and Baraffe, I.: 2000, *Ann. Rev. Astron. Astrophys.* **38**, 337–377.

Chabrier, G., Saumon, D., Hubbard, W.H., and Lunine, J.I.: 1992, *Astrophys. J.* **391**, 817–826.

Chabrier G., Barman, T., Baraffe, I., Allard F., and Hauschildt, P.: 2004, *Astrophys. J.* **603**, L53–L56.

Charbonneau, D., Brown, T., Latham, D., and Mayor, M.: 2000, *Astrophys. J.* **529**, L45–L48.

Cody, A.M. and Sasselov, D.D.: 2002, *Astrophys. J.* **569**, 451–458.

Conrath, B.J.D. and Gautier, D.: 2000, *Icarus* **144**, 124–134.

Fortney, J.J. and Hubbard, W.B.: 2003, *Icarus* **164**, 228–243.

Guillot, T., Chabrier, Morel, P., and Gautier, D.: 1994, *Icarus* **112**, 354–367.

Guillot, T., Chabrier, G., Gautier, D., and Morel, P.: 1995, *Astrophys. J.* **450**, 463–472.

Guillot, T.: 1999, *Planet. Space Sci.* **47**, 1183–1200.

Guillot, T. and Showman, A.: 2002, *Astron. Astrophys.* **385**, 156–165.

Hubbard, W.H. and DeWitt, H.E.: 1985, *Astrophys. J.* **290**, 388–393.

Hubbard, W.H., Guillot, T., Marley, M.S., Burrows, A., Lunine, J.I., and Saumon, D.S.: 1999, *Planet. Space Sci.* **47**, 1175–1182.

Hubbard, W.H., Burrows, A., and Lunine, J.I.: 2002, *Ann. Rev. Astron. Astrophys.* **40**, 103–136.

Konacki, M., Torres, G., Jha, S., and Sasselov, D.: 2003, *Nature* **421**, 507–509.

Pfaffenzeller, O., Hohl, D., and Ballone, P.: 1995, *Phys. Rev. Lett.* **74**, 2599–2602.

Salpeter, E.E.: 1973, *Astrophys. J.* **181**, L83–L86.

Saumon, D.S. and Chabrier, G.: 1992, *Phys. Review A* **46**, 2084–2100.

Saumon, D.S. and Guillot, T.: 2004, *Astrophys. J.*, in press (astro-ph/0403393).

Saumon, D.S., Chabrier, G., and Van Horn, H.M.: 1995, *Astrophys. J. Suppl.* **99**, 713–741.
Stevenson, D.J.: 1975, *Phys. Lett. A* **58**, 282.
Stevenson, D.J. and Salpeter, E.E.: 1977, *Astrophys. J. Suppl.* **35**, 239–261.
Sudarsky, D., Burrows, A., and Hubeny, I.: 2003, *Astrophys. J.* **588**, 1121–1148.
Torres, G., Konacki, M., Sasselov, D., and Jha, S.: 2003, *Astrophys. J. Lett.*, submitted (astro-ph/0310114).
Winisdoerffer, C., Chabrier, G., and Zérah, G.: 2004, *Phys. Review E*, to be published.

Address for Offprints: Isabelle Baraffe Ecole Normale Supérieure, 69364 Lyon Cedex 07, France; ibaraffe@ens-lyon.fr

FORMATION OF GIANT PLANETS – AN ATTEMPT IN MATCHING OBSERVATIONAL CONSTRAINTS

YANN ALIBERT, CHRISTOPH MORDASINI, OLIVIER MOUSIS and WILLY BENZ
Physikalisches Institut, University of Bern, CH-3012 Bern, Switzerland

Received: 1 June 2004; Accepted in final form: 13 October 2004

Abstract. We present models of giant planet formation, taking into account migration and disk viscous evolution. We show that migration can significantly reduce the formation timescale bringing it in good agreement with typical observed disk lifetimes. We then present a model that produces a planet whose current location, core mass and total mass are comparable with the one of Jupiter. For this model, we calculate the enrichments in volatiles and compare them with the one measured by the *Galileo* probe. We show that our models can reproduce both the measured atmosphere enrichments and the constraints derived by Guillot *et al.* (2004), if we assume the accretion of planetesimals with ices/rocks ratio equal to 4, and that a substantial amount of CO_2 was present in vapor phase in the solar nebula, in agreement with ISM measurements.

Keywords: Stars: planetary systems – stars: planetary systems: formation – solar system: formation

1. Introduction

The current paradigm for the formation of giant gaseous planets is based on the so-called core accretion model in which a growing solid core reaches a critical mass and accretes rapidly a massive atmosphere (Pollack *et al.*, 1996). This model explains for example the global enrichment in heavy elements observed in the giant planets, and can be used to interpret the enrichments in volatiles observed in the atmosphere of Jupiter by the mass spectrometer on-board the *Galileo* probe (Atreya *et al.*, 1999; Mahaffy *et al.*, 2000). However, while this model has many appealing features, it suffers at least from three shortcomings.

First, the timescale (close to 10 Myr) found by Pollack *et al.* (1996) to form Jupiter at its present location is uncomfortably close to the lifetime of protoplanetary disks which is believed to be of the order of 1-10 Myr (Haisch *et al.*, 2001). This timescale problem has led others to look for more rapid formation mechanisms based on direct gravitational collapse (Boss, 2002; 2004). Second, Pollack *et al.* (1996) assumed that the giant planets of our solar system have been formed where they are observed today. However, the discovery over the last decade of extrasolar planets at very short distances to their host star has opened the possibility that planets may actually migrate over large distances (Lin *et al.*, 1996; Trilling *et al.*, 1998; Papaloizou and Terquem, 1999). The time scale of migration is still very uncertain, but conservative estimates give values between 0.1 and 10 Myr.

Space Science Reviews 116: 77–95, 2005.
DOI: 10.1007/s11214-005-1949-z

Finally, the interpretation by Gautier *et al.* (2001a; b) and Hersant *et al.* (2004) of the enrichment in volatiles in Jupiter is not strictly speaking consistent with Pollack *et al.* (1996). These authors assume, for example, that all planetesimals have been accreted by Jupiter during the late hydrodynamical phase (phase 3 in Pollack *et al.*, 1996), although nearly one half are accreted during phase 1 and phase 2.

Since all relevant timescales (planet formation, disk evolution, and migration) are of the same order of magnitude, it appears difficult to obtain a self-consistent model while omitting anyone of these processes. In Section 2 below, we briefly summarize our efforts to develop such a self-consistent model within the framework of the core-accretion scenario. New formation models of giant planets including these processes are presented in Section 3. In Section 4, we will use these models to calculate the corresponding volatile enrichment and will compare them to the observed one in Jupiter. A summary and conclusions are presented in Section 5.

2. The Model

Basically, our model to compute the formation of giant planets follows closely the work by Pollack *et al.* (1996) with some notable addition. It consists in three different modules that calculate: 1) the disk structure and its time evolution, 2) the interaction of planetesimals with the atmosphere of the planet, and 3) the internal structure of the planet. We give here a short description of each module. More details and some tests of the model can be found in Alibert *et al.* (2004a).

2.1. Disk Structure and Evolution

Contrary to Pollack *et al.* (1996), we do not assume a static disk but rather a time evolving one. For simplicity, we assume a so-called α-disk (axisymmetric and with constant α) for which we determine the structure (both vertical and radial) as a function of time using the method described in Papaloizou and Terquem (1999). From the vertical structure, we compute, as a function of distance to the star r, the surface density Σ and subsequently the mid-plane temperature and pressure $T_{\rm mid}(r, \Sigma)$, $P_{\rm mid}(r, \Sigma)$ the mean viscosity $\nu(r, \Sigma)$, and the disk density scale height $H(r, \Sigma)$. The first two quantities are needed as boundary conditions in the calculation of the internal structure of the planet, whereas the two others enter in the calculation of the radial structure of the disk. The time evolution of the disk is governed by a diffusion equation, modified to take into account the momentum transfer between the planet and the disk, as well as the effect of photo-evaporation. The rate of momentum transfer between the planet and the disk is calculated following Lin and Papaloizou (1986)

$$\Lambda(r) = \frac{f_\Lambda}{2r}\sqrt{GM_{\rm star}}\left(\frac{M_{\rm planet}}{M_{\rm star}}\right)^2\left(\frac{r}{\max(|r-a|, H)}\right)^4, \quad (1)$$

where a is the sun-planet distance and f_Λ is a numerical constant. The photo-evaporation term is as in Veras and Armitage (2003).

2.2. MIGRATION

Gravitational interactions between the growing protoplanet and the disk lead to inward migration and possibly gap formation (Lin and Papaloizou, 1986; Ward, 1997; Tanaka *et al.*, 2002). For low mass planets, the migration rate is linear with mass (type I migration, Ward, 1997). Higher mass planets open a gap and the migration rate is set by the viscosity (type II migration, Ward, 1997).

While the general physical understanding of the origin of migration is clear, the actual migration rates obtained for type I migration especially are so short that all planets should actually be destroyed by the central star long before the disappearance of the gaseous disk. Tanaka *et al.* (2002) have performed new analytical calculations of type I migration, in two or three dimensional disks and found longer migration timescales but unfortunately still too short to ensure survival. Further suggestions for increased type I migration timescales can be found in calculations by Nelson and Papaloizou (2003). As suggested by these authors, torques exerted on at least small mass planets ($M_{\rm planet} < 30 M_\oplus$) embedded in turbulent MHD disks are strongly fluctuating resulting in a slow down of the net inward motion. Moreover, as shown by Menou and Goodman (2003), type I migration of low-mass planets can be slowed down by nearly one order of magnitude in regions of opacity transitions.

These considerations seem to indicate that the actual migration timescales may in fact be considerably longer than originally estimated by Ward (1997) or even by Tanaka *et al.* (2002). For these reasons, and for lack of better knowledge, we actually use for type I migration the formula derived by Tanaka *et al.* (2002) reduced by an arbitrary numerical factor f_I (set to $1/30$ in this paper). Tests have shown that provided this factor is small enough to allow planet survival, its actual value *does not* change the formation timescale but just the extend of migration (see Section 3.3).

For type II migration, two cases have to be considered. For low mass planets (when their mass is negligible compared to the one of the disk) the inward velocity is given by the viscosity of the disk. When the mass of the planet becomes comparable to the one of the disk, migration slows down and eventually stops. In this latter case, the variation of the planet's orbital momentum is equal to the angular momentum transport rate (Lin and Papaloizou, 1985; Lin *et al.*, 1996):

$$\frac{d}{dt}\left[M_{\rm planet} a_{\rm planet}^2 \Omega\right] = \frac{3}{2}\Sigma \nu \Omega r^2, \tag{2}$$

where $\Omega^2 = G M_{\rm star}/a_{\rm planet}^3$, and the second term is calculated at the current position of the planet, $a_{\rm planet}$, but using the non perturbed gas surface density. In all cases of type II migration, the migration rate is limited to the viscous velocity of the disk.

Migration type switches from type I to type II when the planet becomes massive enough to open a gap in the disk which occurs when the Hills radius of the planet becomes greater than the density scale height H of the disk.

2.3. THE PLANETESIMALS

In this module we compute the trajectory, the energy and mass loss of planetesimals falling through the atmosphere of the planet under the influence of gravity and aerodynamic drag forces. The drag coefficient is calculated (assuming a sphere) as a function of the local Mach and Reynolds numbers using the equations given by Henderson (1976). The loss in kinetic energy results in a local heating of the planet's atmosphere which enters in the calculation of the internal structure. Given the size of the planetesimals considered here (100 km), ablation is found to be negligible and deposition of mass occurs almost entirely due to fragmentation which occurs when the pressure at the stagnation point becomes larger than the planetesimals tensile strength. We do not take into account any diffusion effects that could bring planetesimals from outside to inside the feeding zone.

Due to the scattering effect of the planet, the surface density of planetesimals is constant within the current feeding zone but decreases with time proportionally to the mass accreted (and/or ejected from the disk) by the planet.

The feeding zone is assumed to extend to a distance of 4 $R_{\rm Hill}$ on each side of the planetary orbit, where $R_{\rm Hill}$ is the Hills radius of the planet. We use the expressions in the Appendix B and C of Greenzweig and Lissauer (1992) to calculate the gravitational enhancement factor.

For the inclination and eccentricities of the planetesimals we adopt the same values as in Pollack *et al.* (1996). For the physical properties of the planetesimals we use the values for ice.

Finally, it is important to take into account the ejection of planetesimals scattered by the planet since the amount of planetesimals ejected from the feeding zone directly determines the final abundance of heavy elements in the planet. To compute the ejection rate, we use the accretion to ejection ratio scaling derived from Ida and Lin (2004):

$$f_{\rm acc} \propto \left(\frac{V_{\rm Kepl}}{V_{\rm esc,planet}} \right)^4, \tag{3}$$

where $V_{\rm Kepl}$ is the disk keplerian velocity at the planet location, and $V_{\rm esc,planet}$ the escape velocity from the planet. This latter formula is an order of magnitude estimate for the ejection rate, and is still subject to some uncertainties. However, work by Guillot and Gladman (2000) suggests that the ejection rate may be high enough to prevent the accretion of more than $\sim 8 M_\oplus$ on a $10 M_\oplus$ core, at the present location of Jupiter. This suggests that the ejection rate may be signicantly higher than the one given by Equation (3) using $f_{\rm acc} = 1$.

Ongoing N-body calculations (Horner *et al.*, 2004) suggest a value of $f_{\rm acc}$ of the order of 10 to 100 depending on the planet's location and planet's mass. We will assume in the results presented here $f_{\rm acc} = 10$.

2.4. Protoplanet Structure and Evolution

The internal structure of the planet is calculated, taking into account a growing core (and the inner luminosity due to the accretion of planetesimals). We use for the models presented here the sinking approximation described in Pollack *et al.* (1996): after dissolution inside the envelope, planetesimals debris are assumed to slowly sink to the core, leading to an extra term in the luminosity. This corresponds to the approximation used in the standard case of Pollack *et al.* (1996). As shown by Alibert *et al.* (2004a), planetesimals are destroyed relatively deep in the envelope. Consequently, the differences between the sinking and the no sinking approximation are found to be much smaller than in Pollack *et al.* (1996).

The equations of planet evolution are solved, using opacities from Bell and Lin (1994) and the equation of state from Chabrier *et al.* (1992). The outer boundary conditions are given by requiring that the disk and the planet join smoothly at the outer radius, i.e. $T_{\rm surf} = T_{\rm mid}(r, \Sigma)$, and $P_{\rm surf} = P_{\rm mid}(r, \Sigma)$. The gas accretion rate onto the planet is determined by the condition: $R_{\rm planet} = min(R_{\rm Hill}, R_{\rm acc})$ where $R_{\rm planet}$ is the outer radius of the planet, and $R_{\rm acc}$ the accretion radius (see Pollack *et al.*, 1996). At each timestep, we calculate the mass of the envelope required to reach this condition. However, in reality, the latter condition can only be satisfied if the disk can actually supply enough gas to the planet. Once a gap in the disk opens, the maximum gas accretion rate is set to the rate given by Veras and Armitage (2003). At this stage, the growth in mass of the planet is set by the disk and no longer by the internal structure of the planet which is no longer computed.

3. New Formation Models

3.1. In Situ Formation

To properly quantity the effect of migration on planet formation, we first compute a model in which migration is turned off. Figure 1 shows the mass of accreted planetesimals as well as the mass of gas as a function of time for a planet at 5.5 AU. The gas and solid surface densities are non evolving in this simulation, and their values are $525{\rm g/cm}^2$ and $10{\rm g/cm}^2$. As in Pollack *et al.* (1996), we do not consider the ejection in this simulation and the next one.

This model corresponds approximately to case J2 of Pollack *et al.* (1996), the corresponding timescale for formation being around 50 Myr in their simulation. The three phases described in Pollack *et al.* (1996) are clearly identified, the timescale for formation is given by the length of phase 2. The formation time is around 30 Myr, somewhat lower than in Pollack *et al.* (1996), but still much longer

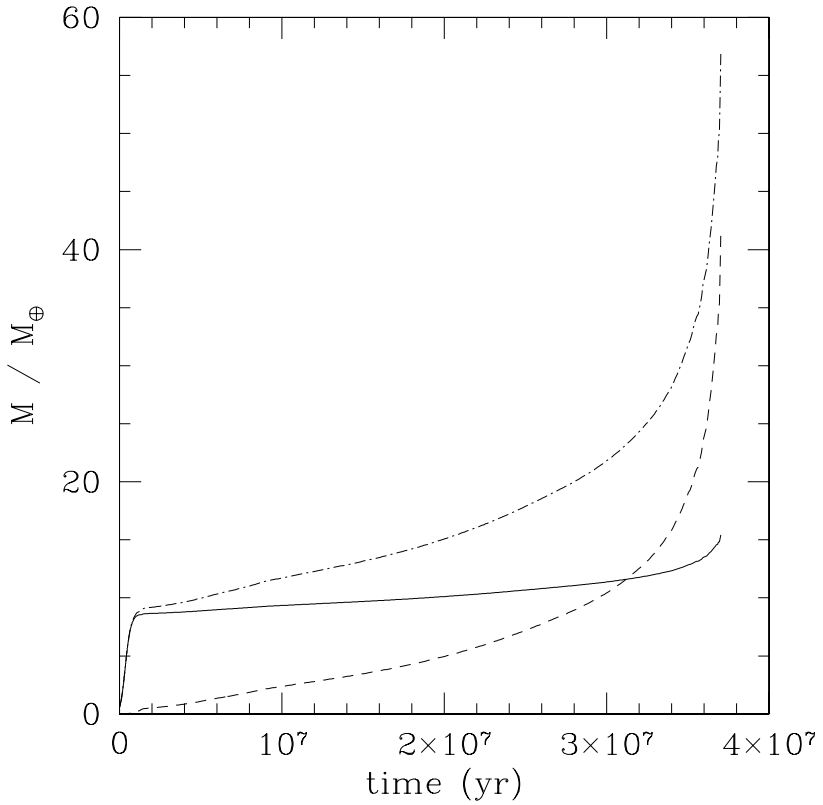

Figure 1. Time evolution of the planet in the case of in-situ formation. *Solid line:* Mass of accreted planetesimals (either in core or dissolved in the envelope), *dashed line:* mass of accreted gas and *dot-dashed line:* total mass.

than typical disks lifetimes. The difference with Pollack *et al.* (1996) provides a measure for the sensitivity of the results to differences in physical and numerical approximations used in both approaches. In particular, we use a different equation of state and opacity law (which has been shown to have a huge influence on the length of phase 2, see Pollack *et al.*, 1996), and our initial model is not exactly the one of Pollack *et al.* (1996).

3.2. Initial Disk Models

To calculate models with migration and disk evolution, we have to specify an initial disk profile, as well as the disk viscosity. We will consider two kinds of initial surface density profiles, $\Sigma \propto r^{-2}$, and $\Sigma \propto r^{-3/2}$, where r is the distance to the sun. The viscosity parameter α is set to 2×10^{-3} which yields a typical evolution time of the disk of a few Myr. The gas-to-dust ratio is equal to 70 for disk mid-plane temperature below 170 K, and 280 in the opposite case. The numerical parameters are f_I (reduction of type I migration) equal to 1/30 and f_Λ, the numerical factor

in the expression of the momentum transfer between the planet and the disk, set to 0.05. This latter choice gives a reduction of Σ due to momentum transfer around 30% when the disk density scale height equals the Roche radius of the planet (corresponding to the moment when migration switches from type I to type II). The main conclusions presented here remain valid if f_Λ is set to 0: the effect of gap formation on formation is essentially due to the limitation of the accretion rate of gas (see Section 2.4), and not due to the variation of the boundary conditions at the surface of the planet.

3.3. Formation with Migration: Timescale to Accrete a Massive Envelope

We first calculate the timescale to reach the crossover mass (mass of accreted planetesimals equal to mass of accreted gas). We consider an initial disk density profile given by $\Sigma \propto r^{-2}$, the constant being chosen to yield $\Sigma = 525\mathrm{g/cm}^2$ at 5.2 AU. As in Pollack *et al.* (1996), this surface density profile is chosen to have isolation masses that do not depend on the distance to the sun. In this section, we do not take into account photo-evaporation nor ejection, and we start with an embryo of $0.6M_\oplus$ initially at 8 AU. Figure 2 shows the mass of planetesimals and the mass of gas accreted by the planet as a function of time. Note that the mass of accreted planetesimals does not correspond to the core mass since some fraction of them are being destroyed while traversing the envelope and never reach the core.

As in Pollack *et al.* (1996), the formation timescale is essentially determined by the time necessary to reach the runaway accretion phase which occurs shortly after the crossover mass (mass of core equals mass of envelope), M_{cross}, has been reached. Allowing for migration and disk evolution, we obtain a formation time of about $\sim$1 Myr, i.e. thirty times faster than in our identical model in which migration and disk evolution have been switched off. The main reason for this speed-up is that owing to migration, the feeding zone is not as severely depleted as in Pollack *et al.* (1996), and hence, the long time needed to reach critical core mass and start runaway gas accretion is suppressed. Taking into account migration, the moving planet always encounters new planetesimals and thus its feeding zone is never emptied. To illustrate this important point, Figure 3 shows the initial and final disk profiles (for both the gaseous and the solid component).

Comparing a planet formed *in situ* or allowed to migrate at times of equal core mass (beginning of the simulation and after 0.7 Myr), we note that the envelope mass is always larger in the migrating case. This effect can also contribute to the speed-up, and can be understood as the combination of two effects (see Papaloizou and Terquem, 1999):

1. for a given core mass and distance to the star, the envelope mass increases when the accretion rate decreases
2. at a fixed accretion rate and core mass, the mass of the envelope is a growing function of the distance to the star.

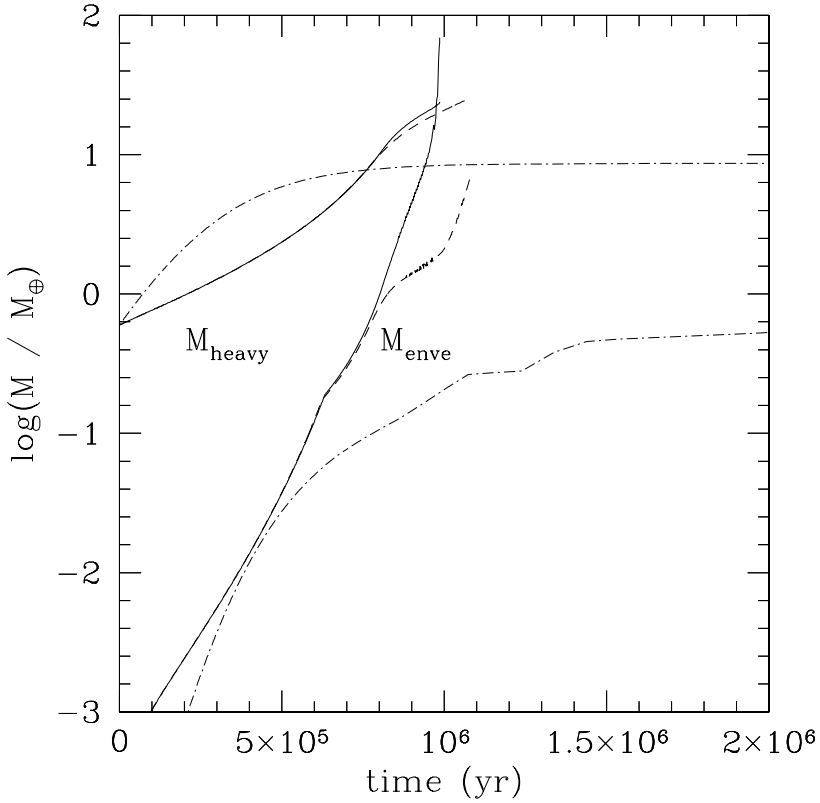

Figure 2. Mass of accreted planetesimals and mass of gas as a function of time for different models (all with initial disk surface density $\Sigma \propto r^{-2}$). *Solid line:* with migration but without gap formation, *dashed line:* with migration and gap formation, *dot-dashed line:* without migration nor gap formation (same as Figure 1).

This speed-up effect appears to be very robust against changes in the value of f_I (reduction of type I migration), provided its value is small enough to ensure survival of the planet. For example, in a calculation in which the reduction of type I migration (f_I) is set to 0.1, an embryo starting at 15 AU undergoes runaway accretion in less than 3 Myr. Reducing type I migration by 0.01 leads an embryo initially at 7 AU to runaway after less than 1 Myr.

3.4. Formation of a Giant Planet at 5 AU

Depending on the different physical parameters used, a wide variety of giant planets can be formed. As an example, we provide here the result of a simulation yielding a giant planet of mass $\sim 350 M_\oplus$ located at about 5 AU within less than 3 Myr. In this example, we consider a density profile, $\Sigma \propto r^{-3/2}$ normalized so that the mass of the disk (between 0.5 AU and 50 AU) is $0.04 M_\odot$, and a disk photo-evaporation rate $10^{-8} M_\odot$/yr. The type I reduction parameter is taken equal

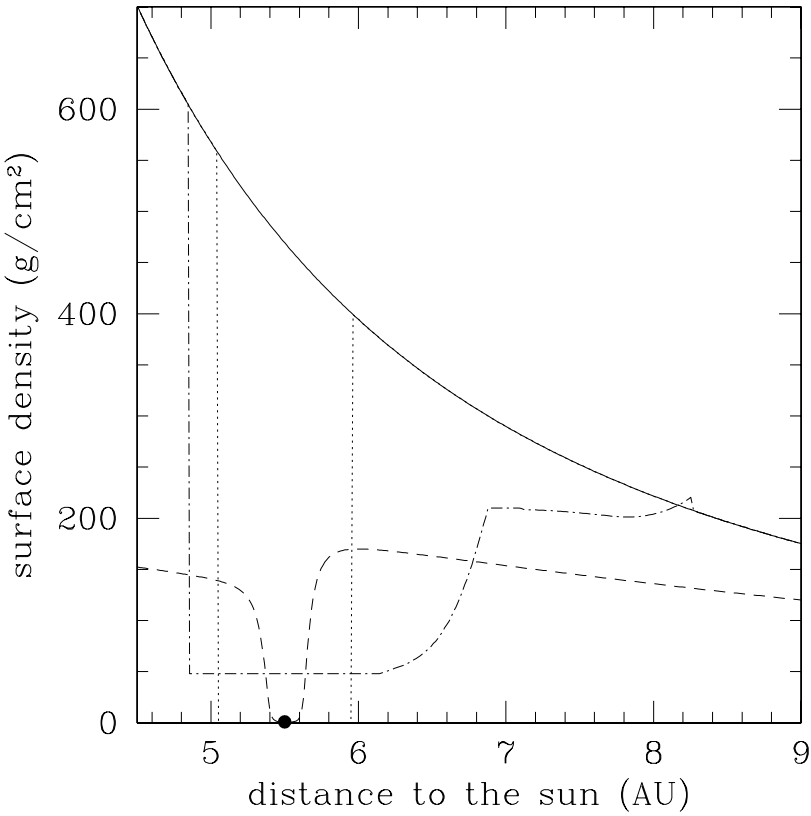

Figure 3. Gas and solid surface densities for the models with and without migration (both with an initial surface density $\Sigma \propto r^{-2}$). *Solid line:* initial surface densities; *dashed line:* gas surface density for model with migration and gap formation, after 1 Myr; *dot-dashed line:* solid surface density for the same model, at the same time; *dotted line:* solid surface density at the same time, but for the in-situ model. The solid surface densities are multiplied by 70, and the big dot gives the position of the planet.

to 1/100, and we do not take into account the effect of gap formation on the boundary conditions at the surface of the planet*. We start the calculation with an embryo at 11.5 AU. Figure 4 shows the evolution of the mass of the gaseous envelope, the mass of accreted planetesimals, as well as the mass of the disk, and Figure 5 gives the distance to the sun as a function of time. The crossover mass is reached after 1.6 Myr, and at the same time, due to gap formation, the accretion rate of gas is limited to its maximum value, which decreases with decreasing disk mass. The formation process ends after less than 3 Myr when the disk has disappeared. The final planet is characterized by a core of $\sim 6M_\oplus$ and an envelope of $\sim 360M_\oplus$ of which $\sim 36M_\oplus$ are accreted planetesimals which were destroyed before reaching the core. This final mass of heavy elements may be slightly increased further during the

* however, the gap has still the effect of limitation of the gas accretion rate

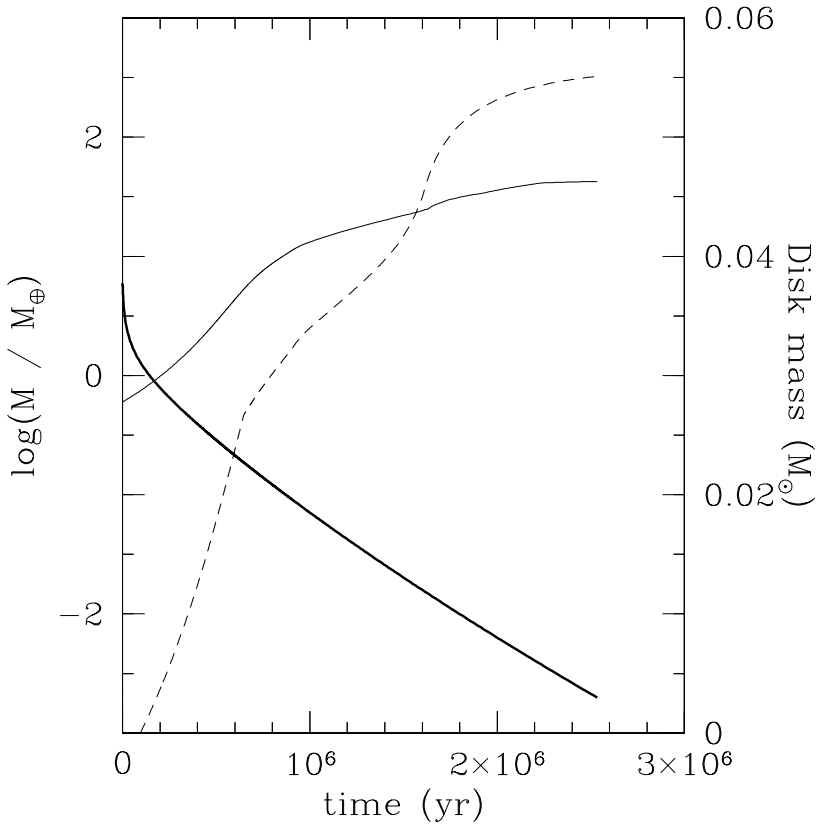

Figure 4. Mass of the different components for model of Section 3.4. *Solid line:* mass of accreted planetesimals, *dashed line:* mass of accreted gas, and *heavy solid line:* mass of the disk.

late stages of the formation, when the planet will accrete and/or eject the remaining planetesimals inside its final feeding zone. However, given the uncertainty on the ejection rate, the final content of heavy elements is not strongly constrained.

The migration of the planet can be divided into three phases. Before ∼1 Myr the planet undergoes type I migration at which time migration switches to type II. Shortly before the end of the formation process, at ∼2.5 Myr, the mass of the planet becomes non negligible compared the disk mass and migration slows down and eventually stops when the disk has disappeared. At the end of the simulation, the planet is located at 5.14 AU, but it is expected that it will move to ∼5 AU before the disk has completely disappeared.

Note that the extent of migration, and therefore the starting location of the embryo for a fixed endpoint, strongly depends upon the type I migration rate (f_I). A higher rate ($f_I = 0.03$) results in the formation of a similar planet from an embryo initially located at ∼ 15 AU. Reducing the type I migration rate would also reduce the starting location of the embryo.

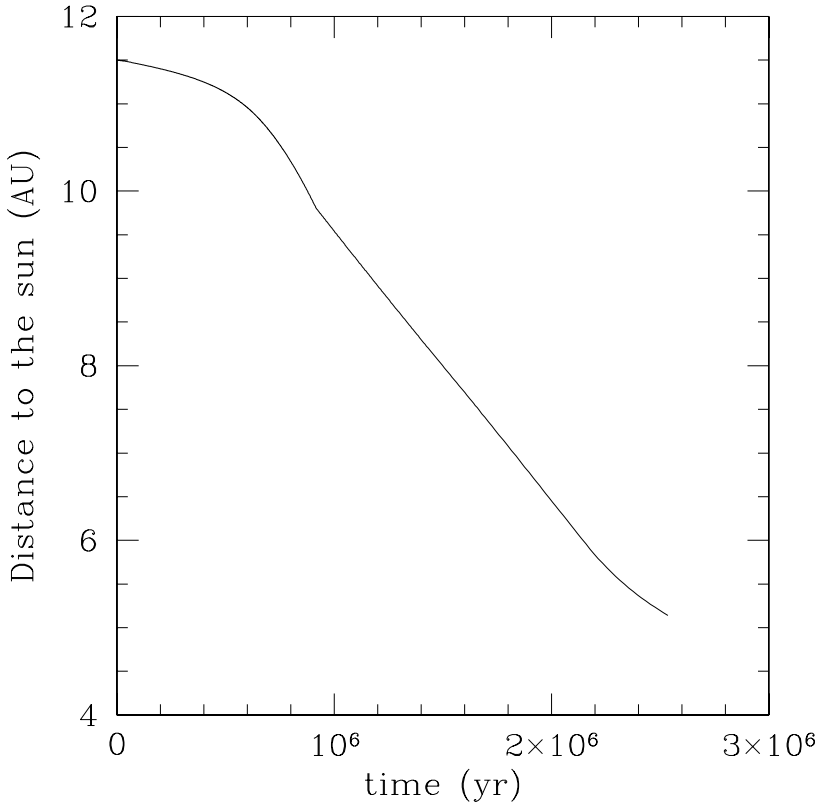

Figure 5. Distance to the sun for model of Section 3.4. The kink around 1 Myr signals the change from type I to type II migration.

4. Comparison with Observational Constraints from Jupiter

We now consider the model of Section 3.4 which has a core and a total mass comparable to Jupiter and is located at a similar distance to the sun.

4.1. Core Mass vs. Total Mass of Heavy Elements

The total mass of heavy elements present inside the atmosphere of the planet is $\sim 36 M_{\oplus}$, coming from the accretion of planetesimals that have been destroyed inside the envelope before reaching the core*. The total mass of heavy elements inside the atmosphere is then compatible with the one derived by Guillot *et al.* (2004), whereas the mass of the core seems slightly too high. We obtain a core mass of $\sim 6 M_{\oplus}$, whereas the maximum core mass compatible with Guillot *et al.*

* One should also take into account some heavy elements accreted with the gas, but their abundance in the gas after planetesimals formation is highly reduced and therefore this contribution remains small.

(2004), for our total mass of heavy elements, is of the order of $\sim 5 M_{\oplus}$. However, this mass depends on the assumed physical properties of the planetesimals. For example, considering some reduced tensile strength (for example due to voids or failures in planetesimals) would reduce this value. Moreover, the mass of the core may be reduced further if it dissolves to some extend during the evolution of the planet (Guillot *et al.*, 2004).

Finally, we note again that the total mass of heavy elements depends on the ratio of planetesimal ejection versus accretion rate which can become quite large at late time.

4.2. Volatile Enrichments in the Atmosphere of Jupiter

In order to interpret the volatile enrichments measured in Jupiter by Atreya *et al.* (1999) and Mahaffy *et al.* (2000), Owen *et al.* (1999) proposed that the heavy elements in Jupiter were acquired from the delivery of planetesimals formed from amorphous ices. Hence, they suggested that either Jupiter was formed beyond 30 AU before migrating to its actual position, or that the solar nebula was substantially cooler at 5 AU than described by popular models, or that the heavy elements were delivered by planetesimals originating from distant regions. On the other hand, Gautier *et al.* (2001a; b) and Hersant *et al.* (2004) taking into account the *in situ* scenario of Pollack *et al.* (1996), proposed that volatiles were trapped as clathrate hydrates or hydrates in planetesimals located in the feeding zone of the giant planet. In order to model the corresponding enrichments of Jupiter's envelope, they assumed that most of solids were collected by the giant planet during the hydrodynamical collapse phase, at the end of the formation process, which is not strictly speaking consistent with Pollack *et al.* (1996).

In this subsection, we calculate the theoretical enrichments of Ar, Kr, Xe, C, N, and S in our Jupiter-like planet computed in section 3.4 and compare these values to those observed for Jupiter. For this, we assume that volatiles rich planetesimals were formed from ices crystalized in the solar nebula. These planetesimals are continuously accreted during the planet migration, as calculated by our code.

Figure 6 describes the mass evolution of proto-Jupiter as a function of the distance to the Sun, for the model of Section 3.4. It can be seen that planetesimals start to accumulate onto proto-Jupiter as soon as migration begins. Accretion lasts until the planet reaches 5 AU. Volatiles are assumed to have been trapped in these planetesimals under the forms of hydrates, clathrate hydrates or pure ices during the initial cooling phase of the solar nebula, which is not modeled yet in our disk calculations. This phase is assumed to occur before the formation of the $0.6 M_{\oplus}$ embryo.

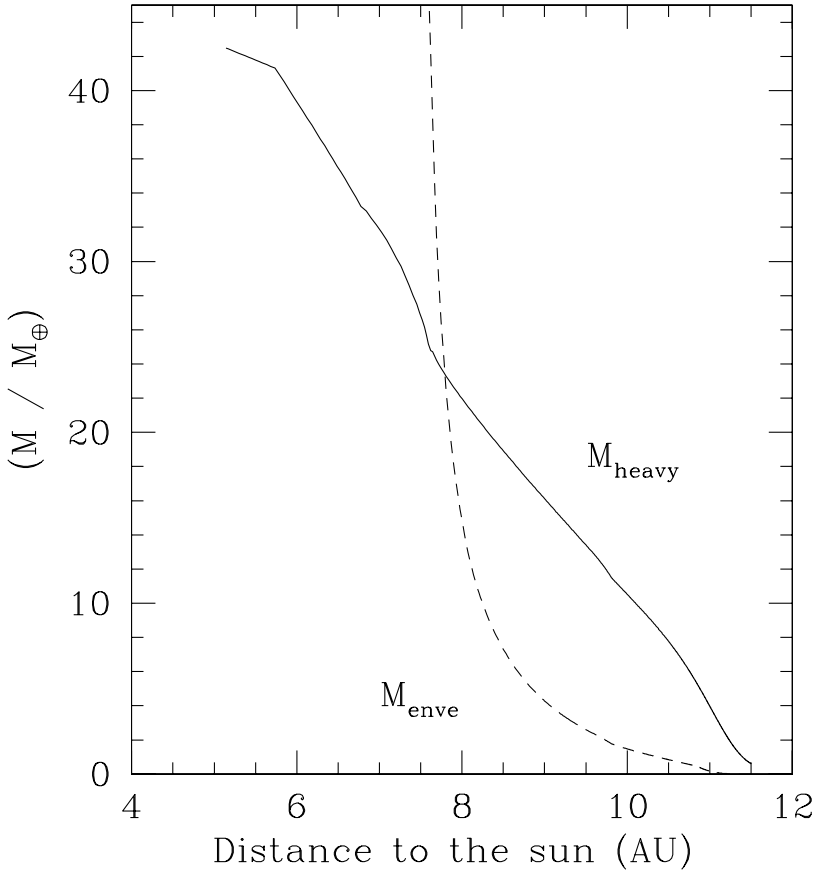

Figure 6. Mass of accreted material onto proto-Jupiter as a function of the distance to the Sun. M_{heavy} and M_{enve} represent respectively the mass of accreted planetesimals and the mass of accreted gas.

4.2.1. *Composition of Planetesimals Accreted During the Formation of Proto-Jupiter*

Current scenarios of formation of the solar nebula consider that ices and gases present in the presolar cloud fell onto the disk during the collapse of the cloud, and that most of ices vaporized in the nebula within 30 AU (Chick and Cassen, 1997). This hypothesis is in agreement with the work of Mousis *et al.* (2002) who have shown that CO/CH_4 and N_2/NH_3 ratios in vapor phase in the solar nebula remain quasi identical to the interstellar values. According to Alibert *et al.* (2004b), we assume that C is present in vapor phase in the subnebula, in three species, namely CO_2, CO and CH_4. The adopted abundances ratio is here equal to 20/10/1. Regarding nitrogen, we assume that it is present in the form of N_2 and NH_3, the ratio N_2/NH_3 being a free parameter (see Alibert *et al.*, 2004b, for a discussion).

We assume that the amount of available water along the migration pathway of proto-Jupiter is at least high enough to allow the trapping of the volatile species

TABLE I

Calculations of the ratios of trapped masses of volatiles to the mass of H_2O ice in planetesimals formed at 5 and 20 AU in the solar nebula. Gas phase abundance of H_2O is given in text and gas phase abundance of volatiles are assumed to be solar (Anders and Grevesse, 1989) with $CO_2/CO/CH_4$ = 20/10/1 and with N_2/NH_3 = 1 or 10 in vapor phase in the solar nebula.

	5 AU	20 AU
	$N_2/NH_3 = 1$ / $N_2/NH_3 = 10$	$N_2/NH_3 = 1$ / $N_2/NH_3 = 10$
CO_2/H_2O	7.12×10^{-1} / 6.90×10^{-1}	6.90×10^{-1} / 6.67×10^{-1}
CO/H_2O	1.53×10^{-1} / 1.48×10^{-1}	1.54×10^{-1} / 1.49×10^{-1}
CH_4/H_2O	1.02×10^{-2} / 9.91×10^{-3}	9.97×10^{-3} / 9.64×10^{-3}
N_2/H_2O	4.78×10^{-2} / 6.66×10^{-2}	4.83×10^{-2} / 6.67×10^{-2}
NH_3/H_2O	4.78×10^{-2} / 6.35×10^{-3}	4.50×10^{-2} / 6.22×10^{-3}
H_2S/H_2O	4.30×10^{-2} / 4.17×10^{-2}	4.23×10^{-2} / 4.09×10^{-2}
Ar/H_2O	4.29×10^{-3} / 4.16×10^{-3}	4.45×10^{-3} / 4.30×10^{-3}
Kr/H_2O	2.29×10^{-6} / 2.22×10^{-6}	2.33×10^{-6} / 2.26×10^{-6}
Xe/H_2O	3.13×10^{-7} / 3.03×10^{-7}	3.12×10^{-7} / 3.02×10^{-7}

considered under the form of hydrates or clathrate hydrates. Assuming N_2/NH_3 = 1 in the gas phase of the solar nebula and solar abundances (Anders and Grevesse, 1989), the minimum required abundance of water at 5 and 20 AU is 1.85 and 1.95 times the solar water abundance ($H_2O/H_2 \sim 5.54 \times 10^{-4}$ in the nebula, with $CO_2/CO/CH_4$ = 20/10/1 in the gas phase), respectively. If N_2/NH_3 = 10 in vapor phase in the solar nebula, the corresponding values are 1.91 and 2.02 at 5 and 20 AU, respectively.

Table I gives the values of the different volatiles to H_2O mass ratios in planetesimals for N_2/NH_3 = 1 and 10 in the gas phase and for the corresponding minimum abundances of water at 5 and 20 AU in the solar nebula. Since these ratios remain practically identical whatever the distance to the Sun between 5 and 20 AU for given abundances of species, one can assume that icy planetesimals that took part in the formation of proto-Jupiter during its migration shared the same composition in volatiles than those formed at 5 AU. The results presented in this section will then not depend on the starting point of the embryo that will form Jupiter, provided it starts its formation process below 20 AU.

4.2.2. *The Enrichment in Volatiles in Jupiter's Envelope*

Knowing the amount of planetesimals accreted, as well as their composition, we can calculate the abundance of C, N, Ar, Xe and S in the atmosphere of our final planet.

TABLE II

Comparison of the observed enrichments in volatiles in Jupiter with values calculated from different masses of ices (water and volatiles) vaporized in the envelope of proto-Jupiter ($M_{\rm ices}$).

Species	Observed	$M_{\rm ices}/M_\oplus = 32$ [c]	$M_{\rm ices}/M_\oplus = 27.6$ [d]
Ar	2.5 ± 0.5 [a]	2.32	2.00
Kr	2.7 ± 0.5 [b]	2.55	2.20
Xe	2.5 ± 0.7 [b]	3.31	2.86
C	2.9 ± 0.5 [b]	3.68	3.18
N	3.6 ± 0.8 [b]	2.80	2.84
S	2.5 ± 0.15 [b]	2.65	2.65

[a] Mahaffy *et al.* (2000), [b] Atreya *et al.* (1999)
[c] mass of ices required to fit the observed enrichments with $N_2/NH_3 = 10$ in vapor phase in the solar nebula
[d] mass of ices required to fit the observed enrichments with $N_2/NH_3 = 1$ in vapor phase in the solar nebula

TABLE III

Calculated masses of water, volatiles (excluding water), total ices, rocks and total mass of heavy elements (M_Z) trapped in the envelope of Jupiter and constraint from Guillot *et al.* (2004). Masses are calculated for $I/R = 4$ and different values of N_2/NH_3 in vapor phase in the solar nebula.

	I/R = 4		Guillot *et al.* (2004)
N_2/NH_3	10	1	
$M_{\rm water}/M_\oplus$	16	13.5	
$M_{\rm volatiles}/M_\oplus$	16	14.1	
$M_{\rm ices}/M_\oplus$	32	27.6	
$M_{\rm rocks}/M_\oplus$	8	6.9	
$M_Z/M_\oplus$	40	34.5	≤ 42

We first adopt $N_2/NH_3 = 10$ in vapor phase. Using the results of our model, we have tried to reproduce the observed abundances of volatiles (see Table II). While the total mass of heavy elements required in the envelope of Jupiter ($40 M_\oplus$ assuming a planetesimal ices/rocks (I/R) ratio equal to 4, see Table III) is almost compatible with our model and is below the upper limit defined by Guillot *et al.* (2004), we cannot fit the measured enrichment in carbon. Moreover, we obtain a

slightly higher value than the upper limit for Xe and an excess of abundance for S. This excess of abundance for S results from the fact that this element was assumed to be exclusively in the form of H_2S in the solar nebula. Since it has been shown that some H_2S may have been consumed in the corrosion of Fe alloy grains at high temperature ranges in the solar nebula to form troilite FeS (Fegley, 2000), one can argue that the abundance of H_2S was subsolar in vapor phase in the solar nebula prior to its incorporation in icy planetesimals. Under this assumption, the abundance of H_2S has been revised down to fit the measured upper value (0.62 times the solar abundance for $N_2/NH_3 = 10$ in vapor phase).

Adopting now $N_2/NH_3 = 1$ in vapor phase in the solar nebula, the minimum mass of ices required to fit the enrichments in volatiles is 27.6 $M_\oplus$, including $13.5M_\oplus$ of water and $14.1M_\oplus$ of volatiles. This corresponds to $34.5M_\oplus$ of heavy elements in the envelope of Jupiter with I/R = 4. This value is compatible with the ones derived from Guillot *et al.* (2004) but is slightly lower than what we obtained in our simulation ($\sim 36M_\oplus$). However, given the uncertainties on the final value of heavy elements, the difference between the two values is probably not significant.

Finally, adopting, as in Hersant *et al.* (2004), $CO_2/CO/CH_4 = 0/10/1$ and $N_2/NH_3 = 10$ in the gas phase of the solar nebula, we can also fit the observed enrichments. However, in that case, at least $37.6M_\oplus$ of water and $10M_\oplus$ of volatiles are required in the envelope of Jupiter. Hence, whatever the adopted I/R ratio, the value of heavy elements required ($> 47.6M_\oplus$) always exceeds the highest mass of heavy elements (42 $M_\oplus$) allowed by the internal structure models of Jupiter by Guillot *et al.* (2004).

5. Summary and Discussion

Our calculations show that the formation of giant planets, can be sped-up if one takes into account the effect of migration. This is mainly due to the suppression of phase 2 described in Pollack *et al.* (1996). We then obtain formation timescales that are compatible with the observed lifetime of protoplanetary disks, without having to consider disks significantly more massive than the minimum mass solar nebula. This effect of course, does not preclude other effects such as reduction of opacity (Hubickyj *et al.*, 2003), formation of vortices prior to planet formation (Klahr and Bodenheimer, 2003) or fragmentation of planetesimals (Inaba *et al.*, 2003) to further reduce this timescale.

Using this model, we are able to model the formation of a Jupiter-like planet, with final properties in good agreement with the ones of Jupiter (core mass, mass of heavy elements, mass of gas, and distance to the sun). We note however that the final mass of heavy elements accreted is a function of the ratio of ejection to accretion rate. A change in this ratio woul modify the accretion rate of solids towards the end of the formation process but not during the early phases. More work is needed to quantify this effect.

The model presented here starts with an embryo located at some arbitrary distance from the star. The precise location depends on the actual type I migration rate, and may be between ∼10 to ∼15 AU for the rates considered here. However one can wonder how likely it is to find embryos at such large distances (Thommes *et al.*, 2003). On the other hand, simulations by Weidenschilling *et al.* (2004) show that an embryo can be ejected from inner regions in a relatively short timescale (of the order or less than 1 Myr).

In our simulation forming Jupiter, at the time the planet reaches the current orbit of Saturn, its mass is $\sim 30 M_{\oplus}$ so that perturbations on other objects (such as the Kuiper Belt Objects) will remain small. A planet formed from an embryo initially located much further away (with an increased type I migration rate) might perturb the exterior part of the solar system, and not be consistent with the existence of a cold Kuiper Belt. More calculations are needed to adress this point, which might set an upper limit on the total migration of the planet. Similarly, the effect of migrating giant planets on the terrestrial planet formation, especially in the case of giant planets crossing this region, remains an important issue.

In the framework of our current model, we can reproduce the results on Jupiter derived by Guillot *et al.* (2004), regarding the mass of the core and the total mass of heavy elements accreted. Moreover, assuming ices/rocks ratio of accreted planetesimals equal to 4, and that CO_2 was present in vapor phase in the outer solar nebula, with $CO_2/CO \sim 2$, a value consistent with ISM measurements (Gibb *et al.*, 2004), we can explain the enrichments in volatiles observed by the *Galileo* probe, while being compatible with Guillot *et al.* (2004).

Finally, it appears very difficult to form a planet, and to prevent it from spiraling into the sun if the amount of type I migration as computed today is not reduced by a factor of at least 10. Our results then strongly suggest that there might still be a serious problem in our understanding of this type of migration.

Acknowledgements

This work was supported in part by the Swiss National Science Foundation. O.M. was supported by an ESA external fellowship, and this support is gratefully acknowledged.

References

Alibert, Y., Mordasini, C., and Benz, W.: 2004a, 'Migration and giant planet formation', *Astron. Astrophys.* **417**, L25–L28.

Alibert, Y., Mousis, O., and Benz, W.: 2004b, 'Volatiles enrichments in Jupiter', in preparation.

Allamandola, L.J., Bernstein, M.P., Sandford, S.A., and Walker, R.L.: 1999, 'Evolution of interstellar ices', *Space Sci. Rev.* **90**, 219–232.

Anders, E., and Grevesse, N.: 1989, 'Abundances of the elements – meteoritic and solar', *Geochim. Cosmochim. Acta* **53**, 197–214.

Atreya, S.K., Wong, M.H., Owen, T.C., Mahaffy, P.R., Niemann, H.B., de Pater, I., Drossart, P., and Encrenaz, T.: 1999, 'A comparison of the atmospheres of Jupiter and Saturn: Deep atmospheric composition, cloud structure, vertical mixing, and origin', *Planet. Space Sci.* **47** 1243–1262.

Bell, K.R. and Lin, D.N.C.: 1994, 'Using FU Orionis outbursts to constrain self-regulated protostellar disk models', *Astrophys. J.* **427**, 987–1004.

Bodenheimer, P. and Pollack, J.B.: 1986, 'Calculations of the accretion and evolution of giant planets: The effects of solid cores', *Icarus* **67**, 391–408.

Boss, A.P.: 2002, 'Evolution of the solar nebula: V. Disk instabilities with varied thermodynamics', *Astrophys. J.* **576**, 462–472.

Boss, A.P.: 2004, 'Rapid formation of outer giant planets by disk instability', *Astrophys. J.* **599**, 577–581.

Chabrier, G., Saumon, D., Hubbard, W.B., and Lunine, J.I.: 1992, 'The molecular-metallic transition of hydrogen and the structure of Jupiter and Saturn', *Astrophys. J.* **391**, 817–826.

Chick, K.M. and Cassen, P.: 1997, 'Thermal processing of interstellar dust grains in the primitive solar environment', *Astrophys. J.* **447**, 398–409.

Fegley, B., Jr.: 2000, 'Kinetics of gas-grain reaction in the solar nebula', *Space Sci. Rev.* **92**, 177–200.

Gautier, D., Hersant, F., Mousis, O., and Lunine J.I.: 2001a, 'Enrichments in volatiles in Jupiter: A new interpretation of the *Galileo* measurements', *Astrophys. J.* **550**, L227–L230.

Gautier, D., Hersant, F., Mousis, O., and Lunine J.I.: 2001b, 'Erratum: Enrichments in volatiles in Jupiter: A new interpretation of the *Galileo* measurements', *Astrophys. J.* **559**, L183–L183.

Gibb, E.L., Whittet, D.C.B., Boogert, A.C.A., and Tielens, A.G.G.M.: 2004, 'Interstellar ice: The infrared space observatory legacy', *Astrophys. J. Supp.* **151**, 35–73.

Greenzweig, Y. and Lissauer, J.J.: 1992, 'Accretion rates of protoplanets. II - Gaussian distributions of planetesimal velocities', *Icarus* **100**, 440–463.

Guillot, T. and Gladman, B.: 2000, 'Delivery of planetesimals and Giant planet formation', in F. Garzón, C. Eiroa, D. de Winter, and T.J. Mahoney (eds.), *Disks, Planetesimals, and Planets*, ASP Conf. Proc. **219**, 475.

Guillot, T., Stevenson, D.J., Hubbard, W.B., and Saumon, D.: 2004, 'The interior of Jupiter', in F. Bagenal, T.E. Dowling, and W.B. McKinnon (eds.), *Jupiter*, in press.

Haisch, K.E., Lada, E.A., and Lada, C.J.: 2001, 'Disk frequencies and lifetimes in young clusters', *Astrophys. J.* **553**, L153–L156.

Henderson, C.B.: 1976, 'Drag coefficient of spheres in continuum and rarefied flows', *AIAA Journal* **14**, 707–707.

Hersant, F., Gautier, D., and Huré, J.M.: 2001, 'A 2-D model for the primordial nebula constrained by D/H measurements in the solar system: implications for the formation of giant planets', *Astrophys. J.* **554**, 391–407.

Hersant, F., Gautier, D., and Lunine J.I.: 2004, 'Enrichment in volatiles in the giant planets of the solar system', *Planet. Space Sci.* **52**, 623–641.

Hills, J.G. and Goda, M.P.: 1993, 'The fragmentation of small asteroids in the atmosphere', *Astron. J.* **105**, 1114–1144.

Horner, J., Alibert, Y., and Benz, W.: 2004, in preparation.

Hubickyj, O., Bodenheimer, P., and Lissauer, J.: 2003, 'Small Core for Jupiter using the Core Instability Model', *Proc.35th DPS meeting*, 25.06.

Inaba, S., Wetherill, G.W., and Ikoma, M.: 2003, 'Formation of gas Giant planets: Core accretion models with fragmentation and planetary envelope', *Icarus* **166**, 46–62.

Ida, S. and Lin, D.N.C.: 2004, 'Toward a deterministic model of planetary formation. I. A desert in the mass and semimajor axis distributions of extrasolar planets', *Astrophys. J.* **604**, 388–413.

Klahr, H. and Bodenheimer, P.: 2003, 'A three phase model for planet formation – the formation of a planet in the eye of a hurricane', in M. Fridlund and T. Henning (eds.), *Earths: DARWIN/TPF and the Search for Extrasolar Terrestrial Planets*, **ESA SP-539**, 481–483.

Lin, D.N.C. and Papaloizou, J.: 1985, 'On the dynamical origin of the solar system', in D.C. Black and M.S. Matthews (eds.), *Protostars and planets II*, Tucson, AZ, University of Arizona Press, 981–1072.

Lin, D.N.C. and Papaloizou, J.: 1986, 'On the tidal interaction between protoplanets and the protoplanetary disk. III - Orbital migration of protoplanets', *Astrophys. J.* **309** 846–857.

Lin, D.N.C., Bodenheimer, P., and Richardson, D.C.: 1996, 'Orbital migration of the planetary companion of 51 Pegasi to its present location', *Nature* **380** 606–607.

Lunine, J.I. and Stevenson, D.J.: 1985, 'Thermodynamics of clathrate hydrate at low and high pressures with application to the outer solar system', *Astrophys. J. Supp.* **58**, 493–531.

Mahaffy, P.R., Niemann, H.B., Alpert, A., Atreya, S.K., Demick, J., Donahue, T.M., Harpold, D.N., and Owen, T.C.: 2000, 'Noble gas abundance and isotope ratios in the atmosphere of Jupiter from the Galileo Probe Mass Spectrometer', *J. Geophys. Res.* **105**, 15,061–15,072.

MacLow, M.M. and Zahnle, K.J.: 1994, 'Explosion of comet Shoemaker-Levy 9 on entry into the Jovian atmosphere', *Astrophys. J.* **434**, L33–L36.

Menou, K. and Goodman, J.: 2003, 'Low-mass proto-planet migration in T-Tauri α-disks', *Astrophys. J.* **606**, 520–531.

Mousis, O., Gautier, D., and Bockelée-Morvan, D.: 2002, 'An evolutionary turbulent model of Saturn's subnebula: Implications for the origin of the atmosphere of Titan', *Icarus* **156**, 162–175.

Mousis, O. and Gautier, D.: 2004, 'Constraints on the presence of volatiles in Ganymede and Callisto from an evolutionary turbulent model of the Jovian subnebula', *Planet. Space Sci.* **52**, 361–370.

Nelson, R.P. and Papaloizou, J.C.B.: 2003, 'The interaction of planets with a disc with MHD turbulence IV: Migration rates of embedded protoplanets', *Mon. Not. Roy. Astron. Soc.* **350**, 849–864.

Owen, T.C., Mahaffy, P.R., Niemann, H.B., Atreya, S.K., Donahue, T.M., Bar-Num, A., and de Pater, I.: 1999, 'A low temperature origin for the planetesimals that formed Jupiter', *Nature* **402**, 269–270.

Papaloizou, J.C.B. and Terquem, C.: 1999, 'Critical protoplanetary core masses in protoplanetary disks and the formation of short-period Giant planets', *Astrophys. J.* **521**, 823–838.

Pollack, J.B., Hubickyj, O., Bodenheimer, P., Lissauer, J.J., Podolak, M., and Greenzweig, Y.: 1996, 'Formation of the giant planets by concurrent accretion of solids and gas', *Icarus* **124**, 62–85.

Tanaka, H., Takeuchi, T. and Ward, W.R.: 2002, 'Three-dimensional interaction between a planet and an isothermal gaseous disk. I. Corotation and Lindblad torques and planet migration', *Astrophys. J.* **565**, 1257–1274.

Thommes, E.W., Duncan, M.J., and Levison, H.F.: 2003, 'Oligarchic growth of giant planets', *Icarus* **161**, 431–455.

Trilling, D.E., Benz, W., Guillot, T., Lunine, J.I., Hubbard, W.B., and Burrows, A.: 1998, 'Orbital evolution and migration of Giant planets: Modeling extrasolar planets', *Astrophys. J.* **500**, 428–439.

Veras, D. and Armitage, P.J.: 2003, 'Outward migration of extrasolar planets to large orbital radii', *Mon. Not. Roy. Astron. Soc.* **347**, 613–624.

Ward, W.R.: 1997, 'Survival of planetary systems', *Astrophys. J.* **482** L211–L217.

Weidenschilling, S.J., Marzari, F., and Davis, D.R.: 2004, 'Accretion of the Outer planets: Oligarchy or monarchy?', *Lunar Planet. Inst. Conf. Abstr.* **35**, 1174.

Zahnle, K.J.: 1992, 'Airburst origin of dark shadows on Venus', *J. Geophys. Res.* **97**, 10243–10255.

Address for Offprints: Yann Alibert, Physikalisches Institut, Hallerstrasse 6, CH-3012 Bern, Switzerland; yann.alibert@phim.unibe.ch

II. NEUTRAL ATMOSPHERES OF THE GIANT PLANETS AND THEIR SATELLITES

NEUTRAL ATMOSPHERES OF THE GIANT PLANETS: AN OVERVIEW OF COMPOSITION MEASUREMENTS

THÉRÈSE ENCRENAZ
LESIA, Observatoire de Paris, 92195 Meudon, France

Received: 17 May 2004; Accepted in final form: 1 September 2004

Abstract. Measurements of the chemical composition of the giant planets provide clues of their formation and evolution processes. According to the currently accepted nucleation model, giant planets formed from the initial accretion of an icy core and the capture of the protosolar gas, mosly composed of hydrogen and helium. In the case of Jupiter and Saturn (the gaseous giants), this gaseous component dominates the composition of the planet, while for Uranus and Neptune (the icy giants) it is only a small fraction of the total mass. The measurement of elemental and isotopic ratios in the giant planets provides key diagnostics of this model, as it implies an enrichment in heavy elements (as well as deuterium) with respect to the cosmic composition.

Neutral atmospheric constituents in the giant planets have three possible sources: (1) internal (from the bulk composition of the planet), (2) photochemical (from the photolysis of methane) and (3) external (from meteoritic impacts, of local or interplanetary origin). This paper reviews our present knowledge about the atmospheric composition in the giant planets, and their elemental and istopic composition. Measurements concerning key parameters, like C/H, D/H or rare gases in Jupiter, are analysed in detail. The conclusion addresses open questions and observations to be performed in the future.

Keywords: neutral atmospheres, giant planets, composition measurements

1. Formation of the Giant Planets

A few decades ago, it was generally accepted that giant planets formed through gravitational instability, from the collapse of a fragment of the protosolar nebula. This model was challenged in the early 1980 by the so-called "nucleation model". According to this scenario (Mizuno, 1980; Pollack *et al.*, 1996), giant planets accreted from an initial core of heavy elements in the form of icy planetesimals. When the cores reach a mass of $10-15$ terrestrial masses ($M_\oplus$), the surrounding gaseous nebula is captured by gravitational collapse. It is possible to discriminate between the two models by measuring their abundances ratios. In the first case (gravitational collapse), the chemical composition of the giant planets should directly reflect the protosolar composition, assumed to follow the cosmic abundances. In contrast, in the case of the nucleation model, an increase in heavy elements is expected in the giant planets.

Assuming cosmic abundances (i.e. 2% in mass for the heavy elements present in the protosolar gas), it is possible to estimate, for the giant planets, the expected enrichment in heavy elements with respect to hydrogen, as compared to the cosmic

Space Science Reviews 116: 99–119, 2005.
DOI: 10.1007/s11214-005-1950-6

TABLE I

Abundances in the tropospheres of the giant planets

Planet	Total Mass ($M_\oplus$)	Mass of heavy elements in the protosolar gas	Total mass of heavy elements	Expected enrichment	Measured enrichment
Jupiter	318	6	18	3	3 (GPMS)
Saturn	95	2	14	7	6 ± 2 (CH_4)
Uranus	15	0.06	12.06	40	$20-50$ (CH_4)
Neptune	17	0.1	12.1	36	$20-50$ (CH_4)

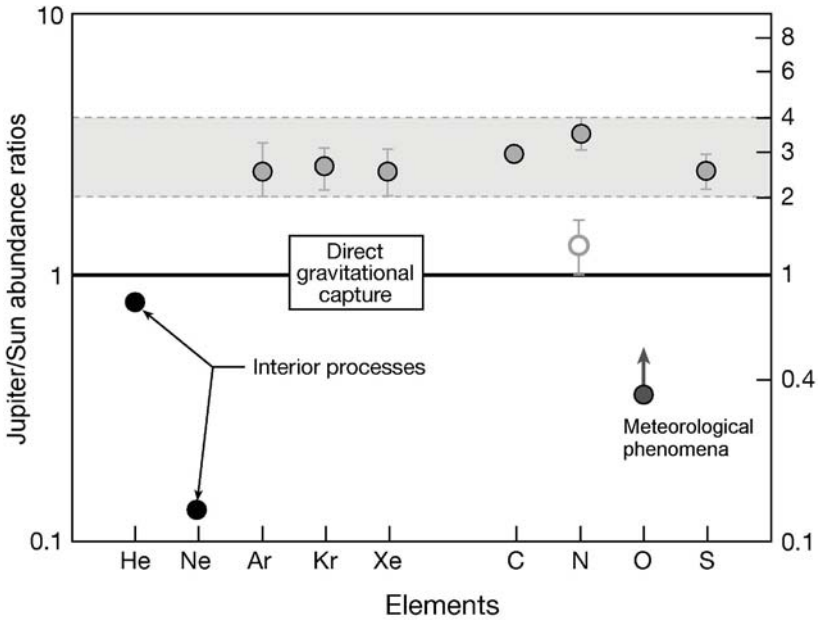

Figure 1. Elemental abundances in Jupiter, relative to hydrogen, with respect to the solar value. Apart from He, Ne and O (which are most likely depleted by internal or dynamical processes), all the elements exhibit enrichments by a factor about 3. The figure is taken from Owen *et al.* (1999).

abundances. Two assumptions are made: (1) all heavy elements are equally trapped in ices (which is a debatable question, as will be discussed below); (2) following the infall of the protosolar gas and the subsequent heating of the protoplanets, all elements are uniformely mixed in the interiors. Table I gives the expected enrichments in heavy elements under these assumptions, compared with the observational data. In the case of Jupiter, several abundance ratios have been measured in situ by the Galileo probe and they globally favor a factor 3 enrichment (Owen *et al.*, 1999; Figure 1); however, this result still raises open questions, as some species like

nitrogen and argon require very low temperatures ($T < 30$ K) to be trapped in ices; such a temperature appears much lower than the expected formation temperature of Jupiter (Owen *et al.*, 1999). For the other giant planets, C/H, measured from CH_4, is the only observable parameter. In spite of the large error bars, the measurements indicate a C/H enrichment which is consistent with the predictions (Gautier and Owen, 1989; Baines *et al.*, 1995; Lellouch *et al.*, 2001).

Another diagnostic of the nucleation model can be inferred from the D/H measurement. This ratio is known to be enriched in ices through ion-molecule and molecule-molecule reactions which favor the formation of deuterated ices at low temperatures (Irvine and Knacke, 1989). In the case of the giant planets, deuterium is mostly in the form of HD and CH_3D. As will be discussed below, the D/H ratio in the giant planets, inferred from both HD/H_2 and CH_3D/CH_4, shows a significant enrichment which also supports the nucleation model.

2. Methods for Measuring Chemical Compositions

Planetary spectra are characterized by two components: a solar component corresponding to the reflected part of the solar flux ($\lambda < 4 - 5\mu$m), and a thermal component ($\lambda > 4 - 5\mu$m) corresponding to the absorbed solar flux, re-emitted at longer wavelengths (with in addition, in the case of giant planets, the possible contribution of an internal flux). The solar contribution shows its maximum at about 0.5μm, and the maximum of the thermal contribution ranges from 30μm (in the case of Jupiter) to 70μm (in the case of Neptune). Emission fluorescence can also be observed in the UV (especially in the Ly α line of hydrogen at 1216 Å), the visible or the near-IR range (in particular CH_4 in the giant planets at 3.3μm).

In the case of the reflected sunlight component, planetary atmospheric signatures are observed in absorption in front of the solar spectrum. CH_4 is predominent in the case of the giant planets (Figure 2). Information is retrieved upon the column density of the atmospheric constituent, and shows, to first order, little dependence upon the atmospheric pressure and temperature. These measurements have been used to determine the column densities of NH_3 in Jupiter and CH_4 in the four giant planets. The penetration level, between the CH_4 absorption bands, can reach the troposphere down to about 1-3 bars. This method has allowed, in particular, the determination of the C/H ratio in all giant planets (Gautier and Owen, 1989; Baines *et al.*, 1995). In the 2.7μm window, the reflected radiation probes the NH_3 cloud level in Jupiter and Saturn, and presumably the H_2S cloud level in the case of Uranus and Neptune (Encrenaz *et al.*, 2000).

In the case of the thermal component, the outgoing flux strongly depends upon the thermal profile of the atmosphere. Giant planets are characterized by a temperature inversion at the tropopause level (0.1 bar) where the temperature ranges from 110 K (Jupiter) down to 50 K (Uranus and Neptune). Molecular species seen below this level, in the troposphere, are observed as absorption features while

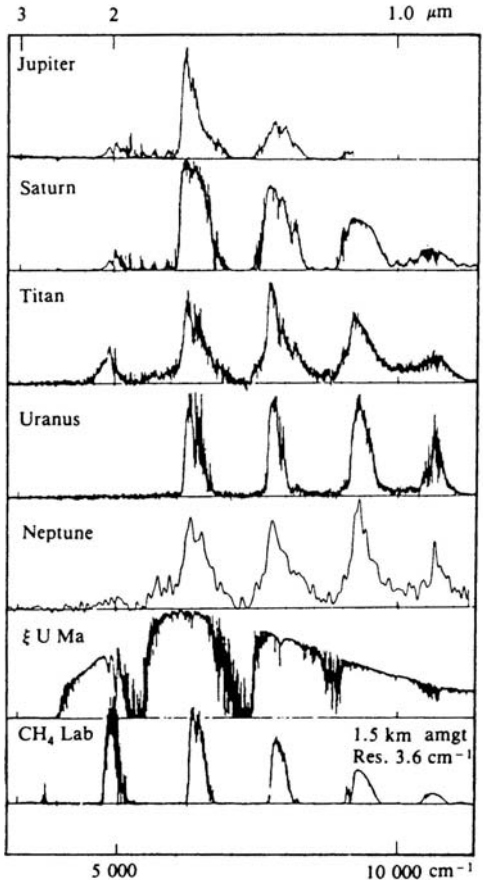

Figure 2. Near-infrared spectra of the giant planets and Titan. A stellar spectrum (ξ U Ma) is shown to identify terrestrial absorptions. Comparison with a laboratory spectrum of CH_4 shows that all spectra are dominated by methane absorptions. The figure is taken from Larson (1980).

stratospheric species, above the tropopause, are seen as emission features (Figure 3; see Encrenaz, 2000, for a review).

The thermal component has been used to identify most of the minor species of the giant planets, and to determine their mixing ratios. Data have come from ground-based and millimeter high-resolution spectroscopy, as well as from space data. Planetary spacecraft have been used (IRIS/Voyager on the giant planets and Titan, NIMS/Galileo on Jupiter, VIMS and CIRS on Cassini on Jupiter, Saturn and Titan) but also Earth-orbiting satellites, in particular the Infrared Space Observatory (ISO) and the HST.

In the case of Jupiter, in-situ mass spectrometry measurements have provided a major contribution about the composition of the neutral atmosphere of the Jovian atmosphere, thanks to the Galileo probe which entered the planet on December 7, 1995.

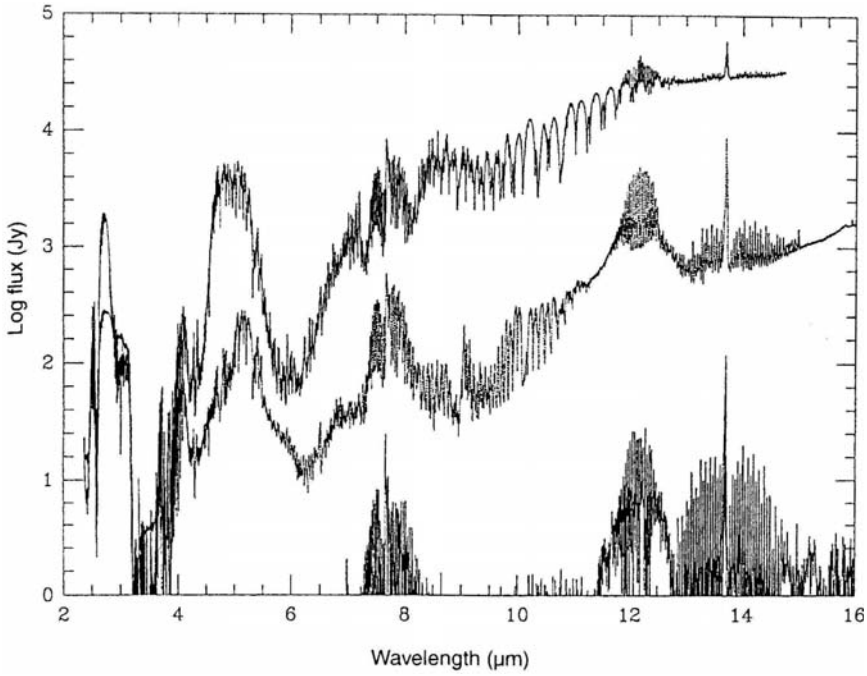

Figure 3. The infrared spectra of Jupiter, Saturn and Neptune observed by the SWS spectrometer of the ISO satellite. The reflected solar flux dominates below 4μm, while thermal emission is observed at higher wavelengths. Molecular features appear there in emission, if formed in the stratospheres (CH_4 at 7.7μm, C_2H_6 at 12μm, C_2H_2 at 13.7μm) or in absorption, if formed in the troposphere (NH_3 at 10μm in Jupiter, PH_3 at $8-9\mu$m in Saturn). The flux of Uranus and Neptune is less than 1 Jy below 7μm. Uranus (not shown in the figure) is detected only in the C_2H_2 emission band at 13.7μm, with a flux equal to one third of that of Neptune. Ground-based imaging spectroscopy can be performed in the L (3.5μm), M (4.8μm) and N (10μm) bands, with resolving powers as high as 10^5. The figure is taken from Encrenaz (1999).

3. Tropospheric Composition of the Giant Planets

Under thermochemical equilibrium, carbon and nitrogen are expected to be mostly in the form of CH_4 and NH_3 respectively in the conditions of high pressure and low temperature which were likely to prevail in the subnebulae of the giant protoplanets (Prinn and Fegley, 1989). In the tropospheres of the giant planets, we thus expect to find minor species in reduced form. The list of observed tropospheric species (Table II), besides H_2 and He, includes both equilibrium species (CH_4, NH_3, H_2O, H_2S, ...) and disequilibrium species (PH_3, GeH_4, AsH_3); the latter are considered as tracers of upward dynamical motions. In the stratospheres, two kinds of species are found: hydrocarbons coming from the methane photodissociation, and oxygenated species coming from an external source of oxygen. Two other species, CO (detected in all giant planets, possibly of internal and external origin) and HCN

TABLE II

Expected enrichment in heavy elements in the giant planets, according to the nucleation model, assuming an initial core mass of $12M_{\oplus}$ (updated from Encrenaz *et al.*, 2004a).

Species	Jupiter	Saturn	Uranus	Neptune
H_2	1	1	1	1
HD	1.8×10^{-5}	2.3×10^{-5}	5.5×10^{-5}	6.5×10^{-5}
He	0.157	0.10-0.16	0.18	0.23
CH_4	2.1×10^{-3}	4.4×10^{-3}	2×10^{-2}	4×10^{-2}
$^{13}CH_4$	2×10^{-5}	4×10^{-5}		
CH_3D	2.5×10^{-7}			
NH_3	2×10^{-4}	3.2×10^{-7}	10^{-5}	2×10^{-5}
$^{15}NH_3$	4×10^{-7}			
PH_3	6×10^{-7}	1.7×10^{-6}		
GeH_4	7×10^{-10}	2×10^{-9}		
AsH_3	3×10^{-10}	2×10^{-9}		
CO	1.5×10^{-9}	2×10^{-9}		10^{-6}
H_2O	1.4×10^{-5}	2×10^{-7}		

(detected in Neptune's stratosphere), are discussed separately. Finally a single ion, H_3^+, has been detected in all giant planets except Neptune.

3.1. The He/H ratio; Ne/H and the Noble Gases in Jupiter

In the absence of any evolutionary process, we would expect the He/H ratio in the giant planets to be representative of its value in the protosolar nebula ($Y = 0.275 \pm 0.01$, with Y being the helium mass fraction). Measurements, however, led to a different result. The He/H ratio in the giant planets has been inferred from Voyager data, using both the radio-occultation experiment and the IRIS far-infrared spectra (which are sensitive to the helium content). First results (Gautier and Owen, 1989) indicated a significant depletion of helium in the case of Jupiter ($Y = 0.18 \pm 0.04$) and a much stronger one in the case of Saturn ($Y = 0.06$). The Jupiter value was refined with the Galileo probe measurement (Von Zahn *et al.*, 1998) which inferred $Y = 0.234 \pm 0.005$. This discrepancy between the Voyager and Galileo results led to a reanalysis of the helium estimate on Saturn ($Y = 0.18 - 0.25$; Conrath and Gautier, 2000), significantly closer to the Jupiter value.

These new results still suggest a depletion of helium in Jupiter and Saturn. The current interpretation (after Stevenson, 1982) is that helium does condense in the form of droplets in the ocean of metallic hydrogen which is expected in the interiors of Jupiter and Saturn. This process develops with time over the history of

the planets, as the interiors cool down. As the droplets fall down toward the center, the helium concentration of the outer layers is depleted accordingly. In the case of Jupiter, the same mechanism is invoked to explain the depletion of Ne with respect to hydrogen measured by the mass spectrometer of the Galileo probe (Owen *et al.*, 1999; Figure 1).

In the case of Uranus and Neptune, the helium differentiation is not expected to take place, because the internal pressure is not high enough for hydrogen to be in metallic form. According to current models of planets' interiors, condensation of helium in molecular hydrogen is not expected. As a result, the value of He/H in Uranus and Neptune should be representative of the protosolar He/H value. Present estimates, derived from Voyager, are not in conflict with it, but the error bars are still very large ($Y = 0.262 \pm 0.048$ for Uranus, $Y = 0.32 \pm 0.05$ for Neptune; Conrath *et al.*, 1987; 1991).

Deriving more accurate estimates of the He/H ratio in the giant planets is thus a major objective for the future. In the case of Saturn, we can expect a more accurate measurement from the coupling of radio-occultation data and far-infrared spectra obtained by CIRS aboard the Cassini specacraft. In the case of Uranus and Neptune, the large error bars of the present estimates are partly due to the low signal-to-noise ratio of the IRIS-Voyager data in the far infrared range. We can thus expect improved He/H measurements with the spectra of the far-infrared observatories which are or will be in Earth orbit, Spitzer and later Herschel. Ultimately, an accurate measurement of helium in the four giant planets will require an in-situ measurement with a descent probe. As illustrated by the Galileo probe, such a device will also provide us with the abundance ratios of Ne and the other noble gases, which are key parameters for constraining the formation processes of the planetesimals which formed the icy cores of the giant planets (Owen *et al.*, 1999).

3.2. Tropospheric Equilibrium Species: CH_4, NH_3, H_2O, H_2S

With the exception of methane in Jupiter and Saturn, these species condense in the tropospheres of the giant planets. In order to determine abundance ratios, measurements have to be performed below the clouds, assuming that the gases are homogeneously mixed at these levels. For Jupiter and Saturn, the cloud structure expected from thermochemical models includes NH_3 at about 0.5-1 bar, NH_4SH at 2-4 bars and H_2O at 3-10 bars (Atreya and Romani, 1985; Atreya and Wong, 2004). The reality, however, is more complex, as illustrated by the results of the Galileo probe which entered a dried hot spot in Jupiter's troposphere. In the case of Uranus and Neptune, a CH_4 cloud is expected at about 1 bar, and possibly an H_2S cloud at 2-5 bars, and mixtures of NH_3, NH_4SH, H_2O and H_2S ices at deeper layers, down to several tens of bars (de Pater *et al.*, 1991; Atreya and Wong, 2004).

In the case of Jupiter, the mass spectrometer of the Galileo probe was able to measure the densities of minor species down to a pressure level of about 20 bars and thus to retrieve reliable abundance ratios. As mentioned above, most of the el-

ements (C, N, S, Ar, Kr, Xe) were found to be enriched versus hydrogen by a factor 3 with respect to cosmic abundances (Owen *et al.*, 1999; Figure 1). Three elements were depleted: He, Ne and O. For He and Ne, as mentioned above, this depletion was attributed to interior processes (condensation in the liquid metallic phase of hydrogen), while the oxygen depletion was assumed to be of meteorological origin (see below). If these interpretations are correct, one can conclude that there is a global enrichement of heavy elements in Jupiter by a factor 3, which implies that Jupiter was apparently made of solar composition icy particles (SCIPs). A major open question is to understand at which temperature these planetesimals formed, and how they could be incorporated in Jupiter, since, according to laboratory measurements, trapping these elements in ices (or in clathrates) requires temperatures as low as about 30 K (Owen *et al.*, 1999). There is no satisfying answer to this question presently.

In the case of the other giant planets, the C/H ratio was derived from both the reflected solar component (C/H in Uranus and Neptune; Baines *et al.*, 1995) and the thermal component (C/H in Saturn, from Voyager and ISO observations of the 7.7μm band; Gautier and Owen, 1989; Lellouch *et al.*, 2001). We have seen (Table I) that the measured enrichment appears consistent with the predictions of the nucleation model of giant planets' formation.

The O/H ratio was determined in the tropospheres of both Jupiter and Saturn using IR spectroscopy at 5μm, from ground-based and Voyager data in the case of Jupiter (Larson *et al.*, 1975; Kunde *et al.*, 1982; Bjoraker *et al.*, 1986; Drossart and Encrenaz, 1982) and from the ISO satellite in the case of Saturn (de Graauw *et al.*, 1997). A significant depletion of the O/H ratio was inferred; this result was confirmed, in the case of Jupiter, by the in-situ measurement of the Galileo probe which inferred a O/H value of 0.4 times the solar ratio at its deepest level ($P = 21$ bars). This result has been interpreted (Atreya *et al.*, 1997; Atreya and Wong, 2004) as the signature of strong downward motions inside the hot spots, devoid of clouds, which are observed at 5μm (the thermal emission coming from hotter levels, dominates the observed outgoing flux as seen from Earth). The in-situ measurement of the Galileo probe, which entered such a hot spot, may thus not be representative of the whole planet, which is probably subject to intense meteorological effects. In the case of Saturn, ISO also found evidence for a strong depletion. We note however that the hot spots on Saturn are not as localized nor as contrasted as in Jupiter, and that the global meteorology is probably different. In the future, one will try to determine the H_2O content outside the hot spots, to obtain a more global measurement; this could be achieved by other probes sent in Jupiter's and Saturn's atmospheres, or by studying their radioemission, as will be discussed below.

Measuring the N/H ratio below the clouds is very difficult in the case of Saturn, and even more for Uranus and Neptune. Indirect estimates, derived from the NH_3 continuum and not from line identification, have been obtained from ground-based radio measurements (de Pater and Massie, 1985).

How to improve the determination of these abundance ratios in the future? We need to probe deep tropospheric layers, below the cloud levels. In the case of Jupiter and Saturn, this requires probing pressures levels of several bars down to about 10 bars. A possible way is to explore the radio emission range of the giant planets, in the millimeter-centimeter range, where the thermal radiation comes from the deep tropospheric layers, down to several bars (de Pater, 1999). At higher wavelengths, this method is no more usable because of non-thermal effects: in the case of Jupiter, synchrotron radiation becomes to be important below about 30 GHz ($\lambda > 1$ cm). Measuring the thermal radiation of the giant planet, in particular from an orbiting spacecraft, could provide valuable constraints on the abundances of H_2O, NH_3 and H_2S which all have continuous absorptions contributing to the shape of the observed spectrum. This determination, however, might be model-dependent, as the line profiles are poorly determined in this spectral range (Encrenaz and Moreno, 2002). In the case of Uranus and Neptune, it is probably impossible to probe below the clouds from remote sensing, as, according to thermochemical models (Atreya and Wong, 2004), these clouds probably extend down to several tens of bars and possibly more. As a conclusion, the only way to measure abundance ratios in Uranus and Neptune will be to send probes in their atmosphere with mass spectrometry in-situ experiments, which will at least measure carbon and noble gas abundances.

3.3. Isotopic Ratios: D/H, $^{12}C/^{13}C$, $^{14}N/^{15}N$

The determination of isotopic ratios can provide important constraints upon formation processes of the giant planets, because these ratios should not have encountered any alteration during their histories. Of special interest are D/H, measured in the four giant planets, and $^{14}N/^{15}N$, measured in Jupiter. In addition, the $^{12}C/^{13}C$ ratio has been determined in both Jupiter and Saturn, in agreement with the terrestrial value.

3.3.1. *D/H*

Deuterium in the Universe was entirely formed by primordial nucleosynthesis, and, since then, is continuously destroyed in stars, where it is converted into ^3He. The value of D/H in the protosolar nebula ($D/H = 2.5 \times 10^{-5}$, as measured from solar wind measurements, see Geiss and Gloeckler, 1998) should thus reflect its value in the local interstellar medium, 4.6 Gy ago. As Jupiter and Saturn are mostly made of protosolar gas (Table I), their D/H values are expected to be representative of the protosolar value. In contrast, Uranus and Neptune are mostly made of ices, where D/H is expected to be enriched by ion-molecule and molecule-molecule reactions at low temperatures, as observed in the interstellar medium and in comets (Irvine and Knacke, 1989); a deuterium enrichment is thus expected.

Deuterium in the giant planets has been measured from two species, HD and CH_3D. HD rotational lines have been observed on the four giant planets by the

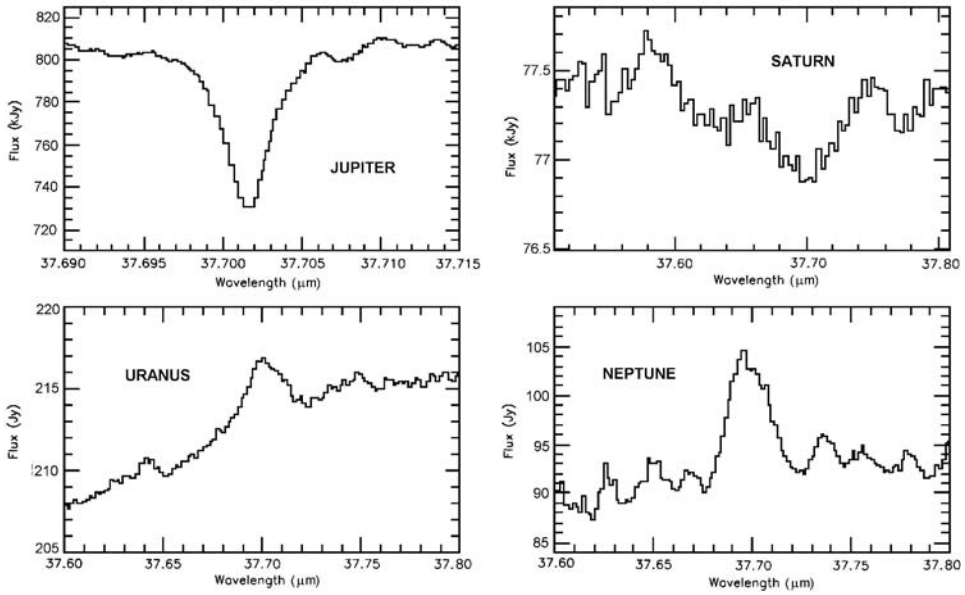

Figure 4. Detection of the HD R(2) rotational line in the four giant planets with ISO-SWS. In the case of Jupiter, the high-resolution Fabry-Perot mode ($R = 30000$) was used because of saturation effects; the grating mode ($R = 1700$) was used for the 3 other planets. Note the the HD lines appear in absorption in Jupiter and Saturn and in emission in Uranus and Neptune, because the continuum level, constrained by H_2-H_2 and H_2-He collision-induced absorption, is formed at higher level when the temperature is colder. Hence the HD line is formed in the upper troposphere on Jupiter and Saturn, and in the lower stratosphere on Uranus and Neptune.

ISO satellite (Figure 4). CH_3D bands have been observed in the near-IR (reflected sunlight) range on all giant planets, and also in the thermal regime on Jupiter, Saturn and Neptune. In addition, D/H has been measured in Jupiter by the GPMS. All measurements have confirmed the expectations (Table III). Jupiter's and Saturn's values are close to the protosolar value, which is slightly higher than the D/H value measured in the local interstellar medium today. In Uranus and Neptune, D/H is close to 5×10^{-5} which corresponds to an enrichment by a factor of about 2 with respect to the protosolar value. In the future, it will be important to get a more accurate measurement of D/H in Saturn (as this measurement is presently quite uncertain), and in Uranus and Neptune. According to the models, D/H should be sightly higher in Saturn than in Jupiter, but there is no evidence of this effect presently, as the error bars are still too large. We can hope to improve this measurement with the Cassini/CIRS measurements. Refining the determination of D/H in Uranus and Neptune will also allow us to compare the deuterium enrichment in the icy giants and in comets, which might have the same composition of the proto-neptunian ices. The D/H ratio has been measured so far in 3 long-period comets, which all show an enrichment by a factor 3 with respect to the protosolar value. An important question in the future will be to determine whether D/H in the icy giants

TABLE III
D/H in solar-system objects and in the interstellar medium.

Object	D/H	Reference
Jupiter (Galileo)	$(2.6 \pm 0.7) \times 10^{-5}$	Mahaffy *et al.* (1998)
Jupiter (ISO, from HD)	$(2.4 \pm 0.4) \times 10^{-5}$	Lellouch *et al.* (2001)
Jupiter (ISO, from CH_3D)	$(2.2 \pm 0.7) \times 10^{-5}$	Lellouch *et al.* (2001)
Saturn (ISO, from HD)	$1.85^{+0.85}_{-0.6} \times 10^{-5}$	Lellouch *et al.* (2001)
Saturn (ISO, from CH_3D)	$1.50^{+1.45}_{-0.65} \times 10^{-5}$	Lellouch *et al.* (2001)
Uranus (ISO)	$5.5^{+3.5}_{-1.5} \times 10^{-5}$	Feuchtgruber *et al.* (1999)
Neptune (ISO)	$6.5^{+2.5}_{-1.5} \times 10^{-5}$	Feuchtgruber *et al.* (1999)
Comet Halley	$(3.16 \pm 0.34) \times 10^{-4}$	Eberhardt *et al.* (1995)
Comet Hyakutake	$(2.9 \pm 1.0) \times 10^{-4}$	Bockelée-Morvan *et al.* (1998)
Comet Hale-Bopp	$(3.3 \pm 0.8) \times 10^{-4}$	Meier *et al.* (1998)
Protoneptunian ices	$5 - 20 \times 10^{-4}$	Feuchtgruber *et al.* (1999)
Protosolar (from solar wind)	$(2.1 \pm 0.5) \times 10^{-5}$	Geiss and Gloeckler (1998)
LISM	$(1.5 \pm 0.1) \times 10^{-5}$	Linsky (1998)

is actually different from the cometary value, and also if D/H in the short-period comets has the same value as previously observed. These data will help us to better understand the possible connection between comets and the planetesimals which formed the outer giant planets.

3.3.2. $^{12}C/^{13}C$

The $^{12}C/^{13}C$ ratio in tropospheric methane has been measured on both Jupiter and Saturn, with results close to the terrestrial ratio (Fox *et al.*, 1972; Combes *et al.*, 1977). An increase in $^{13}CH_4$ was reported in the stratosphere of Jupiter from Voyager measurements at 7.7μm (Courtin *et al.*, 1984), but this result was not confirmed by ISO measurements (Lellouch *et al.*, 2001). An increase of $^{13}C^{12}CH_2$, with respect to the terrestrial value, was also reported from observations of an individual line in the stratosphere of Jupiter (Drossart *et al.*, 1985); this anomaly could be due to non-LTE effects. Current observations seem to indicate that the $^{12}C/^{13}C$ in the bulk of the giant planets (as measured from tropospheric methane) is terrestrial (Owen and Encrenaz, 2003).

3.3.3. $^{14}N/^{15}N$

An unexpected result came from the determination of $^{14}N/^{15}N$ in Jupiter, by two independent methods, IR spectroscopy from ISO (Fouchet *et al.*, 2000) and in-situ mass spectroscopy from the Galileo probe (Owen *et al.*, 2001). Both experiments found a depletion in ^{15}N by a factor of about 2, as compared to the terrestrial value. The current interpretation (Owen *et al.*, 2001) is that the Jovian value might

represent the protosolar value of this ratio, which would thus be different from the value on Earth. This would imply that nitrogen was trapped in Jupiter in the form of N_2, while nitrogen in the terrestrial planets came in the form of NH_3 or HCN. An important measurement in the future will be to determine $^{14}N/^{15}N$ from NH_3 in Saturn (possibly with the Cassini mission, ultimately with a descent probe), and also the nitrogen isotopic ratio in the Sun, where one would expect the jovian value instead of the terrestrial one. Note that we can also measure this ratio in Neptune, as well as Jupiter, from HCN. In the case of Jupiter, these results will be more representative of the infalling material. In the case of Neptune, the result may be diagnostic of the origin of HCN.

3.4. Disequilibrium Species: PH_3, GeH_4, AsH_3

Some molecules have been observed in the tropospheres of Jupiter and Saturn while thermochemical models predict they should not be present; these species are called disequilibrium species. Phosphine PH_3, in particular, has been extensively studied in both Jupiter and Saturn. According to predictions, PH_3 should not be observable as, for $T < 2000$ K, it should react with H_2O and form P_2O_5. Yet PH_3 has been observed on both planets, with a mixing ratio which strongly decreases with altitude in the upper troposphere, independently of saturation effects. The current interpretation is that PH_3 is a tracer of strong vertical upward motions. The abundance of phosphine in Jupiter, at a pressure of several bars, is about the solar value, while it is enriched by a factor 3 in the case of Saturn. The same circulation mechanism is probably responsible for the presence of GeH_4 and AsH_3 (which, according to thermochemical models, should be destroyed in presence of H_2O), both also observed in Jupiter and Saturn.

For future studies, PH_3 is an important molecule as it is observed in many spectral ranges from the near IR to the millimeter range, which allow to probe different altitude levels: lower troposphere (a few bars) at 3μm and 5μm, upper troposphere at 8μm, 10μm and in the far-infrared range. Monitoring PH_3 at different wavelengths at high spatial resolution on both Jupiter and Saturn could be a precious diagnostic of tropospheric dynamics. In the case of Saturn, we can hope to obtain this data set from the VIMS and CIRS instruments aboard the Cassini spacecraft. In the case of Uranus and Neptune, measuring tropospheric PH_3 might be diagnostic of their internal dynamics (see Section 5.3).

4. The Stratospheres of the Giant Planets

Table IV summarizes the stratospheric species detected in the atmospheres of the giant planets.

TABLE IV

Abundances in the stratospheres of the giant planets (updated from Encrenaz *et al.*, 2004a).

Species	Jupiter	Saturn	Uranus	Neptune
CH_4	2.1×10^{-3}	4.4×10^{-3}	$3 \times 10^{-5} - 10^{-4}$	7×10^{-4}
CH_3D				2.2×10^{-7}
C_2H_2		3.5×10^{-6} (0.1mb)	$2 - 4 \times 10^{-7}$	1.1×10^{-7}
		2.5×10^{-7} (mb)	(0.1 − 0.3 mb)	(0.1 mb)
$^{12}C^{13}CH_2$	*			
C_2H_6	4.0×10^{-6}		4.0×10^{-6}	1.3×10^{-6}
	(0.3 − 50 mb)	(< 10 mb)		(0.03 − 1.5 mb)
CH_3C_2H	*	6.0×10^{-10}		
		(< 10 mb)		
C_4H_2	*	9.0×10^{-11}		
C_2H_4	7×10^{-9}	*	*	*
C_3H_8	6×10^{-7}			
C_6H_6	2×10^{-9}	*		
CH_3		$0.2 - 1 \times 10^{-7}$	$2 - 9 \times 10^{-8}$	
		(0.3μb)		(0.2μb)
CO	1.5×10^{-9}	2×10^{-9}	3×10^{-8}	10^{-6}
CO_2	3×10^{-10}	3×10^{-10}		5×10^{-10}
	(< 10 mb)	(< 10 mb)		(< 5 mb)
H_2O	1.5×10^{-9}	$2 - 20 \times 10^{-9}$	$5 - 12 \times 10^{-9}$	$1.5 - 3.5 \times 10^{-9}$
	(< 10 mb)	(< 0.3 mb)	(< 0.03 mb)	(< 0.6 mb)
HCN				3×10^{-10}
H_3^+	*	*	*	*

*: detected

4.1. CH_4 PHOTODISSOCIATION PRODUCTS

Methane photochemistry takes place in the stratospheres of all giant planets. Major photodissociation products are C_2H_2 (observed in all giant planets) and C_2H_6 (in Jupiter, Saturn and Neptune). Minor products include C_2H_4 and CH_3 (in Jupiter, Saturn and Neptune), and CH_3C_2H, C_4H_2 and C_6H_6 (in Jupiter and Saturn). Many of these species were detected by the SWS spectrometer aboard the ISO satellite (de Graauw *et al.*, 1997; Schulz *et al.*, 1999; Bézard *et al.*, 1998; 1999); in addition, CH_3 and C_4H_2 were detected in Jupiter by the CIRS instrument during the Cassini flyby of Jupiter (December 2000; Simon-Miller *et al.*, 2003) and C_2H_4 was identified in both Jupiter and Saturn by high-resolution ground-based spectroscopy at 10.5μm (Bézard *et al.*, 2001a).

While the tropospheres of the giant planets look roughly similar, with a tropopause at 100 mbar in all cases, the stratospheres appear remarkably different in their

thermal structure and their dynamics. In particular, the eddy diffusion coefficient which characterizes the degree of turbulence in the stratosphere, is higher in Saturn and Neptune as in Jupiter, and is significantly lower in the case of Uranus. The reasons for such variations are still unclear. The low value of the eddy diffusion coefficient on Uranus could be at least partly responsible for the absence of detected photodissociation product, apart from C_2H_2 (Encrenaz *et al.*, 1998). In addition, the low temperature of the lower stratosphere makes the detection of minor species in this region more difficult.

4.2. The External Source of Oxygen

An unexpected discovery was the detection of H_2O and CO_2 emission lines observed by the Short Wavelength Spectrometer of the ISO satellite (Feuchtgruber *et al.*, 1997; 1999) on all giant planets (except CO_2 in Uranus). The emissions were found to originate in the upper stratospheres, with a mean H_2O mixing ratio of $10^{-9} - 10^{-8}$ in this region. The mean H_2O incoming flux was estimated using a transport model in which the incoming H_2O material is removed by vertical diffusive and eddy transport, without chemical loss. The derived H_2O incoming flux was about $10^5 - 10^7$ cm^{-2} s^{-1}, with the Uranus value being lower than the other ones (Feuchtgruber *et al.*, 1997). The mean CO_2 mixing ratio was (except for Uranus) $3 - 5 \times 10^{-10}$ above the 10-mbar level.

Because of the low temperature of the tropopause (below 110 K) which acts as a cold trap, H_2O can only be of external origin. CO_2 could also come from the exterior or result from chemical reactions in the stratosphere involving H_2O and CH_3. Two possible sources can be considered for the external source of oxygen: a local source involving rings and satellites, or an interplanetary flux of dust particles or micrometeoroids. In the case of Jupiter, the observed CO_2 and H_2O emissions appear to be at least partly a consequence of the SL9 collision in July 1994 (Lellouch *et al.*, 2002). In the case of Saturn, the rings provide an obvious possible source for external oxygen; the oxygen origin for Uranus and Neptune remains to be understood. We will learn about the water source from the Cassini mission in the case of Saturn (using the CIRS infrared spectrometer with high spatial resolution), and from the Herschel mission for all giant planets (using, in particular, the HIFI high-resolution heterodyne spectrometer).

4.3. Origins of CO and HCN

Another surprising result was, in 1992, the detection of large amounts of CO and HCN in the stratosphere of Neptune (Marten *et al.*, 1991; 1993; Rosenqvist *et al.*, 1992). The inferred CO mixing ratio (about 10^{-6}) was 10^3 times higher than the value expected from thermochemical equilibrium models (Fegley and Prinn, 1989), which had been measured in both Jupiter and Saturn. From a recent ground-based study of CO at high spectral resolution, Bézard *et al.* (2002) have concluded that CO in Jupiter (apart from the SL9 component) had to be of both external and

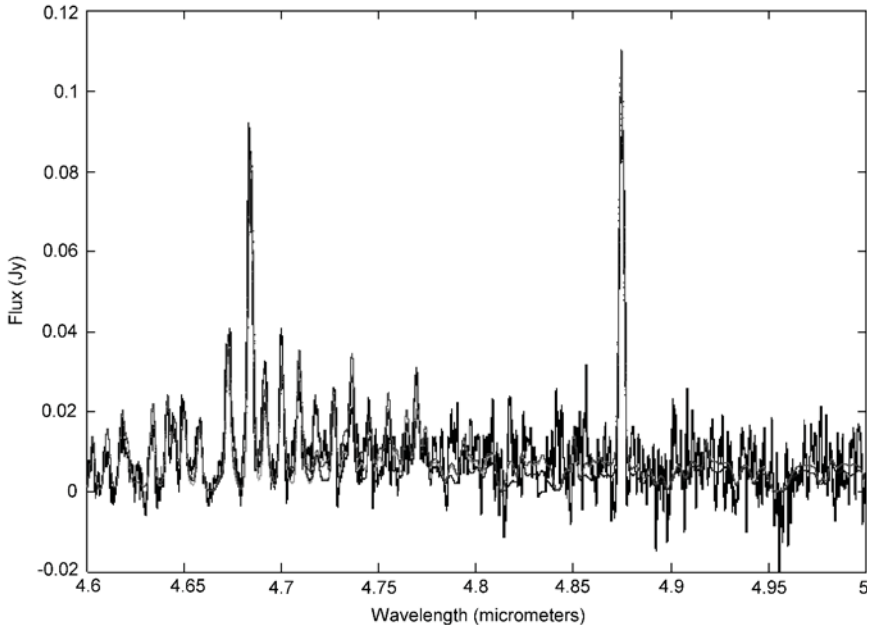

Figure 5. The spectrum of CO in the $5-\mu$m window, observed with the ISAAC infrared imaging spectrometer at the VLT. The emission features at $4.60-4.75\mu$m are due to CO fluorescence. A few H_3^+ emission lines also dominate the spectrum, in particular at 4.657 and 4.875μm. A weak continuum is detected over the spectral range; it is attributed to reflected sunlight above a cloud layer located at 3 bars. The absence of CO and PH_3 absorptions over this continuum provides upper limits of the abundances of these species in the lower troposphere of Uranus (after Encrenaz *et al.*, 2004b).

internal origin. In the case of Saturn, the origin of CO is still an open question. In Uranus, CO has been recently detected through infrared fluorescence at 5μm (Encrenaz *et al.*, 2004b; Figure 5), and seems to be at least partly of external origin, but here again, this conclusion is still uncertain. In the case of Neptune however, the abundance of CO is so high that it would be very difficult to explain it with an external source only. Most likely, CO comes from the interior of Neptune.

4.4. The External Source of Oxygen

An unexpected discovery was the detection of H_2O and CO_2 emission lines observed by the Short Wavelength Spectrometer of the ISO satellite (Feuchtgruber *et al.*, 1997; 1999) on all giant planets (except CO_2 in Uranus). The emissions were found to originate in the upper stratospheres, with a mean H_2O mixing ratio of $10^{-9}-10^{-8}$ in this region. The mean H_2O incoming flux was estimated using a transport model in which the incoming H_2O material is removed by vertical diffusive and eddy transport, without chemical loss. The derived H_2O incoming flux was about 10^5-10^7 cm^{-2} s^{-1}, with the Uranus value being lower than the

other ones (Feuchtgruber *et al.*, 1997). The mean CO_2 mixing ratio was (except for Uranus) $3 - 5 \times 10^{-10}$ above the 10-mbar level.

If this result is confirmed, it may have important implications about the formation scenario of the planet. Indeed, the high abundance of CO in Neptune is to be associated with the high abundance of stratospheric HCN. This molecule has not been detected in any other giant planet, except as a product of the SL9 collision in Jupiter. The presence of HCN in Neptune's stratosphere probably comes from the chemistry of CH_3 radicals with N atoms. These nitrogen atoms could have two possible sources: they could either be ejected from Triton (which is known to have a weak but stable atmosphere of N_2) or result from the dissociation of N_2 molecules coming from Neptune's interior. In the latter case, the implication might be that Neptune's planetesimals might have incorported CO and N_2 in higher abundances than in the other giant planets. This result, if confirmed, could bring important constraints on the physical conditions under which this planet was formed. A possible test would be the measurement of $^{14}N/^{15}N$ in HCN on Neptune, possibly with the ALMA interferometer. The remaining question would be to understand why Uranus was not formed in the same way. In order to resolve these uncertainties about the origin of CO in the giant planets, and the origin of HCN in Neptune, we would need to send probes in the atmospheres of Uranus and Neptune, in order to measure in-situ the vertical distributions of these minor species as a function of depth.

5. Conclusions, Open Questions and Future Observations

Remote sensing spectroscopy and, in the case of Jupiter, in-situ measurements, have allowed us to build a complete picture of the chemical composition of the giant planets. All existing measurements favor the nucleation model of the giant planets, which assumes that they accreted around initial icy cores. However, several open questions remain to be solved. The main following issues can be addressed.

5.1. At which Temperature did Jupiter's Planetesimals Form?

The GPMS measurements aboard Galileo have demonstrated that heavy elements in Jupiter (except for 3 exceptions, presumably due to local or internal processes) are globally enriched by a factor 3 with respect to hydrogen, as compared to the solar values (Owen *et al.*, 1999). This global enrichment fully supports the nucleation model of the giant planets, as first described by Mizuno (1980) and later fully studied by Pollack *et al.* (1996). This result brings the evidence that Jupiter formed from solar composition icy particles (SCIPs), as all elements appear to have been equally trapped in ices. This important result also raises an open question: at what temperature did these icy particles form? Laboratory experiments show that nitrogen and argon cannot be trapped at temperatures higher than about 30 K

(Owen *et al.*, 1999). Still, the temperature around Jupiter's orbit is supposed to have been significantly higher. It is unlikely that Jupiter could have formed in a very cold environment, as the density would not have been sufficient for the planet to accrete such a high mass. Alternatively, if the building blocks of Jupiter were formed at very low temperature, how did they migrate to reach Jupiter's orbit? These questions, presently unanswered, are among the major challenges of today's planetology.

5.2. Were all Giant Planets made of Solar-composition Interplanetary Particles?

There is now strong evidence that Jupiter formed from SCIPs. What about the other planets? Two abundance ratios, C/H and D/H, have been measured in the four giant planets and the results favor the nucleation model. More accurate measurements, however, will be needed to confirm this result; the Cassini mission should be of great help in the case of Saturn. There is little hope to have access to other abundance ratios in the deep tropospheres of Uranus and Neptune, where only descent probes will be able to measure abundance ratios, at least for carbon and rare gases.

5.3. Why are Uranus and Neptune so Different?

In spite of their common status of icy giants, the two planets show significant differences regarding their internal heat (with no internal source detected in the case of Uranus), their turbulence in the stratosphere (with the eddy diffusion coefficient at the homopause being about $10^3 - 10^4$ lower on Uranus than on Neptune), and their stratospheric composition (with CO and HCN being much more abundant in Neptune). Are these differences related to the internal structures, and thus reflect different formation processes, or are they the result of different evolution processes? Another possible source of difference is the peculiar position of Uranus' rotation axis, very close to the ecliptic pole. It has been suggested that convection in Uranus' interior might be inhibited, which would lead to the absence of ascending convective motions and the absence of species like CO or PH_3 in the upper troposphere. However the reason for this inhibition would remain to be explained.

The way to better understand this problem is a search for tropospheric CO and PH_3 in both Uranus and Neptune. CO is probably present in large abundances in Neptune's troposphere (Guilloteau *et al.*, 1994), while, in the case of Uranus, recent measurements of CO suggest that its origin is more likely external (Encrenaz *et al.*, 2004b). In the case of PH_3 we only have upper limits so far on both Uranus and Neptune, derived from the submillimeter range (Encrenaz *et al.*, 1996). Two spectral regions can be used for future observations: the submillimeter range using large bandwidths (with ground-based antennae, and later Herschel and Alma), or the 5-μm window using 8-m class telescopes.

5.4. Which are the Key Measurements for the Future?

In the case of Saturn, CIRS on Cassini will hopefully provide us with new measurements of abundance ratios: C/H (from CH_4), possibly N/H (from NH_3), D/H (from HD and CH_3D), and He/H. CIRS will also allow to study the H_2O stratospheric emission, its spatial distribution and its temporal variations.

The Herschel Earth-orbiting submillimeter observatory, to be launched in 2007, will be best suited for the study of stratospheric water in all giant planets. In particular the HIFI instrument, with its high resolving power, will allow to retrieve the mean vertical distribution of H_2O, and the PACS imaging spectrometer will be able to get some limited spatial resolution on Jupiter; these long-term observations will help answering the question of the water origin. Herschel should also provide us with key measurements on He/H and D/H in all giant planets, as well as a search for tropospheric and stratospheric minor species,

Ground-based high-resolution infrared spectroscopy has been a powerful tool for studying minor atmospheric species. Recent examples include hydrocarbons in the $10 - 13\mu$m range with TEXES at IRTF (with the detection of C_2H_4 in particular), CO in Jupiter (with the FTS at CFHT) and Uranus (with ISAAC at the VLT). In the future, high-resolution instruments like CRIRES at the VLT, with a resolving power of 10^5, will allow to push further the detectability limits. The access to the submillimeter range will also allow to search for minor atmospheric species like H_2S, H_2Se, HCl and other halides. With its high sensitivity and its high resolving power, Alma will be the best means for such a study, in particular for the study of CO and PH_3 in Uranus and Neptune. Alma could also bring information on isotopic abundances of CO (Jupiter and Neptune) and HCN (Neptune).

These observational means, however, will not give us the whole set of abundance ratios, including the noble gases, in the deep tropospheres of the giant planets, which are the key parameters for understanding the formation processes of these planets. What we need in all four giant planets is the equivalent of the GPMS measurements in Jupiter; in addition, the experience of the Galileo probe, entering an atypical region of Jupiter, illustrates that two probes at least should be sent in each planet, in order to separate possible effects due to local meteorology. In summary, the next step of the giant planets' space exploration appears to be a multiple probe mission carrying, in particular, mass spectrometry measurements. Such a set of measurement should bring a major input on the present unanswered questions about the early composition of the giant planets, and, beyond, about formation and evolution processes in the outer solar system.

References

Atreya, S.K. and Romani, P.N.: 1985, 'Photochemistry of the clouds of Jupiter, Saturn and Uranus', in G. Hunt (ed.), *Recent Advances in Planetary Meteorology*, Cambridge Univ. Press, pp. 17–68.

Atreya, S.K., Wong, M.H., Owen, T.C., Niemman, H.B., and Mahaffy P.R.: 1997, 'Chemistry and clouds of Jupiter's atmosphere: a Galileo perspective', in C. Barbieri, J. Rahe, T.V. Johnson, and A.M. Sohus (eds.), *The Three Galileos, The Man, the Spacecraft, the Telescope*, Kluwer Academic Publishers.

Atreya, S.K. and Wong, A.S.: 2004, 'Couples clouds and chemistry of the giant planets – A case for multiprobes', this volume.

Baines, K.H., Mickelson, M.E., Larson, Lee, E., and Ferguson, D.W.: 1995, 'The abundances of methane and ortho/para hydrogen on Uranus and Neptune: implications of new laboratory 4-0 H_2 quadrupole line parameters', *Icarus* **114**, 328–340.

Bézard, B., Feuchtgruber, H., Moses, J.I., and Encrenaz, T.: 1998, 'Detection of methyl radicals (CH_3) on Saturn', *Astron. Astrophys.* **334**, L41–L44.

Bézard, B., Romani, P.N., Feuchtgruber, H., Encrenaz, T.: 1999, 'Detection of the methyl radical on Neptune', *Astrophys. J.* **515**, 868–872.

Bézard, B., Moses, J.I., Lacy, J., Greathouse, T., Richter, M., Griffith, C.: 2001a, 'Detection of Ethylene (C_2H_4) on Jupiter and Saturn in Non–Auroral Regions', *Bull. Am. Astr. Soc.* **33** p. 1079.

Bézard, B., Drossart, P., Encrenaz, T., and Feuchtgruber, H.: 2001b, 'Benzene in the giant planets', *Icarus* **154**, 492–500.

Bézard, B., Lellouch, E., Strobel, D., Maillard, J.-P., and Drossart, P.: 2002, 'Carbon monoxide on Jupiter: evidence for both internal and external sources', *Icarus* **159**, 95–111.

Bjoraker, G.L., Larson, H.P., and Kunde, V.G.: 1986, 'The abundance and distribution of water vapor in Jupiter's atmosphere', *Astrophys. J.* **311**, 1058–1072.

Bockelée-Morvan, D., Gautier, D., Lis, D.C., Young, K., Keene, J., Phillips, T., Owen, T., Crovisier, J., Goldsmith, P.F., and Bergin, E.A.: 1998, 'Deuterated Water in Comet C/1996 B2 (Hyakutake) and Its Implications for the Origin of Comets', *Icarus* **133**, 147–162.

Combes, M., Maillard, J.-P., and de Bergh, C.: 1977, 'Evidence for a telluric value of the $^{12}C/^{13}C$ ratio in the atmospheres of Jupiter and Saturn', *Astron. Astrophys.* **61**, 531–537.

Conrath, B.J. and Gautier, D.: 2000, 'Saturn Helium Abundance: A Reanalysis of Voyager Measurements', *Icarus* **144**, 124–134.

Conrath, B.J., Gautier, D., Hanel, R.A., Lindal, G., and Marten, A.: 1987, 'The helium abundance in Uranus from Voyager infrared measurements', *J. Geophys. Res.* **92**, 15,003–15,010.

Conrath, B.J., Gautier, D., Lindal, G., Samuelson, R.E., and Shaffer, W.E.: 1991, 'The helium abundance of Neptune from Voyager measurements', *J. Geophys. Res.* **96**, 18,907–18,919.

Courtin, R., Gautier, D., Marten, A., Kunde, V.: 1984, 'The $^{12}C/^{13}C$ Ratio in Jupiter from the Voyager infrared investigation', *Icarus* **53**, 121–132.

de Graauw, T., *et al.*: 1997, 'First results of ISO-SWS observations of Saturn : detection of CO_2, CH_3CH_2, C_4H_2 and tropospheric H_2O', *Astron. Astrophys.* **321**, L13–L16.

de Pater, I.: 1999, 'The solar system at radio wavelengths', in P.R. Weissman, L.-A. McFadden, T.V. Johnson, *Encyclopedia of the solar system*, San Diego, Academic Press, pp. 735–772.

de Pater, I. and Massie, S.T.: 1985, 'Models of the millimeter-centimeter spectra of the giant planets', *Icarus* **62**, 143–171.

de Pater, I., Romani, P.N., and Atreya, S.K.: 1991, 'Possible microwave absorption by H_2S in Uranus' and Neptune's atmospheres', *Icarus* **91**, 220–233.

Drossart, P., and Encrenaz, Th.: 1982, 'The abundance of water vapor on Jupiter from the Voyager IRIS data at 5 microns', *Icarus* **52**, 483–491.

Drossart, P., Lacy, J., Serabyn, E., Tokunaga, A., Bézard, B., and Encrenaz, T.: 1985, 'Detection of $^{12}C^{13}CH_2$ on Jupiter at 13 microns', *Astron. Astrophys.* **149**, L10–L12.

Eberhardt, P., Reber, M., Krankowsky, D., Hodges, R.R.: 1995, 'The D/H and $^{18}O/^{16}O$ ratios in water from comet P/Halley', *Astron. Astrophys.* **302**, 301–304.

Encrenaz, T.: 1999, 'The planet Jupiter', *Astron. Astrophys. Rev.* **9**, 171–219.

Encrenaz, T.: 2000, 'ISO observations of solar-system objects', in F. Casoli, J. Lequeux, F. David (eds.), *Infrared Astronomy, today and tomorrow*, Springer-Verlag, Berlin, Paris, pp. 89–150.

Encrenaz, T. and Moreno, R.: 2002, 'The microwave spectra of planets', in M. de Petris and M. Gervasi (eds.), *Experimental Cosmology at Millimetre Wavelengths, 2K1BC Workshop*, Am. Inst. of Physics Conf. Proc. **616**, pp. 330–337.

Encrenaz, T., Serabyn E., and Weisstein, E.W.: 1996, 'Millimeter spectroscopy of Uranus and Neptune: Constraints on CO and PH_3 tropospheric abundances', *Icarus* **124**, 616–624.

Encrenaz, T., *et al.*: 1998, 'ISO observations of Uranus: the stratospheric distribution of C_2H_2 and the eddy diffusion coefficient', *Astron. Astrophys.* **333**, L43–L46.

Encrenaz, T., Schulz, B., Drossart, P., Lellouch, E., Feuchtgruber, H., and Atreya, S.K.: 2000, 'The ISO spectra of Uranus and Neptune between 2.5 and 4.2 μm: constraints on albedos and H_3^+', *Astron. Astrophys.* **358**, L83–L87.

Encrenaz, T., Bibring, J.-P., Blanc, M., Barucci, M.-A., Roques, F., and Zarka, P.: 2004a, *The solar system*, Third Edition, Springer-Verlag.

Encrenaz, T., Lellouch, E., Drossart, P., Feuchtgruber, H., Orton, G.S., and Atreya, S.K.: 2004b, 'First detection of CO in Uranus', *Astron. Astrophys.* **413**, L5–L9.

Fegley, B., Jr. and Prinn, R.G.: 1989, 'Solar nebula chemistry – Implications for volatiles in the solar system', in H.A. Weaver, L. Danly, and M. Fall (eds.): 1989, *The Formation and Evolution of Planetary Systems*, Cambridge Univ. Press, Cambridge and New York, USA, pp. 171–205.

Feuchtgruber, H., Lellouch, E., de Graauw, T., Bézard, B., and Encrenaz, T.: 1997, 'External supply of oxygen to the atmospheres of the giant planets', *Nature* **389**, 159–162.

Feuchtgruber, H., Lellouch, E., Bézard, B., Encrenaz, T., de Graauw, T., and Davis G.R.: 1999, 'Detection of HD in the atmospheres of Uranus and Neptune: a new determination of the D/H ratio', *Astron. Astrophys.* **341**, L17–L21, 1999.

Feuchtgruber, H., Lellouch, E., Encrenaz, T., Bézard, B., Coustenis, A., Drossart, P., Salama, A., de Graauw, T. and Davis, G.R.: 1999, 'Oxygen in the stratospheres of the giant planets and Titan', ESA SP-427, pp. 133–136.

Fouchet, T., Lellouch, E., Bézard, B., Encrenaz, T., Drossart, P., Feuchtgruber, H., de Graauw, T.: 2000, 'ISO-SWS observations of Jupiter: measurements of the ammonia tropospheric profile and of the $^{14}N/^{15}N$ ratio', *Icarus* **143**, 223–243.

Fox, K., Owen, T., Mantz, A.W., Rao, N.K.: 1972, 'A tentative identification of $^{13}CH_4$ and an Estimate of $^{12}C/^{13}C$ in the atmosphere of Jupiter', *Astrophys. J.* **176**, L81–L84.

Gautier, D. and Owen, T.: 1989, 'The composition of outer planet atmospheres', in S.K. Atreya, J.B. Pollack, and M.S. Shapley (eds.), *Origin and evolution of planetary and satellite atmospheres*, S.K. Atreya, J.B. Pollack, and M.S. Shapley (eds.), Univ. Arizona Press, Tucson, pp. 487–512.

Geiss, J. and Gloeckler, G.: 1998, 'Abundances of deuterium and helium-3 in the protosolar cloud', *Space Sci. Rev.* **84**, 239–250.

Guilloteau, S., Dutrey, A., Marten, A., and Gautier, D. : 1994, 'CO in the atmosphere of Neptune: detection of the J=1-0 line in absorption', *Astron. Astrophys.* **279**, 661–667.

Irvine, W. and Knacke, R.F.: 1989, 'The chemistry of interstellar gas and grains', in S.K. Atreya, J.B. Pollack, and M.S. Shapley (eds.), *Origin and evolution of planetary and satellite atmospheres*, Univ. Arizona Press, Tucson, pp. 3–34.

Kunde, V.G., Hanel, R.A., Maguire, W.C., Gautier, D., Baluteau, J.P., Marten, A., Chedin, A., Husson, N., and Scott, N.: 1982, 'The tropospheric gas composition of Jupiter's north equatorial belt (NH_3, PH_3, CH_3D, GeH_4, H_2O) and the jovian D/H isotopic ratio', *Astrophys. J.* **263**, 443–467.

Larson, H.P.: 1980, 'Infrared spectroscopic observations of the outer planets, their satellites, and the asteroids', *Ann. Rev. Astron. Astrophys.* **18**, 43–75.

Larson, H.P., Fink, U., Treffers, R., and Gautier, T.N.: 1975, 'Detection of water vapor on Jupiter', *Astrophys. J.* **197**, L137–L140.

Lellouch, E., Bézard, B., Fouchet, T., Feuchtgruber, H., Encrenaz, T., and de Graauw, T.: 2001, 'The deuterium abundance in Jupiter and Saturn from ISO-SWS observations', *Astron. Astrophys.* **370**, 610–622.

Lellouch, E., Bézard, B., Moses, J.I., Davis, G.R., Drossart, P., Feuchtgruber, H., Bergin, E.A., Moreno, R., and Encrenaz, T.: 2002, 'The origin of water vapor and carbon dioxide in Jupiter's stratosphere', *Icarus* **159**, 112–131.

Linsky, J.L.: 1998, 'Deuterium abundance in the Local Interstellar Medium and possible spatial variations', *Space Sci. Rev.* **84**, 285.

Mahaffy, P.R., Donahue, T.M., Atreya, S.K., Owen, T.C., and Niemann, H.B.: 1998, 'Galileo Probe Measurements of D/H and ^{3}He/^{4}He in Jupiter's Atmosphere', *Space Sci. Rev.* **84**, 251–263.

Marten, A., Gautier, D., Owen, T., Sanders, D., Tilanus, R.T., Deane, J., and Matthews, H.: 1991, B.G. Marsden (ed.), *Neptune*, IAUC 5331.

Marten, A., Gautier, D., Owen, T., Sanders, D.B., Matthews, H.E., Atreya, S.K., Tilanus, R.P.J., and Deane, J.R.: 1993, 'First observations of CO and HCN on Neptune and Uranus at millimeter wavelengths and their implications for atmospheric chemistry', *Astrophys. J.* **406**, 285–297.

Meier, R., Owen, T., Matthews, H.E., Jewitt, D.C., Bockelée-Morvan, D., Biver, N., Crovisier, J., Gautier, D.: 1998, 'A Determination of the HDO/H_2O Ratio in Comet C/1995 O1 (Hale-Bopp)', *Science* **279**, 842–844.

Mizuno, H.: 1980, 'Formation of the giant planets', *Progress of Theoretical Physics* **64**, 544–557.

Owen, T. and Encrenaz, T.: 2003, 'Element abundances and isotopic ratios in the giant planets and Titan', *Space Sci. Rev.* **106**, 121–138.

Owen, T., Mahaffy, P., Niemann, H.B., Atreya, S., Donahue, T., Bar-Nun, A., and de Pater, I.: 1999, 'A low-temperature origin of the planetesimals that formed Jupiter', *Nature* **402**, 269–270.

Owen, T., Mahaffy, P.R., Niemann, H.B., Atreya, S.K., and Wong, M.: 2001, 'Protosolar nitrogen', *Astrophys. J.* **553**, L77–L79.

Pollack, J.B., Hubickyj, O., Bodenheimer, P., Lissauer, J.J., Podolak, M., Greenzweig, Y.: 1996, 'Formation of the giant planets by concurrent accretion of solids and gas', *Icarus* **124**, 62–85.

Prinn, R.G. and Fegley, B.: 1989, 'Solar nebula chemistry: origin of planetary, satellite and cometary volatiles', in S.K. Atreya, J.B. Pollack, and M.S. Shapley (eds.), *Origin and evolution of planetary and satellite atmospheres*, Univ. Arizona Press, Tucson, pp. 78–136.

Rosenqvist, J., Lellouch, E., Romani, P., paubert, G., and Encrenaz, T.: 1992, 'Millimeter-wave observations of Saturn, Uranus and Neptune: CO and HCN on Neptune', *Astrophys. J.* **392**, L99–L102.

Schulz, B., Encrenaz, T., Bézard, B., Romani, P., Lellouch, E., and Atreya, S.K.: 1999, 'Detection of C_2H_4 in Neptune using ISO/PHT-S observations', *Astron. Astrophys.* **350**, L13–L17.

Simon-Miller, A.A., Flasar, F.M., Achterberg, R., Conrath, B., Gierasch, P.J., Kunde, V., Nixon, C.A., Jennings, D.E., Romani, P., Carlson, R., Cassini CIRS Team: 2003, 'Jupiter Observations by Cassini CIRS: Atmospheric Dynamics, Temperatures and Composition', *Bull. Amer. Astron. Soc.* **34**, 659–659.

Stevenson, D.J.: 1982, 'Interiors of the giant planets', *Ann. Rev. Earth Plan. Sci.* **30**, 755–764.

Von Zahn, U., Hunten, D.M., and Lehmacher, G.: 1998, 'Helium in Jupiter's atmosphere: Results from the Galileo probe helium interferometer experiment', *J. Geophys. Res.* **103**, 22,815–22,830.

Address for Offprints: Thérèse Encrenaz, Observatoire de Paris, 5, place Jules Janssen, F-92195 Meudon Cedex, France; `therese.encrenaz@obspm.fr`

COUPLED CLOUDS AND CHEMISTRY OF THE GIANT PLANETS — A CASE FOR MULTIPROBES

SUSHIL K. ATREYA and AH-SAN WONG
Department of Atmospheric, Oceanic, and Space Sciences, The University of Michigan, Ann Arbor, MI 48109-2143, USA

Received: 23 April 2004; Accepted in final form: 4 August 2004

Abstract. In seeking to understand the formation of the giant planets and the origin of their atmospheres, the heavy element abundance in well-mixed atmosphere is key. However, clouds come in the way. Thus, composition and condensation are intimately intertwined with the mystery of planetary formation and atmospheric origin. Clouds also provide important clues to dynamical processes in the atmosphere. In this chapter we discuss the thermochemical processes that determine the composition, structure, and characteristics of the Jovian clouds. We also discuss the significance of clouds in the big picture of the formation of giant planets and their atmospheres. We recommend multiprobes at all four giant planets in order to break new ground.

Keywords: Jupiter, giant planets; chemistry, clouds; chromophores, haze; multiprobes

> That the Planets are not without Water, is made not improbable by the late Observations: For about *Jupiter* are observ'd some spots of a darker hue than the rest of his Body, which by their continual change show themselves to be Clouds: For the spots of *Jupiter* which belong to him, and never remove from him, are quite different from these, being sometimes for a long time not to be seen for these Clouds; and again, when these disappear, showing themselves. ...
>
> Christianus Huygens, In *Kosmotheoros* 1698

1. Introduction

Ever since the invention of *occhiale* (telescope) by Galileo Galilei nearly four centuries ago, Jupiter's clouds have fascinated amateur astronomers and planetary scientists alike. With the availability of modern observing techniques, it has been possible to determine the morphology and characteristics of the upper visible clouds of Jupiter and Saturn. However, the cloud structure of the four giant planets is complex, extending deep into their atmospheres. Galileo Probe is the only entry probe ever deployed at a giant planet. But, the probe entered a meteorologically anomalous region — the Sahara Desert of Jupiter — one of the driest places on the planet. Hence, information on only the very tenuous clouds in the entry site could be gleaned from the Probe nephelometer measurements. These observations could not reveal anything about the cloud structure elsewhere on Jupiter. On the other hand, a good picture of the structure of Jovian clouds has begun to emerge by

Space Science Reviews 116: 121–136, 2005.
DOI: 10.1007/s11214-005-1951-5

combining existing data (nephelometer, mass spectrometer, and remote imaging) with thermochemical models. The model predictions are for a three-layer cloud structure at Jupiter and Saturn, and a 4–5 layer cloud structure in the atmospheres of the icy giants, Uranus and Neptune. We will first discuss the cloud formation model, then compare the results with existing observations. We will then discuss the significance of clouds in the models of formation of the giant planets and their atmospheres, and finally make recommendations for future work.

2. Thermochemical Cloud Model

The equilibrium cloud condensation models (ECCM) of Jupiter date back to the pre-Voyager epoch. The model was first developed by Weidenschilling and Lewis (1973), and has undergone further development as described in Atreya and Romani (1985) and Atreya (1986). The lifting condensation level (LCL), i.e. the base of the cloud, is calculated by comparing the partial pressure (e) and the saturation vapor pressure (e_c) of the condensible volatile. The LCL is reached at the altitude where relative humidity (e/e_c) of 100% is attained. The amount of condensate in the ECCM is determined by the temperature structure at the LCL and vicinity. The release of latent heat of condensation modifies the lapse rate, hence the temperature structure, of the atmosphere. Thus, the composition and structure of the clouds depend on the composition of the atmosphere, and in particular the distribution of condensible volatiles.

Thermochemical equilibrium considerations suggest that NH_3, H_2S and H_2O are the only species likely to condense in the atmospheres of Jupiter and Saturn, if the composition were solar. The presently known "elemental" abundance information for Jupiter, Saturn and the icy giants is given in Table I, and also illustrated for Jupiter in Figure 1. As shown in Table I, N (from NH_3) and S (from H_2S) are enriched relative to solar, but O (from H_2O) is subsolar even at the deepest level in the region of the Galileo Probe entry on Jupiter. O/H is expected to be enriched by a similar factor as the other heavy elements, i.e. 3 ± 1 (Owen *et al.*, 1999; Atreya *et al.*, 1999), since current ideas of the formation of Jupiter favor a core accretion model in which cold planetesimals are the original carriers of heavy elements (heavier than helium). If the heavy elements were delivered by clathrate hydrates, then the water abundance would be more than $9\times$ solar in Jupiter's well-mixed atmosphere (Gautier *et al.*, 2001a; b). In either case, condensation of water both as ice and droplets is inevitable.

For Saturn, tentative information on only one condensible species, NH_3, is available, indicating perhaps a greater enrichment factor compared to that at Jupiter (Table I). In fact, C/H also seems greater than at Jupiter. The progressively larger enrichment in the heavy elements from Jupiter to Neptune is consistent with the predictions of the core accretion model (although this fact is reflected also in Sat-

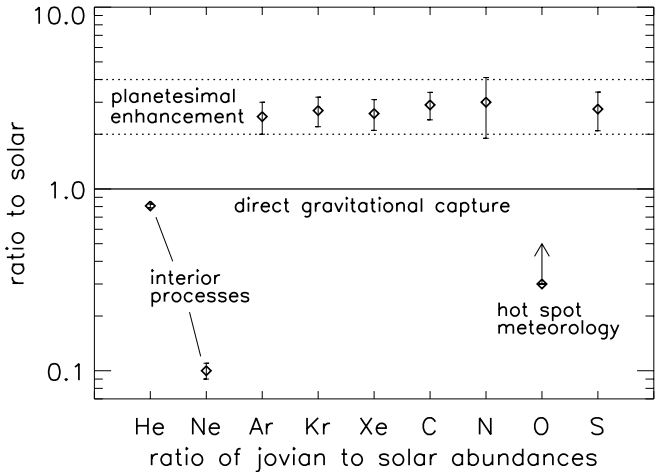

Figure 1. Elemental abundances (relative to H) in Jupiter's atmosphere compared to the solar values. The Jupiter results are those measured by the Galileo Probe Mass Spectrometer (GPMS). Solid horizontal line shows that direct gravitational capture would result in elemental abundances (ratioed to H), same as in the Sun. However, heavy elements, Ar, Kr, Xe, C, N, and S are all found to be enriched by a factor of 3 ± 1. Figure updated from Owen *et al.* (1999).

TABLE I

Elemental and relevant isotopic abundances

Elements	Sun	Jupiter/Sun	Saturn/Sun	Uranus/Sun	Neptune/Sun
He/H	0.0975	0.807 ± 0.02	0.56–0.85	0.92–1.0	0.92–1.0
Ne/H	1.23×10^{-4}	0.10 ± 0.01	?	20–30 (?)	30–50 (?)
Ar/H	3.62×10^{-6}	2.5 ± 0.5	?	20–30 (?)	30–50 (?)
Kr/H	1.61×10^{-9}	2.7 ± 0.5	?	20–30 (?)	30–50 (?)
Xe/H	1.68×10^{-10}	2.6 ± 0.5	?	20–30 (?)	30–50 (?)
C/H	3.62×10^{-4}	2.9 ± 0.5	4–6	20–30	30–50
N/H	1.12×10^{-4}	3.0 ± 1.1 hs	2–4 (?)	20–30 (?)	30–50 (?)
O/H	8.51×10^{-4}	0.29 ± 0.1 hs	?	20–30 (?)	30–50 (?)
S/H	1.62×10^{-5}	2.75 ± 0.66 hs	?	20–30 (?)	30–50 (?)
P/H	3.73×10^{-7}	0.82	5–10	20–30 (?)	30–50 (?)
Isotopes	Sun	Jupiter	Saturn	Uranus	Neptune
$^{15}N/^{14}N$	$< 2.8 \times 10^{-3}$	$2.3 \pm 0.3 \times 10^{-3}$			
D/H$\times 10^{-5}$	2.1 ± 0.5	2.6 ± 0.7	2.25 ± 0.35	$5.5^{+3.5}_{-1.5}$	$6.5^{+2.5}_{-1.5}$

After Atreya (2004). See also Atreya *et al.* (2003), Atreya *et al.* (1999) for references. O/H at Jupiter is from Wong *et al.* (2004a). The solar values are taken from Anders and Grevesse (1989) in order to maintain a standard reference. The heavy element ratios for Uranus and Neptune are taken to be the same as C/H from CH_4 measurements on these planets. Note: hs is 5-micron hotspot.

urn's (5–10)× solar P/H, being a disequilibrium species, phosphine is not a good indicator of the heavy element enhancement factor). Thus, for purposes of cloud structure modeling, it is reasonable to assume a factor of 5 enhancement over solar for all of Saturn's condensible species, ammonia, ammonium hydrosulfide, and water.

The lapse rate, cloud structure and bases, and the cloud density in the outer planet atmospheres can be derived using thermodynamic equilibrium principles. The lapse rate depends both on latent heat released upon condensation and the heat of formation if a gas phase chemical reaction results into a condensate. Whenever the partial pressure of a constituent exceeds its saturated vapor pressure, condensation occurs. This process releases latent heat of condensation, thereby changing the local lapse rate. An expression for the wet adiabatic lapse rate ($\mathrm{d}T/\mathrm{d}z$) can be derived using the principle of energy conservation for adiabatic expansion of a mole of gas.

Hydrogen sulfide does not condense by itself in the atmospheres of Jupiter and Saturn. In the gas phase, it can combine with ammonia to form ammonium hydrosulfide (NH_4SH), or ammonium sulfide ($[NH_4]_2S$) which is less likely, i.e.,

$$NH_3(g) + H_2S(g) = NH_4SH. \tag{1}$$

With the inclusion of this "chemical condensation", the energy conservation equation (from first principle of thermodynamics) is

$$\mathrm{d}Q = 0 = \bar{C}_P\,\mathrm{d}T - v\,\mathrm{d}P + \sum_k L_k\,\mathrm{d}X_k + L_{\mathrm{rx}}\,\mathrm{d}X_{\mathrm{H_2S}} \tag{2}$$

where $\bar{C_P}$ is mean molar heat capacity at constant pressure P, $\mathrm{d}T$ is differential change in temperature, v is molar volume of the gas, $\mathrm{d}X_k$ is the differential change in the number of moles of the k^{th} gas due to condensation, L_k is molar enthalpy of condensation (latent heat) of the k^{th} gas, and L_{rx} is the molar heat of reaction/formation for the Reaction (1).

Ammonium hydrosulfide (or ammonium sulfide, if formed) would condense as a solid in the environmental conditions of all giant planets. The "chemical" condensation of H_2S results in the heat of formation, similar to the latent heat of condensation. The equilibrium constant, K_P, for Reaction (1) is given by:

$$\log_{10} K_P = 14.82 - \frac{4705}{T} = \log_{10}(P_{\mathrm{NH_3}} P_{\mathrm{H_2S}}) \tag{3}$$

from International Critical Tables, where P_k is the partial pressure expressed in atmospheres and T is the temperature in K. Also,

$$P_{\mathrm{NH_3}} = P X_{\mathrm{NH_3}},\ P_{\mathrm{H_2S}} = P X_{\mathrm{H_2S}},\ \mathrm{d}X_{\mathrm{NH_3}} = \mathrm{d}X_{\mathrm{H_2S}} \tag{4}$$

since the rate of concentration change of all species is the same in a mixed atmosphere. Differentiating Equation (3) and employing Equations (4) gives

$$\frac{X_{H_2S} + X_{NH_3}}{X_{H_2S} X_{NH_3}} \, dX_{H_2S} = 10834 \frac{dT}{T^2} - 2\frac{dP}{P} \tag{5}$$

Using the standard gas law $Pv = RT$ (where R is gas constant per mole), $dP = -g\rho \, dz$ (where $\rho = \bar{m}/v$ is mass density, and $\bar{m}$ is mean molecular weight), mixing ratio definition $X_k = P_k/P$, and Clausius-Clapeyron equation $dP_k/dT = L_k/T\Delta v_k \sim L_k/Tv_k$, we obtain

$$dX_k = \frac{1}{P} dP_k - \frac{P_k}{P^2} dP = X_k \left(\frac{L_k \, dT}{RT^2} + \frac{g\bar{m}}{RT} dz \right). \tag{6}$$

Substituting Equations (5) and (6) into Equation (2), the following expression for the wet adiabatic lapse rate of the atmosphere is obtained,

$$\frac{dT}{dz} = -\frac{\bar{m}g}{\bar{C}_P} \left(\frac{1 + \frac{1}{RT} \left[\sum_k L_k X_k + \frac{2(X_{H_2S} X_{NH_3}) L_{rx}}{X_{H_2S} + X_{NH_3}} \right]}{1 + \frac{1}{\bar{C}_P T^2} \left[\sum_k \frac{L_k^2 X_k}{R} + \frac{10834 (X_{H_2S} X_{NH_3}) L_{rx}}{X_{H_2S} + X_{NH_3}} \right]} \right) \tag{7}$$

NH_3 could also dissolve in H_2O, resulting in an "aqueous solution cloud" in the atmosphere. If the concentration of the solution is C (due to NH_3 condensation), then for every mole of solution, $(1 - C)$ mole of H_2O is condensed out, i.e.,

$$dX_{solution} = \frac{dX_{H_2O}}{1 - C}. \tag{8}$$

In Equation (2), $L_k dX_k$ term should therefore reflect the heat due to condensation in solution, i.e.,

$$\frac{L_s \, dX_{H_2O}}{(1 - C)}, \tag{9}$$

where L_s is the average heat of condensation of the solution. This will affect the lapse rate in Equation (7) and subsequently the atmospheric temperature.

The average density of the condensate k between two closely spaced atmospheric levels I and J is given by

$$\bar{D} = \frac{m_k (X_k^I - X_k^J) \bar{P}}{\bar{m} g \, \Delta z} \tag{10}$$

where m_k is the mass fraction of the k^{th} condensate, Δz is the height interval between the two levels, and $\bar{P}$ is the mean atmospheric pressure.

3. Cloud Model Results and Observations

3.1. Clouds of Jupiter and Saturn

Based on the above considerations of equilibrium thermodynamics, it is possible to construct the ECCM for Jupiter and Saturn. Figure 2 shows results of ECCM calculations for Jupiter, with $1\times$ solar and $3\times$ solar condensible volatile abundances in the left panel, and greatly depleted condensible volatiles in the right panel in order to simulate the LCL of the clouds detected in the Galileo Probe Entry Site (PES). Since the Galileo Probe entered a dry region, the condensible volatiles were found to be greatly depleted to levels well below their expected condensation levels. It has been proposed that the depletion is caused by a giant downdraft extending to at least the 22 bar level or 160 km below 1 bar (Atreya *et al.*, 1997; Owen *et al.*, 1997; Atreya *et al.*, 1999; Atreya *et al.*, 2003), or a giant wave whose trough extends to at least the same level (Showman and Dowling, 2000). Neither of these hypotheses can completely explain the volatile distribution in the PES, thus additional investigation is needed. Note that the cloud densities calculated by the ECCM (Figure 2) represent upper limits and are much greater than any densities that would actually be expected in the Jovian atmosphere. This is due to the fact that atmospheric dynamics would not normally support a continuous wet adiabatic ascent through the entire atmospheric column, and microphysical processes lead to a reduction of the cloud density through precipitation. On the other hand, the ECCM is accurate in predicting the LCLs of the condensible volatiles, i.e. the cloud bases. This is clearly evident from a comparison of the ECCM calculations shown in Figure 2 and the observation of clouds.

The Galileo Probe Nephelometer detected a tenuous cloud layer at 1.3 bar, and more tenuous ones at 1.6 bar and 0.55 bar (Ragent *et al.*, 1998). Although the H_2S and H_2O mixing ratios in the PES at pressures less than 9 bar are unknown, their extrapolated values from the measured mixing ratios at pressures greater than 9 bar (Niemann *et al.*, 1998; Atreya *et al.*, 1999; Atreya *et al.*, 2003), together with the NH_3 profile inferred from the attenuation of Galileo Probe radio signal (Folkner *et al.*, 1998), are consistent with those required to simulate the PES cloud bases (Figure 2). This is a strong evidence that the three cloud layers detected in the PES most likely represent the clouds of NH_3-ice, NH_4SH-ice, and H_2O-ice, with their bases at, respectively, 0.5, 1.3, and 1.6 bar level (Atreya *et al.*, 1999).

Outside the Galileo Probe entry site, only remote sensing observations exist. Extensive observations of Jupiter's upper visible clouds at relatively high spatial resolution were done with the Galileo orbiter imaging system at visible and near infrared wavelengths (727, 756, 889 nm). From an analysis of the low-mid latitude data, Banfield *et al.* (1998) identified a nearly ubiquitous cloud cover with its base at 750 ± 200 mb, and cloud optical depth varying between 0 and 20. The atmospheric pressure range of the observed cloud bases is consistent with the range

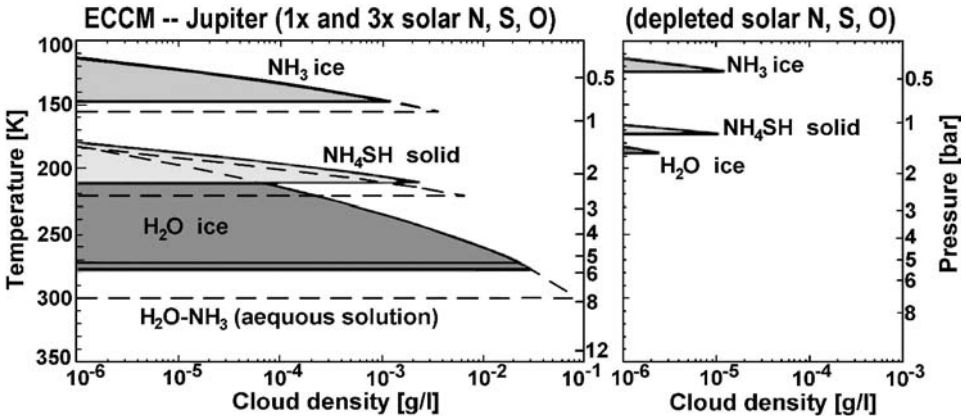

Figure 2. ECCM for Jupiter. *Left panel:* Elemental abundances of condensible volatiles are taken at 1× solar (*solid area*) and 3× solar (*dashed lines*) values. *Right panel:* as left panel, but with the following depleted condensible volatile abundances relative to solar: H_2O: 0.01%; NH_3: 1%; H_2S: 0.5%. The cloud concentrations (in grams per liter) represent upper limits. The temperature profile used in the ECCM is from Seiff *et al.* (1998) for the Galileo PES in right panel, and modified due to condensation in left panel. (After Atreya *et al.*, 1999.)

predicted by the ECCM for 0.01× solar $\leq NH_3 \leq$ 4× solar, which spans the range of ammonia abundance on Jupiter, as measured by the Galileo Probe. The ECCM calculations show that ammonia would condense to ammonia ice at ∼500 mb for 0.01× solar N/H, at 600 mb for 0.5× solar N/H, at 720 mb for 1× solar N/H, at 750 mb for 1.2× solar N/H, at 840 mb for 3× solar N/H, and at 1000 mb for 4× solar N/H (see Figure 2 for some cases). The Galileo Near Infrared Mapping Spectrometer (NIMS) near IR observations (Irwin *et al.*, 2001) and the Galileo Probe and HST observations for the north equatorial belt (Sromovsky and Fry, 2002) indicate cloud opacity variations in the 1–2 bar region. This variability is most likely due to an ammonium hydrosulfide cloud predicted by the ECCM. The belts represent relatively dry, downwelling regions where the cloud locations are expected to be similar to those in the hot/warm spots.

The robustness of the ECCM is further strengthened by the observations of thunderstorms and lightning from the Galileo (Gierasch *et al.*, 2000; Ingersoll *et al.*, 2000) and Cassini (Dyudina *et al.*, 2003) orbiters, attributed to the presence of water clouds *deeper* than 4–5 bars. Indeed, the ECCM calculations show that only water clouds can form in this pressure region (Fig. 2), and that at least 1× solar H_2O is required for the cloud to be at $\geq$ 5 bar level. But, the *base* of the water clouds cannot be determined by the above remote sensing observations. Hence the water abundance in well-mixed atmosphere of Jupiter is still unknown.

ECCM calculations for Saturn are shown in Figure 3, with the condensible volatiles taken as 1× solar and 5× solar. The 5× solar enhancement of the heavy elements is the more likely scenario for Saturn, as discussed in Section 2. Since the atmosphere of Saturn is colder relative to Jupiter, the condensation of the same

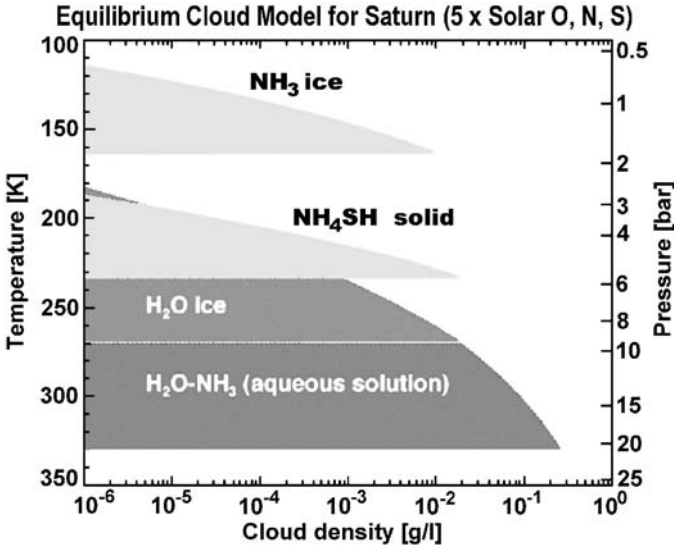

Figure 3. ECCM of Saturn, assuming a five-fold enrichment of the condensible volatiles, so that N/H, S/H, and O/H are each 5× solar. The cloud concentrations (in gram/liter) represent upper limits.

species occurs at much greater pressure levels on Saturn compared to Jupiter. For example, with solar O/H, the base of the water cloud on Saturn (12.6 bars) is at nearly twice the pressure it is at Jupiter (5.7 bar); for 5× solar, the Saturn water cloud begins at 21 bars!

An important consideration of the cloud properties is the presence of a solution cloud on both planets. A droplet cloud due to an aqueous solution of ammonia in water becomes increasingly significant with greater and greater enrichment of ammonia and water, as can be seen for the 3× solar case for Jupiter and 5× solar case for Saturn (Figures 2 and 3). The solution cloud provides a ready loss mechanism for ammonia, followed by its loss in the ammonium hydrosulfide cloud higher up in the atmosphere. There are indications that even outside the hotspots the ammonia mixing ratio may be depleted by up to a factor of two down to the 2–3 bar level, i.e. below its expected condensation level (e.g., de Pater, 1986). The ammonia loss in NH_4SH discussed here can explain some of this loss, but additional loss mechanisms may be necessary.

3.2. Cloud Contaminants

The agreement between the ECCM results on the locations of (i) all cloud layers in a dry region (Galileo PES), (ii) the upper cloud layers (Galileo imaging), and (iii) the purported water clouds (Galileo and Cassini imaging) is a strong evidence for ammonia ice as being the material of Jupiter's visible cloud layer. With the exception of relatively dry regions such as belts and hotspots, clouds

are present everywhere on Jupiter. Yet, ammonia clouds have not been identified spectrally over most of the planet. In fact, Galileo/NIMS (Baines *et al.*, 2002) and Cassini/CIRS (Composite Infrared Spectrometer; Wong *et al.*, 2004a) observations find spectrally identifiable ammonia clouds only in certain locations, covering just ∼1% of Jupiter (Baines *et al.*, 2002). In the case of Saturn, spectral identification of ammonia clouds is non-existent. It has been suggested previously that the lack of spectral identification of (ammonia) clouds on Jupiter and Saturn may be due to dusting by photochemical haze (Tomasko *et al.*, 1984; West *et al.*, 1986). In that case only the short-lived, freshly made plumes (Baines *et al.*, 2002) or high altitude (ammonia) haze (Wong *et al.*, 2004a) could remain uncontaminated and be identified spectrally as ammonia ice. Note that observations with the Infrared Space Observatory (ISO) in the 2.7–3 μm range also indicated the presence of spectrally-identifiable ammonia clouds on Jupiter (Brooke *et al.*, 1998). However, the ISO data provide little information on the actual spatial distribution of the spectrally-identifiable ammonia clouds since the instrumental field-of-view covers some 60° in latitude and 40° in longitude (Baines *et al.*, 2002). Another factor in the spectral obscuration of the upper visible cloud layer of these planets could be cloud properties, including ammonia aerosol particle size effects.

Throughout the atmospheres of Jupiter and Saturn, haze can be produced by photochemical processes. In the stratosphere, haze results primarily from condensation of polycyclic aromatic hydrocarbons (PAHs) and hydrazine (N_2H_4-s). The PAHs are produced in a series of hydrogen abstraction-acetylene addition (HACA) steps that involve, starting with C_6H_6, H-abstraction (by UV photolysis, or reaction with H) followed by C_2H_2-addition (Figure 4). Based on a coupled photochemical-aerosol microphysical model (Friedson *et al.*, 2002; Wong *et al.*, 2003) that includes the production rate of hydrocarbon haze particles, their sedimentation, growth and diffusion through the atmosphere, a hydrocarbon haze deposition rate of ∼10 μm per year is calculated (one year is the average overturning time of the ammonia cloud particles; K. Baines, 2004, personal communication). The haze thickness is larger than the 3 μm wavelength of observations (Baines *et al.*, 2002). Thus, masking of the ammonium spectral signature by the grey hydrocarbon haze material is a distinct possibility.

In fact, the amount of the haze contaminant is expected to be much greater, since the stratospheric hydrocarbon haze would mix with the hydrazine haze particles produced in the photochemistry of ammonia in the region of the tropopause (Strobel, 1973; Atreya *et al.*, 1977). Hydrazine haze is much more abundant than the hydrocarbon haze. A production rate of 6.9×10^{10} hydrazine molecules cm^{-2} s^{-1} is calculated, which amounts to as much as 1.3 mg/m^2 per Jovian day of the hydrazine condensate (Atreya *et al.*, 1977). Being grayish, an admixture of the two can be an ideal contaminant for the ammonia clouds of Jupiter, rather than the white N_2H_4-s alone. The larger bulk of the admixture contaminant than of the PAH-condensate alone is also important for another reason—it can prevent spectral identification of

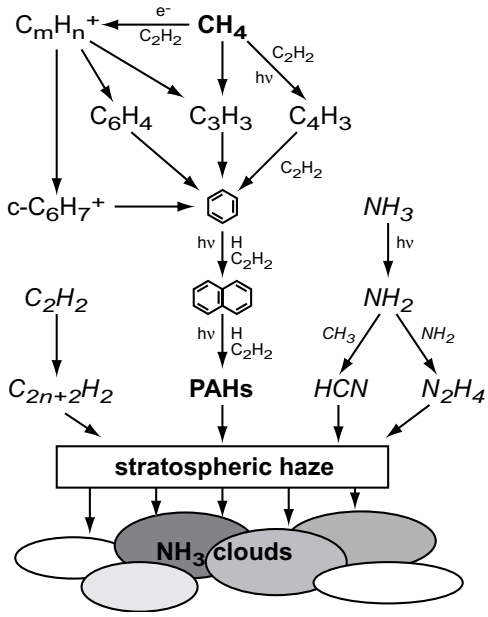

Figure 4. Illustration of important reaction pathways of haze formation on Jupiter. The pathways beginning with C_2H_2 and leading to polyyne polymerization (*lower left branch*) and the HCN polymerization (*right branch*) are minor contributors to haze formation. In the auroral regions of Jupiter, ion chemistry plays a decisive role in the hydrocarbon chemistry, so that nearly all of the "auroral" benzene (precursor to PAH) is produced through the electron recombination of ring ion c-$C_6H_7^+$ (Wong *et al.*, 2003).

the clouds, even if the haze ends up in the core of NH_3-ice particles, i.e. if it is suitable as condensation nuclei for ammonia. It has been suggested that spectral masking can occur if the contaminant is a significant fraction of the total mass (West *et al.*, 1989), which is the case for the contaminant admixture. The same type of admixture is expected to be present in Saturn's atmosphere. Preliminary calculations show that the PAH produced hydrocarbon haze is abundant on Saturn also (Wong and Atreya, 2004), and the quantity of photochemically produced hydrazine is also fairly large (Atreya *et al.*, 1980).

3.3. Clouds of Uranus and Neptune

We show in Figure 5 an ECCM model for Neptune. Uranus is nearly identical. The topmost cloud layer at ∼1 bar level is made up of methane ice, according to the ECCM model. Voyager radio occultation observations did in fact infer a cloud layer at ∼1 bar level. The base of the water-ice cloud for *solar* O/H is expected to be at ∼40 bar level, whereas for the NH_3-H_2O solution clouds it is at approximately twice this pressure. But, the heavy elements are most likely enriched relative to solar. The C/H ratio at Uranus is ∼20–30× solar, and between 30× and 50× solar

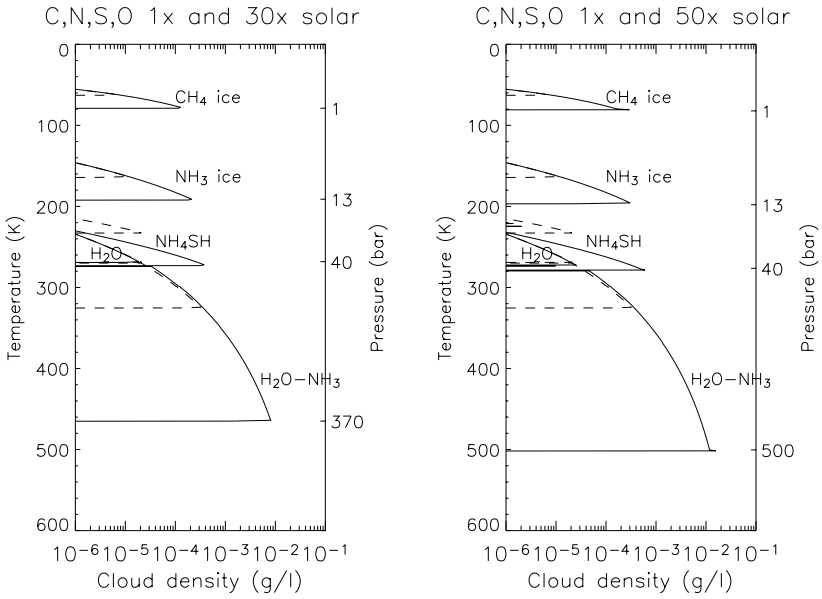

Figure 5. ECCM for Neptune, assuming 1× (*dashed lines*) and 30× enrichment (*left panel*), and 1× (*dashed lines*) and 50× enrichment (*right panel*), of condensible volatiles (CH_4, NH_3, H_2S, H_2O ratioed to H) relative to solar. Cloud bases for 30× solar, 50× solar cases are marked on right ordinates. The cloud concentrations (in gram/liter) represent upper limits. The structure and locations of the clouds at Uranus would be very similar due to similar thermal structure and atmospheric density in the tropospheres of the two planets.

at Neptune, as derived from the measurement of methane. As in the case of Jupiter, the enrichment factor for all other heavy elements is expected to be similar. Thus, O/H, hence water, as well as the other condensibles (NH_3, H_2S) are also expected to be enhanced by factors of 20–30 or more relative to solar in the atmospheres of Uranus and Neptune. For purposes of illustration, we present cases with 1×, 30×, and 50× solar enrichment of the condensible volatiles (CH_4, NH_3, H_2S, H_2O) in Figure 5 for Neptune. The NH_3-H_2O aqueous solution cloud base is calculated to be at 370 bars and 500 bars, respectively for 30× and 50× solar cases, accounting for van der Waals corrections. Some models (e.g. Ree, 1986; Podolak *et al.*, 1991) predict the presence of a water-ammonia ionic ocean in the tens of kilobar region (depth depending upon O/H and N/H). Such an ocean would be much deeper than the aqueous solution cloud of the ECCM discussed above. Therefore NH_3 as well as H_2O will have been depleted well below their ECCM condensation levels.

3.4. Cloud Chromophores

The brownish-orange-yellow colors of the visible clouds of Jupiter and Saturn continue to be a mystery, as there are no measurements available to determine the nature of the chromophore/s. Potential chromophores range from phosphorus

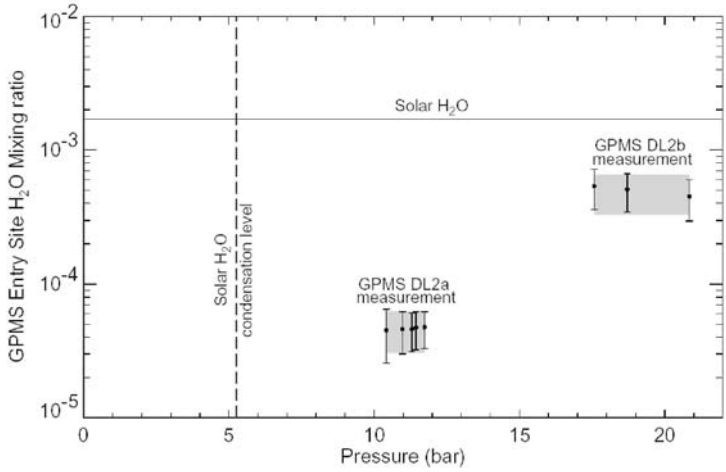

Figure 6. Galileo Probe Mass Spectrometer (GPMS) measured mixing ratio of water vapor as a function of atmospheric pressure. The mixing ratio increased dramatically, by nearly a factor of 10, between 10 and 22 bar levels, but remained subsolar even at the deepest level probed. The condensation level for solar water is shown by broken vertical line, i.e. the base of water ice cloud would be at approximately 5 bar. (After Atreya *et al.*, 2003; Wong *et al.*, 2004b.)

(P_2–yellow; P_4–red) produced in the stratospheric photochemistry of PH_3, to sulfur species (S_8–yellow; ammonium polysulfide, $(NH_4)_xS_y$–orange; hydrogen polysulfide, H_xS_y–brown). In the atmospheres of Jupiter and Saturn, H_2S is sequestered in the NH_4SH cloud in the 2 and 5 bar region, respectively, where the dissociating UV flux does not penetrate. Thus, the sulfur species are less likely to be responsible for the cloud colors, unless H_2S can be dissociated by other means, such as high energy cosmic rays. The aqua-marine color of Uranus and Neptune, on the other hand, is a direct consequence of the scattering of the Sun's bluish-green light by their atmospheres in which the Sun's red light is absorbed effectively by the large quantities of methane. The white clouds on these planets are due to the condensation of methane (Section 3.3).

4. Future

Much still remains mysterious about the clouds of the giant planets. It is only by having access to the region well below the main cloud layers that the abundances of key heavy elements can be determined. In the case of Jupiter, although the noble gases, C, N and S have been measured in the well-mixed atmosphere, the water mixing ratio, hence the oxygen elemental abundance, has not been determined (Table I, Figure 1). The current status of the water measurement is shown in Figure 6. The cloud models discussed in Section 2 show that outside the hotspots, water clouds are expected at 5–8 bar level for (1–3) $\times$ solar O/H. But in the Galileo

PES, the water mixing ratio was still rising at the deepest level probed, 22 bars! The thunderstorm and lightning observations on Jupiter (Section 2) are a good indication that the water abundance in the deep well-mixed atmosphere of Jupiter must be at least solar. But the results are not quantitative enough to be useful for constraining models of the formation of Jupiter and its atmosphere.

Since water is presumably the original carrier of heavy elements to Jupiter, it is the single most critical species remaining in order to constrain the formation models of Jupiter. It is not known at Jupiter, and, unfortunately, Cassini orbiter observations will not be able to yield the water abundance or, for that matter, the abundance of the heavy noble gases and sulfur in Saturn's atmosphere (there is a possibility of measuring N/H, however). Future missions that can accurately determine the water abundance in the deep well-mixed atmospheres of Jupiter and Saturn will be most valuable. Considering the possibility that water may be variable over these planets, it is imperative that measurements be carried out to depths *well below* the expected condensation levels of 5–20 bars, i.e. to pressures of at least 50–100 bars. Since the meteorology of the hotspot entry sites is poorly understood, it is also important to carry out *simultaneous* measurements of other key species even if their mixing ratios were measured previously (e.g. at Jupiter by the Galileo Probe). Other supporting measurements for understanding the atmospheric composition data are winds and cloud particle properties.

A comparative study of the gas giants, when combined with a similar study for the icy giants, can provide the most comprehensive constraints on the models of formation of our solar system and, by extension, the extrasolar planetary systems. But determination of heavy element abundances on Uranus and Neptune becomes much more challenging than that at Jupiter and Saturn if the O and N elemental abundance must be measured also. This is because the water droplet cloud is expected to form at nearly a kilobar level—the kind of pressure encountered at the bottom of the Marianas Trench! But, in fact, even if the technological challenge of the probe and payload survival to and data transmission from kilobar levels, where the temperatures exceed 500 K, could be overcome, the O and N elemental abundances may not be representative of their well-mixed atmospheric values due to the formation of an ionic solution in the tens of kilobar region, as discussed above. Fortunately, unlike Jupiter and Saturn, it is not imperative to measure the N and O abundance at Uranus and Neptune in order to constrain their formation models. The noble gases, C, S, D/H, and $^{15}N/^{14}N$ can provide all the constraints one needs for developing the models of the formation of the icy giants and their atmospheres. And these elements can be easily measured at shallower depths, i.e. at pressures of only 50–100 bars maximum. Unlike Jupiter and Saturn, neon is not expected to be depleted in the tropospheres of Uranus and Neptune, due to the absence of condensation of helium into droplets in which Ne dissolves, or by another fractionation process. In fact, the available measurements yield nearly solar He/H in the atmospheres of Uranus and Neptune, unlike Jupiter (and possi-

bly Saturn), as seen in Table 1. Thus, Ne/H is a critical measurement for Uranus and Neptune. Although the N/H at Uranus and Neptune seems neither easy nor a good discriminator of models, the $^{15}N/^{14}N$ and D/H isotope ratios are important measurements, as they would reveal the role of comets in the formation of these planets, by comparing the value against the cometary value and the "protosolar" $^{15}N/^{14}N$ and D/H already measured at Jupiter by the Galileo Probe.

In summary, the big questions of the formation of the giant planets and the origin of their atmospheres require simultaneously addressing interrelated and intertwined issues of composition and clouds. It is essential to measure the elemental abundances below the cloud levels. For the gas giants, critical elements are: C, N, S, O, He, Ne, Ar, Kr, Xe, D/H and $^{15}N/^{14}N$, whereas N and O are neither easily accessible nor critical for the icy giants. Supporting information on cloud structure and winds is essential also. Because of their disequilibrium nature, PH_3, AsH_3, GeH_4 and CO are not good indicators of heavy element enhancement, nevertheless, their measurement on all giant planets is also desirable as they can reveal much about the interior processes. A comparative planetology approach can provide the best results. Multiple probes to the diverse multiple worlds of the giant planets are recommended for understanding the formation of our solar system and the extrasolar systems. Either in a single grand tour mission or on individual identical spacecraft missions, 2–3 probes deployed to 50–100 bars at each planet are recommended. A grand tour would fully exploit the capabilities of the Prometheus spacecraft, but celestial mechanics considerations might limit the mission to Jupiter, Saturn, and one of the two icy giants. In that case Neptune would be the ideal final target where, in addition to dropping the probes, a fully instrumented orbiter could also be deployed. A visionary approach involving multinational partnership is most desirable to accomplish the immensely challenging exploration of multiple planets by multiple probes. In the shorter term, relatively modest microwave spacecraft missions can help define the more ambitious probe mission/s to the giant planets.

Acknowledgements

We thank Toby Owen, Richard Young and Scott Bolton for illuminating discussions. SKA acknowledges support for this research by a grant from NASA's Planetary Atmospheres Program.

... And at the going off of these clouds, some spots have been taken notice of in him, much brighter than the rest of his Body, which remin'd but a little while, and then were hid from our sight. These Monsieur *Cassini* thinks are only the Reflection from the Snow that covers the tops of the Hills in *Jupiter*: but I should rather think that it is only the colour of the Earth, which chances to be free from those Clouds that commonly darken it.

Christianus Huygens, In *Kosmotheoros* 1698

References

Anders, E. and Grevesse, N.: 1989, 'Abundances of the elements—Meteoritic and solar', *Geochim. Cosmochim. Acta* **53**, 197–214.

Atreya, S.K., Donahue, T.M., and Kuhn, W.R.: 1977, 'The distribution of ammonia and its photochemical products on Jupiter', *Icarus* **31**, 348–355.

Atreya, S.K., Kuhn, W.R., and Donahue, T.M.: 1980, 'Saturn: Tropospheric ammonia and nitrogen', *Geophys. Res. Lett.* **7**, 474–476.

Atreya, S.K. and Romani, P.N.: 1985, 'Photochemistry and clouds of Jupiter, Saturn and Uranus', in G.E. Hunt (ed.), *Planetary Meteorology*, Cambridge University Press, pp. 17–68.

Atreya, S.K.: 1986, *Atmospheres and Ionospheres of the Outer Planets and their Satellites*, Chapter 3, Springer-Verlag, New York-Berlin.

Atreya, S.K., Wong, M.H., Owen, T.C., Niemann, H.B., and Mahaffy, P.R.: 1997, 'Chemistry and clouds of the atmosphere of Jupiter: A Galileo Perspective', in C. Barbieri *et al.* (eds.), *Three Galileos: The Man, The Spacecraft, The Telescope*, Kluwer, Dordrecht, The Netherlands, pp. 249–260.

Atreya, S.K., Wong, M.H., Owen, T.C., Mahaffy, P.R., Niemann, H.B., de Pater, I., Drossart, P., and Encrenaz, Th.: 1999, 'A comparison of the atmospheres of Jupiter and Saturn: deep atmospheric composition, cloud structure, vertical mixing, and origin', *Planet. Space Sci.* **47**, 1243–1262.

Atreya, S.K., Mahaffy, P.R., Niemann, H.B., Wong, M.H., and Owen, T.C.: 2003, 'Composition and origin of the atmosphere—an update, and implications for the extrasolar giant planets', *Planet. Space Sci.* **51**, 105–112.

Atreya, S.K.: 2004, 'Composition, clouds, and origin of Jupiter's atmosphere — a case for deep multiprobes into giant planets', *ESA* **SP-544**, 57–62.

Baines, K.H., Carlson, R.W. and Kamp, L.W.: 2002, 'Fresh ammonia ice clouds in Jupiter. I. Spectroscopic identification, spatial distribution, and dynamical implications', *Icarus* **159**, 74–94.

Banfield, D., Gierasch, P.J., Bell, M., Ustinov, E., Ingersoll, A.P, Vasavada, A.R., West, R.A., and Belton, M.J.S.: 1998, 'Jupiter's cloud structure from Galileo imaging data', *Icarus* **135**, 230–250.

Brooke, T.Y., Knacke, R.F., Encrenaz, Th., Drossart, P., and Crisp, D.: 1998, 'Models of the ISO 3-μm reflectance spectrum of Jupiter', *Icarus* **136**, 1–13.

de Pater, I.: 1986, 'Jupiter's zone-belt structure at radio wavelengths', *Icarus* **68**, 344–369.

Dyudina, U.A., Del Genio, A.D., Ingersoll, A.P., Porco, C., West, R.A., Vasavada, A.R., and Barbara, J.M.: 2003, 'Lightning on Jupiter observed in the H_α line by the Cassini Imaging Science Subsystem', submitted to *Icarus*.

Folkner, W.M., Woo, R., and Nandi, S.: 1998, 'Ammonia abundance in Jupiter's atmosphere derived from attenuation of the Galileo probe's radio signal', *J. Geophys. Res.* **103**, 22,847–22,856.

Friedson, A.J., Wong, A.S., and Yung, Y.L.: 2002, 'Models for polar haze formation in Jupiter's stratosphere', *Icarus* **158**, 389–400.

Gautier, D., Hersant, F., Mousis, O., and Lunine, J.I.: 2001a, 'Enrichment in volatiles in Jupiter: A new interpretation of the Galileo measurements', *Astrophys. J.* **550**, L227–L230.

Gautier, D., Hersant, F., Mousis, O., and Lunine, J.I.: 2001b, 'Erratum: Enrichment in volatiles in Jupiter: A new interpretation of the Galileo measurements', *Astrophys. J.* **559**, L183.

Gierasch, P.J., Ingersoll, A.P., Banfield, D., Ewald, S.P., Helfenstein, P., Simon-Miller, A., Vasavada, A., Breneman, H.H., Senske, D.A., and the Galileo Imaging Team: 2000, 'Observation of moist convection in Jupiter's atmosphere', *Nature* **403**, 628–630.

Huygens, C.: 1698, *Kosmotheoros*, English translation, 'The Celestial Worlds Discover'd: or, Conjectures Concerning the Inhabitants, Plants and Productions of the Worlds in the Planets', Frank Cass & Co. Ltd., England, pp. 25–26.

Ingersoll, A.P., Gierasch, P.J., Banfield, D., Vasavada, A.R., and the Galileo Imaging Team: 2000, 'Moist convection as an energy source for the large-scale motions in Jupiter's atmosphere', *Science* **403**, 630–632.

Irwin, P.G.J., Weir, A.L., Taylor, F.W., Calcutt, S.B., and Carlson, R.W.: 2001, 'The origin of belt/zone contrasts in the atmosphere of Jupiter and their correlation with 5-μm opacity', *Icarus* **149**, 397–415.

Niemann, H.B., *et al.*: 1998, 'The composition of the Jovian atmosphere as determined by the Galileo probe mass spectrometer', *J. Geophys. Res.* **103**, 22,831–22,846.

Owen, T.C., Atreya, S.K., Mahaffy, P., Niemann, H.B. and Wong, M.H.: 1997, 'On the origin of Jupiter's atmosphere and the volatiles on the Medicean Stars', in C. Barbieri *et al.* (eds.), *Three Galileos: The Man, The Spacecraft, The Telescope*, Kluwer, Dordrecht, The Netherlands, pp. 289–297.

Owen, T., Mahaffy, P.R., Niemann, H.B., Atreya, S.K., Donahue, T., Bar-Nun, A., and de Pater, I.: 1999, 'A low-temperature origin for the planetesimals that formed Jupiter', *Nature* **402**, 269–270.

Podolak, M., Hubbard W.B., and Stevenson D.J.: 1991, 'Models of Uranus interior and magnetic field', in J. Bergstralh, *et al.* (eds.), *Uranus*, The University of Arizona Press, Tucson, pp. 48–49.

Ragent, B., Rages, K.A., Knight, T.C.D., Arvin, P., and Orton, G.S.: 1998. 'The clouds of Jupiter: Results of the Galileo Jupiter mission probe nephelometer experiment', *J. Geophys. Res.* **103**, 22,891–22,909.

Seiff, A., Kirk, D.B., Knight, T.C.D., Young, R.E., Mihalov, J.D., Young, L.A., Milos, F.S., Schubert, G., Blanchard, R.C. and Atkinson, D.: 1998, 'Thermal structure of Jupiter's atmosphere near the edge of a 5-μm hot spot in the north equatorial belt', *J. Geophys. Res.* **103**, 22,857–22,889.

Ree, F.H.: 1986, 'A new approach to multiphase equilibria: Applications to high pressure physics problems', *Physica* **139-140B**, 73–78.

Showman, A.P. and Dowling, T.: 2000, 'Nonlinear simulations of Jupiter's 5 micron hotspots', *Science* **289**, 1737–1740.

Sromovsky, L.A. and Fry, P.M.: 2002, 'Jupiter's cloud structure as constrained by Galileo Probe and HST observations', *Icarus* **157**, 373–400.

Strobel, D.F.: 1973, 'The photochemistry of NH_3 in the Jovian atmosphere', *J. Atmos. Sci.* **30**, 1205.

Tomasko, M.G., West, R.A., Orton, G.S., and Tejfel, V.G.: 1984, 'Clouds and aerosols in Saturn's atmosphere', in T. Gehrels and M.S. Matthews (eds.), *Saturn*, The University of Arizona Press, Tucson, pp. 150–194.

Weidenschilling, S.J. and Lewis, J.S.: 1973, 'Atmospheric and cloud structure of the Jovian planets', *Icarus* **20**, 465–476.

West, R.A., Strobel, D.F., and Tomasko, M.G.: 1986, 'Clouds, aerosols, and photochemistry in the Jovian atmosphere', *Icarus* **65**, 161–217.

West, R.A., Orton, G.S., Draine, B.T., and Hubbell, E.A.: 1989, 'Infrared absorption features for tetrahedral ammonia ice crystals', *Icarus* **80**, 220–224.

Wong, A.S., Yung, Y.L., and Friedson, A.J.: 2003, 'Benzene and haze formation in the polar atmosphere of Jupiter', *Geophys. Res. Lett.* **30**, 1447.

Wong, A.S. and Atreya, S.K.: 2004, 'Benzene, and other hydrocarbons on Saturn', *EGS abstract*, EGU04-A-02239, Nice, France.

Wong, M.H., Bjoraker, G.L., Smith, M.D., Flasar, F.M., and Nixon, C.A.: 2004a, 'Identification of the 10-μm ammonia ice feature on Jupiter', *Planet. Space Sci.* **52**, 385–395.

Wong, M.H., Mahaffy, P.R., Atreya, S.K., Niemann, H.B., and Owen, T.C.: 2004b, 'Updated Galileo Probe Mass Spectrometer measurements of carbon, oxygen, nitrogen, and sulfur on Jupiter', *Icarus*, in press.

Address for Offprints: Sushil K. Atreya, Department of Atmospheric, Oceanic, and Space Sciences, The University of Michigan, Ann Arbor, MI 48109-2143, USA; atreya@umich.edu

COMPARATIVE STUDY OF THE DYNAMICS OF THE OUTER PLANETS

RETA F. BEEBE
Department of Astronomy, P.O. Box 30001, MS 4500, New Mexico State University, Las Cruces, NM 88003, USA

Received: 14 April 2004; Accepted in final form: 9 August 2004

Abstract. The two classes of outer planets, Gas Giants and Ice Giants, have distinctly different global circulation patterns and internal structure. Ongoing ground-based observations of the Ice Giants provide clues to better understanding and Galileo and Cassini data will generate constraints for Gas Giant modeling. The composition below the cloud levels, the depths to which the winds penetrate and the processes that sustain the zonal winds and weather systems are not understood. Basic questions concerning the structure, composition and atmospheric dynamics that are sustained on the four giants could be answered by a combination of orbiters and probes. Future missions that could answer these questions are not currently under development.

Keywords: giant planets, atmospheres, composition, proto-planetary disk

1. The Character of the Outer Planets

Current models of disk evolution and solar system formation have been influenced by contrasts in the physical properties of the four giant planets of our outer solar system. Their physical properties indicate that they have considerable differences in bulk composition and that they formed under at least two scenarios. In Table I, comparison of Jupiter with Saturn suggests a trend where density would be related to mass. The same is true for Neptune and Uranus; however, when the masses of the four giants are considered together, it is apparent that the internal structure of the two outer planets differs drastically from that of Jupiter and Saturn. Their density differences and their locations within the solar system suggest that Jupiter and Saturn accumulated their masses in a region of the proto-planetary disk that was richer in hydrogen and helium than was the case for the smaller, relatively denser outer planets. If this were the case, then Uranus and Neptune would be richer in ice-forming elements (carbon, oxygen and nitrogen) and this composition difference would provide a basis for dividing these bodies into two groups: the Gas Giants (Jupiter and Saturn) and the Ice Giants (Uranus and Neptune).

The distinction between Gas and Ice Giants is not just one of internal composition. Consideration of the atmospheric circulation reinforces the idea that the two classes have distinct properties. Transfer of internal heat and the manner in which solar energy is absorbed and redistributed supports two distinct regimes of

Space Science Reviews 116: 137–154, 2005.
DOI: 10.1007/s11214-005-1952-4

TABLE I
Properties of the Giant Planets

	Gas Giants		Ice Giants	
	Jupiter	Saturn	Uranus	Neptune
Solar distance (AU)	5.2	9.6	19.2	30.1
Mass (Earth=1)	317.9	95.2	14.5	17.1
Mean Density (g/cc)	1.33	0.69	1.29	1.64
Rotation Period (hr)	9.84	10.23	17.9	19.2
Max. zonal velocity(m/sec)	175	475	-100	-480
Width of equatorial jet (°)	±15	±45	±25	±50
Insolation (Earth=1)	0.037	0.011	0.003	0.001
Effective temperature (K)	124	95	59	59
Flux out/Solar Flux	1.67	1.78	1.06	2.61

atmospheric circulation in the upper, visible atmospheres of these planets and raises the question of whether the Ice Giants possess oceans. Figure 1 and Table I provide trends and parameters to quantify these regimes. Jupiter and Saturn possess strong eastward equatorial winds and alternating westward and eastward jets that decrease in magnitude with increasing latitude. Uranus and Neptune have broad, westward equatorial jets with less well-defined high latitudinal wind systems. The process that would generate eastward jets is not well understood and must involve upward heat transport driven by internal heat sources in Jupiter and Saturn. And, although a simple model for a solar heated, rotating atmosphere would predict a westward equatorial flow, the lack of correlation of maximum wind speed with available solar heating (see insolation parameter, flux out/solar flux absorbed in Table I) indicates that a simple, solar driven model is inadequate and that knowledge of atmospheric structure, heat transport at greater depths and coupling with the deep interior is needed to understand the energy transport.

Occultations of the radio signal of spacecraft by the planets have provided values for the refractive index as a function of height in the atmosphere that, assuming hydrostatic equilibrium and mean molecular weight, has been interpreted as a relation between pressure and temperature. Although transmission of the radio signal is limited to the upper few bars of the atmosphere, it provides an additional comparison between the two classes of giant planets. Figure 2 reveals the similarity of the Uranian and Neptunian profiles and contrasts them with those of the Gas Giants. Values for the ratio of radiated flux to that absorbed from incident sunlight indicate that transport of internal heat plays a major role in determining atmospheric structure and dynamics and raises the question of what processes control heat loss in the Ice Giants that lead to similar temperature profiles and such a small internal heat source for Uranus.

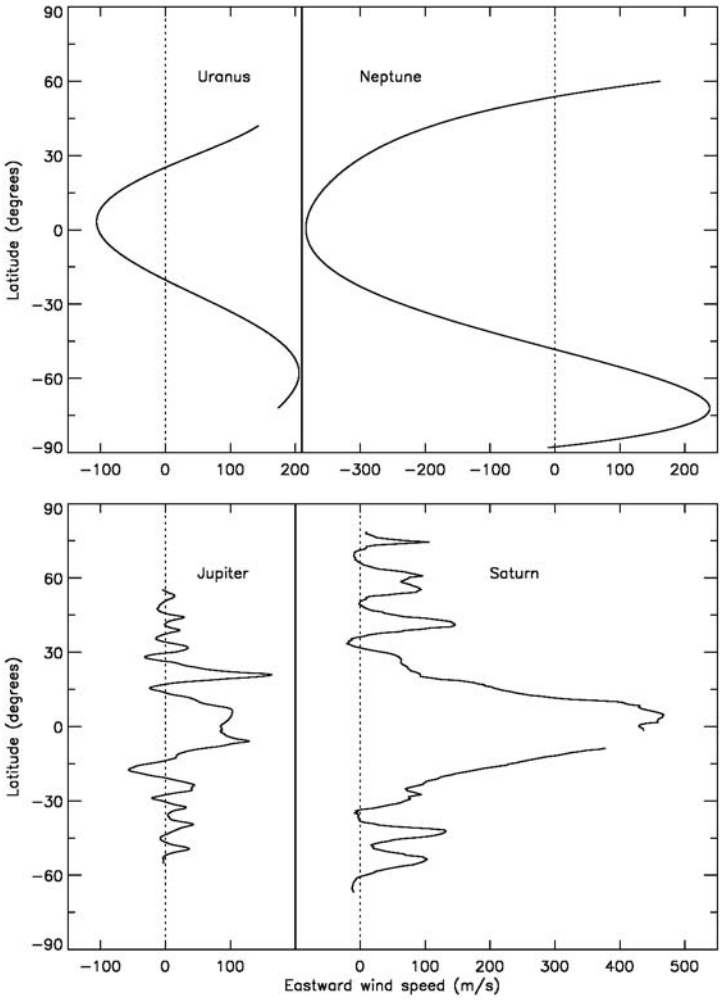

Figure 1. Comparison of prevailing winds obtained from tracking motions of clouds in sequences of Voyager and HST images of the visible cloud decks of the giant planets.

It is apparent that there are two classes of giant planets, each with their own characteristics, but there are many unanswered questions that apply to all four planets. A balanced effort that explores these bodies and a comparative approach to modeling the atmospheres of both the Gas and Ice Giants will be required to acquire the answers. Some of these fundamental questions are:

- What is the balance of energy sources that maintain the zonal winds?
- How stable are the zonal winds and how do they vary with depth?
- What is the composition of the deep atmosphere?
- How is internal heat transported through the atmosphere and what role does water play?

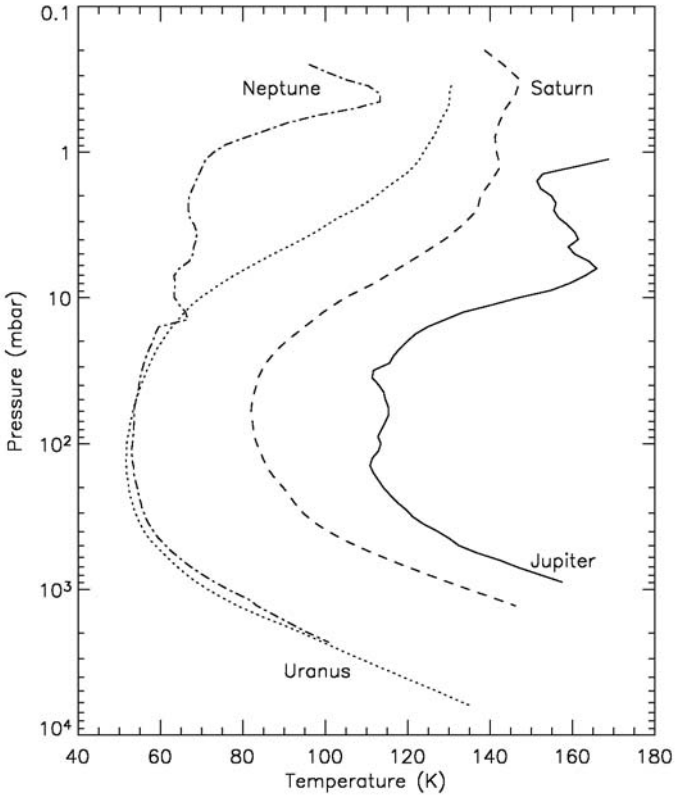

Figure 2. Plots of Temperature versus Pressure profiles derived from radio occultation data illustrate differences among the giant planets.

- How and why does atmospheric temperature vary with depth, latitude and time?
- How is the solar insolation redistributed and at what depth?
- How do large, long-lived systems maintain themselves?

These are fundamental questions that will require a combination of observations with improved frequency and spatial resolution that probe to increasing depths, careful analysis and improved modeling approaches. Constraints of spacecraft mobility, limited payload mass and low transmission capability and the current schedule for exploring the individual planets limit our progress. With the Jupiter/Galileo and Cassini observations concluded and the Saturn/Cassini exploration currently underway, a better understanding of the Gas Giants is anticipated. However, with no plans for missions to Uranus and Neptune, improved understanding of the Ice Giants depends on obtaining ground-based observations and concentration on interpretation and modeling that may provide better insight into the details of Voyager and Hubble Space Telescope observations of Uranus and Neptune.

2. Progress in Understanding Uranus

Although zonal banding had been reported during an equinox (Alexander, 1965), in the pre-Voyager era the nature of the global circulation was unknown. Because of the remoteness and unique orientation of the planet (the 84 yr period of revolution and inclination of the pole (98°) results in alternating 42 years of sunlight and 42 years of polar darkness and an equatorial area receiving less insolation than an equal polar area) it was not obvious what the circulation would be. Failure to detect evidence of an internal heat source and the fact that incident solar flux was one-tenth that at Jupiter further confused the situation.

Based on previous observations that indicated low variability of Uranus and Neptune from 1972 to 1996, Lockwood and Thompson (1999; 2002) assumed that the cloud decks were spatially and temporally nonvariable and used the apparent disks of the planet as reflectors to measure the solar constant. During this interval Uranus passed through solstice in 1985 and some polar brightening occurred, indicating limited seasonal response. In comparison Neptune has brightened more than 10 percent over the same interval.

The Voyager cameras (Smith *et al.*, 1986) obtained data that revealed a faint banded appearance and isolated polar hazes, indicating the presence of an organized zonal flow. Unfortunately, very few isolated cloud features that could be used for wind markers were present. Less than 10 features, ranging from a faint UV cloud feature at $-72°$ latitude to dark spots at $-36°$ and -41° and two long-lived bright plumes at $-27°$ were combined with the oblateness factor, derived from occultation data at $-4.5°$ (Lindal *et al.*, 1987) to reveal a broad westward equatorial flow. This established that the pattern of global circulation on Uranus was distinct from that of Jupiter and Saturn, which have eastward circulation at low latitudes.

As the Voyager spacecraft flew by Uranus, the Infrared Imaging Spectrometer (IRIS) was used to measure temperatures on both the illuminated and shadowed sides of the planet. The data revealed little temperature difference between the illuminated and dark poles, even though the shadowed pole had experienced winter solstice in 1985 and was in darkness (Conrath *et al.*, 1991). Measurement of emitted IR radiation over a large range in phase angle allowed accurate determination of the magnitude of the internal heat source and revealed that the radiated flux was nearly equal to the absorbed solar flux (Conrath *et al.*, 1991).

These results, together with the temperature-pressure profile derived from the occultation data, provided a basis for proposing a model for global circulation. When compared to 1989 Neptune data, major questions remained unanswered:

- Was the bland featureless cloud deck typical or could episodic convection occur?
- What was the nature of vertical heat transport in the atmosphere?
- How constant were the zonal winds?

– How was solar energy redistributed in the atmosphere to yield similar effective temperatures and T/P profiles when the incident solar flux differed by a factor of 3 (see Table I and Figure 2)?

Compared to conditions in 1986 when Voyager observations were made near solstice, Uranus will be at equinox in 2007, thus providing a global view of the planet and allowing study of the effects of changing distribution of insolation with latitude. Although no missions are currently planned for the Uranian system, the Hubble Space Telescope (HST) provides spatially resolved images at visual and IR wavelengths and microwave observations, which probe to greater depths, can be obtained at the Very Large Array (VLA) radio telescope. These visual, IR and microwave observations probe from the stratosphere to as deep as 50 bars, and provide a basis for constraining seasonal variation models.

Karksochka (1998) and Hammel *et al.* (2001) used visible and near IR observations obtained with HST to observe similar cloud features in 1994, 1997, 1998, and 2000, and determined translation rates of the features relative to the period of rotation of Uranus' magnetic field (and presumably its core) and derived the first measurements of winds in the northern hemisphere. These data contain features up to 40 degrees latitude and establish a broad retrograde equatorial jet and prograde motion at mid latitudes that are nearly symmetric about the equator. These results indicated that the winds were approximately constant from 1986 to 2000, but continued monitoring will be needed to provide modeling constraints for understanding the response to seasonal heating of this system with long radiative and frictional time constants.

Hofstadter and Butler (2003) utilized the VLA to obtain latitudinally resolved measurements (5° resolution) of 2 and 6 cm emissions in 1994 and 2002 and retrieved 1980's observations and reduced all the data in a consistent manner. They conclude that the deep atmosphere (5-50 bars) changed significantly between 1989 and 1994. At low latitudes they observed a darker region, caused by excess opacity and/or low temperatures, and an increased pole-to-equator temperature gradient (Figure 3). The authors point out that it is difficult to separate temperature and opacity effects, but they favor an interpretation with opacity as the dominant effect and conclude the temperature gradient is larger at 40 bars than 4 bars, indicating that the adjustment to solar heating occurs at depth in the atmosphere.

Although there is no planned opportunity to obtain high-resolution, space-based data within the foreseeable future, these results indicate that progress will be made in understanding the dynamics of the Uranian atmosphere. Voyager occultation data provided a temperature profile down to 2.3 bars to establish a basic constraint for modeling. And, although the life of HST is limited, increased use of adaptive optics in near IR and access to microwave via VLA during a time of seasonal change will provide challenging constraints for developing dynamical models.

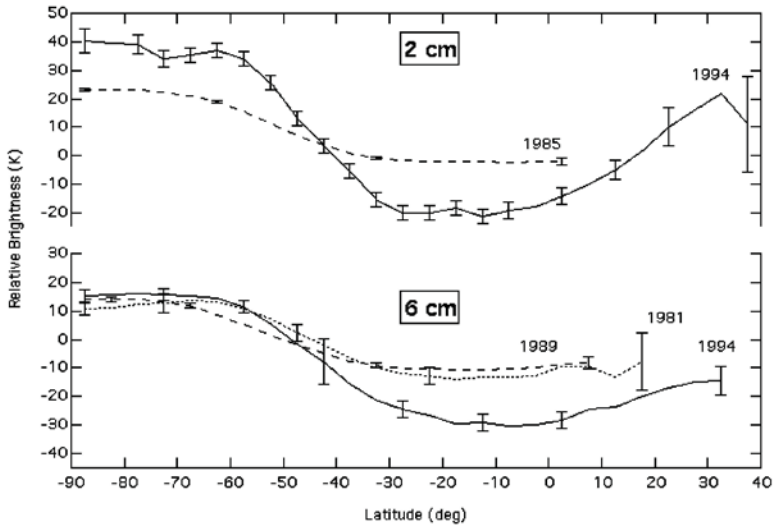

Figure 3. Brightness versus latitude derived from VLA microwave data.

3. Comparison of Neptune with Uranus

Previous to the Voyager 2 fly-by, imaging of Neptune in near IR had progressed to a level that bright features could be distinguished in spatially resolved narrow-band imaging (Hammel, 1989). Selection of filters sounding in frequency intervals within and excluding regions of methane absorption allowed comparison of reflectivity of high altitude regions with lower regions and established the presence of bright high-level clouds. Higher spatial resolution in Voyager images revealed bright clouds associated with localized centers of lower reflectivity. The smaller structures showed surprising temporal variability and were frequently associated with lee waves generated by interaction of zonal winds and the local centers (Smith *et al.*, 1989). As with Uranus, these data revealed a strong retrograde equatorial jet and a lack of well defined, alternating jets at higher latitudes. Determination of the latitudinal position of the "storm" centers in the resulting time series revealed that they migrated with time and that the Great Dark Spot, the largest system, was drifting equatorward (Hammel *et al.*, 1989), possibly toward its destruction. The Voyager data raised several significant questions concerning the temporal variability of the zonal winds and the rate of development of storm centers and their expected lifetimes.

Although the greater distance of Neptune relative to Uranus results in a factor of 5 reduction in spatial resolution, the definition of the clouds and contrast has allowed continued HST monitoring and extension of observations to higher northern latitudes. In 1996 observations revealed large storms near 25° and other features from −61° to 38° latitude. Sromovsky *et al.* (2001) obtained observations that revealed 18 features from that could be tracked to derive wind speeds. These

results agreed with Voyager except near large weather systems. They conclude that the greatest incidence of weather disturbances is near -45° latitude.

The planetary science community would enthusiastically endorse a mission capable of exploring satellites, rings, magnetic field and the atmosphere of Neptune. The richness of the Neptunian system recommends it as target for the first "Ice Giant" mission. However, the cost of such a mission is a formidable obstacle and, as was noted in the NRC Decadal Study (2003), development of technology to provide power and deep, multistage probes would be needed for the mission. Should Uranus' atmosphere display considerable convective activity with considerable change in cloud cover and measurable heat loss, the science community might reconsider its priorities. However, within the context of past schedules and the length of time needed to develop and launch a spacecraft, it is unrealistic to expect a NASA mission to either icy planet within the next decade. Thus, in the near future, the best avenue for better understanding of the ice giants will require that the limited Uranian and Neptunian data be used to constrain realistic physical models.

4. Gas Giant Circulation

Unlike the Ice Giants, the Gas Giants generated cloud structures that were visible in small telescopes. Changes were abrupt enough that naked-eye observers have noted these changed since the development of reflector telescopes. The combination of a long focal length of the combined primary and secondary mirrors and a primary mirror diameter as small as 20 cm yielded spatial resolution and surface brightness that revealed fine detail during brief periods of good seeing. As techniques developed that utilized an etched eyepiece that allowed precise centering of the planetary disk on crosshairs, visual observers recorded times of central meridian crossing of the leading and following edges of cloud features. This approach yielded reliable periods of revolution and allowed observers to map the equatorial jets and the alternating east-west jet structure that was associated with the belted appearance of Jupiter and to a lesser degree on Saturn (Peek, 1958; Sánchez-Lavega *et al.*, 1993).

As IR sensitive detectors were developed, measurements of emerging heat flux revealed that the rate of heat loss exceeded the absorbed incident solar radiation, providing evidence for an internal heat source. Before close-up spacecraft observations were available there were good records of belt-zone variability, rough map of zonal winds, records of the behavior of long-lived features and although it was known that Jupiter was radiating excess heat, a reliable measure of the magnitude of the internal heat source could not be derived until the Pioneer 10 infrared radiometer measured the energy radiated into large phase angles (Chase *et al.*, 1974; Conrath *et al.*, 1991).

Realizing that the resulting global dynamics would be strongly influenced by both solar insolation and convective transport from lower regions of the planet and that the wind patterns differed drastically from those on Earth, investigators (Ingersoll, 1976; Stone, 1976; Williams, 1978) developed initial models. As this work progressed, it led to the formulation of basic questions that influenced the selection and design of spacecraft and instruments. Some of these basic questions were:

- What energy source maintains the zonal winds and generates multiple jets?
- How do the winds vary with depth? Are they related to deep organized cylindrical flows?
- How does the atmospheric temperature vary with depth, latitude and time?
- How do large long-lived systems maintain themselves?
- Why are equatorial winds on Saturn stronger than those on Jupiter?

Ongoing efforts to interpret the dynamic aspects of Jupiter in the post-Galileo epoch are summarized by Ingersoll *et al.* (2004).

5. Investigation of Jupiter's Atmosphere

Although the Pioneer 10 and 11 missions flew by Jupiter in 1973 and 1974 and obtained significant data that characterized the magnetic field and provided excellent photometry of the upper haze layers of the atmosphere, the spin-scan design and collection rate of the photometer allowed the reconstruction of only a few images, which combined with the limited resolution of the IR camera, did not provide a wealth of dynamical data.

When Voyager 1 and 2 arrived at Jupiter in 1979, the improved spatial resolution (500 to 50 km per pixel during periods of global coverage) and enhanced development of infrared instrumentation provided significant time sequences and latitudinal resolution to allow derivation of significant parameters. Global map sequences revealing cloud translations were utilized to generate maps of the global wind pattern and insight into wave phenomena and cloud development (Ingersoll *et al.*, 1981). Within the context of the stability of the zonal winds, the intensity of eddy activity was surprising and highlighted the fact that the manner in which convection was included in models that attempted to generate the global circulation was critical. Infrared observations with IRIS were used to derive equator-to-pole temperature trends and belt-zone temperature differences (Conrath *et al.*, 1981). In addition, these data revealed a latitudinal dependence and equatorial enhancement of the ammonia and hydrogen ortho-para ratio that could be used to constrain equatorial upwelling (Conrath and Gierasch, 1984). Analysis of high-resolution imaging sequences of selected cloud structures provided insight into how long-lived features such as the Red Spot and White Ovals interacted with the surrounding environment and allowed determination of average lifetimes of typical features (Mitchell *et al.*, 1981). Also, temperature-pressure (T/P) relations were

obtained from radio occultation data (Lindal *et al.*, 1981), probing to a depth of about one bar of pressure and revealing a near adiabatic T/P relation in the lower levels. Estimated energies from observations of lightning were large and suggested vigorous convective activity (Borucki *et al.*, 1982) although the mechanism for generation was not understood. These results accentuated the need to understand the composition of the atmosphere, the nature of the deep winds and the role that water played in the atmospheric dynamics and increased interest in the potential of the expected yield from the Galileo Probe.

In response to the announcement that comet Shoemaker-Levy 9 was doomed to plunge into Jupiter, the Space Telescope Science Institute organized a team to optimize the use of the Hubble Space Telescope and other observers acquired access to large ground-based telescopes to carry out an observing campaign to assess the response of the atmosphere to the impacts. From the dynamical point-of-view, the response was disappointing. Most of the material exited from the atmosphere back out along the entry corridor, the ejecta was propelled to high altitudes and accelerated as it fell back, resulting in generation of stratospheric phenomena and no observable perturbation in the underlying troposphere. The dark cooling material dispersed and was weakly entrained in jets and more strongly in the perimeter of cyclonic systems in belts, indicating a decrease of the jet velocity with altitude. A more spectacular phenomenon was the dark expanding rings (Hammel *et al.*, 1995). The observed velocities of expansion were too slow for sound waves and too fast for gravity waves near or below the cloud deck which led Ingersoll and Kanamori (1995) to propose a stratified layer that required enhanced water (10 x solar). This prediction was not validated by the Galileo probe and Walterscheid *et al.* (2000) have argued that the apparent velocity could be explained as stratospheric gravity waves and would not provide a constraint on water abundance.

The Galileo spacecraft was inserted in an equatorial orbit in order to use the Galilean satellites as "tour engines" to optimize global investigations of the four satellites. This required an approach that constrained the probe entry site to low latitudes. Initial plans were to enter near the equator, but delays forced the site northward and, although the Galileo planners were aware that $+7^\circ$ latitude was the most longitudinally variable region on the planet, they had no choice. The probe entered a region that radiated strongly at 5-micron (Orton *et al.*, 1998), indicating below average cloud cover. The transmitted data was used to derive temperature, composition, wind, cloud, and radiation profiles at one point on the planet down to 22 bars.

The noble gases were measured directly by the mass spectrograph (Niemann *et al.*, 1998). Neon was found to be deficient relative to solar abundance while Ar, Kr and Xe were enhanced by about a factor of 2.5 and carbon and nitrogen by a factor of 3. The oxygen abundance was not determined. H_2O, although deficient relative to solar abundance, was still increasing at 19 bars. The lack of detection of multiple cloud layers (Sromovsky *et al.*, 1996) that had been predicted in static chemical equilibrium models (Lewis, 1969) and the fact that the region appeared

to be an anomalous "hot spot" raised questions of interpretation. Characterization of this region as a hot spot was complicated by analysis of the Doppler shift of the transmitted signal by Atkinson *et al.* (1998), who found Doppler velocities that increased strongly with depth from 1 to 4 bars and then remained constant down to 22 bars. This indicates that the increase of winds with depth would exert a strong horizontal shear on the hot spot and that the degree of longitudinal shearing would be such that humidity conditions experienced in the spot should be typical of that latitudinal region. If this downwelling and low humidity is the result of interaction of the prevailing wave pattern with the underlying atmosphere (Showman and Dowling, 2000), this latitudinal region may be anomalously dry. There is no observational evidence of a similar wave pattern in the analogous region in the southern hemisphere. The longitudinal scale of cloud features in the south at -7° latitude is much smaller, possibly due to influence of the Red Spot. No other equatorward edge of a belt displays large-scale longitudinal periodicity in cloud structure. Thus, the conditions in the region of probe entry may or may not characterize typical belt regions. The fact that the Galileo probe entered a latitudinal region that may be nonrepresentative of the Jovian atmosphere and failed to determine the water content in a region that was not modified by prevailing weather conditions provides strong arguments for multiple probe to depths below the weather layer, a technologically challenging task.

Plans for the Galileo orbiter included extensive mapping of cloud structures and motions, mapping lightning sites observed on the dark side of the planet and correlating them with cloud structure and comparing imaging and IR spectra in searches for vertical transport and observable water. The crumpled antenna required that plans be drastically reduced, but many of the science goals were achieved. Observations of thunderstorms west of the Red Spot allowed analysis of the storms and estimates of vertical heat transport combined with the incidence of lightning in the belts led Gierasch *et al.* (2000) and Ingersoll *et al.* (2000) to propose that the excess internal heat is balanced by moist convection in the belts. And, although the data rate greatly inhibited retrieval of data, limited observations in visual and IR provided high resolution data to validate the lack of significant variation in the zonal winds and to progress in understanding the detailed structure and velocities of active regions and long-lived features (Vasavada *et al.*, 1998).

Galileo disappointments were due not only to limited areal and temporal coverage but also evidence that fresh clouds have little vertical scale and emerging structures are quickly contaminated with smog, masking vertical motion. Determinations of cloud depths using filters at visible wavelengths (Banfield *et al.*, 1998) were limited. Mapping of variations in chemical composition were equally disappointing. Using IR mapping, Baines *et al.* (2002) detected NH_3 ice clouds south of the $+7^\circ$ hot spots but encountered a dearth of detections elsewhere. The scarcity of both NH_3 and H_2O ice was consistent with other observations that have indicated that clouds are located in the troposphere and are observed through overlying gas and haze. Historically, new clouds were reported to be white and became

more "belt-like" with time. Attempts to detect upper altitude decay of the zonal jets through methane filters using HST/NICMOS failed to show longitudinal displacement. These data revealed clouds located in the troposphere and, seen through strong methane filters, the clouds showed no vertical distortion, only the effect of overlying extinction.

Data obtained from the HST and the Infrared Telescope Facility in Hawaii provided a global context for the Galileo data and an ongoing time line to seek information about the constancy of zonal winds, evolution of long-lived features and atmospheric disturbances. Merging of the three white ovals (Simon *et al.*, 1998), changes in cloud reflectivity and possible accelerations (Sánchez-Lavega and Gomez, 1996) have been monitored. The Cassini flyby obtained a new data set that will provide spatial and temporal information that will continue to establish a climatological data set when it is released for public use in 2005.

6. Comparison of Saturn with Jupiter

A telescopic view of Saturn reveals distinct banding parallel to the equator or ring plane. When compared with Jupiter, the color is muted and there is little longitudinal variation. Historically, as summarized by Sánchez-Lavega *et al.* (1993), disturbances were rare but had been used to determine that Saturn possessed a broad equatorial that was about three times as strong as that of Jupiter, and that large equatorial storms had occurred in 1933 and 1960.

The Voyager 1 and 2 encountered Saturn in 1980 and 1981. The sensitivity of the high-resolution video cameras did not extend into the red and near IR where extinction due to hazes would have been smaller. Green filtered images revealed longitudinally organized wave structures and limited scattered spots that could serve as wind markers. A zonal wind profile was derived and it was determined that, unlike on Jupiter, the most active convection was associated with maximum retrograde winds, which were also the regions of lowest reflectivity. The IRIS data was used to derive temperatures and ortho/para ratio as function of latitude. Combining this information with temperature-pressure profiles produced a data set that could be compared with that of Jupiter to test proposed dynamical models.

During the 23-year period between Voyager 2 and Cassini, several significant events have been monitored with HST. The 1990 Equatorial storm (Barnet *et al.*, 1992; Beebe *et al.*, 1992) provided markers to study storm dispersal in the equatorial region. This storm appeared to consist of a single convective disturbance that interacted with the surrounding wind field, generating a complex pattern of turbulent clouds and apparent wave structures. The abrupt onset, rapid quenching and the fact that it was the third of a series of similar disturbances, separated by approximately two Saturnian years raised many questions concerning the structure and time response of the atmosphere.

The UV capabilities of the HST were utilized by Edgington *et al.* (2000) to monitor seasonal changes in upper hazes and Sánchez-Lavega *et al.* (2003) have reported observations that indicate a large decrease in the speed of the equatorial prograde jet. If Cassini verifies that this is a change in the velocity of the jet, not a superposed wave phenomenon, it will add additional confusion to our understanding of the circulation of the Gas Giants.

Many approaches to modeling various components of the dynamical phenomena in the Gas Giant atmospheres have been utilized and are reviewed by Ingersoll *et al.* (2004). The Cassini infrared data Russell (2002a; 2002b) will contribute additional information and possibly clarify why the observed cloud motion in Saturn's atmosphere, when referenced to the rotation period of the radio signal, is predominately eastward. Also, interpretation of dynamical data from Titan, a more earthlike atmosphere, subjected to the same seasonal and insolation parameters may influence further modeling of atmospheric responses in the outer Solar System.

7. The Cassini Mission

The Cassini remote sensing that can contribute to our understanding of the dynamics of the Gas Giants includes radio occultations, UV (UVIS), Visual (ISS), and IR (VIMS and CIRS) Russell (2002a; 2002b) observations. In a sequence of gravity assists to reach Saturn, Cassini flew by Jupiter and obtained spatially and temporally resolved data in 2000 - 2001. Using automatic correlation on a time series of global mosaics, Porco *et al.* (2003) measured winds that were similar to those found by Voyager. The ISS team also produced a north polar map defining zonal organization at high latitudes. The time sequence and red sensitivity allow determination of the smaller zonal velocities further defining the global circulation at high latitudes. Enhanced sensitivity of CIRS, relative to IRIS, allowed the production of four 7.1 to 16.7 micron global mapping sequences with 3° latitude resolution and excellent spectral resolution. Utilizing these data Achterberg *et al.* (2003) retrieved NH_3 at the 400-500 mbar level and showed that the mole fraction is strongly anticorrelated with zonal mean temperatures indicating that meridional variations in temperature and ammonia are due to upwelling and subsidence associated with slow meridional circulation.

The Jupiter Cassini observations demonstrated that all four remote sensing instruments are functional and, relative to Voyager, produce improved spatial and spectral resolution for application to Saturn. Enhanced IR capabilities offer promise for better mapping of time-variable atmospheric behavior. The Jovian data set will be compared with that of Saturn to constrain models of the Gas Giants.

Saturn expectations are high. The low scattered light and enhanced near-IR capabilities of the ISS NA/WA cameras and VIMS spatial and frequency resolution promise better mapping of convective activity. The CIRS capabilities will yield Or-

tho/Para observations of 1° latitude resolution, temperature maps with 0.1° latitude resolution and global coverage with high frequency resolution will allow mapping of trace components and their relation to zonal winds and convective activity. UVIS observation will provide information on polar hazes and polar circulation. Early observations are promising, but will Saturn cooperate? Will we see ortho/para disequilibrium and NH_3 at the observable altitudes? Will we get valid cloud markers to separate winds from phase speeds? Has the equatorial jet decreased as reported by Sánchez-Lavega *et al.* (2003) or will we be able to separate wave motion from zonal flow?

8. Beyond Cassini

Information concerning the deep atmospheres and basic interior structures is needed to understand the atmospheric dynamics of the Gas and Ice Giants. Parameters that would characterize the deep atmospheres as well as the interiors include the determination of elemental abundances below the weather deck (O, C, N, S, H and He), measurement of the deep winds and an understanding of the nature of convection as a function of depth, atmospheric properties as a function of latitude and longitude with depth, internal mass distribution and core sizes and the structure of magnetic fields and their depth of formation. A better understanding of these parameters would enhance our understanding of the dynamics and coupling between the deep atmosphere and the interior and would also provide valuable constraints for planetary formation in general.

Detailed measurements of the gravitational and magnetic fields at varying latitudes and distances are needed to characterize the internal mass distribution and to understand at what depth the magnetic field is generated. These are best done from an inclined elliptical orbit with a periapse that is nearly atmospheric grazing that would precess through a range of orbital inclinations. A similar orbit is needed to avoid synchrotron radiation while obtaining global microwave mapping that, when combined with probe data, could provide information concerning the latitudinal distribution and longitudinal variation of water and ammonia over the planet.

Planned NASA missions to the outer solar system are dominated by the Jupiter Icy Moon Orbiter (JIMO). This is a mission that is committed to detailed exploration of the three outer Galilean satellites and scheduled to launch no sooner than 2015. In order to avoid component damage due to Jupiter's intense radiation the minimum distance of approach of the craft to Jupiter will be no closer than the orbit of Europa. Although the design allows large power consumption and high communication rates, the current mass limitation and equatorial orbit will limit its use for atmospheric objectives. Instrumentation will be dominated by requirements to attain satellite goals, and the remoteness of the orbit will not allow detection of detailed gravitational or magnetic fields. An approach to utilize microwave detectors to probe the depths and obtain information about water abundance cannot

be carried out. In addition, the mass constraints and equatorial orbit rule out the possibility of launching and communicating with atmospheric probes.

A second possibility to obtain Gas Giant information was described in the NRC Decadal Report (2003). This mission would utilize a Jupiter polar orbiter with multiple probes and remote microwave sensing. The proposed orbit would be optimized to produce detailed maps of the gravitational and magnetic fields, and to characterize the internal mass distribution and the nature of magnetic field. The probes would measure winds and composition as a function of depth below the weather deck and microwave global mapping would be carried out to map variations in temperature and H_2O. This mission has been included in the current NASA New Frontiers competition. Limited budget and costing policies will dominate the proposed approach and will define what is possible within the New Frontiers line. Whether it will be selected for further development is currently unknown; however if it were, the need for multiple probes would not be addressed, limiting knowledge of the deep atmosphere.

To understand the conditions in the deep atmospheres considerable technology development is needed. Missions that can deliver multiple probes to selected latitudes and place magnetically clean, relatively passive craft in low, near polar elliptical orbits are needed. If the Prometheus program continues to develop capabilities beyond JIMO, a large spacecraft might deliver and serve the individual components of these investigations. How these missions would utilize the nuclear ion drive technology is yet to be determined; however, it is apparent that a range if capabilities of radioisotope generators radioisotope thermoelectric generators (RTGs) would be needed. In order to sound below the weather layer (200 bars or more) to understand the deep atmosphere, probes with multiple stages and adequate power supplies to relay information through the overlying atmosphere will be needed. This will also require development of new heat shields as well as advances in instrumentation to better define composition and structure as a function of depth. Combinations of orbiters and probes, possibly communicating with an orbiting telecommunication station should be considered.

In order to better understand the differences between Gas Giants and Ice Giants, similar missions are needed to at least one of each type of planet. Because of problems of ring avoidance, Jupiter is the favored Gas Giant. It is not clear which Ice Giant would be most interesting. The richness of the Neptunian system and interest in Triton and the complex ring structure would favor a complex mission that could support small orbiters as well as multiple probes. But if Uranus were to show considerable response to seasonal changes, the community involved in solar systems formation and evolution would campaign strongly for a mission to characterize Uranus at equinox.

These missions will not occur in the near future; however, considerable Galileo and Cassini data will be available and will provide constraints for modeling the dynamics of the Gas Giants. And, although there is no mission to the Ice Giants, observations of Uranus promise to provide constraints that will challenge mod-

elers. The combination of visible and IR wind measurements and latitudinally resolved microwave data combined with the approach of Uranian equinox will allow a search for evidence that Uranus is adjusting to the polar radiation that it has received in the last 20 years. Neptune should be included in this effort to provide additional constraints and the results from this combined effort should funnel into optimizing missions to study the dynamics of the Ice Giants.

References

Achterberg, R.K., Conrath, B.J., Gierasch, P.J., and Flasar, F.M.: 2003, 'Cassini CIRS Observations of Ammonia in Jupiter's Upper Troposphere', *BAAS* **34**, 900.

Alexander, A.F.O.: 1965, *The planet Uranus: The history of observation, theory and discovery*, Faber and Faber, London.

Atkinson, D.H., Pollack, J.B., and Seiff, A.: 1998, 'The Galileo probe Doppler Wind Experiment: Measurement of the deep zonal winds on Jupiter', *J. Geophys. Res.* **103**, 22911–22928.

Baines K.H., Carlson, R.W., and Kamp, L.W.: 2002, 'Fresh ammonia ice clouds in Jupiter I. spectroscopic identification, spatial distribution, and dynamical implications', *Icarus* **159**, 74–94.

Banfield, D., Gierasch, P.J., Bell, M., Ustinov, E., Ingersoll, A.P., Vasavada, A.R., West, R.A., and Belton, M.J.S.: 1998, 'Jupiter's cloud structure from Galileo imaging data', *Icarus* **135**, 230–250.

Barnet, C.D., Westphal, J.A., Beebe, R.F., and Huber, L: 1992, 'Hubble Space Telescope observations of the 1990 Equatorial Disturbance on Saturn: Winds and Central Meridian Albedos', *Icarus* **100**, 499–511.

Beatty, J.K., Peterson, C.C., and Chaikin, A. (eds): 1999, *The New Solar System, 4^{th} Edition*, Cambridge University Press, London.

Beebe, R.F., Barnet, C., Sada, P.V., and Murrell, A.S.: 1992, 'The onset and growth of the 1990 equatorial Disturbance on Saturn', *Icarus* **95**, 163–172.

Borucki, W.J., Bar-Nun, A., Scarf, F.L., Cook, A.F., and Hunt, G.E.: 1982, 'Lightning activity on Jupiter', *Icarus* **52**, 492–502.

Chase, S.C., Ruiz, R.D., Munch, G., Neugebauer, G., Schroeder, G., and Trafton, L.M.: 1974, 'Pioneer 10 infrared radiometer experiment: preliminary results', *Science* **183**, 315–317.

Conrath, B.J., Flasar, F.M., Pirraglia, J.A., Gierasch, P.J., and Hunt, G.E.: 1981, 'Thermal structure and dynamics of the Jovian atmosphere. 2. Visible cloud features', *J. Geophys. Res.* **86**, 8769–8775.

Conrath, B.J. and Gierasch, P.J.: 1984, 'Global variation of the para hydrogen fraction in Jupiter's atmosphere and implications for dynamics on the outer planets', *Icarus* **57**, 184–204.

Conrath, B.J., Pearl, J.C., Appleby, J.F., Lindal, G.F., Orton, G.S., and Bezard, B.: 1991, 'Thermal structure and energy balance of Uranus', *in* J. Bergstrahl, E. Miner, and M. Matthews (eds.), *Uranus*, Univ. of Arizona Press, Tucson, pp. 204–252.

Edgington, S.G., West, R.A., Friedson, A.J., and Atreya, S.K.: 2000, 'A 2-D photochemical model with meridional circulation', *BAAS* **32**, 1013.

Gierasch, P.J., Ingersoll, A.P., Banfield, D., Ewald, S.P., Helfenstein, P., Simon-Miller, A., Vasavada, A., Breneman, H.H., Senske, D.A., and the Galileo Imaging team: 2000, 'Observation of moist convection in Jupiter's atmosphere', *Nature* **403**, 628–630.

Hammel, H.B., Beebe, R.F., de Jong, E.M., Hansen, C.J., Howell, C.D., Ingersoll, A.P., Johnson, T.V., Limaye, S.S., Magalhães, J.A., Pollack, J.B., Sromovsky, L.A., Suomi, V.E., and Swift, C.E.: 1989. 'Neptune's wind speeds obtained by tracking clouds in the Voyager images', *Science* **245**, 1367–1369.

Hammel, H.B.: 1989, 'Discrete cloud structure on Neptune', *Icarus* **80**, 14–22.

Hammel, H.B., Beebe, R.F., Ingersoll, A.P., Orton, G.S., Mills, J.R., Simon, A.A., Chodas, P., Clarke, J.T., De Jong, E., Dowling, T.E., Harrington, J., Huber, L.F., Karkoschka, E., Santori, C.M., Toigo, A., Yeomans D., and West R.A.: 1995, 'HST imaging of atmospheric phenomena created by the impact of Comet Shoemaker-Levy 9', *Science* **267**, 1288–1296.

Hammel, H.B., Rages, K., Lockwood, G.W., Karkoschka, E., and de Pater, I.: 2001, 'New Measurements of the Winds of Uranus', *Icarus* **153**, 229–235.

Hofstadter, M.D. and Butler, B.J.: 2003, 'Seasonal change in the deep atmosphere of Uranus', *Icarus* **165**, 168–180.

Ingersoll, A.P.: 1976, 'The atmosphere of Jupiter', *Space Sci. Rev.* **18**, 603–639.

Ingersoll, A.P., Beebe, R.F., Mitchell, J.L., Garneau, G.W., Yagi, G.M., and Muller J.P: 1981, 'Interaction of eddies and mean zonal flow on Jupiter as inferred from Voyager 1 and Voyager 2 images', *J. Geophys. Res.* **86**, 8733–8743.

Ingersoll, A.P. and H. Kanamori: 1995, 'Waves from the collisions of Comet Shoemaker-Levy 9 with Jupiter', *Nature* **374**, 706–708.

Ingersoll, A.P., Gierasch, P.J., Banfield D., and Vasavada A.R.: 2000, 'Moist convection as an energy source for the large-scale motions in Jupiter's atmosphere', *Nature* **403**, 630–632.

Ingersoll, A.P., Dowling, T.E., Gierasch, P.J. , Orton, G.S., Read, P.L., Sanchez-Lavega, A., Showman, A.P., Simon-Miller, A.A., and Vasavada, A.R.: 2004, 'Dynamics of Jupiter's Atmosphere', *in* F. Bagenal, T. Dowling, and W. McKinnon (eds.), *Jupiter: The Planet, Satellites and Magnetosphere*, Cambridge University Press, London.

Karkoschka, E.: 1998, 'Clouds of High Contrast on Uranus', *Science* **280**, 570–572.

Lewis, J.S.: 1969, 'The clouds of Jupiter and the NH_3-H_2O and NH_3-H_2S systems', *Icarus* **10**, 365–378.

Lindal, G.F., Wood, G.E., Levy, G.S., Anderson, J.D., Sweetnam, D.N., Hotz, H.B., Buckles, B.J., Holmes, D.P., Doms, P.E., Eshleman, V.R., Tyler, G.L., and Croft, T.A.: 1981, 'The atmosphere of Jupiter: An analysis of the Voyager radio occultation measurements', *J. Geophys. Res.* **86**, 8721–8727.

Lindal, G.F., Lyons, J.R., Sweetnam, D.N., Eshleman, V.R., and Hinson, D.P.: 1987, 'The atmosphere of Uranus – Results of radio occultation measurements with Voyager 2', *J. Geophys. Res.* **92**, 14987–15001.

Lockwood, G.W. and Thompson, D.T.: 1999, 'Photometric variability of Uranus, 1972-1996', *Icarus* **137**, 2–12.

Lockwood, G.W. and Thompson, D.T.: 2002, 'Photometric variability of Neptune, 1972-2000', *Icarus* **156**, 37–51.

Mitchell, J.L., Beebe, R.F., Ingersoll, A.P., and Garneau: 1981, 'Flow fields within Jupiter's Great Red Spot and White Oval BC', *J. Geophys. Res.* **86**, 8751–8757.

Niemann, H.B., Atreya, S.K., Carignan, G.R., Donahue, T.M., Haberman, J.A., Harpold, D.N., Hartle, R.E., Hunten, D.M., Kasprzak, W.T., Mahaffy, P.R., Owen T.C., and Way, S.H.: 1998, 'The composition of the Jovian atmosphere as determined by the Galileo probe mass spectrometer', *J. Geophys. Res.* **103**, 22831–22845.

NRC Decadal Report Book #0-309-08495-4: 2003, *New Frontiers of the Solar System: An Integrated Exploration Strategy*, National Academies Press, Washington, D.C.

Orton, G.S., Fisher, B.M., Baines, K.H., Stewart, S.T, Friedson, A.J., Ortiz, J.L., Marinova, M., Ressler, M., Dayal, A., Hoffmann, W., Hora, J., Hinkley, S., Krishnan, V., Masanovic, M., Tesic, J., Tziolas, A., and Parija, K.C.:1998, 'Characteristics of the Galileo probe entry site from Earth-based remote sensing observations', *J. Geophys. Res.* **103**, 22791–22814.

Peek, B.M.: 1958, *The Planet Jupiter*, Faber and Faber, London.

Porco, C.C., West, R.A., McEwen, A., Del Genio, A.D., Ingersoll, A.P., Thomas, P., Squyres, S., Dones, L., Murray, C.D., Johnson, T.V., Burns, J.A., Brahic, A., Neukum, G., Veverka, J., Barbara, J.M., Denk, T., Evans, M., Ferrier, J.J., Geissler, P., Helfenstein, P., Roatsch, T., Throop, H.,

Tiscareno, M., and Vasavada, A.R.: 2003, 'Cassini imaging of Jupiter's atmosphere, satellites, and rings', *Science* **299**, 1541–1547.

Russell, C.T. (ed.): 2002a, 'The Cassini/Huygens Mission I', *Space Sci. Rev.* **104**, 1–640.

Russell, C.T. (ed.): 2002b, 'The Cassini/Huygens Mission II', *Space Sci. Rev.* **104**, 509–679.

Sánchez-Lavega, A., Lecacheux, J., Colas, F., and Laques, P.: 1993, 'Temporal behavior of cloud morphologies in Saturn's atmosphere', *J. Geophys. Res* **98**, 18857–18872.

Sánchez-Lavega, A., and Gomez, J.M.: 1996, 'The South Equatorial Belt of Jupiter 1. Its Life Cycle', *Icarus* **121**, 1–17.

Sánchez-Lavega, A., Pérez-Hoyos, S., Rojas, J.F., Hueso, R., and French, R.G.: 2003, 'A strong decrease in Saturn's equatorial jet at cloud level', *Nature* **423**, 623–625.

Showman, A.P., and Dowling, T.E.: 2000, 'Nonlinear simulations of Jupiter's 5-μm hot spots', *Science* **289**, 1737–1740.

Simon, A.A., Beebe, R.F., Gierasch, P.J., Vasavada A.R., and Belton M.J.S.: 1998, 'Global context of the Galileo E6 observations of Jupiter's White Ovals', *Icarus* **135**, 220–229.

Smith, B.A., Soderblom, L.A., Beebe, R., Bliss, D., Boyce, J.M., Brahic, A., Briggs, G.A., Brown. R.H., Collins, S.A., Cook, A.F., Croft, S.K., Cuzzi, J.N., Danielson, G.E., Davies, M.E., Dowling, T.E., Godfrey, D., Hansen, C.J., Harris, C., Hunt, G.E., Ingersoll, A.P., Johnson, T.V., Krauss, R.J., Masursky, H., Morrison, D., Owen, T., Plescia, J.B., Pollack, J.B., Porco, C.C., Rages, K., Sagan, C., Shoemaker, E.M., Sromovsky, L.A., Stoker, C., Strom, R.G., Suomi, V.E., Synnott, S.P., Terrile, R.J., Thomas, P., Thompson, W.R., and Veverka., J.: 1986, 'Voyager 2 in the Uranian system - Imaging science results', *Science* **233**, 43–64.

Smith, B.A., Soderblom, L.A., Banfield, D., Barnet, C., Basilevksy, A.T., Beebe, R.F., Bollinger, K., Boyce, J.M., Brahic, A., Briggs, G.A., Brown, R.H., Chyba, C., Collins, S.A., Colvin, T., Cook, A.F., Crisp, D., Croft, S.K., Cruikshank, D., Cuzzi, J.N., Danielson, G.E., Davies, M.E., De Jong, E., Dones, L., Godfrey, D., Goguen, J., Grenier, I., Haemmerle, V.R., Hammel, H., Hansen, C.J., Helfenstein, C.P., Howell, C., Hunt, G.E., Ingersoll, A.P., Johnson, T.V., Kargel, J., Kirk, R., Kuehn, D.I., Limaye, S., Masursky, H., McEwen, A., Morrison, D., Owen, T., Owen, W., Pollack, J.B., Porco, C.C., Rages, K., Rogers, P., D. Rudy, C., Sagan, C., Schwartz, J., Shoemaker, E.M., Showalter, M., Sicardy, B., Simonelli, D., Spencer, J., Sromovsky, L.A., Stoker, C., Strom, R.G., Suomi, V.E., Synott, S.P., R.J., ; P. Thomas, P., Thompson, W.R., Verbiscer, A., and Veverka, J.: 1989, 'Voyager 2 at Neptune - Imaging science results', *Science* **246**, 1422–1449.

Sromovsky, L.A., Best, F.A., Collard, A.D., Fry, P.M., Revercomb, H.E., Freedman, R.S., Orton, G.S., Hayden, J.L., Tomasko, M.G., and Lemmon, M.T.: 1996, 'Solar and thermal radiation in Jupiter's atmosphere: Initial results of the Galileo Probe Net Flux Radiometer', *Science* **272**, 851–854.

Sromovsky, L.A., Fry, P.M., Dowling, T.E, Baines, K.H., and Limaye, S.S.: 2001, 'Coordinated 1996 HST and IRTF imaging of Neptune and Triton III. Neptune's atmospheric circulation and cloud structure', *Icarus* **149**, 459–488.

Stone, P.H.: 1976, 'The meteorology of the Jovian atmosphere', *in* T. Gehrels (ed.), *Jupiter*, University of Arizona Press, Tucson, 586–615.

Vasavada, A.R., Ingersoll, A.P., Banfield, D., Bell, M., Gierasch, P.J., Belton, M.J.S., Orton, G.S., Klaasen, K.P., De Jong, E., Breneman, H.H., Jones, T.J., Kaufman, J.M., Magee K.P., and Senske D.A.: 1998, 'Galileo imaging of Jupiter's atmosphere: The Great Red Spot, equatorial region, and White Ovals', *Icarus* **135**, 265–275.

Walterscheid, R.L., Brinkman D.G., and Schubert, G.: 2000, 'Wave disturbances from the Comet SL-9 impacts into Jupiter's atmosphere', *Icarus* **145**, 140–146.

Williams, G.P.: 1978, 'Planetary circulations 1. Barotropic representation of Jovian and terrestrial turbulence', *J. Atmos. Sci.* **35**, 1399–1426.

Address for Offprints: Reta F. Beebe, Department of Astronomy, P.O. Box 30001, MS 4500, New Mexico State University, Las Cruces, NM 88003, USA; rbeebe@nmsu.edu

PHOTOCHEMISTRY IN OUTER SOLAR SYSTEM ATMOSPHERES

DARRELL F. STROBEL
Department of Earth and Planetary Sciences, Johns Hopkins University, Baltimore, MD 21218, USA

Received: 21 April 2004; Accepted in final form: 2 September 2004

Abstract. The photochemistries of the H_2-He atmospheres of the gas giants Jupiter, Saturn and ice giants Uranus and Neptune and Titan's mildly reducing N_2 atmosphere are reviewed in terms of general chemical and physical principles. The thermochemical furnace regions in the deep atmospheres and the photochemical regions of the giant planets are coupled by vertical mixing to ensure efficient recyling of photochemical products. On Titan, mass loss of hydrogen ensures photochemical evolution of methane into less saturated hydrocarbons. A summary discussion of major dissociation paths and essential chemical reactions is given. The chapter ends with a overview of vertical transport processes in planetary atmospheres.

Keywords: planetary atmospheres, photochemistry

1. Introduction

The atmospheres in the outer solar system can be divided into two broad classes: 1) the hydrogen/helium atmospheres of the gas giants Jupiter and Saturn and of the ice giants Uranus and Neptune, and 2) the nitrogen atmospheres of Titan, Triton, and Pluto. A first order description of the atmospheric composition of the giant planets can be given by starting with a solar system chemistry set containing the elemental abundances of our Sun and calculating the abundances of gaseous compounds based on thermodynamic equilibrium. Given the range of temperatures and the high pressures in the adiabatic hydrogen-helium envelopes of the giant planets, thermochemistry predicts and observations confirm that the saturated hydrides are the predominant compounds from the reactive elements. Thus H becomes H_2, C, N, O, and S become CH_4, NH_3, H_2O, and H_2S, etc. In the chapter on composition (Encrenaz, 2004), one finds that the gas giants are enriched in the heavier elements by a factor of ~ 3, whereas the ice giants are enriched by a factor of ~ 30, presumably due to the accretion of icy planetesimals to form a core of heavy elements.

Thermochemistry predicts in the opposite limit of low pressures, high temperatures that most abundant forms of C and N are CO and N_2. Nitrogen atmospheres can be form directly from outgassing of N_2 from an ice clathrate or from the photochemical destruction of a primitive NH_3 atmosphere, as discussed by (Lunine, 2004) and for the latter scenario below.

Photochemistry is driven by solar UV, EUV radiation and in a liberal definition of the word, energetic electrons. These drivers may be represented by equiva-

Space Science Reviews 116: 155–170, 2005.
DOI: 10.1007/s11214-005-1953-3

lent temperatures of $T_{\text{photons}} > 6000$ to 2,000,000 K, and $T_{\text{electrons}} > 1$ keV $\sim 10^7$K, which may be compared to the thermochemical furnace regions on the giant planets, where $T \geq 1000$ K. One important consideration in photochemistry is whether atmospheric mass loss of various elements is significant. The relevant non-dimensional parameter for atmospheric mass loss is the Jeans parameter $\lambda = v_{\text{esc}}^2/U^2$, where U is the most probable velocity of a Maxwellian distribution and v_{esc} is the escape velocity at the exobase from the planet/satellite's gravitational potential well. The Jeans parameter can be written as

$$\lambda = \frac{r_{\text{exobase}}}{H} = \frac{\text{gravitational potential energy}}{\text{random kinetic energy}} . \tag{1}$$

For the giant planets the respective values of λ at their exobases are 480, 420, 50, and 120 for Jupiter, Saturn, Uranus, and Neptune (Strobel, 2002). Thus atmospheric mass loss is negligible on the giant planets and chemistry occurs as a closed system. Atmospheric motions couple photochemical regions in atmospheric regions above the cloud tops ($p < 1$ bar) where $T < 1000$ K, with the thermochemical furnace regions at $T > 1000$ K. This ensures recycling and no irreversible destruction of saturated hydrides, with specific emphasis on CH_4.

Generally, for thermal escape to be important, λ must be less than 10. Thus even for Titan, Triton, and Pluto, with their respective λ values for N_2 of 45, 23, and unknown, but possibly ~ 10, escape of N atoms and N_2 is not important for photochemistry and perhaps even photochemical evolution. However the Jeans parameter, which is proportional to mass of the atom or molecule, is very small for H and H_2 at the exobases and their escape occurs at the maximum permissible rate. Thus in the photochemistry of CH_4 the loss of hydrogen leads to the irreversible conversion of CH_4 to less saturated hydrocarbons, C_xH_y, where $y < 4x$, in this open chemical system with escaping hydrogen.

There are three basic approaches to the study of the chemistry in planetary atmospheres. One is thermodynamic equilibrium calculations. For these calculations to be valid, the time scales for approaching equilibrium must be short in comparison to the relevant time scales for solar system formation and geological processes. In addition, the appropriate equilibrium quenching temperatures must be known.

The second approach is laboratory experiments, which require critical compromises in pressure, mixing ratios, etc., to simulate an atmosphere due to constraints on the size of laboratory equipment. The smallest macroscopic length scale in the atmosphere is the scale height which is in the range of $10 - 100$ km, whereas laboratory equipment is typically a few cm to m. Hence experimental results must be scaled appropriately to be applicable to atmospheres.

The third approach is absolute reaction rate kinetics, which is the underpinning of photochemical calculations. Here models require a detailed, accurate description of all important reactions, photochemical processes, transport, and constituents. Omission of one important reaction will lead to spurious results. Current accuracy of laboratory rate coefficients is $\sim \pm 20\%$. A model with many reactions may

require more precision than this to produce accurate results. The bottom line is that atmospheric measurements are extremely important in order to differentiate between what we think is there from what is there and with what abundance and distribution.

For reasons of brevity, the reader is referred to Strobel (1983) for details and citations. Space limitations prevent a discussion of the photochemistry of the N_2 atmospheres of Triton and Pluto. The reader is referred respectively to Strobel and Summers (1995) and Summers *et al.* (1997).

2. Photochemistry of H_2-He Atmospheres

In the atmospheres of the giant planets, the photochemistry of H_2 and CH_4 is common to all, whereas the photochemistry of other hydrides NH_3 and PH_3 is only relevant on Jupiter and Saturn. The UV photons that initiate the photochemistry of these hydrides do not penetrate deeply enough to reach these condensable species in the cold upper tropospheres of the ice giants.

2.1. Photochemistry of H_2

Molecular hydrogen absorbs, principally, solar EUV radiation below 84.5 nm with a typical cross section on the order of 10^{-17} cm^2. Since it is the dominant constituent in these atmospheres, its photochemistry occurs in their thermospheres and leads to the formation of their ionospheres. Specifically, H_2 has an ionization continuum below 80.4 nm and a dissociation continuum below 84.5 nm

$$H_2 + h\nu(\lambda < 84.5\text{nm}) \rightarrow H + H(^2P) \tag{2}$$

$$H_2 + h\nu(\lambda < 80.4\text{nm}) \rightarrow H_2^+ + e \tag{3}$$

$$H_2 + h\nu(\lambda < 80.4\text{nm}) \rightarrow H^+ + H + e \tag{4}$$

In addition, H_2 dissociates by fluorescence after discrete absorption in the Lyman and Werner band systems. For the Lyman band system, $\lambda < 110.9$ nm

$$H_2(X^1\Sigma_g^+) + h\nu \rightarrow H_2(B^1\Sigma_u^+)_{(v=v')} \rightarrow H_2(X^1\Sigma_g^+)_{(v=v'')} + h\nu \tag{5}$$

If $v'' > 14$, H_2 will dissociate into the vibrational continuum of the ground state.

The ionization of He adds to the production of H_2^+ by

$$He + h\nu(\lambda < 50.4\text{nm}) \rightarrow He^+ + e \tag{6}$$

$$He^+ + H_2 \rightarrow H_2^+ + He \tag{7}$$

At least two H atoms are eventually produced as a result of H_2 ionization, because

$$H_2^+ + H_2 \rightarrow H_3^+ + H \tag{8}$$

$$H_3^+ + e \rightarrow H_2 + H \text{ or } 3\,H, \quad \alpha \simeq 5 \times 10^{-8} \left(\frac{300}{T_e}\right)^{0.5} \text{cm}^3\,\text{s}^{-1} \tag{9}$$

At ionospheric pressures recombination of H is extremely improbable and the ionosphere supplies a downward flux of H atoms to the stratosphere. On Jupiter this globally averaged flux is $\sim 10^9$ cm^{-2} s^{-1} including a contribution from auroral H production, whereas on Saturn, Uranus, and Neptune it can be estimated by scaling the solar flux to get the solar produced portion $\sim 1.2 \times 10^8$, $\sim 3 \times 10^7$, and $\sim 1 \times 10^7$ cm^{-2} s^{-1}, respectively.

The electron densities depend critically on whether H^+ or H_3^+ is the major ion (He^+ is rapidly converted to H_2^+ and thus not important) as radiative recombination of protons is much slower than dissociative recombination of H_3^+

$$H^+ + e \rightarrow H + e, \alpha = 4 \times 10^{-12} \left(\frac{250}{T_e}\right)^{0.7} \text{cm}^3\,\text{s}^{-1}\,. \tag{10}$$

The partitioning of H^+ and H_3^+ depends on the vibrational temperature of H_2 through the exothermic reaction

$$H^+ + H_2(v \geq 4) \rightarrow H_2^+ + H \tag{11}$$

when H_2 is at least in vibrational level 4 or higher, and at higher pressure, protons recombine by

$$H^+ + H_2 + H_2 \rightarrow H_3^+ + H_2\,. \tag{12}$$

In the vicinity of the homopause, ion reactions with hydrocarbons become important

$$H^+ + CH_4 \rightarrow CH_3^+ + H_2 \tag{13}$$
$$H^+ + CH_4 \rightarrow CH_4^+ + H \tag{14}$$
$$CH_4^+ + H_2 \rightarrow CH_5^+ + H \tag{15}$$
$$CH_3^+ + CH_4 \rightarrow C_2H_5^+ + H_2 \tag{16}$$
$$C_xH_y^+ + e \rightarrow C_xH_{y-1}^+ + H \tag{17}$$

This sequence of reactions is also an efficient way to dissociate CH_4 in auroral regions, as the rate of CH_4 dissociation proceeds at the ionization rate of H_2 below the CH_4 homopause. In Jupiter's auroral regions, where energetic particles deposit $\sim 10^{14}$ W of power, this dissociation pathway is substantial.

2.2. Photochemistry of Hydrocarbons

The photochemistry of CH_4 is driven principally by the intense solar Lyman α line at 121.6 nm, because UV radiation is absorbed by CH_4 with a significant cross section only below $\sim$ 145 nm, even though only 4.5 eV is needed to break CH_4 apart. The primary dissociation channels at Lyman-α are

$$CH_4 + h\nu \rightarrow CH_3^* + H \rightarrow CH_3 + H \tag{18}$$
$$\rightarrow {}^1CH_2 + H_2 \tag{19}$$
$$\rightarrow {}^{1\,\text{or}\,3}CH_2 + 2\,H \tag{20}$$
$$\rightarrow CH + H + H_2 \tag{21}$$

The net photochemistry of CH_4 in an H_2 atmosphere can be represented by

$$2(CH_4 + h\nu \rightarrow CH_3 + H) \quad (22)$$
$$2(CH_4 + h\nu \rightarrow CH_2 + H_2) \quad (23)$$
$$2(CH_2 + H_2 \rightarrow CH_3 + H) \quad (24)$$
$$2CH_3 + M \rightarrow C_2H_6 + M \quad (25)$$
$$\text{net} \quad 2\,CH_4 \rightarrow C_2H_6 + 2H \quad (26)$$

$$CH_4 + h\nu \rightarrow CH + H + H_2 \quad (27)$$
$$CH + CH_4 \rightarrow C_2H_4 + H \quad (28)$$
$$\text{net} \quad 2\,CH_4 \rightarrow C_2H_4 + H_2 + 2\,H \quad (29)$$

followed by rapid photolysis of C_2H_4 to form C_2H_2

$$C_2H_4 + h\nu \rightarrow C_2H_2 + H_2 \quad (30)$$
$$C_2H_4 + h\nu \rightarrow C_2H_2 + 2\,H\,. \quad (31)$$

Photolysis of C_2H_2 can lead to catalytic dissociation of CH_4 by the following sequence of reactions

$$C_2H_2 + h\nu \rightarrow C_2H + H \quad (32)$$
$$C_2H_2 + h\nu \rightarrow C_2 + H_2 \quad (33)$$
$$C_2H + CH_4 \rightarrow C_2H_2 + CH_3 \quad (34)$$
$$C_2 + CH_4 \rightarrow C_2H + CH_3 \quad (35)$$
$$\text{net} \quad CH_4 + h\nu \rightarrow CH_3 + H \text{ or } \frac{1}{2}H_2 \quad (36)$$

However if the radicals react preferentially with H_2, which occurs when $T > 150$ K in the stratosphere, then

$$C_2H + H_2 \rightarrow C_2H_2 + H \quad (37)$$
$$C_2 + H_2 \rightarrow C_2H + H \quad (38)$$
$$C_2H + H_2 \rightarrow C_2H_2 + H \quad (39)$$
$$\text{net} \quad 2\,H_2 \rightarrow 4\,H \quad (40)$$

and acetylene photolysis leads to catalytic dissociation of H_2. But acetylene can also catalytically recombine H atoms

$$H + C_2H_2 + M \rightarrow C_2H_3 + M \quad (41)$$
$$H + C_2H_3 \rightarrow C_2H_2 + H_2 \quad (42)$$
$$\text{net} \quad 2\,H \rightarrow H_2 \quad (43)$$

Methane can be partially recycled by the following reaction

$$H + CH_3 + M \rightarrow CH_4 + M \quad (44)$$

and

$$H + C_2H_4 + M \rightarrow C_2H_5 + M \quad (45)$$

$$H + C_2H_5 \rightarrow 2\,CH_3 \quad (46)$$

$$2(H + CH_3 + M \rightarrow CH_4 + M) \quad (47)$$

$$\text{net} \quad C_2H_4 + 4\,H \rightarrow 2\,CH_4 \quad (48)$$

Note that in the latter reaction sequence that H reacts with C_2H_5 to break the double carbon bond, which is the key to recycling CH_4.

2.3. Photochemistry of NH_3 and PH_3

The photochemistry of NH_3 and PH_3 is driven by longer wavelength solar UV radiation, as overlying H_2, CH_4, and C_2H_6 absorbs most solar radiation below 165 nm. On Jupiter NH_3 is more abundant than PH_3, whereas on Saturn this situation is reversed for $p < 1$ bar. For $\lambda > 165$ nm, their photochemistries can be summarized as

$$NH_3 + h\nu \rightarrow NH_2 + H \qquad PH_3 + h\nu \rightarrow PH_2 + H \quad (49)$$

$$NH_2 + NH_2 + M \rightarrow N_2H_4 \qquad PH_2 + PH_2 + M \rightarrow P_2H_4 \quad (50)$$

$$NH_2 + H + M \rightarrow NH_3 \qquad PH_2 + H + M \rightarrow PH_3 \quad (51)$$

At the cold temperatures in the tropopause regions of the giant planets, N_2H_4 certainly condenses and, with the possible exception of Jupiter, the same is true for P_2H_4.

$$(N_2H_4)_g \rightarrow (N_2H_4)_s \qquad (P_2H_4)_g \rightarrow (P_2H_4)_s \quad (52)$$

For the few molecules of N_2H_4 and P_2H_4 in gas phase, they are susceptible to photolysis and H atom attack.

$$N_2H_4 + h\nu \rightarrow N_2H_3 + H \qquad P_2H_4 + h\nu \rightarrow P_2H_3 + H$$

$$N_2H_4 + H \rightarrow N_2H_3 + H_2 \qquad P_2H_4 + H \rightarrow P_2H_3 + H_2$$

$$H + N_2H_3 \rightarrow N_2H_2 + H_2 \qquad H + P_2H_3 \rightarrow P_2H_2 + H_2$$

$$N_2H_3 + N_2H_3 \rightarrow N_2H_4 + N_2H_2 \qquad P_2H_3 + P_2H_3 \rightarrow P_2H_4 + P_2H_2$$

$$N_2H_2 \rightarrow N_2 + H_2 \qquad P_2H_2 \rightarrow P_2 + H_2$$

where N_2H_2 and P_2H_2 spontaneously decompose. Another more direct path to the production of elemental phosphorus is the following

$$H + PH_3 \rightarrow PH_2 + H_2 \quad (53)$$

$$H + PH_2 \rightarrow PH + H_2 \quad (54)$$

$$H + PH \rightarrow P + H_2 \quad (55)$$

$$P + PH \rightarrow P_2 + H \quad (56)$$

but the spin forbidden reactions

$$P + H_2 + M \rightarrow PH_2 + M \quad (57)$$
$$PH + H_2 + M \rightarrow PH_3 + M \quad (58)$$

are important, even if their rate coefficients are as small as $\sim 10^{-41}$ cm^6 s^{-1}. Thus the production of significant amounts of elemental phosphorus, P_x, is highly improbable.

2.4. Photochemistry of CO, CO_2, and H_2O

Although the atmospheres of the giant planets are reducing, there are trace amounts of oxygen present in the form of H_2O and CO in the thermochemical furnace regions and also in the upper atmosphere due to ablation of meteoroidal material, infall of ice particles from rings, oxygen ions from the magnetosphere supplied ultimately from surface oxygen on icy satellites, and comets, e. g. Shoemaker-Levy 9. Historically the origin of CO in upper troposphere/stratosphere of Jupiter was posed as an either internal source or external source of the oxygen for the O in CO. Finally in Bézard *et al.* (2002) convincing data were obtained that there are both internal and external sources. For an external source that delivers oxygen in any form, e. g., O^+, O, H_2O, it will ultimately be converted into almost all CO. Oxygen ions are converted to H_2O by the following sequence of reactions

$$O^+ + H_2 \rightarrow OH^+ + H \quad (59)$$
$$OH^+ + H_2 \rightarrow H_2O^+ + H \quad (60)$$
$$H_2O^+ + CH_4 \rightarrow H_3O^+ + CH_3 \quad (61)$$
$$H_3O^+ + e \rightarrow H_2O + H \quad \text{or} \quad OH + H_2 \quad (62)$$

In the stratospheres of the giant planets where solar UV radiation is restricted to longward of 165 nm, CO_2 and H_2O can undergo rapid photolysis with a time constant that is short in comparison to the vertical transport time constant, whereas CO does not dissociate at these wavelengths. Photolysis of H_2O yields OH, which reacts occasionally with CO to form CO_2 and mostly with H_2 to recycle H_2O. But if OH reacts only once with C_2H_2 or C_2H_4 in a cycle of repeated H_2O dissociations as oxygen is mixed downward toward the tropopause, then oxygen is converted irreversibly to CO. Similarly, O atoms reacts with H_2 to form OH, but when they react with CH_3 to form CH_2O, the final product is also CO. CO cannot be photolyzed or attacked by OH to form CO_2 in the lower stratosphere as H_2O condenses there and removes the OH source. Detailed calculations demonstrate that the ultimate fate of external oxygen is the preferential formation of CO as the reservoir oxygen species above the tropopause.

3. Photochemistry of Titan's N_2 Atmosphere

In contrast to the tightly bound atmospheres of the giant planets with negligible loss of atmosphere, Titan has an extended N_2 atmosphere with an exobase at 0.6 Titan radius from the surface, where hydrogen in atomic and molecular form escapes as rapidly as it can be delivered to the exobase. Its escape rate is governed by the CH_4 dissociation rate. The key to understanding photochemistry of Titan's atmosphere is the irreversible photochemical destruction of CH_4 with almost 100% conversion to less saturated hydrocarbons and escaping hydrogen. Thus Titan's atmospheric environment is highly conducive to chemical evolution and possibly including the evolution of its nitrogen atmosphere from an ammonia atmosphere.

3.1. Photochemistry of NH_3 as the Source of N_2

Ammonia is readily dissociated by solar radiation below 230 nm.

$$NH_3 + h\nu \longrightarrow NH_2 + H \tag{63}$$

If the surface temperature of Titan were at least 150 K in the past due to an atmospheric greenhouse , then there would have been sufficient NH_3 in the atmosphere to absorb all solar photons below 230 nm ($\sim 3.5\times10^{11}$ photons cm^{-2} s^{-1}), whereas if the surface temperature were only 115 K, the reduced vapor pressure of NH_3 would lower its column density and reduce the number of absorbed photons by one-half. The radical NH_2 undergoes reactions

$$NH_2 + H + M \longrightarrow NH_3 + M \tag{64}$$

$$NH_2 + NH_2 + M \longrightarrow N_2H_4 + M \tag{65}$$

$$N_2H_4 + h\nu \longrightarrow N_2H_3 + H \tag{66}$$

$$(N_2H_4)_{(g)} \longrightarrow (N_2H_4)_{(s)}, \quad \text{if } T < 150\,\text{K} \tag{67}$$

The condensation of N_2H_4 stops the conversion of NH_3 to N_2. But if the atmospheric greenhouse were warm enough in the region where most of the photolysis took place, then the conversion proceeds via

$$N_2H_3 + N_2H_3 \longrightarrow N_2H_4 + N_2 + H_2. \tag{68}$$

The N_2 yield per NH_3 dissociation event is ~ 0.15 for a net N_2 production rate of $\sim 5 \times 10^{10}$ cm^{-2} s^{-1}, under current solar luminosity conditions. If the current N_2 column density is divided by this production rate, it takes ~ 200 My or 4% of the age of the solar system to convert an ammonia atmosphere into a nitrogen atmosphere. This process is more than sufficient under appropriate greenhouse conditions to account the present N_2 atmosphere. However, if one chooses to invoke the escape of an initially more massive N_2 atmosphere (> 30 bars) to account for the current enhanced isotopic ratio of $^{15}N/^{14}N$ in HCN (Lunine, 1999), one must invoke a direct source of N_2 such as delivery in ice clathrates.

3.2. PHOTOCHEMISTRY OF HYDROCARBONS

As previously discussed, the photochemistry of CH_4 is driven by solar Lyman α radiation with radical products given by Equation (18). These radicals react to form C_2H_y hydrocarbons.

$$CH_3 + CH_3 + M \longrightarrow C_2H_6 + M \tag{69}$$

$$CH + CH_4 \longrightarrow C_2H_4 + H \tag{70}$$

$$^3CH_2 + CH_3 \longrightarrow C_2H_4 + H \tag{71}$$

$$^3CH_2 + {}^3CH_2 \longrightarrow C_2H_2 + H_2 \quad \text{or} \quad 2\,H \tag{72}$$

$$C_2H_4 + h\nu \longrightarrow C_2H_2 + H_2 \quad \text{or} \quad 2\,H \tag{73}$$

While the direct CH_4 photolysis proceeds at pressures $\sim$ nbar, indirect catalytic dissociation of CH_4 via C_2H_2 dissociation (Equation 32) proceeds at mbar pressures followed by

$$C_2H + CH_4 \rightarrow C_2H_2 + CH_3 \tag{74}$$

$$C_2 + CH_4 \rightarrow C_2H + CH_3 \tag{75}$$

$$\text{net} \quad CH_4 + h\nu \rightarrow CH_3 + H \text{ or } \frac{1}{2}H_2 \tag{76}$$

The combination of direct and indirect CH_4 dissociation coupled with the high efficiency for hydrogen escape and irreversible destruction yields a photochemical lifetime for atmospheric CH_4 of only $\sim$ 50 My, which is short in comparison to the age of Titan, and implies that it must be continually resupplied from the interior. Typically, an upward flux of CH_4 on the order of 10^{10} cm^{-2} s^{-1} is required and balanced by downward fluxes of less saturated, C_2, C_3, C_4, etc., hydrocarbons carrying the same total number of carbon atoms. All of these less saturated hydrocarbons condense as liquids or solids in the lower stratosphere and vicinity of Titan's cold tropopause, $\sim$ 71 K, to form pervasive haze layers. Eventually they precipitate from the atmosphere and accumulate on the surface, perhaps as a liquid hydrocarbon, tertiary ocean of C_2H_6, CH_4, and N_2, with icebergs of solid C_2H_2, CO_2 found on the bottom. With a conservative estimate for the efficiency of indirect CH_4 dissociation that yields the above atmospheric lifetime and flux of CH_4, a globally average ocean depth of $\sim$ 200 m would result if the current photochemistry were maintained over the age of Titan.

Synthesis of complex hydrocarbons, e.g. polyacetylenes, proceed via

$$C_{2n}H + C_{2m}H_2 \longrightarrow C_{2(n+m)}H_2 + H \tag{77}$$

but can be defeated by H-atom cracking reactions

$$H + C_{2n}H_2 + M \longrightarrow C_{2n}H_3 + M \tag{78}$$

$$H + C_{2n}H_3 \longrightarrow C_2H_2 + C_{2n-2}H_2 \tag{79}$$

Since the Titan haze is composed of large, condensed molecules with most of the mass contributed by hydrocarbons, Titan must somehow limit the efficiency of these H-atom cracking reactions. The haze particles may play a fundamental role in this process by suppressing the H atom concentration via heterogeneous reactions on the aerosol surfaces.

$$\mathrm{H} + \mathrm{aerosol} \longrightarrow \mathrm{H_{ad}} \cdot \mathrm{aerosol},\ k = \frac{1}{4}\gamma\, A\, v_{\mathrm{th}} \tag{80}$$

$$\mathrm{H} + \mathrm{H_{ad}} \cdot \mathrm{aerosol} \longrightarrow \mathrm{H_2} + \mathrm{aerosol},\ k = \frac{1}{4}\gamma\, A\, v_{\mathrm{th}} \tag{81}$$

which are more than competitive with the cracking reactions (Equation 78) that are slow at Titan's pressures and temperatures. Here $\mathrm{H_{ad}}$ is adsorbed H, γ is the stick coefficient estimated to be ~ 0.1, A is the surface area of the aerosol, which for 0.1 μm particles is 12×10^{-10} cm^2, and v_{th} is the thermal speed for H atoms $\sim 2 \times 10^5$ cm s^{-1}, for a rate of $\sim 6 \times 10^{-6}$ cm^3 s^{-1}.

3.3. Photochemistry of N_2

The N_2 bond at 9.7 eV is extremely difficult to break. With no optically allowed excitation paths into repulsive electronic states, dissociation occurs by indirect paths. Solar radiation below 100 nm can excite predissociating electronic states and yield a minor source of N atoms. The ion chemistry of N_2^+ preserves the N_2 bond. But dissociative ionization of N_2 by either electron impact or solar EUV radiation will produce one N atom and one N^+ ion, which will react with CH_4 to yield either an N atom or an ion (H_2CN^+ or HCN^+). The latter ion reacts with CH_4 to form the former ion and recombination of H_2CN^+ produces the nitrile HCN. Energetic electrons of photolytic and magnetospheric origins can also directly dissociate N_2. We can summarize these processes by

$$\begin{pmatrix} h\nu \\ \mathrm{e}^* \end{pmatrix} + \mathrm{N_2} \longrightarrow \begin{pmatrix} \mathrm{N}(^2\mathrm{D}) + \mathrm{N}(^4\mathrm{S}) \\ \mathrm{N^+} + \mathrm{N} \end{pmatrix} \tag{82}$$

The $N(^2D)$ reacts with CH_4 to produce NH, whereas $N(^4S)$ reacts with radicals $^3CH_2$ and CH_3 to produce HCN directly or via H_2CN. The key consideration is the extent of self destruction of odd nitrogen by the reaction

$$\mathrm{N} + \mathrm{NH} \longrightarrow \mathrm{N_2} + \mathrm{H}\,. \tag{83}$$

Based on the detailed calculations by (Strobel, 1992), the downward flux of N atoms from the thermosphere by reactions (82) referenced to the surface is $\sim (0.5 - 1) \times 10^9$ cm^{-2} s^{-1}, whereas self destruction by the above reaction limits the HCN flux to only $\sim (1 - 2) \times 10^8$ cm^{-2} s^{-1}. Once the CN bond is formed, it is preserved through the stratosphere. Dissociation of HCN yields the CN radical, which can react with various hydrocarbons

$$\mathrm{CN} + \mathrm{CH_4} \longrightarrow \mathrm{HCN} + \mathrm{CH_3} \tag{84}$$

$$CN + C_2H_2 \longrightarrow HC_3N + H \quad (85)$$
$$CN + C_2H_4 \longrightarrow C_2H_3CN + H \quad (86)$$
$$CN + HCN \longrightarrow (CN)_2 + H \quad (87)$$

to maintain the CN bond.

Nitrogen escape processes are non-thermal involving electron impact dissociation of N_2 at or near the exobase which yields a flux of N atoms $\sim 4 \times 10^7$ cm^{-2} s^{-1}, equivalent to removal of 0.02 times the present atmosphere, and ion sputtering of N_2 in the vicinity of the exobase produces a somewhat larger flux $\sim 8 \times 10^8$ cm^{-2} s^{-1}, for a removal of perhaps 40% of the present atmosphere (Lammer and Bauer, 1993).

3.4. PHOTOCHEMISTRY OF CO AND CO_2

The primary carrier of oxygen is CO with a tropospheric mixing ratio of 32 ppmv (Encrenaz, 2004). Its stratospheric mixing ratio is highly contentious. Thus one cannot infer whether the source(s) is internal and/or external. Most probably if the ultimate source of N_2 were direct delivery, then most of the CO would be similarly supplied. An initial atmosphere with considerable CO could be chemically destroyed by energetic magnetospheric and photo-electrons and subsequent reactions, such as

$$e^* + CO \longrightarrow C + O(^1D) + e \quad (88)$$
$$O(^1D) + CH_4 \longrightarrow OH + CH_3 \quad (89)$$
$$CO + OH \longrightarrow CO_2 + H \quad (90)$$

In the cold tropopause region CO_2 condenses out to produce dry ice. This conversion is further augmented by

$$e^* + N_2 \longrightarrow N_2(A^2\Sigma) + e \quad (91)$$
$$N_2(A^2\Sigma) + CO \longrightarrow CO(a^3\Pi) + N_2 \quad (92)$$
$$CO(a^3\Pi) + CO \longrightarrow CO_2 + C \quad (93)$$

The detection of H_2O at the ppbv level in the upper atmosphere implies an external source, most probably, meteorites with a net flux of $\sim 10^6$ cm^{-2} s^{-1}. This oxygen input is then "balanced" by removal in the form of dry ice at the tropopause or non-negligible thermal escape of O atoms at the exobase. However the oxygen half life is $\sim$ 10 By, hence the quotes for balanced. From an external source, CO can be produced by reactions

$$OH + CH_3 \longrightarrow CO + 2\,H_2 \quad (94)$$
$$^3CH_2 + OH \longrightarrow CO + H_2 + H\,. \quad (95)$$

4. Basic Principles and Simple Models

A satisfactory photochemical description of species in planetary atmospheres requires an accurate treatment of transport processes. The ultimate description would be incorporation of the chemistry into a general circulation model of the atmosphere. In many instances our knowledge of the atmosphere is too immature to justify such an elaborate treatment of atmospheric dynamics. Initially it is more reasonable to perform an accurate calculation of vertical density profiles by solution of the steady-state continuity equations for each specie.

$$\frac{\mathrm{d}\phi_i}{\mathrm{d}z} = P_i - L_i n_i \tag{96}$$

where ϕ_i is the vertical flux, P_i is the production rate per unit volume, L_i is the chemical loss rate, n_i is the number density, and z is the altitude. The usual representation of 1D vertical transport is the sum of molecular diffusion represented by an average diffusion coefficient, D_i, and an eddy diffusion coefficient, K_{zz}, which parameterizes macroscopic vertical mixing in the atmosphere by dissipative waves and mean wind systems/meridional circulations. For an isothermal atmosphere

$$\phi_i = -D_i \left[\frac{\mathrm{d}n_i}{\mathrm{d}z} + \frac{n_i}{H_i} \right] - K_{zz} \left[\frac{\mathrm{d}n_i}{\mathrm{d}z} + \frac{n_i}{H_\mathrm{a}} \right] \tag{97}$$

where T is temperature, $H_i = kT/m_i g$ is the scale height of the individual constituent, $H_\mathrm{a} = kT/m_\mathrm{a} g$ is the scale height of the background atmosphere, m_i is the constituent's mass, m_a is the mean molecular mass of the atmosphere, and g is the gravitational acceleration.

The homopause is defined as the level where $D_i \equiv K_{zz}$. At heights substantially above this level, eddy diffusion may be neglected and constituents which do not readily escape the gravitational field of a planet have $\phi_i = 0$ at the top of the atmosphere. In the absence of chemistry above the homopause ($P_i = L_i = 0$), the density varies as

$$n_i \propto \exp\left(-z/H_i\right) \tag{98}$$

in an isothermal atmosphere and depends critically on the constituent's mass. In the opposite limit, at altitudes much below the homopause, molecular diffusion can be neglected and in the absence of chemistry and net transport through the atmosphere, the density varies as

$$n_i \propto \exp\left(-z/H_\mathrm{a}\right) \tag{99}$$

Since $n_\mathrm{a} \propto \exp(-z/H_\mathrm{a})$, the constituent's mixing ratio (molar fraction), μ_i, is

$$\mu_i = \text{constant} \tag{100}$$

It follows that for any family of species whose net chemistry exactly cancels

$$\sum_i (P_i - L_i n_i) \equiv 0 \tag{101}$$

then

$$\sum_i \phi_i = \text{constant} = 0 \tag{102}$$

if their thermal escape or loss to the surface or interior is negligible. Since $\phi_i \propto \mathrm{d}\mu_i/\mathrm{d}z$, then the above equation implies also

$$\sum_i \mu_i = \text{constant} . \tag{103}$$

Hence the total mixing ratio of a chemical element in all forms is conserved in the homosphere, the region below the homopause. This powerful conservation law is very useful to infer the abundance of a constituent that contains substantial quantities of an element, but whose measurement is extremely difficult, if not impossible currently. In the Earth's middle atmosphere, this law is used for elemental hydrogen to infer H_2.

In the limit when $\mathrm{d}\phi_i/\mathrm{d}z = 0$, which implies a constant downward flux, ϕ_0, and set equal to the net column production rate high in the atmosphere is carried through the homosphere, an illuminating solution to the continuity equation is the following:

$$n_i = \frac{\phi_0}{K_{zz}} \left(\frac{1}{H_\mathrm{a}} - \frac{1}{H_K} \right)^{-1} + b \exp\left(-\frac{z}{H_\mathrm{a}} \right) \tag{104}$$

where the eddy diffusion coefficient is assumed to vary as $K_{zz} = K_0 \exp(z/H_K)$, $H_K > H_\mathrm{a}$. When $\phi_0 = 0$, the constituent is fully mixed, $\mu_i = b =$ constant. If the integration constant, b, is zero, then the constituent is transported downward at the maximum rate, $K_{zz}(1/H_\mathrm{a} - 1/H_K)$, and $n_i \propto 1/K_{zz}$, and it follows that n_i is a maximum, where K_{zz} is a minimum and illustrative of why pollutants accumulate in a region of slow mixing. Since ϕ_0 is positive and downwards, it illustrates why an external source of an element, e. g., oxygen delivered by meteoritic infall, will preferentially be concentrated in the region of minimum mixing, generally in the vicinity of the cloud tops on the giant planets. Conversely, if an element in all forms is concentrated preferentially in a region where K_{zz} is a minimum, then it implies that $\phi_0 > 0$, and that an external source for the element exists.

For compounds (e. g., CO) produced in the thermochemical furnaces of the giant planets, which are convective regions with large values of K_{zz} ($\sim 10^7 - 10^9$ cm^2 s^{-1}), they cannot be transported upwards to the tropopause region where K_{zz} is in the range of $\sim 10^3 - 10^4$ cm^2 s^{-1}, and have their mixing ratios increase with altitude. This principle can be illustrated by a solution to the continuity equation for constant $K_{zz} = K_\mathrm{t}$ in the troposphere, constant upward flux, $|\phi_0|$,

$$\mu_t = b_t - \frac{|\phi_0| H_a}{K_t n_0} \exp\left(\frac{z}{H_a}\right) \tag{105}$$

where for convenience the background atmospheric density, n_a, is written as $n_a = n_0 \exp(-z/H_a)$, with $z = 0$ at the interface of the discontinuity in the K_{zz}. Note that with an upward flux the tropospheric mixing ratio must decrease with increasing height as $|\phi_0| = -K_t n_a (d\mu_t/dz)$ and $\mu_t < b_t = lower\ boundary\ value$. At the interface the flux must be continuous, thus

$$|\phi_0| = -K_t n_a \left(\frac{d\mu_t}{dz}\right) = -K_0 n_a \left(\frac{d\mu_s}{dz}\right) , \tag{106}$$

where K_0 is the minimum value of K_{zz} above the cloud tops and μ_s is the mixing ratio above the interface. Clearly

$$\frac{d\mu_s}{dz} = \frac{K_t}{K_0}\frac{d\mu_t}{dz} \approx 10^4 \frac{d\mu_t}{dz} < 0 \tag{107}$$

and hence $\mu_t > \mu_s$.

In the extended atmospheres of the satellites with radius, R, and homopause at z_0, the variation of g must be taken into account and the geopotential height is the preferred height coordinate, written as

$$\zeta = \frac{R^2}{(R + z_0)(R + z)} (z - z_0) \tag{108}$$

and a variable K_{zz} may then be written as

$$K_{zz} = K_0 \exp(\kappa\zeta) . \tag{109}$$

Whereas the eddy diffusion coefficient is widely regarded as nothing more than a "fudge factor" to be empirically inferred from appropriate chemical tracer, the concept of eddy diffusion can be put on a rigorous basis in terms of wave-induced transport and mean vertical wind-induced transport. For a long-lived chemical tracer with a relaxation rate, α_{ri}, back to photochemical equilibrium, μ_{PE}, the continuity equation for zonally averaged mixing ratio, $\overline{\mu_i}$, is

$$\overline{w}\frac{\partial\overline{\mu_i}}{\partial z} = \alpha_{ri} (\overline{\mu_i} - \mu_{PE}) . \tag{110}$$

Here the term on the left represents the tilting of constant mixing ratio surfaces by the mean vertical winds, $\overline{w}$, which is counterbalanced by the strength of the chemical relaxation rate back to photochemical equilibrium. One can define a globally averaged eddy diffusion coefficient to parameterize this process, given by

$$K_{zz} = \frac{\overline{w^2}}{\alpha_{ri}}, \quad \text{where} \quad \langle\overline{w\mu_i}\rangle = -K_{zz}\left\langle\frac{\partial\overline{\mu_i}}{\partial z}\right\rangle \tag{111}$$

where $\langle\rangle$ denotes global average. Note that the eddy diffusion coefficient is applicable only to the chemical tracers with relaxation rate, α_r.

For wave-induced transport, (Strobel, 1981) derived an expression, the 2^{nd} term on the right of the equation below, where k is the zonal wavenumber, $\overline{u}$ is the mean zonal wind, c is the wave zonal phase speed, σ_i is the growth or dissipation rate of the wave, and w' is the vertical wave velocity. The overall effective, globally averaged eddy diffusion coefficient for a specific constituent i is then

$$\langle K_{zz} \rangle_i = \left\langle \frac{\overline{w^2}}{\alpha_{ri}} \right\rangle + \left\langle \frac{L_i + \sigma_i}{k^2(\overline{u} - c)^2 + (L_i + \sigma_i)} \overline{w'^2} \right\rangle \tag{112}$$

Note that each constituent has a specific effective eddy diffusion coefficient, unless it has identical values for α_{ri}, L_i, σ_i as another constituent. The author has explored the consequences of this in West *et al.* (1986) and noted that CO, C_2H_6, and NH_3 profiles in the tropopause region do not yield the same magnitudes of K_{zz}. In spite of this fact, almost all 1D photochemical calculations performed for the atmospheres of the outer planets and satellites have assumed a common K_{zz} vertical profile.

5. Concluding Remarks

There are still significant problems in our understanding of photochemistry in the outer solar system. Some examples include calculating the C_2H_6/C_2H_2 mixing ratios correctly on Jupiter and Saturn with the same chemistry. On Jupiter auroral-induced chemistry is important, as it is driven by the deposition of $\sim 10^{14} W$ of power which is far in excess of solar EUV power of $\sim 8 \times 10^{11}$W, but poorly understood and the subject of active research (Friedson *et al.*, 2002). The inference of a consistent vertical profile for K_{zz} for all species in 1D photochemical transport models is problematical, especially on Neptune and Titan. It could be indicative that each constituent has a specific effective eddy diffusion coefficient based on its chemistry as discussed above or alternatively that we lack a complete understanding of the basic photochemistry in these atmospheres.

This list of problems is not exhaustive and for the reader interested in pursuing the subject in more depth, the following list of references is recommended as a good starting point: Jupiter (Gladstone *et al.*, 1996), Saturn (Moses *et al.*, 2000a; 2000b), Uranus (Summers and Strobel, 1989), Neptune (Romani *et al.*, 1993; Lellouch *et al.*, 1994), Pluto (Summers *et al.*, 1997), and Titan (Banaszkiewicz *et al.*, 2000; Toublanc *et al.*, 1995) but I have a strong preference for the classic paper of Yung *et al.* (1984).

6. Acknowledgements

This research was supported in part by NASA Grant NAG5-12051.

References

Banaszkiewicz, M., Lara, L.M., Rodrigo, R., López-Moreno, J.J., and Molina-Cuberos, G.J.: 2000, 'A coupled model of Titan's atmosphere and ionosphere', *Icarus* **147**, 386–404.

Bézard, B., Lellouch, E., Strobel, D. F., Malliard, J.-P., and Drossart, P.: 2002, 'Carbon monoxide on Jupiter: Evidence for both internal and external sources', *Icarus* **159**, 95–111.

Encrenaz, T.: 2004, 'Overview of composition measurements', this volume, 121–134.

Friedson, A.J., Wong, A.-S., and Yung, Y.L.: 2002, 'Models for polar haze formation in Jupiter's stratosphere', *Icarus* **158**, 389–400.

Gladstone, G.R., Allen, M., and Yung, Y.L.: 1996, 'Hydrocarbon photochemistry in the upper atmosphere of Jupiter', *Icarus* **119**, 1–52.

Lammer, H., and Bauer, S. J.: 1993, 'Atmospheric mass loss from Titan by sputtering', *Planet. Space Sci.* **41**, 657–663.

Lellouch, E., Romani, P.N., and Rosenqvist, J.: 1994, 'The vertical distribution and origin of HCN in Neptune's atmosphere', *Icarus* **108**, 112–136.

Lunine, J. I., Yung, Y. L., and Lorenz, R. D.: 1999, 'On the volatile inventory of Titan from isotopic abundances in nitrogen and methane', *Planet. Space Sci.* **47**, 1291–1303.

Lunine, J.: 2004, 'Formation and evolution of Titan's atmosphere', this book, 177–190.

Moses, J.I., Bézard, B., Lellouch, E., Gladstone, G.R., Feuchtgruber, H., and Allen, M.: 2000a, 'Photochemistry of Saturn's atmosphere. I. Hydrocarbon chemistry and comparisons with ISO observations', *Icarus* **143**, 244–298.

Moses, J.I., Bézard, B., Lellouch, E., Gladstone, G.R., Feuchtgruber, H., and Allen, M.: 2000b, 'Photochemistry of Saturn's atmosphere. II. Effects of an influx of external oxygen', *Icarus* **145**, 166–202.

Romani, P.N., Bishop, J., Bézard, B., and Atreya, S.: 1993, 'Methane Photochemistry on Neptune: Ethane and Acetylene Mixing Ratios and Haze Production', *Icarus* **106**, 442–463.

Strobel, D. F.: 1981, 'Parameterization of linear wave chemical transport in planetary atmospheres by eddy diffusion', *J. Geophys. Res.* **86**, 9806.

Strobel, D. F.: 1983, 'Photochemistry of the reducing atmospheres of Jupiter, Saturn, and Titan', *Intl. Rev. Phys. Chem.* **3**, 145.

Strobel, D. F., Summers, M. E., and Zhu, X.: 1992, 'Titan's upper atmosphere: Structure and ultraviolet emissions', *Icarus* **100**, 512–526.

Strobel, D. F., and M. E. Summers: 1995, 'Triton's upper atmosphere and ionosphere', *in* Neptune and Triton, D. P. Cruikshank (ed.), Univ. Arizona Press, Tucson, pp. 1107–1148.

Strobel, D. F.: 2002, 'Aeronomic systems on planets, moons, and comets', *in* Comparative Aeronomy in the Solar System, M. Mendillo, A. Nagy, and H. Waite (eds.), American Geophysical Union, Geophysical Monograph Series, pp. 7–22.

Summers, M.E. and Strobel, D.F.: 1989, 'Photochemistry of the atmosphere of Uranus', *Astrophys. J.* **346**, 495–508.

Summers, M.E., Strobel, D.F., and Gladstone, G.R.: 1997, 'Chemical models of Pluto's atmosphere', in S.A. Stern and D.J. Tholen (eds.), *Pluto*, Univ. Arizona Press, Tucson, pp. 391–434.

Toublanc, D., Parisot, J.P., Brillet, J., Gautier, D., Raulin, F., and McKay, C.P.: 1995, 'Photochemical modeling of Titan's atmosphere', *Icarus* **113**, 2–26.

West, R.A., Strobel, D.F., and Tomasko, M.G.: 1986, 'Clouds, aerosols, and photochemistry in the jovian atmsophere', *Icarus* **65**, 161–217.

Yung, Y.L., Allen, M., and Pinto, J.P.: 1984, 'Photochemistry of the atmosphere of Titan – Composition between model and observations', *Astrophys. J. Suppl.* **55**, 465–506.

Address for Offprints: D. F. Strobel, Department of Earth and Planetary Sciences, Johns Hopkins University, 3400 North Charles Street, Baltimore, MD 21218, USA; strobel@jhu.edu

FORMATION AND EVOLUTION OF TITAN'S ATMOSPHERE

ATHENA COUSTENIS
LESIA, Paris-Meudon Observatory, 5, place Jules Jannsen, 92195 Meudon Cedex, France

Received: 20 September 2004; Accepted in final form: 20 October 2004

Abstract. The origin and evolution of Titan's enigmatic atmosphere is reviewed. Starting with the present-day volatile inventory, the question of what was the original composition on Titan and how a satellite of similar size to other Galilean moons managed to acquire and hold on to the required material is discussed. In particular the possible sources and sinks of the main mother molecules (nitrogen, methane and oxygen) are investigated in view of the most recent models and laboratory experiments. The answers expected to be provided by the instruments aboard the Cassini-Huygens mission to some of the most prominent current questions regarding Titan's atmosphere are defined.

Keywords: Satellites; Titan; atmospheres; Solar System; infrared; space missions

1. Introduction

Titan's atmosphere is a mystery to this day. In this year of the arrival of the Cassini-Huygens mission in the Saturnian system, one of the questions that scientists will try to answer from the data gathered by the spacecraft and the probe will be : why does Titan have an atmosphere, while other similarly large satellites (and planets for that matter, like more massive Mars) do not and where does this atmosphere come from. Indeed, it is curious to observe that Jupiter's large moons Ganymede and Callisto, although of comparable mass and size to Titan, having also formed in the outer solar system, proved unable to retain a gaseous envelope of any significant size.

This is just one question related to Titan's atmosphere. Another has to do with its origin, how it was formed and maintained. Yet a third one relates to the chemical composition and the inventory of such a major gas envelope.

The subject of the origin of Titan's atmosphere has been extensively addressed over the past decades as new data enriched our knowledge of Titan from space and ground-based measurements. Consequently models and scenarios have evolved. Recently, reviews and novel interpretations have been offered (e.g. Gautier, 1997; Owen, 2000; and references therein).

There are several ways through which Titan could have obtained its atmosphere: one is by capturing it from the solar nebula or from an unfractionated proto-Saturnian nebula during its formation; a second would be by outgassing of the accreted material; volatile contributions from impacting comets have also been invoked. In the first case, Titan would have captured its atmospheric gases from the

Space Science Reviews 116: 171–184, 2005.
DOI: 10.1007/s11214-005-1954-2

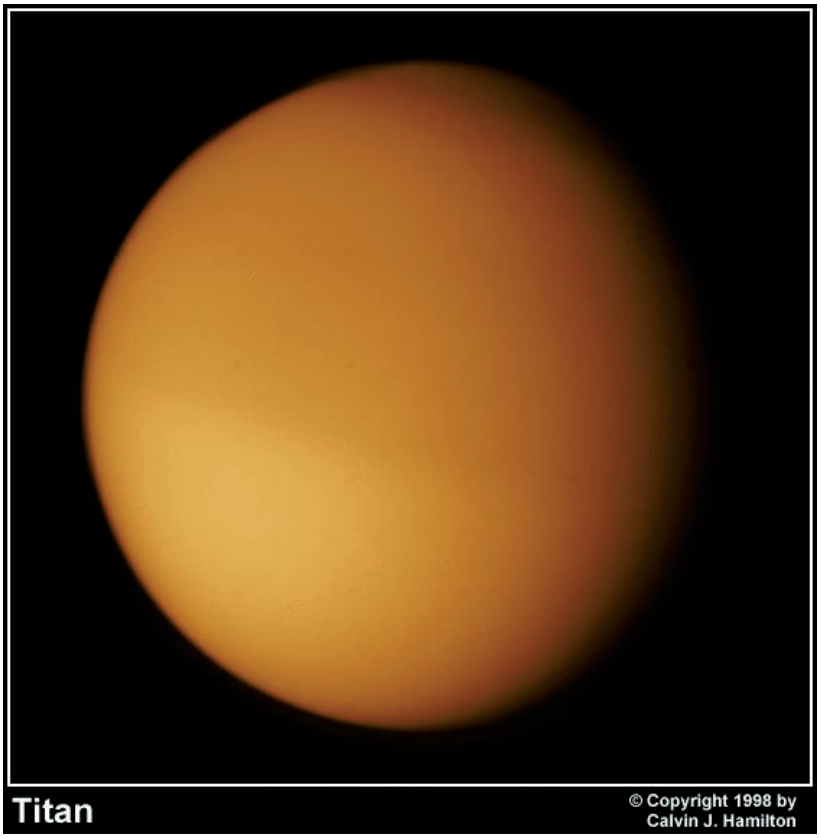

Figure 1. Titan: images from the Voyager mission in the early 80s. The only other body in our solar system with a significantly thick atmosphere mainly composed of nitrogen exhibits here a pronounced north-south asymmetry in the stratospheric haze layers, with the North darker than the South at the time of the Voyager encounter in the visible range.

surrounding Saturnian subnebula (of the same elemental composition as the solar nebula), but in that case – if N_2 was captured – most of the C would have to be in the form of CO while the CO/N_2 ratio on Titan is on the order of 30 ppm (Table I). Titan's atmosphere is most likely the result of the devolatilization of the ices and rocks that accreted to form the satellite.

2. The Formation of Titan and the Origin of its Atmosphere

Titan's atmosphere as we know it today from space and ground-based observations is a remarkably rich environment in which a host of molecules react with each other, photolyze, aggregate and are eventually deposited on the surface after condensation in liquid or solid form. Table I gives an idea of the current chemical composition of Titan's atmosphere. The main constituents today are molecular

TABLE I

Chemical composition of Titan's atmosphere today, adapted and updated from Coustenis and Taylor (1999), and references therein. This Table focuses on mean molecular abundances as found in ground-based observations or by the Infrared Space Observatory (ISO) and reported by Coustenis *et al.* (2003) (referred to as "ISO" in the comments column) rather than Voyager spatially-resolved measurements. The species are listed in decreasing abundance.

Constituent	**Mixing ratio**	**Comments**
N_2	~ 0.98	major constituent (inferred indirectly)
Ar	<0.07	undetected, Samuelson *et al.* (1997a)
CH_4	~ 0.018	in the stratosphere, Flasar *et al.* (2004)
H_2	1.1×10^{-3}	Samuelson *et al.* (1997a)
C_2H_6	2.0×10^{-5}	from ISO
CO	3.2×10^{-5}	in the troposphere, Lellouch *et al.* (2003)
	$5\text{-}7\times10^{-5}$	in the stratosphere, Gurwell and Muhlemann (2000), López-Valverde *et al.* (2004), Flasar *et al.* (2004)
CH_3D	1.1×10^{-5}	from ISO
D/H	8.7×10^{-6}	isotope ratio from CH_3D ISO value
C_2H_2	5.5×10^{-6}	from ISO
HC_3N	3.0×10^{-7}	from ISO
C_3H_8	2.0×10^{-7}	from ISO
C_2H_4	1.2×10^{-7}	from ISO
CO_2	2.0×10^{-8}	from ISO
C_3H_4	1.2×10^{-8}	from ISO
H_2O	8.0×10^{-9}	at 400 km from ISO, Coustenis *et al.* (1998)
C_4H_2	2.0×10^{-9}	from ISO
CH_3CN	1.5×10^{-9}	Bézard *et al.* (1993)
C_6H_6	4.0×10^{-10}	from ISO
C_3H_4	$<2.0\times10^{-9}$	upper limit from ISO (allene isomer)
C_2N_2	$<1.0\times10^{-9}$	upper limit from V1/IRIS Coustenis *et al.* (1991)
C_4N_2		solid phase from V1/IRIS, Samuelson *et al.* (1997b)

nitrogen, methane and molecular hydrogen, followed by 16 detected trace species (hydrocarbon, nitriles and oxygen compounds), one of which is only in solid form (C_4N_2).

There are many unsolved issues regarding the chemical composition of Titan's atmosphere, including the origin of the major constituents, nitrogen and methane. The exact abundances of these two chemical compounds is largely unknown even today (Table I). If we had a better knowledge of the exact quantities of the mother molecules on Titan we might have found the grounds to establish more precise formation theories for the satellite.

As it is, there are still several scenarios proposed for the creation of Titan and for the acquisition of its atmosphere. One suggestion was that Titan captured its atmosphere from the gases contained in the surrounding nebula during its accretion period. A problem with this idea is that the Kronian subnebula at the time of Titan's formation must have had the same elemental composition as the solar nebula. In that case, the noble gases abundance ratios (and in particular that of Ne/H for instance) should be similar on Titan as in the Sun. The solar abundance of Ne/H is found to be almost identical to that of N/H (Anders and Grevesse, 1989), whereas no Ne has been detected to date on Titan. It follows that direct capture of the gaseous envelope around Titan must be excluded.

There remain two sources of volatiles available for Titan's atmosphere : accretion from planetesimals condensed within the Saturnian subnebula and input from comets which condensed outside the Saturnian subnebula. It is logical to assume that the atmosphere we witness today around Titan should be a combination of both: outgassing from the ices composing the interior following the accretion period and the delivery by cometary impacts (the latter was proposed by Griffith and Zahnle, 1995). The latter hypothesis was shown to be able to explain the atmosphere around Titan and the lack of one around Ganymede and Callisto by virtue of the different impact energies in the Jovian and the Kronian systems, which would cause the creation of an atmosphere in the case of Titan and the erosion of those acquired initially by the Galilean moons. Comets should have condensed directly from the material available in the solar nebula. They contain nitrogen both in molecular form and as part of organic molecules, but very little methane. If Titan's atmosphere was the result of cometary impacts, the N_2 may have been produced from the breakdown of complex organic material during the impact. Although this hypothesis is attractive in that it offers an explanation as to why other large moons are not favored with an atmosphere, it is contradicted by the large variations observed in the D/H ratio in comets (e.g. Bockelée-Morvan *et al.*, 1998; Meier *et al.*, 1998a, b) and Titan (Coustenis *et al.*, 2003). For the additional problem of the methane input through this method see the following section.

A further consideration in the problems of the origin of nitrogen in Titan's atmosphere and the lack of an atmosphere around the Jovian satellites has to do with the solar evolution of X-ray and extreme ultraviolet radiation, the radiation which is absorbed in the upper planetary atmospheres, heating them. From recent studies dealing with such problems (Penz *et al.*, 2004, and references therein) it would appear that the young Sun provided considerably higher X-ray and EUV flux thus causing (by effect of the atmosphere being heated to blow off temperatures during the first 100 My or so) the nitrogen isotope anomaly by large evaporation of the nitrogen atmosphere. By the same token, this theory provides an alternative scenario (vs cometary impact studies such as the one by Griffith and Zahnle, 1995) for the lack of a nitrogen atmosphere around the Galilean satellites.

As concerns the contribution of planetesimal degassing to the atmosphere of Titan, one needs to examine the nature of the gases which condense in such material

initially. This was shown to depend on the temperature and pressure at which the ice formed (Bar-Nun *et al.*, 1985; 1988). Laboratory measurements thus show that very low temperatures (less than 75 K) are required to allow for a substantial trapping of highly volatile species such as CH_4, CO and N_2. There is no indication that the subnebula around Saturn could have become that cold prior to the accretion period on Titan. Therefore, we are led to the conclusion that the dominant carrier for nitrogen on Titan was rather NH_3 and other volatiles that can be trapped efficiently at higher temperatures (Owen, 2000, and references therein). Subsequent photolysis of NH_3 on early Titan could easily produce the present amount of N_2.

2.1. Origin of Nitrogen

The issue of discriminating between the primary original source of the current N_2 on Titan (whether it was delivered in the form of N_2 or NH_3, can be tackled by considering the temperatures prevailing during Titan's accretion. A test for the two hypotheses can be provided by considering the argon abundance on Titan. Indeed, laboratory experiments (Bar-Nun *et al.*, 1988) show that N_2 and Ar are similarly trapped in ice forming at temperatures near 75 K. Then, if nitrogen on Titan was originally in the form of N_2, it would have been trapped to about the same extent as argon (or perhaps slightly less). On the other hand, if the nitrogen originally came in the form of ammonia, as said previously we would expect the atmospheric value of Ar/N_2 to be relatively low (about 1%). The current upper limit for Ar on Titan is around 0.06 (e.g. Samuelson *et al.*, 1997a), which tends to be near the limit value expected for direct capture of N_2. We can not exclude, on this basis alone, one or the other scenarios.

However, one other consideration needs to be invoked: it appears from recent estimates of the $^{12}C/^{13}C$ and $^{15}N/^{14}N$ isotopic ratios on Titan (Hidayat *et al.*, 1997; Marten *et al.*, 1997) that the Titan atmosphere has allowed large amounts of nitrogen to escape, while the carbon is maintained by an unseen reservoir. Indeed, while the $^{12}C/^{13}C$ ratio is practically terrestrial, the $^{15}N/^{14}N$ one is more than 4 times larger than the one observed on the Earth. From a study of non-thermal loss processes by Lammer *et al.* (2000), it would seem that Titan could originally have denser atmosphere than today but that due to an also much denser solar wind during the early stage of the young Sun, an important nitrogen loss could have been caused and led to the currently observed nitrogen isotope fractionation (similar fractionation of argon from N_2 is also observed on Mars, Earth and Venus, suggesting the incorporation of nitrogen in other forms than N_2 in these planets as well (Owen and Bar-Nun, 1995). However, solar wind estimations of young solar-like stars indicate that the early solar wind may indeed have been much higher, but could not fractionate the nitrogen in Titan's upper atmosphere in contrast to higher EUV radiation of the young Sun (see Penz *et al.*, 2004, and references therein). If we take into account the lost N_2 amounts, then it appears that the original outgassed Ar/N_2 ratio should have been far below the solar value, which means that only a

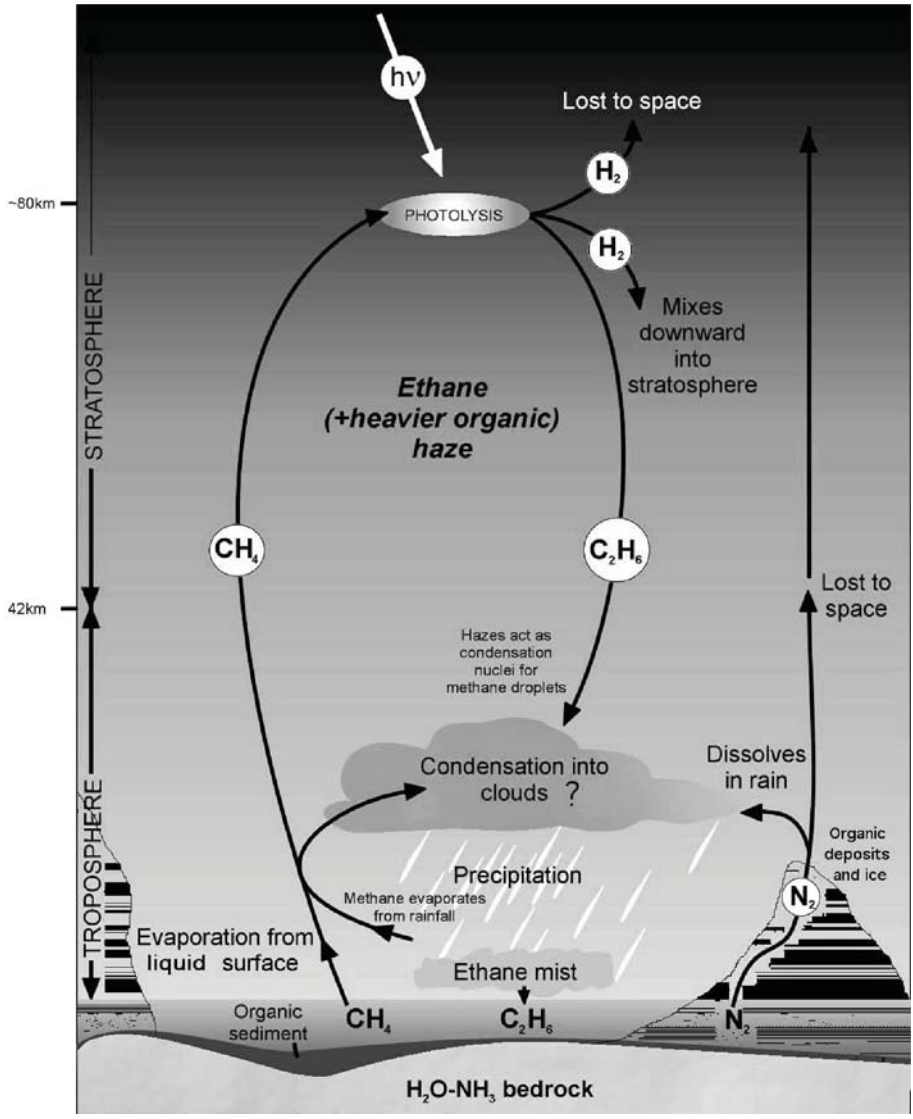

Figure 2. Titan's complex atmospheric system.

small amount (if any) of N_2 could have been trapped in the ices that formed Titan. Then the nitrogen on Titan must have originated as ammonia. One might question this inference simply because ammonia must also have been present around Jupiter as well, and we do not find nitrogen atmospheres around the Jovian moons. Also, the upper limit for argon on Titan is not stringent enough.

It then seems that we need to wait for more precise observations of the major constituent abundances on Titan before we can infer the real origin of its atmosphere.

2.2. ORIGIN OF METHANE

The question of how much methane was there originally in Titan's atmosphere and how much can there be left today (the current methane abundance remains to be determined but should be around 2% (Flasar *et al.*, 2004, from recent Cassini/CIRS meaasurments; see also Samuelson and Mayo, 1997, for CH_4 supersaturation) is an important issue since it will give a handle on the chemistry of methane loss for the past four billion years.

Compared to what we find in comets or in the Interstellar Medium, there seems to be a lot of methane on Titan ($CH_4/CO > 1000$; Gautier and Raulin, 1997), whereas CO is believed to have been more abundant than CH_4 in the protosolar nebula. Prinn and Fegley (1981) have suggested in their evolutionary scenario that in a dense subnebula of Saturn CO was converted into CH_4 which was then trapped in the form of clathrate hydrates by the condensing water vapor in the planetesimals that formed Titan and its primitive atmosphere (Owen 1982; 2000). Since the solar photolysis irreversibly converts all of the atmospheric methane in hydrocarbons in a relatively short time compared to Titan's age of about 50 My (Strobel, 2004, this volume), CH_4 must then be continuously replenished from a local reservoir either on or under Titan's surface (Lunine and Stevenson, 1987; Stevenson, 1992; Gautier, 1997). These various authors have suggested that some form of volcanism may exist on Titan allowing the delivery of atmospheric methane from a subsurface reservoir, or simple exchanges between the subsurface and the atmosphere through a porous regolith. These ideas are difficult to test remotely (one possibility would be that clouds observed from the ground – if confirmed on Titan with Cassini – could be located above such volcanos.

This scenario explains the value of the D/H ratio inferred on Titan (the most recent one from ISO measurements: $8.75\ ^{+3.25}_{-2.25} \times 10^{-5}$, Coustenis *et al.*, 2003, is in agreement with ground-based observations by Orton, 1992). This D/H ratio is lower by factors 3-4 than the one measured in water in Halley, Hyakutake and Hale-Bopp comets (Balsiger *et al.*, 1995; Eberhardt *et al.*, 1995; Bockelée-Morvan *et al.*, 1998; Meier *et al.*, 1998a, b). Should we assume, as currently admitted, that ices which formed comets acquired their enrichment in deuterium from hydrogen in the presolar cloud, the D/H ratio in water and in methane ices should have been near the values measured at equilibrium at the temperature of the cloud. Theoretical calculations predict that, at equilibrium, D/H in CH_4 is still higher than D/H in water. Even if interstellar grains were partly re-equilibrated with hydrogen in the nebula prior to forming comets (Gautier, 1997), the difference in deuterium enrichments between the two species should have remained approximately the same since the isotopic exchange coefficient between CH_4 and HD is not very different from that between H_2O and HD (Lécluse and Robert, 1994; Lécluse *et al.*, 1996). In other words, in comets D/H in CH_4 is probably higher than D/H in H_2O. Therefore, the large difference between the D/H ratio in water in comets on one hand and the D/H in methane in Titan on the other hand rules out a formation of the atmosphere

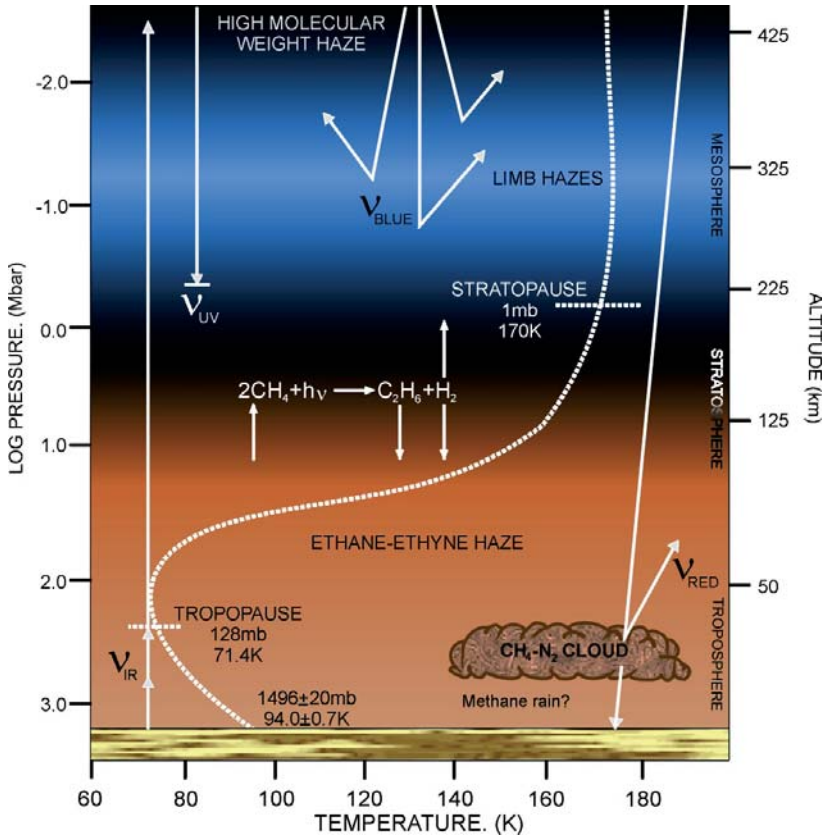

Figure 3. The cycle of methane in Titan's atmosphere

of the satellite by impacts from external icy planetesimals ("comets") alone, contrary to a scenario advocated by some authors (Zahnle *et al.*, 1992; Griffith and Zahnle, 1995). However, exterior contribution of volatiles may have played a part in the formation of Titan's atmosphere as these authors show that it would favor the creation such an atmosphere around Titan but not around the Jovian satellites. Nevertheless, this scenario does not explain the large excess of CH_4 with respect to CO observed in Titan, since CH_4 is currently less abundant than CO in comets (Table 5 of Iro *et al.*, 2003).

On the other hand, this D/H ratio is consistent with the scenario of the formation of the atmosphere by degassing from the interior of the satellite (Gautier, 1997; Owen, 2000; and references therein). As to the origin of the deuterium enrichment observed on Titan in the methane with respect to the protosolar value $2.35\pm0.3 \times 10^{-5}$, calculated as the weighted mean of the D/H ratios in hydrogen estimated by Geiss and Gloecker (1998), Mahaffy *et al.* (1998), and Lellouch *et al.* (2001), there have been suggested at least two interpretations. According to the original Prinn and Fegley (1981) scenario and subsequent works of these au-

thors, the CO conversion to CH_4 in Saturn's subdisk was accompanied by isotope exchange between CH_4 an HD prior to clathrate formation, while an additional significant fractionation mechanism followed the accretion and outgassing processes (Pinto *et al.*, 1986; Lunine and Tittemore, 1993).

A different story is proposed through an evolutionary model of Saturn's subnebula developed by Mousis *et al.* (2002a, b). These authors find that no substantial conversion of CO to CH_4 occurred in the subnebula. They argue that CH_4 ices infalling from the presolar cloud vaporized in the solar nebula. Subsequently, methane isotopically exchanged deuterium with hydrogen in the nebula until the temperature was low enough to permit the formation of solid clathrate hydrates of CH_4 around 10 AU (Hersant *et al.*, 2004; Gautier and Hersant, 2005, this volume). These clathrates, incorporated in planetesimals which formed Titan did not decompose in the interior of the satellite, except near the surface where the freed CH_4 could escape to the atmosphere through cracks (Lunine and Stevenson, 1987). Calculating the evolution of D/H in CH_4 in the solar nebula from plausible ISM values, allowed Mousis *et al.* (2002b) to reproduce the values measured in the atmosphere of Titan by ISO. The scenario implies that the fractionation of the deuterated methane over 4.5 billions of years was quite small, if any. This suggests that the replenishment of the atmospheric methane comes from the interior of the satellite, through cryovolcanism.

Both scenarios reproduce the large atmospheric CH_4 mass, the low CO/CH_4 ratio and the mass estimations of N_2 converted from NH_3 in the primitive atmosphere. The higher X-ray and EUV flux of the young Sun theory invoked previously can also explain the D/H ratio measurements on Titan (Penz *et al.*, 2004).

2.3. Origin of Oxygen

Three oxygen compounds have been detected on Titan to date: CO, CO_2 and H_2O. Carbon dioxide was identified on Titan by Samuelson *et al.* (1983) and the CO_2 abundance from Voyager/IRIS measurements was inferred to be on the order of 10^{-8} (Table I). CO was discovered on Titan from ground-based observations (de Bergh *et al.*, 1988). Its profile in Titan's atmosphere is a controversial subject even today: it appears that recent observations from the ground report CO amounts in the stratosphere on the order of 50-60 ppm (Gurwell and Muhlemann, 2000; López-Valverde *et al.*, 2004), whereas the values found for CO in the troposphere seem to be consistently around 32 ppm (Lellouch *et al.*, 2003), that is two times lower than in the stratosphere, so that a higher mixing ratio for CO is found in the stratosphere than in the troposphere. This is difficult to understand since the chemical lifetime of CO on Titan is very long (about 10^9 years) compared with the atmospheric transport time scales and hence CO is expected to be well mixed in the atmosphere. The non-constant vertical profile then implies that either CO is destroyed on Titan and/or that an external source for CO must be invoked (López-Valverde *et al.*, 2004).

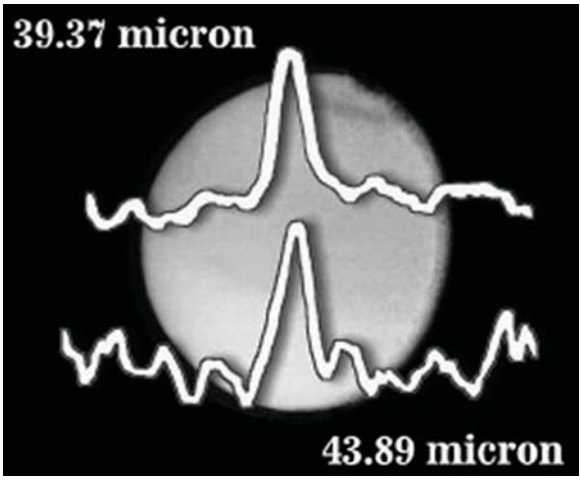

Figure 4. Water detection in Titan's atmosphere with ISO.

H_2O was detected on Titan from ISO observations around 40 micron (Coustenis *et al.*, 1998). A photochemical profile was tested against the observations and adjusted so as to provide a satisfactory fit. It then yields a mole fraction of about 8 $\times 10^{-9}$ at 400 km of altitude on Titan. The water influx deduced from these observations at 700 km (ablation level) is (0.8-2.8) $\times 10^6$, which is surprisingly close to the water influx inferred on Saturn from ISO observations also (Feuchtgruber *et al.*, 1997) by factors of 0.5-6.2, suggesting that local and interplanetary components in supplying water to the atmospheres of Saturn and Titan (which were evaluated to be significantly in favor of Saturn) may not be very well understood. In the case of Titan the origin of the water vapor remains to be elucidated (whether local or interplanetary). The presence of CO_2 and H_2O in Titan's atmosphere requires an external source for oxygen, at least in the form of H_2O, presumably delivered by micrometeoritic ablation. There must be a balance between the oxygen input, the escape of O atoms and the oxygen compounds' initial abundances (Owen, 2000).

Owen *et al.* (1999) reported the detection of $C^{18}O$ on Titan and derived a value of the $^{18}O/^{16}O$ ratio of about two times the terrestrial one. This implies that where no significant isotopic enrichment is found for C in Titan's atmosphere, fractionation is observed for H, N and O. Recent theoretical considerations on the evolution of CO on Titan by considering the enrichment observed in the heavy isotopomers of CO (^{13}CO and $C^{18}O$) relative to $^{12}C^{16}O$, suggest that a rapid exchange of C atoms between CH_4 and CO reservoirs could have taken place (within 800 My), and thus the original isotopic enrichment of ^{13}CO in CO may have been diluted by the exchange process (Wong *et al.*, 2002). These authors have reassessed the Titan oxygen chemistry and found that through a less efficient process to form CO than initially believed, the CO equilibrium value would only be around 2 ppm. The CO observed values (much larger) seem to then suggest that CO is not in equilibrium

in Titan's atmosphere, but was subject to massive loss in a permanently non-steady state. Regular meteoritic supply of CO (Lara *et al.*, 1996) or episodic delivery by comets (Griffith and Zahnle, 1995) constitute viable additional external sources for the CO observed on Titan.

3. Conclusion: Answers Expected from Cassini-Huygens

In the case of the origin of Titan's atmosphere, the Cassini-Huygens mission will be of value, since many of the instruments on board will address questions related to this subject. It appears that the main player here will be the gas chromatograph mass spectrometer (GCMS) on the Huygens probe which will measure with precision the abundances of deuterium and noble gases (such as argon) and their isotopes on Titan. Abundances of ^{36}Ar and ^{38}Ar will provide an upper limit for the amount of nitrogen delivered as N_2, while the ^{40}Ar abundance will inform on the outgassing from the interior. The examination of the Ar/Kr/Xe pattern should permit us to discriminate between the various scenarii proposed for the origin of Titan's atmosphere (Mousis *et al.*, 2002a). The surprising $^{14}N/^{15}N$ value discussed in Section 2.1 was obtained in HCN, which is produced from photochemical processes occuring in the high atmosphere. The GCMS instrument will permit us to measure it in N_2.

However, uncertainties on these measurements and the importance of acquiring high precision calls for additional information, which could be provided by observations from other instruments, such as the Composite Infrared Spectrometer (CIRS) on board the orbiter which will measure the CH_3D abundance at 1150 cm^{-1} giving access to the D/H ratio when dividing by the CH_4 abundance. A measurement of the D/H ratio in other molecules than CH_4 (such as for instance in H_2O if Huygens can make a measurement after landing on water ice) would also help to define if methane is indeed affected by isotope exchange in the atmosphere (Owen, 2000). The D/H ratio and a better assessment of the $^{12}C/^{13}C$ ratio should help better define the nature of a methane reservoir on Titan. The Cassini orbiter will also provide a mapping of the ground which will allow us to estimate the craters and evaluate the impacts to which the satellite has been subjected. If the crater basins are filled with liquid hydrocarbons, then we may get a chance to elucidate the mystery of the methane reservoir. In the event where we observe giant impact basins on Titan's surface, one may want to consider the theory of the origin of Titan's atmosphere from impacts by proto-Hyperion fragments, as suggested by Farinella *et al.* (1997).

On a different topic, the mapping of Titan's surface by Cassini may also bring clues as to the possible collapse and re-inflation of Titan's atmosphere (as was suggested by Lorenz *et al.*, 1997). In such a case, the surface maps might reveal the presence of U-shaped valleys near the poles (formed during glacial erosion), small-crater population or evidence of cryoclastic volcanism.

CIRS will also provide a better analysis of the H_2 dimer features and allow the detection of the H_2-Ar Van der Waals molecule (Gautier, 1997). This will allow to either detect argon or infer a more stringent upper limit for its abundance.

Cassini/VIMS observations should provide a better understanding and modeling of the CO fluorescent emission in the near-infrared, by detecting the CO emission lines even though at a low resolution. Without the terrestrial atmospheric interference, these observations should allow a mapping of the temperature field and the CO abundance as a function of latitude. The Cassini/CIRS instrument will observe the CO rotational lines in the sub-mm range and hence infer a more precise determination of the stratospheric mixing ratio.

Whatever the scenario proposed currently, it appears that Titan "was at the right place at the right moment" and benefited from conditions which allowed it to acquire sufficient of valuable material to build a dense atmosphere. The Cassini-Huygens mission will help us in the coming months to bring answers to the questions regarding the particular existence of this atmosphere.

Acknowledgements

I am grateful to D. Gautier, D. Strobel, and reviewer H. Lammer for valuable comments on the manuscript.

References

Anders, E. and Grevesse, N.: 1989, 'Abundances of the elements: meteoritic and solar', *Geochim. Cosmochim. Acta* **53**, 197–214.

Balsiger, H., Altwegg, K., and Geiss, J.: 1995, 'D/H and $^{18}O/^{16}O$ ratio in the hydronium ions and neutral water from in situ measurements in comet Halley', *J. Geophys. Res.* **100**, 5827–5834.

Bar-Nun, A., Herman, G., Laufer, D., and Rappaport, M.L.: 1985, 'Trapping and release of gases by water ice and implications for icy bodies', *Icarus* **63**, 317–332.

Bar-Nun, A., Kleinfeld, I., and Ganor, E.: 1988, 'Shape and optical properties of aerosols formed by photolysis of acetylene, ethylene and hydrogen cyanide', *J. Geophys. Res.* **93**, 8383–8387.

Bézard, B., Marten, A., and Paubert, G.: 1993, 'Detection of Acetonitrile on Titan', *Bull. Am. Astron. Soc.* **25**, 1100 (abstract).

Bockelée-Morvan, D., *et al.*: 1998, 'Deuterated water in Comet C/1996 B2 (Hyakutake) and its implication for the origin of comets', *Icarus* **133**, 147–162.

Coustenis, A., Bézard, B., Gautier, D., Marten, A., and Samuelson, R.: 1991, 'Titan's atmosphere from Voyager infrared observations: III. The vertical distributions of hydrocarbons and nitriles near Titan's North pole', *Icarus* **89**, 152–167.

Coustenis, A., Salama, A., Lellouch, E., Encrenaz, Th., Bjoraker, G., Samuelson, R.E., de Graauw, Th., Feuchtgruber, H., Kessler, M.F.: 1998, 'Evidence for water vapor in Titan's atmosphere from ISO/SWS data', *Astron. Astroph.* **336**, L85–L89.

Coustenis, A. and Taylor, F.: 1999, *Titan: the Earth-like Moon*, WSP Publishers Eds, Singapore.

Coustenis, A., Salama, A., Schulz, B., Ott, S., Lellouch, E., Encrenaz, Th., Gautier, D., and Feuchtgruber, H.: 2003, 'Titan's atmosphere from ISO mid-infrared spectroscopy', *Icarus* **161**, 383–403.

de Bergh, C., Lutz, B. L., Owen, T., and Chauville, J.: 1988, 'Monodeuterated methane in the outer Solar Ssytem. III. Its abundance on Titan', *Astrophys. J.* **329**, 951–955.

Eberhardt, P., Reber, M., Krankowsky, D., Hidges, R. : 1995, 'The D/H and $^{18}O/^{16}O$ ratios in water from comet P/Halley', *Astron. Astrophys.* **302**, 301–316.

Farinella, P., Marzari, F., and Matteoli, S.: 1997, 'The disruption of Hyperion and the origin of Titan's atmosphere', *Astron. J.* **113**, 2312–2316.

Feuchtgruber, H., Lellouch, E., de Graauw, Th., Bézard, B., Encrenaz, T., and Griffin, M.: 1997, 'External supply of oxygen to the atmospheres of the giant planets', *Nature* **389**, 159–162.

Flasar, F.M., *et al.*: 2004, 'Temperatures, winds and composition in the Saturn system', *Science*, in press.

Gautier, D.: 1997, 'The aeronomy of Titan', ESA SP-1177.

Gautier, D. and Raulin, F.: 1997, 'Chemical composition of Titan's atmosphere', in A. Wilson (ed.), *Huygens: Science, Payload and Mission*, ESA Special report SP-1177, 359–364.

Gautier, D. and Hersant, F.: 2005, 'Formation and composition of planetesimals: trapping volatiles by clathration', this volume.

Geiss, J. and Gloecker, G.: 1998, 'Abundances of deuterium and helium-3 in the proto-solar cloud', *Space Sci. Rev.* **82**, 239–250.

Griffith, C.A. and Zahnle, K.: 1995, 'Influx of cometary volatiles to planetary moons: the atmospheres of 1000 possible Titans', *J. Geophys. Res.* **100**, 16,907–16,922.

Gurwell, M.A. and Muhlemann, D.O.: 2000, 'CO on Titan: more evidnece for a well-mixed vertical profile', *Icarus* **145**, 653–656.

Hersant, F., Gautier, D., and Lunine, J.I.: 2004, 'Enrichments in volatiles in the giant planets of the Solar System', *Plan. Space Sci.* **52**, 623–624.

Hidayat, T. and Marten, A.: 1998, 'Evidence for a strong $^{15}N/^{14}N$ enrichment in Titan's atmosphere from millimeter observations', *Icarus* **126**, 170–182.

Hidayat, T., Marten, A., Bézard, B., Gautier, D., Owen T., Matthews, H.E., and Paubert, G.: 1997, 'Millimeter and submillimeter observations of Titan: retrieval of the vertical profile of HCN and the $^{12}C/^{13}C$ ratio', *Icarus* **126**, 170–182.

Iro, N., Gautier, D., Hersant, F., Bockelée-Morvan, D., and Lunine, J.I.: 1997, 'An interpretation of the nitrogen deficiency in comets', *Icarus* **161**, 511–532.

Lammer, H., Stumptner, W., Molina-Cuberos, G.J., Bauer, S.J., and Owen, T.: 2000, 'Nitrogen isotope fractionation and its consequence for Titan's atmospheric evolution', *Plan. Space Sci.* **48**, 529–543.

Lara, L.M, Lellouch, E., López-Moreno, J.J., Rodrigo, R.: 1996, 'Vertical Distribution of Titan's Atmospheric Neutral Constituents', *J. Geophys. Res.* **101**, 23,262–23,283.

Lécluse, C. and Robert, F.: 1994, 'Hydrogen istope exchange rates: origin of water in the inner solar sytem', *Geochim. Cosmochim. Acta* **58**, 2297–2939.

Lécluse, C., Robert, F., Gautier, D., and Guiraud, M.: 1996, 'Deuterium enrichment in giant planets', *Plan. Space Sci.* **44**, 1579–1592.

Lellouch, E., Bézard, B., Fouchet, T., Feuchtgruber, H., Encrenaz, T., and de Graauw, T.: 2001, 'The deuterium abundance in Jupiter and Saturn from ISO-SWS observatons', *Astron. Astrophys.* **370**, 610–622.

Lellouch, E., Coustenis, A., Sebag, B., Cuby, J.-G., López-Valverde, M., Fouchet, Th., Crovisier, J., and Schmitt, B.: 2003, 'Titan's 5-micron window: observations with the Very Large Telescope', *Icarus* **162**, 156–169.

López-Valverde, M.A., Lellouch, E., and Coustenis, A.: 2004, 'Carbon monoxide fluorescence from Titan's atmosphere', *Icarus*, submitted.

Lorenz, R.D., McKay, C.P., and Lunine, J.I.: 1997, 'Photochemically-induced collapse of Titan's atmosphere', *Science* **275**, 642–644.

Lunine, J. and Tittemore, W.C.: 1993, 'Origins of outer-planet satellites', in E.H. Levy and J.L. Lunine (eds.), *Protostars and Planets III*, University of Arizona Press, pp. 1177–1252.

Lunine, J.I. and Stevenson, D.J.: 1987, 'Clathrate and ammonia hydrates at high pressure: Application to the origin of methane on Titan', *Icarus* **70**, 61–77.

Lunine, J.I., Yung, Y.I., and Lorenz, R.D.: 1999, 'On the volatile inventory of Titan from isotope abundances in nitrogen and methane', *Plan. Space Sci.*, **47**, 1291–1303.

Mahaffy, P.R., Donahue, T.M., Atreya, S.K., Owen, T.C., and Niemann, H.B.: 1998, 'Galileo probe measurements of D/H and ^{3}He/^{4}He in Jupiter's atmosphere', *Space Sci. Rev.* **84**, 251–263.

Marten, A., Hidayat, T., Moreno, R., Paubert, G., Bézard, B., Gautier, D., and Owen, T.: 1997, 'Saturn VI (Titan)', in D.W.E. Green (ed.), *IAU Circular* **6702**, 19 July.

Meier, R., Owen, T.C., Matthews, H.E., Jewitt, D.C., Bockelée-Morvan, D., Biver, N., Crovisier, J., and Gautier, D.: 1998a, 'A determination of the HDO/H_2O ratio in comet C/1995 01 (Hale-Bopp)', *Science* **279**, 842–844.

Meier, R., Owen, T.C., Jewitt, D.C., Matthews, H. E., Senay, M., Biver, N., Bockelée-Morvan, D., Crovisier, J., and Gautier, D.: 1998b, 'Deuterium in Comet C/1995 01 (Hale-Bopp): detection of DCN', *Science* **279**, 1707–1710.

Mousis, O., Gautier, D., and Bockelée-Morvan, D.: 2002a, 'An evolutionary turbulent model of Saturn's subnebula: Implications for the origin of the atmosphere of Titan', *Icarus* **156**, 162–175.

Mousis, O., Gautier, D., and Coustenis, A.: 2002b, 'The D/H ratio in methane in Titan. Origin and history', *Icarus* **159**, 156–169.

Orton, G.: 1992, 'Ground-based observations of Titan's thermal spectrum', in B. Kaldeich (ed.), *Symposium on Titan*, ESA-SP 338, 81–85.

Owen, T.C.: 1982, 'The composition and origin of Titan's atmosphere', *Plan. Space Sci.* **30**, 833–838.

Owen, T. and Bar-Nun, A.: 1995, 'Comets, impacts, and atmospheres', *Icarus* **116**, 215–226.

Owen, T., Biver, N., Marten, A., Matthews, H., and Meier, R.: 1999, *IAU Circ.* **703**, 11 November.

Owen T.C.: 2000, 'The origin of Titan's atmosphere', *Plan. Space Sci.* **48**, 747–752.

Penz, T., Lammer, H., and Biernat, H.K.: 2004, 'The influence of the solar particle and radiation environment on Titan's atmosphere evolution', *Adv. Space Res.*, submitted.

Pinto, J.P, Lunine, J.I., Kim, S.J., and Yung, Y.L.: 1986, 'D to H ratio and the origin and evolution of Titan's atmosphere', *Nature* **319**, 388–390.

Prinn, R.G. and Fegley, B.Jr.: 1981, 'Kinetic inhibition of CO and N_2 reduction in circumplanetary nebulae – Implications for satellite composition', *Astrophys. J.* **249**, 308–317.

Samuelson, R.F., Maguire, W.C., Hand, R.A., Kunde, V.G., Jennings, D.F., Yung, Y.L., and Aikin, A.C.: 1983, 'CO_2 on Titan', *J. Geophys. Res.* **88**, 8709–8715.

Samuelson, R.E. and Mayo, L.A. : 1997, 'Steady-state model for methane condensation in Titan's troposphere', *Planet. Space Sci.* **45**, 949–958.

Samuelson, R.E., Nath, N.R., and Borysow, A.: 1997a, 'Gaseous abundances and methane supersaturation in Titan's troposphere', *Planet. Space Sci.* **45**, 959–980.

Samuelson, R.E., Mayo, L.A., Knuckles, M.A., and Khanna, R.J.: 1997b, 'C_4N_2 ice in Titan's north polar stratosphere', *Planet. Space Sci.* **45**, 941–948.

Stevenson, D. J.: 1992, 'Interior of Titan', in B. Kaldeich (ed.), *Symposium on Titan*, ESA-SP 338, 29–33.

Strobel, D.F.: 2004, 'Photochemistry in outer solar system atmospheres', this volume.

Wong, A., Morgan, C.G., Yung, Y.L., and Owen, T.C.: 2000, 'Evolution of CO on Titan', *Icarus* **155**, 382–392.

Zahnle, K., Pollack, J.B., Grinspoon, D., and Dones, L.: 1992, 'Impact Generated Atmospheres over Titan, Ganymede and Callisto', *Icarus* **95**, 1–23.

Address for Offprints: Athena Coustenis, Paris-Meudon Observatory, 5, place Jules Jannsen, 92195 Meudon Cedex, France; athena.coustenis@obspm.fr

AEROSOLS ON THE GIANT PLANETS AND TITAN

RÉGIS COURTIN (regis.courtin@obspm.fr)
LESIA, CNRS/Observatoire de Paris, 92195 Meudon P^{al} CEDEX, France

Received: 1 June 2004; Accepted in final form: 30 August 2004

Abstract. On the giant planets and Titan, like on the terrestrial planets, aerosols play an important part in the physico-chemistry of the upper atmosphere ($P \leq 0.5$ bar). Above all, aerosols significantly affect radiative transfer processes, mainly through light scattering, thus influencing the atmospheric energy budget and dynamics. Because there is usually significant coupling between atmospheric circulation and haze production, aerosols may constitute useful tracers of atmospheric dynamics. More generally, since their production is directly linked to some kind of energy deposition, their study may also provide clues to external sources of energy as well as their variability. Finally, aerosols indirectly influence other processes such as cloud formation and disequilibrium chemistry, by acting either as condensation nuclei or as reaction sites for surface chemistry. Here, I present a review of observational and modeling results based on remote sensing data, and also some insights derived from laboratory simulations. Despite our knowledge of the effects of aerosols in outer planetary atmospheres, however, relatively little is understood about the pathways which produce them, either endogenously (as end-products of gas-phase photochemical or shock reactions) or exogenously (as residues of meteroid ablation).

Keywords: Aerosols, hazes, particulates, atmospheres, giant planets, Titan

1. Introduction

'Aerosols' is a general term describing solid or liquid particles of arbitrary shape that are suspended in a gaseous medium. In the case of planetary atmospheres, they are often referred to as haze particles (or simply haze), but also as particulates, dust, mist, smog, etc. Here, I will use indifferently the terms 'aerosols' and 'haze'.

One may distinguish between dispersion and condensation aerosols (Fuchs, 1964). The first category may be the result of grinding or atomization of solids or liquid particles (*e.g.* meteoroid ablation) or the consequence of the transfer of solid particles in the atmosphere through turbulent eddies (*e.g.* dust storms on Mars). The second category of aerosols may be formed through the condensation of supersaturated vapors (*e.g.* polar stratospheric clouds on Earth) or chemical reactions leading to non-volatile products (*e.g.* Titan's organic haze). The main difference between the two classes is that dispersion aerosols usually contain a wider range of particle sizes. There are also noticeable differences with regards to thermodynamical phase. Aerosols in solid-phase usually consist of individual or slightly aggregated particles of irregular form (dispersion aerosols) or of loose aggregates of a very large number of regular crystals or spherical particles (con-

Space Science Reviews 116: 185–199, 2005.
DOI: 10.1007/s11214-005-1955-1

densation aerosols). Conversely, aerosols in liquid phase are spherical and collision between them may produce spherical particles of larger dimensions. In any case, it is important to remember that the majority of natural aerosols are considerably polydisperse, *i.e.* the distribution of particle sizes is a certain function $f(r)$ characterized by a mean particle size r_0 and a variance b. Other important parameters are the number density as a function of altitude $N(z)$, and the scattering properties (extinction cross-section, phase function).

For spherical particles, depending on the magnitude of the size parameter $x = 2\pi r/\lambda$, where λ is the wavelength and r is the particle radius, Rayleigh ($x << 1$) or Mie ($x \sim 1$) theories allow a straightforward computation of the scattering properties of aerosols from their optical constants. For non-spherical particles (ovoids, tetrahedres, aggregates), specific methods have been developed which are more adapted to certain of the conditions encountered in planetary atmospheres. Caution needs to be exercized in this respect since most of the results derived to-date have been obtained under the assumption of sphericity.

On the giant planets and Titan, the general wisdom is that, regardless of their origin or phase, aerosols consist of the various particulates present in the atmospheric layers located above the tropospheric cloud deck, *e.g.* the NH_3 cloud on Jupiter and Saturn, the putative H_2S cloud on Uranus and Neptune, and the CH_4 cloud or rain on Titan. By virtue of the cloud formation process itself, in which the aerosols play the role of nucleation sites for the cloud particles, the borderline between the tropospheric haze and the condensation cloud is very tenuous. Characterizing the tropospheric aerosols often amounts to characterizing the cloud particles.

1.1. Significance of Aerosols

What is the significance of aerosols for the physico-chemistry of outer planetary atmospheres? For one thing, aerosols constitute a blurring veil through which we try to observe (and sometimes *cannot* observe) the deep layers of an atmosphere. More precisely, aerosols may be efficient scatterers of both sunlight and thermal radiation, thus exerting a strong and sometimes determinant influence on the distribution of energy throughout an atmosphere. In terms of thermal balance, their influence may be characterized as that of an anti-greenhouse layer: they absorb/scatter incoming solar radiation, whereas they are (almost) transparent to thermal emission radiated to space by deeper atmospheric layers or by the surface. Thus, haze particles contribute to the heating of upper atmospheric layers and to the maintenance of a thermal inversion above the tropopause.

Aerosols may also be useful tracers of dynamics, since there is usually significant coupling between atmospheric circulation and haze microphysics. This is particularly true in the case of Titan, but also evidenced in the case of the giant planets. More generally, the production of aerosols is related to some kind of energy deposition, either from solar UV radiation, or from impacting magnetospheric

particles and cosmic rays, or else from meteroid ablation. Therefore, the distribution of aerosols and their physico-chemical properties may be good indicators for the study of such external sources of energy and of their variability.

Finally, there are two areas in which the influence of aerosols is thought to be important but for which we have only scant information: cloud formation and disequilibrium chemistry. It could be said that without aerosols there would be no clouds, because aerosols provide the condensation nuclei for the formation and growth of tropospheric cloud particles from supersaturated gaseous constituents. These processes occur at levels much deeper than those at which aerosols are formed; therefore, this implies an efficient vertical transport of aerosols by turbulent diffusion and sedimentation. Finally, chemical reactions at the surface of haze particles are thought to provide alternate channels for complex chemical synthesis. One favorable factor is that stratospheric haze particles are more exposed to UV solar radiation and energetic particles than cloud particles.

1.2. Experimental Investigations

1.2.1. *Remote Sensing Observations*

The vast majority of observational results on aerosols have been obtained through the analysis of remote sensing data gathered in the UV–visible–IR range (roughly from 0.2 to 50 μm) from extensive Earth-based observations and from experiments on board the Pioneer, Voyager and Galileo probes. At UV, visible and near-IR wavelengths, the characteristics of aerosols are derived from measuring the scattered solar radiation, and by modeling the geometric albedo or spectral reflectivity of the planet. Most observations are obtained at low phase angles, but space probes have provided crucial opportunities for high phase angle measurements. At infrared wavelengths, some information may be derived on aerosols from modeling the thermal emission spectrum, provided the temperature structure and gaseous opacity are known with good accuracy. Section 2 presents several examples of what can be learned from such observations.

1.2.2. *In Situ Measurements*

So far, in situ measurements have contributed very little information on aerosols in the outer planets and Titan. One notable exception is the nephelometry experiment performed on Jupiter in December 1995 by the Galileo probe (Ragent *et al.*, 1996; 1998). However, this experiment obtained information in the range 0.46–12 bar, moreover in a relatively particle-free 5 micron "hot spot." Therefore, its results are much less relevant to the Jovian aerosols than to the cloud structure. In the near future (January 2005), thanks to the Huygens probe, collection and pyrolytic analysis of the Titan aerosols will be attempted (ACP experiment), as a set of spectrophotometric and polarimetric measurements are carried out simultaneously from the blue to the near-infrared against the solar radiation background (DISR

experiment). This unique combination of investigation techniques should provide crucial insights on both the chemical and optical properties of the aerosols.

1.2.3. *Laboratory Simulations*

An impressive body of (sometimes conflicting) information has been gathered in the last twenty years on outer planetary aerosol analogs from simulation experiments carried out in the laboratory. The synthesis of haze particles or material has been achieved through a wide range of energy deposition processes: UV photolysis, coronal or radio-frequency discharges, cold plasma discharge, shock chemistry, etc. Because of the upcoming Cassini-Huygens mission, investigation of the Titan aerosol analogs has been at the forefront of this effort (Khare *et al.*, 1984; Bar-Nun *et al.*, 1988; McDonald *et al.*, 1991; Thompson *et al.*, 1991; Sagan *et al.*, 1992; Scattergood *et al.*, 1992a; Scattergood *et al.*, 1992b; Khare *et al.*, 1993; Sagan *et al.*, 1993; McDonald *et al.*, 1994; Coll *et al.*, 1997; Khare *et al.*, 2001; Khare *et al.*, 2002; Ramirez *et al.*, 2002; Tran *et al.*, 2003), but some results are also relevant to Uranus and Neptune (Khare *et al.*, 1987). The information obtained from such experiments concern particle size, shape, complex index of refraction, electrostatic charging, stickiness and chemical composition. It should be noted that different schemes of energy deposition usually lead to different characteristics of the aerosols.

2. Characteristics of Aerosols in the Outer Planets

Early attempts at interpreting the geometric albedo of Jupiter at UV and visible wavelengths concluded to the presence of absorbing particles above the main cloud deck (Axel, 1972). For a while, this led to an awkward denomination for the Jovian aerosols which were dubbed "Axel dust." Similar inferences of the presence of stratospheric UV aborbing material were made by Scattergood and Owen (1977) in the case of Titan and the outer planets. To date, there have only been partial reviews of the characteristics of aerosols on the giant planets and Titan: for instance, Tejfel (1992) published such a review for the giant planets, and topical reviews also exist for each planet (as referenced in the following sub-sections). Below, I will only discuss some of the most recent works.

2.1. JUPITER

The Jovian areosols have been studied in much detail. The review by Tomasko (1976) summarized the results obtained from ground-based observations prior to the Pioneer fly-bys, while the Pioneer results themselves have been published by Smith and Tomasko (1984) and Tomasko *et al.* (1978). Contributions from the Voyager photopolarimeter experiment were presented by West *et al.* (1981). The International Ultraviolet Explorer also provided many insights on stratospheric aerosols (Tomasko *et al.*, 1986).

2.1.1. *The General Picture*

The present description of the Jovian aerosols derives from the summary compiled by West *et al.* (1986), as well as more recent ground-based spectrophotometric observations (Banfield *et al.*, 1998a). Assuming spherical particles with the refractive index of NH_3, one finds that the mean radius is within a factor of 2 of 0.2 μm. A nearly homogeneous stratospheric haze extends from $\sim$ 70 mbar to pressures less than 20 mbar (limit of sensitivity). This stratospheric haze becomes thicker and higher (P $\leq$ 10 mbar) poleward of 60°. The tropospheric haze is falling off above $\sim$ 400 mbar, but it extends higher ($\sim$ 200 mbar) in the North Equatorial Zone and over the Great Red Spot. Poleward of 45° North and South, it thins considerably. The two haze layers are separated by a relatively clear region at $\sim$100 mbar. This clearing is likely to be associated with coagulation of aerosols in the lower stratosphere, leading to an increased fall-out. This implies that the source of the stratospheric aerosols is located above 10 mbar.

More detailed information on the local and regional distribution of aerosols were gathered during the Galileo orbital mission (Banfield *et al.*, 1998b). First, these results confirmed that a stratospheric haze with an optical depth of $\sim$0.1–0.2 and an upper tropospheric haze of optical depth varying between 1 and 6 exist over all regions. These haze layers contain little lateral structure on scales smaller than the planetary jets. On scales of the jets and ovals, the pressure limits of the upper tropospheric haze vary regionally, although the concentration of particles is roughly constant. The majority of the albedo constrasts visible on Jupiter originate over a narrow height range centered at $\sim$750 mbar, where the NH_3 condensation cloud is expected.

Furthermore, Galileo high-phase angle images in the violet (417 nm) and near-IR (756 nm) revealed a more complex structure (Rages *et al.*, 1999). A detached haze layer was observed at 60° North in both filters. The extinction on the discrete haze layer is enhanced by a factor of $\sim$ 2 over its surroundings. The particle radius varies slightly from 0.27–0.32 μm near $\sim$ 20 mbar (from the violet filter) to 0.45 μm near $\sim$ 100 mbar (from the near-IR filter). In addition, a population of very small particles (0.02 μm) is needed to fit the violet limb profile. Aerosols may then be best represented as fluffy aggregates. Finally, the aerosol number density increases by an order of magnitude between 9° and 60° North.

One particularly interesting result came out of the Cassini fly-by which occured in December 2000, namely the detection of the NH_3-ice absorption feature at 10 μm by the Composite Infra-Red Spectrometer (Wong *et al.*, 2004), confirming the long-suspected nature of the tropospheric aerosols and upper cloud.

2.1.2. *Polar Regions and Auroral Zones*

The polar regions are covered with a thicker and higher stratospheric haze. At visible wavelengths, the polar regions appear dark, the Northern Polar Hood ($\phi \sim 46 - 90°$) being slightly more extended than the Southern one ($\phi \sim 57 - 90°$), whereas in strong methane bands, at 727 and 889 nm, and in the 2 μm continuum,

the polar hoods appear bright but less extended than at visible or UV wavelengths, suggesting a thickening of the haze near the poles. (West, 1979; 1988; Kim *et al.*, 1991). Furthermore, the polar hoods appear dark in the UV, implying the presence of UV-absorbing material such as hydrocarbon chains or hydrazine possibly associated with the deposition of energy and the chemistry involved in auroral phenomena (Pryor and Hord, 1991). The latter processes have been explored by Friedson *et al.* (2002) and Wong *et al.* (2003), who conclude that efficient pathways will lead to the formation of benzene and other complex hydrocarbons, including multi-ring compounds which subsequently condense to form aerosols.

2.1.3. *Aftermath of the SL9 Collision*

A unique opportunity to study the injection of aerosols in the atmosphere of a planet was offered to us by the impact of comet Shoemaker-Levy 9 with Jupiter in July 1994. A worldwide observing campaign brought forth many interesting results on the physical properties of the debris (Moreno *et al.*, 1995; Ortiz *et al.*, 1995; Rosenqvist *et al.*, 1995; Banfield *et al.*, 1996; Muñoz *et al.*, 1996; Molina *et al.*, 1997; Pryor *et al.*, 1997b). The review by West (1996) indicates the following characteristics: The mean particle radius is in the range 0.1–0.3 μm. Particles were distributed over a wide altitude range, between about 1 mbar and 200 mbar or deeper. Color and volatility of the aerosols suggest that they were formed from organic material recondensed on more refractory material, such al Al_2O_3, magnesium and iron silicates and soot, although the silicate material represented about 10–20% of the total volume of the particles. The latitudinal spread of the aerosols was on the order of 20° over one year and significant sedimentation occured over the same period.

2.2. SATURN

Excellent reviews of the characteristics of the Saturnian aerosols were published by Tomasko *et al.* (1984) and Tomasko and Doose (1985), based on the observational data gathered prior and during the Voyager encounters. Since then, new insights have been obtained from HST imaging (Karkoschka and Tomasko, 1993), airborne spectroscopy near 3μm (Kerola *et al.*, 1997), and ground-based near-IR spectrophotometry (Stam *et al.*, 2001).

The work by Karkoschka and Tomasko (1993) yielded the following general picture: stratospheric aerosols appear uniformely mixed with the top 10 km-amagat of gas ($P \leq 90 - 130$ mbar) above a uniformely mixed distribution of tropospheric aerosols. The optical thickness of the stratospheric aerosols increases from equator to pole ($\tau \sim 0.2$–0.4 at 70–90° N), and the mean particle radius is ~ 0.15 μm. In the polar region, they appear much darker than the tropospheric aerosols. The optical thickness of the latter decreases from equator to pole, and it is correlated with the wind speed pattern. Their optical properties are consistent with that of

NH_3 particles. The mean particle radius is $1.5\pm$ 0.3 μm, except maybe around southern mid-latitudes where it is smaller ($\sim$ 0.3 μm).

According to Kerola *et al.* (1997), however, the particles seen at 3 μm cannot be pure ice crystals. In their model, if an NH_3 haze extends much above the 700 mbar level, it becomes incompatible with the observed spectrum. Examination of other plausible haze materials which have diagnostic spectral features coincident with Saturn's 2 and 3 μm windows resulted in no positive identification of the composition of the tropospheriuc particles. In particular, both N_2H_4 and C_2H_2 can be ruled out. Thus, a scheme involving sedimentation of photochemically produced particles (*e.g.* P_2H_4) supersedes the notion that the convective uplift of solid NH_3 fills the 400–1400 mbar region with an extended haze of pure ammonia ice particles.

Using an inversion method independent of assumptions on the microphysical properties of the scatterers, Stam *et al.* (2001) found the following: the stratospheric and tropospheric haze layers are separated by a relatively clear region, and the latter is also separated from the NH_3 cloud; the bottom of the stratospheric haze varies between 20 mbar near the equator and 40 mbar at mid-latitudes; the largest stratospheric haze optical thickness is found at northern (fall) mid-latitudes, not in the polar regions; the tropospheric haze shows a strong hemispheric asymmetry: its extension varies from 80–400 mbar at southern mid-latitudes to 100–600 mbar at northern mid-latitudes, suggesting seasonal variations in the photochemical and condensation processes; the optical thickness of the tropospheric haze shows latitudinal variations, with the largest values found between 10° S and 15° N.

2.3. URANUS

The review published by West *et al.* (1991) summarized our post-Voyager knowledge on the Uranian aerosols. More detailed results derived from the Voyager imaging data were later pubished by Rages *et al.* (1991) and those from the photopolarimeter instrument by Pryor *et al.* (1997b). Subsequent studies were carried out by Baines *et al.* (1996) with ground-based spectrophotometric observations, by Baines *et al.* (1998) with HST imaging, and by Courtin (1999) with HST UV spectroscopy. From these works, the following structure has been derived: A three-tier stratospheric haze layer composed of condensed hydrocarbons and distributed uniformely across the disk, and a tropospheric methane haze with an optical thickness significantly enhanced south of $\sim$60°. Photochemical considerations predict that the stratospheric aerosols are made of C_4H_2 (at $\sim$0.2–2.5 mbar), C_2H_2 (at $\sim$2.5–14 mbar) and C_2H_6 (at $\sim$14–100 mbar), whereas the CH_4 haze extends from 100 to 1230 mbar. The mean particle radii are respectively 0.02, 0.05, 0.26 and 0.4 μm. Finally, the UV optical properties of the stratospheric haze material show some similarity with that of the Saturnian stratospheric haze, although they appear less absorbing (Figure 1).

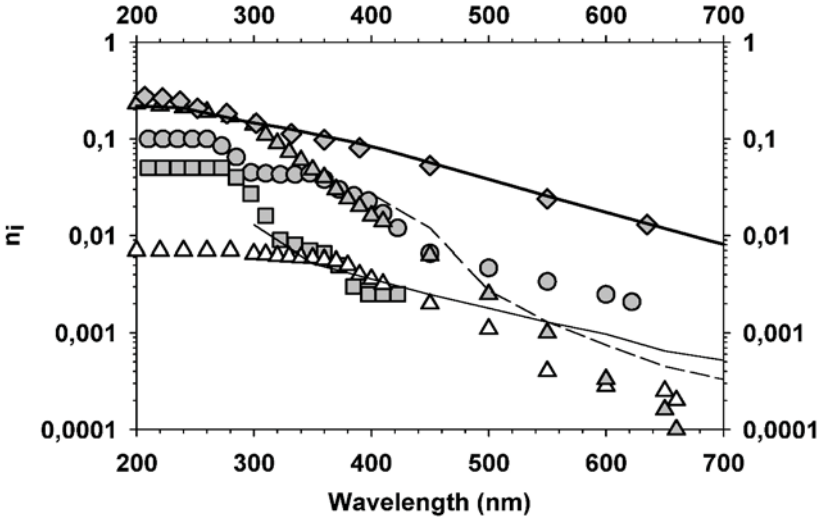

Figure 1. Imaginary index of refraction inferred for the Saturnian stratospheric (*filled triangles*) and tropospheric (*open triangles*) aerosols, for the Uranian (*circles*) and Neptunian (*squares*), aerosols (undistinguished stratospheric and tropospheric material), and for the Titan stratospheric aerosols (*diamonds*). Also plotted, are the laboratory measurements of Khare *et al.* (1984) for the Titan analogs (*thick solid line*), and those of Khare *et al.* (1987) for the Uranian and Neptunian analogs (*thin dashed line*: 93% H_2 + 7% CH_4 ; *thin solid line*: 99.5% H_2 + 0.5% CH_4).

2.4. NEPTUNE

Most of what we know on the Neptunian aerosols has been derived from the Voyager data (Conrath *et al.*, 1991; Pryor *et al.*, 1992; Moses *et al.*, 1995), and also from Earth-based observations carried out after the encounter. The review published by Baines *et al.* (1996) represents a good summary of our present understanding. From the analysis of ground-based spectrophotometric data by Baines and Hammel (1994), hazes on Neptune exhibit a structure grossly similar to that on Uranus, although the specifics are quite different in terms of particle size and number densities. The three stratospheric haze layers, thought to be composed of C_4H_2 (at ∼1.4–5.8 mbar), C_2H_2 (at ∼5.8–10 mbar) and C_2H_6 (at ∼10–20 mbar), are separated from the CH_4 haze extending from 340 to 1540 mbar. The mean particle radii are respectively 0.2, 0.2, 0.2 and 2.5 μm. From the analysis of HST spectroscopic observations, Courtin (1999) found that the stratospheric haze material are much less absorbing in the UV than on Uranus (Fig. 1).

High-phase angle images from Voyager 2 reveal a comparable picture with slightly different parameters, at least locally (28–30° S): A distinct haze layer is visible around 12 mbar, probably composed of condensed C_2H_6. The total atmospheric extinction in the 0.5–5 mbar range significantly exceeds the extinction due to Rayleigh scattering alone, suggesting the presence of high-altitude hazes. There is no evidence for methane condensation in the stratosphere, confirming the notion

that CH_4 is supersaturated there. The mean particle radius in the 0.5–5 mbar and at 28 mbar is $\sim$0.1 μm. The visible optical depth at 15 mbar is $1–4\times10^{-3}$, mostly from scattering. Hence, the hazes cannot account for the stratospheric temperature inversion, which is probably supported by the absorption due to supersaturated CH_4.

Also note that detailed studies have been published on the link between the photochemical production of hydrocarbons in Neptune's stratosphere and the nucleation processes leading to the formation of aerosols (Moses *et al.*, 1992; Romani *et al.*, 1993).

2.5. TITAN

The case of Titan is unique in the solar system. No other planetary satellite possesses such a dense and physico-chemically active atmosphere. From the point of view of aerosol synthesis, Titan could be nicknamed as the "ultimate tholins factory." A wealth of observational results concerning the aerosols have been obtained since the Voyager era (West and Smith, 1991; Courtin *et al.*, 1991; Samuelson and Mayo, 1991; Courtin, 1992; Samuelson, 1992; McKay and Toon, 1992; Toon *et al.*, 1992; Courtin *et al.*, 1995; Rannou *et al.*, 1995; Karkoschka and Lorenz, 1997; Lorenz *et al.*, 1997; Rannou *et al.*, 1997; McGrath *et al.*, 1998; Coustenis *et al.*, 1999; Lorenz *et al.*, 1999; Rannou *et al.*, 2000; Rannou *et al.*, 2003). Recent modeling works have been focused on the formation of the aerosols from gaseous compounds (Lebonnois *et al.*, 2002; Wilson and Atreya, 2003; Wilson and Atreya, 2004), and on their electrostatic charging (Bakes *et al.*, 2002; Dimitrov and Bar-Nun, 2003). Others have modeled the influence exerted by the ubiquitous haze on the thermal structure, the dynamics and associated seasonal changes, or the chemistry of minor species (McKay *et al.*, 1991; Hutzell *et al.*, 1993; Hutzell *et al.*, 1996; Rannou *et al.*, 2002; Bakes *et al.*, 2003).

Most of the results derived by the above-mentioned authors have been summarized in a thorough review by McKay *et al.* (2001). I will only recall a few important properties: the Titan haze is optically thick in the UV-visible ($\tau \sim 3$ at 0.5 μm) ; the optical depth decreases with increasing wavelength and the haze is almost purely scattering beyond 1 μm; the haze varies with latitude and season, the main features being a dark Polar Hood and an alternating hemispheric albedo contrast with a discontinuity at the equator; the particles in the main haze deck are probably fractal in nature with an equivalent volume radius of 0.2 μm; the optical properties of the aerosol material match that of laboratory analogs (or tholins) in the UV-visible-IR range; the haze material is probably composed of organic heteropolymers, but its stochiometry remains uncertain (C/N$\sim$2–11 and C/H$\sim$1 for analogs obtained by plasma discharge ; C/N$\sim$18–24 for photochemical analogs); haze particles may act as condensation nuclei for methane rain showers in the lower troposphere; the haze has a significant influence on the thermal balance (anti-greenhouse effect near the surface $\sim$-9 K + stratospheric heating $\sim$20 K);

there is a strong positive feedback between the haze and the circulation pattern which may explain the vertical structure (a detached haze around 400 km) and the seasonal cycle.

2.6. Comparative Results

The bonanza of observational results summarized above allows us to use a comparative approach to try and understand the physico-chemistry of aerosols on the outer planets and Titan. I will only touch on a few highlights.

Regarding the relationships between vertical structure and formation processes on the giant planets, one can surmise that distinct aerosol layers probably reflect distinct formation processes and compositions: stratospheric aerosols, generated at high altitude through photochemistry and auroral precipitation, are brought downwards by diffusion and sedimentation; upper tropospheric aerosols also appear to contain photochemical products (although less absorbing), rather than being made of pure NH_3 or CH_4 condensates. It is quite possible that a vertical composition gradient exists between the top of the tropospheric haze (ice crystals coated with photochemical products) and the bottom of the condensation cloud (ice crystals).

In terms of the coupling between aerosol formation and thermo-dynamical processes: on Titan, the vertical structure and seasonal cycle of the haze indicate a strong coupling between haze microphysics and atmospheric dynamics; on the giant planets, this coupling appears to be somewhat weaker. Is it only related to the magnitude of the mass-loading of the Titan haze which is 10 times larger than on Jupiter (25 against 3 μg.cm^{-2}) ?

As far as the optical properties of the aerosols are concerned, general trends may be derived from a comparison between the inferred absorptivities and that of laboratory analogs. Figure 1 represents the imaginary index of refraction of aerosols in Saturn, Uranus, Neptune, and Titan. First, it is remarkable that the observed values match the corresponding laboratory data so closely, at least in the 300-500 nm range. For Titan, this match extends even further into the infrared. All haze materials exhibit an increasing absorptivity towards the UV, the strongest variation being displayed by the stratospheric aerosols on Saturn, which are almost transparent in the red but are as dark as the Titan organic aerosols at 200 nm. It would be interesting to confirm and elucidate this behavior from more detailed measurements with Cassini. Contrary to expectations, aerosols on Neptune are more transparent than on Uranus, despite the fact that they are produced in a more methane-rich environnement. This may reflect the influence of a more vigorous mixing in the atmosphere.

3. Concluding Remarks

First, I would like to recall a word of caution from Karkoschka and Tomasko (1993): "One must be careful not the be fooled by exploring too small a class of atmospheric structures." This is to draw attention on the fact that most of our interpretations of remote sensing data still rely on certain assumptions, either about particle shape and size, haze vertical structure, or optical properties of the material. We need more "ground truth" from in situ measurements. The upcoming Huygens mission will certainly fill that hiatus in the case of Titan. It is hoped that the next couple of decades will see the advent of a multi-probe mission carrying nephelometers into the atmospheres of all four giant planets.

We have been rather successful at building realistic seasonal 2-D coupled models of the photochemical, microphysical and dynamical processes involved in shaping the structure and composition of the haze on Titan. Similar efforts need to be developed for the giant planets with an obvious priority for Saturn. Finally, we have just begun to explore the photochemical pathways leading to the formation of UV-dark material in the polar regions of the giant planets, and those leading to the formation of organic heteropolymers on Titan. Both modeling topics promise to be very fruitful in the context of the interpretation of the Cassini-Huygens data.

References

Axel, L.: 1972, 'Inhomogeneous models of the atmosphere of Jupiter', *Astrophys. J.* **173**, 451–468.

Baines, K.H. and Hammel, H.B.: 1994, 'Clouds, hazes, and the stratospheric methane abundance in Neptune', *Icarus* **109**, 20–39.

Baines, K.H., Hammel, H.B., Rages, K.A., Romani, P.N., and Samuelson, R.E.: 1996, 'Clouds and hazes in the atmosphere of Neptune', in D.P. Cruikshank (ed.), *Neptune and Triton*, The University of Arizona Press, Tucson, USA, pp. 489–546.

Baines, K.H., Yanamandra-Fisher, P.A., Lebofsky, L.A., Momary, T.W., Golisch, W., Kaminski, C. and Wild, W.J.: 1998, 'Near-infrared absolute photometric imaging of the Uranian system', *Icarus* **132**, 266–284.

Bakes, E.L.O., Lebonnois, S., McKay, C.P., and Bauschlicher, C.W.: 2002, 'Photoelectric charging of submicron aerosols and macromolecules in the Titan haze', *Icarus* **157**, 464–475.

Bakes, E.L.O., Lebonnois, S., Bauschlicher, C.W., and McKay, C.P.: 2003, 'The role of submicrometer aerosols and macromolecules in H_2 formation in the Titan haze', *Icarus* **161**, 468–473.

Banfield, D., Gierasch, P.J., Squyres, S.W., Nicholson, P.D., Conrath, B.J., and Matthews, K.: 1996, '2 μm spectrophotometry of Jovian stratospheric aerosols – scattering opacities, vertical distributions, and wind speeds', *Icarus* **121**, 389–410.

Banfield, D., Conrath, B.J., Gierasch, P.J., Nicholson, P.D., and Matthews, K.: 1998, 'Near-IR spectrophotometry of Jovian aerosols – meridional and vertical distributions', *Icarus* **134**, 11–23.

Banfield, D., Gierasch, P.J., Bell, M., Ustinov, E., Ingersoll, A.P., Vasavada, A.R., West, R.A. and Belton, M.J.S.: 1998, 'Jupiter's cloud structure from Galileo imaging data', *Icarus* **135**, 230–250.

Bar-Nun, A., Kleinfeld, I., and Ganor, E.: 1988, 'Shape and optical properties of aerosols formed by photolysis of acetylene, ethylene, and hydrogen cyanide', *J. Geophys. Res.* **93**, 8383–8387.

Coll, P., Cosia, D., Gazeau, M.-C., and Raulin, F.: 1997, 'New planetary atmosphere simulations: Application to the organic aerosols of Titan', *Adv. Space Res.* **19**, 1113–1119.

Conrath, B.J., Gautier, D., Lindal, G.F., Samuelson, R.E., and Shaffer, W.A.: 1991, 'The Helium Abundance of Neptune from Voyager Measurements', *J. Geophys. Res. Suppl.* **96**, 18,907–18,919.

Courtin, R., Wagener, R., McKay, C.P., Caldwell, J., Fricke K.-H., Raulin, F. and Bruston, P.: 1991, 'UV spectroscopy of Titan's atmosphere, planetary organic chemistry and prebiological synthesis. II. Interpretation of new IUE observations in the 220-335 nm range', *Icarus* **90**, 43–56.

Courtin, R.: 1992, 'Titan's UV albedo: Observations and modeling', *Symposium on Titan*, **ESA-SP 338**, pp. 59–67.

Courtin, R., Gautier, D. and McKay, C.P.: 1995, 'Titan's thermal emission spectrum: Reanalysis of the Voyager infrared measurements', *Icarus* **114**, 144–162.

Courtin, R.: 1999, 'The Raman signature of H_2 in the UV spectra of Uranus and Neptune: Constraints on the haze optical properties and on the para-H_2 fraction', *Planet. Space Sci.* **47**, 1077–1100.

Coustenis, A., Schmitt, B., Khanna, R.K., and Trotta, F.: 1999, 'Plausible condensates in Titan's stratosphere from Voyager infrared spectra', *Planet. Space Sci.* **47**, 1305–1329.

Dimitrov, V. and Bar-Nun, A.: 2003, 'Hardening of Titan's aerosols by their charging', *Icarus* **166**, 440–443.

Friedson, A.J., Wong, A.-S., and Yung, Y.L.: 2002, 'Models for polar haze formation in Jupiter's stratosphere', *Icarus* **158**, 389–400.

Fuchs, N.A.: 1964, *The Mechanics of Aerosols*, Pergamon Press, Oxford, England, 1964.

Hutzell, W.T., McKay, C.P., and Toon, O.B.: 1993, 'Effects of time-varying haze production on Titan's geometric albedo', *Icarus* **105**, 162–174.

Hutzell, W.T., McKay, C.P., Toon, O.B., and Hourdin, F.: 1996, 'Simulations of Titan's brightness by a two-dimensional haze model', *Icarus* **119**, 112–129.

Karkoschka, E. and Tomasko, M.G.: 1993, 'Saturn's upper atmospheric hazes observed by the Hubble Space Telescope', *Icarus* **106**, 428–441.

Karkoschka, E. and Lorenz, R.D.: 1997, 'Latitudinal variation of aerosol sizes inferred from Titan's shadow', *Icarus* **125**, 369–379.

Khare, B.N., Sagan, C., Arakawa, E.T., Suits, F., Callcott, T.A. and Williams, M.W.: 1984, 'Optical constants of organic tholins produced in a simulated Titanian atmosphere – from soft X-ray to microwave frequencies', *Icarus* **60**, 127–137.

Khare, B.N., Sagan, C., and Thompson, W.R.: 1987, 'Solid hydrocarbon aerosols produced in simulated Uranian and Neptunian stratospheres', *J. Geophys. Res.* **92**, 15,967–15,082.

Khare, B.N., Thompson, W.R., Cheng, L., Chyba, C., Sagan, C., Arakawa, E.T., Meisse, C. and Tuminello, P.S.: 1993, 'Production and optical constraints of ice tholin from charged particle irradiation of (1:6) C_2H_6/H_2O at 77 K', *Icarus* **103**, 290–300.

Khare, B.N., Bakes, E.L.O., Cruikshank, D., and McKay, C.P.: 2001, 'Solid organic matter in the atmosphere and on the surface of Outer Solar System bodies', *Adv. Space Res.* **27**, 299–307.

Khare, B.N., Bakes, E.L.O., Imanaka, H., McKay, C.P., Cruikshank, D.P. and Arakawa, E.T.: 2002, 'Analysis of the time-dependent chemical evolution of Titan haze tholin', *Icarus* **160**, 172–182.

Kerola, D.X., Larson, H.P., and Tomasko, M.G.: 1997, 'Analysis of the near-IR spectrum of Saturn: A comprehensive radiative transfer model of its middle and upper troposphere', *Icarus* **127**, 190–212.

Kim, S.J., Goorvitch, D., Drossart, P., Moorwood, A., and Caldwell, J.: 1991, 'The 2-micron polar haze of Jupiter', *Icarus* **91**, 145–153.

Lebonnois, S., Bakes, E.L.O., and McKay, C.P.: 2002, 'Transition from gaseous compounds to aerosols in Titan's atmosphere', *Icarus* **159**, 505–517.

Lorenz, R.D., Smith, P.H., Lemmon, M.T., Karkoschka, E., Lockwood, G.W., and Caldwell, J.: 1997, 'Titan's North-South asymmetry from HST and Voyager imaging: Comparison with models and ground-based photometry', *Icarus* **127**, 173–189.

Lorenz, R.D., Lemmon, M.T., and Smith, P.H.: 1999, 'Seasonal change on Titan observed with the Hubble Space Telescope WFPC-2', *Icarus* **142**, 391–401.

McDonald, G.D., Khare, B.N., Thompson, W.R., and Sagan, C.: 1991, '$CH_4/NH_3/H_2O$ spark Tholin: Chemical analysis and interaction with Jovian aqueous clouds', *Icarus* **94**, 354–367.

McDonald, G.D., Thompson, W.R., Heinrich, M., Khare, B.N., and Sagan, C.: 1994, Chemical Investigation of Titan and Triton Tholins, *Icarus* **108**, pp. 137–145

McGrath, M.A., Courtin, R., Smith, T.E., Feldman, P.D., and Strobel, D.F.: 1998, 'The ultraviolet albedo of Titan', *Icarus* **131**, 382–392.

McKay, C.P., Pollack, J.B., and Courtin, R.: 1991, 'The greenhouse and antigreenhouse effects on Titan', *Science* **253**, 1118–1121.

McKay, C.P. and Toon, O.B.: 1992, 'Titan's organic haze', *Symposium on Titan*, **ESA-SP 338**, 185–190.

McKay, C.P., Coustenis, A., Samuelson, R.E, Lemmon, M.T., Lorenz, R.D., Cabane, M., Rannou, P., and Drossart, P.: 2001, 'Physical properties of the organic aerosols and clouds on Titan', *Planet. Space Sci.* **49**, 79–99.

Molina, A., Moreno, F., and Muñoz, O.: 1997, 'Aerosol debris in the core and crescent-shaped regions of Comet P/Shoemaker-Levy 9 H and G fragment impact sites on Jupiter', *Icarus* **127**, 213–220.

Moreno, F., Muñoz, O., Molina, A., López-Moreno, J.J., Ortiz, J.L., Rodríguez, J., López-Jimenez, A., Girela, F., Larson, S.M., and Campins, H.: 1995, 'Physical properties of the aerosol debris generated by the impact of fragment H of Comet P/Shoemaker-Levy 9 on Jupiter', *Geophys. Res. Lett.* **22**, 1609–1612.

Moses, J.I., Allen, M., and Yung, Y.L.: 1992, 'Hydrocarbon nucleation and aerosol formation in Neptune's atmosphere', *Icarus* **99**, 318–346.

Moses, J.I., Rages, K., and Pollack, J.B.: 1995, 'An analysis of Neptune's stratospheric haze using high-phase-angle Voyager images', *Icarus* **113**, 232–266.

Muñoz, O., Moreno, F., and Molina, A.: 1996, 'Aerosol properties of debris from fragments E/F of Comet Shoemaker-Levy 9', *Icarus* **121**, 305–310.

Ortiz, J.L., Muñoz, O., Moreno, F., Molina, A., Herbst, T.M., Birkle, K., Böhnhardt, H. and Hamilton, D.P.: 1995, 'Models of the SL9 collision-generated hazes', *Geophys. Res. Lett.* **22**, 1605–1608.

Pryor, W.R. and Hord, C.W.: 1991, 'A study of photopolarimeter system UV absorption data on Jupiter, Saturn, Uranus and Neptune: Implications for auroral haze formation', *Icarus* **91**, 161–172.

Pryor, W.R., West, R.A., Simmons, K.E., and Delitsky, M.: 1992, 'High-phase-angle observations of Neptune at 2650 and 7500 Å – haze structure and particle properties', *Icarus* **99**, 302–317.

Pryor, W.R., Na, C.Y., Cochran, A.L., Cochran, W.D., Barker, E.S., Armosky, B.J., and Pulliam, C.E.: 1997a, 'McDonald observatory data on the Comet Shoemaker-Levy 9 impacts on Jupiter and the resulting haze particles', *Planet. Space Sci.* **45**, 1299–1313.

Pryor, W.R., West, R.A., and Simmons, K.E.: 1997b, 'High-phase angle observations of Uranus at 2650 Å: Haze structure and particle properties', *Icarus* **127**, 508–522.

Ragent, B., Colburn, D.S., Avrin, P., and Rages, K.A.: 1996, 'Results of the Galileo probe nephelometer experiment', *Science* **272**, 854–856.

Ragent, B., Colburn, D.S., Rages, K.A., Knight, T.C.D., Avrin, P., Orton, G.S., Yanamandra-Fisher, P.A., and Grams, G.W.: 1998, 'The clouds of Jupiter: Results of the Galileo Jupiter mission probe nephelometer experiment', *J. Geophys. Res.* **103**, 22891–22910.

Rages, K., Pollack, J.B., Tomasko, M.G., and Doose, L.R.: 1991, 'Properties of scatterers in the troposphere and lower stratosphere of Uranus based on Voyager imaging data', *Icarus* **89**, 359–376.

Rages, K., Beebe, R., and Senske, D.: 1999, 'Jovian stratospheric hazes: The high-phase angle view from Galileo', *Icarus* **139**, 211–226.

Ramirez, S.I., Coll, P., Da Silva, A., Navarro-Gonzalez, R., Lafait, J., and Raulin, F.: 2002, 'Complex refractive index of Titan's analogues in the 200–900 nm domain', *Icarus* **156**, 515–529.

Rannou, P., Cabane, M., Chassefière, E., Botet, R., McKay, C.P., and Courtin, R.: 1995, 'Titan's geometric albedo: Role of the fractal structure of the aerosols', *Icarus* **118**, 355–372.

Rannou, P., Cabane, M., Botet, R., and Chassefière, E.: 1997, 'A new interpretation of scattered light measurements at Titan's limb', *J. Geophys. Res.* **102**, 10,997–11,013.

Rannou, P., Ferrari, C., Rages, K., Roos-Serote, M., and Cabanes, M.: 2000, 'Characterization of aerosols in the detached haze layer of Titan', *Icarus* **147**, 267–281.

Rannou, P., Hourdin, F., and McKay, C.P.: 2002, 'A wind origin for Titan's haze structure', *Nature* **418**, 853–856.

Rannou, P., McKay, C.P., and Lorenz, R.D.: 2003, 'A model of Titan's haze of fractal aerosols constrained by multiple observations', *Planet. Space Sci.* **51**, 963–976.

Romani, P.N., Bishop, J., Bézard, B., and Atreya, S.: 1993, 'Methane photochemistry on Neptune: Ethane and acetylene mixing ratios and haze production', *Icarus* **106**, 442–463.

Rosenqvist, J., *et al.*: 1995, 'Four-micron infrared observations of the Comet Shoemaker-Levy 9 collision with Jupiter at the Zelenchuk observatory: Spectral evidence for a stratospheric haze and determination of its physical properties', *Geophys. Res. Lett.* **22**, 1585–1588.

Sagan, C., Thompson, W.R., and Khare, B.N.: 1992, 'Titan's organic chemistry: Results of simulation experiments', *Symposium on Titan*, **ESA-SP 338**, 161–165.

Sagan, C., Khare, B.N., Thompson, W.R., McDonald, G.D., Wing, M.R., Bada, J.L., Vo-Dinh, T. and Arakawa, E.T.: 1993, 'Polycyclic aromatic hydrocarbons in the atmospheres of Titan and Jupiter', *Astrophys. J.* **414**, 399–405.

Samuelson, R.E., and Mayo, L.A.: 1991, 'Thermal infrared properties of Titan's stratospheric aerosols', *Icarus* **91**, 207–219.

Samuelson, R.E.: 1992, 'Infrared properties of Titan's clouds and aerosols', *Symposium on Titan*, **ESA-SP 338**, 191–195.

Scattergood, T. and Owen, T.: 1977, 'On the sources of ultraviolet absorption in spectra of Titan and the Outer planets', *Icarus* **30**, 780–788.

Scattergood, T.W., Lau, E.Y., and Stone, B.M.: 1992a, 'Titan's aerosols. I - Laboratory investigations of shapes, size distributions, and aggregation of particles produced by UV photolysis of model Titan atmospheres', *Icarus* **99**, 98–105.

Scattergood, T.W., Stone, B.M., and Lau, E.Y.: 1992b, 'Laboratory investigations of the aerosols in the stratosphere of Titan', *Symposium on Titan*, **ESA-SP 338**, 377–381.

Smith, P.H., and Tomasko, M.G.: 1984, 'Photometry and polarimetry of Jupiter at large phase angles. II - Polarimetry of the South tropical zone, South equatorial belt, and the polar regions from the Pioneer 10 and 11 missions', *Icarus* **58**, 35–73.

Stam, D.M., Banfield, D., Gierasch, P.J., Nicholson, P.D., and Matthews, K.: 2001, 'Near-IR spectrophotometry of Saturnian aerosols – meridional and vertical distribution', *Icarus* **152**, 407–422.

Tejfel, V.G.: 1992, 'Aerosol component of the atmospheres of the Giant planets', *Astronomicheskii Vestnik* **26**, 3–27.

Thompson, W.R., Henry, T.J., Schwartz, J.M., Khare, B.N., and Sagan, C.: 1991, 'Plasma discharge in $N_2 + CH_4$ at low pressures – experimental results and applications to Titan', *Icarus* **90**, 57–73.

Tomasko, M.G.: 1976, 'Photometry and polarimetry of Jupiter', *Jupiter*, The University of Arizona Press, Tucson, USA, pp. 486–515.

Tomasko, M.G., West, R.A., and Castillo, N.D.: 1978, 'Photometry and polarimetry of Jupiter at large phase angles. I - Analysis of imaging data of a prominent belt and a zone from Pioneer 10', *Icarus* **33**, 558–592.

Tomasko, M.G., West, R.A., Orton, G.S., and Tejfel, V.G.: 1984, 'Clouds and aerosols in Saturn's atmosphere', *Saturn*, The University of Arizona Press, Tucson, USA, pp. 150–194.

Tomasko, M.G. and Doose, L.R.: 1985, 'Clouds and aerosols on Saturn', *The Atmospheres of Saturn and Titan*, **ESA-SP 241**, 53–61.

Tomasko, M.G., Karkoschka, E., and Martinek, S.: 1986, 'Observations of the limb darkening of Jupiter at ultraviolet wavelengths and constraints on the properties and distribution of stratospheric aerosols', *Icarus* **65**, 218–243.

Toon, O.B., McKay, C.P., Griffith, C.A., and Turco, R.P.: 1992, 'A physical model of Titan's aerosols', *Icarus* **95**, 24–53.

Tran, B.N., Joseph, J.C., Ferris, J.P., Persans, P.D., and Chera, J.J.: 2003, 'Simulation of Titan haze formation using a photochemical flow reactor. The optical constants of the polymer', *Icarus* **165**, 379–390.

West, R.A.: 1979, 'Spatially resolved methane band photometry of Jupiter. I. Absolute reflectivity and center-to-limb variations in the 6190-, 7250- and 8900-Å bands', *Icarus* **38**, 12–33.

West, R.A., Hord, C.W., Simmons, K.E., Coffeen, D.L., Sato, M., and Lane, A.L.: 1981, 'Near-ultraviolet scattering properties of Jupiter', *J. Geophys. Res.* **86**, 8783–8792.

West, R.A., Strobel, D.F., and Tomasko, M.G.: 1986, 'Clouds, aerosols, and photochemistry in the Jovian atmosphere', *Icarus* **65**, 161–217.

West, R.A.: 1988, 'Voyager 2 imaging eclipse observations of the Jovian high altitude haze', *Icarus* **75**, 381–398.

West, R.A. and Smith, P.H.: 1991, 'Evidence for aggregates particles in the atmosheres of Titan and Jupiter', *Icarus* **90**, 330–333.

West, R.A., Baines, K.H., and Pollack, J.B.: 1991, 'Clouds and aerosols in the Uranian atmosphere', *Uranus*, The University of Arizona Press, Tucson, USA, pp. 296–324.

West, R.A.: 1996, 'Particles in Jupiter's atmosphere from the impacts of Comet P/Shoemaker-Levy 9', *IAU Colloquium 156: The Collision of Comet Shoemaker-Levy 9 and Jupiter*, Cambridge University Press, Cambridge, USA, pp. 269–292.

Wilson, E.H. and Atreya, S.K.: 2003, 'Chemical sources of haze formation in Titan's atmosphere', *Planet. Space Sci.* **51**, 1017–1033.

Wilson, E.H. and Atreya, S.K.: 2004, 'The current state of modeling the photochemistry of Titan's mutually-dependent atmosphere and ionosphere', *J. Geophys. Res.* **109**, E06002.

Wong, A.-S., Yung, Y.L., and Friedson, A.J.: 2003, 'Benzene and haze formation in the polar atmosphere of Jupiter', *Geophys. Res. Lett.* **30**, 1–4.

Wong, M.H., Bjoraker, G.L., Smith, M.D., Flasar, F.M., and Nixon, C.A.: 2004, 'Identification of the 10-μm ammonia ice feature on Jupiter', *Planet. Space Sci.* **52**, 385–395.

Address for Offprints: Régis Courtin, LESIA, CNRS/Observatoire de Paris, 92195 Meudon P^{al} CEDEX, France; Regis.Courtin@obspm.fr

THE CHANGING FACE OF TITAN'S HAZE: IS IT ALL DYNAMICS?

ROOS-SEROTE, M.
Lisbon Astronomical Observatory, Tapada da Ajuda, 1349-018, Lisbon, Portugal

Received:16 April 2004; Accepted in final form: 22 June 2004

Abstract. Titan's atmosphere shows some similarities with that of the Earth, in terms of composition and surface pressure. Also, its seasonal cycle is similar, as Titan's obliquity is about 27° (23°,5 for the Earth), although it is about 30 times as long.

Titan's haze exhibits an albedo contrast (NSA for North-South Asymmetry) that is changing seasonally. From the analysis of Voyager and Hubble Space Telescope data, we learned that at short visible wavelengths, the albedo of the winter hemisphere is lower by 10-20% than that of the summer hemisphere. This asymmetry peaks at 450 nm and reaches maximum amplitude around Titan's equinoxes. It reverses in about five years, faster than a season which spans seven years. At longer wavelengths, longward of 700 nm, the asymmetry is inverted. The NSA reversal process in the red and in the UV seems to lead the reversal in the blue by 1 or 2 years. No valid explanation exists for this lag, at least in the red.

The results from a recent model which couples atmospheric dynamics, haze microphysics and transport, as well as photochemistry, show that the NSA and its seasonal changes can be explained by an accumulation of haze particles at the winter pole. This is due to the pole-to-pole Hadley circulation pattern that is present during most of Titan's year and rapidly disrupts at the time of the equinoxes. This model can also explain the observed cooler stratospheric temperatures and higher abundances of heavy hydrocarbons and nitriles in the winter polar region. In addition, it provides a mechanism for the formation of a detached haze layer around 300-400 km altitude, as well as the existence of a polar hood.

Thus, it appears that the latitudinal contrasts we observe on Titan are conveniently tracing for us the dynamical behavior of its atmosphere.

Keywords: Titan, haze, season, dynamics

1. Summary of the Haze Properties

Titan's seasonal cycle spans 29.46 Earth years, the time for Saturn to complete an orbit around the Sun at an average distance of 9.54 Astronomical Units. Titan's obliquity is 26°.7, very similar to that of the Earth. The illumination of Titan by the Sun therefore changes in a similar way as for the Earth, in particular both north and south polar regions experience long polar nights. Figure 1 summarizes the seasons on Titan.

An excellent review on the physical characteristics of Titan's haze has been published by McKay *et al.* (2001). The haze is the result of photochemistry taking place in the high atmosphere of Titan, mostly between 500 and 800 km altitude. At these altitudes both molecular nitrogen, the main component of Titan's atmosphere

Space Science Reviews 116: 201–210, 2005.
DOI: 10.1007/s11214-005-1956-0

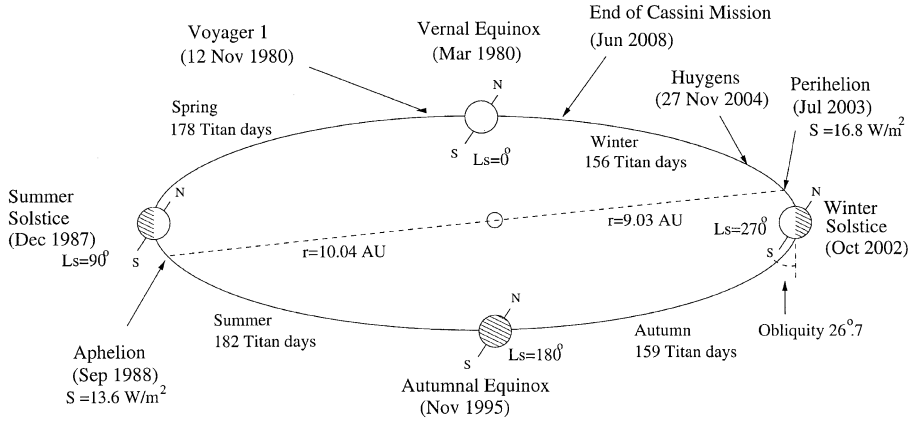

Figure 1. Orbital motion of Titan and Saturn around the Sun during one Saturn year. L_S denotes the Kronocentric orbital longitude of the Sun that characterises the season. Reprinted from *Planetary and Space Science* **47**, Tokano et al., 'Seasonal variation of Titan's atmospheric structure simulated by a general circulation model', pp. 493–520, Copyright 1999, with permission from Elsevier.

(98 %) and methane are photolysed by UV radation from the Sun and are dissociated by energetic particles. Complex reactions betweens ions and radicals thus result in a host of higher organic molecules and nitriles (see for example Wilson and Atreya, 2000, for an overview). Polymerization also takes place, leading to the formation of aerosols. Cabane *et al.* (1992) present a detailed model for the formation and growth of these particles, and conclude that there are two stages. In the first stage small spherical particles form (radius on the order of 0.1 micron) in the 500-600 km altitude range. Upon settling, these particles stick together to form aggregates, which are best described by fractals (West and Smith, 1991; Cabane *et al.*, 1993). It is these aggregate particles that constitute the hazes in the stratosphere (40 to 300 km altitude). The haze production rate is on the order of $0.5 - 2 \times 10^{-14}$ g cm^{-2} s^{-1}.

The detailed vertical haze profile can not be uniquely determined from remote sensing data. For example Rannou *et al.* (2003) use measurements of Titan's geometric albedo between 0.6 and 0.9 micron to constrain the haze vertical profile. They find that the haze extinction decreases with increasing altitude starting at a 100 km and with a scale height about equal to the atmospheric scale height. Below a 100 km, the extinction should decrease down to 30 km, which is slightly into the troposphere.

No measurements, either direct or remote, exist on the composition of the haze particles. Laboratory simulations show that particles forming under Titan conditions, have a C/N ratio of about 1.5 - 18 and a C/H ratio of about 1 (see Table 1 in Lebonnois *et al.*, 2002, for a summary and references, Tran *et al.*, 2003).

Particles that precipitate from the stratosphere into the troposphere could act as consensation nuclei for the formation of methane droplets and clouds. Methane

can be supersaturated in the troposphere (Samuelson *et al.*, 1997; McKay *et al.*, 1997; Tokano *et al.*, 2001). There is clear evidence for tropospheric clouds (Griffith *et al.*, 1998), yet they are either very thin, very patchy and/or transient. Precipitation from these cloud is not expected to reach the surface as total evaporation should occur just above it (Tokano *et al.*, 2001). Slow settling of small fog particles may bring material to the surface, and modify its composition. In any case, the process is not cyclic, and methane is effectively removed from the atmosphere. In fact, the present amount of methane will be completely destroyed in a time several orders of magnitude shorter than the age of the Solar System. Several ideas have been proposed for the source of methane in Titan's atmosphere. Certainly, the Cassini/Huygens mission will bring more insight into this question.

When the Voyager spacecraft flew by Saturn and Titan in the late 1980 and mid 1981, they discovered a Titan completely embedded in an inpenetrable haze layer (at least at visible wavelengths). Nothing could be revealed about the surface. Titan's haze opacity is large at visible wavelengths (about 3 at 0.5 micron), but becomes more and more transparent toward the Near InfraRed (NIR). Several windows in the near-infrared (NIR) are now known and are now used to monitor the lower atmosphere and surface of Titan using Earth-based observatories.

The haze affects the thermal balance of the atmosphere, which in turn affects the circulation and the chemistry, which then feeds back into the haze distribution, and so on. A complete model of Titan's atmosphere should therefore include dynamics, radiative transfer, haze formation and transport, and chemistry. Only recently has such a model become available.

2. The Changing Face of Titan's Haze

2.1. The North-South Asymmetry

At the time of the Voyager encounters (Voyager 1 in November 1980, Voyager 2 in August 1981) Titan had just passed Vernal Equinox (see Figure 1). One of the features observed was an asymmetry of the albedo at visible wavelengths between the northern and the southern hemisphere: the southern hemisphere was about 20% brighter than the northern (Smith *et al.*, 1981; 1982). This effect became known as the North-South Asymmetry (NSA). Before the Voyager encounters, ground based observations of the unresolved disk of Titan had shown that the albedo changes by about 10% at blue and yellow wavelengths over a 7-year period, tentatively attributed to a possible relationship between atmospheric chemistry and the 11-year solar cycle (Lockwood and Thompson, 1979). However, in the years after the Voyager mission, it became clear that the albedo changes are related to the season of Titan (Sromovsky *et al.*, 1981; Lockwood *et al.*, 1986). The cause of the changes must be related to the haze, probed at visible wavelengths.

With the coming of the Hubble Space Telescope (HST) in the late 1980's it became possible to resolve Titan's disk well enough and to monitor its albedo changes

at different wavelengths. Several observing campaigns were performed. Caldwell *et al.* (1992), and Lorenz *et al.* (1997; 1999, 2001) report on the results from HST sessions performed during the 1990s. Caldwell *et al.* (1992) were the first to report that the NSA had reversed at blue (440 nm) and yellow (550 nm) wavelengths, *i.e.* the northern hemisphere was about 10% brighter than the southern. They observed Titan with the HST in August of 1990. However, from images taken at 889nm, in the center of a strong methane absorption band for which no Voyager equivalent exists, the NSA seemed to be inverse relative to the shorter wavelengths. Further observations were performed (Lorenz *et al.*, 1997; 1999; 2001) and the following characteristics of the NSA can be listed:

- The NSA is a function of wavelength: it is strongest at blue wavelengths (with a peak around 450 nm) and at 889 nm (but reversed), weaker at UV and it reverses at red and NIR wavelengths (longward of 700 nm). This could be explained by the increasing albedo of the haze particles with wavelength (Lorenz *et al.*, 1997). At blue wavelengths the particles are dark. In addition, the light from the atmosphere is dominated by Rayleigh scattering which is predicted to have a similar or higher column optical depth than the haze (Figure 9 in (McKay *et al.*, 1989)). Here we may be seeing mainly sunlight scattered back by the atmosphere. At red wavelengths, in particular at the methane bands, the atmosphere is dark. High altitude haze (higher than 60 km altitude) will show up bright. Spatial changes in the haze quantity will then produce contrasts.
- The NSA's phase depend on wavelength: It reaches maximum during the equinox periods, and reverses in the years after the equinoxes. The reversal takes place in about five year, which is faster than the seven year period between equinox and solstice. There is a phase lag of the NSA of about 90° relative to the solar forcing (maximum at the solstices) (Sromovsky *et al.*, 1981; Lorenz *et al.*, 1997). Also, the NSA change in the blue lags behind the change at shorter (UV) and longer wavelengths (> 600 nm) by about 1 or 2 years.

  For the UV, this can be explained by an earlier change in the haze structure at higher altitudes, sounded at these wavelengths. The same is true for the methane absorption bands at 619 nm and 889 nm. However, no good explaination is available for the lag at red continuum wavelengths, which sound deeper atmospheric levels.

  In HST images obtained in 2000, the NSA had inversed again, back to the situation Voyager had encountered (Figure 1 and Lorenz *et al.*, 2001). During the Cassini/Huygens mission the NSA is expected to be stable. It may start to change again somewhere during the extended mission, beyond 2008.

Several mechanisms were proposed to explain the NSA, but a dynamical origin appears most plausible. This is discussed in the next section. Other mechanisms can either be ruled out or can contribute, but not in a dominant way (Lorenz *et al.*, 1997; 1999):

- If a difference in particle sizes between hemispheres was causing the NSA, then the NSA would change as a function of phase angle, *i.e.* it should disappear at small phase angles and reverse near 90° phase angle (Sromovsky *et al.*, 1981 based on the optical properties derived by Rages and Pollack, 1980). This effect was not at all observed. Instead, the NSA remains constant for phase angles at least up to 90° (Sromovsky *et al.*, 1981; Lorenz *et al.*, 1997; Sromovsky and Fry, 1989).
- Sromovsky *et al.* (1981) also considered a deep cloud layer as a possible candidate to explain the NSA. In order for this cloud to fit Titan's geometric albedo as derived by Rages and Pollack (1980), it would have to be more absorbing at short wavelengths, making the NSA stronger at longer wavelengths. However, the opposite is observed, *i.e.* a decrease and reversal of the NSA occurs at longer wavelengths.
- A change of the optical properties due to condensation of materials onto the haze particles is proposed by Courtin *et al.* (1992). He notes a correlation between the increased HCN and C_2H_4 abundances in the northern polar region, as determined from Voyager 1 spectroscopic measurements, and the lower albedo in this region. Voyager 2 data analysis shows that the abundance of other heavier hydrocarbons, likely to condense onto haze particles, have decreased relative to Voyager 1 in high northern latitudes. This would tend to increase the NSA contrast in the UV (Courtin *et al.*, 1992), which is not observed. Even though this process may take place, it cannot be dominant. In addition, Toon *et al.* (1992) point out that this would not cause the observed reversal at longer wavelengths.
- Hutzell *et al.* (1993) and Lorenz *et al.* (1997) test a model in which the cause of the NSA is a change in the number density of haze particles. They model this change by varying the production rate, which modifies the number of particles higher in the atmosphere, and a change in rain-out altitude, which changed the particle density at lower altitudes. The results are promising, but not satisfactory. It is noted that the time scales of the changes in production rate are much longer than the seasonal time scale.

2.2. Detached Haze Layer and Polar Hood

In the Voyager 1 images, an additional haze layer was detected at higher altitudes than the main haze (Rages and Pollack, 1983) and detached from it. Hence, its denomination as the "the detached haze layer". This layer is clearly visible in high phase angle images as presented for example by Rannou *et al.* (1997). Karkoschka and Lorenz (1997) infer the existence of the detached haze layer from the analysis of images of the shadow of Titan seen on Saturn obtained with the HST in 1995. The detached haze layer seems to be a permanent feature.

In addition, the Voyager images show the existence of a polar hood, a darkening in the north polar region. A closer examination of high and low phase angle

images clearly show that the detached haze layer and the polar hood are physically connected: the whole of Titan is covered by a detached haze layer, and this layer is more opaque over the north (winter) polar region, forming the hood. In the low phase angle image, the polar hood can be clearly seen to be located above the main haze. In the high phase angle image, the physical connection between the detached haze and the polar hood can be neatly distinguished: the detached haze merges into the polar hood near about 65-70 degrees north latitude.

The Voyager 2 images showed that the polar hood seen in Voyager 1 images some nine months earlier had now become more a polar collar. Karkoschka and Lorenz (1997), from HST data obtained in 1995, detected a polar hood at the south pole, as expected. Lorenz *et al.* (2001) report on the detection of a polar collar around 60° south latitude at UV wavelengths in HST images taken in 2000. They refer to possible detection of a polar hood in HST 1995 images. Yet, non-optimal viewing conditions of the south polar region make it impossible to draw any firm conclusions. Roe *et al.* (2002) detect the collar at NIR wavelengths. Both Lorenz *et al.* (2001) and Roe *et al.* (2002) invoke polar night chemistry to explain the polar collar and hood. They refer to the work of Samuelson *et al.* (1997), who identified C_4N_2 ice clouds which form during the polar nights and are still present during early spring. The formation and condensation of these compounds can continue during the early spring, as the temperature of the stratosphere continues to decrease during this period (Bézard *et al.*, 1995).

2.3. Composition and Temperature Contrasts

In addition to the haze NSA, both a temperature asymmetry and a latitudinal contrast in composition were observed by the Voyagers. Flasar *et al.* (1981) infer a cooler stratosphere (mbar level, about 200 km altitude) at high nothern latitudes. Coustenis and Bézard (1995) report on a significant (factors 2 - 15) higher abundance of several species (HCN and higher hydrocarbons) in the north polar region. The colder temperatures and the increased abundance in gaseous species appear related and Bézard *et al.* (1995) suggest the first is the consequence of the second. They theorize that the explanation for the latitudinal variation of the chemical species could be related to the seasonal change in solar illumination.

3. Is it all Dynamics?

In order to explain the North-South Asymmetry Hutzell *et al.* (1993) and Lorenz *et al.* (1997) hypothesized a time-variable haze production rate with an otherwise steady-state model. However, a change in the number density of haze particles can also be achieved by dynamics. Lorenz *et al.* (1999) point out that the most probably mechanism to explain the NSA involves meridional circulation. They develop a very simple model and show that an effective increase in albedo (at short

wavelengths) of the summer hemisphere relative to the winter hemisphere takes places if there is transport of haze from the summer to the winter hemispheres. At longer wavelengths, where the radiation probes deeper into the stratosphere, this model does not work well, and Lorenz *et al.* (1999) refer to the need for coupled haze/circulation models.

Hourdin *et al.* (1995) develop a General Circulation Model (GCM) for the atmosphere of Titan that produces the observed strong zonal winds in the stratosphere (superrotation). They show that seasonal effects on the dynamics are important: a single Hadley cell meridional circulation, from the summer to the winter pole, exists during some 80% of the Titan year, whereas a double Hadley cell circulation, centered around the equator takes place at the equinoxes.

Tokano *et al.* (1999) report on the results of GCM runs under different conditions, including the transport of haze. They conclude that the latitudinal haze distribution and composition contrast seen at the time of the Voyager encounters are due to the circulation pattern which consists of one pole-to-pole cell during the equinox, rising in the south and sinking in the north (their Figure 22). They recognize the necessity for a model that combines dynamics, haze microphysics and photochemistry.

This model has now become available and is described by Luz *et al.* (2003). It couples the dynamics model of Hourdin *et al.* (1995), including the latitudinal eddy mixing by barotropic instabilities developed by Luz and Hourdin (2003), to the radiative transfer scheme of McKay *et al.* (1989), the model of the optical properties of fractal haze particles from Rannou *et al.* (1997) and the simplified photochemistry from Lebonnois *et al.* (2001).

Rannou *et al.* (2002) use a version of this model to calculate the haze distribution and its variation with season. They find that the meridional winds at the altitude of aerosol production (around 450 km) are much faster than the vertical settling velocity. As a consequence, aerosols are transported towards the winter pole well before they can fall over one atmospheric scale height. At the winter pole they then fall to lower altitudes and coagulate to form aggregates. This produces the polar hood. During the short transition period just after the equinoxes the circulation is broken into two cells, and then changes direction. In this period, the fractal aggregate haze particles redistribute at lower altitudes (lower than about 200 km) over the rest of the planet, maintaining the main haze. Also, the reversal process decreases the polar hood to a polar collar and eventually the polar hood starts to grow at the other pole.

This circulation mechanism explains the North-South Asymmetry. It effectively transports haze from one pole to the other. As already noted by Lorenz *et al.* (1999), this gives rise to an effective darkening of the winter pole at short wavelengths. At longer wavelengths, since the haze becomes brighter than the underlying atmosphere, the effect is inverse, as observed.

In addition, the accumulation of haze in the winter polar region results in strong cooling of the atmosphere, as observed. This has a positive feedback on the meri-

onal circulation, which in turn increases the accumulation of the haze. It also increases the strength of the zonal winter jet.

Luz *et al.* (2003) report in more detail on these and other model results. They observe that the stratospheric zonal wind jet, which forms around the winter pole, dynamically isolates this region from lower latitudes and prevents species poleward of the jet to diffuse to lower latitudes. There is strong eddy mixing equatorward of the jet and in the summer hemisphere. This can explain the increase in heavy hydrocarbons and nitriles at these altitudes and latitudes: the model reproduces well the Voyager-derived composition contrasts. It also matches the temperature contrast observed by Voyager. It supports the idea that it is of radiative origin, due to asymmetric distribution of infrared opacity.

Luz *et al.* (2003) suggest that the jet could be the border of the polar hood or the polar collar. They also find that the pole-to-pole travel time of the haze is on the order of 2.6 years which is compatible with the observed turnover time of the NSA of about 5 years.

A wind inversion is produced at lower altitudes (from winter to summer). This could be the cause for the observed wavelength (and thus altitude) dependence of the NSA, especially at longer visible wavelengths, were deeper levels are sounded. However, Luz *et al.* (2003) note that there is no phase lag in the circulation pattern, so that the 1-2 year lead of the NSA change in the red relative to the blue as reported by Lorenz *et al.* (2001) still needs an explanation.

The coupled dynamics-microphysics-photochemistry model appears to be able to explain many features at once. If true, then the latitudinal contrasts we observe are all related to the dynamics of the atmosphere of Titan. The Cassini mission will very soon bring many new data against which to test our models and theories.

Acknowledgements

MRS thanks the organization of the ISSI Workshop 'A comparative study of the giant planets before the exploration of Saturn by Cassini-Huygens' for the invitation to participate and for the excellent Workshop. MRS thanks an anonymous referee for very useful input and editing corrections.

References

Bézard, B., Coustenis, A., and McKay, C.P.: 1995, 'Titan's stratospheric temperature asymmetry: a radiative origin?', *Icarus* **113**, 267–276.

Cabane, M., Chassefière, E., and Israel, G.: 1992, 'Formation and growth of photochemical aerosols in Titan's atmosphere', *Icarus* **96**, 176–189.

Cabane, M., Rannou, P., Chassefière, E., and Israel, G.: 1993, 'Fractal aggregates in Titan's atmosphere', *Planet. Space Sci.* **41**, 257–267.

Caldwell, J.D, Smith, P.H., Tomasko, M.G., and Weaver, H.: 1992, 'Titan: evidence for seasonal change – A comparison of Voyager and Hubble Space Telescope images', *Icarus* **103**, 1–9.

Courtin, R.: 1992, 'Titan's UV albedo: observation and modeling', *ESA-SP* **338**, 59–67.
Coustenis, A. and Bézard, B.: 1995, 'Titan's atmosphere from Voyager infrared observations. IV. Latitudinal variations of temperature and composition', *Icarus* **115**, 126–140.
Flasar, F.M., Samuelson, R.E., and Conrath, B.J.: 1981, 'Titan's atmosphere: temperature and dynamics', *Nature* **292**, 693–698.
Griffith, C.A., Owen, T., Miller, G.A, and Geballe, T.: 1998, 'Transient clouds in Titan's lower atmosphere', *Nature* **395**, 575–578.
Hourdin, F., Talagrand, O., Sadourny, R., Courtin, R., Gautier, D., and McKay, C.P.: 1995, 'Numerical simulation of the general circulation of the atmosphere of Titan', *Icarus* **117**, 358–374.
Hutzell, W.T., McKay, C.P., and Toon, W.B.: 1993, 'Effects of time-varying haze production on Titan's geometric albedo', *Icarus* **105**, 162–174.
Karkoschka, E. and Lorenz, R.D.: 1997, 'Latitudinal variation of aerosol sizes inferred from Titan's shadow', *Icarus* **125**, 369–379.
Lebonnois, S., Bakes, E.L.O., and McKay, C.P.: 2002, 'Transition from gaseous compounds to aerosols in Titan's atmosphere', *Icarus* **159**, 505–517.
Lenonnois, S., Toublanc, M., Hourdin, F., and Rannou, P.: 2001, 'Seasonal variations of Titan's atmospheric composition', *Icarus* **152**, 384–406.
Letoureur, B. and Coustenis, A.: 1993, 'Titan's atmosphere from Voyager 2 infrared spectra', *Planet. Space Sci.* **41**, 593–602.
Lockwood, G.W. and Thompson, D.T.: 1979, 'A relationship between solar activity and planetary albedos', *Nature* **280**, 43–45.
Lockwood, G.W., Lutz, B.L., Thompson, D.T., and Bus, E.A.: 1986, 'The albedo of Titan', *Astrophys. J.* **303**, 511–520.
Lorenz, R.D., Smith, P.H., Lemmon, M.T., and Karkoschka, E.: 1997, 'Titan's North-South Asymmetry from HST and Voyager imaging: comparison with models and ground-based photometry', *Icarus* **127**, 173–189.
Lorenz, R.D., Lemmon, M.T., and Smith, P.H.: 1999, 'Seasonal change on Titan observed with the Hubble Space Telescope WFPIC-2', *Icarus* **142**, 391–401.
Lorenz, R.D., Young, E.F., and Lemmon, M.T.: 2001, 'Titan's smile and Collar: HST observations of seasonal change 1994-2000': *Geoph. Res. Let.* **28**, 4,453–4,456.
Luz, D. and Hourdin, F.: 2003a, 'Latitudinal transport by barotropic waves in Titan's atmosphere. I. General propertier from a horizontal shallow-water model', *Icarus* **166**, 328–342.
Luz, D., Hourdin, F., Rannou, P., and Lebennois, S.: 2003b, 'Latitudinal transport by barotropic waves in Titan's atmosphere. II. Results from a coupled dynamics-microphysics-photochemistry GCM', *Icarus* **166**, 343–358.
McKay, C.P., Coustenis, A., Samuelson, R.E., Lemmon, M.T., Lorenz, R.D., Cabane, M., Rannou, P., and Drossart, P.: 2001, 'Physical Properties of the organic aerosols and clouds on Titan', *Plan. Space Sci.* **49**, 79–99.
McKay, C.P., Pollack, J.B. and Courtin, R.: 1989, 'The thermal structure of Titan's atmosphere', *Icarus* **80**, 23–53.
McKay, C.P. and Martin, S.C.: 1997, 'Temperature lapse rate and methane in Titan's troposphere' *Icarus* **129**, 498–505.
Rages, K., and Pollack, J.B.: 1983, 'Titan aerosols: optical properties and vertical distribution', *Icarus* **55**, 50–62.
Rages, K., and Pollack, J.B.: 1980, 'Titan aerosols: optical properties and vertical distribution', *Icarus* **41**, 119–130.
Rannou, P., McKay, C.P, and Lorenz, R.D.: 2003, 'A model of Titan's haze of fractal aerosols constrained by multiple observations' *Plan. Space Sci.* **51**, 963–976.
Rannou, P., Hourdin, F., and McKay, C.P.: 2002, 'A wind origin for Titan's haze structure', *Nature* **418**, 853–856.

Rannou, P., Cabane, M., Botet, R., and Chassefière, E.: 1997, 'A new interpretation of scattered light measurements at Titan's limb', *J. Geoph. Res.* **102**, 10,997–11,013.

Roe, H.G., de Pater, I., Mactintosh, B., Gibbard, S.G., Max, C.E., and McKay, C.P.: 2002, 'Titan's atmosphere in later southern spring observed with adaptive optics on the W.M. Keck II 10-meter telescope', *Icarus* **157**, 254–258.

Samuelson, R.E., Mayo, L.A., Knuckles, M.A., and Khanna, R.J.: 1997a, 'C_4N_2 ice in Titan's north polar stratosphere', *Planet. Space Science* **45**, 941–948.

Samuelson, R.E., Nath, N.R., and Borysow, A.: 1997b, 'Gaseous abundances and methane supersaturation in Titan's troposphere' *Planet. Space Science* **45**, 959–980.

Smith, B.A., *et al.*: 1981, 'Encounter with Saturn: Voyager 1 imaging results', *Science* **212**, 163–182.

Smith, B.A., *et al.*: 1982, 'A new look at the Saturn system: the Voyager 2 images': *Science* **215**, 504–537.

Sromovsky, L.A. and Fry, P.M.: 1989, 'The phase variation of Titan's brightness contrast: implied constraints on properties of haze particles', *Bull. Am. Astron. Soc.* **21**, 959.

Sromovsky, L.A., Suomi, V.E., Pollack, J.B., Kraus, R.J., Limaye, S.S., Owen, T., Revercomb, H.E., and Sagan, C.: 1981, 'Implications of Titan's North-South Asymmetry', *Nature* **292**, 698–702.

Tokano, T., Neubauer, F.M., and Laube, M.: 2001, 'Three-dimensional modeling of the tropospheric methane cycle on Titan', *Icarus* **155**, 130–147.

Tokano, T., Neubauer, F.M., Laube, M., and McKay, C.P.: 1999, 'Seasonal variation of Titan's atmospheric structure simulated by a general circulation model', *Plan. Space Sci.* **47**, 493–520.

Toon, O.B., McKay, C.P., Griffith, C.A., and Turco, R.P.: 1992, 'A physical model of Titan's aerosols', *Icarus* **95**, 24–53.

Tran, B.N., Joseph, J.C., Ferris, J.P., Persans, P.D., and Chera, J.J.: 2003, 'Simulation of Titan haze formation using a photochemical flow reactor. The optical constants of the polymer', *Icarus* **165**, 379–390.

West, R.A. and Smith P.H.: 1991, 'Evidence for aggregate particles in the atmospheres of Titan and Jupiter', *Icarus* **90**, 330–333.

Wilson, E.H. and Atreya, S.K.: 2000, 'Sensitivity studies of methane photolysis and its impact on hydrocarbon chemistry in the atmosphere of Titan', *J. Geoph. Res.* **105, E8**, 20,263–20,273.

Address for Offprints: M. Roos-Serote, Lisbon Astronomical Observatory, Tapada da Ajuda, 1349-018, Lisbon; roos@oal.ul.pt

IO'S ATMOSPHERE AND SURFACE-ATMOSPHERE INTERACTIONS

EMMANUEL LELLOUCH
LESIA, Observatoire de Paris, F-92195 Meudon

Received: 10 May 2004; Accepted in final form: 11 August 2004

Abstract. Our knowledge of Io's atmosphere has improved dramatically in the last fifteen years, with a wealth of new observational data at millimeter, UV and IR wavelengths, and the development of numerous models describing its horizontal and vertical structure, composition, photochemistry and plasma interaction. Io's atmosphere is dominantly composed of SO_2, present mostly at low-to-mid latitudes with column densities of a few 10^{16} cm^{-2} and important (factors of 5-10) longitudinal variations. Minor compounds include SO, S_2, and NaCl. Sublimation equilibrium with SO_2 frost and direct volcanic output coexist to maintain Io's atmosphere against condensation, photolytic and escape losses.

Keywords: Io, atmosphere, sublimation equilibrium, volcanism

1. Introduction

Jupiter's satellite Io, shaped by active volcanism, is certainly one of the most unusual bodies of the Solar System. Volcanism on Io manifests itself in different ways, including a variety of landforms, IR hot spots and outbursts, and the most spectacular eruptive plumes (Spencer and Schneider, 1996). Volcanism is also the ultimate source of an atmosphere which bears unique properties, in terms of composition, distribution, structure and maintenance, and which is the subject of this chapter. Section 2 recalls the initial discovery of Io's atmosphere, outlines the essential question it raised, and summarizes the early answers to this question. Section 3 contains an overview of recent datasets, and discusses our current observational understanding of Io's atmosphere. Recent models are discussed in Section 4. Finally, a synthesis on the nature of Io's atmosphere is proposed in Section 5. Earlier and more extended reviews on Io's atmosphere can be found in Spencer and Schneider (1996), Lellouch (1996), and Trafton *et al.* (1998), McGrath *et al.* (2004), in which the reader is directed for more references that can be given in this short paper.

2. Early Observations, Early Models, and Associated Questions

Although Pioneer 10 had detected an ionosphere around Io in 1973, it is *Voyager* in 1979 which gave the first quantitative information on the composition and pressure

Space Science Reviews 116: 211–224, 2005.
DOI: 10.1007/s11214-005-1957-z

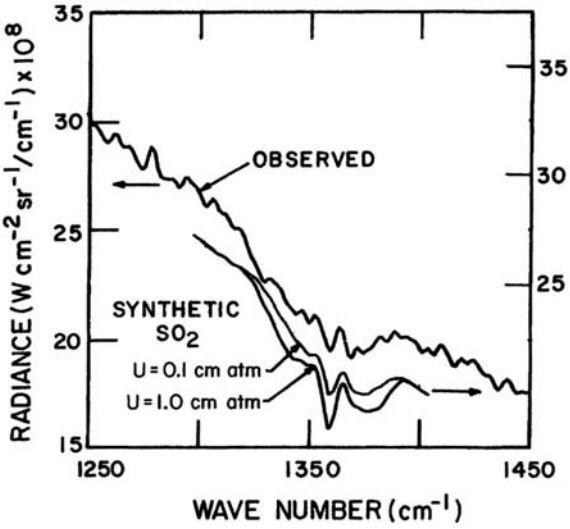

Figure 1. The historical detection of SO_2 gas on Io by IRIS/Voyager (from Pearl *et al.*, 1979)

of Io's neutral atmosphere. Simultaneously to the discovery of active volcanism, Voyager achieved the mid-IR detection of gaseous SO_2 around the volcanic hot spot Loki (Pearl *et al.*, 1979), at a local pressure of about 0.1 μbar (Figure 1). This detection also permitted the interpretation of Io's ground-based spectra as indicating the presence of SO_2 frost on Io's surface (e.g. Smythe *et al.*, 1979). This triple discovery was of course an enormous step forward, but it immediately raised the essential question that is still probably focussing most research efforts on Io's atmosphere. Was SO_2 gas detected around Loki because Loki emitted a SO_2-rich volcanic plume, or rather because the SO_2 frost in that region was able to sustain a significant atmosphere? Indeed, given the SO_2 sublimation vapor pressure curve, a 0.1 μbar atmosphere is in equilibrium with SO_2 frost at 130 K, which is a reasonable temperature for Io's dayside surface. Extending this issue to Io's atmosphere as a whole, the basic question is: is Io's atmosphere primarily supported by sublimation equilibrium, or dynamically maintained by volcanic output?

The 1980–1989 decade saw no new positive detection of Io's atmosphere, but a blossoming of models trying to answer this question. Buffered models favored the first explanation, stipulating that the atmospheric pressure reflects local equilibrium with the surface. The main issue is then to determine the location and appropriate temperature of the frosts. A variety of such models were developed (e.g. Fanale *et al.*, 1982; Matson and Nash, 1983), altogether covering six orders of magnitude in pressure. A remark that was made is that equilibrium models imply huge horizontal pressure variations and as such are inherently unstable (Ingersoll *et al.*, 1985). Planetary wide winds must occur and modify the pressure distribution. Strict equilibrium cannot be maintained and depending on the regions, there must condensation or sublimation exchanges with the surface. Furthermore, the frost

distribution on Io is likely to be non-uniform, and in that case, it was shown (Ingersoll, 1989) that a regional control of the atmosphere must occur, namely that there exists a characteristic dimension L of order 100 km ($L = \sqrt{2\pi}\, H/\alpha$, where H is the atmospheric scale height and α a sticking coefficient) over which individual frosts control the atmospheric pressure. In volcanic models, the atmospheric pressure reflects a dynamical equilibrium with volcanic venting. A relationship between the magnitude of the volcanic venting flux (E_s) and the local increase in pressure was established ($\Delta P \approx \sqrt{2\pi}\, E_s v_s/\alpha$, where v_s is a speed of sound), and it was shown that over a cold surface, a volcanic atmosphere will decrease exponentially over the same characteristic dimension.

These analyses thus indicate a similarity in the behaviour of volcanic and sublimation atmospheres. In addition, Io's atmosphere escapes to the torus at a rate of $\approx$ 1 ton/sec (Spencer and Schneider, 1996). Therefore sublimating frosts lose mass which must be resupplied by the volcanos, so volcanism is the ultimate source of Io's atmosphere and one may be tempted to regard the volcanic/sublimation distinction as artificial. Although this point of view is valid to some extent, it must be recognized that sublimation and volcanic atmospheres must have quite different vertical structures, one being hydrostatic, and the other "plume-like" with significant gas horizontal and vertical velocities.

In addition, the two types of atmospheres have different lifetimes, therefore must show different responses to radiative and photochemical processes. Overall a possible approach is to define a volcanic component as one which locally does not vary with the surface temperature, and in particular is maintained on the nightside.

For completeness, one must also mention the sputtering models, in which a tenuous atmosphere is generated from impact of energetic magnetospheric particles with the surface (see e.g. Cheng *et al.*, 1986). Such atmospheres are self-limited to at most a column density of $\approx 10^{16}$ cm^{-2}, i.e. pressure of 0.2 nanobar, and as such cannot explain the Voyager observation, but nonetheless may be important on some specific regions, particularly on the nightside away from volcanic sources. Note that sputtering of the atmosphere itself also occurs, producing atmospheric heating and escape to the neutral clouds and the plasma torus (e.g. Johnson, 1989).

With these theoretical aspects, the key questions to be answered by observations were the following: what is the typical pressure of Io's atmosphere? What is its horizontal distribution, its characteristic temperature and its vertical structure? Does it vary with time? Finally, are there other components besides SO_2 that could provide information on the atmospheric nature?

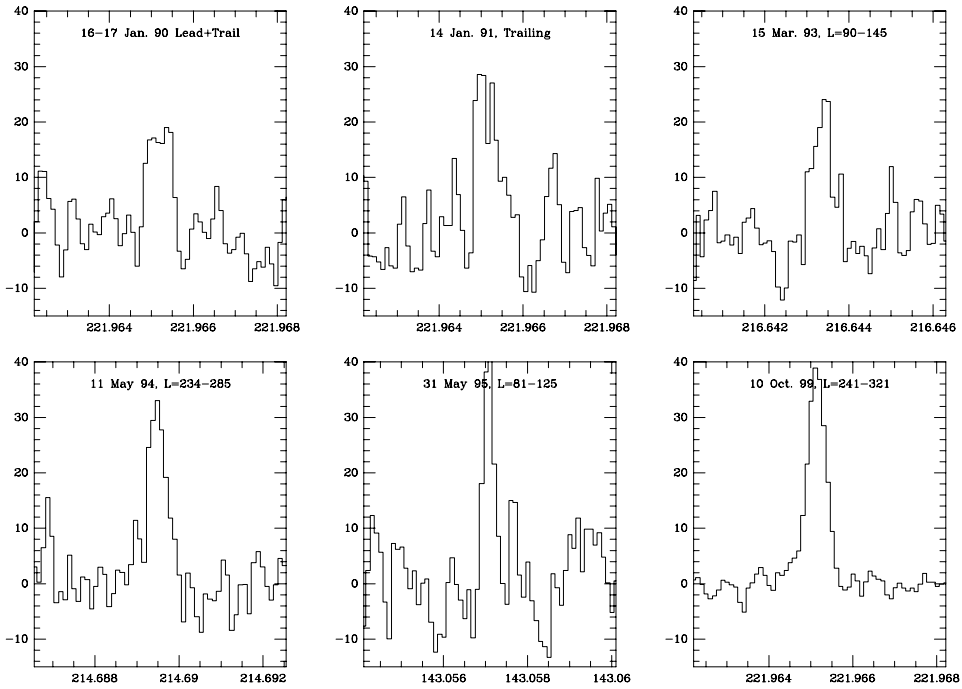

Figure 2. Sample millimeter observations of SO_2 emission from Io. The date and orbital longitude of Io are indicated.

3. Recent Observational Progress

3.1. The SO_2 Atmosphere

3.1.1. *Data*

In contrast to the previous decade, the last 15 years have seen an explosion of new observations. Millimeter observations, illustrated in Figure 2, consist of disk-average observations of rotational lines (e.g. Lellouch *et al.*, 1992; 2003). For SO_2, a dozen of such lines have been observed in emission. Line profiles are fully resolved, and show typical widths of 0.8 km/s, but the broadening mechanism is uncertain. It could reflect thermal Doppler broadening, or bulk velocity dispersion within plumes. Therefore, the data can be intepreted in two different ways: a hydrostatic equilibrium atmosphere – which in effect represents a sublimation atmosphere – or a volcanic plume atmosphere. The millimeter observations have also provided the first detection of two species, SO and NaCl (see below).

SO_2 is a strong absorber in the UV, either as a line or a continuum absorber. This was succesfully exploited since 1992 in several disk-averaged and disk-resolved UV observations, mostly from HST spectroscopy and imaging (FOS, GHRS, FOC, and STIS). Unlike in the millimeter range, the UV observations are primarily sensitive to the absorber column, with little influence by the gas temperature. Figure 3

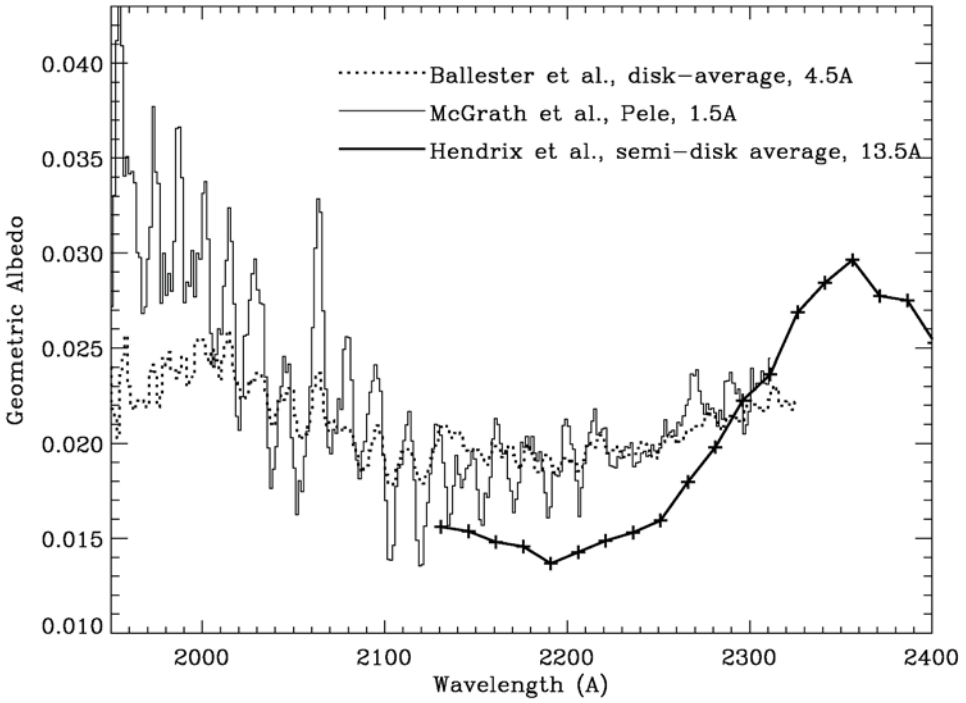

Figure 3. Several disk-averaged or disk-resolved UV spectra of Io, showing absorption by SO_2 gas.

shows a collection of UV spectra around 2200 Å, at various resolutions, clearly showing the individual SO_2 electronic bands. Disk-resolved UV spectroscopic observations include measurements of SO_2, SO, S (McGrath *et al.*, 2000; Jessup *et al.*, 2004), and S_2 (Spencer *et al.*, 2000). UV imaging observations have also been performed (e.g. Sartoretti *et al.*, 1996). Their interpretation is complicated by the competing effects of SO_2 frost and gas at low spectral resolution. An exception is the Ly α images (e.g. Strobel and Wolven, 2001) which provide a relatively direct "negative view" of Io's atmosphere, since SO_2 is a strong continuum absorber at 1215 Å.

In the infrared, while no positive result was achieved during more than 20 years, ground-based mid-IR observations obtained in 2001, 2002, and 2004 finally permitted the disk-average detection of SO_2 at 19 μm in absorption (Spencer *et al.*, 2004). These observations showed in particular a dramatic longitudinal variability of the SO_2 19 μm spectrum, with much deeper absorptions on the anti-Jupiter hemisphere than at $L = 300$. They also suggest secular variability of the absorption depths, but at some longitudes only. The quantitative interpretation of these spectra in terms of the SO_2 column is complex as it involves non-LTE issues and a strong dependence on temperature.

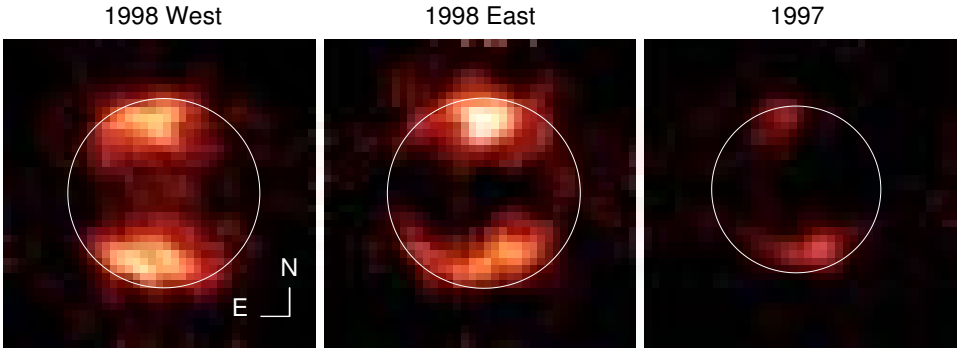

Figure 4. Images of Io in Ly α. Dark regions indicate the presence of SO_2 gas.

3.1.2. *Interpretation*

As is perhaps not surprising, the disk-averaged observations do not lead to a unique description of the SO_2 atmosphere, and their interpretations range between two "end-member" situations: (i) a dense, hot and localized atmosphere or (ii) a more tenuous, cool and extended atmosphere. For example, the 1993–1994 millimeter observations could be interpreted as a 5×10^{17} cm^{-2} SO_2 column at T=600 K, covering 3% of the surface, or a thinner and colder atmosphere (2×10^{16} cm^{-2} at $T = 250$ K) covering 30% of the surface (Lellouch, 1996). Similarly the 1992 UV observations could be modelled in terms of a relatively dense (2×10^{17} cm^{-2}) but patchy (11%) atmosphere, or a thinner (1×10^{16} cm^{-2}) global atmosphere (Ballester *et al.*, 1992). In spite of this ambiguity, disk-average column densities of a few 10^{16} cm^{-2} are consistently indicated by these observations, with evidence for a somewhat denser atmosphere on Io's trailing side than on the leading (Trafton *et al.*, 1996). Evidence for temporal variability is also present, although it is noteworthy that Io's SO_2 atmosphere is always detected when searched for. Finally, these data do not provide a good handle on the atmospheric temperatures, and even less on the vertical thermal structure, although recent datasets, both in the UV and in the mm, suggest rather low temperatures (< 250 K).

The presence of horizontal variations in the SO_2 pressure was definitely established from the UV disk-resolved observations. HST/FOS observations (McGrath *et al.*, 2000) in which the aperture of the instrument was centered of three different regions, indicated variations in the local SO_2 columns by a factor of $\approx$5. HST/Ly α images (Figure 4) provide a more global view of the SO_2 gas distribution. They show an atmosphere mostly confined to low latitudes ($< 30-40°$), with SO_2 columns of $\approx 10^{16}$ cm^{-2}, strongly decreasing towards the poles (Strobel and Wolven, 2001). The latitudinal boundary of the SO_2 atmosphere varies strongly with longitude. In contrast, these images do not show obvious variations with local time in the equatorial zone. Temporal variability is also present. Finally, HST/STIS spectra taken on Io's anti-jovian hemisphere (Jessup *et al.*, 2004) indicate larger SO_2 abundances than inferred previously from the HST/FOS spectra. All together,

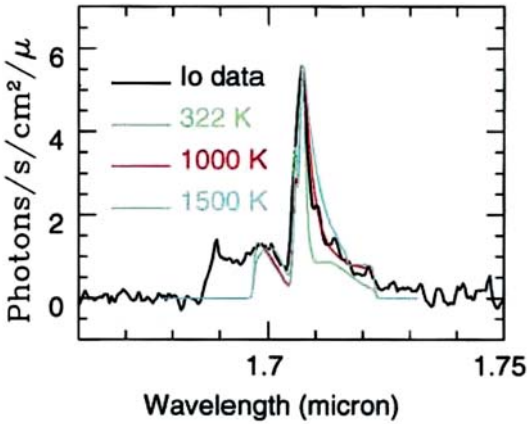

Figure 5. Detection of SO emission from Io in eclipse. The band structure indicates a rotational temperature of ∼1000 K. From De Pater *et al.* (2002).

the UV spectra imply longitudinal variations by a factor of about 20, in reasonable agreement with the mid-IR observations. The HST/STIS spectra of Jessup *et al.* (2004) further show a smooth variation of SO_2 away from the subsolar point, with the SO_2 abundance decreasing regularly with either latitude or solar zenith angle. They also reveal that the SO_2 abundance at the active plume Prometheus is only $\approx$ 40% larger than in surroundings region. The last two aspects suggest a general dominance of the sublimation component, except at high latitudes or large solar zenith angles.

3.2. Minor compounds

Regarding the global composition of Io's atmosphere, three minor molecular species have been detected in addition to SO_2. Sulfur monoxide (SO) was detected in millimeter observations (Lellouch *et al.*, 1996). It constitutes globally 3–10% of SO_2, but its horizontal distribution is uncertain. In particular, it is unknown whether SO is colocated with SO_2 or if the SO atmosphere is more global. SO was also detected in IR observations as an emission at 1.7 μm observed during eclipse (De Pater *et al.*, 2002, Figure 5). The SO emission seems to originate from the Loki volcano. The only mechanism that seems viable to explain this observation is the de-excitation of SO directly injected in an excited state by volcanic emission. Given the SO abundance derived from the mm observations, the band structure and strength of the IR emission together indicate a rotational temperature of $\approx$ 1000 K, and a vibrational temperature of $\approx$ 1500 K. This observation may thus actually probe the physical conditions of volcanic emission. Disulfur (S_2) was detected in the Pele plume against Jupiter's continuum at the terminator (Spencer *et al.*, 2000), with a mixing ratio $S_2/SO_2 = 8 - 30\%$. S_2 is certainly variable, as it was not detected in more recent similar observations. Finally, sodium chloride (NaCl) was recently detected in millimeter observations (Lellouch *et al.*, 2003).

It constitutes globally about 0.4% of SO_2. NaCl is most probably of direct volcanic origin. Due to increased condensation and photolytic losses, NaCl must have a shorter atmospheric lifetime than SO_2.

Volcanic emission rates are estimated to be (2-8)$\times 10^{28}$ NaCl molecules s^{-1}, i.e. 0.3-1.3 % of SO_2. NaCl is also an important source for the sodium neutral clouds. Finally, Io's atmosphere includes a number of atomic species (O, S, Cl, Na, K), as reviewed in McGrath *et al.* (2004).

4. Recent models

All these new observations have prompted the development of new models, which can be classified in six categories.

- *Modern buffered models*. These are again sublimation equilibrium models, but which include a variety of physical processes that were ignored by the early sublimation models (latent heat of SO_2 frost, thermal conduction, internal flow, solid state greenhouse). These models (Kerton *et al.*, 1996) are thus expected to depict the surface temperatures more reliably. The main result is that compared to the earlier models, they predict lower surface temperatures and therefore equilibrium pressures. In addition, the temperature fields they predict are no longer symmetric with respect to the subsolar point, resulting from the inclusion of thermal conduction and thermal inertia.
- *Volcanic gas composition models*. The basic idea of these models is that eruption temperatures on Io – which have been measured to be as high at 1700 K – are high enough that volcanic gases are chemically equilibrated in the vent vicinity, and in contrast quenched in the cooling expanding plumes. This allows one to calculate an atmospheric composition as a function of the eruption conditions, or, vice versa, to use a measured composition to infer physical conditions in volcanic eruptions. Some of the results are the following: (i) SO is an expected volcanic gas (Zolotov and Fegley, 1998), (ii) NaCl is the expected dominant Na- and Cl- bearing volcanic gas (Fegley and Zolotov, 2000), (iii) many other species, such as S_2O or KCl are predicted, and (iv) the composition of the Pele plume, namely the SO_2/S_2 ratio measured by HST, can be used to infer the magma temperature and the vent pressure at Pele (Zolotov and Fegley, 2000).
- *Radiative models* are concerned with calculating the atmospheric vertical profile from an analysis of the heat budget. They have been developed mostly in 1-D and for the case of an hydrostatic SO_2 atmosphere. Heating sources include solar heating in the UV and IR bands of SO_2, as well as plasma and Joule heating. Radiative losses are due to non-LTE IR cooling and rotational cooling. These models (e.g. Strobel *et al.*, 1994) find that the lower atmosphere is cold, due to intense IR cooling, but that the upper atmosphere can be very hot, perhaps up to 2000 K, essentially due to Joule heating. Figure 6

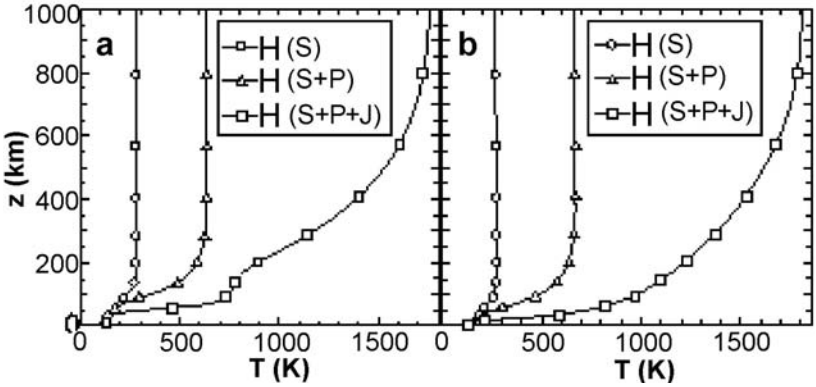

Figure 6. Effects of solar, solar+plasma, and solar+plasma+Joule heating on the temperature structure of Io's atmosphere. *Panel a.* Surface pressure = 130 nbar. Note the presence of a mesosphere. *Panel b.* Surface pressure = 3.5 nbar. From Strobel *et al.* (1994).

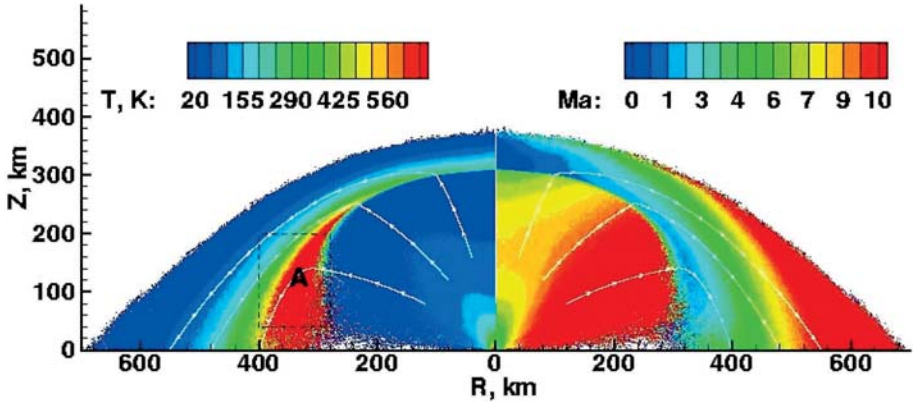

Figure 7. Model of an isolated volcanic plume. Contours of the temperature and Mach number are shown. From Zhang *et al.* 2003.

shows the separate effects of solar, plasma and Joule heating in warming the atmosphere for two different values of the surface pressure. Recently, thermal calculations have been extended plume atmospheres. These complex models (Zhang *et al.*, 2003) consist of Monte-Carlo simulations of gas dynamics and describe phenomena such are plume expansion and re-entry shock, including the effect of radiative cooling. They consider the case of nightside isolated plumes, and the case of dayside plumes erupting in a background atmosphere. Figure 7 shows model results for gas temperature and Mach number for the case of an isolated plume.

– *Photochemical models*. The goal of these models (e.g. Summers and Strobel, 1996; Moses *et al.*, 2002a; 2002b), also mostly developed in the context of 1-D hydrostatic atmospheres, is to predict an equilibrium atmospheric composition. Photochemistry in a SO_2 atmosphere predicts SO to be the most

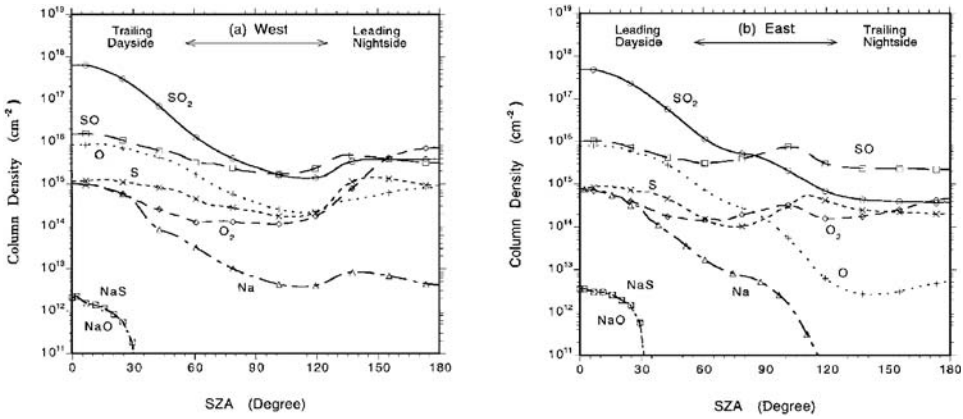

Figure 8. Model calculations of the solar zenith angle dependence of the major gases of Io's atmosphere at Eastern and Western elongation. The model assumes that SO is non-condensible. From Wong and Smyth (2000).

important secondary component, although the observed SO/SO_2 ratio of 3-10% is not easy to reproduce in the case of a plume atmosphere with short (flight) lifetime (Summers and Strobel, 1996). Another finding is that a very tenuous oxygen atmosphere is naturally produced from SO_2 photochemistry and might dominate on the nightside. The case of an atmosphere enriched in minor compounds by volcanic output was also studied, in order to determine the fate and stability of these species vs. photolytic and transport losses. A conclusion was that purely volcanic species such as S_2 and NaCl have relatively short lifetimes (several hours only), therefore their observation requires an active volcanic source.

- *"Unified" models* (e.g. Wong and Johnson, 1996; Wong and Smyth, 2000) attempt to combine, in the framework of the sublimation atmosphere, descriptions of the vertical structure, horizontal transport and photochemistry in order to predict the two dimensional atmospheric structure as a function of altitude and solar zenith angle, including the atmospheric composition. Figure 8 is an example of model output, showing how SO and O_2 progressively become major atmospheric species when one moves away from the subsolar point and towards the nightside, if they are non-reactive and/or non-condensible on the surface.
- The subject of plasma interaction with the atmosphere is a full subject in itself (Saur *et al.*, 2004) and well beyond this review. Nonetheless, it is worth mentioning here a recent result from an *electrodynamic interaction model* (Saur and Strobel, 2004), related to the nature of the atmosphere. Far-UV emissions (e.g. OI at 1356 Å), driven by electron impact, decrease by a factor of about three when Io is in eclipse (Clarke *et al.*, 1994)). This behaviour is not straightforward to understand because intensities of the FUV emissions do not vary monotonically with the SO_2 column densities, as too dense an

atmosphere limits the atmospheric penetration of the electrons. Saur and Strobel (2004) modelled the evolution of radiation in eclipse and found that the non-condensible atmospheric component must remain below $\sim(3\text{-}5)\times10^{14}$ cm^{-2}; otherwise, the emissions would *brighten* during eclipse. They conclude that sublimation dominates over volcanic emission by at least an order of magnitude in maintaining the SO_2 atmosphere.

5. Synthesis and Prospects

Coming back to the "essential" question that arose after the initial discovery of SO_2 in Io's atmosphere, the present collection of data and models suggests that Io's atmosphere has a dual nature. A number of its remarkable features are consistent both with sublimation equilibrium and with dynamic volcanic maintenance of the atmosphere. This includes (i) the surface pressure order of magnitude (ii) the latitudinal distribution of SO_2 gas, which exhibits a low-latitude concentration and a smooth variation with latitude and (iii) its longitudinal distribution, which shows a peak on the anti-jovian hemisphere. *Galileo*-derived maps of the SO_2 frost distribution (Douté *et al.*, 2001) indicate that SO_2 frost is nearly ubiquitous on Io, but most abundant on the anti-jovian hemisphere. However, the same is true for active volcanic plumes, and in general regions of high frost content correlate well with plume longitudes.

A few observational aspects favor a sublimation-driven atmosphere. This includes the fact that the HST/STIS data show only a modest increase of the SO_2 gas abundance around Prometheus. This may indicate a global atmosphere supplied by sublimation, with only local enhancements due to volcanic output. The interpretation by Saur and Strobel (2004) of the eclipse behaviour of the FUV features is qualitatively consistent with that conclusion, although the role it assigns to volcanic emissions is even much more minor.

Conversely, there are observations that clearly favour the volcanic atmosphere concept. This includes (i) the detection of SO_2 in the Pele plume at the terminator – i.e. in a place where the surface temperature is cold (ii) the presence of species that have a negligible vapor pressure (NaCl, S_2) and (iii) the interpretation of the SO IR observations in terms of hot excited SO directly emitted by Loki. Finally, the existence of short-term variability may also be viewed in support on a volcanic atmosphere, although such a variability remains insufficiently documented.

Future progress will require further observations, some of which can be already identified. Local time vs. geographical effects must be disentangled in longitudinal variations, possibly by tracking a given region when it rotates from dawn to dusk. Abundance profiles must be determined systematically as a function of distance from volcanic centers, and individual volcanos must be resolved. All efforts must also be made to determine reliably the characteristic temperature of the atmosphere and its variation with height. Local wind measurements would be of extremely

high value as providing clues on local and global atmospheric dynamics. Current millimeter-data provide disk-averaged wind measurements, but their interpretation is uncertain (see McGrath *et al.*, 2004). Finally, observing the nightside molecular atmosphere would also provide very strong constraints on the atmospheric nature. Some of the above measurements can be already (or will soon) performed from the Earth or Earth-orbit, but several will require the operation of an Io orbiter.

Io's atmosphere and surface-atmosphere interactions are clearly unique in the Solar System. Enormous progress in its knowledge has been achieved since our virtual state of ignorance at the end of the 80's. Important questions do remain, but at least they seem to be now well posed, and a roadmap to solve them may be drawn.

References

Ballester, G.E., McGrath, M.A., Strobel, D.F., Zhu, X., Feldman, P.D., and Moos, H.W.: 1992, 'Detection of the SO_2 atmosphere on Io with the Hubble Space Telescope', *Icarus* **88**, 1–23.

Cheng, A.F., Haff, P.K., Johnson, R.E., and Lanzerotti, L.J.: 1986, 'Interactions of planetary magnetospheres with icy satellites surfaces', *in* J.A. Burns and M.S. Matthews (eds.), *Satellites*, The University of Arizona Press, pp. 403–406.

Clarke, J., Ajello, J., Luhmann, J., Schneider, N., and Kank, I.: 1994, 'Hubble Space Telescope UV spectral observations of Io passing into eclipse', *J. Geophys. Res.* **99**, 8387–8402.

De Pater, I., Roe, H., Graham, J.R., Strobel, D.F., and Bernath, P.: 2002, 'Detection of the forbidden SO $a^1\Delta - X^3\Sigma^-$ rovibronic transition on Io at 1.7 μm', *Icarus* **156**, 296–301.

Douté, S., Schmitt, B., Lopes-Gautier, R., Carlson, R., Soderblom, L., Shirley, J., and the *Galileo*-NIMS team: 2001, 'Mapping SO_2 frost on Io by the modeling of NIMS hyperspectral images', *Icarus* **149**, 107–132.

Fanale, F.P., Banerdt, W.B., Elson, L.S., Johnson, T.V., and Zurek, R.W.: 1982, 'Io's surface - its phase composition and influence on Io's atmosphere and Jupiter's magnetosphere', *in* D. Morrison (ed.), *Satellites of Jupiter*, The University of Arizona Press, pp. 756–781.

Fegley, B. Jr. and Zolotov, M.Yu.: 2000, 'Chemistry of sodium, potassium, and chlorine in volcanic gases on Io', *Icarus* **148**, 193–210.

Ingersoll, A.P.: 1989, 'Io meteorology – How atmospheric pressure is controlled locally by volcanos and surface frost', *Icarus* **81**, 298–313.

Ingersoll, A.P., Summer, M.E., and Schlipf, S.G.: 1985, 'Supersonic meteorology of Io – Sublimation-driven flow of SO_2', *Icarus* **64**, 375–390.

Jessup, K.L., Spencer, J.R., Ballester, G.E., Howell, R., Roessler, F., Vigel, M., and Yelle, R.: 2004, 'The atmospheric signature of Io's Prometheus plume and anti-jovian hemisphere: Evidence for a sublimation atmosphere', *Icarus* **169**, 197–215.

Johnson, R.E.: 1989, 'Plasma heating of an SO_2 atmosphere on Io', *Geophys. Res. Lett.* **16**, 1117–1120.

Kerton, C.R., Fanale, F.P., and Salvail, J.R.: 1996, 'The state of SO_2 on Io's surface', *J. Geophys. Res. 101*, 7555–7564.

Lellouch, E.: 1996, 'Io's atmosphere: not yet understood', *Icarus* **124**, 1–21.

Lellouch, E., Belton, M., De Pater, I., Paubert, G., Gulkis, S., and Encrenaz, T.: 1992, 'The structure, stability, and global distribution of Io's atmosphere', *Icarus* **98**, 271–295.

Lellouch, E., Strobel, D.F., Belton, M.J., Summers, M.E., Paubert, G., and Moreno, R.: 1996, 'Detection of sulfur monoxide in Io's atmosphere', *Astrophys. J.* **459**, L107–L110.

Lellouch, E., Paubert, G., Moses, J.I., Schneider, N.M., and Strobel, D.F.: 2003, 'Volcanically emitted sodium chloride as a source for Io's neutral clouds and plasma torus', *Nature* **421**, 45–47.

Matson, D.L. and Nash, D.B.: 1983, 'Io's atmophere: pressure control by regolith cold trapping and surface venting', *J. Geophys. Res.* **88**, 4771–4783.

McGrath, M.A., Belton, M.J.S., Spencer, J.R., and Sartoretti, P.: 2000, 'Spatially resolved spectroscopy of Io's Pele plume and SO_2 atmosphere', *Icarus* **146**, 476–493.

McGrath, M.A., Lellouch, E., Strobel, D.F., Feldman, P.D., and Johnson, R.E.: 2004, 'Satellite atmospheres', *in* F. Bagenal (ed.), *Jupiter: the Planet, Satellites, Magnetosphere*, Cambridge University Press, in press.

Moses, J.I., Zolotov, M.Yu., and Fegley, B.: 2002a, 'Photochemistry in a volcanically driven atmosphere on Io: sulfur and oxygen species from a Pele-type eruption', *Icarus* **156**, 76–106.

Moses, J.I., Zolotov, M.Yu., and Fegley, B.: 2002b, 'Alkali and chlorine photochemistry in a volcanically driven atmosphere on Io', *Icarus* **156**, 107–135.

Pearl, J., Hanel, R., Kunde, V., Maguire, W., Fox, K., Gupta, S., Ponnamperuma, C., and Raulin, F.: 1979, 'Identification of gaseous SO_2 and new upper limits for other gases on Io', *Nature* **280**, 755–758.

Sartoretti, P., Belton, M.J.S., and McGrath, M.A.: 1996, 'SO_2 distributions on Io', *Icarus* **122**, 273–287.

Saur, J. and Strobel, D.F.: 2004, 'Relative contributions of sublimation and volcanoes to Io's atmosphere inferred from its plasma interaction during solar eclipse', in press.

Saur, J., Neubauer, F.M., Connerney, J.E.P., Zarka, P., and Kivelson, M.G.: 2004, 'Plasma interaction of Io with its plasma torus', *in* F. Bagenal (ed.), *Jupiter: the Planet, Satellites, Magnetosphere*, Cambridge University Press, in press.

Smythe, W.D., Nelson, R.M., and Nash, D.B.: 1979, 'Spectral evidence for SO_2 frost or adsorbate on Io's surface', *Nature* **280**, 766–767.

Spencer, J.R., and Schneider N.M.: 1996, 'Io on the eve of the *Galileo* mission', *Ann. Rev. Earth Planet. Sci.* **24**, 125–190.

Spencer, J.R., Jessup, K.L., McGrath, M.A., Ballester, G.E., and Yelle, R.V.: 2000, 'Discovery of S_2 in Io's Pele plume', *Science, 288*, 1208–1210.

Spencer, J.R., Lellouch, E., Richter, M., Lopez-Valverde, M.-A., Jessup, K.L., Greathouse, T., and Flaud, J.-M.: 2004, 'Mid-infrared detection of large longitudinal asymetries in Io's SO_2 atmosphere', submitted.

Strobel, D.F., Zhu, X. and Summers, D.F.: 1994, 'On the vertical thermal structure of Io's atmosphere', *Icarus* **111**, 18–30.

Strobel, D.F. and Wolven, B.C.: 2001, 'The atmosphere of Io: abundances and sources of sulfur dioxide and atomic hydrogen', *Astrophys. Space Sci.* **277**, 271–287.

Summers, M.E. and Strobel, D.F.: 1996, 'Photochemistry and vertical transport in Io's atmosphere and ionosphere', *Icarus* **120**, 290–316.

Trafton, L.M., Caldwell, J.J., Barnet, C., and Cunningham, C.C.: 1996, 'The gaseous sulfur dioxide abundance over Io's leading and trailing hemispheres: HST spectra of Io's C^1B_2-X^1A_1 band of SO_2 near 2100 Å', *Astrophys. J., 456*, 384–392.

Trafton, L.M., Matson, D.L., and Stansberry, J.A.: 1998, 'Surface/atmosphere interactions and volatile transport (Triton, Pluto, and Io)', *in* B. Schmitt, de Bergh, C., and Festou, M. (eds.), *Solar System Ices*, Kluwer Academic Publishers, pp. 773–812.

Wong, M.C. and Johnson, R.E.: 1996, 'A three-dimensional azimuthally symmetric model atmosphere for Io. 1. Photochemistry and the accumulation of a nightside atmosphere', *J. Geophys. Res.* **101**, 23243–23254.

Wong, M.C. and Smyth, W.H.: 2000, 'Model calculations for Io's atmosphere at eastern and western elongation', *Icarus* **146**, 60–74.

Zhang, J., Goldstein, D.B., Varghese, P.L., Gimelshein, N.E., Gimelshein, S.F. and Levin, D.A.: 2003, 'Simulation of gas dynamics and radiation in volcanic plumes on Io', *Icarus* **163**, 182–197.

Zolotov, M.Yu. and Fegley, B., Jr.: 1998, 'Volcanic production of sulfur monoxide (SO) on Io', *Icarus* **132**, 431–434.

Zolotov, M.Yu. and Fegley, B., Jr.: 2000, 'Eruption conditions of Pele volcano on Io inferred from chemistry of its volcanic plume', *Geophys. Res. Lett.* **27**, 2789–2791.

Address for Offprints: Emmanuel Lellouch, LESIA, Observatoire de Paris, F-92195 Meudon, France; emmanuel.lellouch@obspm.fr

III. AURORAE AND MAGNETOSPHERES

SOLAR SYSTEM MAGNETOSPHERES

M. BLANC[1], R. KALLENBACH[2] and N.V. ERKAEV[3]
[1]*Observatoire Midi Pyrénées, 14, av. Edouard Belin, F-31400 Toulouse, France*
[2]*International Space Science Institute, Hallerstrasse 6, 3012 Bern, Switzerland*
[3]*Institute of Computational Modelling, Russian Academy of Sciences, Krasnoyarsk 660036, Russia*

Received: 24 November 2004; Accepted in final form: 30 November 2004

Abstract. This article proposes a short review of our present knowledge of solar system magnetospheres, with the purpose of placing the study of Saturn's magnetosphere in the context of a comparative approach. We describe the diversity of solar system magnetospheres and the underlying causes of this diversity: nature and magnetization state of the planetary obstacle, presence or not of a dense atmosphere, rotation state of the planet, existence of a system of satellites, rings and neutral gas populations in orbit around the planet. We follow the "russian doll" hierarchy of solar system magnetospheres to briefly describe the different objects of this family: the heliosphere, which is the Sun's magnetosphere; the "elementary" magnetospheres of the inner planets, Earth and Mercury; the "complex" magnetospheres of the giant planets, dominated by planetary rotation and the presence of interacting objects within their magnetospheric cavities, some of which, like Ganymede, Io or Titan, produce small intrinsic or induced magnetospheres inside the large one. We finally describe the main original features of Saturn's magnetosphere as we see them after the Voyager fly-bys and before the arrival of Cassini at Saturn, and list some of the key questions which Cassini will have to address during its four-year orbital tour.

1. The Variety of Solar System Magnetospheres

1.1. EARTH'S MAGNETOSPHERE

The term 'magnetosphere' has first been used for the cavity in the magnetized solar wind plasma which is created by the dipolar terrestrial magnetic field. The existence of this cavity had been anticipated before the space age through its magnetic and ionospheric manifestations, but it is really with the advent of the exploration of space in the 1960's, starting with the discovery of the Van Allen radiation belts and the detection of the external boundary of the magnetosphere, the magnetopause, by NASA's Explorer 12 (Cahill and Amazeen, 1963), that it became the subject of an intense and long-lasting investigation. This cavity has a rather sharp boundary at which the magnetic pressure $p_B = B^2/(2\mu_0)$ of the terrestrial magnetic field B balances the hydrodynamic pressure of the solar wind. The 'obstacle' in the solar wind – the terrestrial magnetosphere – is preceded by a bow shock where much of the dynamic pressure $p_\mathrm{d} = \rho V_\mathrm{d}^2/2$ (V_d: drift speed of the plasma in the reference frame of the shock; ρ: mass density of the solar wind fluid) of the upstream supersonic solar wind is converted into thermal pressure $p_\mathrm{T} = nk_\mathrm{B}T$ (n:

Space Science Reviews 116: 227–298, 2005.
DOI: 10.1007/s11214-005-1958-y

number density of the plasma fluid, T: plasma temperature) of the downstream magnetosheath region. The plasma in the hot magnetosheath is mainly fed by the solar wind. However, only a little fraction of the magnetosheath plasma is fed into the magnetosphere because the magnetopause is an almost tangential magnetic field discontinuity, and the plasma flow is 'frozen' to the magnetic field lines and therefore diverted around the magnetopause. The plasma inside the magnetopause is in fact fed by a majority of ions from the terrestrial ionosphere, H^+, He^+ and a variable fraction of singly charged oxygen ions created by solar UV ionisation or electron impact ionisation of atmospheric oxygen. Protons and other ions from the solar wind seem to be only a secondary source of the plasma in the terrestrial magnetosphere, although this is still debated (Hultqvist *et al.*, 1999).

With the development of planetary exploration, it became evident that the Earth's magnetosphere is only one particular example of a family of objects that can be called "magnetospheres" in a generic way. Indeed, space exploration of planets and comets showed that sharp boundaries similar to the Earth's bow shock and magnetopause tend to form in front of planetary/cometary obstacles to the solar wind flow. The result of the interaction is that the interplanetary magnetic field and to some extent the solar wind plasma tend to be excluded from a region of space around the obstacle which can be designated as its "magnetosphere." The structure and dynamics of these "magnetospheres" depend very strongly upon several specific characteristics of each planet: the nature of the obstacle, the nature of the internal sources of plasmas and momentum, the spin period of the planet, the relative geometries of the spin axis, magnetic dipole axis, and solar wind flow velocity vector which leads to to a division of this class of objects into two main categories.

1.2. Nature of the Obstacle: Intrinsic vs. Induced Magnetospheres

In front of all planets, the solar wind flow is stopped at some distance by the planetary obstacle, and its flow is diverted around the planetary obstacle. This solar-wind stand-off distance, upstream of the planet or comet, is the distance at which the solar wind total pressure (magnetic + flow dynamic pressure) is matched by the opposing pressure of the planetary obstacle. This obstacle can be one of three objects: the planet solid surface (in the absence of a dense atmosphere), its atmosphere/ionosphere, or the planetary magnetic field itself. It is when, as in the case of Earth, giant planets and Mercury, the main obstacle to solar wind flow is the planetary magnetic field, that we speak of "intrinsic magnetospheres."

When the planetary magnetic field is dominated by its dipole component, the calculation of the distance at which this field can stand off the solar wind pressure is well known, and leads to the so-called Chapman-Ferraro distance

$$R_{CF} = R_P \left(\frac{B_{surf}^2}{\mu_0 \rho V_{SW}} \right)^{1/6}, \tag{1}$$

TABLE I
Classification scheme of planetary magnetospheres.

Planet's or satellite's envelope:	$R_{CF} \gg R_P$	$R_{CF} \ll R_P$
Solid surface	Obstacle = planetary field	Obstacle = solid surface
	Mercury	Moon
	(Ganymede)	(Europa, Callisto, Saturnian icy satellites)
dense atmosphere	Obstacle = planetary field	Obstacle = planetary atmosphere/ionosphere
	Earth	Venus
	Giant planets	(Io, Titan)

which is calculated as the distance at which the magnetic pressure of the planetary field on the Sun-planet line (taking into account the additional effect of currents flowing on the magnetopause) balances the total solar wind pressure. In this formula R_P represents the planetary radius, B_{surf} the surface magnetic field at the planet's equator, and V_{SW} the solar wind speed. One sees that the different types of obstacles met by the solar wind depend on the relative magnitudes of R_P and R_{CF}:

1. If $R_{CF} \gg R_P$, the solar wind interacts with the planetary field, we have an "intrinsic magnetosphere."
2. If $R_{CF} \ll R_P$, the solar wind is not deviated by the planetary magnetic field, and it interacts directly with the planet's atmosphere/ionosphere, or its surface if it has no significant atmosphere. We then speak of an "induced magnetosphere," as it is the draping of the solar wind magnetic field around the planetary obstacle which creates a cavity and a wake.
3. The case $R_{CF} \approx R_P$ is an interesting one: the planet and its magnetic field can both contribute to the planetary obstacle. Mars, where magnetic anomalies extending into the ionosphere have been detected, may be of this type (Winterhalter *et al.*, 2004).

Table I summarizes the different cases of planetary obstacles to the solar wind, and how they are determined by the relative magnitudes of R_P and R_{CF} and by the nature of the planet's (or satellite's) envelope. The solar system nicely offers to us all different cases to explore.

In the case of induced magnetospheres, their structure and dynamics further depend on the nature of the planetary envelope, atmosphere/ionosphere or solid surface. Venus, which has a dense atmosphere, is the reference example of the case of an atmospheric interaction. The induced magnetospheres of Titan and of comets also very likely belong to this category. Near comets a "contact surface" divides the

region where the pressure of the gas and dust originating from the comet dominates from the region where the solar wind plasma pressure and magnetic field dominates (Neubauer *et al.*, 1986). A cometary magnetosphere also has a second interface, the cometary bow shock, where the solar wind slows down from supersonic to subsonic streaming. The region between the cometary bow shock and the contact surface is called cometosheath in correspondence to the terrestrial magnetosheath. Not only comets, but all induced magnetospheres in a supersonic flow are expected to usually have two interfaces that correspond to the comet's contact surface and bow shock. However, it has been discussed during the time of the Giotto mission to comet Halley whether strong mass-loading could lead to fluid solutions without a shock.

Our moon is an example of a surface interaction with the solar wind. It results in the formation of a plasma wake, and a plasma cavity downstream of the lunar obstacle. Several of the poorly known cases of satellite interactions in giant planets' magnetospheres also fall in this category. Particularly interesting as an induced magnetosphere is the case of the volcanic satellite Io in the Jovian magnetosphere, which will be described in Section 4.

In the remainder of the text we are going to deal with the heliosphere, intrinsic magnetospheres of planets, the intrinsic magnetosphere of Ganymede – the only satellite with an intrinsic "mini-magnetosphere" (Kivelson *et al.*, 2004) – , and with the induced magnetospheres of Io and Titan.

1.3. Magnetospheric Motions: The Interplay of Solar Wind and Planetary Rotation

Planetary magnetosphere are very dynamic objects (Kivelson and Bagenal, 1999). Their plasma and trapped particle populations experience large scale motions under the influence of three dominant momentum sources:

1. the solar wind bulk motion, characterized by its flow velocity vector $\mathbf{V}_{SW}$;
2. planetary rotation, characterized by the planet's spin vector $\vec{\Omega}$;
3. the Keplerian motions of orbiting objects, which are dominantly in or very near the planet's equatorial plane, and therefore provide an angular momentum aligned with $\vec{\Omega}$.

The solar wind momentum source acts on the interior motions of the magnetospheric cavities through a variety of processes, inducing a general circulation pattern called magnetospheric convection which has best been documented at Earth. Frictional transfer of momentum (as initially proposed by Axford and Hines, 1960) probably plays some role, but the most efficient mechanism seems to be the reconnection of solar wind and magnetospheric field lines on the front side of the magnetopause, initially proposed by Dungey (1961). In the MHD description, this opening of field lines and their subsequent transport over the poles and into the magnetotail lobes by the solar wind flow establish, through the magnetopause, a direct connection between solar wind and interior magnetospheric flows. A fraction

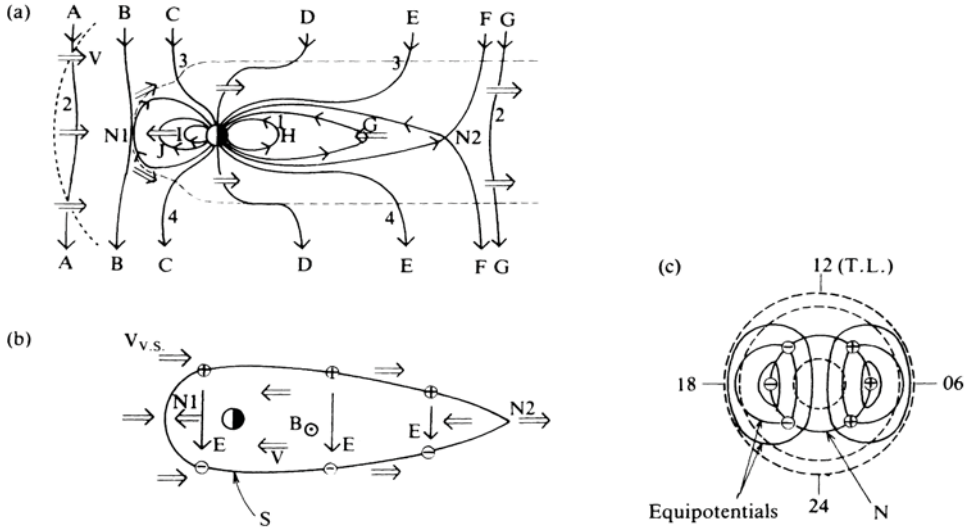

Figure 1. The "Dungey cycle" of magnetic flux and plasma circulation in the Earth's magnetosphere (from Encrenaz *et al.*, 2004).

of the solar wind electric field is transmitted inside the magnetosphere along magnetic field lines, producing a large-scale electrostatic potential difference between the dawn and dusk flanks of the cavity. As schematically explained in Figure 1, the same electric field which induces the anti-sunward motion of open field lines and magnetic flux tubes shown in panel a) also induces the return flow of plasma and closed magnetic field lines shown in the equatorial cross-section of panel b).

One of the open questions of magnetospheric physics is to determine to what extent this mechanism and the resulting magnetospheric convection pattern also apply to other planets. To address it, let us return to the general case of the geometry of the interaction of a planet with the solar wind.

As this terrestrial example very well shows, a planet's charged particle motions are controlled by the geometry of the magnetic field through which they move. For a dipole field, this geometry is best characterized by the magnetic dipole moment, M. The relative orientations of three vectors ($\mathbf{V}_{SW}$; $\vec{\Omega}$; and $\mathbf{M}$, the magnetic dipole moment) thus constrain to a large extent the dynamical regime which each planetary environment tends to enforce on its charged particles. The solar system provides us with an interesting excursion into this parameter space, as shown in Figure 2 which represents the geometry of these three vectors for the Earth and our four outer planets.

The proper motion of the planetary body is at the origin of diurnal and seasonal variations of each magnetosphere and its dynamical regime: whereas the seasonal variation intensity is, as usual, governed by the planet's obliquity, the importance of its diurnal variation really depends on the angle between the spin axis and magnetic dipole moment.

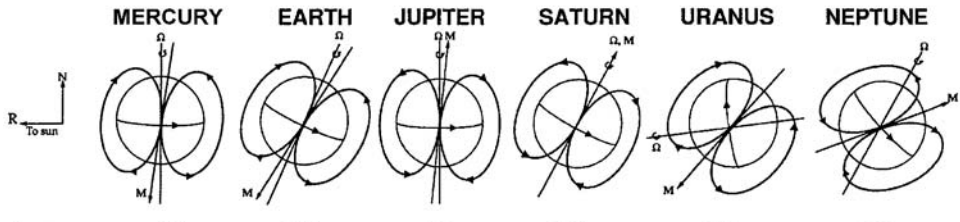

	MERCURY	EARTH	JUPITER	SATURN	URANUS	NEPTUNE
Obliquity $\cos^{-1}(\Omega \cdot N) =$	0.0°	23.5°	3.1°	26.7°	97.9°	29.6°
Dipole Tilt $\cos^{-1}(\Omega \cdot M) =$	+11.0°	+11.7°	-9.6°	-0.0°	-59°	-47°
Solar Wind Angle $\cos^{-1}(\Omega \cdot R) =$	90.0°	66.5 - 113.5°	86.9 - 93.1°	63.7 - 116.5°	7.9 - 172.1°	60.4 - 119.6°
Angle Parker Spiral	21°	45°	79°	84°	87°	88°

Figure 2. The relative geometries of the solar wind direction (opposite to vector **R** here), planetary spin vectors $\vec{\Omega}$ and dipole moments **M** are illustrated in this figure for Earth and the giant planet. They play an important role in the way solar-wind forcing and planetary motion interplay to determine a global pattern of plasma and magnetic flux circulation in each magnetosphere. In addition the planetary obliquity angle determines the importance of seasonal variations in magnetospheric phenomena, and the angle between **M** and $\vec{\Omega}$ determines the importance of diurnal variations in magnetospheric flows (from Bagenal, 1992).

As one can guess from Figure 2, the Uranus and Neptune cases are very different from the other cases, because of the strong angle existing between their spin and magnetic dipole axes. As a result, their magnetic field experiences a very strong rotational modulation, and so do all their magnetospheric phenomena. This rotational modulation is the dominant feature of magnetospheric dynamics there.

At the opposite, Saturn, Jupiter and Earth have small angles between **M** and $\vec{\Omega}$. Except for the possible effects of higher order components in the magnetic field, their magnetic field geometry is relatively stationary in the solar wind frame of reference over a diurnal period, and one can first, in a very rough approximation, consider the resulting plasma circulation pattern as relatively steady in a reference frame using $\vec{\Omega}$ as the Z axis and the projection of the Sun's direction on the equatorial plane as the X axis. Following a standard description, let us look at the motion of low energy plasma – and associated magnetic flux – in the equatorial plane of this reference plane. The two ingredients are two flow systems that are approximately superimposed. Planetary rotation produces a circular motion at all radial distances, whereas solar-wind induced plasma convection produces an approximately uniform flow towards the sun in that plane (see panel b) of Figure 1). The superposition of the two flow patterns produces a stagnation point in the flow, somewhere near the dusk meridian. This stagnation point (see also Kivelson, 2005, this volume) is located at a distance

$$R_{\rm stag} \approx \left(\Omega_{\rm P} B_0 R_{\rm P}^3 / E_{\rm conv}\right)^{1/2} \quad ; \quad E_{\rm conv} \approx 0.1 V_{\rm SW} B_{\rm IMF} \, . \tag{2}$$

from the planet's center. The flow line passing through this point is a flow separatrix. Inside this separatrix, plasma flows on closed flow lines, essentially coro-

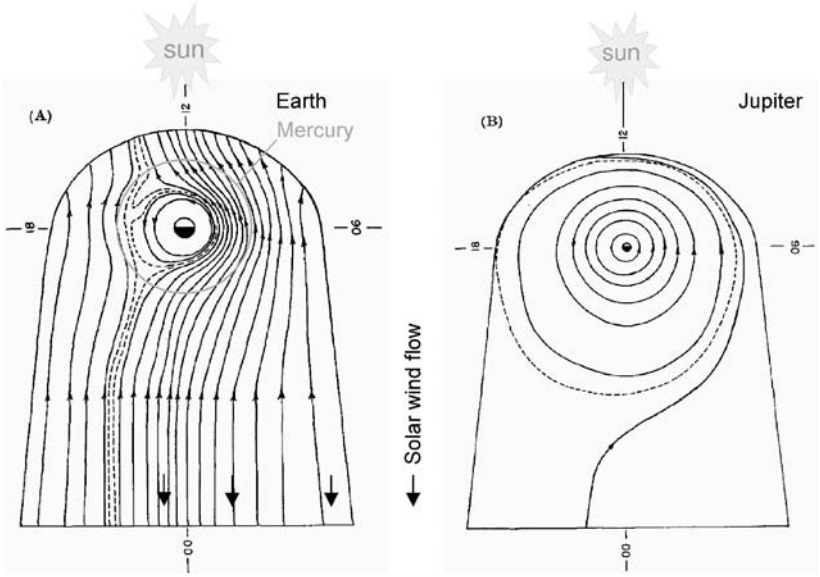

Figure 3. Schematic of the convection pattern in Earth's and Mercury's magnetospheres (*panel A*) and in the magnetosphere of a fast rotator (*panel B*).

tating with the planet. Outside of it, it is dragged on flow lines originating from the nightside and tail region, and which cross the magnetosphere boundary, the magnetopause, on the dayside.

The relative magnitudes of the stagnation point distance R_{stag} and of the magnetopause distance R_{CF} make it possible to identify two very different flow regimes for planetary magnetospheres with small diurnal modulation.

In planets like Earth or Mercury (see the values of the characteristic parameters in Table III), R_{stag} is significantly smaller than R_{CF}. A large fraction of the plasma in the equatorial plane experiences sunward convection under the effect of the interaction with the solar wind. The effect of planetary rotation is dominant only in the innermost part of the magnetosphere, as shown in Figure 3, panel (A). One speaks of "slow rotators" for such planets. Mercury corresponds to an extreme case in this category, as the region of corotation is nearly entirely covered by the solid body of the planet (green circle in panel A of Figure 3). If this prediction is correct, one can speak of a "convection only" magnetosphere.

On the contrary, in the case of Jupiter and other giant planets, planetary rotation is dominant over solar wind forcing over a very large fraction of the magnetospheric cavity, and magnetospheric dynamics is essentially that of a fast rotating magnet trapping and energizing plasmas, as illustrated in panel (B) of Figure 3. One speaks of "fast rotators" for this family of magnetospheres.

TABLE II
Plasma and momentum sources in planetary magnetospheres.

Source	Dominant ions	Flow induced on plasma and magnetic flux tubes
Solar wind	H^+, He^{++}	- Antisunward flow over magnetic poles and along flanks - Return "convection" flow
Planetary envelope	Ionized atmospheric or sputtered neutrals	- Planetary rotation
Orbital sources (satellites, rings, dust ions, neutral gas clouds)	Ions from sublimated gas, gas clouds, sputtered neutrals	- Keplerian motion

1.4. Sources, Sinks and Transport of Magnetospheric Plasma

Planetary magnetospheres are populated with a variety of plasma and charged particles populations. These populations are produced by different sources, located in different regions, before experiencing transport processes which bring them to sink regions where they are lost. During their life as charged species, they move and are transported under the effect of the three main sources of magnetospheric motions we just identified: solar wind flow, planetary rotation, orbital (Keplerian) motions. There are actually also three major sources of plasma, each one related to one of the three sources of momentum (see Table II).

The solar wind is a plasma source for all intrinsic magnetospheres, because a small fraction of the solar wind particles and plasma interacting with a magnetosphere makes its way through its magnetopause, introducing mainly H^+ and He^{++} ions inside the cavity. The bulk motion of the solar wind constitutes the momentum source associated to it.

The planetary envelope (solid surface or atmosphere) constitutes the second source of plasma. When the planet has an atmosphere dense enough to stop the external UV and particle radiations, the interaction of these radiations with the atmospheric atoms and molecules produces charged particles whose composition reflects in an indirect way the composition of the atmosphere. Similarly, when these same radiations interact with a solid surface, surface sputtering, photodetachment, evaporation and further ionisation also produce charged particles whose composition is related to that of the planetary surface. Quite naturally, the source of momentum associated with the planetary source is the planet's spin motion. It is a source of momentum for magnetospheric motions for two reasons: fresh ionospheric ions enter the system with a speed close to the local planetary rotation

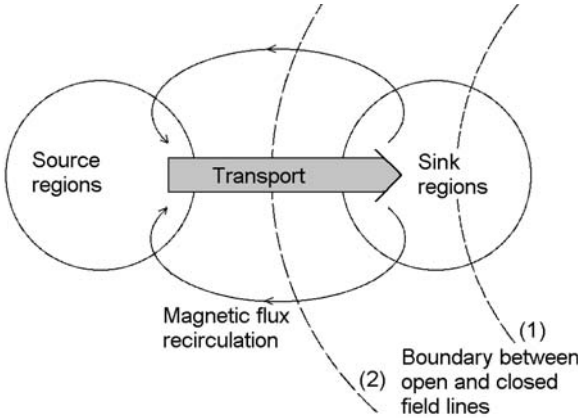

Figure 4. A key problem of magnetospheric physics – plasma transport vs. magnetic flux recirculation.

and, more importantly, ionospheric ions and electrons remain dynamically coupled to the rotational motion of the planet (in fact, of its upper atmosphere) through collisions with the ambient gas particles.

Orbital sources constitute the third category: In the worlds of giant planets, which really are small planetary systems in the solar system, a large number of objects orbit the planet, generally near its geographic equatorial plane and in most cases inside its magnetosphere: ring particles, dust and gas clouds, satellites. All of them are additional sources of plasma populations, with chemical compositions reflecting that of their parent bodies. The associated momentum source is the orbital motion of the parent bodies, which generally tend to follow a Keplerian near-circular motion. All fresh plasma produced by these orbital sources tends to enter the system with the local Keplerian speed before interacting with magnetospheric particles and fields.

1.5. A Key Problem of Magnetospheric Physics: Plasma Transport vs. Magnetic Flux Recirculation

During their lifetime as charged particles, plasma particles are transported over some distance before being lost in sink regions. Determining the "history" of the different charged particle species, how they are transported, how and where they are lost (by recombination, absorption by a solid surface or loss to interplanetary space or to another charged particle reservoir) is one of the major themes of magnetospheric research. Figure 4 illustrates this theme and the main difficulty associated with it: the coupling of plasma transport to magnetic flux circulation. As shown in the diagram, the plasma transport problem essentially implies connecting source regions to sink regions via a flow field or, more generally, transport processes involving motions at different spatial and temporal scales and their coupling. For low energy particles, plasma motions are tied to magnetic flux motions by elec-

trodynamic forces, so that plasma transport implies some kind of magnetic flux transport at the same scale and connecting the same source and sink regions. But unlike plasma populations, magnetic flux is not lost or created in magnetospheric environments, but only transported. For this reason any plasma transport scenario must consider not only how the magnetic flux is transported from source to sink regions, but also must explain how it is recirculated back towards the source region.

Each specific transport case must find a specific solution to this problem. In the case of the solar wind source and transport at Earth, Figure 1 shows how the problem was solved by Dungey: the flow that transports part of solar wind particles inside the magnetosphere through the magnetotail also brings solar magnetic flux impinging on the magnetopause back to the magnetopause after crossing twice a surface separating closed and open magnetic field lines. This scenario implies magnetic flux reconnection, and associated energy dissipation and particle acceleration, both at the magnetopause (near N1 in Figure 1) and in the magnetotail median plane (near N2). Section 4.2 of this article will illustrate the difficulty of finding the corresponding solution for plasma transport at Jupiter. More generally, a very serious difficulty deals with the problem of the flow of magnetic flux across topological magnetic field boundaries. We have drawn as dashed lines in Figure 4 two possible locations for the separatrix between closed and open planetary magnetic field lines. In case (1), plasma transport does not cross this boundary. Magnetic field recirculation can remain confined inside the closed field lines domain, for instance in a vortex loop often called magnetic flux interchange. In case (2), on the contrary, plasma transport crosses the boundary between closed and open field lines, as in the example of Figure 1. The recirculation of magnetic flux then has to involve a reconfiguration of the magnetic field geometry and, in a long term average, a balanced transfer of magnetic flux in both directions through the closed/open field lines boundary via magnetic reconnection.

1.6. Summary: The "Russian Doll" Structure of Solar System Magnetospheres

The variety of solar system magnetospheres we just overlooked here can be described in another systematic way if we consider their hierarchic organisation, which is summarized in Figure 5.

Starting from the largest object in the solar system, the heliosphere, one may really consider it as the Sun's magnetosphere, since it is the cavity blown up by the hydrodynamic pressure of the solar wind inside the Local Interstellar Medium (LISM). The heliospheric interface also has two boundaries, the termination shock, located at about 100 AU, where the supersonic solar wind is slowed down and becomes subsonic, and the heliopause. The heliopause is expected to be located at approximately between 100 and 200 AU and marks the outer boundary to where the solar wind remains tied (frozen-in) to the heliospheric magnetic field originating in the Sun. At the heliopause, the solar wind pressure is presumably balanced

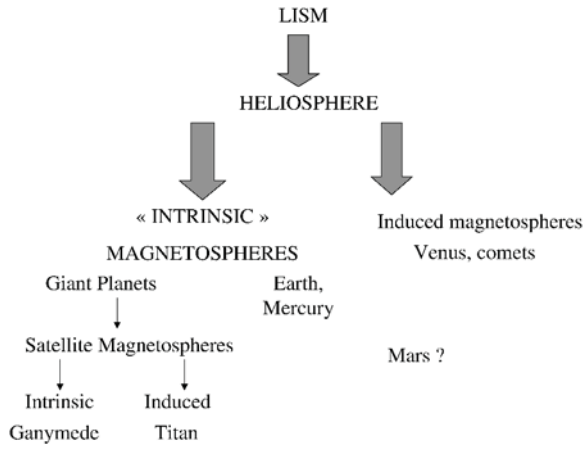

Figure 5. Russian doll hierarchy in solar system magnetospheres: the heliosphere, which is the Sun's magnetosphere carved in the flow of the interstellar medium, contains all solar system magnetospheres, induced or intrinsic. While the magnetospheres of comets and inner planets are "elementary," i.e. contain no other magnetosphere, giant planets magnetospheres are complex ones, inside which planetary satellites may form their own magnetospheres.

by the dynamic pressure of mainly the neutral component of the LISM. In fact, the heliosphere may have a third boundary, the helio-bow shock, if the LISM is supersonic.

Inside the heliosphere we find all planetary and cometary magnetospheres, with their division between intrinsic and induced magnetospheres. The hierarchic tree stops there in the inner solar system, but in the outer solar system giant planets' magnetospheres are shelters to other magnetospheres internal to their cavities. Though most of them are induced magnetospheres, Ganymede offers the particularly interesting and, to this day, unique case of an intrinsic magnetosphere imbedded in another intrinsic magnetosphere.

This short review will focus on intrinsic magnetospheres, with the objective of providing a general context for the detailed study of Saturn's magnetosphere which Cassini-Huygens will undertake in the coming years. The main characteristics of known intrinsic magnetospheres are summarized in Table III.

Our description of solar system magnetospheres will follow the Russian doll diagram of Figure 5, from top to bottom. We shall first briefly describe the heliosphere and explain how Cassini-Huygens, on its way to Saturn, has been able to observe some of its internal characteristics (Section 2). Then we shall describe the inner planets' magnetospheres, using Mercury and Earth as two "end members" of this category of "simple" magnetospheres (Section 3). Section 4 will focus on giant planets magnetospheres, and Section 5 will describe satellite interactions within them. Finally, in the light of this overview, we shall summarize some of the specific characteristics of Saturn's magnetosphere first observed by the Pioneer

TABLE III

Basic parameters of planetary magnetospheres (Bagenal, 1992; Blanc *et al.*, 2002).

	Mercury	Earth	Jupiter	Saturn	Uranus	Neptune
R_P [km]	2 440	6 373	71 398	60 330	25 559	24 764
T_{spin} [h]	59×24	24	9.9	10.7	17.2	16.1
$\|\mathbf{M}_P\|$	0.0003	:=1[a]	600	50	25	
B_{surf} [μT]	0.25	31	428	22	23	14
Θ_R	0°	23.5°	3.1°	26.7°	97.9°	29.6°
$\Delta\Theta_M$	-11.0°	+11.3°	-9.6°	-0.0°	-59°	-47°
R_h [AU]	0.3−0.4	1	5.2	9.5	19	30
n_{SW} [cm^{-3}]	70	10	0.4	0.1	0.03	0.005
B_{IMF} [nT]	30	6	1.0	0.5	0.25	0.15
$I_{Ly\alpha}$	≈ 7	:= 1[b]	0.04	0.011	0.0027	0.0011
R_{CF}	$1.4R_M$	$8R_E$	$30R_J$	$14R_S$	$18R_U$	$18R_N$
R_{stag}	$< R_M$	$\approx 4R_E$	$\gg R_{CF}$	$\gg R_{CF}$	$\gg R_{CF}$	$\gg R_{CF}$
R_{MS}	$1.9R_M$	$11R_E$	$50-100R_J$	$16-22R_S$	$18R_U$	$23-26R_N$
n_{max} [cm^{-3}]	1000	1−4000	>3000	−100	3	2
Sources	dominant sources marked by *					
Planet	? Exosphere/ surface	O^+, H^{+}* Ionosphere	H^+ Ionosphere		H^{+}* H cloud	
Solar wind	H^+ ?	H^+			H^+	H^+
Orbital sources	−	−	O^{n+}, S^{n+}* Io	O^+, H_2O^+, H^{+}* Dione, Thetys N^+, H^+ Titan		N^+, H^{+}* Triton
S_{ions} [s^{-1}]	?	2×10^{26}	$>10^{28}$	10^{26}	10^{25}	10^{25}
lifetime of plasma ions	?	days hours	10−100 days	30 days − years	1−30 days	∼ 1 day
ENAs [cm^{-2} s^{-1}]	?	∼ 100	∼ 440	∼ 240	< 12	< 4

[a] $|\mathbf{M}|_\oplus = 7.906\times10^{15}$ T m^3; [b] $I_{Ly\alpha;\oplus} \approx 10^6$ cm^{-2} s^{-1}; $R_{stag} \approx \left(\Omega_P B_0 R_P^3 / E_{conv}\right)^{1/2}$: distance of stagnation point with solar wind driven convective electric field $E_{conv} \approx 0.1 V_{SW} B_{IMF}$; R_P: radius of planetary body; T_{spin}: spin period; $|\mathbf{M}_P|$: magnetic moment of planetary body; B_{surf}: surface magnetic field at equator; Θ_R: Angle between rotation axis and normal to ecliptic; $\Delta\Theta_M$: dipole tilt and sense with respect to rotation axis; R_h: heliocentric distance; n_{SW}: solar wind density; B_{IMF}: Interplanetary magnetic field; $I_{Ly\alpha}$: solar Lyman-α radiation; R_{CF}: distance to subsolar point of magnetopause; R_{MS}: size of magnetosphere; n_{max}: maximum plasma density; S_{ions}: source strength of plasma ions; ENAs: Energetic neutral atom fluxes.

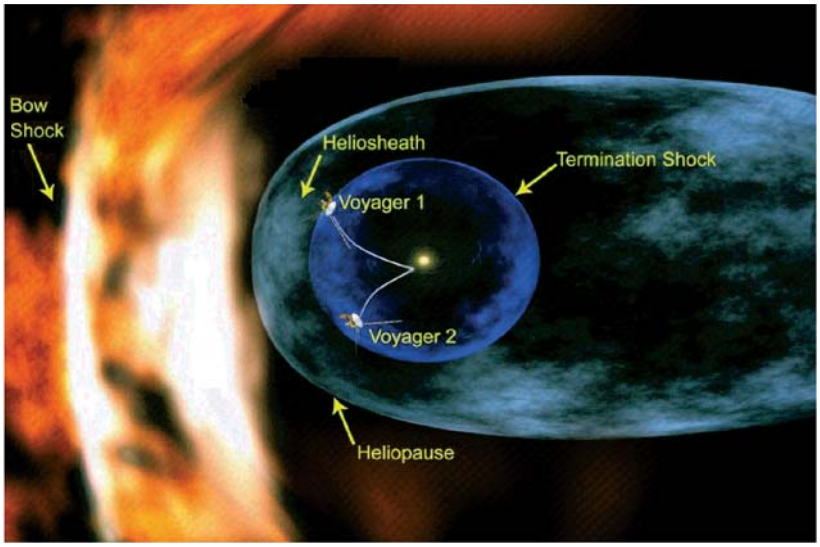

Figure 6. Artist's view of the heliosphere, the magnetosphere of our sun carved by the solar wind into the flow of the interstellar medium.

and Voyager spacecraft, and list some of the key scientific questions which are waiting for the Cassini-Huygens mission to address and hopefully solve.

2. The Heliosphere

The heliosphere (Figure 6) is the cavity carved into the local interstellar medium by the solar wind flow. Though the overall structure of the outskirts of this object is still poorly known, it is expected that the supersonic regime of the solar wind is terminated at some boundary, the "termination shock," to become subsonic and be compressed between the shock and the outer limit of the heliosphere, the heliopause (Parker, 1961; Baranov *et al.*, 1971). If the LISM is supersonic a shock (helio-bow shock) is expected to form outside the heliopause. The Voyager spacecraft are flying towards this boundary, and some indications that it is near the shock or has already crossed it have been reported at the time of our writing (Krimigis *et al.*, 2003; 2004; McDonald *et al.*, 2003) on the basis of the analysis of the observed variations of the fluxes of $\sim$1 MeV protons measured by the CRS and LECP instruments on board of the two Voyager spacecraft near 90 AU. The interpretation of these first detection signatures is complex and still under discussion in conjunction with the data from the other instruments and from other space missions (Kallenbach *et al.*, 2004).

The interaction of the heliosphere with the Local Interstellar Medium (LISM), is indeed very complex, as the LISM itself is a multi-phasic medium comprising interstellar neutrals (mostly H and He), ions, interstellar dust and galactic cosmic

rays. All components interact in different ways with the heliosphere, and a fraction of the particle fluxes actually penetrates the heliosphere, as summarized in Figure 7.

While the plasma component of the LISM is essentially deviated around the heliospheric cavity, galactic cosmic rays penetrate inside the cavity, where they follow complex trajectories under the effect of the geometry of the interplanetary magnetic field. For that reason their fluxes are modulated by the solar cycle and solar activity in general.

As explained in the legend of Figure 6, non-ionized particles (neutrals and interstellar dust particles) can penetrate directly into the heliospheric cavity, where they experience the combined effects of solar gravity, solar wind and radiation pressures, and (for charged grains) the interplanetary electric and magnetic fields which bends their trajectory past the sun. The pick-up ions of interstellar origin discovered first were singly charged He^+ ions (Möbius *et al.*, 1985). Subsequently, a whole set of elements has been detected (Gloeckler *et al.*, 1993; see e.g. Kallenbach *et al.*, 2000, for a review).

During its interplanetary cruise to Saturn via Venus, the Earth and Jupiter, the Cassini-Huygens spacecraft was also able to detect some of these "messengers" of the interstellar space into our solar system. For neutral hydrogen and helium, they were detected by the CAPS plasma instrument in the form of the pick-up ions which these neutrals produce when ionized by solar radiation. McComas *et al.* (2004) observed these ions over an extended period between Jupiter and Saturn (Figure 8, *upper panel*). According to trajectory calculations, the combined effects of gravity, radiation pressure, and loss of neutrals due to ionisation near the Sun produce opposite effects on the trajectories of helium and hydrogen. Helium has fairly low probability to be ionised, and its trajectories are bent inwards to form a "focusing cone" which has already been observed in-situ at 1 AU (Gloeckler *et al.*, 2004). Hydrogen forms an "interstellar hydrogen shadow" in the region behind the Sun where pickup H^+ is depleted both because the outward force due to radiation pressure exceeds gravitational attraction at this time and because H atoms have a high probability of being ionised by the solar Lyman-α radiation and swept out with the solar wind. As a result, one was expecting a gradual increase of hydrogen fluxes (*lower left panel*) and a decrease of helium fluxes (*lower right panel*) along the Cassini-Huygens trajectory, as actually observed. This measurements represents the first in-situ detection of the "interstellar hydrogen shadow" downstream of the Sun.

Cassini-Huygens was also able to detect a component of interstellar dust during the inner part of its interplanetary cruise near 1 AU, using the CDA dust analyser (Altobelli *et al.*, 2004). Out of 189 events transmitted, 29 dust impacts were identified, out of which 14 could be attributed unambiguously to interstellar dust. The separation of interplanetary impacts from interstellar ones was based on a combined analysis of the impact charge signals together with geometric and kinematic spacecraft data. The dust flux has been compared to the heliocentric velocity and direction of interstellar dust detected by Ulysses (Landgraf *et al.*,

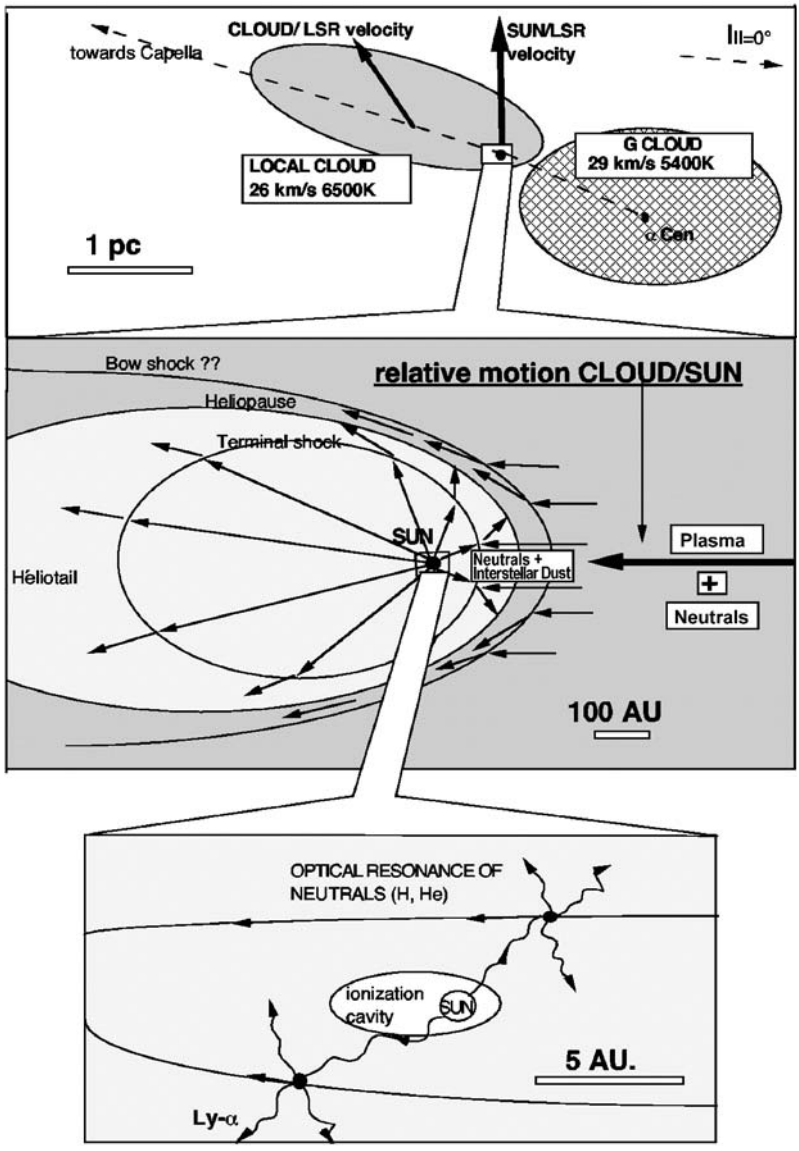

Figure 7. Schematic representation of the interaction of the Local Interstellar Medium (LISM) with the solar system (courtesy of R. Lallement). *Top*: The Sun is presently traversing the "local cloud" of the LISM with a relative velocity of 26 km/s. *Middle*: This relative motion is at the origin of the formation of two shocks (outer and inner) and a contact discontinuity, the heliopause, between the solar wind and the plasma and magnetic field component of the outer medium. But the non-ionized components of the LISM (neutrals and dust) can penetrate directly inside the heliospheric cavity. *Bottom*: H Neutrals can be seen there through their optical resonance with solar Ly alpha radiation. Some of these interstellar neutrals are ionized, and then dragged by the electromagnetic field into the solar wind flow, producing a population of hot ions with a chartacteristic shell velocity distribution function known as "interstellar pick-up ions."

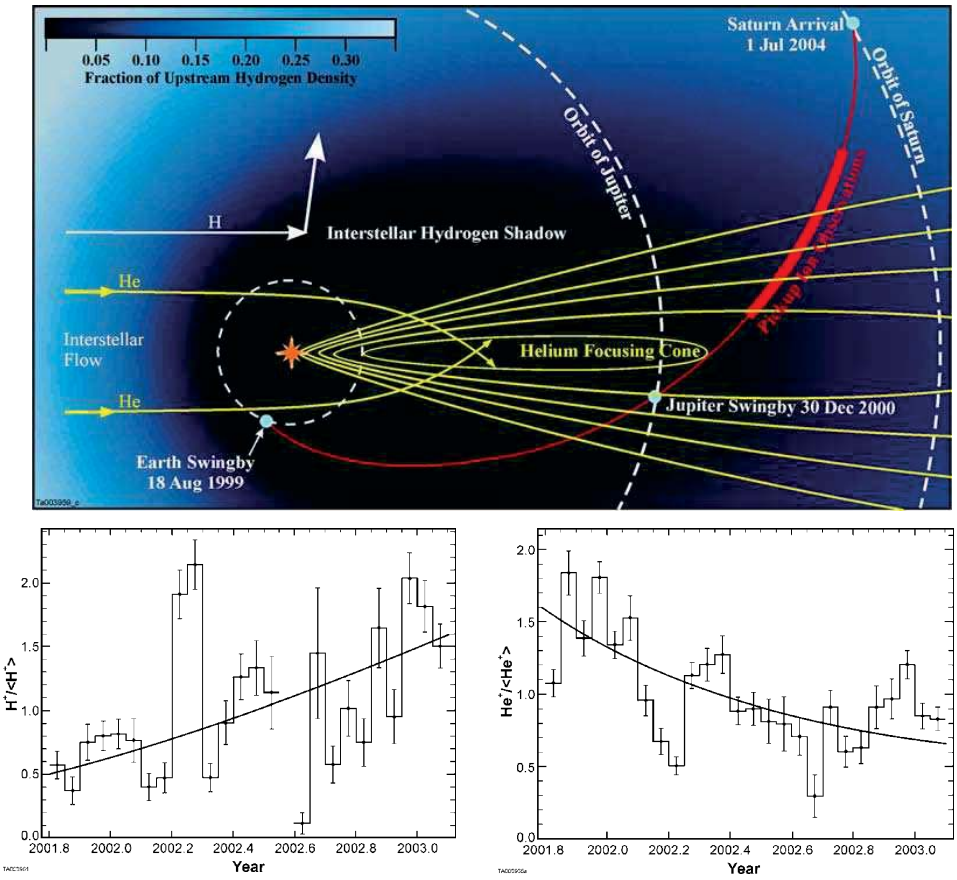

Figure 8. Observations of the fluxes of interstellar pick-up ions were performed by McComas *et al.* (2004), using the CAPS plasma instrument on board Cassini-Huygens, along part of the trajectory between Jupiter and Saturn. They show that the fluxes of hydrogen (*lower left panel*) decrease along the trajectory, while the fluxes of helium increase (*lower right panel*), an observation fully consistent with the expected focusing and defocusing effects exerted by the Sun's gravity and radiation pressure on these two species (*upper panel*).

2003). The directions of arrival determined (shown in Figure 9) illustrate again the effects of gravitational focusing and radiation pressure on particle trajectories. These detections, closest to the Sun among all those detected until now, stimulated a broader study of the complete set of detections achieved in previous years by the Helios, Galileo and Ulysses spacecraft and are an important contribution to our knowledge of the penetration of solid interstellar particles into our solar system.

Overall, it is interesting to note that, even before reaching Saturn, Cassini-Huygens will have contributed to a better knowledge of the largest – and maybe the most complex – of all solar system magnetospheres: our heliosphere!

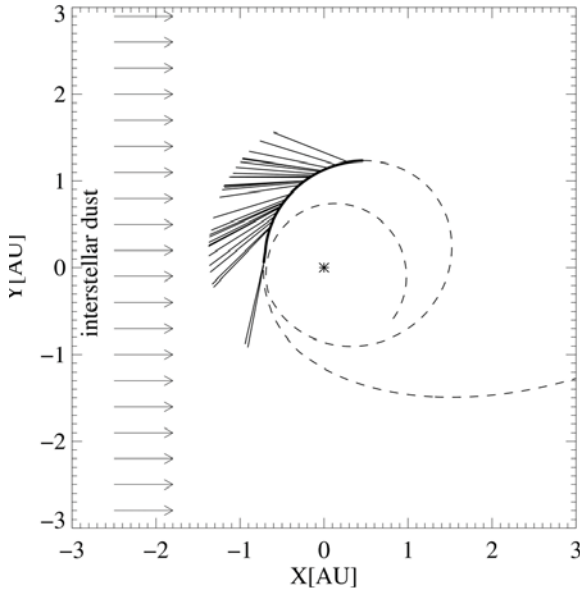

Figure 9. Detections of interstellar dust particles near 1 AU by the CDA instrument of Cassini-Huygens during its interplanetary cruise. The ∼14 particles detected unambiguously are analysed jointly with previous data from Helios, Galileo and Ulysses to produce a better understanding of how and where interstellar dust penetrates into our solar system.

3. The Interplay of Planetary and Solar Wind Sources: Inner Planets Magnetospheres

3.1. Earth and Mercury: Similarities and Differences

The first and dominant large difference between the terrestrial and Hermean magnetospheres is the level of detailed knowledge we have of them. If Earth evidently has the best explored magnetosphere, Mercury shares with Uranus and Neptune, at the other end of the solar system, the very poor knowledge we have of its magnetosphere, limited to what we learnt from two of the three Mariner 10 fly-by's of this planet in 1974 and 1975. Both the plasma instrument and the magnetometer indicated a bow shock and a magnetopause (Ogilvie *et al.*, 1974; Ness *et al.*, 1974). Extrapolation of the interface locations to the subsolar direction yielded a shock stand-off distance of $1.9 \pm 0.2 R_{\mathrm{M}}$ and a magnetopause distance of $1.35 \pm 0.2 R_{\mathrm{M}}$. The magnetic moment of Mercury has been determined to be 1/3000 that of Earth (Table III). The exosphere consists of He with a surface density of 600 cm^{-3} and of atomic H with 8 cm^{-3} (Broadfoot *et al.*, 1974). Subsequently, Na, K, and Ca have been detected spectroscopically from ground-based observations (Potter and Morgan, 1985; 1986; Bida *et al.*, 2000). The upper limit of the electron density derived from Mariner data is 10^3 cm^{-3} in the ionosphere, 0.1 cm^{-3} in the polar cap (Ogilvie *et al.*, 1977), and 1 cm^{-3} at higher altitudes in the magnetotail.

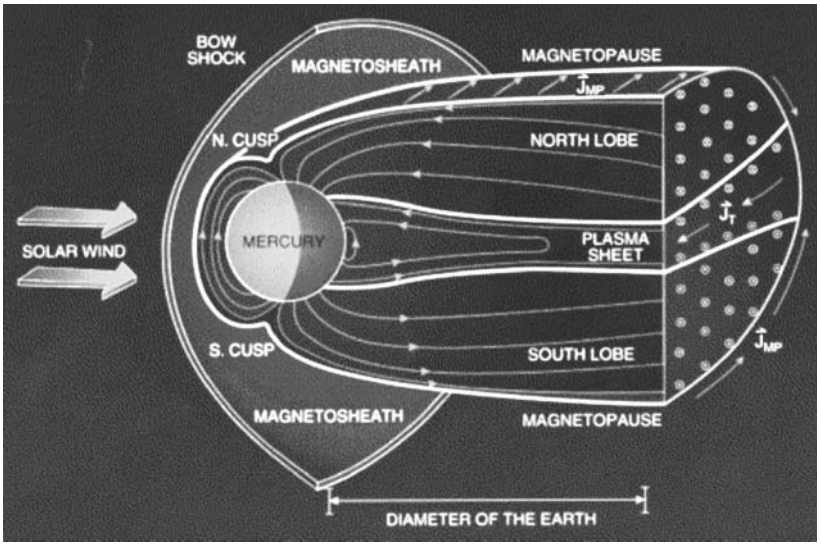

Figure 10. A schematic view of Mercury's magnetosphere can be derived, to a first approximation, by a downscaling of the Earth's magnetosphere by a factor of 7 to 8 (measured in planetary radii), showing some of its unique characteristics: due to the weak planetary magnetic field, the solid body of Mercury occupies a very large fraction of its magnetosphere; due to the lack of an atmosphere, magnetospheric and solar wind plasmas and particles probably interact directly with the Hermean surface and tiny exosphere, which constitute themselves an additional plasma source. From Slavin (2004).

This means that the ionospheric conductivity does not influence significantly the structure of the plasma. From these original data, additional review articles (in particular by Russell *et al.*, 1988) and modelling works, a better understanding of the Hermean magnetosphere emerged with time, as reported in the recent review article by Slavin (2004), from which we extract the schematic view of Figure 10.

To a very first approximation Mercury's magnetosphere can be described by applying a factor of 7 to 8 reduction (in planetary radii) to a model of the Earth's magnetosphere. There is indeed a large similarity between the two magnetospheres:

1. their morphology is dominated by the solar wind interaction, which generates a shock, a magnetopause and a magnetic tail with two lobes separated by a plasma sheet; - they are both slow rotators (e.g., from the comparison of R_M and R_{stag} in Table III), so that magnetospheric flows are expected to be dominated by solar-wind-induced convection, as shown in Figure 3.
2. in the absence of any satellite inside the magnetosphere, they are fed by only two plasma sources, the solar wind and the internal planetary source,
3. finally, there seems to be some evidence that magnetospheric substorms, e.g. the sporadic spontaneous relaxation of the tail magnetic field configuration towards a more dipole-like geometry which releases energy and accelerates particles, exist at both planets: the evidence for magnetospheric substorms at Mercury has been discussed by Christon (1989) from a detailed analysis of

magnetic field and electron flux data during one of the Mariner 10 fly-by's. There is not, however, a general consensus on this: an alternative interpretation of the same data in terms of a direct driven response of Mercury's magnetosphere to changes in solar wind conditions was presented by Luhmann *et al.* (1998).

The list of similarities ends there, because two other characteristics make the Hermean magnetosphere a very different object from Earth's:

1. the importance of the volume occupied by the solid body inside the magnetospheric cavity, which implies that neither the corotation region, which produces a plasmasphere at Earth, nor the region of stable charged particle trapping which is responsible for the maintenance of a terrestrial radiation belt are present at Mercury;
2. the absence of an atmosphere and an ionosphere, which play a very important role in the Eartht's magnetosphere.

To summarize, both magnetospheres are convection-dominated magnetospheres in which only two of the three major plasma sources are present: the solar wind and the source produced by the planetary envelope. But in one case – Earth – the planetary source is its atmosphere, and in the other one – Mercury – it has to be provided by the solid surface and the overlying tiny exosphere. A comparative study of the two planets will therefore be a very unique opportunity to better understand the interplay of the solar wind and planetary sources in a convecting magnetosphere, and at the same time will make it possible to better understand, among the dynamical features of the terrestrial magnetosphere, those which are specifically produced by the presence of a dense atmosphere and its associated ionosphere. To start this comparison, Figure 11 shows the circulation of plasmas from the two sources in the magnetic noon-midnight meridian planes of Earth (panel a) and of Mercury (panel b).

In both cases, for a southward orientation of the interplanetary magnetic magnetic field, solar wind plasma enters the magnetosphere near the cusps and downstream along the magnetopause, while planetary plasma escapes from the planetary envelope along field lines. Both populations, after being convected over the polar caps, are transported towards the night and downstream along the tail, and also partly converge towards the tail mid-plane where they contribute to feeding the plasma sheet. The fraction of this plasma of the two origins which reaches this plasma sheet planetward of the distant tail neutral line may be accelerated planetward and recirculated towards and around the planets. This planetward motion, in the case of Earth, largely takes place during substorms, when the magnetic tail equilibrium itself breaks up. Much of the Earth picture of this basic "Dungey cycle" of plasma convection assigns an important role to the ionospheric plasma, and a key question for magnetospheric physics is to determine whether this role is essential or marginal in the substorm and convection scenarios, and whether it can be played by another type of planetary envelope: after identifying the specific role attributed to

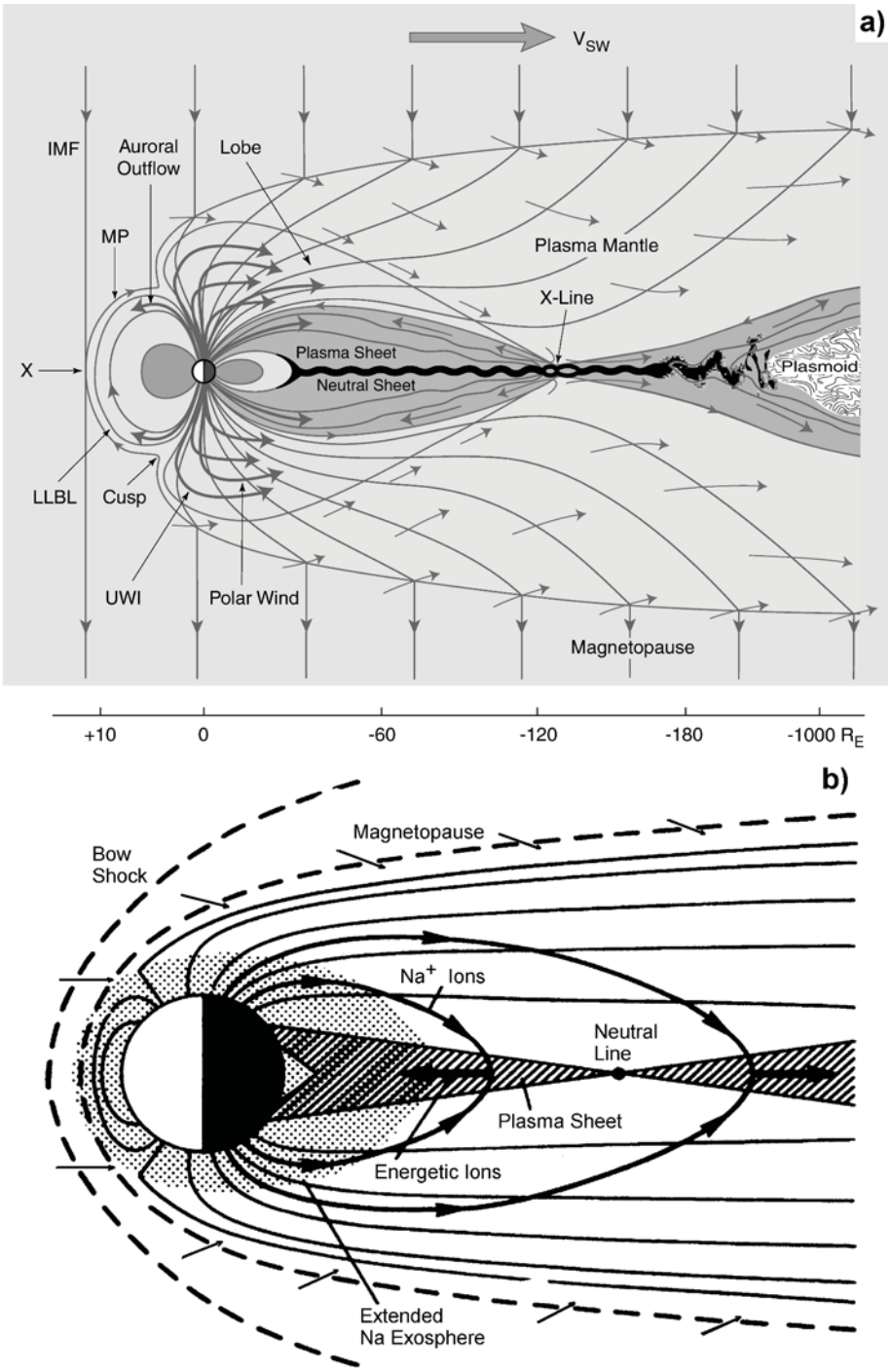

Figure 11. A comparison of the flows of plasmas from the penetrating solar wind and from the planetary source for the cases of a) Earth (from Hultqvist *et al.*, 1999) and b) Mercury (adapted from Ip, 1987).

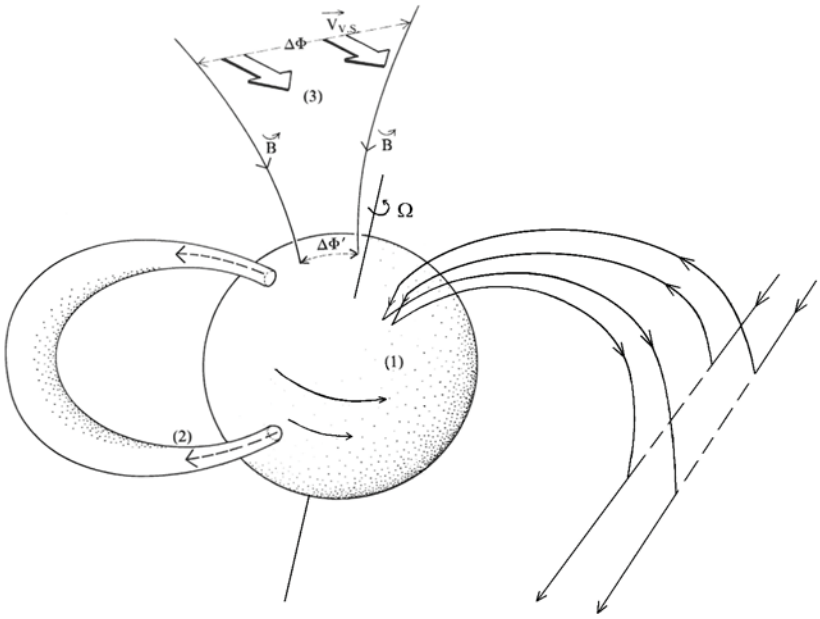

Figure 12. A schematic representation of the roles played by the ionosphere in the dynamics and electrodynamics of the Earth's magnetosphere. (1) Conducting shell following the planetary rotation and dragging the feet of magnetospheric field lines into corotation; (2) plasma reservoir feeding magnetic flux tubes with cold plasma, and contributing to the flow of downward field-aligned electric currents via cold ionospheric electrons; (3) mapping of the large-scale interplanetary electric field to the ionosphere and subsequent formation of the large-scale magnetic convection vortices, (4) conducting path for the disruption of the cross-tail electric current during substorm break-up and formation of the so-called substorm current wedge. (adapted from Encrenaz *et al.*, 2004).

the ionosphere in our present understanding, let us examine the possible alternative role of the surface and tiny exosphere of Mercury in the plasma convection cycle.

3.2. The Role of a Planetary Ionosphere: The Lesson from Earth

Figure 12 illustrates the different roles which the ionosphere plays in magnetospheric flows at Earth. First, the ionosphere covers the altitude region of the atmosphere where collisions between charged and neutral particles are important enough to produce a resistivity in the atmospheric medium: this is the so-called dynamo region of the ionosphere. This ionospheric dynamo layer constitutes a conducting shell which entirely covers the globe and electrically connects all magnetic field lines. This conductor mostly follows the rotation of the terrestrial atmosphere, dragging all field lines into this rotational motion at the angular velocity Ω of the planet. In addition, the ionospheric plasma has access by upward diffusion and other processes to the whole magnetic flux tube to which it is connected. This is the origin of the ionospheric plasma source of planetary magnetospheres. Ions, and even more the much lighter electrons from the ionosphere, provide poten-

tial charge carriers for the flow of electric currents along magnetic field lines. These "magnetic-field-aligned currents" make it possible to connect electric current sources in the distant magnetosphere or in the solar wind to the electric conductor we just described. One consequence of this (3) is that the large-scale electrostatic potential differences generated in the Earth's reference frame by the solar wind flow generate currents which close into the polar ionosphere and partly apply the solar-wind potential difference across the terrestrial polar caps. Another important consequence (4) is that the instability in the cross-tail electric current which is believed to be at the origin of substorms in one of the leading models can develop into a complete disruption of a section of the cross-tail current along magnetic field lines and into the nightside auroral ionosphere (Galand and Chakrabarti, 2002), where it is observed as the substorm "current wedge." The possibility of this short-circuit of the cross-tail current by the ionospheric conductor may therefore play a role in the development of the substorm scenario itself: we don't really know, but the study of the opposite case of a planet where there is no ionospheric conductor may provide part of the answer: this is one of the main interests of studying the case of Mercury.

3.3. The Possible Roles of the Regolith and Exosphere at Mercury

What is the alternative to an ionosphere at Mercury? The only possibility resides in the solid surface and subsurface, mainly the planetary regolith, and its gas-phase extension in space, the hermean exosphere. Figure 13 shows a cross-section of this system, illustrating the coupling processes between its adjacent superposed layers.The tiny exosphere of Mercury, which has been observed from Earth as a highly variable medium comprising such atmospheric species as Na, K and Ca, is the likely product of the superposed effects of surface sputtering (by solar photons, solar wind ions, solar energetic particles and the recirculation of magnetospheric ions to the surface) and vaporization produced by meteoritic impact. It constitutes in itself the planetary source for the magnetosphere. Ions such as O^+, Na^+, K^+, Mg^+, ..., produced by photoionozation and electron impact are picked up into the magnetospheric convection flow and also partly outflow along field lines. Together with the associated electron population, exospheric ions provide a very limited cross-field conductance, which Cheng *et al.* (1987) and Glassmeier (1997) estimated to be at most a few tenths of mhos. Some of them, after their transport into the magnetosphere, impact back the surface where they contribute to surface sputtering and the production of fresh exospheric particles. Below the exosphere, the regolith and underlying layers also provide some degree of conductance across magnetospheric field lines. The value of this conductance is very difficult to estimate, but it is unlikely to be sufficient to carry the amount of current expected from a phenomenon such as a substorm current wedge, if it exists at Mercury. An intriguing fact, however, is that high-Q field line resonance has been identified

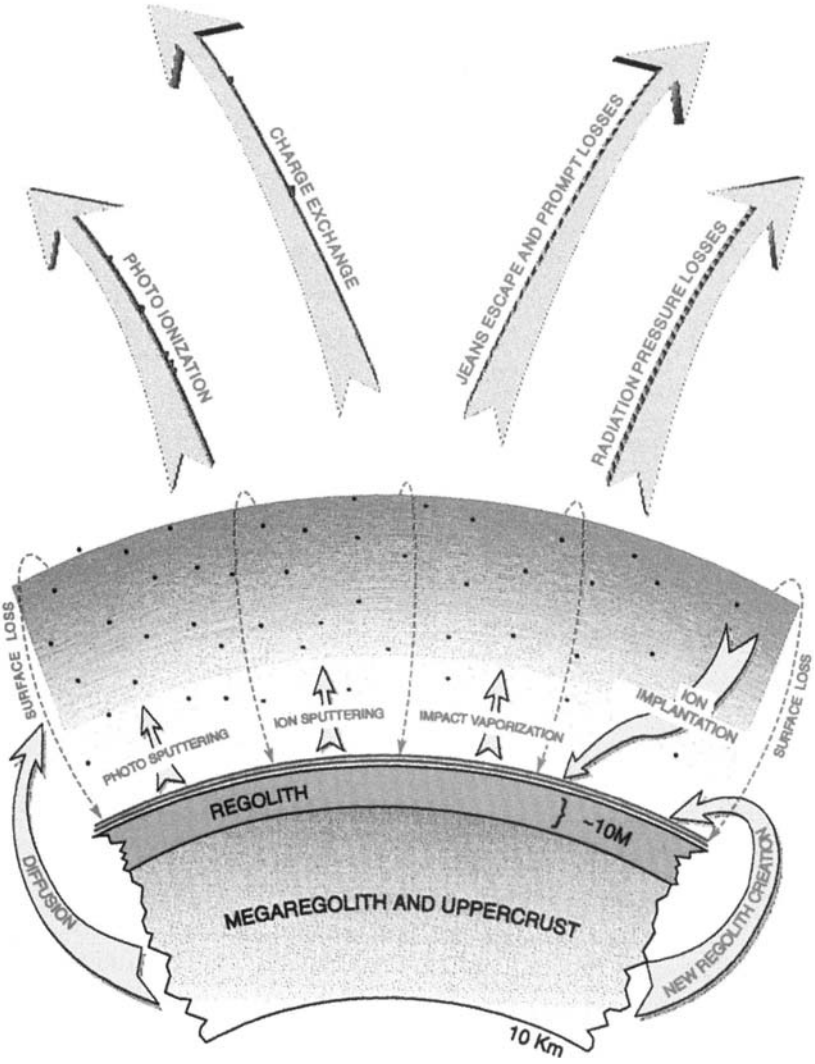

Figure 13. Surface/exosphere/magnetosphere interactions are the very original features of the Hermean magnetosphere, and they may play an important role in the overall dynamics and electrodynamics of this object in the absence of any ionosphere (from Morgan and Killen, 1997).

in the ULF wave band of the magnetic field fluctuations at Mercury by Russell (1989), implying that a good reflector exists for Alfvén waves at the two ends of Hermean magnetic field lines. The nature of this reflector and of the associated conducting layer remains to be discovered: this is but one of the many problems which Messenger and BepiColombo investigators will have to solve in the coming years.

3.4. Sputtering Processes: Lessons from Cassini?

Similarities presumably exist for the sputtering and subsequent ionisation processes at the surface of Mercury and at the surfaces of the icy satellites in the Saturn system. Three processes have been invoked to reconcile the exospheric densities of Mercury: (i) sputtering by solar wind protons or energetic particles through open magnetic field lines e.g. near the cusp, (ii) photo-sputtering by solar ultraviolet radiation, (iii) meteoroid bombardment of the regolith. In particular, process (ii) offers an explanation for the variability of the sodium densities observed by Killen *et al.* (2001) during a CME event. Lammer *et al.* (2003) give a recent overview on the particle release processes at the surface of Mercury. Modeling process (i) they obtain escape fluxes of $1.3 - 1.6 \times 10^5$ cm^{-2} s^{-1} for Na assuming a solar wind proton flux of 4×10^8 cm^{-2} s^{-1}, and $1.0 - 1.4 \times 10^4$ cm^{-2} s^{-1} for K. Process (ii) yields 3×10^6 cm^{-2} s^{-1} for Na and about 10^4 cm^{-2} s^{-1} for K with 1.4×10^{15} photons cm^{-2} s^{-1} below 248 nm. Process (iii) delivers escape fluxes of the same order as those from the other processes under quiet solar wind conditions if the meteoroid flux is of order 4.4×10^7 kg y^{-1} to Mercury's exosphere. The escape speeds of the Na and K atoms are of order 1 km s^{-1}. The three processes and the subsequent ionisation processes are discussed in more detail in Section 4.4.1 in the context of the plasma source processes at the icy satellites of Saturn.

4. Giant Planets Magnetospheres

4.1. General Features of Giant Planets' Magnetospheres

Giant planets magnetospheres display the largest diversity of phenomena by all points of view. The diversity of their plasma and momentum sources, and their mutual interplay, produce a host of mechanisms which was progressively recognized over the years. Jupiter was studied first as a radio emitter, because of the intensity and complexity of its emissions which already revealed some of its characteristics: irregular behavior, rotational modulation, Io phase control of a component of the decametric emission. With space exploration by the Pioneer, Ulysses and Voyager spacecraft, and in particular thanks to Voyager 2's "Grand Tour" of the solar system, the existence of giant planets magnetospheres as a real family of similar objects was definitely established (see the beautiful review by Bagenal, 1992). As illustrated in Figure 14, all four giant planets have intrinsic magnetic fields which carve magnetospheric cavities of varying sizes into the solar wind. All of them have radiation belts, radio emissions and auroras, showing that they behave as giant charged particle accelerators (Bhardwaj and Gladstone, 2000).

Unlike at Earth, where the energy source for particle acceleration is extracted from the solar wind, it is essentially planetary rotation which provides the energy source for these outer solar system particle accelerators: a complex interaction

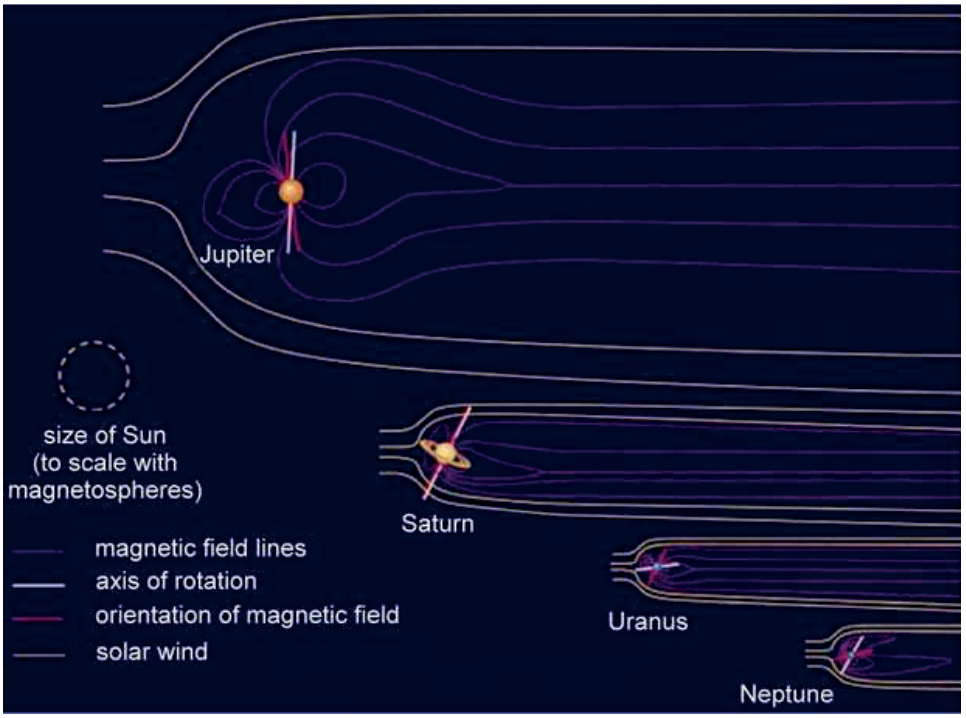

Figure 14. Illustration of relative sizes of giant planet magnetospheres, as they were revealed to us by the Voyager spacecraft (from Bennet, 2004).

between the rotation of the central magnetic field, coupled to the planetary rotation via the ionospheric conductor, and orbital sources of material and momentum, produces momentum and energy for the transport and energisation of plasmas and the associated radio and auroral emissions. In this short review, we will focus on this interaction as our main theme, as it is indeed the one which is unique at outer planets:

1. The three momentum sources described in the introduction are present at giant planets, but *the planetary spin momentum source is by far dominant* as shown by the comparison of R_{CF} and R_{stag} in Table III. Giant planets are fast rotators, or corotation dominated magnetospheres. They can be described to some extent as fast rotating magnets trapping and accelerating plasmas, but the solar wind interaction is not absent and actually plays an important role at least in the external zones of these magnetospheres. Neptune plays a special role, though, because its magnetosphere is completely reconfigured during each planetary rotation period.
2. The three plasma sources are present as well, but *the orbital plasma sources are dominant*, except for the case of Uranus. The orbital plasma sources are associated with the presence of a host of objects, satellites, rings, gas and dust clouds, in the geographic equatorial plane.

Thus, in an attempt to understand how these systems work, the primary effort must focus on the interaction processes between planetary rotation and the plasma sources, in particular the orbital sources. These interactions must be described and understood in connection with the magnetic field interactions, and from this point of view giant planets offer us a unique opportunity to explore to some significant extent the role of the relative orientations of the magnetic dipole and of planetary pin, described in the ($\mathbf{M}$, $\vec{\Omega}$) parameter space illustrated in Figure 2. Along this line of research, several key questions have emerged, out of which we would like to stress the following ones:

1. Do we physically understand in their diversity the wealth of interaction processes taking place between orbital objects and planetary rotation: interactions with the planetary rings, with the different types of satellites (magnetized or not, with or without a dense atmosphere, ...) and with the clouds of dust and gas orbiting the central planet (Io torus, gas clouds and E ring at Saturn, etc.)?
2. How do giant planets "solve" the basic problem of plasma transport vs. magnetic flux recirculation described in the introduction? This problem is particularly serious there: if we focus on the orbital plasma sources which are indeed dominant, their source regions are all on regions dominated by the corotation flow, or at least by closed flow lines encircling the planet, whereas an important potential sink region is the outer magnetosphere, with the magnetopause and the very extended magnetic tail where some fraction of the magnetic flux is probably open and plasma can also be evacuated down the tail. The processes allowing the plasma to be transported outward from the orbital sources to these sink regions and providing at the same time the necessary recirculation of the magnetic flux is still essentially unresolved.
3. How is this transport of the plasma from the orbital sources connected to the apparently inverse transport of a more energetic charged particle population towards the inner regions of these magnetospheres which seems to provide energetic particles and maintain radiation belts? Do we deal with two independent phenomena, or rather with a unique giant magnetic confinement machine which partly recycles and accelerates inwards a fraction of the orbital plasma? This question is still open.
4. How does the complex interaction between charged particles and fields generate the diversity of planetary emissions observed? We shall not touch on this subject here, but refer the reader to the chapter by Zarka and Kurth (2005) in this book.

We can take full advantage of the variety of situations discovered in the different magnetospheres during the last thirty fascinating years of outer planets exploration to summarize what we understand of these questions just at the start of the comprehensive study of Saturn's magnetosphere by Cassini-Huygens. In the remainder of this section we shall give a short description of each magnetosphere before focusing on Saturn. Besides the many commonalities, we will also try to emphasize the differences between the systems of the four giant planets:

1. The Jovian magnetosphere, studied in detail during recent years by the *Galileo* spacecraft, and Saturn's magnetosphere, at present explored by the Cassini spacecraft, are the reference cases of magnetospheres of "fast rotators," where plasma is concentrated near the equatorial plane and rigidly co-rotates in the inner magnetosphere. They differ significantly in their plasma properties, though: For Jupiter one single orbital source, the volcanic satellite Io, is dominant, it emits about 1 ton/s, mainly SO_2. For Saturn, the rings and icy satellites are more radially distributed sources of neutrals and ions. Titan, the solar wind, interplanetary and interstellar neutrals, as well as cosmic ray albedo neutron decay (CRAND; Hess, 1968) all contribute. The plasma density is much lower than in the Jovian magnetosphere, and the neutral populations play an important role.
2. Mainly because of the lower plasma density in the Kronian magnetosphere, Jupiter and Saturn differ in the sources of their main auroral emissions. In the case of Jupiter, the main auroral oval connects magnetically to the region near $20R_J$, where the plasma co-rotation breaks down (Hill, 1979). At Saturn, there is some evidence that the main aurorae are solar-wind driven (Prangé *et al.*, 2004; Kivelson, 2005, this volume), but the recent results from the HST observation campaign at the beginning of 2004 showed a very dynamic Saturnian aurora which may also be driven partly by planetary rotation and internal phenomena.
3. The densities of the neutral populations dominate in the case of Saturn and probably in the cases of Uranus and Neptune, while the plasma is still important for the dynamics of the Kronian magnetosphere, and certainly dominant in the case of Jupiter.
4. The relative orientations of the rotation and the magnetic dipole axis and the direction of the solar wind flow in the ecliptic plane lead to important differences. While in the case of Jupiter and Saturn, rotation axis and magnetic dipole axis are rather aligned and almost perpendicular to the ecliptic plane, the rotation axis of Uranus is almost aligned with the ecliptic plane, and the orientation of its magnetic dipole axis is significantly off the orientation of the rotation axis. Therefore, in average the solar-wind driven convection may dominate in the magnetosphere of Uranus, although it is a fast rotator. The orientations of the rotation and magnetic dipole axis of the magnetosphere of Neptune suggests that the magnetosphere is completely reconfigures during every half rotation period. So far, we only had one snapshot to test models on the magnetospheres of Uranus and Neptune – the data of the Voyager 2 mission.

Finally, in Section 5 we will review the satellites interactions at giant planets, as an introduction to Titan's poorly known magnetospheric interaction.

4.2. JUPITER

The Jovian magnetosphere has been a subject of considerable interest for a very long time, since the discovery of its strong decametric radio emission by Burke and Franklin (1955), and of the Io control of this emission by Bigg (1964). It is also the one we know best, since it has been visited by five interplanetary probes (Pioneer 10 and 11, Voyager 1 and 2, *Ulysses*) and one orbiter (*Galileo*) which brought an impressive set of information that can be analysed together with the remote sensing observations of the radio emissions and of the aurora from Earth.

A comprehensive and up-to-date description of the Jovian magnetosphere as we know it at the end of the *Galileo* mission can be found in the new book "Jupiter: The planet, satellites and magnetosphere" (Bagenal *et al.*, 2004). We shall essentially refer to it in this short description, which is divided into subsections on the large-scale structure of the Jovian magnetosphere, its aurora, and the phenomena of plasma transport. The large-scale current systems of the Jovian magnetosphere are discussed in this volume by Kivelson (2005).

4.2.1. *The Large-scale Structure of the Jovian Magnetosphere*

Jupiter's magnetosphere is usually divided into the inner ($< 10R_J$), the middle ($10 - 40R_J$), and the outer ($> 40R_J$) magnetosphere:

1. *The inner magnetosphere* contains the so-called Io torus ($5.2 - 10R_J$, see Section 5.1) and the inner radiation belts. Because of the low plasma temperature ($k_B T < 100$ eV), the plasma β ($\beta = 2\mu_0 n k_B T/B^2$) is usually below 0.2, and, therefore, the plasma dynamics are dominated by the magnetic field. Due to the friction with the ionosphere the plasma co-rotates with Jupiter. The co-rotation, the dominance of the magnetic forces and stresses, and the fact that the magnetic dipole of Jupiter is tilted by 9.6° with respect to the rotation axis leads to the 'rotating-beacon' type modulation of the plasma (Krupp *et al.*, 2004) with the planetary rotation frequency.
2. *The middle magnetosphere* contains the transition region at about $20R_J$ (Hill, 1979), where the plasma β in the thin equatorial plasma sheet exceeds unity, and, thus, the plasma increasingly lags behind co-rotation with increasing radial distance. Beyond $\approx 20R_J$, the plasma's thermal pressure, the centrifugal force, and, further out, the solar wind pressure have comparable importance. The 'link' between the plasma and the rotating magnetic field becomes more and more delayed, the plasma sheet oscillates in the form of an outward spiral wave. The effective propagation speed of this wave has initially been determined to be 840 km/s or $43R_J$/h (Kivelson *et al.*, 1978, updated by Khurana *et al.*, 2004).

   An extremely disturbed plasma region is found at about $15R_J$ on the dayside of Jupiter. It is called the "cushion region," where cloudlets of iogenic plasma enclosed in magnetic bubbles break off to serve as a source of plasma for the outer magnetospheric flux tubes.

3. *The outer magnetosphere* has plasma speeds up to a factor 2 below the ideal co-rotation speed. In the nightside outer magnetosphere, an additional current system, the magnetotail current, connects the magnetodisc current to the magnetopause current. This further stretches the magnetic field lines, creating a long magnetotail region (length $> 7000 R_J$), which has been known to extend to the orbit of Saturn. The magnetospheric regions above and below the current sheets are depleted of plasma ($n_e < 0.01$ cm^{-3}) and are referred to as lobes in analogy to Earth's magnetosphere.
   A 'flashing-type' modulation has been observed in form of modulations in the intensity and spectral shapes of relativistic electrons ejected from the Jovian magnetosphere to interplanetary space (Simpson *et al.*, 1974). This kind of modulation presumably comes from the interaction of an azimuthally asymmetric rotating object – the Jovian magnetosphere – and an azimuthally asymmetric fixed structure – the outer magnetosphere which is strongly asymmetric with respect to the fixed solar wind flow direction. So far, mostly the concept of 'active sectors' (Vasyliunas, 1975), the longitudes that face the magnetotail, has been discussed in order to explain the 'flashing-type' events.

4.2.2. *The Jovian Aurora*

The complex dynamics of the Jovian magnetosphere are reflected in the Jovian aurora, whose morphology, dynamics and magnetospheric connection has been reviewed in great detail by Clarke *et al.* (2004). Hubble Space Telescope and IR images reveal that Jovian auroral features can be divided into three components: the main oval, the satellite footprints (dominated in brightness by the Io footprint) and the polar emission (see Figure 9 of Kivelson, 2005, in this volume). As pointed out by Kivelson (2005), each of the aurora components generally corresponds to the ionospheric footprints of regions of upward magnetic-field aligned electric currents in electric current loops connecting the ionosphere to the magnetosphere. These current loops transfer momentum between the two levels, in much the same way as the current loop shown in Figure 12 transfers momentum between the solar wind/distant magnetosphere and the terrestrial ionosphere. At Jupiter, the aurora connects to the three types of momentum sources identified in Section 4.1.

1. *The planetary spin source* is responsible for the generation of the main oval. It seems to map to the region of the middle magnetosphere around $20 R_J$, where the co-rotation breaks down. The radial currents which reinforce partial co-rotation of the plasma connect through field-aligned currents to the ionosphere of Jupiter. and cause aurorae. These field-aligned currents, which transfer angular momentum from the ionosphere to the magnetospheric plasma, cause aurorae in Jupiter's ionosphere. The main oval is the brightest component of the Jovian aurora, just as planetary spin is the most important of the three momentum sources at Jupiter.
2. *The orbital momentum source* is represented here by the Galilean satellites, whose magnetic projection onto the polar ionosphere is traced by an auroral

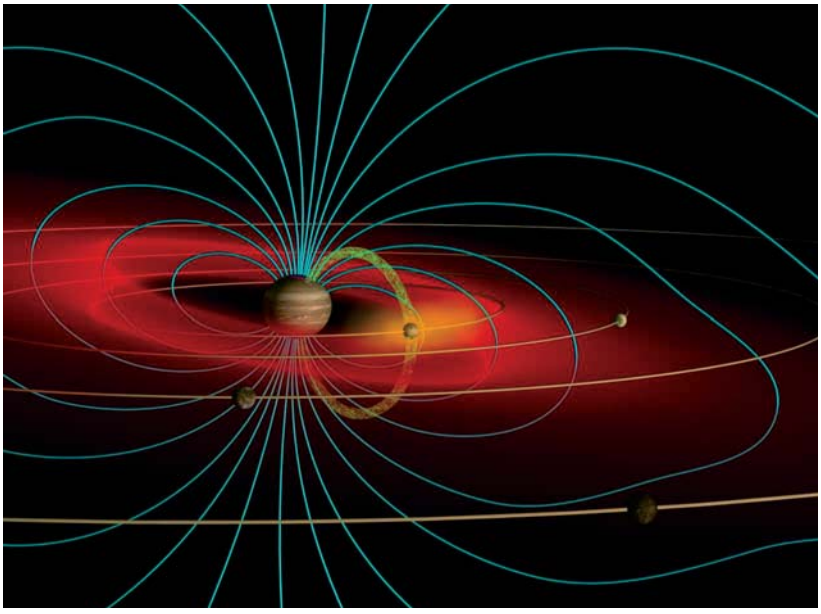

Figure 15. Artist's view of Jupiter's magnetosphere, showing the central role played in its dynamics and plasma sources by planetary rotation and the interaction with the Galilean satellites, mostly Io (adapted from Bennet, 2004).

emission spot. The Galilean satellites move slower than the co-rotation speed and leave an extended plasma wake which in turn leaves an extended trace of auroral emissions in Jupiter's ionosphere.

3. *The solar wind momentum source* is also believed to cause at least some components of the very complex polar emissions. They are believed to map to the external boundaries of the magnetosphere and to magnetic topological boundaries in the magnetic tail as in the case of the terrestrial aurora.

4.2.3. *Plasma Sources and the Resulting Charged Particle Populations*

Jupiter is characterized by the presence of one dominant plasma source, strongly localized near Io's orbit, illustrated in Figure 15, the Io torus (Thomas *et al.*, 2004). This torus of neutrals and ions is produced by the satellite's volcanic emissions, which release a cloud of neutrals along its orbit. Under the effect of photoionization and electron impact ionization of this volcanic gas, dominated by O and S neutrals, approximately 1 ton of fresh iogenic ions are added to the magnetosphere every second and accelerated to the local corotation speed. This intense source is estimated to be larger than the solar wind source by one order of magnitude, and than the ionosphere source and the sources associated with the other satellites by about 2 orders of magnitude (e.g., Hill *et al.*, 1983). It has a very strong effect on the structure and dynamics of the Jovian magnetosphere (reviewed by Khurana *et al.*, 2004, and Krupp *et al.*, 2004). It maintains the plasma torus

near Io's orbit, feeds the region of dipolar field lines extending outwards of it up to about $10R_J$, through which the iogenic thermal plasma must diffuse outward at a rate balancing the Io source rate, and is responsible for the formation of the extended plasma and magnetic disk which is the dominant feature of Jupiter's magnetosphere from $10R_J$ up to at least 60 or $80R_J$ outwards. Voyager observations showed that, superposed to this so-called thermal population (McNutt *et al.*, 1981), a distinct high-energy population is present throughout the middle magnetosphere and plasma disk (Krimigis *et al.*, 1981). Inward of Io's orbit, one finds the maximum fluxes of the Jovian radiation belts, which are revealed in particular by their strong synchrotron emission (Bolton *et al.*, 2004).

4.2.4. *Radial Plasma Transport*

Figure 16, from Krupp *et al.* (2004), provides a nice framework to discuss the main transport processes at Jupiter. What we really know is limited by the spatial coverage of Galileo data, which does not go beyond approximately $150R_J$ in the antisolar direction. The main problem is to explain:

1. how the ton/s of thermal iogenic ions is evacuated by outward radial transport to the outer magnetosphere, magnetic tail and solar wind;
2. how the energetic plasma is generated (what is its source, where?) and transported inwards as observed.

On the second problem, simulation studies of the radiation belts seem to prove that the radiation belts present in the inner magnetosphere are fed by inward transport of plasma from the middle magnetosphere (e.g., Santos-Costa and Bourdarie, 2001) and can reproduce the observed synchrotron emission (Santos-Costa *et al.*, 2001; Bolton *et al.*, 2004). This, in addition to direct evidence for inward diffusion of energetic plasma (see the next paragraph) builds-up a picture in which the energetic component of the Jovian plasma population experiences essentially an inward diffusion from a distant external source to the inner magnetosphere where it feeds the radiation belts. This is the meaning of the narrow inward arrows in Figure 16, upper panel.

The first problem is probably farther from being solved. It really looks as if *Galileo* observations have brought many pieces of the puzzle, which, when assembled, will provide the full picture of how the iogenic plasma finds its way from the Io torus to some distant source regions. But the puzzle clearly remains to be assembled. Here are some of its pieces, which can be found in greater detail in Krupp *et al.* (2004). They can be ordered along the radial distance to the planet. As we move outwards, we move from a region of low β, high density plasma rigidly corotating with the planet, to regions of increasing plasma β, decreasing densities and increasing flux tube volume, which progressively decouple their motions from rigid corotation with the planet. At large distances, they tend to move under the influence of their own inertia, and of specific stresses exerted in the regions of the magnetopause and magnetotail. It is therefore not surprising that the modes

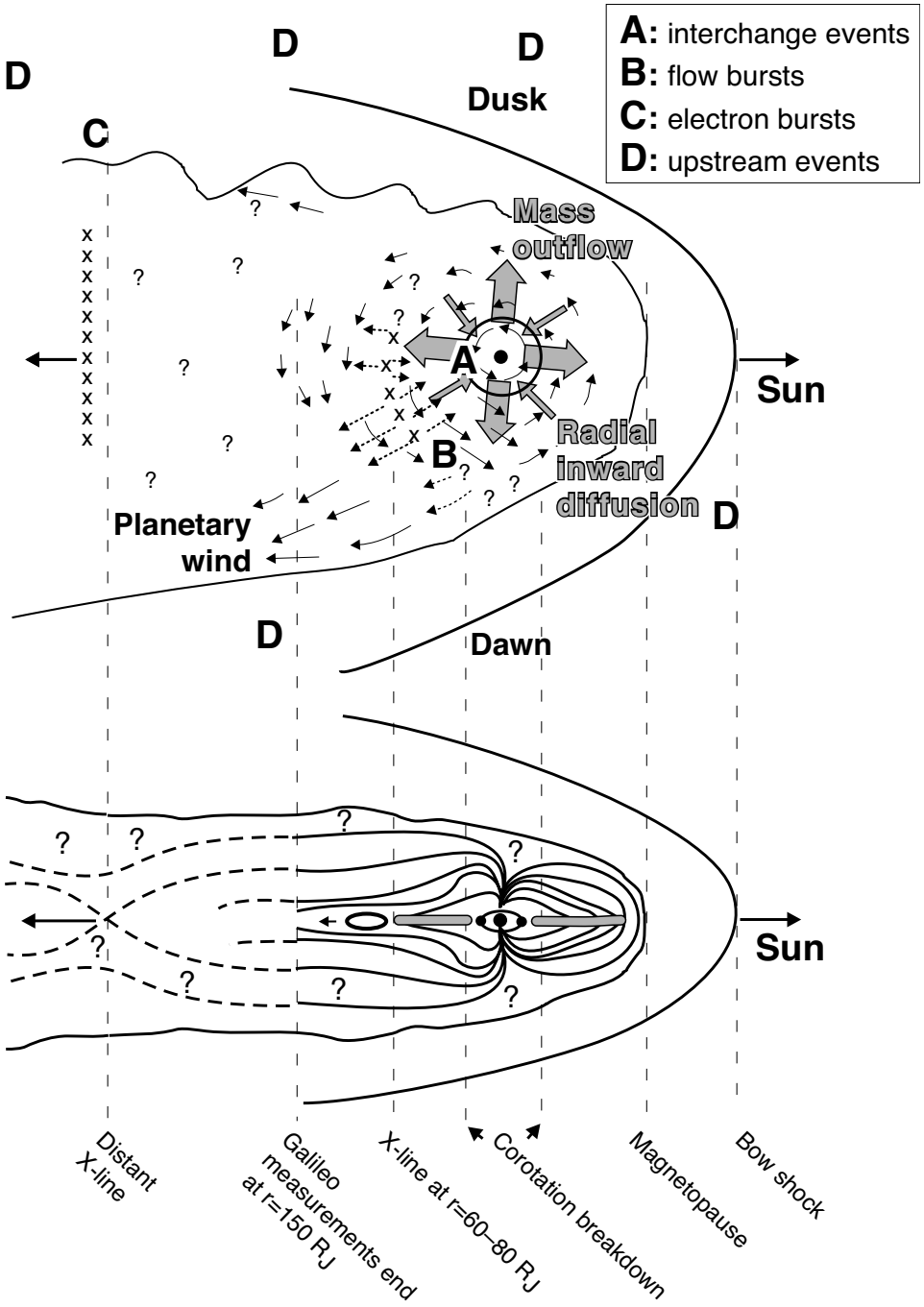

Figure 16. Scheme of the main dynamic phenomena detected in the Jovian magnetosphere, represented by Krupp *et al.* (2004) in the equatorial (*top*) and meridian noon-midnight magnetic planes.

and spatial scales involved in plasma transport change continuously with radial distance:

1. In the outer Io torus, in the region of quasi-dipolar field extending from 6 to about $10R_J$ where the main plasma reservoir of the planet stands, evidence for magnetic flux interchange has been found (e.g., Bolton *et al.*, 1997; Kivelson *et al.*, 1997b; Thorne *et al.*, 1997) in the form of the inward motion of small-scale flux tubes empty of cold plasma but filled with a hot particle population. These observations support the idea that the magnetospheric interchange instability is responsible at least for part of the radial transport there. This idea was first formulated for a magnetosphere by Gold (1959), and later developed by Southwood and Kivelson (1987). It was more recently revisited by Ferrière *et al.* (1999; 2001) and Ferrière and André (2002) who identified the corresponding underlying MHD modes and established some stability conditions. These observations provide some observational material to check these theoretical predictions, but it is interesting to note they show only the inward motion of flux tubes empty of cold plasma, and the compensating outward motion of flux tubes filled with iogenic plasma remains to be observed.
2. Further out, in the "intermediate" region extending approximately to the distance of $20R_J$ where rigid corotation starts to break down, "injection events," occurring in the form of bursts of enhanced energetic ion and electron fluxes dispersed in time were observed by Mauk *et al.* (1999). They were identified by these authors as the Jovian analogs of the "magnetic storms" which cause a rapid growth of the trapped hot particle population of the Earth's inner magnetosphere. These Jovian injection events affect a broad local time sector and correspond to inward motions of the hot particle population by a few R_J.

   In both cases, all the observational evidence bears upon the inward transport of energetic plasma and low-density flux tubes, but no direct evidence of the balancing outward transport of thermal plasma has been reported!
3. In the magnetodisk itself, out to radial distances of 60 to $80R_J$, large-scale "energetic magnetospheric events" have been reported and analysed by Louarn *et al.* (2000), suggesting that a global reconfiguration of the magnetic structure of the disk develops simultaneously with rapid increases in its plasma content and enhanced electromagnetic emissions. These events may be the Jovian analogs (in a rotation-driven magnetosphere) of the terrestrial substorms which develop in a solar-wind driven magnetosphere. A detailed analysis of the PWS data (the electromagnetic field detector on board Galileo) schematically represented in Figure 17 suggests that these energetic events are related to an instability developing in the external part of the Io torus or in the inner part of the magnetodisk that sporadically injects new plasma from the inner magnetosphere in the more distant magnetodisk. Additional multi-instrument studies (Louarn *et al.*, 2001) strongly suggest that these "energetic magnetospheric events" in the distant disk are directly related to the injection events observed in the outer part of the Io torus.

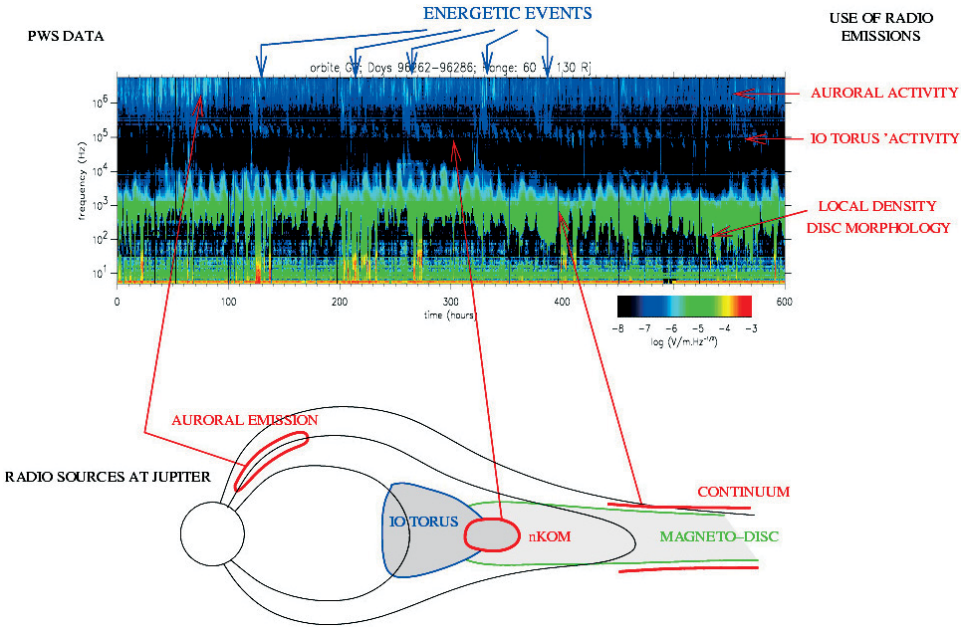

Figure 17. A careful analysis of Galileo radio and plasma waves data allowed Louarn *et al.* (1998; 2000) to show the existence of a mode of large-scale relaxation of the magnetic configuration of Jupiter's magnetic and plasma disk in which a fraction of this magneto-disk is ejected outwards. While locally generated plasma waves make it possible to survey the evolution of the local electron density, the different types of radio emissions received at the spacecraft position provide a simultaneous and remote diagnostic on the dynamical evolution of key regions of the magnetospheric system: the magnetodisk boundary, the outer edge of the Io torus, and auroral zones.

To summarize, there is some partial evidence that radial transport may involve interchange of small-scale flux tubes in the quasi-dipolar region of the magnetosphere, near the torus (see Section 4.4 for a more detailed description), while another process involving sporadic large-scale instabilities near the transition between the outer torus and the magnetodisk governs the outward transfer of iogenic material, and the inward transfer of hot plasma, between these two reservoirs. This does not tell us yet how the iogenic plasma is ultimately lost to the outer magnetosphere, tail and interplanetary space. This ultimately involves a description of plasma flows in the external magnetosphere and tail. Some mechanism, such as the formation and ejection of plasmoids and/or the opening of closed flux tubes to the distant tail, is needed to cross the closed/open field lines boundary of Figure 4. A formal solution to this problem was proposed in 1983 by Vasyliunas (Figure 18). This representation of the evolutions of magnetic field geometries, critical points/lines and plasma flows in a magnetic meridian at different local times of the night sector suggests how a plasmoid filled with iogenic plasma might form in the evening sector, break from the main magnetodisk and be ejected down the tail during its transit towards dawn, while the closed section of the reconnected flux

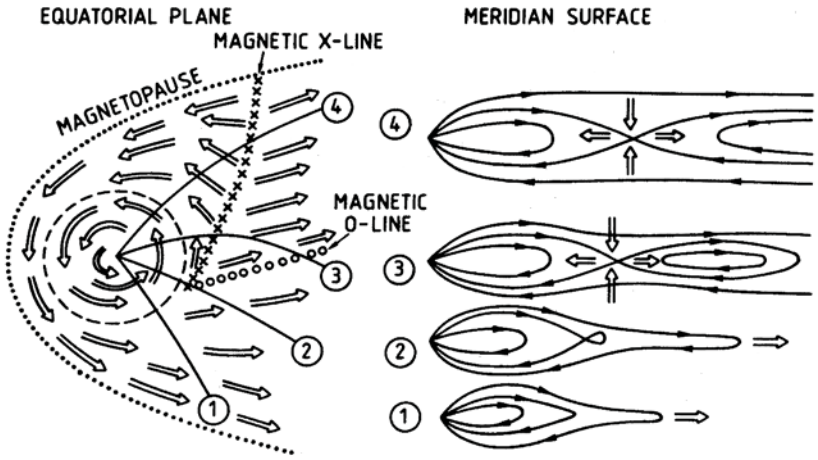

Figure 18. Vasyliunas (1983) proposed this scenario for the evolution of Jovian outer magnetosphere flux tubes between dusk and dawn during a transit of the tail region. In the absence of the confining effect of the magnetopause, a flux tube filled with plasma is elongated into the tail under the effect of the inertia of its mass content, until a plasmoid forms. The subsequent reconnection of tail lobes field lines sunwards of the plasmoid allows the plasmoid to be ejected, carrying its plasma content down the tail while the empty newly created closed flux tube can be convected back towards the planet and dayside near dawn. This "Vasyliunas cycle" is likely to be the Jovian equivalent to the Dungey cycle of the Earth's magnetosphere.

tube, emptied from its plasma, would convect back towards the dayside morning magnetosphere. It is the rotation-driven analog of the solar-wind-driven "Dungey cycle" shown in Figure 1, and is often called the "Vasyliunas cycle" for this reason.

It remains to be checked if this diagram corresponds to the observed magnetic field, particle acceleration and flow behaviors in the external parts of the magnetosphere. The average flow of plasmas has been derived from energetic particle fluxes anisotropies by Krupp *et al.* (2001), showing the dominance of subcorotating types of flows there with a substantial local time modulation. Sporadic tailward and sunward plasma flows have also been observed at different local times in the distant night sector, near the boundaries of the region explored. Further out and at high latitudes, the best signatures we have of flows and magnetic field topological changes must be found in the auroral morphology and dynamics. As reported by Clarke *et al.* (2004), polar emissions are very complex and difficult to interpret (would it be only because of the poor accuracy of magnetic field models when used to map polar regions to the distant equator and tail). Even so, they seem to indicate an increasingly important influence of the solar wind with increasing radial distance and latitude, and that some degree of mixing of the Dungey and Vasyliunas cycles is required to reach a reasonable interpretation of all observed auroral signatures.

Evidently, the full puzzle of plasma and magnetic flux transport at Jupiter still remains to be assembled. Maybe, we shall have to go back there!

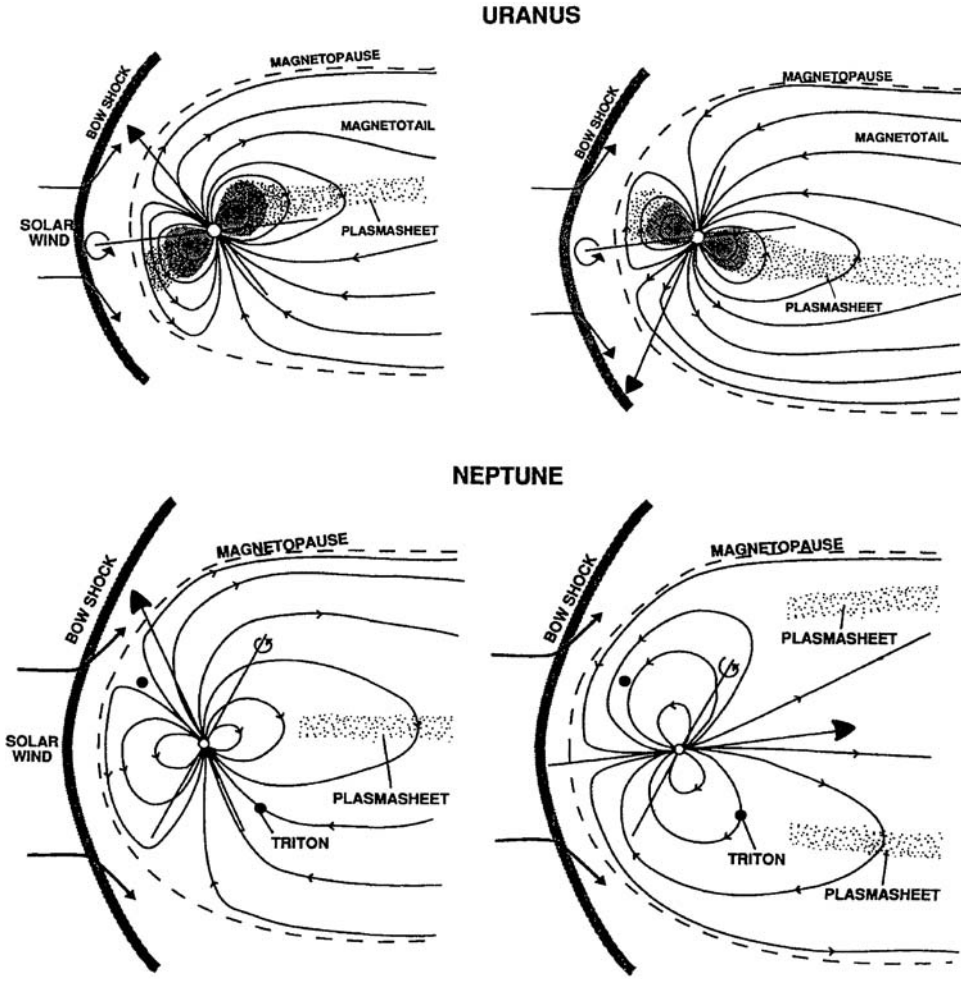

Figure 19. Structure of the magnetospheres of Uranus and Neptune (from Bagenal, 1992).

4.3. Structure of the Magnetospheres of Uranus and Neptune

The knowledge obtained on the asymmetric magnetospheres of Uranus and Neptune has been reviewed by Bagenal (1992). Both planets have a considerable tilt between their rotation axis and their magnetic dipole axis (Figure 19). Therefore, the convection electric field in the inertial frame is not steady.

In the case of **Uranus** the rotation axis is tilted by only 7.9 degrees from the ecliptic plane. For this reason the rotation axis assumes orientations from almost parallel to the solar wind flow to almost perpendicular during Uranus' orbit period of 84 years. At the time of the Voyager 2 fly-by the rotation axis was almost parallel to the solar wind flow. In the frame co-rotating with Uranus, the solar wind convection field is therefore steady Viewed from the inertial frame, the plasma in

Uranus' magnetosphere co-rotates with the intrinsic rotation period of 17 hours. Because of the large tilt of the magnetic dipole axis the plasma structure revolves around the planet-Sun line. The magnetic field topology and trajectories of plasma parcels are described in detail by Selesnick (1988), Belcher *et al.* (1991), and Ness *et al.* (1991). A traditional plasmasphere is only stable if the rotation and magnetic dipole axes are approximately aligned (Selesnick and Richardson, 1986; Vasyliunas, 1986). This is not the case at Uranus. The solar-wind driven convection can penetrate deep into the inner magnetosphere, so the lifetime of plasma within the magnetosphere is a few days. This explains the lack of a significant plasmasphere at Uranus. The surfaces of Uranus' rings and moons are very dark, suggesting that very little sputtering occurs (see Bergstrahl *et al.*, 1991, for a review). Only H^+ is observed, again consistent with a lack of sputtering from the moons/rings. Electron impact ionisation of the large neutral H corona is the main plasma source (Belcher *et al.*, 1991). A convection boundary forms at $4-5R_U$, analogous to Earth (Selesnick, 1988).

Aurorae are observed at Uranus in radio emissions (Zarka and Kurth, 2005, this volume), but also in the infrared at $3-4$ μm from H_3^+ (Miller *et al.*, 2005, this volume) and in the ultraviolet wavelength range (see Bhardwaj and Gladstone, 2000, for an overview). There is no emission detected yet from hydrocarbons between 7 and 14 μm. Cheng *et al.* (1991) report on transient structures based on energetic particle and plasma wave observations. Medium energy protons show inward radial diffusion.

In the case of **Neptune**, the planetary rotation axis is neither aligned with the magnetic dipole axis nor with the solar wind flow. The main source of plasma is probably the moon Triton, which has a substantial ionosphere with peak ion densities near 50000 cm^{-3} (Tyler *et al.*, 1989). Most of the escaping particles are neutral with a total source of 10^{26} s^{-1}, with 2/3 H and 1/3 N (Summers and Strobel, 1989). Roughly 10–20% of the neutrals escaping from Triton are ionized in the magnetosphere (Decker and Cheng, 1994), so the plasma source is 0.1 to 0.2 times the neutral source. Given the source rate and observed plasma density, the transport time can be estimated and is about 13 hours at Triton's orbit (Richardson *et al.*, 1995).

This fast plasma removal rate suggests convective, solar wind driven transport. In a number of articles the peculiarities of Neptune's magnetosphere, arising from the orientations of the rotation and the magnetic dipole axis, are described. Since the planetary rotation axis is neither aligned with the magnetic dipole axis nor with the solar wind flow, there is no reference frame in which the plasma flow is steady (Selesnick, 1990). The magnetic dipole axis changes from 20 degrees to 114 degrees over 16.1 hours. At 90 degrees Neptune's magnetosphere momentarily looks symmetric. At small angles between magnetic dipole axis and solar wind flow the magnetosphere looks completely different (Figure 19). Therefore, the magnetosphere is reconfigured during every planetary rotation. The reconfiguration means that the convection electric field does not average to zero as Neptune rotates, so that

solar-wind driven convection has a cumulative net effect (Selesnick, 1990). In the magnetic equatorial plane, there is a net sunward transport of plasma. Reconnection is strongest when the magnetospheric configuration is Earth-like and weakest for the pole-on configuration (Figure 19, *lower right*) because there are only small regions with the interplanetary and planetary magnetic field being anti-parallel. In the pole-on configuration, the magnetotail has a cylindrical configuration with planetward-directed field on the outside and field lines leaving the planet on the inside separated by a cylindrical current sheet (Bagenal, 1992). Auroral emissions of Neptune are also confined in longitude. So far, only ultraviolet and radio emissions have been observed (Bhardwaj and Gladstone, 2000).

4.4. Saturn's Magnetosphere in the Solar System

The basic morphology of Saturn's magnetosphere has been explored by Pioneer 11 (Frank *et al.*, 1980; Van Allen, 1984; Scarf *et al.*, 1984; Connerney *et al.*, 1984; Schardt *et al.*, 1984) and Voyager 1 (Bridge *et al.*, 1981) and 2 (Bridge *et al.*, 1982). Saturn has a dipolar magnetic field rapidly rotating with a period of 10 hours and 39 minutes, as determined from the rotational modulation of its radio emissions at the Voyager epoch (Kaiser *et al.*, 1984; see Table III for basic parameters of the Saturn system). It is aligned with the spin axis with no low order azimuthal anisotropy. This configuration is unique in the solar system. Neither the magnetic structure nor the plasma distributions of the magnetosphere are expected to be significantly modulated by the planetary rotation as in the case of Jupiter (Krupp *et al.*, 2004). There are nonetheless variations in the radio emission (Desch and Kaiser, 1981; Zarka and Kurth, 2005, in this volume) and vortical perturbations of the field (Espinosa and Dougherty, 2000) with a period that corresponds to Saturn's rotation period. For a discussion of the auroral emissions, we refer to the articles by Zarka and Kurth (2005) and Miller *et al.* (2005) in this volume. The latter authors also present recent theoretical work on convection patterns and auroral currents by Cowley *et al.* (2004). Asymmetries between the convection patterns of the day/dawn side and the night/dusk side can be expected, although recent observations from Cassini show that the auroral ring closes around the night side (Prangé *et al.*, 2004). The same work shows that Saturn's main aurora is driven by the solar wind as predicted by Kivelson (2005) in this volume. We refer to her article for a description of the expected large-scale current systems of the Kronian magnetosphere, which will be researched during Cassini's tour at Saturn. A comprehensive review on the properties of the plasma embedded in Saturn's magnetic field has been given by Richardson (1998) based on the results of the Voyager missions, and Krupp (2005) gives an overview on the energetic particle populations.

Figure 20 succinctly explains the structure of the plasma in the Kronian magnetosphere (see also Krupp, 2005, in this volume). At first glance, there are similarities to the Jovian magnetosphere. However, the diversity of plasma sources and sinks as well as the dominance of the neutral populations make the Kronian

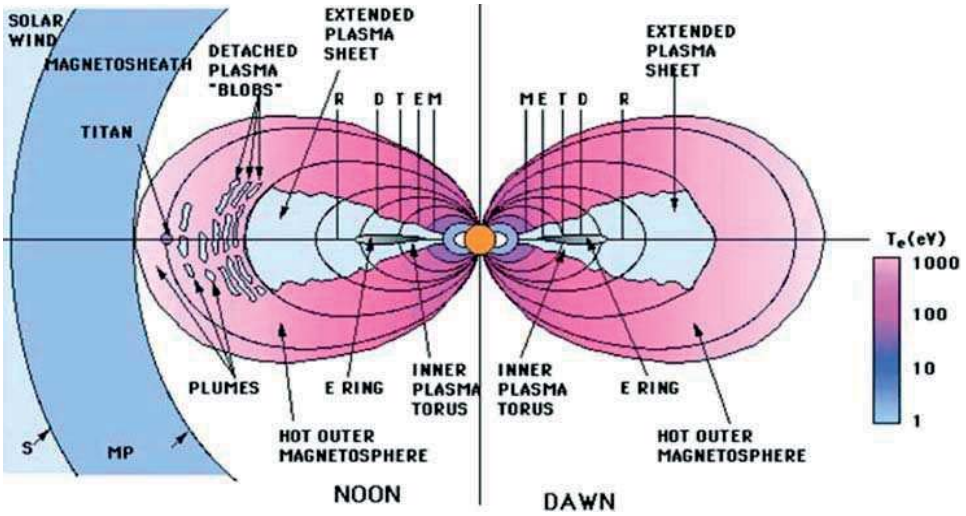

Figure 20. Simplified view of Saturn's magnetic field configuration and main plasma domains as seen by the two Voyager spacecraft in the noon and dawn meridian planes, the only two explored so far (Richardson, 1998). The satellite positions are denoted by M for Mimas, E for Enceladus, T for Thetys, D for Dione, and R for Rhea. The E ring opacity is illustrated by the gray shading. The schematic only shows electron temperatures. The electron densities in the hot outer magnetosphere, the so-called plasma mantle are between 0.02 and 0.2 cm^{-3}. At the boundary between the mantle and the plasmasphere (plasma sheet), the density increases by a factor 10 and ranges up to 10 cm^{-3}.

magnetosphere more complex. We therefore give more detailed information on the microscopic source, loss, and transport processes as a reference for scientists studying Saturn.

The sources of the neutral and charged plasma particles inside the Kronian magnetosphere are Saturn's atmosphere, Titan's atmosphere, the rings, the inner icy satellites Mimas, Enceladus, Tethys, Dione, and Rhea, and the interstellar neutral wind. Neutral atoms and molecules are sputtered from the surfaces of the ring particles and the icy satellites by energetic ions, by photons, and through meteoroid bombardment. Gravitationally bound neutral particles follow Keplerian orbits until they collide with other neutrals, ions, ring particles, moons, or with Saturn, or until they are ionised. Many of these neutrals atoms and molecules are ionised by solar ultraviolet radiation or via collisions with energetic electrons or ions. The plasma is also fed by solar wind ions entering through the magnetotail and ions escaping from the ionospheres of Titan and Saturn. The charged particles of the plasma are lost by collisions with neutrals, electrons (via recombination), the rings, satellites, the atmospheres of Saturn and Titan.

Measurements from ground- and space-based telescopes indicate that Saturn's magnetosphere is dominated by its neutral component. The Faint Object Spectrograph (FOS) on board the Hubble Space Telescope (HST) was used to determine the column density of OH along a line-of-sight at $4.5 R_S$, between Tethys and Ence-

ladus (Shemansky *et al.*, 1993). Jurac *et al.* (2001) combined these and subsequent HST observations of OH to show that the peak OH density was over 700 cm^{-3}.

The charged plasma component is tied (frozen-in) to the magnetic field lines and co-rotates due to friction with Saturn's atmosphere and ionosphere. The centrifugal force confines the plasma close to the equatorial plane. The distribution of the pressure of species i parallel ($P_{\parallel,i}$) and perpendicular ($P_{\perp,i}$) to the dipolar magnetic field line, parametrised by the variable s, is given by Vasyliunas (1983) as

$$\frac{\partial P_{\parallel}}{\partial s} - \left(P_{\parallel} - P_{\perp}\right)\frac{1}{B}\frac{\partial B}{\partial s} - n_i m_i \frac{\partial}{\partial s}\left(\frac{1}{2}\Omega^2 r^2\right) + n_i \frac{\partial}{\partial s}\left(\frac{G M_S m_i}{r}\right) + n_i Z_i e \frac{\partial \phi}{\partial s} = 0, \quad (3)$$

where r is the distance from the spin axis, Ω is the rotation rate of the plasma, n_i, m_i, and $Z_i e$ are the number density, mass, and charge of species i, G is the gravitational constant and $M_S = 5.68 \times 10^{26}$ kg is the mass of Saturn. The potential ϕ describes ambipolar fields that are created due to different scale heights of electrons and ions of different mass and charge above the equatorial plane. In the Kronian magnetosphere, the mirror force, described by the second term in the above equation, can be quite important. The ion distributions are typically anisotropic with $T_{\perp,i}/T_{\parallel,i} = P_{\perp,i}/P_{\parallel,i}$ up to 10 inside Rhea (Richardson and Eviatar, 1988). The process of ionising atoms and molecules, which are picked up by the co-rotating plasma, imparts large perpendicular but small parallel temperatures to the ions.

If small-scale motions dominate over large-scale circulation eddies, the radial motion of ions and electrons can be described by a diffusion equation of the form

$$\frac{\partial N_i L^2}{\partial t} = L^2 \frac{\partial}{\partial L}\left[\frac{D_{LL}}{L^2}\frac{\partial\left(N_i L^2\right)}{\partial L}\right] + S_i - R_i \,, \quad (4)$$

where N_i is the number of ions of species i in a magnetic flux shell per unit L, S_i and R_i are the ion sources and sinks, and $D_{LL} = D_0 L^n$ is the diffusion rate of low-energy particles across L-shells (Birmingham *et al.*, 1967; Fälthammar, 1968). The diffusion coefficient D_{LL} includes and parameterizes all the physics of the small-scale motions which drive the radial transport. Following Young *et al.* (2003), the diffusion coefficient D_{LL}, which is usually assumed to have a simple L-dependence of the form $D_{LL} = D_0 L^n$, may describe the following processes: (A) "terrestrial" radial diffusion mechanisms including (A1) magnetic impulses yielding $D_{LL} \propto L^{10}$, (A2) electrostatic pulses of magnetospheric origin with $D_{LL} \propto L^6$ for magnetic moments $\mu << L^2$ MeV/G and $D_{LL} \propto L^{10}/\mu^2$ for $\mu >> 20L^2$ MeV/G, and (B) "Jovian" radial diffusion via (B1) the ionospheric dynamo mechanism (Brice and McDonough, 1973; Coroniti, 1974) or (B2) the centrifugal interchange (mass interchange between flux tubes in turbulent eddies) instability in regions of strong negative radial plasma density gradients (Siscoe, 1978; Siscoe and Summers, 1981; Southwood and Kivelson, 1987; Ferrière *et al.*, 1999; 2001).

From the outward transport of the ions originating in the Io torus at Jupiter a diffusion parameter $D_{LL} \approx 2.1 \times 10^{-6} R_J^2\ s^{-1}$ has been found scaling as L^n with

$n \approx 2...4$. The interchange process responsible for the plasma transport outward from Io still is not known (Krupp *et al.*, 2004).

As in the case of the Jovian magnetosphere, diffusion coefficients D_{LL} have been determined from observations in the Kronian magnetosphere. A lower limit for the diffusion parameter D_{LL} has been found by Hood (1983; 1985; 1989) from satellite "sweeping" signatures of the inward propagating plasma between $L = 12$ and $L = 5$. Assuming that the only loss mechanisms of energetic particles in the range $0.6 < \mu < 3$ GeV/G are collisions with satellites such as Dione, the radial depletion profile yields $D_{LL} \approx 10^{-9} - 10^{-8} L^3 R_S^2\ \mathrm{s}^{-1}$. The exponent of L may range up to 6 for the higher energetic particles when including maximal absorption by the E ring. Paonessa and Cheng (1986) derived upper limits of D_{LL} from the presumed maximum loss rate to Saturn's atmosphere. This loss rate is constrained by the auroral emissions, i.e., by the fact that for most L-shells no aurorae are observed. Together with the observed phase space densities of energetic particles this yields the maximum pitch-angle scattering rate into the so-called loss cone (ions at low pitch-angle are not reflected in the magnetic field tubes before they reach Saturn's atmosphere). Paonessa and Cheng (1986) obtained an upper limit $D_{LL} \approx 2 \times 10^{-9\pm1} L^3 R_S^2\, s^{-1}$. The exponent of L suggests that process (B2), atmospherically driven diffusion, dominates the radial transport. Changes of the neutral wind couple to the ionospheric plasma and consequently drive motions of the magnetic field lines.

The temperature of the plasma in Saturn's magnetosphere generally increases radially outside of $L = 4$ (Figure 20; Richardson, 1986; Krupp, 2005, in this volume). This indicates that the plasma is dominated by local source and loss processes, otherwise the temperature would vary as $L^{-8/3}$. The $L^{-8/3}$ power law follows from the conservation of the magnetic moment (first adiabatic invariant) $\mu_i = -m_i \langle v_{\perp;i}^2 \rangle \mathbf{B}_0/(2B_0^2)$ of particles moving across L-shells. The perpendicular temperature then scales as $T_\perp(L)/T_\perp(L_0) = B_0(L)/B_0(L_0) = L_0^3/L^3$. The second adiabatic invariant, $m_i l \langle v_\parallel \rangle$, requires the parallel temperature to change as $T_\parallel(L)/T_\parallel(L_0) = l_0^2/l^2 = L_0^2/L^2$. If the distribution is isotropised quickly, the temperature should scale as $\left(T_\perp^2 T_\parallel\right)^{-1/3} \approx L^{-8/3}$.

However, the plasma temperature rather seems to represent the local pick-up energy which increases with L. The co-rotation speed V_{cor} increases with L, whereas the speed V_{n} of neutrals before they are ionised decreases slowly with L. After ionisation the ion temperature of species i approximately corresponds to $(V_{\mathrm{cor}} - V_{\mathrm{n}})^2 / (2k_{\mathrm{B}} m_i)$. The observed increase of ion temperature with L therefore indicates that the thermal plasma is created from the neutral population but also lost by in situ processes.

Among the microscopic source and loss processes in the inner magnetosphere (Figure 21), we would like to emphasize three main groups: (i) the sputtering of neutrals off the surfaces of the rings and icy satellites, (ii) the loss of neutrals to the rings and icy satellites, and (iii) the ionisation processes for neutrals.

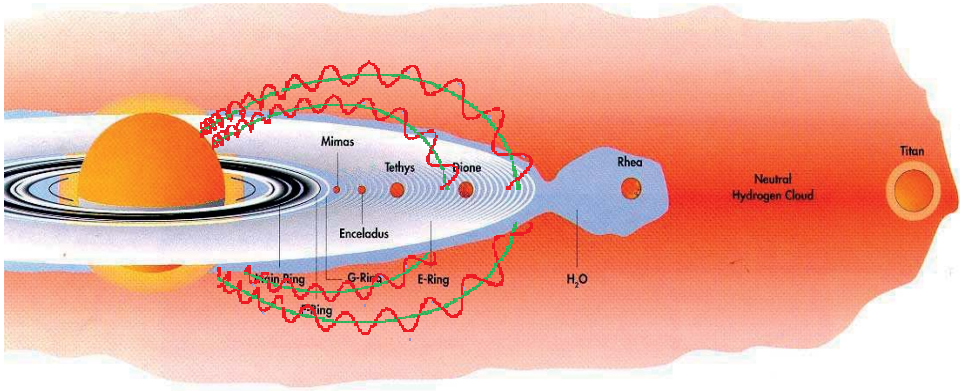

Figure 21. Schematic representation of the inner part of Saturn's magnetosphere. The water distribution is not fully shown above the equatorial plane near the rings. See Figure 24 for the modelled (and observed) distribution.

4.4.1. *Sputtering Processes at the Surfaces of Icy Satellites and Ring Particles*
Three main sputtering processes have been discussed to reconcile the observed neutral release from the icy satellites and rings: (i) photosputtering, (ii) sputtering by magnetospheric particles, and (iii) meteoroid bombardment.

1. *Photosputtering* ejects H and OH from the icy surfaces of the satellites at a rate of 5×10^6 cm^{-2} s^{-1} (Harrison and Schoen, 1967). This rate is lower than the escape fluxes of H_2O determined using Voyager 1 and 2 data of up to 5×10^8 cm^{-2} s^{-1} at Thetys and Dione.
2. *Sputtering by magnetospheric ions* has been invoked by Richardson *et al.* (1986) to produce these escape fluxes. Laboratory experiments have shown that one co-rotating O^+ ion colliding with a water ice surface creates 10 H_2O, 10 H, 5 O_2, and 5 H_2 particles at Rhea and about one third of that at Enceladus (Bar-Nun *et al.*, 1982). These sputtering yields rise by up to two orders of magnitude for ion energies of 100 keV (Shi *et al.*, 1995). Therefore, energetic magnetospheric ions are the main sputtering source at Enceladus, while at Rhea the co-rotating ions dominate because of the higher co-rotation speed.

   Generally, the neutral flux from ion sputtering is $j_n = f_e n_i \langle v_i Y(v_i) \rangle$ (Johnson *et al.*, 1989) where n_i is the density of the sputtering ions, $\langle v_i Y(v_i) \rangle$ the average of the sputtering yield over the incident speed, and f_e is the escape fraction. The latter is estimated from the gravitational escape speed v_G from the satellites and from the energy distribution $f(E)$ of the sputtered neutrals, $f(E) = EU/(E+U)^3/2$; $U = m_i v_U^2/2 = m_p A_i v_U^2/2$. The parameter U is empirically found to be of order 0.05 eV, corresponding to $v_U \sim 3 \times 10^5$ cm s$^{-1}\sqrt{A_i}$. For all the icy satellites of Saturn, the relation $V_{\rm cor} \gg v_U \gg v_G$ (i.e. $E \gg U \gg E_{\rm esc}$) applies. As 10 H_2O molecules and 10 H atoms are released by an impacting O^+, and $V_{\rm cor} \approx 3L v_U(H_2O)$, one expects a neutral density near the satellites of at most $15L$ times the heavy ion density. The density of

O^+, observed in the equatorial plane at Dione's L-shell, is about 25 cm^{-3}. To estimate the mean neutral densities in the L-shells near the moons, one needs to know the transport and loss processes for the neutrals and their dissociation and ionisation products (see below). Detailed models show that the sputtering by energetic ions even with revised rates falls short by at least a factor 2 to reconcile observed neutral OH densities (Richardson, 1998).

3. *Meteoroid erosion* (e.g., Northrop and Connerney, 1987) is another process that may sputter about 3×10^{26} s^{-1} molecules at Dione and Thetys and 10^{26} s^{-1} molecules at Rhea. The latter source strengths are concluded from Figure 2 (*left*) of Pospieszalska and Johnson (1991) and for a micrometeorite flux of 3×10^{-16} g cm^{-2} s^{-1} near Saturn, which has the same order of magnitude as the flux given by Love and Brownlee (1993). These source strengths at Dione-Thetys and Rhea are comparable to or even larger than the maximum strengths due to magnetospheric ion sputtering calculated by Shi *et al.* (1995).

4.4.2. *Loss of Neutral Water Products*

Loss mechanisms for the neutral particles are (i) physical adhesion to icy ring particles, (ii) transport, i.e., flying out of the magnetosphere, (iii) dissociation by impact of magnetospheric charged particles, and (iv) dissociation by solar photons. The processes (iii) and (iv) create other neutral particles, some of which have enough energy to escape Saturn. The ionisation processes are also loss processes for the neutrals. However, in the inner magnetosphere near the rings the ionisation processes are slower than processes (i) − (iv). They are described separately in the following subsection.

1. *Adhesion* rates to icy ring particles was estimated by Hall *et al.* (1996) and Carlson (1980) The optical depth of Saturn's inner rings (A and B) is close to 1 (Pollack, 1975), and the reflection coefficient of hydrogen on low-temperature ice has been derived from laboratory experiments to be about 0.78 (Brackmann and Fite, 1961). The Kepler period of particles near the inner rings is about 4×10^4 s, so that it takes only about $\tau_{adh} \sim 3 \times 10^5$ s for a neutral to be absorbed.
2. *Transport of neutrals* is given by their velocity, their lifetime for any destructive process, the gravitational force and to less extent the radiation pressure. The gravitational escape speed from Saturn's equatorial plane is $3.6 \times 10^6 \sqrt{L}$ cm s^{-1}. As the typical speed of neutrals after sputtering from the icy moons amounts to $v_U \sim 3 \times 10^5$ cm $s^{-1}/\sqrt{A_i}$, only the neutrals in the high-energy tail of the distribution are able to leave Saturn's gravitational field. Most neutrals will stay on Keplerian orbits for a typical time τ_{Kep} of a few 10^6 s in the case of H_2O (Richardson, 1998), if the neutrals are released outside the main rings.
3. *Photodissociation* of H_2O caused by the Lyman-α radiation of the solar spectrum, has a time scale of $\sim 10^5$ s at 1 AU and, therefore, of about $\tau_{diss,Ly} \sim 10^7$ s near Saturn. The branching ratio to hydroxyl formation is 0.874 and to O(1D) is 0.073 (Budzien *et al.*, 1994).

4. *Dissociation by electron impact* has a cross section of order 2×10^{-16} cm^2 at electron energies larger than 50 eV (Harb *et al.*, 2001). With a density of 3 cm^{-3} of the dissociation time scale is of order $\tau_{\mathrm{e-imp,diss}} \sim 3 \times 10^6$ s.
5. *Dissociation by proton impact* is less efficient than by electron impact. It has a cross section of $0.9^{+1.8}_{-0.6} \times 10^{-16}$ cm^2 (Budzien *et al.*, 1994). With a proton flux of order 10^7 cm^{-2} s^{-1} the dissociation time scale is of order $\tau_{\mathrm{p-imp,diss}} \approx \times 10^9$ s.

4.4.3. *Ionisation of Water Molecules*

The ionization processes include (i) ionisation by charge exchange with magnetospheric ions, (ii) ionisation by solar photons, and (iii) ionisation by impact of magnetospheric charged particles.

1. *Charge exchange* cross sections are given in e.g. Budzien *et al.* (1994) for the charge exchange between cometary neutrals and solar wind ions. For H_2O the cross-section is $1.9^{+1.9}_{-1.0} \times 10^{-15}$ cm^2. With a proton flux of order 10^7 cm^{-2} s^{-1} the charge exchange lifetime would be $\tau_{\mathrm{ex}} \sim 5 \times 10^7$ s. However, solar wind has and H^+ energy of 1 keV, much more than corotating H^+ in Saturn's magnetosphere, so that $\tau_{\mathrm{ex}} \sim 10^8$ s at $L = 5$ (Figure 22).
2. *Photoionisation* of H_2O by solar photons has a time scale of $\tau_{\mathrm{UVion}} \sim 2 \times 10^8$ s near Saturn (Budzien *et al.*, 1994).
3. *Impact ionization* of H_2O has cross sections of $2.5^{+2.5}_{-1.3} \times 10^{-16}$ cm^2 for protons (Budzien *et al.*, 1994) impacting with solar wind energies and at most 5×10^{-16} cm^2 (Rao *et al.*, 1995) for electrons with energies of 100 eV, corresponding to the temperature in Saturn's outer magnetosphere. Fluxes of at least 10^7 cm^{-2} s^{-1} are required for impact ionisation to be faster than photoionisation. This condition is usually fulfilled in Saturn's magnetosphere. The rates derived from actual electron fluxes in the Kronian magnetosphere are shown in Figure 22.

4.4.4. *Numerical Models on Source, Loss, and Transport Processes*

Many of the above mentioned rates are a function of the densities of protons and electrons and their velocity distributions. These parameters again depend on L, i.e. the radial location. Richardson *et al.* (1998) have modelled the most important of these rates and lifetimes as a function of the L-parameter (Figure 22). Furthermore, the sources and sinks of the plasma are a complicated function of L. Understanding of the ion and neutral distributions in the Kronian magnetosphere thus requires a self-consistent numerical model. Richardson and Jurac (2004) and Jurac and Richardson (2004) have calculated the complex neutral cloud morphology and the structure of the ion tori near the icy satellites and rings of Saturn. Figure 23 may serve as a simplified scheme for the processes responsible for the distribution of neutral water products and hydrogen as well as their ions. For their model, Jurac and Richardson (2004) took measurements of OH column densities with HST (Shemansky and Hall, 1992; Hall *et al.*, 1996; Jurac *et al.*, 2001) and Voyager plasma measurements as constraints. Neutral distributions were derived from a

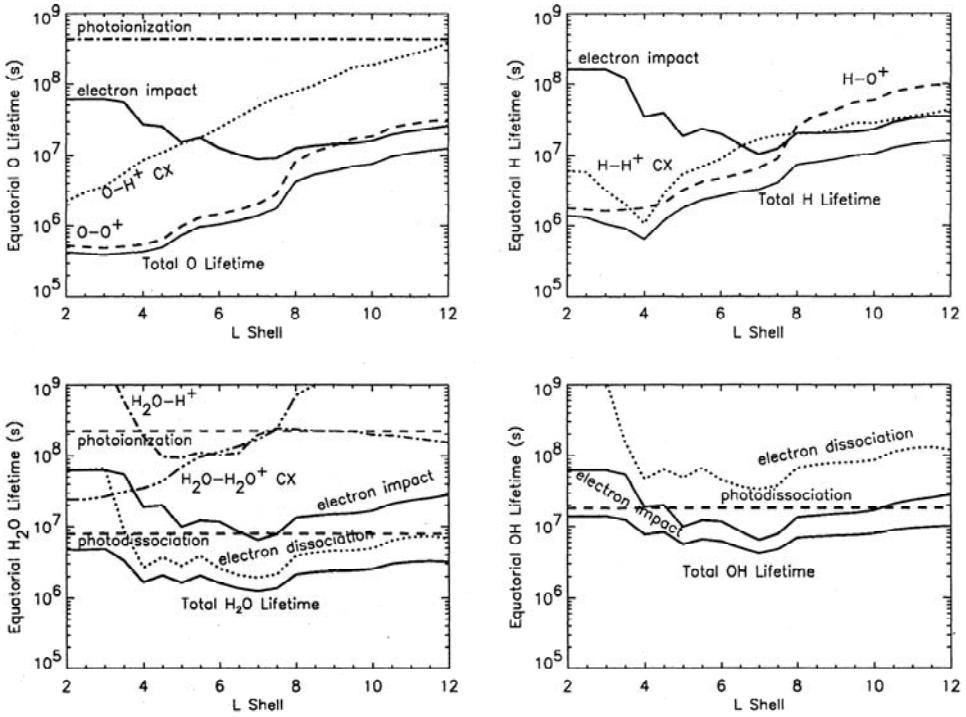

Figure 22. The lifetime of O, H, H_2O, and OH in the Kronian magnetosphere as a function of the *L*-parameter (adapted from Richardson *et al.*, 1998).

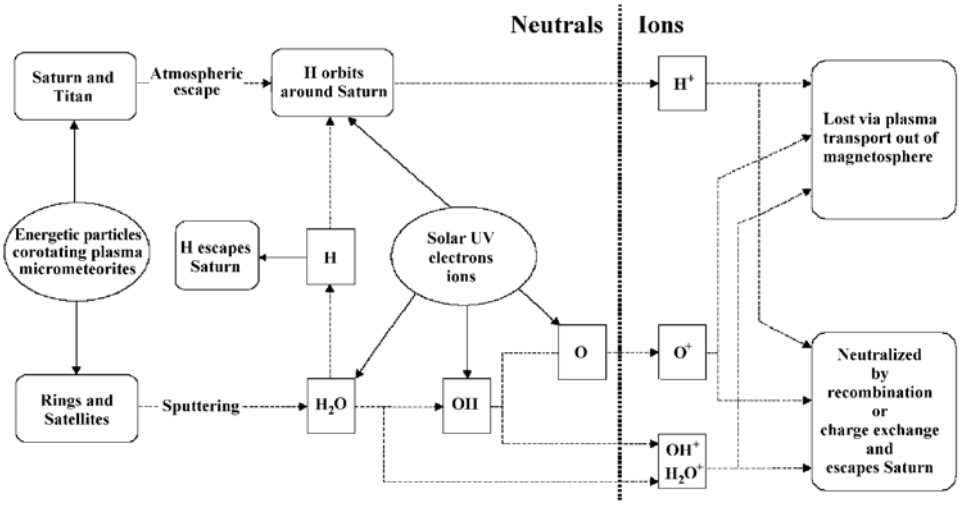

Figure 23. Sputtering, ionisation, and recombination processes in Saturn's magnetosphere (adapted from Blanc *et al.*, 2002).

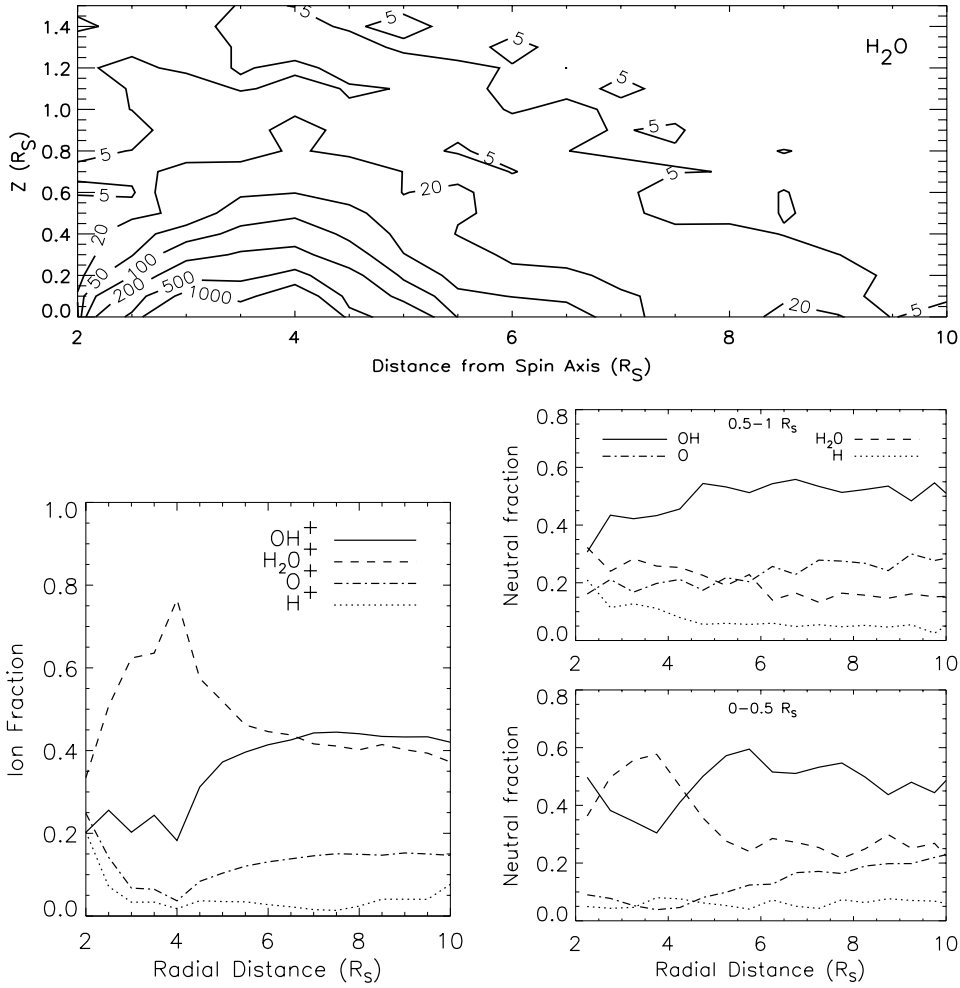

Figure 24. Density of water molecules in cm^{-3} (*upper panel*), relative ion densities (*lower left*), and relative neutral densities far off and near the equatorial plane (*lower right panels*) from the model of Jurac and Richardson (2004).

Monte Carlo model and the plasma transport is described by the above transport equations (3) and (4). The results are shown in Figure 24. The density of H_2O molecules is higher than that of OH molecules. As OH fluoresces more efficiently, it was observed by HST. The scale height of OH (and H_2O) above the equatorial plane modelled by Jurac and Richardson (2004) approximately corresponds to that observed edge-on by Hall *et al.* (1996). The water source needed near Enceladus ($L = 3.95$, within the E ring) to match the data needs to be 10^{28} s^{-1}, which cannot be produced by the sputtering process as can be checked with the above efficiencies and heavy ion densities of O^+. Jurac *et al.* (2002) show that the erosion by micrometeoroids (Pospieszalska and Johnson, 1991) cannot produce the extra H_2O since

the spatial distribution would be different; the larger satellites would be the biggest sources whereas most material seems to come from near Enceladus. Jurac *et al.* (2002) suggest that collisions of small pieces of icy debris near Enceladus are a possible source.

4.4.5. *Source and Loss Processes in Saturn's Atmosphere and Ionosphere*
In several articles in this volume the composition (Encrenaz, 2005), cloud structure (Atreya and Wong, 2005), dynamics (Beebe, 2005), photochemistry (Strobel, 2005), ion-neutral coupling (Miller *et al.*, 2005), and auroral emissions (Zarka and Kurth, 2005) of Saturn's atmosphere and ionosphere are discussed. Here, we only give a brief overview on observations of Saturn's atmosphere and ionosphere.

The spatial distribution of the Lyman-α emission of neutral hydrogen in Saturn's magnetosphere has been imaged by the Voyager Ultraviolet Spectrometer (UVS). After encountering Saturn Voyager 1 had the view down to the equatorial plane near Saturn. The neutral hydrogen density is higher on the duskside of Saturn and closer to the planet suggesting that the main source is Saturn's sunlit atmosphere. Saturn's ionosphere, however, contains a wide variety of species due to photo- and ion chemistry that is initiated by energetic electrons in the auroral zones. The presence of energetic electrons in aurorae had first been presumed by Judge *et al.* (1980) based on Pioneer 11 data. Sporadic enhancements in polar Lyman-α emission have also been observed with the short-wavelength spectrograph aboard the International Ultraviolet Explorer (IUE) by Clarke *et al.* (1981). With the Ultraviolet Spectrometer UVS of Voyager 1 it became feasible to unambigously observe the morphology of aurorae near Saturn's poles (Sandel and Broadfoot, 1981). Near the south pole, the auroral emission extends between 78 and 81.5 °S and has an average brightness of $\sim$ 5 kR based on the 110.5 nm H_2 band feature. Similarly, the northern aurora lies poleward of 76 °N. The 110.5 nm H_2 band emission is correlated with the Saturn kilometric radiation (SKR) (Kaiser *et al.*, 1980; Gurnett *et al.*, 1981; Zarka and Kurth, 2005, this volume).

A particularly interesting phenomenon is the formation of dark hazes in auroral zones, found by Voyager 2 UV observations near Jupiter and Saturn (Pryor and Hord, 1991). These hazes are thought to be caused by the formation of aerosols, including heavy hydrocarbons, by photo- and ion chemistry (Wong *et al.*, 2003). Even the formation of benzene has been observed with the Short-Wavelength Spectrometer (SWS) aboard ISO. A dark auroral oval in Saturn's magnetosphere has unambiguously been detected in reflected sunlight in the near UV (220 nm) with the European Faint Object Camera (FOC) of HST by Ben-Jaffel *et al.* (1995). This confirms that Saturn's aurorae not only produce emission of light but also UV-dark material near the poles, probably hydrocarbon polymers created in reactions that are initiated by energetic auroral electrons.

The destruction of methane, CH_4, by energetic particles or by UV-radiation plays a pivoting role for the chemistry in Saturn's ionosphere. The cross sections for impact ionization of CH_4 peaks at electron energies of about 40 eV and is given

as $\sigma_e \approx 3 \times 10^{-16}$ cm^2 (e.g., Kim *et al.*, 1997), while the cross section for Lyman-α absorption of CH_4 amounts to $\sim 3 \times 10^{-17}$ cm^2 (e.g., Mordaunt *et al.*, 1993). Assuming a solar Lyman-α flux of 10^6 cm^{-2} s^{-1} at 1 AU (Hinteregger *et al.*, 1981), the flux of electrons at energies of more than a few tens of electron volts needs to be at least 10^3 cm^{-2} s^{-1} at Saturn (9.539 AU) to compete with solar Lyman-α radiation in ionizing CH_4.

4.4.6. *Source and Loss Processes in Titan's Atmosphere and Ionosphere*
Titan is the only satellite in the solar system which has a substantial atmosphere characterized by an exobase well above the planetary surface (Hunten *et al.*, 1984). It is an obstacle in the plasma flow which is intermediate between the 'hard' target Venus and the very 'soft' target of a comet with substantial gas production (Blanc *et al.*, 2002). There is a number of articles in this volume on Titan's atmosphere and ionosphere (Roos-Serote, 2005; Coustenis, 2005; Strobel, 2005; Raulin, 2005). We shortly summarize that in the upper atmosphere, where the ionosphere forms, molecular nitrogen and methane are the dominant neutrals below and above an altitude of about 1700 km, respectively. Further out in the exosphere, molecular hydrogen (H_2) and atomic N and H become dominant. Most of our knowledge of Titan's ionosphere is based on models (see, e.g. Krupp, 2005, in this volume). The only observational evidence of its existence is the possible detection of the ionospheric peak region near the terminator by the radio occultation experiment onboard Voyager, with a peak electron density of 2400 cm^{-3} at an altitude of 1175 km (Bird *et al.*, 1997).

As a source of plasma in Saturn's magnetosphere Titan is very variable. Near 12:00 in Saturn local time Titan is sometimes outside the magnetopause, sometimes in the magnetosheath, or at times of high solar wind pressure it can even be exposed to the supersonic solar wind plasma. During these times the Anomalous and Galactic cosmic ray radiation is higher. At Titan, both photoionisation by solar EUV radiation and electron impact ionisation associated with magnetospheric electrons (Figure 25) are thought to contribute to the creation of the ionosphere (cf., Cravens *et al.*, 1992. Gan *et al.* (1992) used a twostream electron transport code and Galand *et al.* (1999) used a multistream code to study how magnetospheric electrons, or atmospheric photoelectrons, interact with Titan's ionosphere and atmosphere. The relative proportion of the two ionization mechanisms (EUV or magnetospheric electrons) at a particular location on Titan and at a particular time is a function of altitude, latitude and longitude, and also depends on the orbital position of Titan. A detailed description of these processes is beyond the scope of this overview paper. However, Figure 25 summarizes the input of the various types of ionising radiation and particles, which also initiate chemical processes which may be relevant for the creation of pre-biotic molecules (Raulin, 2005, this volume). The detection of organic matter by Voyager IRIS on Titan is reviewed by Sagan *et al.* (1984). Poulet and Cuzzi (2002) suggest that Saturn's rings contain Tholin, which may originate from Titan (Cabane and Chassefière, 1995; Chassefière and Cabane, 1995). It is

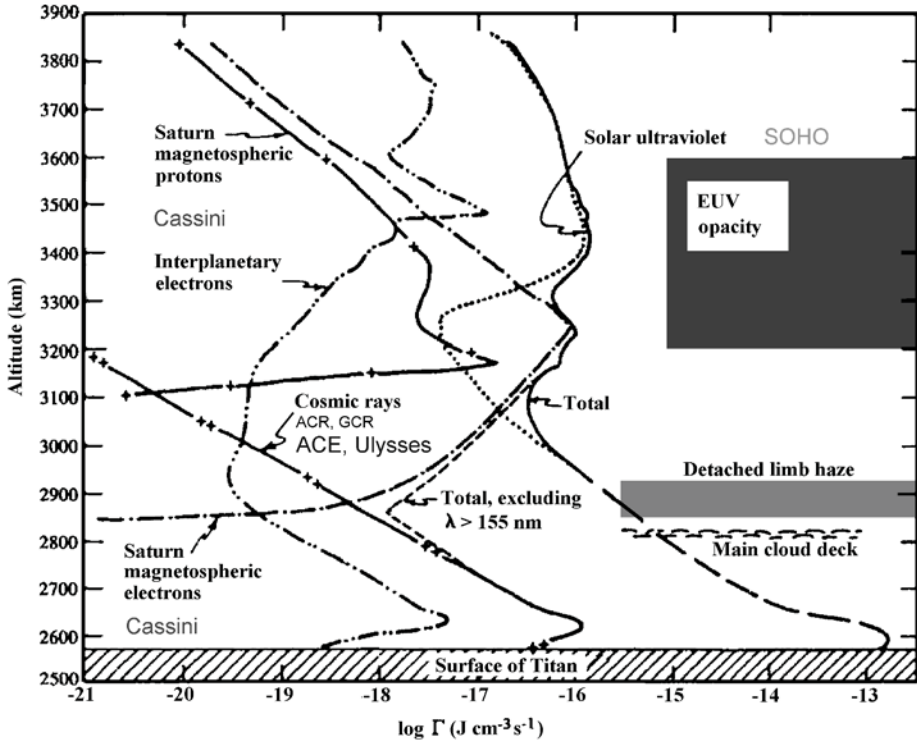

Figure 25. Input of ionising photons, ions, and electrons into Titan's atmosphere according to Sagan and Thompson (1984). At present there is a fleet of spacecraft to monitor the various kinds of optical and particle radiation to which Titan is exposed.

certainly an interesting topic for Cassini/Huygens research to study the pick-up of organic molecules in Titan's wake.

The plasma dynamics near Titan, however, are mainly influenced by the loss of 10^{24} s^{-1} N^+ and/or N_2^+/H_2CN^+ ions, which have been detected during the Voyager 1 flyby in 1980. These ions may form a wake which wraps around Saturn (Eviatar *et al.*, 1982), as will be discussed in the next section. Escape of H, H_2, and N from Saturn's atmosphere creates large clouds of neutrals in the outer magnetosphere which are also important plasma sources for the magnetosphere. Since ions picked up in the outer magnetosphere have high pickup energies and gain energy when they move inward, these Titan neutrals could be an important source of energetic ions.

5. Satellite Interactions in Giant Planets Magnetospheres

Key parameters for the interaction of satellites with the magnetospheric plasma (Figure 26) of the giant planets is their relative speed V_1 with respect to the undistorted magnetospheric plasma and their effective cross-section. This effective cross

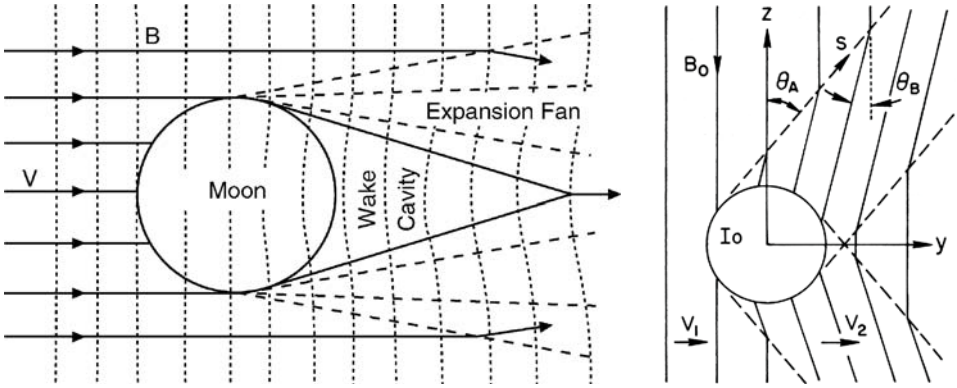

Figure 26. Left: Schematic of the interaction of the solar wind with the Moon, which has low internal and surface conductivity and lacks a significant atmosphere or an ionosphere (Russell, 2001). *Right:* For a satellite with significant internal or surface conductivity or an ionosphere such as Io at Jupiter, the situation is different. The distortion in the plasma due to the satellites propagates in form of an "Alfvén wing" (Hill *et al.*, 1983).

section can simply be their geometric size for the case of a non-conducting satellite with neither an intrinsic magnetic field nor an atmosphere/ionosphere. The Moon is such an example where the solar wind simply runs into its surface.

However, if there is an intrinsic magnetic field, and/or an atmosphere or ionosphere, or significant internal and surface conductivity of the satellite, then the convective electric field of the plasma viewed in the rest frame of the satellite leads to a diversion of the plasma flow. This convective electric field is $\mathbf{E} = \mathbf{V}_1 \times \mathbf{B}$ with $\mathbf{V}_1$ the velocity of the plasma in the frame of the satellite and $\mathbf{B}$ the planetary magnetic field near the satellite. The effective cross-section of the satellite is then much larger, and may be expressed in terms of a magnetic distortion. Key parameters are then the magnetohydrodynamic (MHD) Mach numbers M_s and M_A. The sonic Mach number M_s is given by the ratio of the relative speed of the satellite with respect to the co-rotating plasma V_1 and the sound speed $c_\mathrm{s} = \gamma k_\mathrm{B} T/m_i$ with T the plasma temperature, γ its adiabatic index, and m_i the mass of the dominant ions. The Alfvén Mach number is $M_\mathrm{A} = V_1/V_\mathrm{A}$ with the Alfvén speed $V_\mathrm{A} = B/\sqrt{\mu_0 n_i m_i}$ given by the planetary magnetic field B near the location of the satellite and the number density n_i of the ions which dominate the mass density. Table IV gives an overview of these numbers for the Jovian and Kronian satellites. Far away from the obstacle, the satellite, the distortion of the plasma can be described by a superposition of standing MHD waves i.e. waves with zero frequency in the reference frame of the satellite (Neubauer, 1980). It is important to note that the Alfvén mode will dominate at large distance from the obstacle because it has the least dispersion among the MHD wave modes. Furthermore, it is the only mode that can carry field-aligned (Birkeland) currents. The area in which the Alfvén mode propagates is called the Alvén wing (Figure 26). The Alfvén wing originates at the plasma distortion caused by the obstacle and propagates under an

TABLE IV

Main parameters of satellite interactions in the magnetospheres of Jupiter and Saturn (from Blanc *et al.*, 2002, and references therein).

	Nature of obstacle			
	M_S	M_A	Atmosphere, ionosphere/ solid surface	Magnetized or not
Jovian satellites				
Io	1.65	0.30	Yes/yes	?
Ganymede	2.4	0.48	No/yes	Yes
Europa	1.75	0.39	Yes/yes	**Probably not**
Callisto	2.4	0.94	No/yes	No
Kronian satellites				
Titan	0.57	1.9	Yes/solid + lakes or oceans ?	No
Tethys	1.24	0.25	No/yes	unknown
Dione	1.31	0.46	No/yes	unknown
Rhea	1.29	0.56	No/yes	unknown
Enceladus	2.4	0.14	No/yes	unknown

angle $\theta = \arctan(V_1/V_A)$. Within the Alfvén wing the plasma speed is slowed down to speed V_2 by the interaction with the ionosphere and atmosphere of the satellite (collisions, convective electric field in the conductive ionosphere, etc.).

The first observation of a standing Alfvén wave current system at Io in the Jovian magnetosphere has been observed by Voyager 1 (Acuña *et al.*, 1981).

5.1. Interaction of Io with the Jovian Magnetosphere

As mentioned in Section 4.2, Io is the dominant source of plasma in the Jovian magnetosphere. As the magnetic dipole of Jupiter is tilted by 10° with respect to its rotation axis, the material left in the plasma forms a precessing torus, the Io plasma torus. Its ion composition is dominated by the volcanic material erupting at Io's surface (Belcher, 1983). Io's atmosphere and surface-atmosphere interactions are reviewed by Lellouch (2005) in this volume. Singly and doubly charged sulfur pick-up ions as well as oxygen pick-up ions O^+, O^{2+}, O^{3+}, and O^{4+} from the Io torus have been detected by SWICS on board Ulysses (Geiss *et al.*, 1992). Along the magnetic field lines the scale height of this torus is approximately $R_T \approx 50 - 100 R_{Io}$.

Io has an orbit speed of about 17 km/s while the speed for plasma co-rotation with Jupiter at Io's orbit is about 74 km/s. Io loads about a ton per second from its cold neutral gas cloud to the plasma in the Jovian magnetosphere. Therefore,

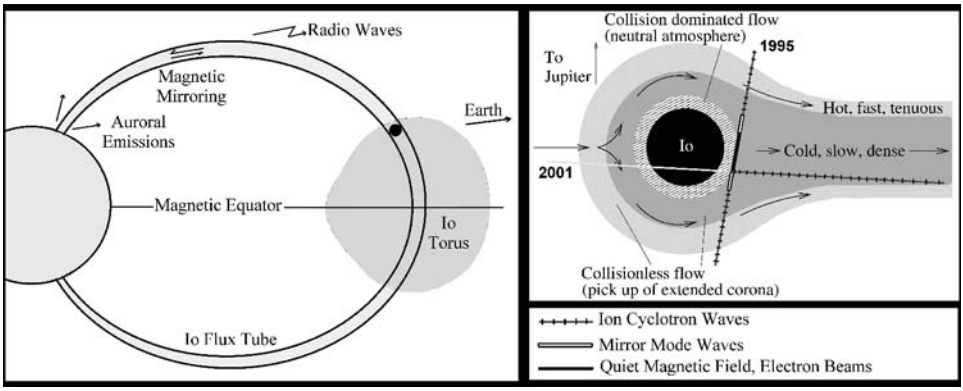

Figure 27. Interaction of Io's ionosphere with the plasma of Jupiter's magnetosphere.

it leaves a plasma wake in its vicinity. The peak density of ionized neutrals in the wake has been measured to be 3×10^3 cm^{-3} (Frank *et al.*, 1996; Gurnett *et al.*, 1996). The plasma speed is slowed in the wake of Io to about 30 km/s in the frame of Io at $3R_{\rm Io}$ ($R_{\rm Io} = 1815$ km) and approaches co-rotation speed at about $7R_{\rm Io}$ down in the wake (Hinson *et al.*, 1998). As described above, in the slowed-down plasma a convective electric field is built up. The distribution of this electric field depends on the conductivity of the plasma, Io's ionosphere, and Io's surface and interior. The resulting electric field in the distorted plasma accelerates ions and electrons.

The velocity difference between the neutrals and the plasma is approximately perpendicular to the Jovian magnetic field which has a strength of about 1835 nT near Io (Kivelson *et al.*, 1996). After their ionization the ions gyrate about the magnetic field. In velocity space the ion distribution is described by a ring with a radius which equals the velocity difference between the neutrals and the plasma. These distributions appear to drive ion cyclotron waves as observed during the two passes of the *Galileo* spacecraft in 1995 and 2001 (Russell *et al.*, 2003). For the 1995 Galileo fly-by (Figure 27), Russell *et al.* (1999) report on the observation of mirror mode waves. The latter are instable in high-beta plasmas with high ratio of perpendicular to parallel temperature. This condition seemed to be fulfilled in Io's wake during the 1995 fly-by (Huddleston *et al.*, 1999). The plasma is slowest with respect to Io close to Io and faster with respect to Io farther away. For this reason the amplitude of the ring distribution of the pick-up ions is lower close to Io which means ion temperatures are lower close to Io.

Inside the cool dense region of Io's wake electron beams have also been observed (Williams and Thorne, 2003). They appear to be accelerated at low altitudes, at about $0.5R_{\rm J}$ in the flux tube connecting to Jupiter's ionosphere. In this context we refer to an article by Chiu and Schulz (1978) on electron precipitation and parallel electric fields in terrestrial auroral regions. The radio emissions of electrons spiraling up and down the flux tubes between Jupiter and Io are described by Zarka

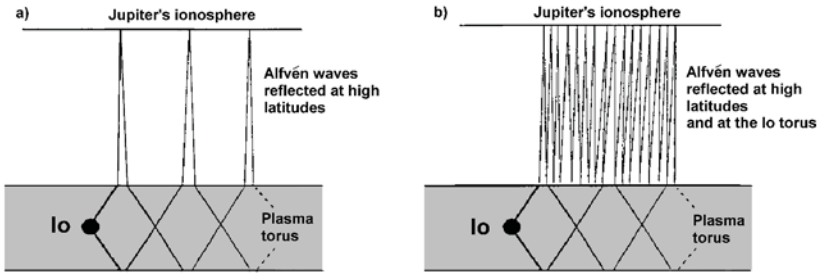

Figure 28. Multiple reflections of Alfvén waves at high latitudes (*panel a*, Gurnett and Goertz, 1981) and standing Alfvén waves between Jupiter's ionosphere and the Io plasma torus (*panel b*, Crary and Bagenal, 1997).

and Kurth (2005) in this volume. We also refer to a recent review by Labelle and Treumann (2002).

As pointed out in this volume by Kivelson (2005), the magnetic flux tube intersecting with Io also maps onto the Jovian ionosphere in the form of auroral ultraviolet emissions. The auroral trace in Jupiter's ionosphere has a primary component extending about 12° in Jovian longitude and a weaker secondary component extending about 100° in Jovian longitude (Clarke *et al.*, 2002; Hill and Vasyliunas, 2002). This distance which corresponds approximately to the longitude over which the primary auroral emission is observed approximately corresponds to the longitudinal distance within which the wake plasma reaches co-rotation speed. This suggests that the primary auroral emission at Io's magnetic footprints is the emission of an Alfvén aurora driven by field-aligned Alfvén currents.

The longitudinal extent of the secondary component of auroral emissions may be explained by the reflection of Io's Alfvénic distortion at the boundaries of the torus, where the plasma density changes abruptly (Clarke *et al.*, 2002). Multiple reflections at the torus boundary extend the region of magnetic field line slippage downstream of Io (see Delamere *et al.*, 2003, for recent models). A fraction of the Alfvén wave amplitude is transmitted to larger latitudes outside the Io torus. Gurnett and Goertz (1981), Bagenal and Leblanc (1988) and Crary and Bagenal (1997) had already modelled standing Alfvéen waves between the Io torus and Jupiter's ionosphere in order to explain radio emission patterns, the 'Jovian decametric arcs' (Figure 28). The propagation of these transmitted Alfvén waves in the narrowing flux tubes to Jupiter's ionosphere and the related auroral emissions have been modelled by Su *et al.* (2003) and are reviewed by Kivelson (2005) in this volume.

The peculiarities of the Alfvén wave propagation along the narrowing magnetic flux tube outside the Io torus were also studied by Erkaev *et al.* (2004). Here, we follow the lines of their work. In particular, these authors also have studied the analogies between the case of Io near Jupiter and the case of Titan near Saturn. The strong disturbances of the corotating plasma, loaded by the newly created ions which form a dense layer around Io, may also occur near Titan in the Kronian

magnetosphere. In the frame of both Io and Titan, the magnetospheric plasma flow is subsonic. However, the magnetospheric flow near Titan is highly variable and Alfvén times are much longer so that the Alfvénic structure may be more difficult to maintain.

The model of Erkaev *et al.* (2004) is based on the idea that the length scale of Alfvén perturbations propagating along the converging magnetic field lines increases proportionally to the magnetic field strength. The amplitudes of velocity and magnetic field perturbations do not change much as long as the wave does not arrive at the reflection zone. This leads to a strong enhancement of the electric field amplitude during the wave propagation in the direction of the magnetic pressure gradient.

The reflection stage starts as soon as the length scale of the wave front becomes of the order of the distance from the planet. The wave is reflecting from a very narrow "hole" of the magnetic tube, and thus it does not reach the conducting ionosphere in cases of sufficient large wave length scales as well as large ratios of $\Sigma_{\max}/\Sigma_{\min}$, where $\Sigma_{\max}$ and $\Sigma_{\min}$ are the maximal and minimal cross sections of the magnetic tube. In such cases, the wave energy flux to the conducting surface at $r = r_{\min}$ is rather small, and thus the dissipation of the wave perturbations is very weak despite the finite conductivity of the boundary. Because of this effect, the Alfvén wave pulse can have many reflections without a noticeable damping.

As mentioned above, the wavelength scale δ is a crucial parameter for the wave propagation along a strongly narrowing magnetic flux tube. It is increasing proportionally to the magnetic field strength in the course of the wave propagation $\delta \sim \delta_0 B(r)/B_0$. Reflection takes place when δ is of order of r, and thus the reflection zone can be estimated from the condition $\delta_0 B(r')/B_0 \sim r'$. For a dipole magnetic field, $B(r')/B_0 \sim (r_{\max}/r)^3$, the reflection condition yields the estimation $r' \sim r_{\max}(\delta/r_{max})^{1/4}$. The ionospheric boundary has a minor influence on the wave reflection if it has a sufficiently small radius r_{min} with respect to r', i.e., $r_{\min}/r_{\max} \ll (\delta/r_{max})^{1/4}$. Here the scale δ is of the order of the diameter of the satellite, $r_{\max}$ is the radial distance to the satellite, and $r_{\min}$ is the radius of the planet. Compared to Io, this condition is fulfilled much better for the case of Titan. Therefore, the effect of the converging magnetic field lines is expected to be much stronger in the case of the Alfvén wave pulses propagating from Titan towards Saturn.

In addition to the Alfvén waves, a local enhancement of the plasma pressure in the vicinity of the satellite can produce slow magnetosonic waves which can also propagate along the Io magnetic flux tube. Slow mode perturbations in the neighborhood of Io have been investigated in several publications (Kopp, 1996; Linker *et al.*, 1991; Krisko and Hill, 1991; Wright and Schwartz, 1990). The intensity of the slow magnetosonic wave is expected to be strongly dependent on the ion production rates.

There exists a direct observation of the plasma pressure in the vicinity of Io (Frank *et al.*, 1996). According to this observation, the plasma pressure has two

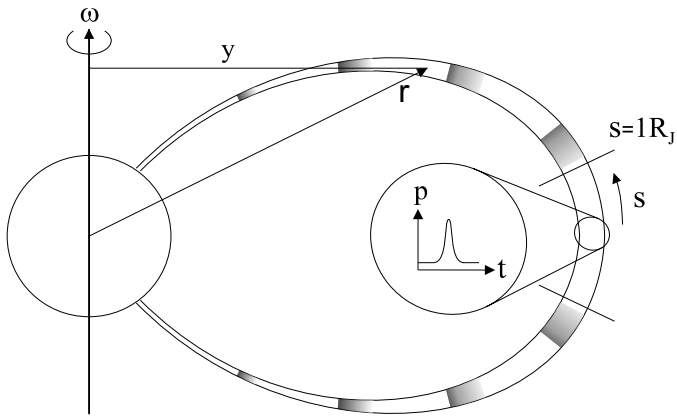

Figure 29. Schematic illustration of the development of a nonlinear slow–mode wave due to a pressure enhancement at Io.

peaks with enhancement factor $\sim$ 3 which can produce the slow magnetosonic waves propagating along the Io flux tube.

The slow magnetosonic waves produced by the pressure enhancements in the vicinity of Io and propagating along the Io magnetic flux tube towards the Jovian ionosphere were investigated by Erkaev *et al.* (2002) using a thin magnetic tube approximation. To describe nonsteady wave perturbations of the magnetic field and plasma parameters, the system of ideal MHD equations was applied. The background plasma parameters used in the calculations of Erkaev *et al.* (2002) are based on the empirical model of Mei *et al.* (1995).

The plasma pressure enhancement in the vicinity of the satellite produces two nonlinear slow waves propagating along the flux tube in opposite directions. The amplitudes of these waves are decreasing in the course of time, the leading fronts are getting more and more steep, and eventually the slow waves are converted into shocks. It is important that the flux tube cross section is inversely proportional to the magnetic field strength and therefore, it has to decrease as r^3 due to the dipole field configuration. Hence, the plasma flow has to move into a more and more narrow flux tube.

Figure 29 illustrates the development of a nonlinear slow–mode wave due to a pressure enhancement in vicinity of Io.

Figure 30 shows distributions of the plasma velocity and pressure as functions of the distance along the magnetic flux tube for different initial parameters. Here P_1 is the amplitude of the initial pressure pulse, and P_0 is the initial background plasma pressure, β_0 is the initial background plasma beta parameter, and κ is the polytropic index. The different shock positions are corresponding to the different times scaled to R_J/V_{A0}, where R_J is the radius of Jupiter, and V_{A0} is the Alfvén speed at the Io position. The distance S is measured from the equator along the magnetic flux tube. Comparing the first and the second panels (from top to bottom), one can see

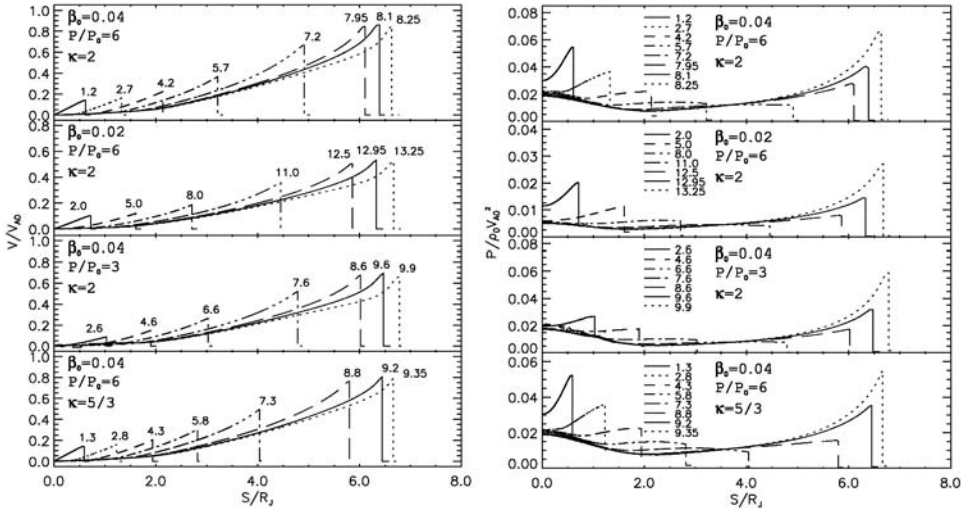

Figure 30. Left: Propagation of the slow shock along the flux tube. The distribution of the plasma velocity are shown as functions of the distance along the magnetic tube for different times. *Right*: Distributions of the plasma pressure as functions of the distance along the tube for different times.

the effect of variation of the initial background beta parameters ($\beta_0 = 0.04$, and $\beta_0 = 0.02$) for a fixed amplitude of pressure pulse (P_1/P_0=6). An increase of the initial plasma beta brings about an enhancement of the velocity maximum with respect to the initial Alfvén speed.

Comparing the first and the third panels, one can see the effect of variation of the pressure pulse amplitude. An increase of the initial pressure pulse amplitude leads to an enhancement of the velocity maximum. The ratio of the velocity maxima is a bit less than the square root of the ratio of the pressure pulse amplitudes.

Comparing panels 1 and 4, one can see that a variation of the polytropic exponent does not affect much on the results of calculations.

There are three stages of the wave evolution in the course of its propagation along the magnetic flux tube. At the first stage ($S < 0.5R_J$), the nonlinear MHD slow wave produced by the pressure pulse is evolved into the shock. At the second stage ($0.5R_J < S < 2R_J$), the wave amplitude characterized by the plasma velocity behind the shock, is nearly constant. At this stage, a shock damping is compensated by two factors: the decrease of the background density due to the centrifugal effect, and the gradual decrease of the magnetic tube cross section. During this period, the plasma pressure behind the shock decreases due to the fall in the background pressure caused by the centrifugal force. At the third stage, the wave amplitude starts to enhance due to a rapid increase of the magnetic field strength and a corresponding decrease of the magnetic tube cross section. The result obtained in the numerical study shows that the intensity of the MHD slow shock increases very much while the shock is propagating along the narrowing magnetic flux tube.

The centrifugal force caused by rotation of the magnetic flux tube plays an important role in the process of slow wave evolution. In the rotating magnetic tube, the background density and plasma pressure increase along the magnetic tube towards the equator. This behavior of the background plasma parameters provides a fast formation of the slow shock wave propagating from the equator along the magnetic flux tube. A strong converging of the magnetic flux tube leads to increase of the strength of the slow shock propagating from the satellite.

The slow shock effects simulated for the case of Io are expected also for Titan because it has similar conditions for the following reasons: 1) Titan has a large ion production rate, 2) a fast rotation of the surrounding plasma, and 3) a very strong convergence of the magnetic field lines in the Titan magnetic tube.

5.2. Interaction of Ganymede with the Jovian Magnetosphere

The case of Ganymede is interesting because it is so far the only known satellite with an intrinsic magnetic field forming its own magnetosphere within a planetary magnetosphere (Kivelson *et al.*, 1997b). In fact, it is the ideal case – more than Earth – to test models on reconnection. The Jovian magnetic field does not considerably change its orientation at Ganymede's location and the magnetic fields of Ganymede and Jupiter are relatively oriented such that reconnection should occur as predicted by Dungey (1961). The interaction between Ganymede's wake and the Jovian ionosphere appears to be similar to the case of Io. Neubauer (1998) describes the stationary distortion of the Jovian magnetosphere in terms of standing Alfvén waves (in the frame of the satellite), the so-called Alfvén wings. Near Ganymede, however, reconnection volumes and a slow-mode shock associated with the formation of a polar wind additionally develop due to the intrinsic magnetic field of Ganymede (Figure 31).

In analogy to the terrestrial magnetosphere, the reconnection is expected to drive aurorae at high latitudes of Ganymede. Such aurorae have in fact been observed (Feldman *et al.*, 2000; Figure 32). However, Eviatar *et al.* (2001) suggest that the tenuous nature of Ganymede's atmosphere precludes excitation of the aurora by precipitating high-energy electrons. Rather, a local acceleration mechanism generates both the continuous background emission and the auroral bright spots. Among these mechanisms are Birkeland-type currents and associated magnetic field-aligned electric fields or stochastic heating of plasma electrons by the Landau damping of electron plasma oscillations generated by precipitated energetic electrons.

5.3. Interaction of Titan with the Kronian Magnetosphere

In this volume, Krupp (2005) presents an overview of the results from Voyager data and shows model results on the Titan torus in the Kronian magnetosphere. As mentioned in Section 4.4.6, this torus is created by 10^{24} s^{-1} N^+ and/or N_2^+/H_2CN^+ loaded to Saturn's magnetosphere in Titan's plasma wake. Here, we try to give an

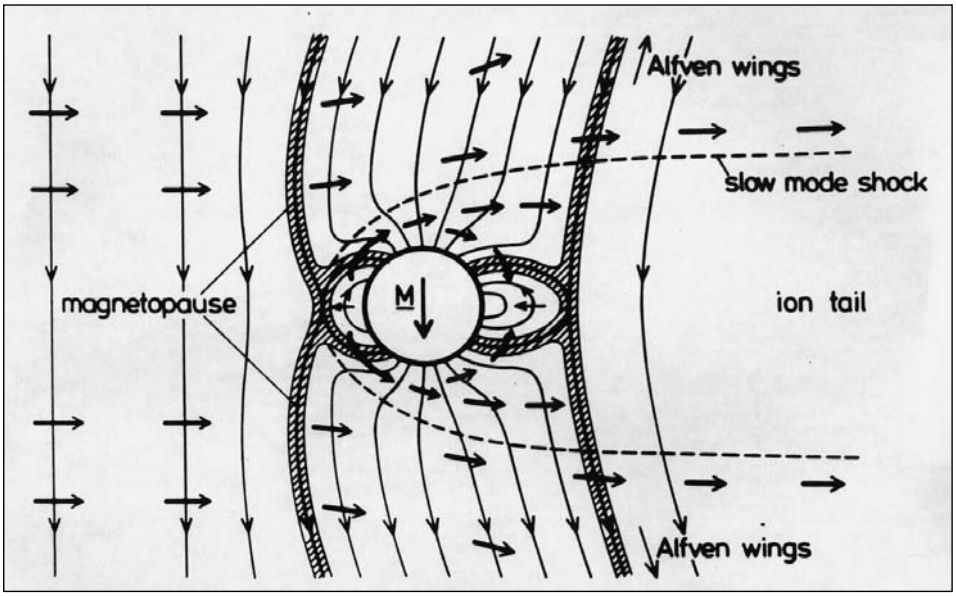

Figure 31. Neubauer's (1998) model of Ganymede's magnetosphere shows its magnetic field lines and topological boundaries in the plane containing the magnetic moment of the satellite and the velocity vector of the impinging Jovian magnetospheric plasma.

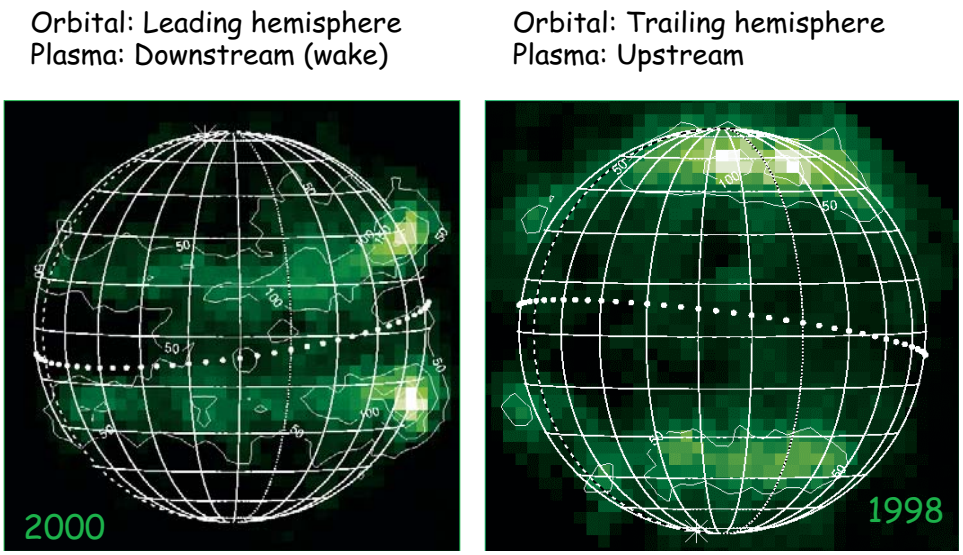

Figure 32. Ganymede's aurora is revealed by these images taken in 1998 (*right*; Feldman *et al.*, 2000) and 2000 (*left*; McGrath, 2002) by the Hubble Space Telescope (HST/STIS).

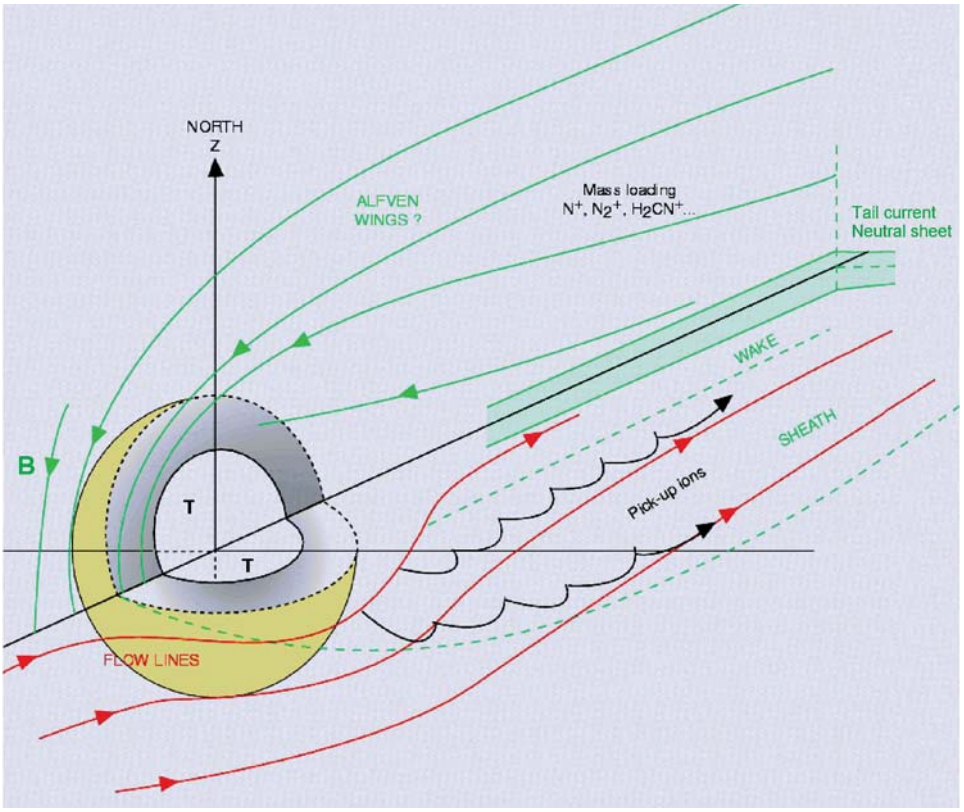

Figure 33. Simplified scheme of the induced ionosphere of Titan, as deduced from the unique encounter of Voyager 1 with this object. Adapted by Blanc *et al.* (2002) from the original data analysis papers and from Neubauer *et al.* (1984).

overview of the results of models on the plasma environment near Titan's ionosphere (Figure 33). Titan is unique, because it may be engulfed in the magnetospheric plasma with the Alfvén velocity and the speed of sound approximately equal to the flow velocity, or in the magnetosheath of Saturn, or even in the solar wind. The plasma around Titan and its atmosphere are intimately linked. At high altitudes the atmosphere is substantially influenced by the incident plasma flow (Neubauer *et al.*, 1984), while in turn the plasma flow fixes the outer boundary condition of the atmosphere of Titan and contributes to the mass budget of the atmosphere. Another unique aspect of the mass-loading near Titan is the fact that the gyroradii of newly created heavy pickup ions are larger than the satellite's radius and are expected to lead to special flow effects in addition to substantial asymmetries (Blanc *et al.*, 2002).

Figure 33 represents a typical configuration when Titan is inside the magnetosphere of Saturn. The figure shows a magnetic field line as it is convected through Titan's atmosphere, as well as horizontal flow lines around the obstacle and the

region of pick-up ions on the anti-Saturn side. The wake of Titan qualitatively looks similar to that of Io at Jupiter. The plasma is loaded by pick-up ions derived from atmospheric neutrals by photoionisation and electron collisional ionisation or by ionospheric escape. The plasma wake of Titan is very cold with thermal speeds of 3 km/s for heavy ions and 12 km/s for H^+ (Hartle *et al.*, 1982; Neubauer *et al.*, 1984). This seems more consistent with ionospheric escape than pickup. At Titan, mass also may not only be lost by classical atmospheric loss mechanisms but in addition via a neutral particle flux due to elastic collisions between fast ions and atmospheric neutrals (atmospheric sputtering) and via charge-exchange reactions.

An ionopause, separating a region free of Saturn's magnetic field and a magnetized region, has been observed by Voyager 1 (Hartle *et al.*, 1982). If there is no ionopause the magnetic field penetrates the atmosphere. An ionopause may only form at high ionisation rates and/or low momentum flux of the plasma. An asymmetry is caused by the convective electric field. On the side of Titan opposite to Saturn, the convective electric field accelerates ions out of the exosphere so that they are diverted around Titan. On the side facing Saturn, the ions are accelerated to penetrate the atmosphere. Asymmetries among the sides facing the Sun and those opposite to the Sun are caused by the solar UV radiation. In the tail region, there is a current sheet, as observed by Voyager 1, separating the northern and southern parts of the tail with opposite magnetic field directions. In addition the tail will contain a north-south trending boundary between field lines draped over different hemispheres of Titan, as the incoming field lines separate at the stagnation point.

For studies of the ionopause and the surrounding regions, flyby orbits with very low altitudes at closest approach are important like the nominal 950 km minimum altitude orbits of the Cassini mission. To evaluate the mass losses through the ion tail, good coverage of the plasma flow on the wake side is necessary as a function of chemical species.

The interaction picture will be different if the magnetosphere is sufficiently compressed for Titan to be located in the magnetosheath or the solar wind. In the latter case a pronounced bow shock is expected.

6. Summary and Cassini-Huygens Perspectives

We just completed a short and very special journey through the solar system, following the paths of Mariner 10 to Mercury, of Pioneer, Ulysses, Voyager and Galileo to the outer planets and heliosphere, and Cassini's seven-year cruise to Saturn. This journey showed the rich diversity of solar system magnetospheres, these "magnetic shelters in space" of our planets. In the same way as our Earth's magnetosphere protects our planet and its living organisms from the most aggressive radiations of interplanetary space, all magnetized planets interact with the interplanetary medium through a cavity carved into the solar wind flow by their magnetic field. The solar system itself, as a whole, has its magnetosphere, the

heliosphere. This magnetic cavity is maintained in the Local Interstellar Medium (LISM) by the expanding solar wind and coronal magnetic field. Solar system magnetospheres thus appear to be a family of objects organized in a "Russian doll hierarchy," with all planetary magnetospheres generated inside the heliosphere by the effect of the solar wind, and some satellite magnetospheres generated by magnetospheric plasma flows around giant planets. Space exploration showed us that the diversity among this family of objects is as broad as the spectacular diversity found among planets and satellites themselves. Studying this diversity is one of the most fruitful approaches we may use to understand in depth what basic processes are at work in a magnetosphere and how their coupling determines the dynamics of these objects.

The heliosphere is probably the most complex of all these magnetospheres. At a time when the Voyager spacecraft are still cruising towards its "inner shock," where the supersonic solar wind flow is expected to terminate, and further out towards its boundary with the LISM, the heliopause, much remains to discover and understand about it. Ulysses and the deep space probes taught us a lot about this object, and Cassini-Huygens also made its contribution. It measured some of the components of the local interstellar medium which penetrate deep into the heliosphere, particularly Interplanetary Dust Particles (IDP's) and the ionized products of interstellar hydrogen and helium atoms, and confirmed the focusing or defocusing effect exerted by the Sun's gravity on their trajectories.

In this review, which focuses on the transport of plasma populations and magnetic flux, we remarked as a starting point that solar system magnetospheres are populated by three main plasma sources: the solar wind which is at the origin of their confinement, a source originating in the planetary envelope, and – for giant planets – sources originating in their orbital systems: rings, satellites, dust and gas clouds. There are also three main momentum sources, each related to one of the plasma sources: the solar wind bulk motion, planetary spin, and finally the orbital motions of satellites, ring particles and orbiting clouds. The geometry of the resulting transport of plasmas and magnetic flux is also a function of the relative orientations of the interplanetary magnetic field, planetary spin and planetary magnetic moment. While plasma populations are transported from source to sink regions, the transport of magnetic flux tubes associated with plasma flowing out of the source regions must preserve flux conservation, and it is therefore constrained to a closed flow pattern in which magnetic flux is recirculated out of the sink regions and back to the source regions. Magnetospheric systems find different solutions to this problem for different situations of dominant plasma and momentum sources.

At the terrestrial planets (Earth and Mercury) the solar wind is the dominant momentum source compared to planetary spin, and we speak of "slow rotators." At Earth this results in the dominance of the so-called "Dungey cycle" of magnetospheric convection in the transport of solar wind and planetary plasmas, at least during periods of strong magnetic activity. It remains entirely to confirm its existence

as the main plasma transport mode at Mercury, where it is only conjectured from models of the solar wind/planet interaction. Since at Earth the planetary plasma source is provided by the upper atmosphere in the form of the ionosphere, while it is provided by the solid surface and tenuous exosphere interacting with external irradiation sources at Mercury, a comparative study of the two planets is particularly interesting. This will become possible with the Messenger and BepiColombo missions in the coming years. They will help to better understand the specific role played by an ionosphere in the regulation of magnetospheric convection and in the triggering and development of substorms. The alternative properties of a planetary regolith, or more generally of a solid surface, as an electrical conductor and as a plasma sources will also be clarified.

Giant planets are, just at the opposite, "fast rotators." Their dominant momentum source is the planetary spin. Their dominant plasma sources are orbital sources, and this is no surprise since giant planet's systems can be seen as miniature planetary systems which happen to reside and move inside their magnetospheric cavities. They can be essentially regarded as rotating magnets trapping an internal plasma population, dragging it partly into planetary rotation, and interacting with the external confining plasma flow – the solar wind – in a large variety of geometries. One can best experience the effects of this variety of geometries at Uranus and Neptune, where the large angles existing between planetary spin, magnetic dipole orientation and/or planetary orbital plane generate very large diurnal and seasonal variations in the coupling of planetary rotation to the solar wind flow. The limited information provided by the fly-bys of these planets by Voyager 2 essentially provided a preliminary idea of the complexity of the resulting configurations and dynamics. At Jupiter the Io torus is by far the dominant plasma source, and this offers to us the very interesting case of a single intense source, strongly peaked in radial distance near Io's orbit, which provides up to one ton per second of fresh thermal ions to the inner magnetosphere. The sink regions are likely to reside essentially in the external magnetosphere and magnetic tail, where magnetic field lines may be partly open and plasma may flow down the tail. Some outward transport of thermal iogenic plasma from Io's orbit to the distant magnetosphere is needed to connect sources and sinks in this situation, but it is apparently superposed to an opposite inward motion of hotter plasma populations, which ultimately maintain the very intense radiation belts observed at the center of the system inside Io's orbit. Some pieces of this puzzle have been identified, in particular by Galileo Orbiter studies, but much more remains to be found and the full puzzle still has to be assembled. Satellite interactions in the Jovian system are also quite fascinating. The Io interaction, with its Alfvén wings, intense currents flowing to and from the Jovian ionosphere along field lines, and associated acceleration processes, represents a very complex electrodynamic generator/load system and produces the spectacular Io auroral spot. Galileo discovered at Ganymede the only known intrinsic magnetosphere of a planetary satellite. Its interaction with the Jovian corotating plasma mimics in

many respects the Dungey cycle of Earth, and generates spectacular auroral circles which have been nicely documented by Hubble Space Telescope observations.

The in-depth orbital exploration of Saturn's magnetosphere and of its satellite interactions which formally started on July 1st, 2004, can be anticipated in the perspective of this overview of solar system magnetospheres, which sheds an even stronger light on the diversity of magnetic geometries, dominant plasma sources and plasma circulation regimes from one object to another. Saturn is probably going to be unique by the diversity of situations and dynamical regimes in a single magnetospheric system we expect to find there. First it materializes the full spectrum of magnetospheric interactions with orbital objects: rings, gas and dust clouds, satellites with a dense atmosphere (Titan, the only one in the solar system) or without (all the icy satellites). Understanding these interactions is not only interesting in itself; it is also the key to an accurate determination of plasma sources at Saturn. Among them the Titan interaction has a special place: it happens to be super-Alfvénic and sub-sonic and to take place most of the times in the magnetosphere, but sometimes also in the solar wind or magneto sheath. This case, which is still unique in the solar system, will stimulate progress in our understanding of the interaction between a supercritical magnetized flow and an obstacle. Saturn is also, like Jupiter, a fast rotator dominated by orbital plasma sources. These sources are significantly less intense than the Io source, but they are probably more diverse and display a much broader distribution in radial distance. This makes Saturn a more complex system in a way, where radial transport and particle acceleration are expected to affect different ionized species and different sources at a variety of radial distances. In addition, in the absence of an equivalent to the Jovian magneto disk, the solar wind effects may interact in the outer regions of the magnetosphere with those of the internal sources of momentum and plasma. It may very well be that, in order to apprehend and understand Saturn's magnetosphere, we shall need to combine all the experience gained in previous studies of other magnetospheres, slow rotators like Earth or "ideal" fast rotators like Jupiter. What we are going to explore at Saturn during the four years (or more) of Cassini's orbital tour is likely to be a really different and very exciting object in the broad family of solar system magnetospheres.

Acknowledgements

This work was supported by grants 04–05–64088, 03–05–20014 BNTS_a from the Russian Foundation of Basic Research and by INTAS grant WP 01-270. We gratefully acknowledge the very dedicated reviewer of this article, John D. Richardson, who worked with us online during the last hours before submitting the whole volume.

References

Acuña, M.H., Neubauer, F.M., and Ness, N.F.: 1981, 'Standing Alfvén wave current system at Io: Voyager 1 observations', *J. Geophys. Res.* **86**, 8513–8521.

Altobelli, N., Kempf, S., Landgraf, M., Srama, R., Dikarev, V., Krüger, H., Moraga-Klostermeyer, G., and Grün, E.: 2004, 'Cassini between Venus and Earth: Detection of interstellar dust', *J. Geophys. Res.* **108**, LIS 7-1, CiteID 8032.

Atreya, S., and Wong, A.-S.: 2005, 'Coupled clouds and chemistry of the giant planets – a case for multiprobes', this volume.

Axford, W.I., and Hines, : 1960,

Bagenal, F.: 1992, 'Giant planet magnetospheres', *Annu. Rev. Earth Planet. Sci.* **20**, 289–320.

Bagenal, F., and Y. Leblanc: 1988, 'Io's Alfvén wave pattern and the Jovian decametric arcs', *Astron. Astrophys.* **197**, pp. 311–319.

Bagenal, F., Dowling, T.E., and McKinnon, W.B. (eds.): 2004, *Jupiter. The planet, satellites and magnetosphere*, Cambridge University Press, Cambridge, UK.

Baranov, V.B., Krasnobaev, K.V., and Kulikovksy, A.G.: 1971, 'A model of the interaction of the solar wind with the interstellar medium', *Sov. Phys. Dokl.* **15**, 791–793.

Bhardwaj, A. and Gladstone, G.R.: 2000, 'Auroral emissions of the giant planets', *Rev. Geophys.* **38**, 295.

Bar-Nun, A.G., Herman, G., Rappaport, M.L., and Mekler, Y.: 1982, 'Sputtering of water ice at 30–40 K by 0.5–6.0 keV H^+ and Ne^+ ions', *Surface Sci.* **150**, 193–201.

Beebe, R.: 2005, 'Comparative study of the dynamics of the outer planets', this volume.

Belcher, J.W.: 1983, 'The low-energy plasma in the Jovian magnetosphere', in A.J. Dessler (ed.), *Physics of the Jovian magnetosphere*, Cambridge Univ. Press, New York, pp. 68–106.

Belcher, J.W., McNutt, R.L., Jr., Richardson, J.D., Selesnick, R.S., Sittler, E.C., and Bagenal, F.: 1991, 'The plasma environment of Uranus', in J.T. Bergstralh, E.D. Miner, and M.S. Matthews (eds.), Univ. of Arizona Press, Tucson, pp. 780–830.

Ben-Jaffel, L., Leers, V., and Sandel, B.: 1995, 'Dark auroral oval on Saturn discovered in Hubble Space Telescope ultraviolet images', *Science* **269**, 951–953.

Bennett, J.O.: 2004, *The Cosmic Perspective: The Solar System*, Addison Wesley.

Bergstrahl, J.T., Miner, E.D., and M.S. Matthews (eds.): 1991, *Uranus*, Univ. Arizona Press, Tucson.

Bhardwaj, A. and Gladstone, G.R.: 2000, 'Auroras on Saturn, Uranus, and Neptune', *Adv. Space Res.* **26**, 1551–1558.

Bida, T.A., Killen, R.M., and Morgan, T.H.: 2000, 'Discovery of calcium in Mercury's atmosphere', *Nature* **404**, 159–161.

Bigg, E.K.: 1964, 'Influence of the satellite Io on Jupiter's decametric emission', *Nature* **203**, 1008.

Bird, M.K., Dutta-Roy, R., Asmar, S.W., and Rebold, T.A.: 1997, 'Possible detection of Titan's ionosphere from Voyager 1 radio occultation observations', *Icarus* **130**, 426–436.

Birmingham, T.J., Northrop, T., and Fälthammar, C.-G.: 1967, 'Charged particle diffusion by violation of the third adiabatic invariant', *Phys. Fluids* **10**, 2389–2398.

Blanc, M., *et al.*: 2002, 'Magnetospheres and plasma science with Cassini-Huygens', *Space Sci. Rev.* **104**, 253–346.

Bolton, S.J., Thorne, R.M., Gurnett, D.A., Kurth, W.S., and Williams, D.J.: 1997, 'Enhanced whistler-mode emissions: Signatures of interchange motion in the Io torus', *Geophys. Res. Lett.* **24**, 2123.

Bolton, S.J., Thorne, R.M., Bourdarie, S., Depater, I., and Mauk, B.: 2004, 'Jupiter's inner radiation belts', in F. Bagenal, T.E. Dowling, and W.B. McKinnon (eds.), *Jupiter. The planet, satellites and magnetosphere*, Cambridge University Press, Cambridge, UK, pp. 671–688.

Brackmann, R.T., and Fite, W.L.: 1961, *J. Chem. Phys.* **34**, 1572.

Brice, N.M., and McDonough, T.R.: 1973, 'Jupiter's radiation belts', *Icarus* **18**, 206–219.

Bridge, H.S., *et al.*: 1981, 'Plasma observations near Saturn – initial results from Voyager 1', *Science* **212**, 217–224.

Bridge, H.S., *et al.*: 1982, 'Plasma observations near Saturn – initial results from Voyager 2', *Science* **215**, 563–570.

Broadfoot, A.L., Kumar, S., Belton, M.J.S., and McElroy, M.B.: 1974, 'Mercury's atmosphere from Mariner 10: Preliminary results', *Science* **185**, 166–169.

Budzien, S.A., Festou, M.C., and Feldman, P.D.: 1994, 'Solar flux variability and the lifetimes of cometary H_2O and OH', *Icarus* **107**, 164–188.

Burke, B.F. and Franklin, K.L.: 1955, 'Observations of a variable radio source associated with the planet Jupiter', *J. Geophys. Res.* **60**, 213.

Cabane, M., and Chassefière, E.: 1995, 'Laboratory simulations of Titan's atmosphere: organic gases and aerosols', *Planet. Space Sci.* **43**, 47–65.

Cahill, L.J. and Amazeen, P.G.: 1963, 'The boundary of the geomagnetic field', *J. Geophys. Res.* **68**, 1835–1843.

Carlson, R.W.: 1980, 'Photo-sputtering of ice and hydrogen around Saturn's rings', *Nature* **283**, 461.

Chassefière, E., and Cabane, M.: 1995, 'Two formation regions for Titan's hazes: indirect clues and possible synthesis mechanisms', *Planet. Space Sci.* **43**, 91–103.

Cheng, A.F., Johnson, R.E., Krimigis, S.M., and Lanzerotti, L.J.: 1987, 'Magnetosphere, exosphere and surface of Mercury', *Icarus* **71**, 430–440.

Cheng, A.F., Krimigis, S.M., and Lanzerotti, L.J.: 1991, 'Energetic particles at Uranus', in J.T. Bergstralh, E.D. Miner, and M.S. Matthews (eds.), Univ. Arizona Press, Tucson, pp. 831–893.

Chiu, Y.T. and Schulz, M.: 1978, 'Self-consistent particle and parallel electrostatic field distributions in the magnetospheric-ionospheric auroral region', *J. Geophys. Res.* **83**, 629–642.

Christon, S.P.: 1989, 'Plasma and energetic electron flux variations in the Mercury 1 C event – evidence for a magnetospheric boundary layer', *J. Geophys. Res.* **94**, 6481–6505.

Clarke, J.T., Moos, H.W., Atreya, S.K., and Lane, A.L.: 1981, 'IUE detection of bursts of H Ly-alpha emission from Saturn', *Nature* **290**, 226–227.

Clarke, J.T., Ajello, J., Ballester, G., Ben-Jaffel, L., Connerney, J., Gérard, J.-C., Gladstone, G.R., Pryor, W., Trauger, J., and Waite, J.H., Jr.: 2002, 'Ultraviolet emissions from the magnetic footprints of Io, Ganymede, and Europa on Jupiter', *Nature* **415**, 997–1000.

Clarke, J.T., Grodent, D., Cowley, S.W.H., Bunce, E.J., Zarka, P., Connerney, J.E.P., and Satoh, T.: 2004, 'Jupiter's aurora', in F. Bagenal, T.E. Dowling, and W.B. McKinnon (eds.), *Jupiter. The planet, satellites and magnetosphere*, Cambridge University Press, Cambridge, UK, pp. 639–670.

Connerney, J.E.P., and Ness, N.F.: 1988, 'Mercury's magnetic field and interior', in F. Vilas, C.R. Chapman, and M.S. Matthews (eds.), *Mercury*, Univ. Arizona Press, Tucson, pp. 494–513.

Connerney, J.E.P., Davis, L., Jr., and Chenette, D.L.: 1984, 'Magnetic field models', in T. Gehrels and M.S. Matthews (eds.), *Saturn*, Univ. of Arizona Press, Tucson, pp. 354–377.

Coroniti, F.V.: 1974, 'Energetic electrons in Jupiter's magnetosphere', *Astrophys. J. Suppl. Ser.* **27**, 261–281.

Coustenis, A.: 2005, 'Formation and evolution of Titan's atmosphere', this volume.

Cowley, S.W.H., Bunce, E.J., and Prangé, R.: 2004, 'Saturn's polar ionospheric flows and their relation to the main auroral oval', *Ann. Geophysicae* **22**, 1379.

Crary, F.J. and Bagenal, F.: 1997, 'Coupling the plasma interaction at Io to Jupiter', *Geophys. Res. Lett.* **24**, 2135–2138.

Cravens, T.E., Keller, C.N., and Gan, L.: 1992, 'The ionosphere of Titan and its interaction with Saturnian magnetospheric electrons', ESA SP-338, pp. 273–278.

Decker, R.B. and Cheng, A.F.: 1994, 'A model of Triton's role in Neptune's magnetosphere', *J. Geophys. Res.* **99**, 19027–19045.

Delamere, P.A., Bagenal, F., Ergun, R., and Su, Y.-J.: 2003, 'Momentum transfer between the Io plasma wake and Jupiter's ionosphere', *J. Geophys. Res.* **108**,SMP 11-1, CiteID 1241.

Desch, M.D., and Kaiser, M.L.: 1981, 'Saturn's kilometric radiation – satellite modulation', *Nature* **292**, 739–741.

Dungey, : 1961, 'Interplanetary magnetic field and auroral zones', *Phys. Rev. Lett.* **6**, 47.

Encrenaz, T.: 2005, 'Neutral atmospheres of the giant planets: an overview of composition measurements', this volume.

Encrenaz, T., Bibring, J.-P., Blanc, M., Barucci, M.-A., Roques, F., and Zarka, P.: 2004, *The Solar System*, Springer.

Erkaev, N.V., Shaidurov, V.A., Semenov, V.S., and Biernat, H.K.: 2002, 'Effects of MHD slow shocks propagating along magnetic flux tubes in a dipole magnetic field', *Nonlinear Processes in Geophysics* **9**, 163.

Erkaev, N.V., Shaidurov, V.A., Semenov, V.S., Langmayr, D., Biernat, H.K.: 2004, 'Peculiarities of Alfvén wave propagation along a nonuniform magnetic flux tube', *Phys. Plasmas*, in press.

Espinosa, S.A., and Dougherty, M.K.: 2000, 'Periodic perturbations in Saturn's magnetic field', *Geophys. Res. Lett.* **27**, 2785–2788.

Eviatar, A., Siscoe, G.L., Scudder, J.D., Sittler, E.C., Jr., and Sullivan, J.D.: 1982, 'The plumes of Titan', *J. Geophys. Res.* **87**, 8091–8103.

Eviatar, A., Strobel, D.F., Wolven, B.C., Feldman, P.D., McGrath, M.A., and Williams, D.J.: 2001, 'Excitation of the Ganymede ultraviolet aurora', *Astrophys. J.* **555**, 1013–1019.

Fälthammar, C.-G.: 1968, 'Radial diffusion by violation of the third adiabatic invariant', *in* B.M. McCormac (ed.), *Earth's Particles and Fields*, Reinhold, New York, pp. 157–169.

Feldman, P.D., McGrath, M.A., Strobel, D.F., Moos, H.W., Retherford, K.D., and Wolven, B.C.: 2000, 'HST/STIS UV imaging of polar aurora on Ganymede', *Astrophys. J.* **535**, 1085–1090.

Ferrière, K.M. and André, N.: 2002, 'A mixed magnetohydrodynamic-kinetic theory of low-frequency waves and instabilities in homogeneous, gyrotropic plasmas', *J. Geophys. Res.* **107**, SMP 7-1, CiteID 1349.

Ferrière, K.M., Zimmer, C., and Blanc, M.: 1999, 'Magnetohydrodynamic waves and gravitational/centrifugal instability in rotating systems', *J. Geophys. Res.* **104**, 17335–17356.

Ferrière, K.M., Zimmer, C., and Blanc, M.: 2001, 'Quasi-interchange modes and interchange instability in rotating magnetospheres', *J. Geophys. Res.* **106**, 327–344.

Frank, L.A., Burek, B.G., and Ackerson, K.L.: 1980, 'Plasmas in Saturn's magnetosphere', *J. Geophys. Res.* **85**, 5695–5708.

Frank, L.A., Paterson, W.R., Ackerson, K.L., Vasyliunas, V.M., Coroniti, F.V., and Bolton, S.J.: 1996, 'Plasma observations at Io with the Galileo spacecraft', *Science* **274**, 394–395.

Galand, M. and Chakrabarti, S.: 2002, 'Auroral processes in the solar system', in *Atmospheres in the Solar System: comparative aeronomy*, Geophys. Monograph **130**, AGU.

Galand, M., Lilensten, J., Toublanc, D., and Maurice, S.: 1999, 'The ionosphere of Titan: Ideal diurnal and nocturnal cases', *Icarus* **140**, 92–105.

Gan, L., Keller, C. N. and Cravens, T.E.: 1992, 'Electrons in the ionosphere of Titan', *J. Geophys. Res.* **97**, 12137–12151.

Geiss, J., *et al.*: 1992, 'Plasma composition in Jupiter's magnetosphere – initial results from the Solar Wind Ion Composition Spectrometer', *Science* **257**, 1535–1539.

Glassmeier, K.-H.: 1997, 'The Hermean magnetosphere and its ionosphere-magnetosphere coupling', *Planet. Space Sci.* **45**, 119–125.

Gloeckler, G., Geiss, J., Balsiger, H., Fisk, L.A., Galvin, A.B., Ipavich, F.M., Ogilvie, K.W., von Steiger, R., and Wilken, B.: 1993, 'Detection of interstellar pick-up hydrogen in the solar system', *Science* **261**, 70–73.

Gloeckler, G., *et al.*: 2004, 'Observations of the helium focusing cone with pickup ions', *Astron. Astrophys.* **426** 845–854.

Gold, T.: 1959, 'Plasma and magnetic fields in the solar system', *J. Geophys. Res.* **64**, 1665.

Gurnett, D.A. and Goertz, C.K.: 1981, 'Multiple Alfvén wave reflections excited by Io: Origin of the Jovian decametric arcs', *J. Geophys. Res.* **86**, 717–722.

Gurnett, D.A., Kurth, W.S., and Scarf, F.L.: 1981, 'Plasma waves near Saturn – Initial results from Voyager 1', *Science* **212**, 235–239.

Gurnett, D.A., Kurth, W.S., Roux, A., Bolton, S.J., and Kennel, C.F.: 1996, 'Galileo plasma wave observations in the Io plasma torus and near Io', *Science* **274**, 391–392.

Gurnett, D.A., *et al.*: 2002, 'Control of Jupiter's radio emission and aurorae by the solar wind', *Nature* **415**, 985–987.

Hall, D.T., Feldman, P.D., Holberg, J.B., and McGrath, M.A.: 1996, 'Fluorescent hydroxyl emissions from Saturn's ring atmosphere', *Science* **272**, 516–518.

Harb, T., Kedzierski, W., and McConkey, J.W.: 2001, 'Production of ground state OH following electron impact on H_2O', *J. Chem. Phys.* **115**, 5507–5512.

Harrison, H., and Schoen, R.I.: 1967, 'Evaporation of ice in space: Saturn's rings', *Science* **157**, 1157–1176.

Hartle, R.E., Sittler, E.C., Jr., Ogilvie, K.W., Scudder, J.D., Lazarus, A.J., and Atreya, S.K.: 1982, 'Titan's ion exosphere observed from Voyager 1', *J. Geophys. Res.* **87**, 1383–1394.

Haynes, P.L., Balogh, A., Dougherty, M.K., Southwood, D.J., and Fazakerley, A.: 1994, 'Null fields in the outer Jovian magnetosphere: Ulysses observations', *Geophys. Res. Lett.* **21**, 405–408.

Hess, W.N.: 1968, *The Radiation Belt and Magnetosphere*, Blaisdell Publishing Company.

Hill, T.W.: 1979, 'Inertial limit on co-rotation', *J. Geophys. Res.* **84**, 6554–6558.

Hill, T.W. and Vasyliunas, V.M.: 2002, 'Jovian auroral signature of Io's corotational wake', *J. Geophys. Res.* **107**, SMP 27-1.

Hill, T.W., Dessler, A.J., and Goertz, C.K.: 1983, 'Magnetospheric models', in A.J. Dessler (ed.), *Physics of the Jovian magnetosphere*, Cambridge Univ. Press, New York, pp. 353–394.

Hinson, D.P., Kliore, A.J., Flasar, F.M., Twicken, J.D., Schinder, P.J., and Herrera, R.G.: 1998, 'Galileo radio occultation measurements of Io's ionosphere and plasma wake', *J. Geophys. Res.* **103**, 29343–29358.

Hinteregger, H.E., Fukui, K., and Gilson, B.R.: 1981, 'Observational, reference and model data on solar EUV, from measurements on AE-E', *Geophys. Res. Lett.* **8**, 1147–1150.

Hood, L.L.: 1983, 'Radial diffusion in Saturn's radiation belts – a modeling analysis assuming satellite and ring E', *J. Geophys. Res.* **88**, 808–818.

Hood, L.L.: 1985, 'Radial diffusion of low-energy ions in Saturn's radiation belts – a combined analysis of phase space density and satellite microsignature data', *J. Geophys. Res.* **90**, 6295–6303.

Hood, L.L.: 1989, 'Radial diffusion and losses of energetic protons in the 5 to 12 R_S region of Saturn's magnetosphere', *J. Geophys. Res.* **94**, 8721–8730.

Huddleston, D.E., Strangeway, R.J., Blanco-Cano, X., Russell, C.T., Kivelson, M.G., and Khurana, K.K.: 1999, 'Mirror-mode structures at the Galileo-Io flyby: Instability criterion and dispersion analysis', *J. Geophys. Res.* **104**, 17479–17490.

Hultqvist, B., Oieroset, M., Paschmann, G., and Treumann, R. (eds.): 1999, *Magnetospheric Plasma Sources and Losses*, Space Sci. Ser. ISSI **6**, Springer, 496 pp; reprinted from *Space Sci. Rev.* **88**.

Hunten, D.M., Tomasko, M.G., Flasar, F.M., Samuelson, R.E., Strobel, D.F., and Stevenson, D.J.: 1984, 'Titan', in T. Gehrels and M.S. Matthews (eds.), *Saturn*, Univ. Arizona Press, Tucson, pp. 671–759.

Ip, W.-H.: 1987, 'Mercury's magnetospheric irradiation effect on the surface', *Geophys. Res. Lett.* **14**, 1191–1194; 'Dynamics of electrons and heavy ions in Mercury's magnetosphere', *Icarus* **71**, 441–447.

Johnson, R.E., Pospieszalska, M.K., Sittler, E.C., Cheng, A.F., Lanzerotti, L.J., and Sieveka, E.M.: 1989, 'The neutral cloud and heavy inner torus at Saturn', *Icarus* **77**, 311–329.

Judge, D.L., Wu, F.-M., and Carlson, R.W.: 1980, 'Ultraviolet photometer observations of the Saturnian system', *Science* **207**, 431–434.

Jurac, S. and Richardson, J.D.: 2004, 'A self-consistent model of plasma and neutrals at Saturn: Neutral cloud morphology', *J. Geophys. Res.*, in press.

Jurac, S., Johnson, R.E., Richardson, J.D., and Paranicas, C.: 2001, 'Satellite sputtering in Saturn's magnetosphere', *Planet. Space Sci.* **49**, 319–326.

Jurac, S., McGrath, M.A., Johnson, R.E., Richardson, J.D., Vasyliunas, V.M., and Eviatar, A.: 2002, 'Saturn: Search for a missing water source', *Geophys. Res. Lett.* **29**, 25-1, CiteID 2172.

Kaiser, M.L., Desch, M.D., Kurth, W.S., Lecacheux, A., Genova, F., Pedersen, B.M., and Evans, D.R.: 1984, 'Saturn as a radio source', in T. Gehrels and M.S. Matthews (eds.), *Saturn*, Univ. Arizona Press, Tucson.

Kallenbach, R., Geiss, J., Gloeckler, G., and von Steiger, R.: 2000, 'Pick-up ion measurements in the heliosphere – a review', *Astrophys. Space Sci.* **274**, 97–114.

Kallenbach, R., Hilchenbach, M., Chalov, S.V., and Bamert, K.: 2004, 'On the origin of energetic neutral atoms detected by the SOHO/CELIAS/HSTOF sensor', in V. Florinsky, N.V. Pogorelov, and G.P. Zank (eds.), *Physics of the Outer Heliosphere*, AIP Conf. Proc. **719**, pp. 229–236.

Kaiser, M.L., Desch, M.D., Warwick, J.W., and Pearce, J.B.: 1980, 'Voyager detection of nonthermal radio emission from Saturn', *Science* **209**, 1238–1240.

Khurana, K.K., Kivelson, M.G., and Russell, C.R.: 1997, 'Interaction of Io with its torus: Does Io have an internal magnetic field?' *Geophys. Res. Lett.* **24**, 2391–2394.

Khurana, K.K., Kivelson, M.G., Vasyliunas, V., Krupp, N., Woch, J., Lagg, A., Mauk, B.H., and Kurth, W.S.: 2004, 'The configuration of Jupiter's magnetosphere', in F. Bagenal, T.E. Dowling, and W.B. McKinnon (eds.), *Jupiter. The planet, satellites and magnetosphere*, Cambridge University Press, Cambridge, UK, pp. 593–616.

Killen, R.M., Potter, A.E., Reiff, P., Sarantos, M., Jackson, B.V., Hick, P., and Giles, B.: 2001, 'Evidence for space weather at Mercury', *J. Geophys. Res.* **106**, 20509–20526.

Kim, Y.-K., Hwang, W., Weinberger, N.M., Ali, M.A., and Rudd, M.E.: 1997, 'Electron-impact ionization cross sections of atmospheric molecules', *J. Chem. Phys.* **106**, 1026–1033.

Kivelson, M.G.: 2005, 'The current systems of the Jovian magnetosphere and ionosphere and predictions for Saturn', this volume.

Kivelson, M. and Bagenal, F.: 1999, 'Planetary magnetospheres', in *Encyclopedia of the Solar System*, Academic Press, p. 477.

Kivelson, M.G., Coleman, P.J., Froidevaux, L., and Rosenberg, R.L.: 1978, 'A time dependent model of the Jovian current sheet', *J. Geophys. Res.* **83**, 4823–4829.

Kivelson, M.G., Khurana, K.K., Walker, R.J., Linker, J.A., Russell, C.R., Southwood, D.J., and Polanskey, C.: 1996, 'A magnetic signature at Io: Initial report from the Galileo magnetometer', *Science* **273**, 337–340.

Kivelson, M.G., Khurana, K.K., Russell, C.T., and Walker, R.J.: 1997a, 'Intermittent short-duration magnetic field anomalies in the Io torus: Evidence for plasma interchange?', *Geophys. Res. Lett.* **24**, 2127.

Kivelson, M.G., Khurana, K.K., Coroniti, F.V., Joy, S., Russell, C.T., Walker, R.J., Warnecke, J., Bennett, L., and Polanskey, C.: 1997b, 'Magnetic field and magnetosphere of Ganymede', *Geophys. Res. Lett.* **24**, 2155–2158.

Kivelson, M.G.: 2004, 'Moon-magnetosphere interactions: a tutorial', *Adv. Space Res.* **33**, 2061–2077.

Kopp, A.: 1996, 'Modification of the electrodynamic interaction between Jupiter and Io due to mass loading effects', *J. Geophys. Res.* **101**, 24943–24954.

Krimigis, S.M., *et al.*: 1979, 'Hot plasma environment at Jupiter – Voyager 2 results', *Science* **206**, 977–984.

Krimigis, S.M., Carbary, J.F., Keath, E.P., Bostrom, C.O., Axford, W.I., Gloeckler, G., Lanzerotti, L.J., and Armstrong, T.P.: 1981, 'Characteristics of hot plasma in the Jovian magnetosphere – Results from the Voyager spacecraft', *J. Geophys. Res.* **86**, 8227–8257.

Krimigis, S.M., Decker, R.B., Hill, M.E., Armstrong, T.P., Gloeckler, G., Hamilton, D.C., Lanzerotti, L.J., and Roelof, E.C.: 2003, 'Voyager 1 exited the solar wind at a distance of ~85 AU from the Sun', *Nature* **426**, 45–48.

Krimigis, S.M., Decker, R.B., Roelof, E.C., and Hill, M.E.: 2004, 'Energetic particle observations near the termination shock', V. Florinski, N.V. Pogorelov, and G.P. Zank (eds.), *Physics of the Outer Heliosphere*, AIP Conf. Proc. **719**, pp. 133–138.

Krisko, P.H. and Hill, T.W.: 1991, 'Two-dimensional model of a slow-mode expansion fan at Io', *Geophys. Res. Lett.* **18**, 1947–1950.

Krupp, N.: 2005, 'Energetic particle populations in the magnetospheres of Jupiter and Saturn', this volume.

Krupp, N., Woch, J., Lagg, A., Wilken, B., Livi, S., and Williams, D.J.: 1998, 'Energetic particle bursts in the predawn Jovian magnetotail', *Geophys. Res. Lett.* **25**, 1249–1253.

Krupp, N., Lagg, A., Livi, S., Wilken, B., Woch, J., Roelof, E.C., and Williams, D.J.: 2001, 'Global flows of energetic ions in Jupiter's equatorial plane: First-order approximation', *J. Geophys. Res.* **106**, 26017–26032.

Krupp, N., *et al.*: 2004, 'Dynamics of the Jovian magnetosphere', in F. Bagenal, T.E. Dowling, and W.B. McKinnon (eds.), *Jupiter. The planet, satellites and magnetosphere*, Cambridge University Press, Cambridge, UK, pp. 617–638.

Labelle, J. and Treumann, R.: 2002, 'Auroral radio emissions, 1. Hisses, roars, and bursts', *Space Sci. Rev.* **101**, 295–440.

Lammer, H., Wurz, P., Patel, M.R., Killen, R., Kolb, C., Massetti, S., Orsini, S., and Milillo, A.: 2003, 'The variability of Mercury's exosphere by particle and radiation induced surface release processes', *Icarus* **166**, 238–247.

Landgraf, M., Krüger, H., Altobelli, N., and Grün, E.: 2003, 'Penetration of the heliosphere by the interstellar dust stream during solar maximum', *J. Geophys. Res.* **108**, LIS 5-1, CiteID 8030.

Lellouch, E.: 2005, Io's atmosphere and surface-atmosphere interactions', this volume.

Linker, J.A., Kivelson, M.G., and Walker, R.J.: 1991, 'A three–dimensional MHD simulation of plasma flow past Io', *J. Geophys. Res.* **96**, 21037–21053.

Louarn, P., Roux, A., Perraut, S., Kurth, W.S., and Gurnett, D.: 1998, 'A study of the large-scale dynamics of the jovian magnetosphere using the Galileo plasma wave experiment', *Geophys. Res. Lett.* **25**, 2905–2908.

Louarn, P., Roux, A., Perraut, S., Kurth, W.S., and Gurnett, D.: 2000, 'A study of the Jovian "energetic magnetospheric events" observed by *Galileo*: Role in the radial plasma transport', *J. Geophys. Res.* **105**, 13073–13088.

Louarn, P., Mauk, B.H., Kivelson, M.G., Kurth, W.S., Roux, A., Zimmer, C., Gurnett, D.A., and Williams, D.J.: 2001, 'A multi-instrument study of a Jovian magnetospheric disturbance', *J. Geophys. Res.* **106**, 29883–29898.

Love, S., and Brownlee, D.E.: 1993, 'A direct measurement of the terrestrial mass accretion rate of cosmic dust', *Science* **262**, 550–553.

Luhmann, J.G., Russell, C.T., and Tsyganenko, N.A.: 1998, 'Disturbances in Mercury's magnetosphere: Are the Mariner 10 "substorms" simply driven?', *J. Geophys. Res.* **103**, 9113–9120.

Mauk, B.H., Williams, D.J., McEntire, R.W., Khurana, K.K., and Roederer, J.G.: 1999, 'Storm-like dynamics of Jupiter's inner and middle magnetosphere', *J. Geophys. Res.* **104**, 22759–22778.

McComas, D.J., *et al.*: 2004, 'The interstellar hydrogen shadow: Observations of interstellar pickup ions beyond Jupiter', *J. Geophys. Res.* **109**, CiteID A02104.

McDonald, F.B., Stone, E.C., Cummings, A.C., Heikkila, B., Lal, N., and Webber, W.R.: 2003, 'Enhancements of energetic particles near the heliospheric termination shock', *Nature* **426**, 48–51.

McGrath, M.A.: 2002, 'Hubble Space Telescope observations of Europa and Ganymede', *AGU Fall Meeting 2002*, abstract # P52C-05.

McNutt, R.L., Belcher, J.W., and Bridge, H.S.: 1981, 'Positive ion observations in the middle magnetosphere of Jupiter', *J. Geophys. Res.* **86**, 8319–8342.

Mei, Y., Thorne, R.M., and Bagenal, F.: 1995, 'Analytic model for the density distribution in the Io plasma torus', *J. Geophys. Res.* **100**, 1823–1828.

Miller, S., Aylward, A., and Millward, G.: 2005, 'Giant planet ionospheres and thermospheres: the importance of ion-neutral coupling', this volume.

Möbius, E., Hovestadt, D., Klecker, B., Scholer, M., and Gloeckler, G.: 1985, 'Direct observation of He^+ pick-up ions of interstellar origin in the solar wind', *Nature* **318**, 426–429.

Mordaunt, D.H., Lambert, I.R., Morley, G.P., Ashfold, M.N.R., Dixon, R.N., Western, C.M., Schnieder, L., and Welge, K.H.: 1993, 'Primary product channels in the photodissociation of methane at 121.6 nm', *J. Chem. Phys.* **98**, 2'054–2'065.

Morgan, T.H., and Killen, R.M.: 1997, 'A non-stochiometric model of the composition of the atmospheres of Mercury and the Moon', *Planet. Space Sci.* **45**, 81–94.

Ness, N.F., Connerney, J.E.P., Lepping, R.P., Schulz, M., and Voigt, G.-H.: 1991, 'The magnetic field and magnetospheric configuration of Uranus', in J.T. Bergstralh, E.D. Miner, and M.S. Matthews (eds.), Univ. Arizona Press, Tucson, pp. 739–779.

Neubauer, F.M.: 1980, 'Nonlinear standing Alfvén wave current system at Io: Theory', *J. Geophys. Res.* **85**, 1171–1178.

Neubauer, F.M.: 1998, 'The sub-Alfvénic interaction of the Galilean satellites with the Jovian magnetosphere', *J. Geophys. Res.* **103**, 19843–19866.

Neubauer, F.M., Gurnett, D.A., Scudder, J.D., and Hartle, R.E.: 1984, 'Titan's magnetospheric interaction', in T. Gehrels and M.S. Matthews (eds.), *Saturn*, Univ. Arizona Press, Tucson, pp. 760–787.

Neubauer, F.M., *et al.*: 1986, 'First results from the Giotto magnetometer experiment at comet Halley', *Nature* **321**, 352–355.

Ness, N.F., Behannon, K.W., Lepping, R.P., Whang, Y.C., and Schatten, K.H.: 1974, 'Magnetic field observations near Mercury: preliminary results from Mariner 10', *Science* **185**, 153–162.

Northrop, T.G. and Connerney, J.E.P.: 1987, 'A micrometeorite model and the age of Saturn's rings', *Icarus* **70**, 124–137.

Ogilvie, K.W., Scudder, J.D., Hartle, R.E., Siscoe, G.L., Bridge, H.S., Lazarus, A.J., Asbridge, J.R., Bame, S.J., and Yeates, C.M.: 1974, 'Observations at Mercury encounter by the plasma science instrument on Mariner 10', *Science* **185**, 146–152.

Ogilvie, K.W., Scudder, J.D., Vasyliunas, V.M., Hartle, R.E., and Siscoe, G.L.: 1977, 'Observations of the planet Mercury by the plasma electron experiment: Mariner 10', *J. Geophys. Res.* **82**, 1807–1824.

Paonessa, M. and Cheng, A.F.: 1986, 'Limits on ion radial diffusion coefficients in Saturn's inner magnetosphere', *J. Geophys. Res.* **91**, 1391–1396.

Parker, E.N.: 1961, 'The stellar-wind regions', *Astrophys. J.* **134**, 20–27.

Phan, T.D., *et al.*: 2000, 'Extended magnetic reconnection at the Earth's magnetopause from detection of bi-directional jets', *Nature* **404**, 848–850.

Pollack, J.B.: 1975, 'The rings of Saturn', *Space Sci. Rev.* **18**, 3–93.

Potter, A. and Morgan, T.H.: 1985, 'Discovery of sodium in the atmosphere of Mercury', *Science* **229**, 651–653.

Potter, A. and Morgan, T.H.: 1986, 'Potassium in the atmosphere of Mercury', *Icarus* **67**, 336–340.

Poulet, F. and Cuzzi, J.N.: 2002, 'The composition of Saturn's rings', *Icarus* **160**, 350–358.

Pospieszalska, M.K. and Johnson, R.E.: 1991, 'Micrometeorite erosion of the main rings as a source of plasma in the inner Saturnian plasma torus', *Icarus* **93**, 45–52.

Prangé, R., Pallier, L., Hansen, K.C., Howard, R.. Vourlidas, A., Courtin, R., and Parkinson, C.: 2004, 'A CME-driven interplanetary shock traced from the Sun to Saturn by planetary auroral storms', *Nature*, in press.

Pryor, W.R. and Hord, C.W.: 1991, 'A study of photopolarimeter system UV absorption data on Jupiter, Saturn, Uranus, and Neptune: implications for auroral haze formation', *Icarus* **91**, 161–172.

Rao, M.V.V.S., Iga, I., and Srivastava, S.K.: 1995, 'Ionization cross-sections for the production of positive ions from H_2O by electron impact', *J. Geophys. Res.* **100**, 26421–26425.

Raulin, A.: 2005, 'Exo-astrobiological aspects of Europa and Titan: from observations to speculations', this volume.
Richardson, J.D.: 1986, 'Thermal ions at Saturn: Plasma parameters and implications', *J. Geophys. Res.* **91**, 1381–1389.
Richardson, J.D.: 1998, 'Thermal plasma and neutral gas in Saturn's magnetosphere', *Rev. Geophys.* **36**, 501–524.
Richardson, J.D. and Eviatar, A.: 1988, 'Observational and theoretical evidence for anisotropies in Saturn's magnetosphere', *J. Geophys. Res.* **93**, 7297–7306.
Richardson, J.D. and Jurac, S.: 2004, 'A self-consistent model of plasma and neutrals at Saturn: The ion tori', *J. Geophys. Res.*, in press.
Richardson, J.D., Eviatar, A., Siscoe, G.L.: 1986, 'Satellite tori at Saturn', *J. Geophys. Res.* **91**, 8749–8755.
Richardson, J.D., Belcher, J.W., McNutt, R.L., Jr., and Szabo, A.: 1995, 'The plasma environment of Neptune', in D.P. Cruikshank and M.S. Matthews (eds.), *Neptune*, Univ. Arizona Press, Tucson.
Richardson, J.D., Eviatar, A., McGrath, M.A., Vasyliuñas, V.M.: 1998, 'OH in Saturn's magnetosphere: Observations and implications', *J. Geophys. Res.* **103**, 20245–20256.
Roos-Serote, M.: 2005, 'The changing face of Titan's haze: is it all dynamics?', this volume.
Russell, C.T.: 1989, 'ULF waves in the Mercury magnetosphere', *Geophys. Res. Lett.* **16**, 1253–1256.
Russell, C.T.: 2001, 'The dynamics of planetary magnetospheres', *Planet. Space Sci.* **49**, 1005–1030.
Russell, C.T., Baker, D.N., and Slavin, J.A.: 1988, 'The magnetosphere of Mercury', in F. Vilas, C.R. Chapman, and M.S. Matthews (eds.), *Mercury*, Univ. Arizona Press, Tucson, pp. 514–561.
Russell, C.T., *et al.*: 1999, 'Mirror mode structures at the Gallileo-Io flyby: Observations', *J. Geophys. Res.* **104**, 17471–17478.
Russell, C.T., Blanco-Cano, X., and Kivelson, M.G.: 2003, 'Ion cyclotron waves in Io's wake region', *Planet. Space Sci.* **51**, 233–238.
Sagan, C., and Thompson, W.R.: 1984, 'Production and condensation of organic gases in the atmosphere of Titan', *Icarus* **59**, 133–161.
Sagan, C., Khare, B.N., and Lewis, J.S.: 1984, 'Organic matter in the Saturn system', *in* T. Gehrels and M.S. Matthews (eds.), *Saturn*, Univ. Arizona Press, pp. 788–807.
Sandel, B.R. and Broadfoot, A.L.: 1981, 'Morphology of Saturn's aurora', *Nature* **292**, 679–682.
Santos-Costa, D. and Bourdarie, S.A.: 2001, 'Modeling the inner Jovian electron radiation belt including non-equatorial particles', *Planet. Space Sci.* **49**, 303–312.
Santos-Costa, D., Sault, R., Bourdarie, S., Boscher, D., Bolton, S., Thorne, R., Leblanc, Y., Dulk, G., Levin, S., and Gulkis, S.: 2001, 'Synchrotron emission images from three-dimensional modeling of the Jovian electron radiation belts', *Adv. Space Res.* **28**, 915–918.
Scarf, F.L., Frank, L.A., Gurnett, D.A., Lanzerotti, L.J., Lazarus, A., and Sittler, E.C., Jr.: 1984, 'Measurements of plasma, plasma waves, and suprathermal charged particles in Saturn's inner magnetosphere', in T. Gehrels and M.S. Matthews (eds.), *Saturn*, Univ. Arizona Press, Tucson, pp. 318–353.
Schardt, A.W., Behannon, K.W., Lepping, R.P., Carbary, J.F., Eviatar, A., and Siscoe, G.L.: 1984, 'The outer magnetosphere', in T. Gehrels and M.S. Matthews (eds.), *Saturn*, Univ. Arizona Press, Tucson, pp. 416–459.
Selesnick, R.S.: 1988, 'Magnetospheric convection in the non-dipolar magnetic field of Uranus', *J. Geophys. Res.* **93**, 9607.
Selesnick, R.S.: 1990, 'Plasma convection in Neptune's magnetosphere', *Geophys. Res. Lett.* **17**, 1681–1684.
Selesnick, R.S., and Richardson, J.D.: 1986, 'Plasmasphere formation in arbitrarily oriented magnetospheres', *Geophys. Res. Lett.* **13**, 624–627.
Shemansky, D.E., and Hall, D.T.: 1992, 'The Distribution of Atomic Hydrogen in the Magnetosphere of Saturn', *J. Geophys. Res.* **97**, 4143–4161.

Shemansky, D.E., Matheson, P., Hall, D.T., Hu, H.-Y., and Tripp, T.M.: 1993, 'Detection of the hydroxyl radical in the Saturn magnetosphere', *Nature* **363**, 329–331.

Shi, M., Baragiola, R.A., Grosjean, D.E., Johnson, R.E., Jurac, S., and Schou, J.: 1995, 'Sputtering of water ice surfaces and the production of extended neutral atmospheres', *J. Geophys. Res.* **100**, 26'387–26'396.

Simpson, J.A., Hamilton, D., Lentz, G., McKibben, R.B., Mogro-Campero, A., Perkins, M., Pyle, K.R., Tuzzolino, A.J., and O'Gallagher, J.J.: 1974, 'Protons and electrons in Jupiter's magnetic field: Results from the University of Chicago experiment on Pioneer 10', *Science* **183**, 306–309.

Siscoe, G.L.: 1978, 'Jovian plasmaspheres', *J. Geophys. Res.* **83**, 2118–2126.

Siscoe, G.L., and Summers, D.: 1981, 'Centrifugally driven diffusion of iogenic plasma', *J. Geophys. Res.* **86**, 8471–8479.

Slavin, J.A.: 2004, 'Mercury's magnetosphere', *Adv. Space Res.* **33**, 1859–1874.

Southwood, D.J. and Kivelson, M.G.: 1987, 'Magnetospheric interchange instability', *J. Geophys. Res.* **92**, 109–116.

Strobel, D.F: 2005, 'Photochemistry in outer solar system atmospheres', this volume.

Su, Y., Ergun, R., Bagenal, F., and Delamere, P.: 2003, 'Io-related auroral arcs: Modelling parallel electric fields', *J. Geophys. Res.* **108**, 1094.

Summers, M.E. and Strobel, D.F.: 1989, 'Triton's atmosphere – A source of N and H for Neptune's magnetosphere', *Geophys. Res. Lett.* **18**, 2309–2312.

Thomas, N., Bagenal, F., Hill, T.W., and Wilson, J.K.: 2004, 'The Io neutral clouds and plasma torus', in F. Bagenal, T.E. Dowling, and W.B. McKinnon (eds.), *Jupiter. The planet, satellites and magnetosphere*, Cambridge University Press, Cambridge, UK, pp. 561–591.

Thorne, R.M., Armstrong, T.P., Stone, S., Williams, D.J., McEntire, R.W., Bolton, S.J., Gurnett, D.A., and Kivelson, M.G.: 1997, 'Galileo evidence for rapid interchange transport in the Io torus', *Geophys. Res. Lett.* **24**, 2131.

Tyler, G.L., *et al.*: 1989, 'Voyager radio science observations of Neptune and Triton', *Science* **246**, 1466–1473.

Van Allen, J.A.: 1984, 'Energetic particles in the inner magnetosphere of Saturn', in T. Gehrels and M.S. Matthews (eds.), *Saturn*, Univ. Arizona Press, Tucson, pp. 281–317.

Vasyliunas, V.M.: 1975, 'Modulation of Jovian interplanetary electrons and the longitude variation of decametric emissions', *Geophys. Res. Lett.* **2**, 87–88.

Vasyliunas, V.M.: 1983, 'Plasma distribution and flow', in A.J. Dessler (ed.), *Physics of the Jovian magnetosphere*, Cambridge Univ. Press, New York, pp. 395–453.

Vasyliunas, V.M.: 1986, 'The convection-dominated magnetosphere of Uranus', *Geophys. Res. Lett.* **13**, 621–623.

Williams, D.J. and Thorne, R.M.: 2003, 'Energetic particles over Io's polar caps', *J. Geophys. Res.* **108**, SMP 7-1, CiteID 1397.

Winterhalter, D., Acña, M., and Zakharov, A. (eds.): 2004, *Mars' Magnetism and its Interaction with the Solar Wind*, *Space Sci. Rev.* **111**, Kluwer Academic Publsihers, Dordrecht, NL.

Wong, A.-S., Yung, Y.L., Friedson, A.J.: 2003, 'Benzene and haze formation in the polar atmosphere of Jupiter', *Geophys. Res. Lett.* **30**, 30-1, CiteID 1447, DOI 10.1029/2002GL016661.

Wright, A.N. and Schwartz, S.J.: 1990, 'The equilibrium of a conducting body embedded in a flowing plasma', *J. Geophys. Res.* **95**, 4027–4038.

Young, D.T., *et al.*: 2003, 'Cassini Plasma Spectrometer Investigation', *Space Sci. Rev.*, in press.

Zarka, P. and Kurth, W.S.: 2005, 'Radio wave emission from the outer planets before Cassini', this volume.

Address for Offprints: Michel Blanc, Observatoire Midi Pyrénées, 14, av. Edouard Belin, F-31400 Toulouse, France; `blanc@obs-mip.fr`

THE CURRENT SYSTEMS OF THE JOVIAN MAGNETOSPHERE AND IONOSPHERE AND PREDICTIONS FOR SATURN

MARGARET GALLAND KIVELSON
Institute of Geophysics and Planetary Physics and Department of Earth and Space Sciences, University of California, Los Angeles, CA 90095, USA

Received: 8 July 2004; Accepted in final form: 17 August 2004

Abstract. Magnetized plasmas in motion inevitably generate currents and the magnetized plasmas that form the magnetospheres of the outer planets are no exception. Although a focus on the current systems tends to distract from the underlying dynamics, many elements of magnetospheric structure can be organized by discussing them in terms of the large scale currents present in the system. This paper starts with a digression on the pitfalls of a current-based description of a planetary magnetosphere but then proceeds to characterize the magnetospheres of Jupiter, Earth, and to some extent Saturn by the currents that flow within them. Emphasis is placed on the field-aligned currents that couple the equatorial magnetospheres to the ionospheres and the conditions that call for the development of field-aligned electric fields.

Keywords: outer planets, magnetosphere, ionosphere, current systems

1. Introduction

In discussions of the magnetospheres of Earth and other planets, it is common to identify large scale current systems that account for the observed plasma and magnetic structure. In discussions of the terrestrial magnetosphere, we talk of the Chapman-Ferraro currents that flow on the magnetopause, the tail current sheet that separates the northern and southern lobes of the magnetotail, the Region 1 and Region 2 currents that link the ionosphere to other parts of the large scale system, the ring current that forms at times of geomagnetic activity, and the substorm currents that link the equatorial plasma to the auroral zones of the ionosphere where they create both beauty and havoc in the upper atmosphere. It seems natural to believe that with currents establishing magnetospheric structure, an electric field is responsible for the plasma motions through the familiar "frozen-in field" picture of magnetohydrodynamics using the relation $\mathbf{u} = \mathbf{E} \times \mathbf{B}/B^2$. Here $\mathbf{u}$ is the bulk flow velocity and $\mathbf{E}$ ($\mathbf{B}$) is the electric (magnetic) field. This approach is referred to as the $E - j$ description.

It seems reasonable, then, that a compendium of papers on the outer planets should include a paper describing and contrasting the current systems that characterize the giant planets Jupiter and Saturn, and indeed that is the topic of this chapter. There is, nonetheless, a powerful caveat that must be considered, so Sec-

Space Science Reviews 116: 299–318, 2005.
DOI: 10.1007/s11214-005-1959-x

tion 2 addresses the objections to an $E - j$ description of a magnetosphere as discussed by Parker (1996; 2000).

Magnetohydrodynamics (MHD) tells us that changing flows, pressure gradients, or inertial stresses generate currents. For example, an azimuthal current develops in Jupiter's equatorial plasma at all local times in response to centrifugal stresses. Also heavy ions from Io diffuse outward and the plasma flow slows below corotation speed. Slowing is greatest near the equator, causing the magnetic field lines to curl backward if the magnetic flux is frozen into the plasma motion. The curl of B implies an additional current in the radial direction that closes at its inner and outer boundaries through field-aligned currents linking the equatorial currents to Jupiter's ionosphere. The ultimate source of the radial current is the shear in the azimuthal flow. Surface currents flow on the magnetopause in response to the change of pressure of the plasma across the boundary.

The magnetosphere also responds to temporal variations, whether the source of the variation is internal or external. There is a direct link between the changes of flow and changes of the currents that control the magnetic configuration. Examples of current systems arising from changing flows are familiar from Earth. During substorms, bursty bulk flows (Angelopoulos *et al.*, 1992; 1997; Baumjohann *et al.*, 1990) and other substorm-related flows (Lyons *et al.*, 1999) drive currents into the auroral ionosphere where they can be observed as brightenings. At Jupiter (and surely at Saturn) the interactions of the moons with magnetospheric plasma drives currents, once again linked to changing the plasma flow. One doesn't have to talk about "generators" and "loads". If the flow is dynamic, or if special pressure gradients are present, currents naturally arise (current is generated). The current flows to a part of the system where it is dissipated as it acts to change the motion of the remote plasma.

Plasma currents require current carriers. If there are not enough current carriers (usually electrons) to carry the current, either the available electrons must be accelerated or additional electrons must be sucked out of a source region. This is why field-aligned electric fields develop. We are lucky that such electric fields develop because electrons accelerated by **E** "light up" the auroral ionosphere and give us indirect evidence of where currents are flowing. The aurora is therefore an important tool in a study of currents.

In the following sections, the currents important at Jupiter and Earth are described. In many ways, Saturn is likely to be more similar to Earth than to Jupiter, but we can learn about both Earth and Saturn by examining phenomena that may be subtle at Earth (or Saturn) but appear in extreme form at Jupiter and we can consider what parallels are likely to be found at Saturn.

2. Currents: Inconveniences and Caveats

The topic of this chapter is currents, but Parker warns us (1996; 2000) that analysis starting from currents is at the very least intractable and often misleading. Why? Underlying our analysis are Newton's laws and Maxwell's equations (simplified for MHD limit in which scales are large compared with gyroradii, etc.). Fields and flows are related through

$$\frac{\mathrm{d}\,(\rho\mathbf{u})}{\mathrm{d}t} = -\nabla\cdot\tilde{\mathbf{P}} + \mathbf{j}\times\mathbf{B}\,. \tag{1}$$

Here ρ is the mass density, $\tilde{\mathbf{P}}$ the pressure tensor and $\mathbf{j}$ is the current density. In the MHD limit, currents are determined by the magnetic field structure through

$$\mathbf{j} = \nabla\times\mathbf{B}/\mu_0\,. \tag{2}$$

Equation (2) can be inverted to give $\mathbf{B}$ in terms of $\mathbf{j}$ but only through a highly non-local and mathematically complex relationship

$$\mathbf{B}\,(\mathbf{r}) = \frac{\mu_0}{4\pi}\overset{\text{all space}}{\iiint}\mathrm{d}\mathbf{r}'\;\frac{\mathbf{j}\left(\mathbf{r}'\right)\times\left(\mathbf{r}-\mathbf{r}'\right)}{|\mathbf{r}-\mathbf{r}'|^3} \tag{3}$$

that can lead into a morass. We must know $\mathbf{j}$ everywhere in order to determine $\mathbf{B}$. Everywhere is not an exaggeration. Even very distant currents may matter. For example, an infinite plane current sheet generates a field perturbation that is independent of distance from the sheet! The current flowing on the dayside magnetopause (a large if not infinite current sheet) can therefore not be neglected if one proposes to determine $\mathbf{B}$ anywhere in the equatorial magnetosphere inside of $10R_{\mathrm{E}}$. Yet global knowledge of $\mathbf{j}$ at an instant of time, essential to an accurate determination of $\mathbf{B}$, is not provided by spacecraft measurements. On the other hand, strictly local measurements of $\mathbf{B}$ can be obtained by a small number of closely spaced spacecraft such as those that comprise the Cluster mission (Escoubet *et al.*, 2001), and such measurements provide an excellent approximation to the local $\mathbf{j}$ through Equation (2), a much more convenient situation.

Researchers particularly like to think about currents because they feel comfortable with circuit analogies. However, circuit analogies must be treated with caution. Circuits provide useful insight when we wish to consider how different parts of the system are linked and they are often used to infer "what drives what." But Parker warns: "Electric circuit equations are not derived. They are declared by casual analogy between the time dependent net current in the magnetic field and the current in a fixed electric circuit in the laboratory." And there are several possible pitfalls in circuit analysis. For example, because plasmas at rest can be thought of as electrically neutral, it is acceptable to assume $\nabla\cdot\mathbf{j} = 0$, as is normally done when analyzing circuits. However, this assumption applies strictly only in the plasma rest frame. In frames with finite charge density ρ_q there is no guarantee that

$\mathbf{j}$ is divergenceless. The transformations to a frame moving with velocity $u \ll c$ (the velocity of light) are given by

$$\mathbf{E}' = \mathbf{E} + \mathbf{u} \times \mathbf{B}/c; \qquad \mathbf{B}' = \mathbf{B} \tag{4}$$

$$\rho_q' = \rho_q - \mathbf{u} \cdot \mathbf{j}/c^2; \qquad \mathbf{j}' = \mathbf{j} - \mathbf{u}\rho_q \tag{5}$$

where the Gaussian system is used for clarity of the argument. In the plasma rest frame,

$$\mathbf{E}' = 0; \quad \rho_q' = 0; \quad \nabla \cdot \mathbf{j} = 0 \,. \tag{6}$$

In the frame moving at velocity $\mathbf{u}$,

$$\rho_q = \mathbf{u} \cdot \mathbf{j}/c^2 \,. \tag{7}$$

The continuity equation, a frame-independent relationship requires

$$\nabla \cdot \mathbf{j} + \partial \rho_q / \partial t = 0 \tag{8}$$

and correspondingly

$$\nabla \cdot \mathbf{j} + \mathbf{u} \cdot \partial \mathbf{j} / \partial t / c^2 = 0 \,. \tag{9}$$

For spatial scales and flow speeds typically found in the terrestrial magnetosphere, the right side is very much smaller than the individual terms on the left side but it may not be negligible in all space plasmas.

A more pertinent concern in using circuit analogies is that coupling between the magnetosphere and the ionosphere is described as if the current diverted from equatorial paths flows strictly along field lines and into the ionosphere. Yet nothing constrains the current to remain on a flux tube. Indeed flux tubes may well "leak" current. The point is illustrated in Figure 1. In (a), the current flows onto the flux tube near the equator, flows along the field and diverges in the ionosphere. In (b), the current flows onto the flux tube as for (a), but flows off in a distributed manner so that only a small fraction of the equatorial current reaches the ionosphere. Circuit analogies don't consider this possibility!

Another oversimplification is found in cartoons such at that of the familiar McPherron substorm current wedge illustrated in Figure 2 (McPherron, 1991). Wire circuits can bend sharply, changing the direction of the current abruptly. The tail current does not discontinuously change direction thereafter remaining guided along a flux tube from equator to ionosphere (nor does it flow in extremely thin sheets).

So, there are many reasons not to address the properties of planetary magnetospheres by describing the current systems that they contain, but I shall cheerfully ignore all the good advice just given. In conclusion of this digression and in advance of overlooking all of its sensible warnings, I recommend reading Parker's papers on the subject.

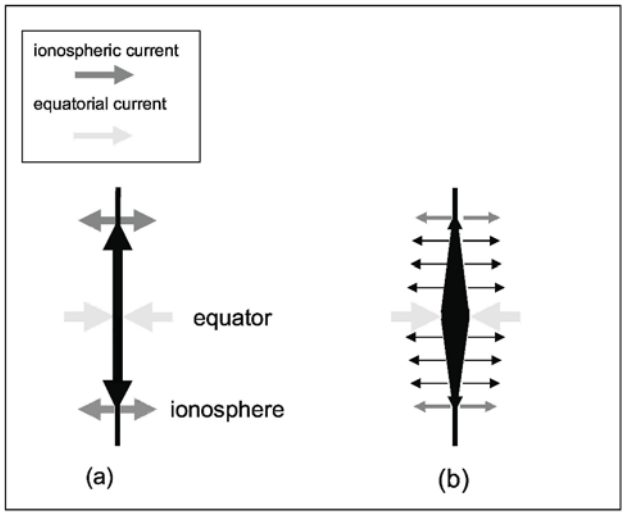

Figure 1. Currents linking magnetosphere and ionosphere. (a) currents confined to flux tube, (b) currents diverge from flux tube between equator and ionosphere.

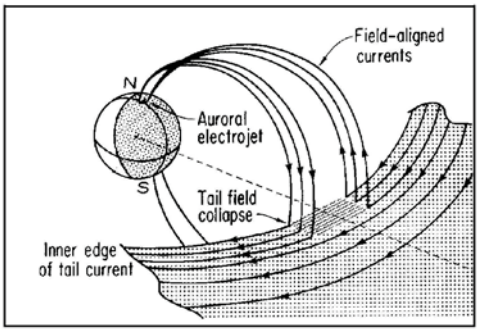

Figure 2. Substorm current wedge as discussed by McPherron (1991).

3. Large Scale Current Systems at Jupiter and Saturn

Most of the large scale current systems at Jupiter or Saturn have analogues at Earth. In all of the magnetospheres, the magnetic field is largely confined within a cavity in the solar wind by interaction of field and flow. The confinement drives surface current on the magnetopause, the magnetopause current. In the magnetotail, the surface current closes through a tail current sheet. Figure 3 shows schematically a cross-section through the magnetotail in which the current closing above and below flows on the magnetopause and returns through the center of the magnetotail.

The magnetopause and tail currents, shown here for Earth, are reversed at Saturn or Jupiter because of the different dipole orientations. The ring current, carried by energetic particles, has no direct analogy at Jupiter.

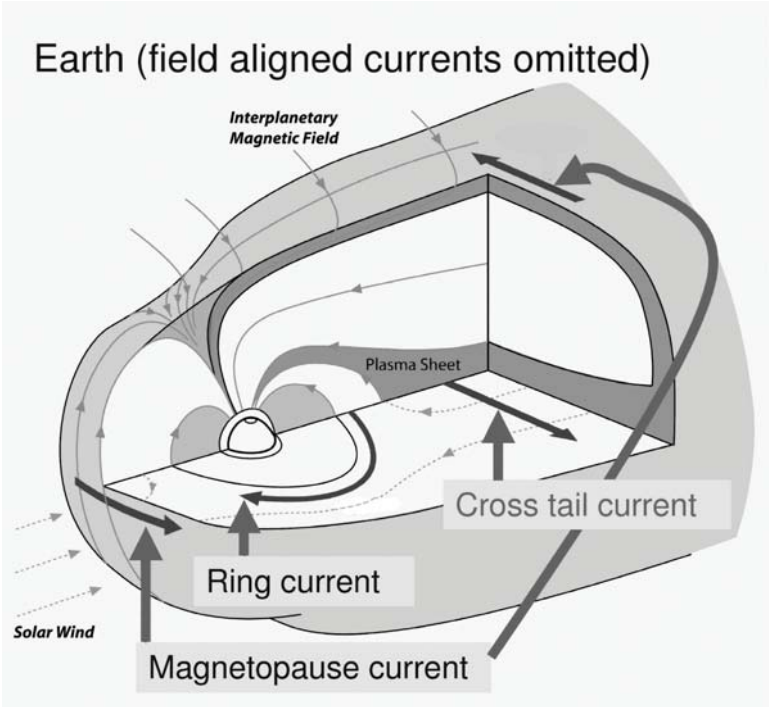

Figure 3. Schematic of currents in the terrestrial magnetosphere (courtesy of K. Khurana, 2004).

TABLE I

Important parameters and basic scale lengths for magnetospheres.

Planet	B_0 (Gauss)	R_p (km)	τ_p (hours)	B_{SW} (nT)	R_{mp} (R_p)	R_{stag} (R_p)
Earth	0.31	6,373	24	$\approx$10	$\approx$10	$\approx$6
Jupiter	4.28	71,398	9.92	$\approx$2	$50-100$	$\approx$250
Saturn	0.22	60,330	10.65	$\approx$1	$\approx$19	$\approx$74

Possibly the most striking differences between the magnetosphere of Earth and those of the outer planets is the spatial scale. Earth's radius is an order of magnitude smaller than the radii of Jupiter and Saturn. But spatial scale is relevant only in relation to the dynamics of the system. One critical scale length is established by the distance to the nose of the magnetopause, R_{mp}. This distance can be estimated in terms of solar wind dynamic pressure as discussed by Walker and Russell (1995), or taken from observations (Kivelson and Bagenal, 1999) as in Table I.

However, there is another length scale of importance that arises because plasma motions are controlled through both external and internal stresses. In the absence of external forces and assuming large ionospheric conductivity, currents flowing from

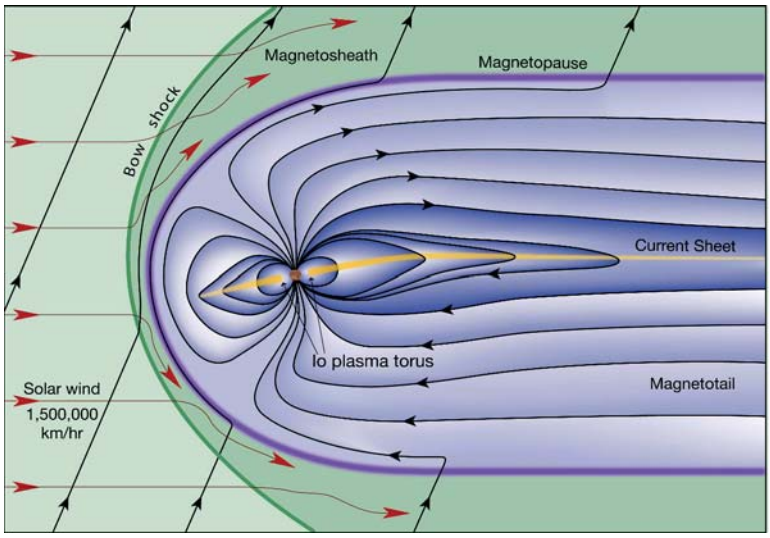

Figure 4. Noon-midnight cut of the Jovian magnetosphere (courtesy of Steve Bartlett and Fran Bagenal, 2004).

the ionosphere to the magnetosphere cause the plasma to rotate at the angular speed of the central planet, a pattern referred to as corotation. Concurrently, flow patterns imposed by magnetic reconnection with the solar wind can result in sunward flows through much of the equatorial magnetosphere (Dungey, 1961). A flow stagnation point can then develop where the rotational flow opposes that imposed by the solar wind. The distance at which this occurs establishes another important length scale for a magnetosphere. That distance ($R_{\rm stag}$) can be determined (Wolf, 1995) from

$$\begin{aligned} R_{\rm stag} &= \left(\Omega_{\rm p} B_0 R_{\rm p}^3 / E\right)^{1/2} \\ R_{\rm stag} &\approx \left(\Omega_{\rm p} B_0 R_{\rm p}^3 / 0.1 V_{\rm SW} B_{\rm SW}\right)^{1/2} \end{aligned} \tag{10}$$

where $\Omega_{\rm p}$ is the angular velocity of the planet, B_0 is the surface magnetic field at the equator of the planet, $R_{\rm p}$ is the planetary radius, and $\mathbf{E}$ is the average cross-magnetosphere electric field. We approximate $\mathbf{E}$ as $0.1\mathbf{V}_{\rm SW} \times \mathbf{B}_{\rm SW}$ in terms of the solar wind speed $V_{\rm SW} \approx 400$ km/s and the magnetic field at the distance of the planet, $\mathbf{B}_{\rm SW}$.

For Jupiter and Saturn, rotational stresses dominate the effects of the solar wind ($R_{\rm stag} \gg R_{\rm mp}$), whereas at Earth, $R_{\rm stag} < R_{\rm mp}$ and solar wind control becomes critical. At Jupiter, the effects of rotation are particularly notable in the region referred to as the middle magnetosphere (Smith *et al.*, 1976). In Jupiter's middle magnetosphere the field lines are stretched radially, as contrasted with the relatively dipolar configuration typical of Earth inward of roughly $R_{\rm mp}$ (compare the noon-midnight magnetic structure in Figure 3 with Figure 4).

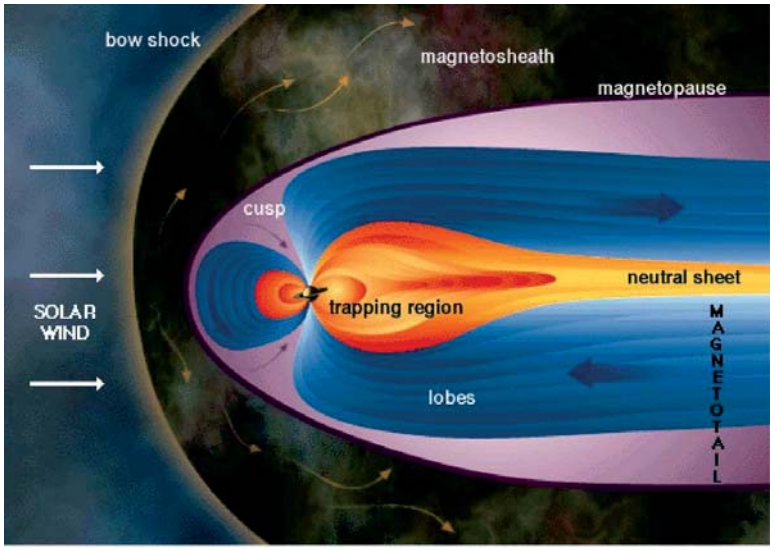

Figure 5. Cut through Saturn's magnetosphere in the noon-midnight meridian (`http://www.windows.ucar.edu/saturn/images/rg.jpg`).

A key to the special properties of Jupiter's magnetospheric field configuration is the heavy ion plasma introduced into the magnetosphere at a rate of 1 ton/s near Io's orbit (at $6R_J$). Radial stresses imposed by the rapidly rotating magnetospheric plasma greatly distort the underlying dipolar magnetic configuration. A large $\partial B_r/\partial z$ develops and accordingly an azimuthal current $j_\phi \approx \mu_0^{-1}\partial B_r/\partial z$. appears. The azimuthal currents flow in a warped current sheet that is indicated schematically in Figure 4. On the day side, the current sheet extends typically about 2/3 of the distance to the magnetopause (Kivelson and Southwood, 2003).

Beyond the azimuthal current sheet the field lines become the quasi-dipolar field lines of the low density outer magnetosphere. The current disk is ring-like in the sense that it encircles the planet, but unlike Earth's ring current it extends over a large radial range, remains confined close to the equatorial plane, and the current carriers are low energy particles.

Effects of rotation are also present at Saturn and in the inner portion of Earth's magnetosphere but they do not distort the magnetic configuration as they do at Jupiter (see Figure 5). This is because at Earth/Saturn, the plasma density is low and neither the rotational stress nor possible contributions of energy particle pitch angle anisotropy affect **B** significantly.

Returning to Jupiter, we note that rotating plasma with a negative radial gradient of flux tube content may be unstable to the interchange instability; at Jupiter this instability leads to outward radial transport of plasma (Cheng, 1985; Southwood and Kivelson, 1987; 1989). Conservation of angular momentum density ($\rho\omega r^2$ in terms of the density ρ, the angular velocity ω, and the cylindrical radial distance r) implies that outward-moving plasma, initially corotating, will lag corotation

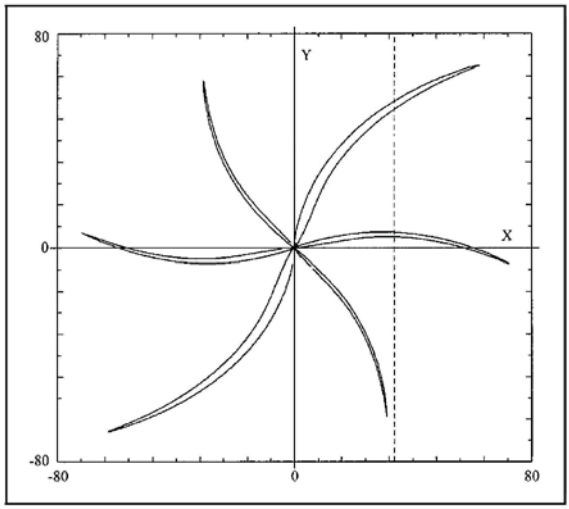

Figure 6. Selected field lines viewed from above (north) in Khurana's (1997) model of Jupiter's middle magnetosphere. Field line bending or "curling" as illustrated here implies radial currents ($\nabla \times \mathbf{B}/\mu_0$) flowing near the equator.

increasingly with radial distance. Because the lag depends on r, which increases along the flux tube from the surface to the equator, the field, "frozen" to the flow, becomes twisted. Figure 6 illustrates this point by showing field lines from a model of the middle magnetosphere viewed from above (Khurana, 1997). The field lines move radially out from the ionosphere and twist or bend back from the radial direction as they approach the equator. As noted, the cause of the bendback is the lag of the plasma relative to corotation as it moves outward. The result is that $\partial B_\phi/\partial r$ is non-zero (especially near the equator) and thus $j_r > 0$ in the near equatorial region. Because the current must be divergenceless, the radial current must close along field lines where they link to the ionosphere as illustrated in Figure 7 from Hill (1979). The radially outward current at the equator can be identified as a corotation-enforcement current because it exerts a $\mathbf{j} \times \mathbf{B}$ force that acts to accelerate the angular speed of the plasma. The closure current at high latitude acts to slow the angular motion of the ionosphere, which can be maintained in corotation through interaction with the collisional atmosphere provided the flux of momentum is sufficient (Vasyliunas, 1994). The current system described, which has no analogue at Earth, has been modeled in detail by K. K. Khurana (1997, and in preparation 2004 with a full magnetopause added). Khurana particularly stresses the role of field-aligned currents that link the equatorial magnetosphere with Jupiter's ionosphere.

Jupiter's ionosphere acts like a TV screen that may light up in some places where currents flow in and out. For example, in Figure 8, an infrared (IR) image of Jupiter, the bright emissions ringing the poles (referred to as the main auroral oval) reveal regions heated by the ionospheric closure of the radial currents that we have

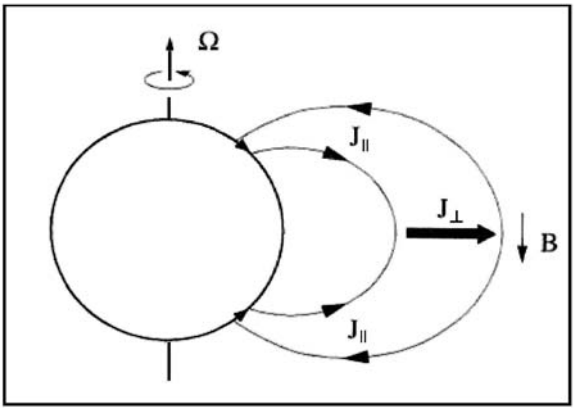

Figure 7. Schematic of currents flowing radially outward in the equatorial plane and closing through the ionosphere (Hill, 1979).

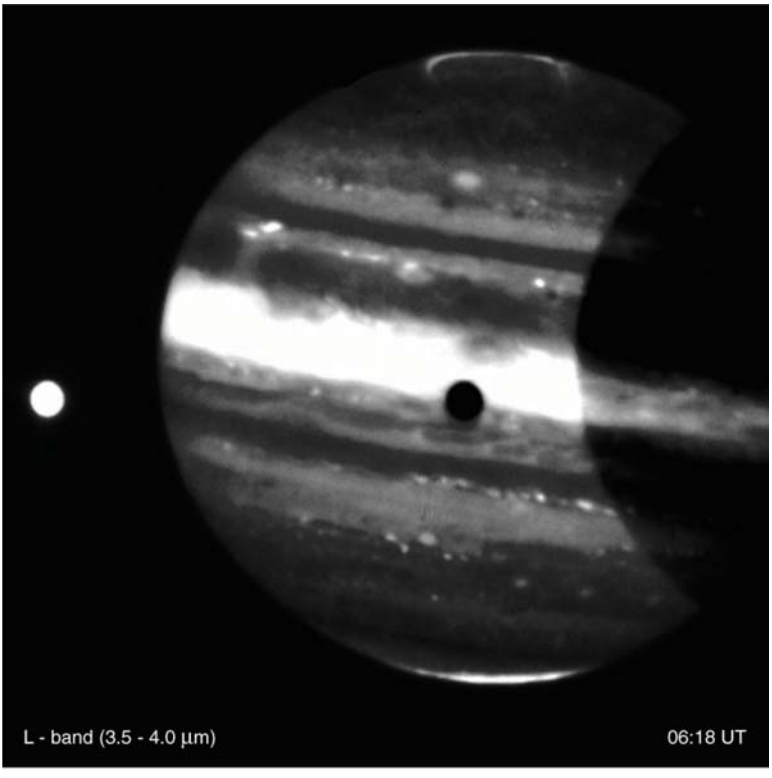

Figure 8. Infrared image of Jupiter (photo from European Southern Observatory).

discussed. The magnetic linkage to the middle magnetosphere is consistent with the flux crossing the middle magnetosphere (Southwood and Kivelson, 2001). In the ionosphere $\mathbf{E} = \eta\mathbf{j}$ where η is the resistivity, which implies that heat ($\mathbf{j} \cdot \mathbf{E} = \eta j^2$) is locally generated in the region of closure currents. Resistive heating produces IR radiation but not emissions in the ultraviolet (UV). IR and UV images need not appear similar. However, Figure 9 shows a high degree of correspondence to the patterns of radiation in the lower frequency bands. Currents are normally carried by the electrons of the low energy plasma whereas UV emissions require excitation by relatively energetic electrons or ions. Hence we are led to ask why energetic charged particles are so closely linked to the ionospheric signatures of currents. For insight, we turn to the signatures associated with currents in the auroral ionosphere at Earth.

In the interpretation of UV aurora at Earth, it has long been accepted that the excitations are driven in regions where upward currents couple the plasma of the magnetotail to the ionosphere. Upward currents require ions to move up from the ionosphere or electrons to move down into the ionosphere. Ionospheric ions are comparatively massive and therefore require large acceleration if they are to move upward as current carriers. Magnetospheric electrons are light and plentiful, but motion towards the ionosphere brings them into an increasingly intense magnetic field and they mirror before they reach the ionosphere. Thus at low altitudes there may not be enough electrons to carry the current. The dilemma of providing current carriers is resolved if an $\mathbf{E}_\parallel$ develops above the ionosphere. With singly charged ions assumed, the field-aligned current density is given by

$$j_\parallel = en_\mathrm{e}\left(v_{\parallel\mathrm{i}} - v_{\parallel\mathrm{e}}\right) \approx -en_\mathrm{e}v_{\parallel\mathrm{e}} \tag{11}$$

where n_e is the electron number density and $v_{\parallel\mathrm{i}}$ and $v_{\parallel\mathrm{e}}$ the field-aligned ion and electron velocity, respectively. If there are too few electrons to carry the required current density along a portion of a flux tube, Equation (11) tells us that either additional electrons or an increase in the speed with which the available electrons move along the flux tube can compensate. Acceleration by the field-aligned electric field produces the required increase of velocity. Indeed, parallel electric fields are routinely observed in conjunction with auroral arcs. Remarkably, observations by the Fast spacecraft (and earlier polar orbiting s/c) reveal that parallel electric fields are observed not only in the upward current region but may also appear in the downward current region, reflecting the fact that the ionosphere, although a plentiful source of low energy electrons, may need help in providing sufficient numbers of current carriers (Ergun *et al.*, 2000).

The acceleration of current-carrying electrons explains the presence of relatively high energy (10s of keV) electrons in the auroral ionosphere, particularly in the regions where electrons are accelerated downward. The Fast team reports that the structure of field-aligned currents at Earth is often latitude dependent. As illustrated in Figure 10, Alfvénic fluctuations (with both upward and downward currents) are observed at the highest latitude in regions where currents are changing

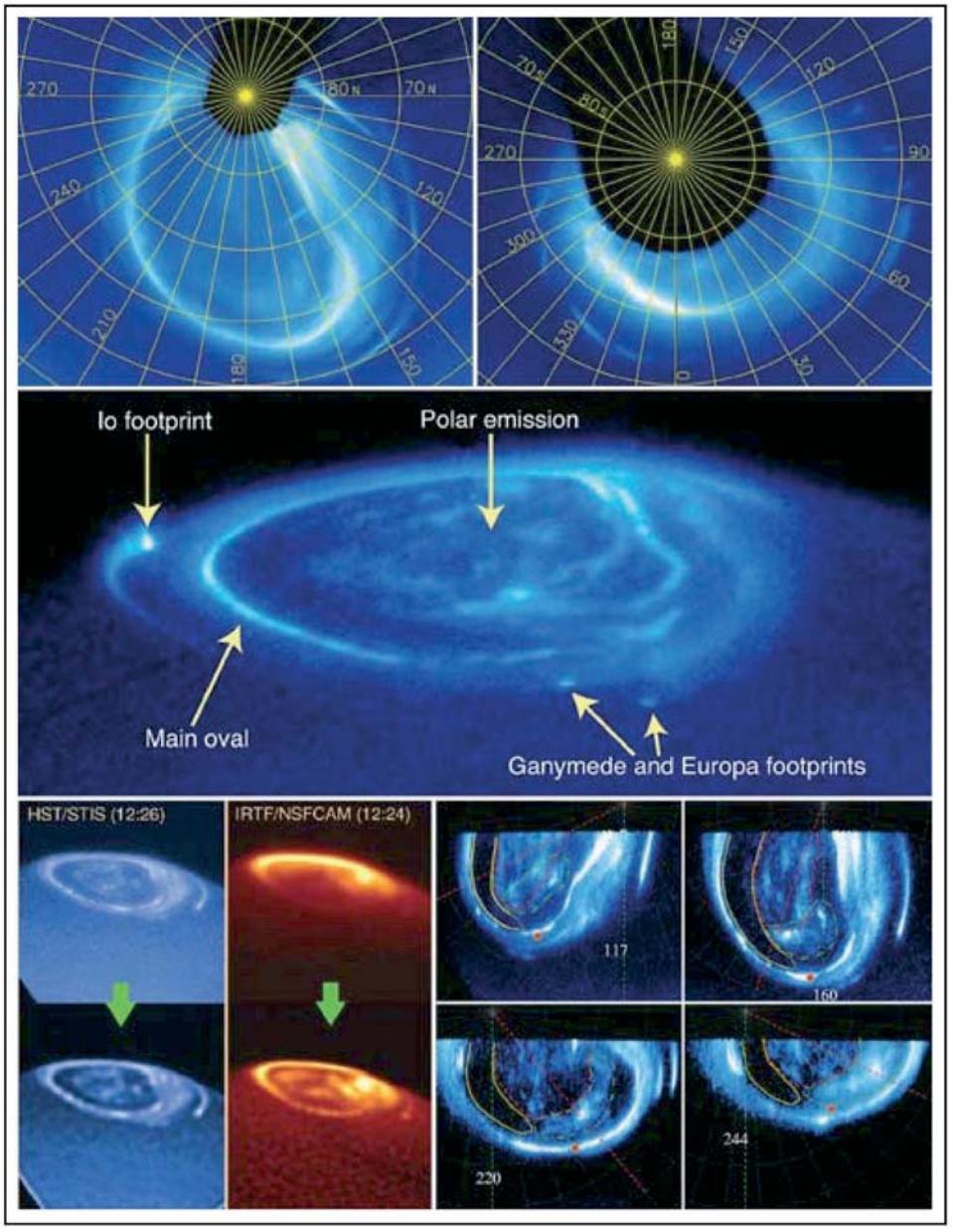

Figure 9. Hubble space telescope images of the auroral atmosphere of Jupiter in UV (blue) and in IR (red). The correspondence of the polar emissions at the two wavelengths supports the view that both types of emission are linked to ionospheric currents.

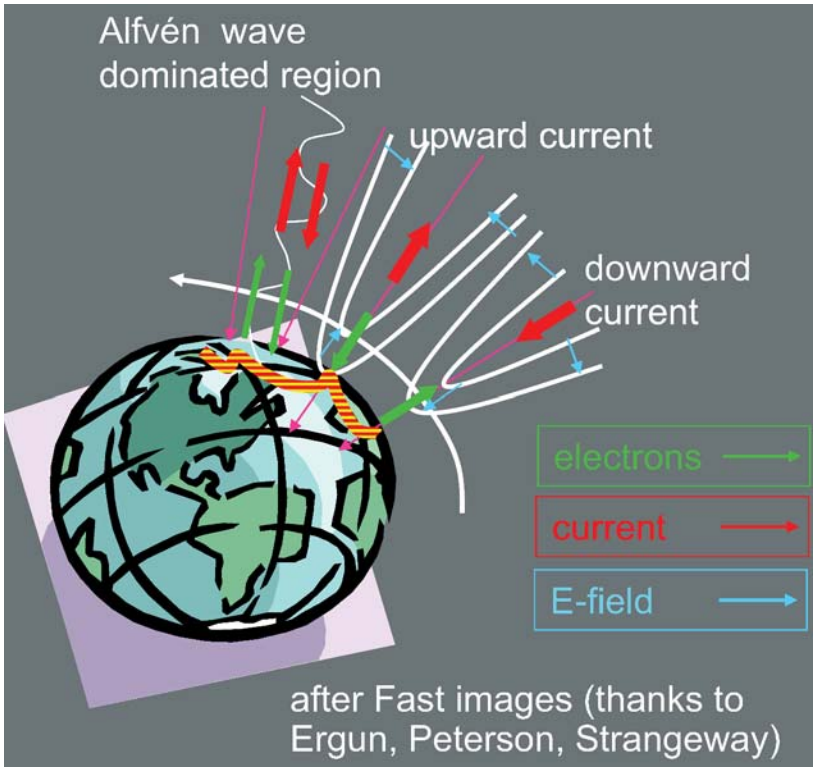

Figure 10. Structure of currents and fields in the auroral region as described in the text. Pink lines represent the magnetic field direction.

in time. At lower latitudes, more stable upward and downward currents appear. The equipotential contours illustrated (white curves) show that the electric fields change direction from being transverse to the magnetic field at high altitudes to being parallel or antiparallel at lower altitudes where the magnetic mirror has excluded a large fraction of the magnetospheric electron population.

The association of parallel electric fields with regions of field-aligned current flow must apply at Jupiter as well as at Earth, even though the processes that cause the currents to flow may differ for the different planets. At Earth, the aurora is linked to magnetotail dynamics. At Jupiter, the main oval is linked to the currents arising from corotation lag. But in both cases field-aligned currents must flow in regions where there is a deficiency of electrons and the problem is solved by imparting acceleration to the available electrons. Estimates by Cowley *et al.* (2004) indicate that at Saturn the plasma lagging corotation drives only weak currents that do not require $\mathbf{E}_{\|}$ and do not produce aurora. It is only when acceleration of electrons is required to carry current into the ionosphere that one finds UV aurora in the regions where the heated ionosphere also glows in the infrared.

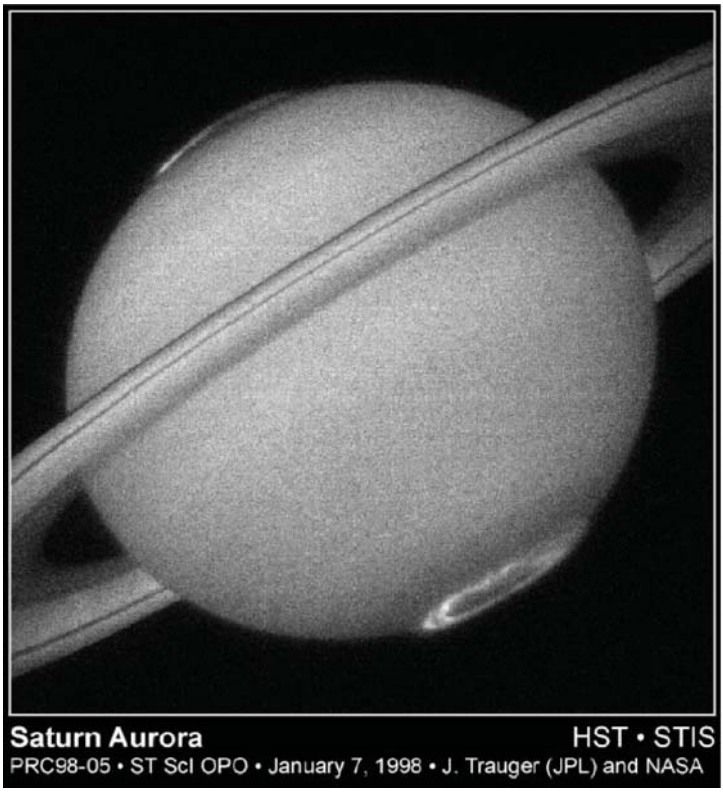

Figure 11. Saturn's aurora imaged in UV by the Hubble Space Telescope.

Field-aligned currents also flow at the boundary between open and closed field lines, both at Earth and Jupiter. These are the currents that drive dayside polar emissions at Earth. Careful examination of the images at the lower left of Figure 9 shows emissions in a ring fully contained within the main oval and these emissions have been identified as the open-closed field line boundary at Jupiter (Pallier and Prangé, 2004). Assuming that the polar oval is the boundary between open and closed field lines, it is reasonable to assume that its intensity will vary as the characteristics of the solar wind, particularly the orientation of its magnetic field, change. Thus it is not unexpected that the intensity of Jupiter's high latitude oval is not constant. In particular, images taken by the Chandra spacecraft revealed impulsive X-ray bursts with variable intensity at a period of 40 minutes (Gladstone *et al.*, 2002), possibly the repetition period of intermittent magnetic reconnection at the dayside magnetopause. At Saturn, Cowley *et al.* (2004) have associated the auroral oval evident in Figure 11 with the open-closed field line boundary, arguing that only at that boundary are the currents sufficiently intense to require parallel electric fields to accelerate electrons. Variable emissions from the auroral oval at Saturn have been reported by Grodent *et al.* (2004) although the link to the interplanetary field

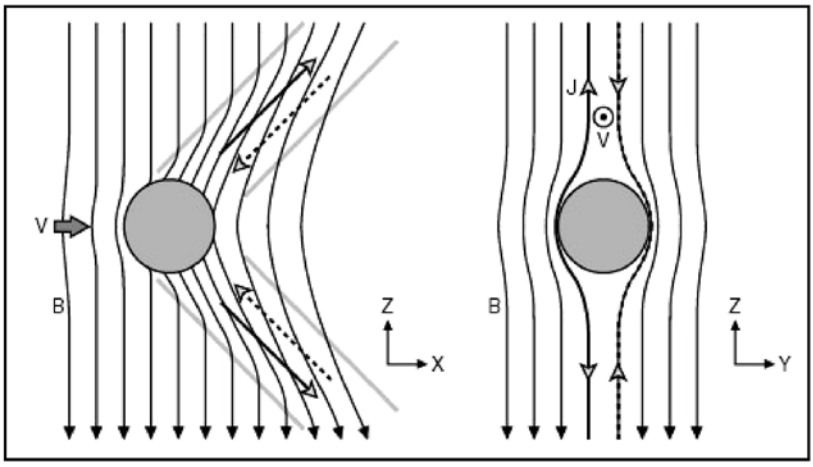

Figure 12. Interaction of a moon with magnetospheric field lines. *Left:* a section containing the field and the flow. *Right:* a section through the field and the radial direction to the planet. The bends of the field and the sense of the field-aligned currents are indicated.

direction has not been established for either Saturn or Jupiter. Some of the variable emissions reported may be linked to substorm-like activity in the magnetotail.

4. Some Current Systems at Jupiter and Saturn Lacking Terrestrial Analogues

A most important feature of the magnetospheres of Jupiter and Saturn that has no terrestrial analogue arises because of the interaction of magnetospheric plasma with the large moons whose orbits lie for the most part within the magnetopause. The Keplerian speed of these moons is lower than the rotational speed of the magnetospheric plasma within which they are embedded, so, in the rest system of a moon, plasma sweeps towards the side that trails its orbital motion. The interaction of the flowing plasma with a moon generates disturbances of various sorts. Of greatest importance for the topic at hand is the bending of field lines linked to the slowing of the plasma by the moon and its atmosphere and by interactions with newly created ions (referred to as pick-up ions) that form a cloud around it (Kivelson *et al.*, 2004). As discussed previously, field bending and currents are linked through Equation (2), thus producing a field and current configuration illustrated in Figure 12. A cross-field current flows radially outward through the moon and/or its ionosphere. Field-aligned currents link the moon and its surroundings to the planetary ionosphere as shown schematically in Figure 13 for some of the Galilean moons of Jupiter. The radial current, analogous to that described in the context of corotation lag, exerts forces to accelerate Io's motion (quite unsuccessfully) and to slow down Jupiter's ionosphere to the orbital speed of Io (also not successfully).

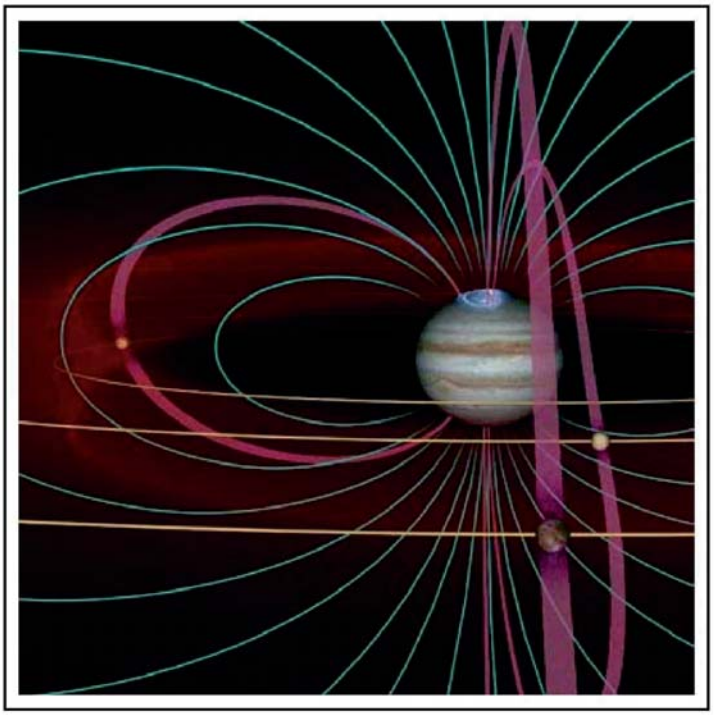

Figure 13. Schematic figure showing currents linking Io (*left*), Ganymede, and Europa (*right*) along field lines to Jupiter's ionosphere.

Like the other current circuits at Jupiter, the currents linking the moons and the ionospheres must flow through regions of low carrier density, regions where the centrifugal stress outward is pushing plasma towards the equatorial point of the field line and regions where the huge gravitational field of Jupiter is pushing plasma towards the ionosphere. This requires that the electrons be accelerated by field-aligned electric fields which accelerate them to energies high enough to produce the UV glow at the feet of the flux tubes of Io, Europa, and Ganymede in Figure 9.

Su *et al.* (2003) take lessons from Earth and apply them to the Io-associated ionospheric signatures (see Figure 14). They attribute the ionospheric emissions at Io's footprint and the trail that leads the footprint in the direction of Io's motion (middle panel of Figure 9) to the effects of $\mathbf{E}_{\|}$. The parallel electric field may be implicated in generating Io-controlled decametric radio emissions (Kivelson *et al.*, 2004).

The low altitude electric field in the downward current region can accelerate electrons out of Jupiter's ionosphere, producing highly collimated electron beams that have been observed in passes across Io's wake and its polar cap (Williams and Thorne, 2003). Europa and Ganymede as well as Io link to Jupiter's ionosphere through field-aligned currents. At Saturn, one anticipates evidence of field-

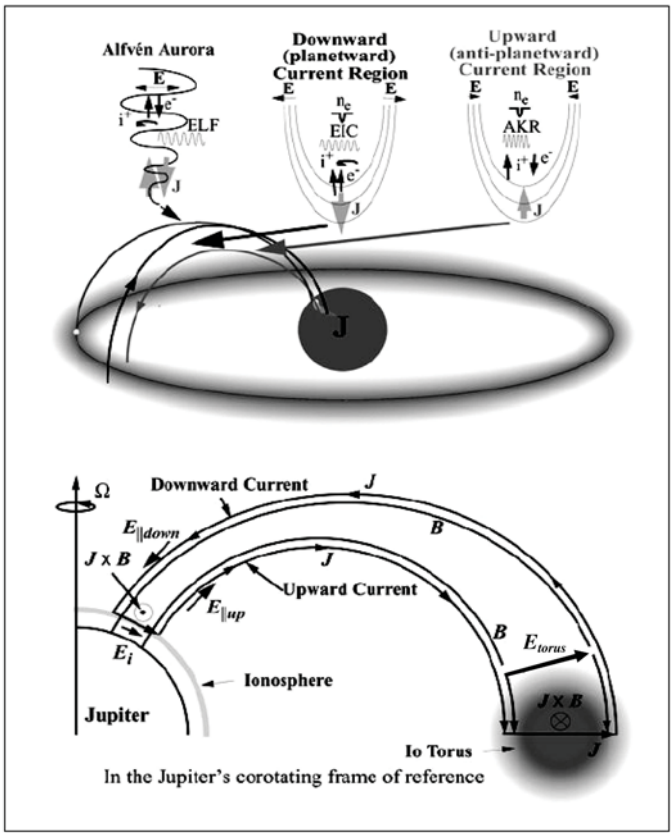

Figure 14. From Su *et al.* (2003) showing the Io-linked currents and proposed structures at low altitude on the flux tubes.

aligned currents and possibly electron beams in the vicinity of the larger moons, particularly at the largest moon, Titan!

An evident feature of the environment of Saturn without parallel at Earth is its ring system. The rings significantly affect Saturn's magnetosphere with strong effects on particle fluxes but details of ring-associated currents remain to be investigated. Rings are present but play a much less significant role in modifying the magnetospheric plasma at Jupiter.

5. The Ring Current – a Terrestrial Current System

In discussing the currents of importance at Jupiter and speculating on currents present in Saturn's magnetosphere, no mention has been made of a ring current. The corotation enforcement currents do flow azimuthally and therefore in a ring around Jupiter, but this current is not an analogue of the terrestrial ring current. At Earth the ring current is important primarily during and following disturbed

intervals (storms). The current waxes and wanes in response to solar wind input. It is carried by moderately energetic particles (10s to hundreds of keV ions). The symmetric part of the current is carried by ions trapped on closed drift paths as a result of temporal variations of the convective flow speed. The asymmetric ring current is carried by energetic ions flowing from night to day on open drift paths. There is no clear analogue at Jupiter, probably because effects of the solar wind are less important in a rotation-dominated magnetosphere. At Saturn there is an equatorial current (Giampieri and Dougherty, 2004) probably more like the disk current of Jupiter's middle magnetosphere than like the ring current of the terrestrial magnetosphere. Cassini measurements may reveal if a current-carrying energetic ion population appears at Saturn during disturbed intervals, but this seems unlikely in a rotation-dominated magnetosphere.

6. Summary Remarks

Magnetospheres, like other magnetized plasmas, are coupled over vast spatial domains by currents generated in response to flows and pressure gradients. Particularly dramatic evidence of magnetospheric currents are found in auroral images where the regions coupled to strong upward current flow often are marked by emission of energetic UV photons. At Earth, such strong currents flow principally in response to solar wind-driven geomagnetic activity with some additional signatures marking the open-closed field line boundary. At Jupiter, currents flow into the main oval from a source not present at Earth, the sub-corotating plasma disk. Field aligned currents/electric fields arise naturally wherever currents perpendicular to the background field diverge (for example, at Jupiter near the inner and outer edges of the equatorial plasma disk or in the vicinity of one of the moons). If there are not enough current carrying particles to carry the current, $\mathbf{E}_{\|}$ (along $\mathbf{B}$) develops to speed along the available carriers sufficiently for them to complete the current circuit. The presence of unique current systems such as that arising from corotation lag at Jupiter and that arising from the ring current at Earth are useful as diagnostics of the relative importance of rotational and solar wind influences on the magnetosphere. Saturn is rotationally dominated and in that sense closer to Jupiter than Earth. Despite being rotationally dominated, Saturn's azimuthal currents are comparatively weak, meaning the field is stretched much less than Jupiter's relative to the dipole field, because Saturn lacks a strong source of pick-up ions like Io.

Acknowledgements

The author thanks various colleagues with whom she has discussed the roles of currents in magnetosphere and the relative importance of rotation and solar wind input over the years. Thanks are owed especially to Krishan Khurana, David Southwood, Fran Bagenal, Raymond Walker and Renée Prangé. Figure 9 was provided

by R. Prangé. The work was supported in part by the National Science Foundation under grant ATM02-05958 and by NASA under JPL contract 1238965.

References

Angelopoulos, V., Baumjohann, W., Kennel, C.F., Coroniti, F.V., Kivelson, M.G., Pellat, R., Walker, R.J., Lühr, H., and Paschmann, G.: 1992, 'Bursty bulk flows in the inner central plasma sheet', *J. Geophys. Res.* **97**, 4027–4039.

Angelopoulos, V., *et al.*: 1997, 'Magnetotail flow bursts: association to global magnetospheric circulation, relationship to ionospheric activity, and direct evidence for localization', *Geophys. Res. Lett.* **24**, 2271–2275.

Baumjohann, W., Paschmann, G., and Lühr, H.: 1990, 'Characteristics of high-speed ion flows in the plasma sheet', *J. Geophys. Res.* **95**, 3801–3809.

Cheng, A.F.: 1985, 'Magnetospheric interchange instability', *J. Geophys. Res.* **90**, 9900–9904.

Cowley, S.W.H., Bunce, E.J., and O'Rourke, J.M.: 2004, 'A simple quantitative model of plasma flows and currents in Saturn's polar ionosphere', *J. Geophys. Res.* **109** (A05212), doi:10.1029/2003JA010375.

Dungey, J.W.: 1961, 'Interplanetary magnetic field and the auroral zones', *Phys. Rev. Lett.* **6**, 47–48.

Ergun, R.E., Carlson, C.W., McFadden, J.P., Mozer, F.S., and Strangeway, R.J.: 2000, 'Parallel electric fields in discrete arcs', *Geophys. Res. Lett.* **27**, 4053–4057.

Escoubet, C.P., Fehringer, M., and Goldstein, M.: 2001, 'The Cluster mission', *Annales Geophysicae* **19**, 1197–1200.

Giampieri, G. and Dougherty, M.K.: 2004, 'Modelling of the ring current in Saturn's magnetosphere', *Annales Geophysicae* **22**, 653–659.

Gladstone, G.R., *et al.*: 2002, 'A pulsating auroral X-ray hot spot on Jupiter', *Nature* **415**, 1000–1003.

Grodent, D., Gérard, J.-C., Saglam, A., and Gustin, J.: 2004, 'The main characteristics of Saturn's UV aurora', in EGU, Geophys. Res. Abs. 02250.

Hill, T.W.: 1979, 'Inertial limit on corotation', *J. Geophys. Res.* **84**, 6554–6558.

Khurana, K.K.: 1997, 'Euler potential models of Jupiter's magnetospheric field', *J. Geophys. Res.* **102**, 11,295–11,306.

Kivelson, M.G. and Bagenal, F.: 1999, 'Planetary magnetospheres', *in* P.R. Weissman, L.-A. McFadden, and T.V. Johnson (eds.), *Encyclopedia of the Solar System*, Acad. Press, San Diego, pp. 477–497.

Kivelson, M.G., Bagenal, F., Kurth, W.S., Neubauer, F.M., Paranicas, C., and Saur, J.: 2004, 'Magnetospheric interactions with satellites', *in* F. Bagenal, T. Dowling, and W. McKinnon (eds.), *Jupiter: The Planet, Satellites and Magnetosphere*, Cambridge Univ. Press, New York, NY, in press.

Kivelson, M.G. and Southwood, D.J.: 2003, 'Losing the Io plasma: Local time variations of Jupiter's magnetospheric structure and the development of the outer magnetosphere maelstrom', IGPP UCLA Publication # 5778, Los Angeles, CA.

Lyons, L., Nagai, T., Blanchard, G., Samson, J., Yamamoto, T., Mukai, T., Nishida, A., and Kokobun, S.: 1999, 'Association between Geotail plasma flows and auroral poleward boundary intensifications observed by CANOPUS photometers', *J. Geophys. Res.* **104**, 4485–4500.

McPherron, R.L.: 1991, 'Physical processes producing magnetospheric substorms and magnetic storms', *in* J. Jacobs (ed.), *Geomagnetism*, Acad. Press, San Diego, pp. 593–639.

Pallier, L. and Prangé, R.: 2004, 'Detection of the southern counterpart of the jovian northern polar cusp: Shared properties', *Geophys. Res. Lett.* **31(6)**, Art. No. L06701.

Parker, E.N.: 1996, 'The alternative paradigm for magnetospheric physics', *J. Geophys. Res.* **101**, 10,587–10,626.

Parker, E.N.: 2000, 'Newton, Maxwell, and Magnetospheric Physics', *in: Magnetospheric Current Systems*, AGU, Washington, DC.

Smith, E.J., Davis, J.L., and Jones, D.E.: 1976, 'Jupiter's magnetic field and magnetosphere', *in* T. Gehrels (ed.), *Jupiter, Studies of the interior, atmosphere, magnetosphere and satellites*, Univ. Ariz. Press, Tucson, AZ, pp. 788.

Southwood, D.J. and Kivelson, M.G.: 1987, 'Magnetospheric interchange instability', *J. Geophys. Res.* **92**, 109–116.

Southwood, D.J. and Kivelson, M.G.: 1989, 'Magnetospheric interchange motions', *J. Geophys. Res.* **94**, 299–308.

Southwood, D.J. and Kivelson, M.G.: 2001, 'A new perspective concerning the influence of the solar wind on the Jovian magnetosphere', *J. Geophys. Res.* **106**, 6123–6130.

Su, Y., Ergun, R., Bagenal, F., and Delamere, P.: 2003, 'Io-related auroral arcs: Modelling parallel electric fields', *J. Geophys. Res.* **108**, Art. No. 1094.

Vasyliunas, V.M.: 1994, 'Role of plasma acceleration time in the dynamics of the Jovian magnetosphere', *Geophys. Res. Lett.* **21**, 401–404.

Walker, R.J. and Russell, C.T.: 1995, 'Solar-wind interactions with magnetized planets', *in* M.G. Kivelson and C.T. Russell (eds.), *Introduction to Space Physics*, Cambridge University Press, New York, pp. 164–182.

Williams, D.J. and Thorne, R.M.: 2003, 'Energetic particles over Io's polar caps', *J. Geophys. Res.* **108**, Art. No. 1397.

Wolf, R.A.: 1995, 'Magnetospheric configuration', *in* M.G. Kivelson and C.T. Russell (eds.), *Introduction to Space Physics*, Cambridge University Press, New York, pp. 288–329.

Address for Offprints: Margaret Galland Kivelson, Institute of Geophysics and Planetary Physics and Department of Earth and Space Sciences, University of California, Los Angeles, CA 90095, USA; mkivelson@igpp.ucla.edu

GIANT PLANET IONOSPHERES AND THERMOSPHERES: THE IMPORTANCE OF ION-NEUTRAL COUPLING

STEVE MILLER, ALAN AYLWARD and GEORGE MILLWARD
Atmospheric Physics Laboratory, Department of Physics and Astronomy, University College London, London WC1E 6BT, U.K.

Received: 15 April 2004; Accepted in final form: 11 July 2004

Abstract. Planetary upper atmospheres – coexisting thermospheres and ionospheres – form an important boundary between the planet itself and interplanetary space. The solar wind and radiation from the Sun may react with the upper atmosphere directly, as in the case of Venus. If the planet has a magnetic field, however, such interactions are mediated by the magnetosphere, as in the case of the Earth. All of the Solar System's giant planets have magnetic fields of various strengths, and interactions with their space environments are thus mediated by their respective magnetospheres. This article concentrates on the consequences of magnetosphere-atmosphere interactions for the physical conditions of the thermosphere and ionosphere. In particular, we wish to highlight important new considerations concerning the energy balance in the upper atmosphere of Jupiter and Saturn, and the role that coupling between the ionosphere and thermosphere may play in establishing and regulating energy flows and temperatures there. This article also compares the auroral activity of Earth, Jupiter, Saturn and Uranus. The Earth's behaviour is controlled, externally, by the solar wind. But Jupiter's is determined by the co-rotation or otherwise of the equatorial plasmasheet, which is internal to the planet's magnetosphere. Despite being rapid rotators, like Jupiter, Saturn and Uranus appear to have auroral emissions that are mainly under solar (wind) control. For Jupiter and Saturn, it is shown that Joule heating and "frictional" effects, due to ion-neutral coupling can produce large amounts of energy that may account for their high exospheric temperatures.

Keywords: giant planets, ionosphere, thermosphere, ion-neutral coupling

1. Introduction

Although typically less than one part in a million of the mass of a planet's atmosphere is represented by the uppermost layers – the coexisting thermosphere and ionosphere – they form an important boundary between the planet itself and interplanetary space. The solar wind and radiation from the Sun may react with the upper atmosphere directly, as in the case of Venus. If the planet has a magnetic field, however, such interactions are mediated by the magnetosphere, as in the case of the Earth. All of the Solar System's giant planets have magnetic fields of various strengths, and interactions with their space environments are thus mediated by their respective magnetospheres.

The neutral thermosphere absorbs solar extreme ultraviolet (EUV) radiation and is subject to a flux of precipitating particles. These precipitating particles may come directly from the solar wind, if the planet is unmagnetised, or be accelerated by

Space Science Reviews 116: 319–343, 2005.
DOI: 10.1007/s11214-005-1960-4

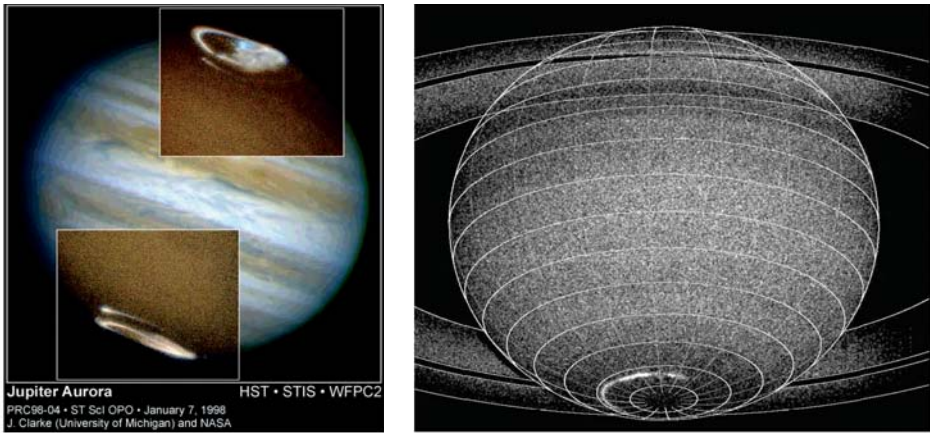

Figure 1. (a) UV images of Jupiter's aurorae superimposed on an optical image of the planet (courtesy J. Clarke, University of Michigan). (b) UV image of Saturn's southern aurora (from Cowley *et al.*, 2004).

fields generated in the magnetosphere, if there is one. Both the absorption of EUV radiation and particle precipitation can cause dissociation and ionisation of the main thermospheric species, and subsequent chemistry can modify the resulting atmospheric composition. The ionosphere refers to that part of the atmosphere where there is a significant proportion of ions and electrons, enough to affect the propagation of radio waves.

Recent work imaging the upper atmospheres of Jupiter, Saturn and Uranus in ultraviolet (e.g. Gérard *et al.*, 1995; Ballester *et al.*, 1998; Clarke *et al.*, 1998; Prangé *et al.*, 1998; Trauger *et al.*, 1998; Vincent *et al.*, 2000; Pallier and Prangé, 2001; Pryor *et al.*, 2001; Waite *et al.*, 2001; Grodent *et al.*, 2003), visible (Vasavada *et al.*, 1999) and infrared (e.g. Satoh *et al.*, 1996; Lam *et al.*, 1997a; Satoh and Connerney, 1999; Trafton *et al.*, 1999) radiation has shown that emission from neutral and ionised species is an important way of tracing the location of energy inputs into the upper atmospheres (Figures 1-2). For the purposes of this chapter, an approximate definition of "auroral emission" is "atmospheric emission in response to particle precipitation" (although this does not cover everything that may be called "auroral"). Thus auroral emission is generally linked to the injection into the atmosphere of particles capable of exciting and ionising atmospheric species. An extensive review of the auroral emissions of all four giant planets is given by Bhardwaj and Gladstone (2000).

Particular progress has been made in understanding how the jovian magnetosphere, and the particle fluxes it produces, map onto the upper atmosphere (Kivelson *et al.*, 1997; Cowley and Bunce, 2001; Hill, 2001; Southwood and Kivelson, 2001). As well as the major magnetospheric signatures, it has even been possible to detect emission due to the perturbations caused by orbiting moons (Connerney *et al.*, 1993; Clarke *et al.*, 1998; Prangé *et al.*, 1998; Clarke *et al.*, 2002). It has

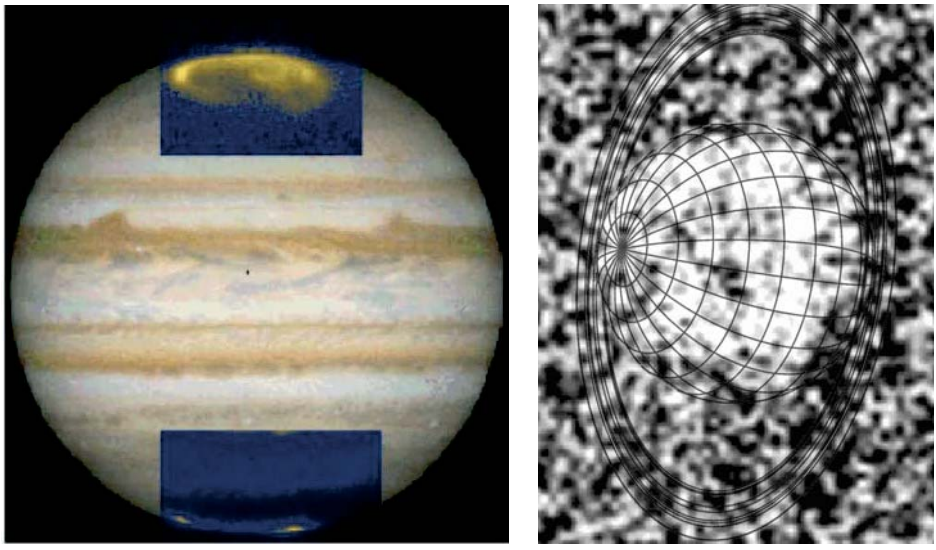

Figure 2. (a) IR images of Jupiter's aurorae taken at 3.953 μm (sensitive to H_3^+ emission) superimposed on an optical image of the planet (courtesy N. Achileos, UCL). (b) IR image of Uranus taken at 3.953 μm (Trafton, Miller and Stallard, unpublished data).

been especially fruitful to link in situ spacecraft measurements of magnetospheric fields and particles to atmospheric emissions. This has led to some referring to the upper atmosphere as a "television screen" for viewing magnetospheric processes.

While not downplaying the importance of this "viewing facility", this article concentrates on the consequences of magnetosphere-atmosphere interactions for the physical conditions of the thermosphere and ionosphere. In particular, we wish to highlight important new considerations concerning the energy balance in the upper atmosphere and the role that coupling between the ionosphere and thermosphere may play in establishing and regulating energy flows and temperatures there. Given the emphasis of this volume on the Cassini/Huygens mission, we will also concentrate on drawing comparisons between Saturn and Jupiter, although other worthwhile comparisons will also be highlighted. In the next two sections, we look at some basic features of the upper atmosphere that will be useful for putting the rest of this chapter in context.

2. Basic Thermospheric Parameters

The thermosphere is the uppermost region of a planet's neutral atmosphere. It is characterised as a region in which the temperature steadily increases with altitude until a maximum (exospheric) limit is reached. Mean free path lengths for thermospheric species are long - sometimes up to hundreds of kilometres - and the mixing of the atmosphere by convection is almost non-existent. The level at which

TABLE I
Key thermospheric parameters for Earth, Jupiter and Saturn

	Earth	**Jupiter**	**Saturn**
Homopause temperature	200 K	200 K	140 K
Homopause pressure	10^{-6} bar	2×10^{-6} bar	1×10^{-7} bar
Homopause density	$3.7 \times 10^{19}\mathrm{m}^{-3}$	$7.3 \times 10^{19}\mathrm{m}^{-3}$	$5.2 \times 10^{18}\mathrm{m}^{-3}$
Homopause scale height[a]	6.0 km	35.7 km	64.5 km
Exospheric temperature	1000 K	940 K	420 K
Exospheric scale height[b]	52.6 km	335.6 km	387.0 km
Critical density	$10^{14}\mathrm{m}^{-3}$	$2.5 \times 10^{13}\mathrm{m}^{-3}$	$2.5 \times 10^{13}\mathrm{m}^{-3}$
Critical pressure	4×10^{-12} bar	10^{-12} bar	10^{-12} bar

[a] Scale height for N_2 for Earth and H_2 for Jupiter and Saturn.
[b] Scale height for O for Earth and H for Jupiter and Saturn.

convective mixing is no longer important is known as the homopause. Above the homopause, atmospheric atomic and molecular species settle out diffusively; each species has its own scale height, H_S, given by:

$$H_S = kT/gm_S \tag{1}$$

where k is Boltzman's constant, T is the thermospheric temperature, g the acceleration due to gravity and m_S is the atomic or molecular weight of species S. At higher altitudes, the thermosphere merges into the exosphere. The base of the exosphere – the *exobase* – is characterised by a critical density, $N_C(S)$, at which the horizontal mean free path of the main thermospheric species, S, is equal to the scale height. $N_C(S)$, is given by:

$$N_C(S) = \left(\pi d_S^2 H_S\right)^{-1} \tag{2}$$

where d_S is the diameter of species S. Some approximate values for key parameters for the Earth, Jupiter and Saturn are compared in Table I.

The above considerations enable more detailed vertical profiles of the thermosphere to be developed. These are shown below for Jupiter (Figure 3; Grodent *et al.*, 2001) and for Saturn (Figure 4; Smith *et al.*, 2004). They show that, except at the very bottom of the thermosphere, where hydrocarbon molecules still have some abundance, the atmosphere is composed mainly of molecular and atomic hydrogen, with helium as a minor species. Diffusive separation ensures that the proportion of H/H_2 increases monotonically with altitude.

To a first approximation, conditions at the homopause are regulated by the balance between the upward convection of heat in the mesosphere and downward conduction of heat in the thermosphere, and the radiation to space of heat from emitting species in the homopause region. More detailed consideration of these

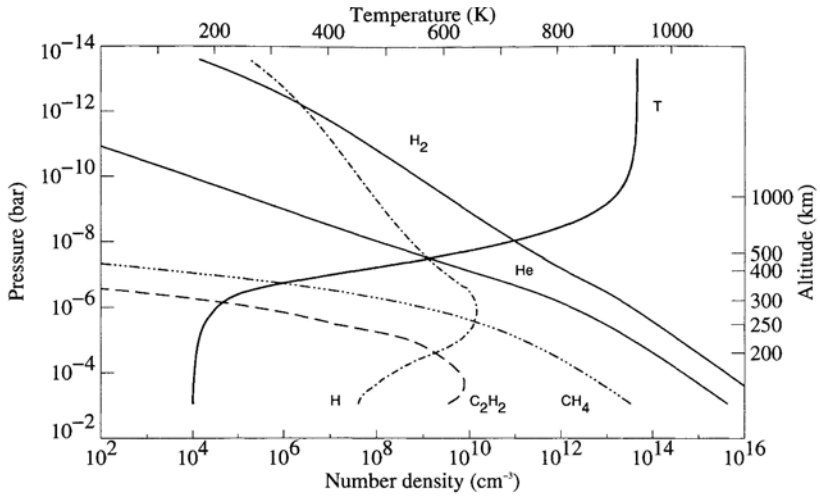

Figure 3. Profile of the composition and temperature profile of the jovian upper atmosphere (from Grodent *et al.*, 2001).

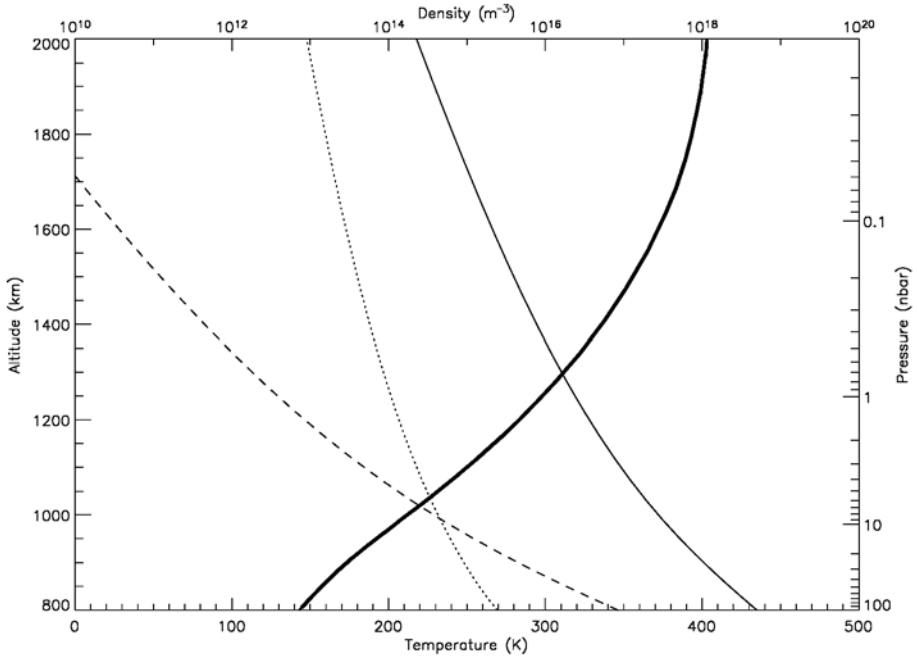

Figure 4. Profile of the composition and temperature profile of the saturnian upper atmosphere (from Smith *et al.*, 2004). *Dark line:* temperature; *light line:* H_2 density; *dashed line:* He density; *dotted line:* H density.

issues can be found in Atreya (1986). In the case of Jupiter, Drossart *et al.* (1993) have shown that hydrocarbons are extremely efficient radiators, emitting some 10^{13} W and controlling the homopause temperature. Above the homopause, the exact temperature profile is determined by a balance between energy inputs as a function of altitude, the downward conduction of heat, and the radiation of heat to space. For Jupiter, this last is due mainly to the efficient radiation of the H_3^+ molecular ion (see Section 3 below; Lam *et al.*, 1997b; Miller *et al.*, 1997; Waite *et al.*, 1997). One key question for all studies of the upper atmospheres of the giant planets is that measured exospheric temperatures are several hundred degrees higher than can be produced by the effects of solar EUV heating alone (Strobel and Smith, 1973; Yelle and Miller, 2004).

3. Basic Ionospheric Considerations

Ionospheres are produced by the impact of ionising radiation and precipitating particles on the neutral atmosphere, and the chemical reactions that ensue. Most of the relevant chemistry for giant planets is summarised in the chapter in this volume by Strobel (2005). More details are given in Waite *et al.* (1983), Majeed and McConnell (1991), and Kim *et al.* (1992). There have also been several reviews, e.g. Atreya (1986), Majeed *et al.* (2004a), Yelle and Miller (2004). Moses and Bass (2000) and Moses *et al.* (2000) have produced an extensive chemical scheme, including all the major reactions involving hydrocarbons, which is particularly appropriate to the lower ionosphere, around and below the homopause. For the purposes of this chapter, however, we shall (mainly) consider only that part of the ionosphere that coexists with the thermosphere. For Jupiter and Saturn that very much simplifies the situation; except at the very bottom of the thermosphere, the chemistry that produces the ionic species is very simple, consisting of reactions between atomic and molecular hydrogen, and helium, and their ionised products. The most important, primary ionisation reactions for the production of the (upper) ionosphere are then:

$$\mathrm{H} + \mathrm{h}\nu/\mathrm{e}^* \rightarrow \mathrm{H}^+ + \mathrm{e}\ (+\mathrm{e}) \quad \text{(I1)}$$

$$\mathrm{H_2} + \mathrm{h}\nu/\mathrm{e}^* \rightarrow \mathrm{H_2^+} + \mathrm{e}\ (+\mathrm{e}) \quad \text{(I2a)}$$

$$\rightarrow \mathrm{H}^+ + \mathrm{H} + \mathrm{e}\ (+\mathrm{e}) \quad \text{(I2b)}$$

$$\mathrm{H_2^+} + \mathrm{H_2} \rightarrow \mathrm{H_3^+} + \mathrm{H} \quad \text{(I3)}$$

$$\mathrm{He} + \mathrm{h}\nu/\mathrm{e}^* \rightarrow \mathrm{He}^+ + \mathrm{e}\ (+\mathrm{e}) \quad \text{(I4)}$$

Reaction I3 follows on so rapidly from reaction I2a that H_2^+ is almost non-existent in the jovian and saturnian ionospheres. The effect is that H_3^+ is the main molecular ion (Figure 5), and – in the auroral regions in particular – can be the major ionospheric species. A further reaction of importance involves charge exchange:

$$\mathrm{H}^+ + \mathrm{H_2}\ (\mathrm{v} \geq 4) \rightarrow \mathrm{H_2^+} + \mathrm{H} \quad \text{(E1)}$$

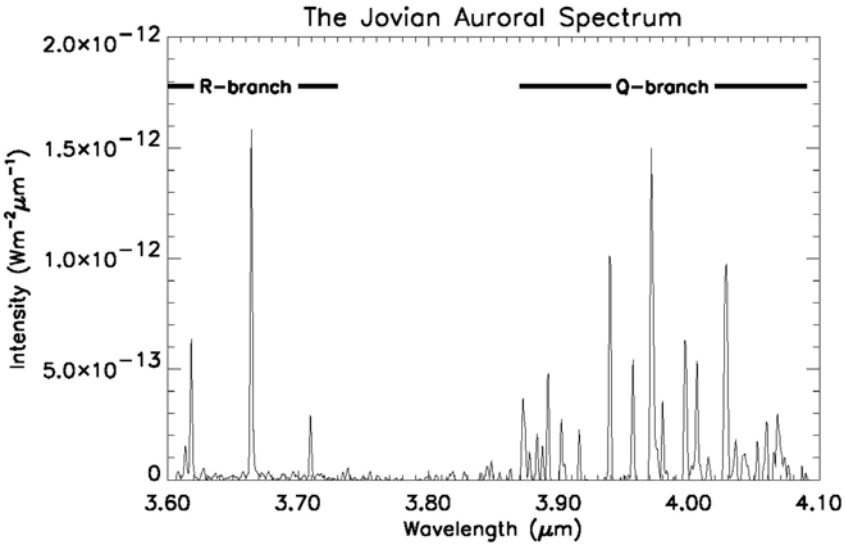

Figure 5. Spectrum of Jupiter's northern aurora in the 3.5 to 4 μm region showing the strong H_3^+ emission (Stallard and Miller, unpublished data).

in which the difference in ionisation energy of H (13.6 eV) and H_2 (15.4 eV) is made up by making use of vibrationally excited molecular hydrogen. Since E1 leads into I3, the net result is to enhance the concentration of H_3^+ at the expense of H^+. Majeed *et al.* (1991) show that this is an important reaction, if levels of vibrationally excited H_2 are overpopulated, compared with what could be expected from LTE, by resonant fluorescence. Unfortunately, the rate of charge exchange for E1 is not well constrained, even to within an order of magnitude (see discussion by Moses and Bass, 2000). Recent work by Moore *et al.* (2004) has shown that this reaction rate can make a large difference to the H^+/H_3^+ balance in the ionosphere. The final component in determining ionospheric concentrations is recombination. For H^+ and He^+, only radiative attachment, the reverse of I1 and I4, is significant:

$$H^+/He^+ + e \rightarrow H/He + h\nu \qquad \text{(R1)}$$

But for H_3^+, as for other (hydrocarbon) molecular ions, dissociative recombination is the main mechanism for re-neutralising the ionosphere:

$$\begin{aligned} H_3^+ + e &\rightarrow H_2 + H \\ &\rightarrow H + H + H \end{aligned} \qquad \text{(R2)}$$

This latter reaction is much faster than R1. The main effect of this is that, while on the dayside the predominant equatorial ion may be H^+ or H_3^+, the predominant nightside ion is H^+, with H_3^+ column densities several times lower. Table II shows typical modelled ion column densities for Jupiter and Saturn, calculated for simple $H/H_2/He$ atmospheres.

TABLE II
Modelled Column Densities of H^+ and H_3^+.

	Equatorial Noon	Equatorial Midnight
Jupiter[a]		
H^+	$5 \times 10^{15} m^{-2}$	$5 \times 10^{15} m^{-2}$
H_3^+	$9 \times 10^{15} m^{-2}$	$2 \times 10^{15} m^{-2}$
Saturn[b]		
H^+	$6 \times 10^{15} m^{-2}$	$6 \times 10^{15} m^{-2}$
H_3^+	$2 \times 10^{15} m^{-2}$	$0.2 \times 10^{15} m^{-2}$

[a] From Achilleos *et al.* (1998).
[b] From Smith *et al.* (2004).

In the auroral regions, where particle precipitation is important, ion column densities are often an order of magnitude greater than those produced by solar EUV ionisation. The altitude at which the maximum numbers of ions are produced depends critically on the individual energy of the incoming particles; the number of ions depends on the number of incoming particles. These effects are shown for Jupiter in Figures 6 and 7 (Millward *et al.*, 2002), for electron energies in the range of $10 - 100$ keV and fluxes of 0.1 to 1000 mW m^{-2}. Reviews of the comparison of model electron and ion density profiles and spacecraft measurements may be found in Atreya (1986) and in Majeed *et al.* (2004a).

The combination of solar EUV ionisation and particle precipitation gives rise to spatial variations in ion column densities. Figure 8 shows that the column density of jovian H_3^+, measured at local noon, varies by more than an order of magnitude between the auroral regions and the equator (Lam *et al.*, 1997b; Miller *et al.*, 1997). The temperature structure is closely correlated with ionospheric variations, since many of the processes associated with ion chemistry are exothermic. However, there can also be heat transport from one region to another that complicates the picture. A jovian temperature map corresponding to Figure 8 is shown in Figure 9. The highest temperatures are to be found in the auroral/polar regions, > 900 K. But then there is a mid-to-low latitude region that is 150 K or more cooler, before the temperature rises again around the equator. The cooling effect of H_3^+ can be obtained from calculating the overall emission, and ranges from a few milliwatts per square metre in the auroral regions to an order of magnitude less at the equator.

4. Auroral and Polar Cap Mechanisms

Bright aurorae are produced when charged particles are accelerated along magnetic field lines and precipitate from the magnetosphere into the upper atmosphere; the

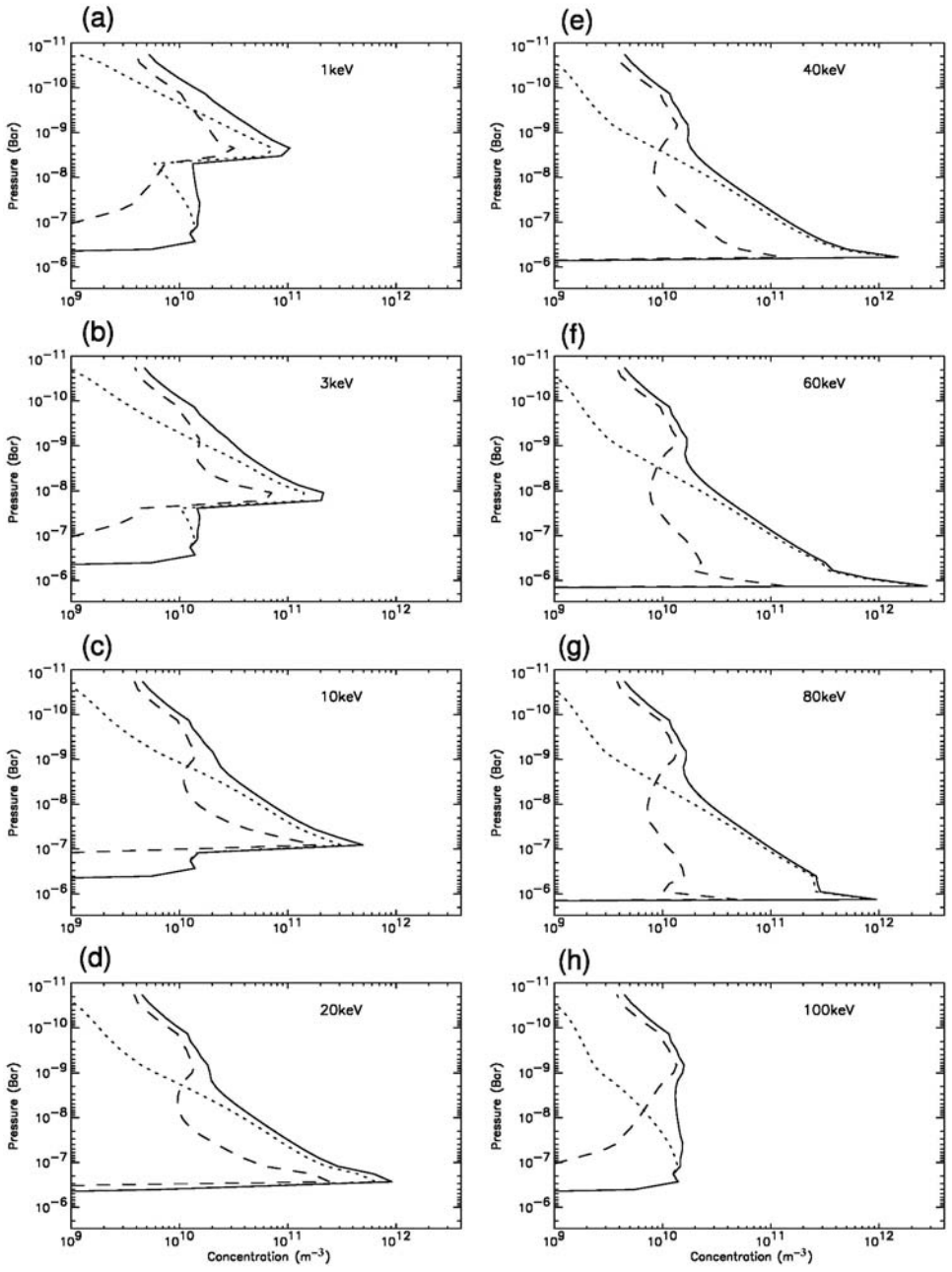

Figure 6. Jovian ion and electron density profiles modelled for a flux of $6.25 \times 10^{12}\text{cm}^{-2}\text{s}^{-1}$ precipitating electrons of various energies. *Full line:* electron density; *dashed line:* H^+ density; *dotted line:* H_3^+ density (from Millward *et al.*, 2002).

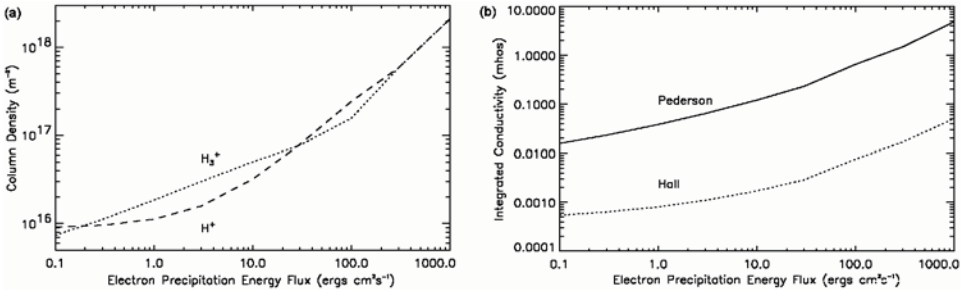

Figure 7. Jovian ion column densities (*top panel*) and conductivities (*lower panel*) modelled for varying total energy fluxes of 10keV electrons (from Millward *et al.*, 2002).

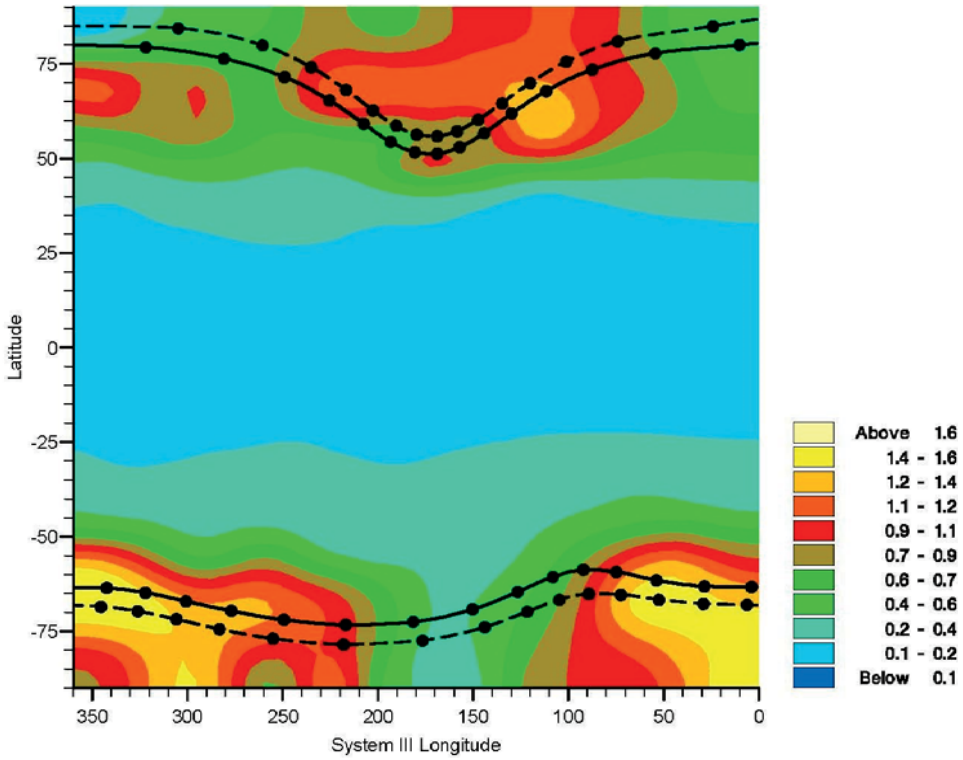

Figure 8. Measured H_3^+ column densities at local noon as a function of location on Jupiter. The units are 10^{12} cm^{-2} (from Lam *et al.*, 1997b).

locations of these aurorae map to the footprints of the fields lines along which the particles have been accelerated. Issues concerning acceleration are dealt with in the chapter by Kivelson (2005), but it is worth considering a few basic points here.

The precipitated particles required to power the Earth's aurorae are equivalent to around 10^{11} W – 10^{12} W (100 GW – 1 TW), and the energy radiated is $\sim$ 1 – 300 GW (see Waite and Lummerzheim, 2002). The main auroral oval on

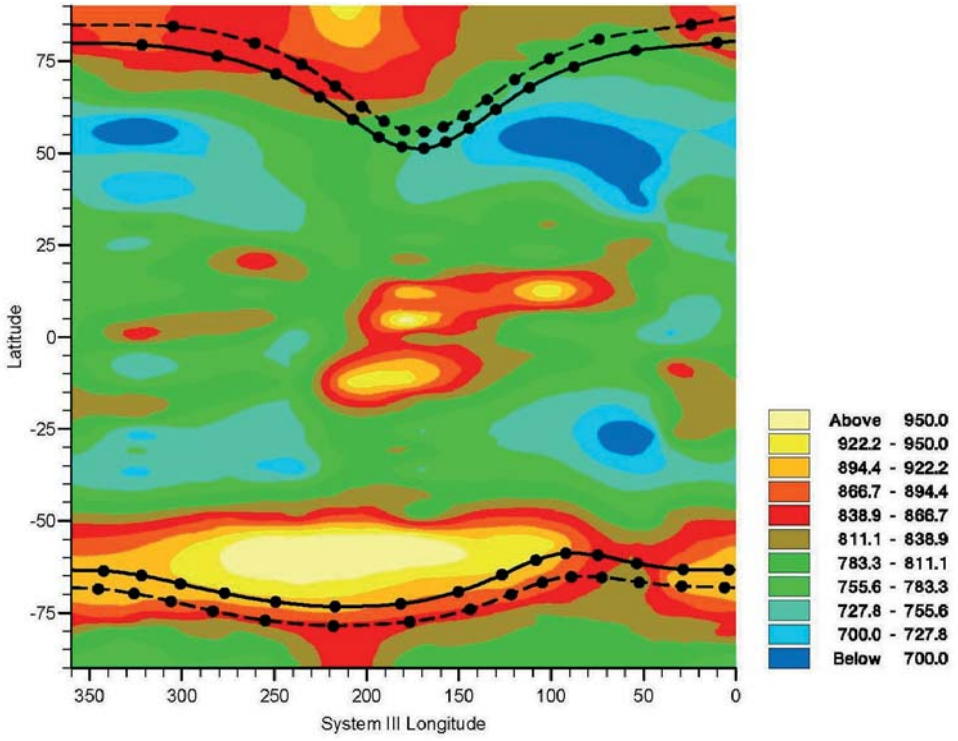

Figure 9. Measured H_3^+ temperatures at local noon as a function of location on Jupiter (from Lam *et al.*, 1997b).

the Earth occurs close to the footprint of the boundary between open and closed magnetic field lines where, in the magnetosphere, currents are generated due to the discontinuity in the flow of plasma. The location of this boundary depends on the solar wind and the interplanetary magnetic field. The main driver of the Earth's aurorae is the interaction with the external medium of the solar wind. In the upper atmosphere, poleward of the main oval – i.e. in the polar cap – field lines are dragged anti-sunward by the solar wind across the poles, returning in the sunward direction along the flanks of the oval. This Dungey cycle (Dungey, 1961) lasts about 3 hours, around an eighth of the Earth's rotation period. The Earth's aurora and polar cap are thus said to be solar wind controlled.

This is not the situation for Jupiter. The innermost Galilean moon, Io, which orbits at 5.9 jovian radii (R_J, $1\,R_J = 71,343$ km) emits about 1 tonne per second from its volcanoes. The neutral gases emitted are initially rotating with the Keplerian orbital period, ≈ 42.5 hours, and are subsequently ionised. The ions so produced are then swept up by Jupiter's magnetic field into an equatorial plasma sheet, which co-rotates with the planet once every 9 hours 55 minutes, and driven centrifugally outwards, a process which requires angular momentum to be transferred from the ionosphere, via a current system. At a radial distance between $\sim\ 20 - 30 R_J$,

corotation begins to break down (Hill, 1979). Field-aligned voltages are generated above the ionosphere that accelerate (mainly) electrons to keV energies along the field lines connecting to the region of corotation breakdown in the plasma sheet, generating the main auroral oval (Cowley and Bunce, 2001; Hill, 2001). Thus the driver for the main auroral oval on Jupiter is internal – the equatorial plasma sheet. Jupiter's aurorae are therefore said to be controlled rotationally, rather than by the solar wind. The energy input of precipitated particles ($\sim 10 - 100$ TW) and the radiated auroral energy ($3 - 10$ TW) are both ~ 100 times greater than the situation for the Earth (Atreya, 1986; Clarke *et al.*, 1987; Waite and Lummerzheim, 2002). Equatorward of the main oval, aurorae due the Galilean moons have been discovered (Connerney *et al.*, 1993, Clarke *et al.*, 1998; 2002; Prangé *et al.*, 1998). Around the magnetic poles, regions equivalent to the Earth's polar cap, i.e. under the control of the solar wind, have been identified (Pallier and Prangé, 2001; Stallard *et al.*, 2003) and analysed (Cowley *et al.*, 2003). Between the main oval and the polar cap, other auroral emissions are seen (see Figures 1a and 2a, and chapter by Kivelson, 2005).

The Voyager 2 spacecraft found auroral emission on Uranus, located around the magnetic poles (Broadfoot *et al.*, 1986; see Herbert and Sandel, 1994, for a full analysis). Unlike Jupiter, however, Uranus does not appear to exhibit localised auroral emission in the H_3^+ infrared (Figure 2b). Instead it has a rather uniform distribution across the disk, peaking at the sub-solar point, with any auroral enhancement probably not more than 20% of the average disk emission (Trafton *et al.*, 1999). As Figure 1b shows, Saturn has a well defined, if variable and non-uniform, auroral oval visible in UV radiation. Until recently, the origin of this oval was unknown. However, recent theoretical work has proposed that it corresponds – as in the case of the Earth – to the closed-open field line boundary (Cowley *et al.*, 2004). Typically, some ~ 100 GW of precipitating electrons are required to produce the ~ 10 GW aurorae, although these may be as feeble as 100×10^6 W (100 MW) on occasions (Trauger *et al.*, 1998). Poleward of the main auroral oval may be flows corresponding to the Dungey cycle, and that predicted by Vasyliunas (1983) (Figure 10). Cowley *et al.* (2004) predict that the Dungey cycle on Saturn takes ≈ 50 hrs, about five times longer than the planetary rotation period.

5. Measurement and Modelling of Ion and Neutral Dynamics

In the past few years there have been significant developments in the measurement and modelling of dynamics in the upper atmospheres of giant planets. In particular, high resolution infrared spectra of Jupiter have revealed the presence of ion winds. These can be driven by magnetospherically generated fields (Rego *et al.*, 1999; Stallard *et al.*, 2001) and by the solar wind (Cowley *et al.*, 2003; Stallard *et al.*, 2003). Three-dimensional modelling, using the Jovian Ionospheric Model (JIM; Achilleos *et al.*, 1998), has demonstrated that such ionospheric flows can couple

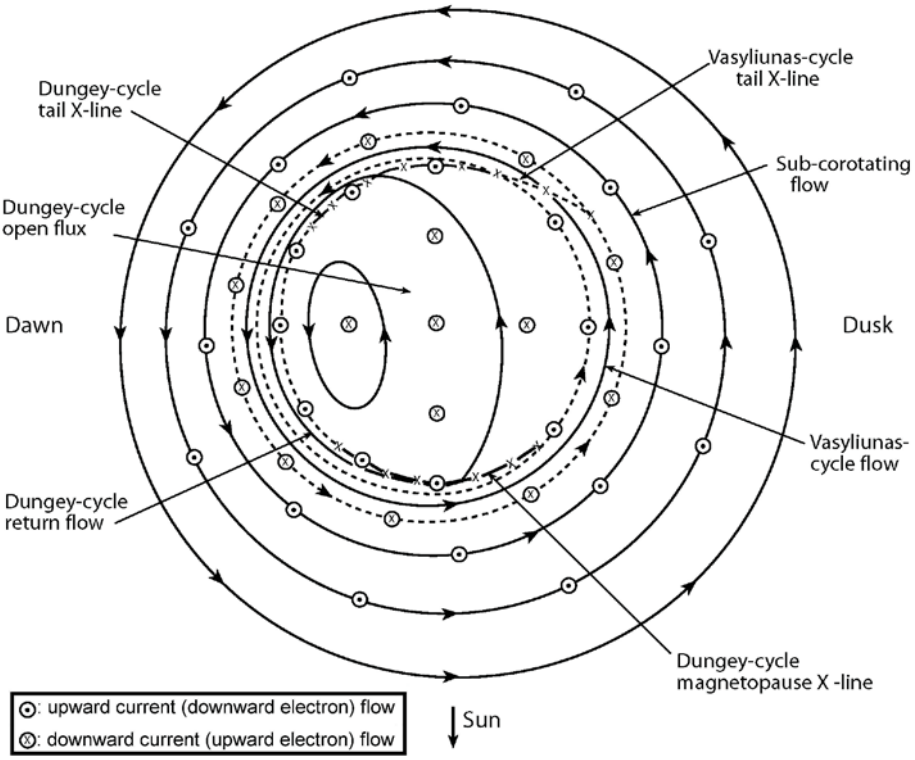

Figure 10. Predicted polar ion flows on Saturn (from Cowley *et al.*, 2004).

to the neutral atmosphere to produce strong wind systems (Millward *et al.*, 2004), which may be responsible for transporting energy from the auroral/polar regions as originally suggested some twenty years ago by Waite *et al.* (1983). Similar results have been obtained using the Jupiter Thermosphere Global Circulation Model of Majeed *et al.* (2004b).

The measurement of ion winds has been achieved by looking at the Doppler shifting of infrared emission from the H_3^+ molecular ion, using NASA's Infrared Telescope Facility and the high-resolution, long-slit spectrometer. Much work has been carried out on Jupiter (Rego *et al.*, 1999; Stallard *et al.*, 2001; 2003) during the time of the Galileo Mission. Figure 11 shows an intensity profile of the $H_3^+ \nu_2 Q(1, 0^-)$ line at 3.953 μm, measured west-east across the auroral oval and polar cap. The profile shows structure corresponding to the auroral oval (Rising and Setting Auroral Oval; RAO and SAO) and regions poleward of that (Dark and Bright Polar Regions; DPR and BPR). It is still unexplained as to why even the DPR still has some 40% of the brightness of the auroral oval when viewed in H_3^+ emission, although this region is very dark when viewed in the UV (Pallier and Prangé, 2001). Figure 12 shows the corresponding line-of-sight (l.o.s.) velocity profiles in the frame of reference that corotates with the planet. It is immedi-

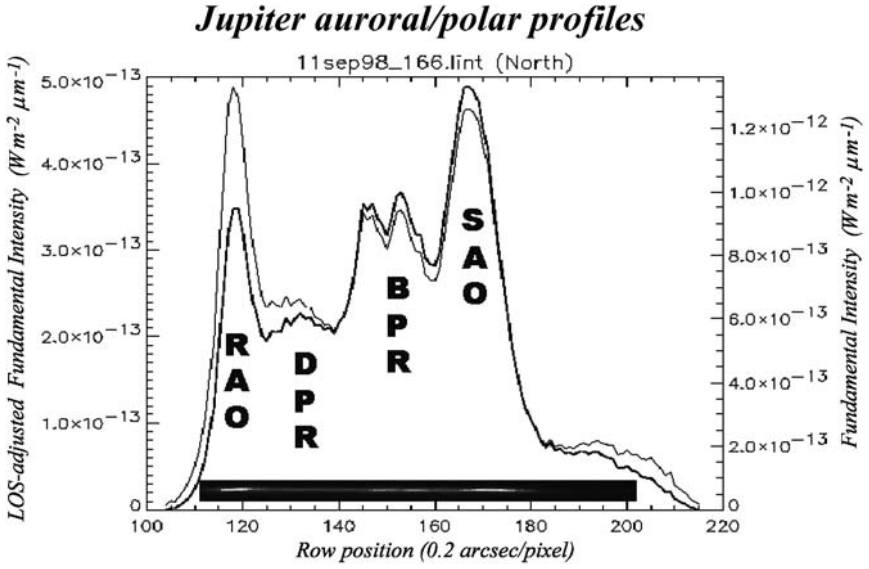

Figure 11. Measured H_3^+ emission profile across the jovian auroral oval (from Stallard *et al.*, 2001). The light line shows the intensity of the 3.953 μm emission as measured; the dark line shows the emission corrected for line-of-sight. RAO: Rising Auroral Oval; DPR: Dark Polar Region; BPR: Bright Polar Region; SAO: Setting Auroral Oval.

ately noticeable that the SAO is blue-shifted and the RAO red-shifted, each by ≈ 1 km s^{-1}. This corresponds to an auroral electrojet with a velocity ≈ 1.5 km s^{-1} flowing (clockwise as viewed from above the north pole) around the auroral oval, counter to the rotation of the planet.

The explanation of this electrojet flows naturally from the Hill (1979) mechanism by which the main auroral oval emission is generated. The electric field, $\mathbf{E}_{\rm eqw}$, that drives the equatorward current through the ionosphere, to close the plasma sheet/field-line/atmosphere circuit, couples with the (near-vertical) jovian auroral magnetic field, $\mathbf{B}_{\rm aur}$, to produce a retrograde Hall ion drift at right angles to both $\mathbf{E}_{\rm eqw}$ and $\mathbf{B}_{\rm aur}$:

$$\mathbf{v}_{\rm ion} = \mathbf{E}_{\rm eqw} \times \mathbf{B}_{\rm aur}/|\mathbf{B}_{\rm aur}|^2 \quad . \tag{3}$$

Since the magnetic field in the auroral regions is $\sim 10^{-3}$ Tesla, a velocity of 1.5 km s^{-1} corresponds to $E_{\rm eqw} \approx 1.5$ V m^{-1}. Higher velocities, up to twice this amount, have also been noted (Rego *et al.*, 1999). Integrated across the width of the auroral oval, which can easily be between 500 km and 1000 km as measured by the H_3^+ intensity profiles, it is clear to see that $V_{\rm eqw}$ – the potential difference generated across the oval by the fields in the plasma sheet – can be of the order of a megavolt or more. Such potential differences are in line with those predicted by theory (Cowley and Bunce, 2001).

Millward *et al.* (2004) have used JIM (Jovian Ionospheric Model; Achilleos *et al.*, 1998) – which is a fully coupled ionosphere-thermosphere global circulation

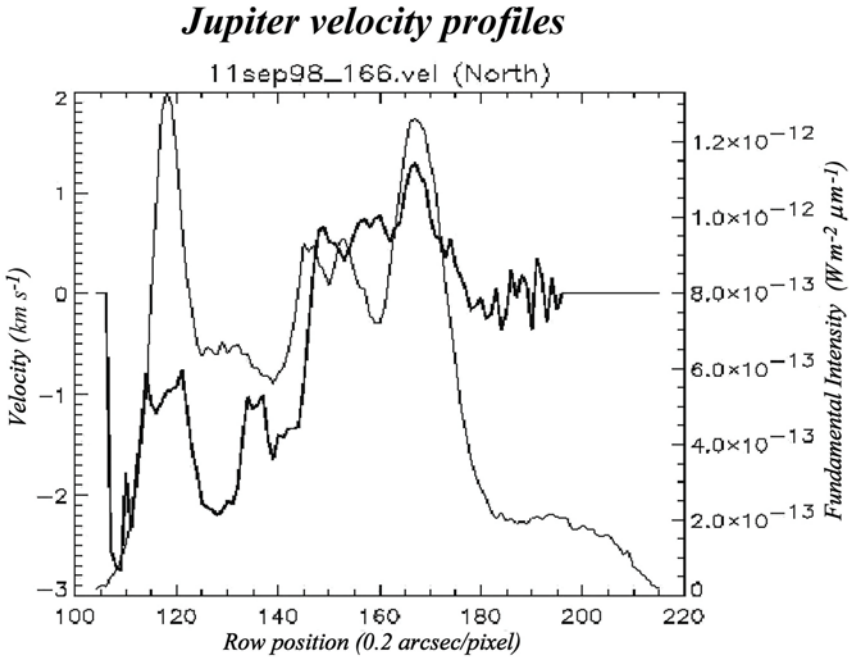

Figure 12. Measured H_3^+ l.o.s. velocity profile across the jovian auroral oval (from Stallard *et al.*, 2001) (*dark line*). The intensity profile (*light line*) is overplotted to aid visualisation. The RAO is red-shifted and the SAO blue-shifted in the planetary reference frame denoting the retrograde auroral electrojet. The strong re-shifting of most of the DPR is consistent with ions that are held near-stationary in the frame of reference that rotates with the magnetic pole (Stallard *et al.*, 2003).

model – to calculate the dynamics of the upper atmosphere under the influence of such equatorward voltages. Coupling to the local magnetic field, electric fields of 2.0 V m^{-1} produce an ion drift of $\approx$ 1.6 km s^{-1} in the rest frame of the planet. At the peak of the ion concentration – around 1 μbar for 60 keV electron precipitation (see Figure 6) – the neutrals are entrained by collisions with ions so efficiently that a neutral wind of $\approx$ 1 km s^{-1} is produced. For smaller voltages, e.g. 0.6 V m^{-1}, the Hall drift is around 500 m s^{-1} and the neutral wind $\approx$ 350 m s^{-1}. A parameter $K(h)$ may be defined such that:

$$K(h) = |v_{\text{neut}}(h)/v_{\text{ion}}(h)| \tag{4}$$

for any altitude, h (Huang and Hill, 1989). $K(h)$ thus represents the fraction of the ion velocity, in the planetary reference frame, that is acquired by the neutrals via ion-neutral collisions. For the upper atmosphere, where eddy diffusion is almost negligible, JIM results show that $K(h)$ peaks strongly at the level that the ion density peaks, with a value of 0.5 or greater. This parameter is used by Cowley and Bunce (2001) in a height-independent form to modify the height-integrated

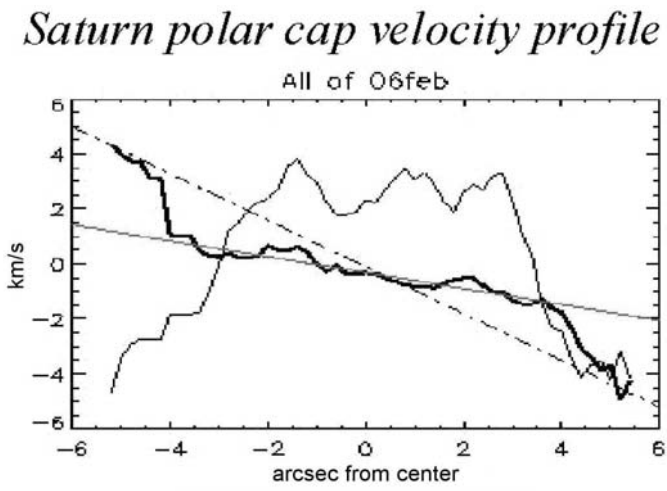

Figure 13. Measured H_3^+ l.o.s. velocity profile across the saturnian auroral oval (from Stallard *et al.*, 2001) (*dark line*) in the inertial reference frame. The intensity profile (*light line*) is overplotted to aid visualisation. The dash-dot line shows the line of corotation with the planet; the red line shows the best straight line fit to the measured velocity profile, only 0.34 of the planetary angular velocity.

Pedersen conductivity of the ionosphere, to allow for the relative motions of ions in the rest frame of the neutral atmosphere in which they are located by:

$$\Sigma_P^* = (1 - K)\Sigma_P \ . \tag{5}$$

With a view to the Cassini Mission, Stallard *et al.* (2004) have recently extended their technique for measuring ion winds on Jupiter to Saturn. Unfortunately, Saturn's auroral emissions – in both UV and IR (H_3^+) – are only a few percent of those of Jupiter. For high resolution IR spectroscopy, this means that exposure times for Saturn are ≈ 1 hour, or more, compared with ≈ 1 minute for Jupiter. Such long exposure times would not be feasible for Jupiter, because of the large offset of the magnetic and rotational poles: auroral intensity and velocity features would be "smeared out" by the rotation of the planet ($\approx 0.6°$ of longitude per minute, or 36° in an hour) to such an extent as to defy analysis. Fortunately, the magnetic and rotational poles of Saturn are near-coincident, and average parameters may still be obtained from hour-long exposures, without longitudinal smearing being too problematic.

Figure 13 shows the velocity profile of Saturn obtained in 2003. This led Stallard *et al.* (2004) – independently – to the same conclusion that Cowley *et al.* (2004) had reached from theoretical considerations: the polar cap region of Saturn is largely under solar wind control, causing the ions there to rotate much more slowly than the planet (in the Sun-Saturn reference frame). The measured average angular velocity of the polar cap ionosphere was $0.34\Omega_S$, where Ω_S is the angular velocity of Saturn, compared with a theoretical prediction of $0.24\Omega_S$. The interpretation of these ion winds is that an equatorward field is imposed by the tendency of

TABLE III
Comparison of predicted and measured exospheric temperatures.

	Jupiter	**Saturn**	**Uranus**	**Neptune**
Heliocentric distance (AU)	5.20	9.57	19.19	30.07
Absorbed solar flux (W m^{-2})	3.7×10^{-5}	1.1×10^{-5}	2.7×10^{-6}	1.1×10^{-6}
T_{exo} (observed) [K]	940	420	800	600
T_{exo} (calculated) [K]	203	177	138	132
ΔT_{exo} (obs-calc) [K]	737	243	662	468

the solar wind to sweep open field lines down the magnetotail, and prevent them rotating with the planet. At the edge of the polar cap, which extends to a colatitude of $\approx 15°$, the ion wind is ≈ 1.7 km s^{-1}. With Saturn's auroral magnetic field being $\approx 6.5 \times 10^{-5}$ Tesla (Cowley *et al.*, 2004), Equation (3) gives the field strength ≈ 0.1 V m^{-1}. Cowley *et al.* (2004) also relate the measured ion angular velocity to the solar wind velocity and the effective Pedersen conductivity:

$$\Omega_{ion} = \Omega_S \mu_0 \Sigma_P^* V_{SW} / \left[1 + \mu_0 \Sigma_P^* V_{SW}\right] \tag{6}$$

where μ_0 is the permeability of free space, and V_{SW} is the solar wind velocity. This important relationship, first derived by Isbell *et al.* (1984), holds out the prospect of correlating the measured ion velocities with Cassini measurements of the solar wind velocity, and thereby measuring conductivities, which can be modelled to derive particle precipitation fluxes. Alternatively, in the absence of available spacecraft data, the measured values of Ω_{ion} may be used, with modelled conductivities, to obtain values of V_{SW}.

6. Energy Considerations

Yelle and Miller (2004) have recently compared the measured exospheric temperatures of the giant planets with those calculated from solar EUV inputs alone. Globally, the solar EUV absorbed at Jupiter is ≈ 2.4 TW, while at Saturn it is ≈ 0.5 TW. Table III shows that considerable additional energy sources are required to produce the observed temperatures.

Particle precipitation in Jupiter's auroral/polar regions is estimated to provide an additional 10 to 100 TW (Clarke *et al.*, 1987), a considerable increase on the solar EUV input, although a large fraction of that may be deposited below the homopause, from where much of the UV auroral radiation emanates; below the homopause – as already noted – hydrocarbons radiate away the energy very efficiently (Drossart *et al.*, 1993). That means that the actual direct energy input into the upper atmosphere (above the homopause) is probably less than 10 TW globally. Grodent

et al. (2001) have produced a 1-dimensional self-consistent model of the jovian upper atmosphere from 20 mbar – i.e. below the homopause – to 10^{-13} bar, well into the lower exosphere (see Figure 3). Their model requires $\approx 3 \times 10^{-2}$ W m^{-2} to produce an auroral temperature profile consistent with UV and IR observations and the low latitude temperature profile measured by the Galileo probe (Seiff *et al.*, 1998). The energy, in the form of keV electrons for the most part, has to be deposited at various altitudes in order to produce the correct temperature profiles. If one approximates the jovian auroral oval to a circle at co-latitude 15° and 500 km wide, the Grodent *et al.* inputs correspond to $3 - 4$ TW globally. There is probably a similar amount from what they term "diffuse aurora", found (mainly) poleward of the main auroral oval.

To produce the high temperatures measured globally, Waite *et al.* (1983) proposed that thermally driven winds could distribute the large amounts of energy deposited in the auroral regions. But such winds have powerful Coriolis forces to overcome as a result of Jupiter's rapid rotation. A solution to the "energy gap" that may be available globally is breaking waves, generated in the lower atmosphere and depositing their energy in the thermosphere (Young *et al.*, 1997). Matcheva and Strobel (1999), however, have questioned whether waves can deposit enough energy to account for the high jovian thermospheric temperatures measured by the Galileo probe (Seiff *et al.*, 1998), and there are even claims that gravity waves may actually cool the upper atmosphere (Hickey *et al.*, 2000). The situation for Saturn, with respect to wave propagation from the lower atmosphere, is currently unclear. But, without identifying what the source of heating is, Mueller-Wodarg *et al.* (2004) have shown that a global energy input to the lower thermosphere of Saturn can increase the exospheric temperature from the ≈ 180 K predicted from solar heating alone to ≈ 410 K, in close agreement with the measurements of Smith *et al.* (1983).

There is some evidence from UV (Feldman *et al.*, 1993), IR (Miller *et al.*, 1997; Rego *et al.*, 2000) and X-ray (Waite *et al.*, 1997) emissions from Jupiter that particle precipitation occurs equatorward of the jovian auroral regions to latitudes as low as 20°, or even to the equator. Such low latitude particle precipitation has been modelled recently by Abel and Thorne (2003) for relativistic particles; they find that IR emission patterns in the northern hemisphere are fairly well reproduced by their model. Such precipitation would heat the atmosphere outside of the auroral regions, and it is worth noting that Grodent *et al.* (2001) require a low energy electron "drizzle" to keep their upper thermospheric temperatures in agreement with the Galileo probe profile. On the other hand, Liu and Dalgarno (1996) modelled the equatorial UV dayglow from Jupiter (Feldman *et al.*, 1993) and found that solar EUV radiation alone could generate the observed spectrum, without the need for additional excitation, such as would be produced by particle precipitation. Planetwide precipitation is probably required to produce the distribution of H_3^+ emission (Figure 2b) observed on Uranus (Trafton *et al.*, 1999). Theoretical

considerations also indicate that low-intensity particle precipitation may occur on Saturn at latitudes lower than the main auroral oval (Cowley *et al.*, 2004).

However, there are two other sources of energy that may be produced within the upper atmosphere, above the homopause, close to the ionisation peak, which would not generate additional UV radiation: Joule heating and "frictional" heating. These are not readily incorporated into 1-D models such as that of Grodent *et al.* (2001).

Joule heating is generated by the passage of currents in the ionosphere. An early attempt to quantify its significance was carried out by Heaps (1975), who concluded that it was less important for Jupiter than for the Earth. However, these calculations were based on relatively low values of electric fields and ionospheric conductivity, more suitable to non-auroral latitudes. The amount of heating produced in the jovian auroral oval by the equatorward electric field discussed above is given by:

$$H_{\mathrm{J}} = |(1-K)E_{\mathrm{eqw}}|^2\,\Sigma_{\mathrm{P}}\,A_{\mathrm{oval}} \tag{7}$$

where A_{oval} is the area of the oval, and the factor $(1-K)$ is required to calculate the Joule heating produced by the current flowing in the rest frame of the neutral atmosphere. Millward *et al.* (2002; 2004) have shown that plausible electron fluxes produce values of Σ_{P} of 1-8 mho. Approximating the oval as before – which gives $A_{\mathrm{oval}} = 5.7 \times 10^{13}$ m^2 – and taking E_{eqw} to be 1.5 V m^{-1} in the planetary rest frame and $K = 0.5$ (Millward *et al.*, 2004), Joule heating can be seen to produce 130 TW per hemisphere for $\Sigma_{\mathrm{P}} = 4$ mho. This is about 200 times more than that first considered by Heaps (1975). (Note that in calculating this figure we have not taken into account any Joule heating produced poleward of the auroral oval by the fields that must exist there to produce the observed ion flows.)

It is possible to carry out a similar calculation for the auroral/polar regions of Saturn, making use of the measured magnetic field and ion lag to corotation, and estimating the effective conductivity. Approximating the auroral oval to a circle centred on the rotational pole with a co-latitude of 15°, we have:

$$\begin{aligned} H_{\mathrm{J}} &= \int_0^{R_{\mathrm{oval}}} |(1-K)E_{\mathrm{eqw}}(r)|^2 \Sigma_{\mathrm{P}} 2\pi r \mathrm{d}r = \int_0^{R_{\mathrm{oval}}} |(1-K)Bv_{\mathrm{ion}}(r)|^2 \Sigma_{\mathrm{P}} 2\pi r \mathrm{d}r \\ &= \int_0^{R_{\mathrm{oval}}} |(1-K)B\Omega_{\mathrm{ion}} r|^2\,\Sigma_{\mathrm{P}}\,2\pi r \mathrm{d}r = \frac{\pi}{2}|(1-K)B\Omega_{\mathrm{ion}}|^2\,\Sigma_{\mathrm{P}}\,R_{\mathrm{oval}}^4 \end{aligned} \tag{8}$$

where we have assumed that B, Ω_{ion} and Σ_{P} are constant across the polar cap, and R_{oval} is $R_S \sin(15°)$ ($R_S = 60,268$ km). For the measured ion angular velocity, and assuming $B = 6.5 \times 10^{-5}$ T and $\Sigma_{\mathrm{P}} = 1$ mho, we have $H_{\mathrm{J}} \approx 4$ TW in each hemisphere, if $K = 0.1$. This is similar to the value calculated by Cowley *et al.* (2004), using a more sophisticated model of the magnetic field and plasma flows. (Note values of K have not been modelled for Saturn yet, and this low value is taken since the degree of ionisation in the saturnian ionosphere is lower than for Jupiter.)

Modelling the effects of ion-neutral collisions has shown that, while the ions respond immediately to the imposition of an equatorward electric field, neutrals take $\sim$ 1000 s to reach their terminal velocity, and a similar time to decelerate when the field is removed (Miller *et al.*, 2000; Millward *et al.*, 2004). This prompted Miller *et al.* (2000) to ask whether the mechanical (kinetic) energy stored up in large-scale neutral wind flows could also provide a source of energy for heating the upper atmosphere, via some sort of "frictional" effect. For Jupiter, the total kinetic energy in the auroral oval is given by:

$$\text{K.E.} = \frac{1}{2} m_{\text{oval}} v_{\text{neut}}^2 = \frac{1}{2} A_{\text{oval}} \rho_{\text{air}} (K v_{\text{ion}})^2 \tag{9}$$

where ρ_{air} is the column mass of jovian air above the ion peak, which is 4×10^{-2} kg m^{-2}, for ion peak produced by 60keV electron precipitation. Using the parameters given above, and $K = 0.5$, we get K.E. $= 5.7 \times 10^{17}$ Joules per hemisphere. The half-life of 1000 s for neutrals to accelerate and decelerate suggests that this could provide $\approx$300 TW per hemisphere, if all of the energy dissipated ended up as heat. For Saturn's polar cap the kinetic energy is given by:

$$\text{K.E.} = \frac{1}{2} \int_0^{R_{\text{oval}}} 2\pi r \rho_{\text{air}} (r \Omega_{\text{ion}} K)^2 \, \mathrm{d}r = \frac{1}{4} \pi \rho_{\text{air}} \Omega_{\text{ion}}^2 R_{\text{oval}}^4 K^2 \quad . \tag{10}$$

Taking ρ_{air} as 10^{-3} kg m^{-2} for Saturn and the parameters used previously, we have K.E. $= 5.5 \times 10^{17} \times K^2$ J per hemisphere. Taking again $K = 0.1$, one would have K.E. $= 5.5 \times 10^{15}$ J per hemisphere. This could produce – using arguments similar to those used for Jupiter above – a contribution of 3 TW per hemisphere of additional energy.

Recent calculations using JIM have demonstrated that ion-neutral coupling in Jupiter's auroral oval can generate waves that transport energy to low latitudes. These are shown in Figure 14, for a model run in which the equatorward potential difference across the auroral oval was set to 3 MV, equivalent to $\approx$0.6 V m^{-1}. Smith *et al.* (2004) have modelled the effect of putting energy into the polar cap of Saturn at various altitudes. They take into account the measured temperatures of $350 - 500$ K at the ion peak in the auroral/polar region (Melin *et al.*, 2004) and the equatorial exospheric temperature of 420 K (Smith *et al.*, 1983). They find that a few TW input at the ion peak can produce heating of the entire thermosphere to give the measured equatorial exospheric temperature, as a result of conduction and adiabatic heating. The latitudinal temperature profile is similar to that measured for Jupiter (Lam *et al.*, 1997b; Miller *et al.*, 1997). Thus auroral/polar heating, produced by Joule heating or "frictionally", may well heat the entire upper atmosphere for Jupiter and Saturn.

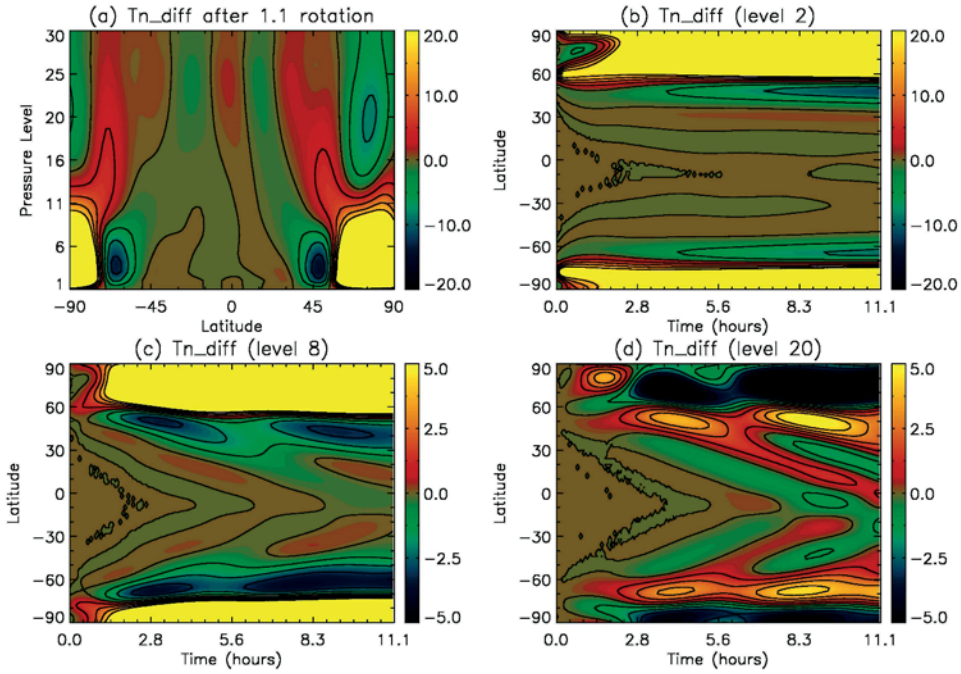

Figure 14. JIM prediction of planet-wide temperature waves generated by the coupling between accelerated ions in the auroral oval and the co-existing thermosphere, as a function of pressure level (*top left*) and time. The plots show the difference between a run carried out with a 3 MV potential difference across the auroral oval (≈ 0.6 V m^{-1}) and one with no p.d. For JIM, Pressure Level 1, $P(1)$, corresponds to 2 mbar, and the models runs on a logarithmic pressure scale such that $P(n) = P(1)\exp[-0.4(n-1)]$. This gives $P(2) = 1.34$ mbar, $P(8) = 0.12$ mbar, and $P(20) = 1.00$ nbar.

7. Conclusions

This brief overview of the upper atmospheres of Jupiter and Saturn shows that, while much has been learned in recent years, there are many outstanding issues for both planets (as for all of the outer planets). One area of great interest is the role of the solar wind in determining the strength and morphology of auroral features in the giant planets – in Jupiter's case, inside the main oval in the polar cap, and for Saturn, the main oval itself. This area of research has been given more impetus with the discovery of a solar wind modulation of Jupiter's radio emission (Gurnett *et al.*, 2002). During the Cassini mission, work on the upper atmosphere of the planet can be tied into the *in situ* magnetospheric and solar wind measurements of the spacecraft. That will enable us to test the empirical relationships developed by Cowley and others. The availability both of observational data and modelling results means that many of the questions of ion-neutral coupling and the dynamics that engenders in the upper atmosphere, which we have only touched on in this chapter, can be investigated in detail. These studies can lead to a situation where

we can understand all of the factors, involved in the atmospheric energy balance, that go into determining the high exospheric temperatures of the giant planets. It may also be that progress can be made in reconciling observed electron profiles and those produced by models.

Acknowledgements

Global circulation model calculations for Jupiter and Saturn referred to in this chapter were carried out using the Miracle High Performance Computer Suite, which is part of the HiPerSPACE Centre at UCL, and funded by the UK Particle Physics and Astronomy Research Council. PPARC is also thanked for supporting the authors in various ways. Miller was a Visiting Astronomer at the IRTF, which is operated for NASA by the Institute for Astronomy, University of Hawaii.

References

Abel, B. and Thorne, R.M.: 2003, 'Relativistic charged particle precipitation into Jupiter's sub-auroral atmosphere', *Icarus* **166**, 311–319.

Achilleos, N., Miller, S., Tennyson, J., Aylward, A.D., Mueller-Wodarg, I., and Rees, D.: 1998, 'JIM: a time-dependent, three-dimensional model of Jupiter's thermosphere and ioniosphere', *J. Geophys. Res.* **103**, 20089–20112.

Atreya, S.K.: 1986, *The Atmosphere and Ionospheres of the Outer Planets and Their Satellites*, Springer Verlag, New York.

Ballester, G.E., and 21 other colleagues: 1998, 'Time-resolved observations of Jupiter's far ultraviolet auroras', *Science* **274**, 409–413.

Baron, R., Joseph, R.D., Owen, T., Tennyson, J., Miller, S., and Ballester, G.E.: 1991, 'Imaging Jupiter's aurorae from H_3^+ emissions in the 3–4 mm band', *Nature* **353**, 539–542.

Bhardwaj, A. and Gladstone, G.R.: 2000, 'Auroral emissions of the giant planets', *Rev. Geophys.* **38**, 295–353.

Broadfoot, A.L., and 18 others: 1986, 'Ultraviolet spectrometer observations of Uranus', *Science* **233**, 74–79.

Clarke, J.T., Caldwell, J., Skinner, T., and Yelle, R.: 1987, 'The aurora and airglow of Jupiter', *in* M.J.S. Belton, R.A. West, and J. Rahe (eds.), *Time Variable Phenomena in the Jovian System* NASA, Washington, pp. 211–228.

Clarke, J.T., and 10 co-workers: 1998, 'Hubble Space Telescope imaging of Jupiter's UV aurora during the Galileo orbiter mission', *J. Geophys. Res.* **103**, 20217–20236.

Clarke, J.T., and 11 co-workers: 2002, 'Ultraviolet emissions from the magnetic footprints of Io, Ganymede and Europa on Jupiter', *Nature* **415**, 997–1000.

Connerney, J.E.P., Baron, R., Satoh, T., and Owen, T.: 1993, 'Images of excited H_3^+ at the foot of the Io flux tube in Jupiter's atmosphere', *Science* **262**, 1035–1038.

Cowley, S.W.H. and Bunce, E.J.: 2001, 'Origin of the main auroral oval in Jupiter's coupled magnetosphere-ionosphere system', *Planet. Space Sci.* **49**, 1067–1088.

Cowley, S.W.H., Bunce, E.J., Stallard, T.S., and Miller, S.: 2003, 'Jupiter's polar ionospheric flows: theoretical interpretation', *Geophys. Res. Lett.* **30**, 1220.

Cowley, S.W.H., Bunce, E.J., and Prangé, R.: 2004, 'Saturn's polar ionospheric flows and their relation to the main auroral oval', *Ann. Geophysicae* **22**, 1379.

Drossart, P., Bézard, B., Atreya, S.K., Bishop, J., and Waite, J.H., Jr., and Boice, D.: 1993, 'Thermal profiles in the auroral regions of Jupiter', *J. Geophys. Res.* **98**, 18803–18810.

Dungey, J.W.: 1961, 'The interplanetary magnetic field and auroral zones', *Phys. Rev. Lett.* **6**, 47.

Feldman, P.D., McGrath, M.A., Moos, H.W., Durrance, S.T., Strobel, D.F., and Davidson, A.F.: 1993, 'The spectrum of the jovian dayglow observed at a 3A resolution with the Hopkins Ultraviolet Telescope', *Astrophys. J.* **406**, 279–284.

Gérard, J.-C., Dols, V., Grodent, D., Waite, J.H., Jr., and Prangé, R.: 1995, 'Simultaneous observations of the saturnian aurora and polar haze with the HST/FOC', *Geophys. Res. Lett.* **22**, 2685–2688.

Grodent, D., Waite, J.H., Jr., and Gérard, J.-C.: 2001, 'A self-consistent model of the jovian auroral thermal structure', *J. Geophys. Res.* **106**, 12933–12952.

Grodent, D., Clarke, J.T., Kim, J., Waite, J.H., Jr., and Cowley, S.W.H.: 2003, 'Jupiter's main auroral oval observed with HST-STIS', *J. Geophys. Res.* **108**, 9921–9937.

Gurnett, D.A., and 16 co-workers: 2002, 'Control of Jupiter's radio emission and aurorae by the solar wind', *Nature* **415**, 985–987.

Heaps, M.G.: 1975, 'The roles of particle precipitation and Joule heating in the energy balance of the jovian thermosphere', *Icarus* **29**, 273–281.

Herbert, F. and Sandel, B.R.: 1994, 'The uranian aurora and its relationship to the magnetosphere', *J. Geophys. Res.* **99**, 4143–4160.

Hickey, M.P., Walterscheid, R.L., and Schubert, G.: 2000, 'Gravity wave heating and cooling in Jupiter's thermosphere', *Icarus* **148**, 266–281.

Hill, T.W.: 1979, 'Inertial limit on corotation', *J. Geophys. Res.* **84**, 6554–6558.

Hill, T.W.: 2001, 'The jovian auroral oval', *J. Geophys. Res.* **106**, 8101–8107.

Hill, T.W. and Dessler, A.J.: 1991, 'Plasma motions in planetary magnetospheres', *Science* **252**, 410–415.

Huang, T.S. and Hill, T.W.: 1989, 'Corotation lag of the jovian atmosphere, ionosphere and magnetosphere', *J. Geophys. Res.* **94**, 3761–3765.

Isbell, J., Dessler, A.J., and Waite, J.H., Jr.: 1984, 'Magnetospheric energization by interaction between planetary spin and solar wind', *J. Geophys. Res.* **89**, 10716–10722.

Kim, Y.H., Fox, J.L., and Porter, H.S.: 1992, 'Densities and vibrational distribution of H_3^+ in the jovian auroral ionosphere', *J. Geophys. Res.* **97**, 6093–6101.

Kivelson, M.G., and 13 colleagues: 1997, 'Galileo at Jupiter: changing states of the magnetosphere and first look at Io and Ganymede', *Adv. Space Res.* **20**, 129.

Kivelson, M.G.: 2005, 'The current systems of the jovian magnetosphere and ionosphere and predictions for Saturn', this volume.

Lam, H.A., Miller, S., Joseph, R.D., Geballe, T.R., Trafton, L.M., Tennyson, J., and Ballester, G.E.: 1997a, 'Variation in the H_3^+ emission of Uranus', *Astrophys. J.* **474**, L73–L76.

Lam, H.A., Achilleos, N., Miller, S., Tennyson, J., Trafton, L.M., Geballe, T.R., and Ballester, G.E.: 1997b, 'A baseline spectroscopic study of the infrared auroras of Jupiter', *Icarus* **127**, 379–393.

Liu, W. and Dalgarno, A.: 1996, 'The ultraviolet spectrum of the jovian dayglow', *Astrophys. J.* **462**, 502–518.

Majeed, T. and McConnell, J.C.: 1991, 'The upper ionospheres of Jupiter and Saturn', *Planet. Space Sci.* **39**, 1715–1732.

Majeed, T., McConnell, J.C., and Yelle, R.V.: 1991, 'Vibrationally excited H_2 in the outer planets thermosphere: fluorescence in the Lyman and Werner bands', *Planet. Space Sci.* **39**, 1591–1605.

Majeed, T., Waite, J.H., Jr., Bougher, S.W., Yelle, R.V., Gladstone, G.R., McConnell, J.C., and Bhardwaj, A.: 2004a, 'The ionospheres-thermospheres of the giant planets', *Adv. Space Res.* **33**, 197–211.

Majeed, T., Waite, J.H., Bougher, S.W., and Gladstone, G.R.: 2004b, 'Jupiter thermosphere general circulation model I. Equatorial thermal structure', *J. Geophys. Res.*, submitted.

Matcheva, K.I. and Strobel, D.F.: 1999, 'Heating of Jupiter's thermosphere by dissipation of gravity waves due to molecular viscosity and heat conduction', *Icarus* **140**, 328–340.

Melin, H., Stallard, T., and Miller, S.: 2004, 'A new determination of Saturn's upper atmospheric temperature in the auroral/polar region', *Astrophys. J. Lett.*, in preparation.

Miller, S., Achilleos, N., Ballester, G.E., Lam, H.A., Tennyson, J., Geballe, T.R., and Trafton, L.M.: 1997, 'Mid-to-low latitude H_3^+ emission from Jupiter', *Icarus* **130**, 57–67.

Miller, S., and 10 other colleagues: 2000, 'The role of H_3^+ in planetary atmospheres', *Phil. Trans. Roy. Soc.* **358**, 2485–2502.

Millward, G., Miller, S., Stallard, T., Aylward, A.D., and Achilleos, N.: 2002, 'On the dynamics of the jovian ionosphere and thermosphere III: the modelling of auroral conductivity', *Icarus* **160**, 95–107.

Millward, G., Miller, S., Stallard, T., Achilleos, N., and Aywlard, A.D.: 2004, 'On the dynamics of the jovian ionosphere and thermosphere IV: ion-neutral coupling', *Icarus*, in press.

Moore, L., Mendillo, M., Mueller-Wodarg, I., and Murr, D.: 2004, 'Photochemical modelling of global variations and ring shadowing in Saturn's ionosphere', *Icarus*, submitted.

Moses, J.I. and Bass, S.F.: 2000, 'The effects of external material on the chemistry and structure of Saturn's ionosphere', *J. Geophys. Res.* **105**, 7013–7052.

Moses, J.I., Bézard, B., Lellouch, E., Gladstone, G.R., Feuchtgruber, H., and Allen, M.: 2000, 'Photochemistry of Saturn's atmosphere I. Hydrocarbon chemistry and comparisons with ISO observations', *Icarus* **143**, 244–298.

Mueller-Wodarg, I.C.F., Mendillo, M., Yelle, R.V., and Aylward, A.D.: 2004, 'A global circulation model of Saturn's thermosphere', *Icarus*, in press.

Pallier, L. and Prangé, R.: 2001, 'More about the structure of the high latitude jovian aurorae', *Planet. Space Sci.* **49**, 1159–1173.

Prangé, R., Rego, D., Pallier, L., Connerney, J.E.P., Zarka, P., and Quenniec, J.: 1998, 'Detailed study of FUV jovian auroral features with the post-COSTAR HST faint object camera', *J. Geophys. Res.* **103**, 20195–20215.

Pryor, W.R., Stewart, A.I.F., Simmons, K.E., Ajello, J.M., Tobiska, W.K., Clarke, J.T., and Gladstone, G.R.: 2001, 'Detection of rapdily varying H_2 emissions in Jupiter's aurora from the Galileo orbiter', *Icarus* **151**, 314–317.

Rego, D., Achilleos, N., Stallard, T., Miller, S., Prangé, R., Dougherty, M., and Joseph, R.D.: 1999, 'Supersonic winds in Jupiter's aurorae', *Nature* **399**, 121–124.

Rego, D., Miller, S., Achilleos, N., Prangé, R., and Joseph, R.D.: 2000, 'Latitudinal profiles of the jovian IR emission of H_3^+ at 4 microns using the NASA Infrared Telescope Facility', *Icarus* **147**, 366–385.

Satoh, T., Connerney, J.E.P., and Baron, R.L.: 1996, 'Emission source model of Jupiter's H_3^+ aurorae: a generalised inverse analysis of images', *Icarus* **122**, 1–23.

Satoh, T. and Connerney, J.E.P.: 1999, 'Jupiter's H_3^+ emissions viewed in corrected jovimagnetic coordinates', *Icarus* **141**, 236–252.

Seiff, A., and 10 co-workers: 1998, 'Thermal structure of Jupiter's atmosphere near the edge of a 5-mm hot spot in the north equatorial belt', *J. Geophys. Res.* **103**, 22857–22890.

Smith, G.R., Shemansky, D.E., Holberg, J.B., Broadfoot, A.L., Sandel, B.R., and McConnell, J.C.: 1983, 'Saturn's upper atmosphere from the Voyager 2 EUV solar and stellar occultations', *J. Geophys. Res.* **88**, 8667–8678.

Smith, C., Aylward, A., Miller, S., and Mueller-Wodarg, I.C.F.: 2004, 'Polar heating in Saturn's thermosphere', *Ann. Geophysicae*, submitted.

Southwood, D.J. and Kivelson, M.G.: 2001, 'A new perspective on the influence of the solar wind on the jovian magnetosphere', *J. Geophys. Res.* **106**, 6123–6130.

Stallard, T., Miller, S., Millward, G., and Joseph, R.D.: 2001, 'On the dynamics of the jovian ionosphere and thermosphere I: the measurement of ion winds', *Icarus* **154**, 475–491.

Stallard, T.S., Miller, S., Cowley, S.W.H., and Bunce, E.J.: 2003, 'Jupiter's polar ionospheric flows: measured intensity and velocity variations poleward of the main auroral oval', *Geophys. Res. Lett.* **30**, 1221.

Stallard, T.S., Miller, S., Trafton, L.M., Geballe, T.R., and Joseph, R.D.: 2004, 'Ion winds in Saturn's southern auroral/polar region', *Icarus* **167**, 204–211.

Strobel, D.F. and Smith, G.R.: 1973, 'On the Temperature of the Jovian Thermosphere', *J. Atmos. Sci.* **30**, 718.

Strobel, D.F.: 2005, 'Photochemistry in outer solar system atmospheres', this volume.

Trafton, L.M., Miller, S., Geballe, T.R., Tennyson, J., and Ballester, G.E.: 1999, 'H_2 quadrupole and H_3^+ emission from Uranus: the uranian thermosphere, ionosphere and aurora', *Astrophys. J.* **524**, 1059–1083.

Trauger, J.T., and 16 co-workers: 1998, 'Saturn's hydrogen aurora: wide field planetary camera 2 imaging from Hubble Space Telescope', *J. Geophys. Res.* **103**, 20237–20244.

Vasavada, A.R., Bouchez, A.H., Ingersoll, A.P., Little, B., Anger, C.D., and the Galileo SSI Team: 1999, 'Jupiter's visible aurora and Io footprint', *J. Geophys. Res.* **104**, 27133–27142.

Vasyliunas, V.M.: 1983, 'Plasma distribution and flow', *in* A.J. Dessler (ed.), *Physics of the jovian magnetosphere*, Cambridge University Press, pp. 395–453.

Vincent, M.B., and 18 co-workers: 2000, 'Jupiter's polar regions in the ultraviolet as imaged by HST/WIFPC2: auroral aligned features and zonal motions', *Icarus* **143**, 205–222.

Waite, J.H., Jr., Cravens, T.E., Kozyra, J.U., Nagy, A.F., Atreya, S.K., and Chen, R.H.: 1983, 'Electron precipitation and related auronomy of the jovian thermosphere and ionosphere', *J. Geophys. Res.* **88**, 6143–6163.

Waite, J.H., Jr., Gladstone, G.R., Lewis, W.S., Drossart, P., Cravens, T.E., Maurelis, A.N., Mauk, B.H., and Miller, S.: 1997, 'Equatorial X-ray emissions: implications for Jupiter's high exospheric temperatures', *Science* **276**, 104–108.

Waite, J.H., Jr., and 10 co-workers: 2001, 'An auroral flare at Jupiter', *Nature* **410**, 787–789.

Waite, J.H., Jr. and Lummerzheim, D.: 2002, 'Comparison of auroral processes: Earth and Jupiter, *in* M. Mendillo, A. Nagy, and J.H. Waite (eds.), *Atmospheres in the Solar System*, AGU Geophysical Monograph **130**, 115–139.

Yelle, R.V. and Miller, S.: 2004, 'Jupiter's thermosphere and ionosphere *in* F. Bagenal, T.E. Dowling, and W.B. McKinnon (eds.), *Jupiter: The Planet, Satellites and Magnetosphere* Cambridge University Press.

Young, L.A., Yelle, R.V., Young, R.E., Seiff, A., and Kirk, D.B.: 1997, 'Gravity waves in Jupiter's thermosphere', *Science* **276**, 108–111.

Address for Offprints: Steve Miller, Atmospheric Physics Laboratory, Department of Physics and Astronomy, University College London, London WC1E 6BT, UK; ucapt0s@ucl.ac.uk

ENERGETIC PARTICLES IN THE MAGNETOSPHERE OF SATURN AND A COMPARISON WITH JUPITER

NORBERT KRUPP (krupp@mps.mpg.de)
Max-Planck-Institut für Sonnensystemforschung, Katlenburg-Lindau, Germany

Received: 17 September 2004; Accepted in final form: 7 October 2004

Abstract. Observations of energetic particles in planetary magnetospheres are a very useful tool to investigate processes in the vicinity of magnetized planets. In-situ measurements of neutral and charged particles can provide information about plasma sources and sinks, magnetic topology and dynamical processes in these magnetospheres. Saturn with the second largest magnetosphere in our solar system is unique. Fast rotating plasma is interacting with the ringsystem, with the icy satellites, and, especially, with Titan, the only moon in our solar system with a dense atmosphere.

1. Introduction

The magnetospheres of Jupiter and Saturn are gigantic plasma laboratories in space. The dimensions of the largest entities in our solar system encompass tens of planetary radii or millions of kilometers around the planets. The sizes of the two largest magnetospheres in our solar system are shown in Figure 1 (the size of the solar disk is drawn on the same scale for comparison). The distances of the noses of the magnetosphere towards the Sun's direction are $24R_S$ ($1R_S = 60330$ km) and $82R_J$ ($1R_J = 71400$ km), respectively. Towards the flanks of the magnetospheres the magnetopauses are found at considerably larger distances as indicated in the sketch.

Most of the knowledge we have about these magnetospheres come from in-situ measurements of spacecraft. They provide snapshots of the magnetospheric configuration during the time of the encounter. Jupiter has been investigated by 6 flyby missions (Pioneer 10 and 11, Voyager 1 and 2, Ulysses and Cassini). The duration of these flybys was a few days only. Jupiter has been explored in great detail by Galileo. The results of this first spacecraft orbiting an outer planet in our solar system provided unprecedented information over an extended time interval. The spacecraft spent nearly eight years in Jupiter's magnetosphere and performed 35 elliptical orbits between $5R_J$ and $150R_J$ in the equatorial plane of the system. Energetic particle measurements taken onboard Galileo changed our view of the Jovian magnetosphere quite extensively. In contrast Saturn was so far visited only by three spacecraft which flew by the planet through its magnetosphere (Pioneer 11, Voyager 1 and 2). As shown in Figure 2, this limits the regions from which magnetospheric data are currently available. Only recently on July 1, 2004 Cassini

Space Science Reviews 116: 345–369, 2005.
DOI: 10.1007/s11214-005-1961-3

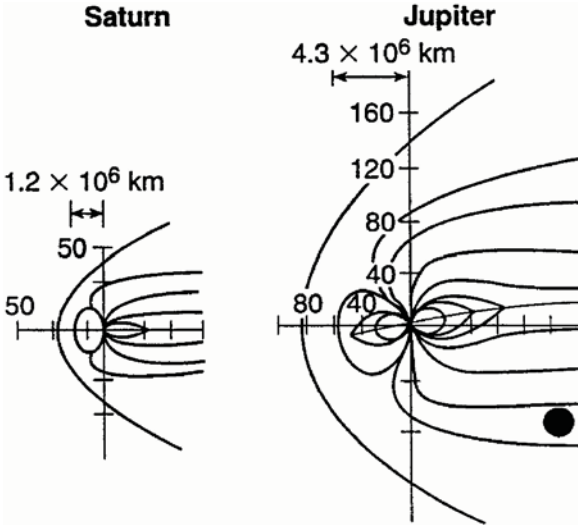

Figure 1. Comparison of the sizes of the Jovian and Kronian magnetospheres. The black dot represents the diameter of the solar disk for comparison.

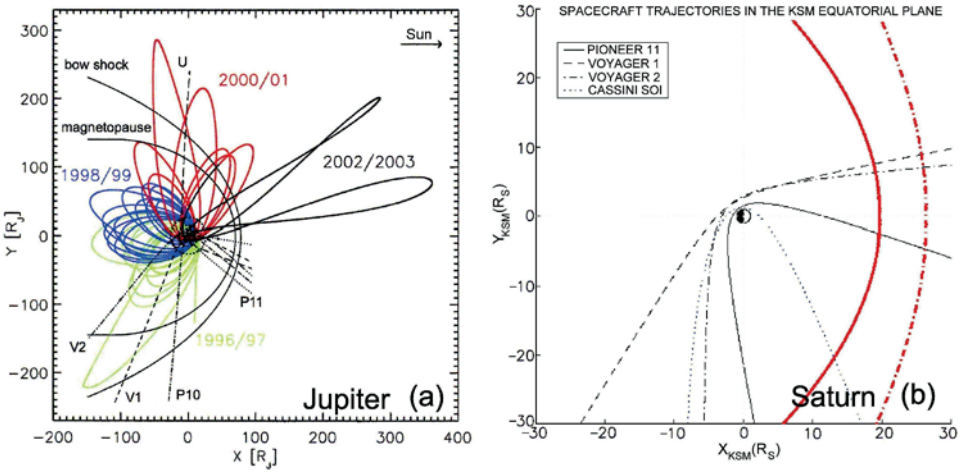

Figure 2. Trajectories of spacecrafts (Pioneer 10 and 11; Voyager 1 and 2, Ulysses, Galileo, and Cassini) that visited the magnetospheres of Jupiter (*top*) and Saturn (*bottom*).

went successfully into orbit around Saturn and will provide nearly global coverage of the Kronian magnetosphere.

One of the most valuable measurements to get information about a planet's magnetosphere besides magnetic field and plasma waves is the observation of energetic particle distributions. The analysis of particle parameters is a very useful tool to investigate the invisible magnetosphere, its global configuration and the dynamical processes, e.g. the motion of plasma and energetic particles inside the magnetosphere. Measured anisotropies of energetic particles allow to study inten-

sity gradients, flow or drifts of particles in the magnetosphere can be studied. The knowledge of the charged particle population offers also the opportunity to study the magnetic field configuration of the planet. The pitch angle distribution (PAD) of these particles provide detailed information about the magnetic topology. Changes of the PADs can be used to quantitatively determine loss processes occurring in the magnetosphere.

Another parameter is the energy spectrum of energetic particles. Differences in the spectra between different ion species and/or changes of the spectral form as a function of latitude or radial distance from the planet classify acceleration mechanisms or composition changes.

Furthermore energetic particles interact with the the atmosphere/exosphere of a planet, with the moons' surfaces and ring particles of the planet, and with existent gas tori along the orbits of moons. These interactions as well as the interaction with waves in the magnetosphere (see chapter of P. Zarka in this book) are often used to study a whole variety of questions in planetary research. Neutral and charged particles originating inside the planet's magnetosphere can be observed remotely outside the magnetic cavity from very large distances from the planet.

However, in-situ particle observations from spacecraft are often limited in energy, spatial coverage, and other constraints. Flybys of spacecraft essentially provide snapshots of the state of the planetary magnetosphere at a given time and at a given point in the magnetosphere. An orbiting spacecraft can investigate the magnetosphere on longer time scales and at multiple points gathering additional information. Nevertheless it is not possible to fully describe the system with the data sets available. Computer simulations have developed quite extensively and could help to understand the interpretation of the real data and extend them into unencountered parts of a planetary magnetosphere.

Potential sources of energetic particles in planetary magnetospheres may be classified as sources from inside or from outside the system (from Van Allen, 1984). External sources are

- the solar wind;
- solar energetic particles;
- cosmic rays including secondary particles from interactions with the atmosphere; rings and satellites;

whereas internal sources can be

- ionized gas from the ionosphere;
- gas sputtered from rings and satellites;
- gas emitted volcanically or outgassed from satellites.

Before the arrival of Cassini it was still under discussion whether the Saturnian magnetosphere is a neutral-dominated magnetosphere. Evidence exists that the interaction of neutrals with the charged particle population dramatically influences the processes in the magnetosphere.

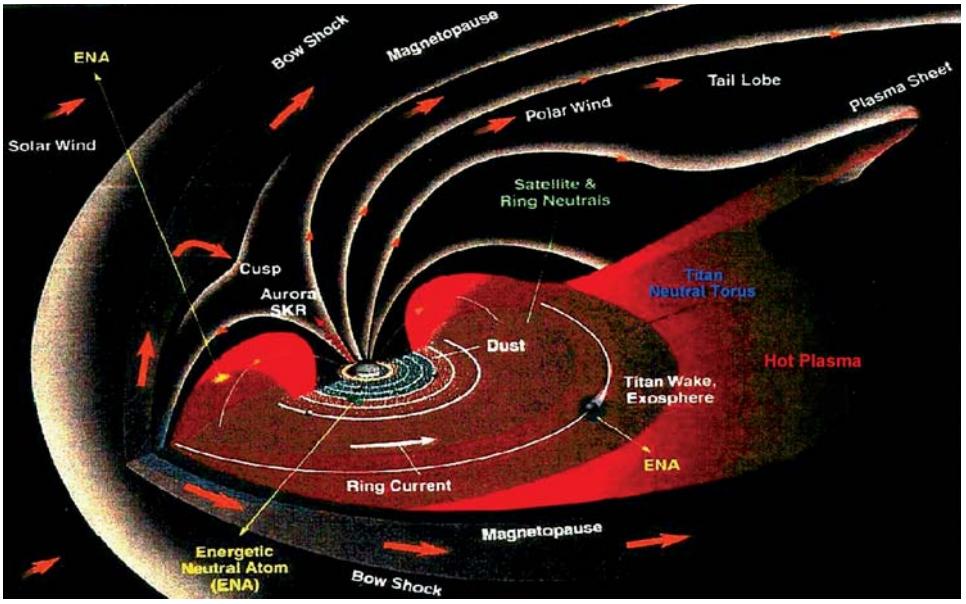

Figure 3. Sketch of Saturn's magnetosphere. (Courtesy APL art department.)

2. Global Configuration of the Kronian Magnetosphere

The first concepts of a magnetosphere at Saturn were developed in 1973 (Kennel, 1973; Scarf, 1973). However, the first and definitive proof of an existing Saturnian magnetosphere was provided by Pioneer 11 measurements in 1979. Our present knowledge about Saturn's magnetosphere is mainly based on the plasma, particle, waves and field observations from the three flyby missions mentioned above. The results are summarized in the review articles, e.g. Schardt (1983) and in Gehrels and Matthews (1984). It is believed that Saturn's magnetospheric characteristics are intermediate between those of Earth and Jupiter (Bridge et al., 1981; Bridge *et al.*, 1982; Lazarus and McNutt, 1983; Sittler *et al.*, 1983; Richardson, 1986; Van Allen, 1984; Simpson *et al.*, 1980). The current picture of the magnetosphere of Saturn is shown in Figure 3.

2.1. Intensities and Energy Spectra

Figure 4 shows energetic particle observations from the Low Energy Charged Particle instrument (LECP) onboard the Voyager 2 spacecraft during its encounter with Saturn in 1981 (Krimigis, 1982).

The magnetosphere of Saturn is populated by low-energy (soft) electrons in the outer region and more energetic electrons closer in. Inside the orbits of Enceladus and Mimas substantially higher counting rates of protons ($E > 80$ MeV) was observed, indicative of very energetic particles in the radiation belts of the

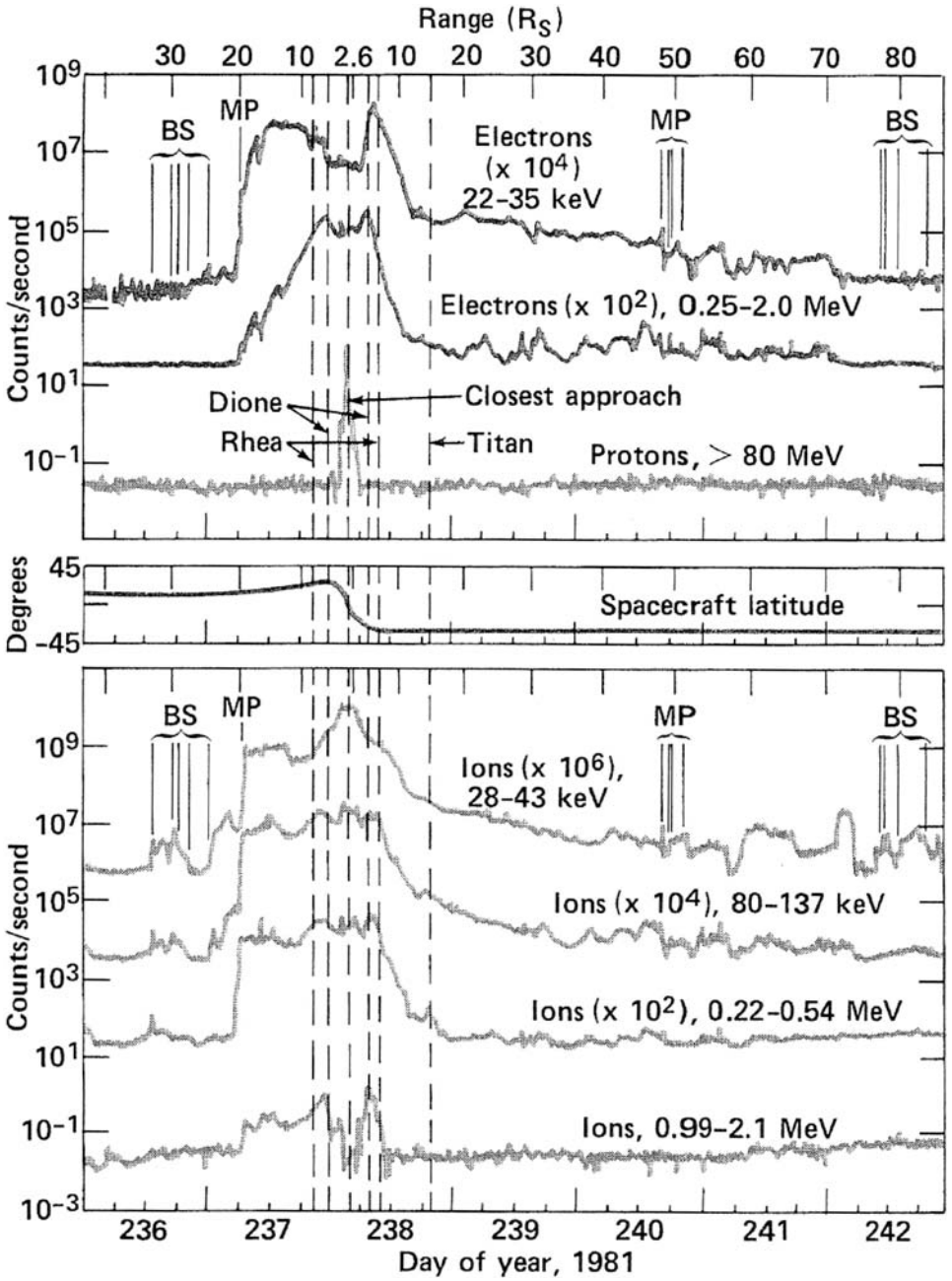

Figure 4. Count rates of selected electron (top panel) and ion channels (bottom panel) of the LECP instrument onboard Voyager2 during the Saturn encounter in 1981. In addition the latitude of the spacecraft along its trajectory is shown in the middle panel (from (Krimigis, 1982)).

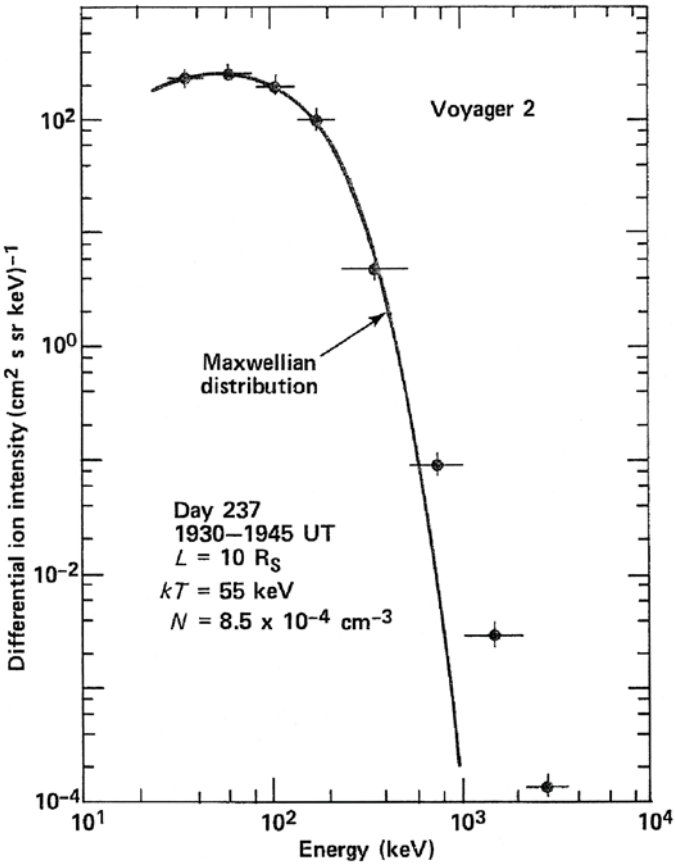

Figure 5. Typical ion energy spectrum in Saturn's magnetosphere measured by the LECP instrument on Voyager 2 at $10R_S$ (from (Krimigis, 1982)).

planet. The time profile of low-energy ions is substantially different from the high-energy ion measurements. Obviously the energy spectra of ions change inside the magnetosphere as a function of radial distance as well as a function of local time.

The spectral shape of these ion energy spectra can be described by a Maxwellian distribution for lower energies and a power-law distribution for energies above a few hundred keV. These two spectral forms can be combined in a kappa-distribution. From these spectral fits a characteristic temperature kT was found at 6×10^8 K (or about 55 keV) which is the highest temperature in the solar system (Krimigis, 1982). Two-component proton spectra were found in the inner Saturnian magnetosphere (Krimigis and Armstrong, 1982), a low-energy population ($<$ 500 keV) described by a power-law with index 2.5, and a high-energy part ($>$ 16 MeV) with a spectral form similar to that expected from cosmic ray neutron albedo decay (CRAND; Fillius and McIlwain, 1980; Krimigis, 1982). This is indicative of different sources of particles present in the Saturnian system.

Other features in the particle observations of the inner magnetosphere inside of $5R_S$ are the absorption signatures from the rings and the inner moons (Simpson *et al.*, 1980; see below).

The trapped radiation characteristics of Saturn fall between those of Earth and Jupiter, both in terms of energies observed as well as peak intensities. Saturn's radiation belts have been modeled recently by Santos-Costa *et al.* (2003) and compared with Voyager 2 energetic particle data. The simulation could reproduce the observations reasonably well within some limitations. In their three-dimensional model of the radiation belts they could show that absorption of dust is the dominant loss effect in the innermost region (1-2.3 R_S) while local losses from satellites play a more important role in the region between 2.3 and 6 R_S in the inner magnetosphere. Their results suggest strong energetic neutral atom (ENA) emissions which so far have not yet been detected directly. If present, the Ion Neutral Camera INCA, part of the Magnetospheric Imaging instrument MIMI onboard Cassini, will be able to detect these ENAs directly.

The boundary between the inner and the outer magnetosphere of Saturn is not sharp and covers the range between 6 and $10R_S$ (Schardt *et al.*, 1984). Based on the three flyby data sets the energetic particle population in the outer Kronian magnetosphere mainly consists of electrons, protons and some heavier ions with energies < 2 MeV at 10 R_S and < 1 MeV near the magnetopause. Inside about 16 R_S (Voyager 2 time period) or inside 10 R_S (Voyager 1 time period) an equatorial current sheet is well established The variability of the particle fluxes outside that region is quite high.

2.2. Ion Composition

In addition to the particle intensities, ion composition in the Kronian magnetosphere can also help better understand the hot plasma. The LECP instrument on Voyager made the first ion composition measurements of Saturn's magnetosphere (Krimigis *et al.*, 1981a; Hamilton *et al.*, 1983). LECP measured the mass histogram shown in Figure 6 for ion energies above 200 keV (Krimigis, 1982).

It was found that H_2^+ and H_3^+ from the planet's ionosphere as well as Helium ions (most probably from the solar wind) are sources of energetic particles in the Kronian magnetosphere. The heavier ion component of the Kronian plasma is shown on the right of Figure 6. Two major constituents were found (carbon and oxygen). At the time of Voyager the solar wind was assumed to be the major source for carbon and that oxygen could either originate from the solar wind or from a secondary oxygen source of water ice dissociation at the surfaces of the satellites and rings. From that reason it was suggested that the satellite interaction with the energetic particle population in the Saturnian system plays a very important role.

Voyager also found that the proton/Helium ratio at equal energy/nucleon is up to values of 5000, much larger than in other magnetospheres (Krimigis *et al.*, 1981b), consistent with an additional source for protons than the solar wind.

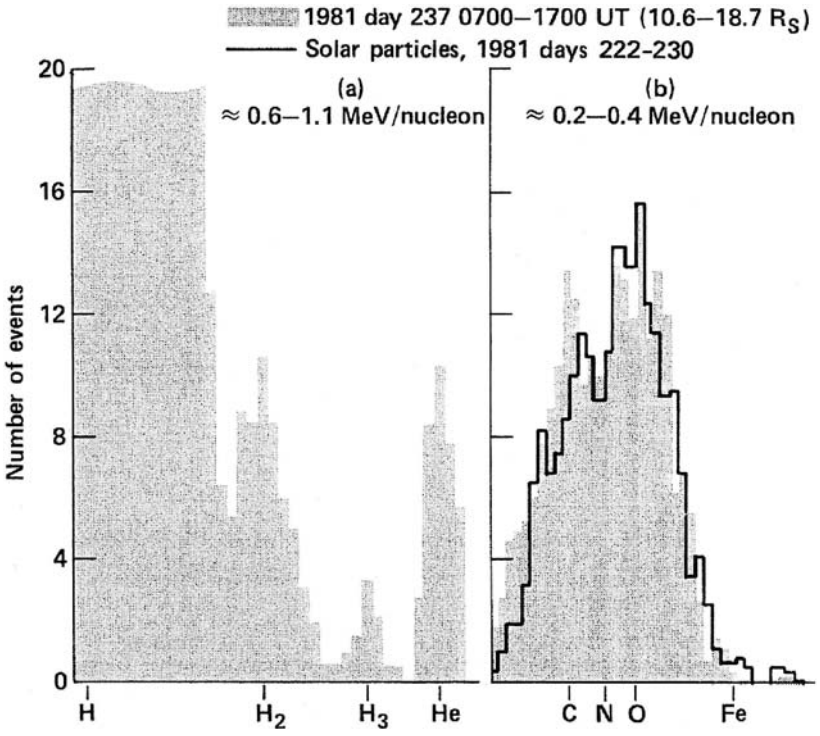

Figure 6. Mass histogram of the Kronian magnetosphere as derived from LECP energetic particle measurements on Voyager 2 (from Krimigis, 1982.)

Recent studies by (Paranicas *et al.*, 2004) showed that the interpretation of charged particle distribution could be affected by the presence of neutral gas. Further investigations by Cassini are needed to fully describe the Voyager measurements.

2.3. Particle Motion and Corotation

The Saturnian magnetosphere is corotation dominated. Plasma and particles corotate (partly) with the planet. Similar to the Jovian case (for details see Vasyliūnas, 1983) magnetospheric plasma moves with the neutral atmosphere. The particle motion in the Kronian magnetosphere has been determined by using particle data from Pioneer 11 applying the technique from (Northrop and Thomsen, 1980). Thomsen *et al.* (1980) and Bastian *et al.* (1980) showed the particle pitch angle distributions peaked at 90 degrees (pancake distribution). From these measurements and the derived directional anisotropies the corotation velocities can be derived. They concluded nearly exact corotation velocity throughout the magnetosphere. Other studies by Frank *et al.* (1980) found plasmas rigidly corotating out to distances of at least $10R_S$. Beyond $10R_S$ the velocities vary between 30 and 80% of the rigid corotation speed presumably due to viscous drag from the solar wind and/or mass

loading from the magnetospheric plasma. Some evidence for additional velocity components radially and in north-south directions exists. It is also seen that just outside the orbits of Dione and Rhea the flow speed of the plasma drops significantly. Carbary et al. (1983b) showed using Voyager low-energy ion data that the derived first-order anisotropies and inferred flows often deviate significantly from the corotation direction. On the nightside the amplitudes are consistent with full corotation out to $20R_S$. Within a radial distance of $9R_S$ the anisotropy direction deviate at times from corotation by nearly 180 degrees and maybe related to the moon Rhea. From particle data on Voyager it was also concluded that the two measured ion species (H^+ and O^+ or N^+) partially corotate with the planet. Figure 7 shows the derived ion velocity components together with temperature and density along the Voyager 1 trajectory in a Saturn-centered cylindrical coordinate system (Richardson, 1986).

Figure 8 shows the derived anisotropy vectors from the Voyager 1 measurement (Krimigis *et al.*, 1981b).

The inset shows the detailed anisotropies around the Titan orbit crossing. The vectors are directed in the sense of corotation pointing to a convective motion in an $\mathbf{E} \times \mathbf{B}$-field configuration inside the magnetopause. Around the Titan L-shell crossing significant deviations from the nominal corotation direction have been observed indicative of a Titan wake signature seen in energetic particle parameters. The sense of particle motion changes with the exit through the dawn magnetopause into the magnetosheath. Here the ansisotropy amplitude increased significantly and the direction of motion was consistent with a slightly diverted anti-sunward motion of the particles.

Modeling of the azimuthal plasma flow velocity in Saturn's magnetosphere by Saur *et al.* (2004) included radial mass transport, friction between magnetospheric ions and neutrals, and ion pickup. The latter two processes could be described in a quantity magnetospheric conductance. They found that two conductance maxima in the calculations are necessary to explain the measured dips in the azimuthal velocity profiles slightly outside the orbits of Dione and Rhea. It was concluded from the model that the net plasma flow is radially inward at some regions within $L = 10$. Inward transport spins up the plasma sometimes exceeding rigid corotation (superrotation). In steady state this inward motion is only possible when plasma is converted into neutrals or if the plasma is absorbed otherwise. Saur *et al.* (2004) followed that material within $10R_S$ can only leave that region as neutrals.

The coupling currents between the ionosphere-magnetosphere system resulting from sub-corotation of the magnetospheric plasma has been studied recently by Bunce *et al.* (2003) and Cowley and Bunce (2003; 2004). The currents involved in these processes are discussed by Kivelson (2005) in this book.

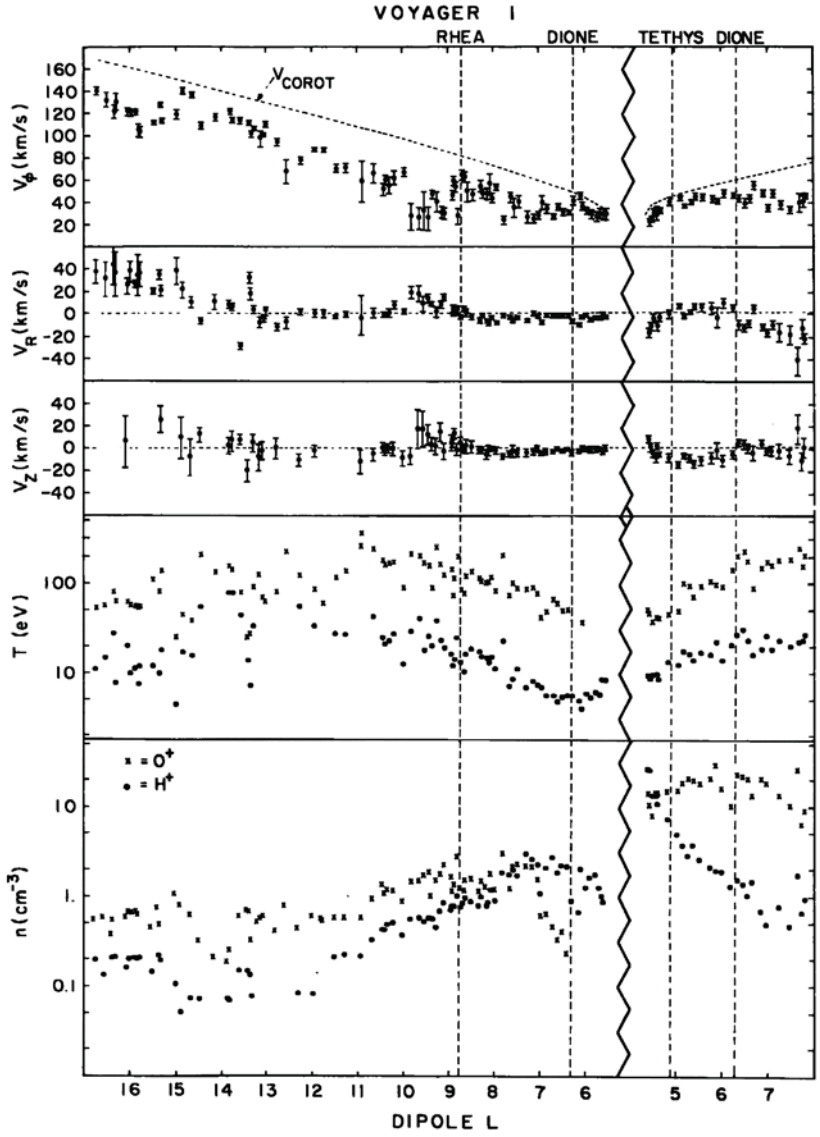

Figure 7. Velocity components, temperature and density of low-energy plasma deduced from PLS data along the Voyager 1 trajectory (from Richardson, 1986, reproduced by Blanc *et al.*, 2002).

2.4. Titan Interaction and its Torus

It is known that Titan possesses a thick atmosphere and up to now this second largest moon in our solar system has no intrinsic magnetic field. The interaction of Titan with its surrounding plasma therefore has some similarities but also differences with the interaction of Venus or a comet with the solar wind. Titan may be located in the solar wind, in the magnetosheath or in the magnetosphere of

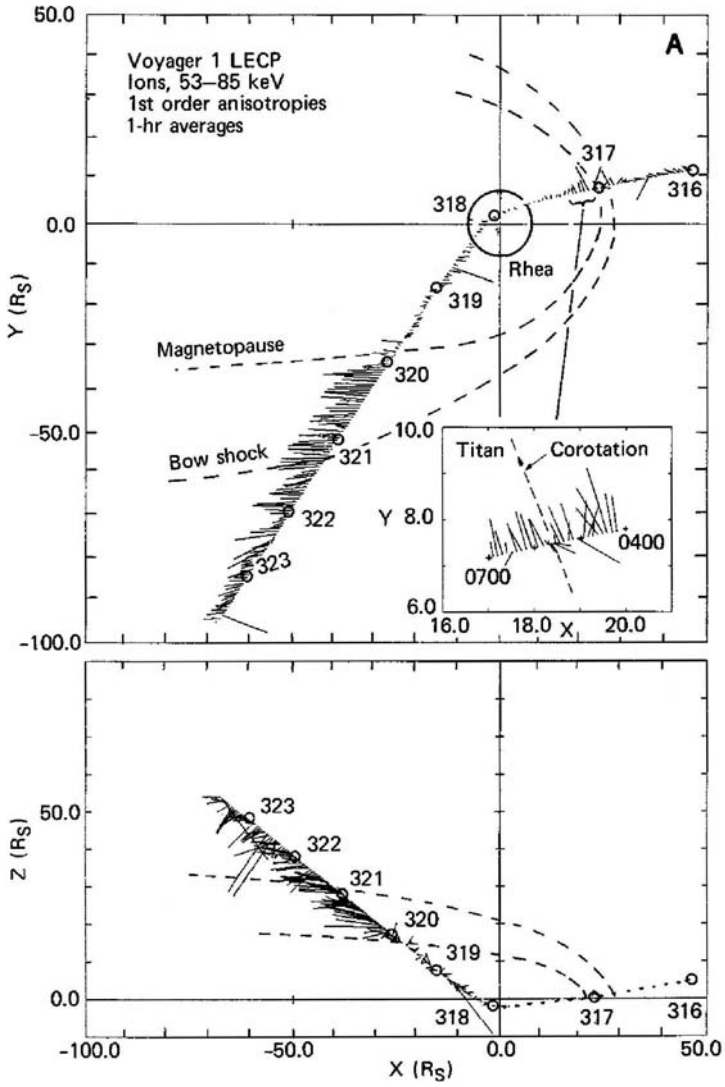

Figure 8. First-order anisotropy vectors of ions (53-85 keV) from Voyager 1 LECP measurements. Projected into the equatorial plane of Saturn (*top*) and in the plane perpendicular to the equator (*bottom*) (from Krimigis *et al.*, 1981b.)

Saturn, depending on the dynamic pressure of the solar wind and the orbital phase of the moon. Our knowledge about the interaction between the moon Titan and the surrounding plasma in the magnetosphere is based on one flyby from Voyager 1 on November 12, 1980, shown in Figure 9.

The results are summarized by (Neubauer *et al.*, 1984). The encounter occurred close to local noon. The moon was inside the magnetosphere at that time. As shown in Figure 10 the derived flow speed close to Titan was between 80 and 150 km/s

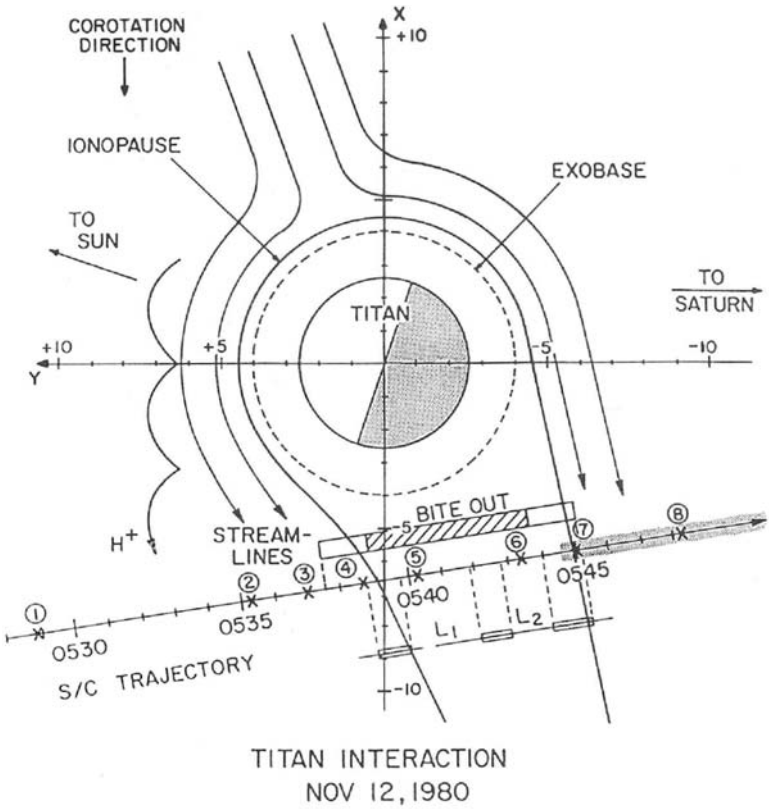

Figure 9. Titan encounter geometry of the Voyager 1 spacecraft after Hartle *et al.* (1982).

compared to 200 km/s rigid corotation speed. The flow direction was found 20 degrees off the nominal corotation direction directed radially inward. This deviation has been interpreted as a motion of the entire magnetosphere during the time of the Titan flyby. The comet-like interaction can be described as a slow-down of plasma deviated around Titan related to mass loading effects and pickup processes (for details see Neubauer *et al.*, 1984). In the moon's wake the velocity of ions dropped to very small values (Maclennan *et al.*, 1982), suggestive that the corotation of plasma is disrupted by the presence of the moon.

Titan's orbit around Saturn is close to the location of a nominal magnetopause position so that the moon could sometimes be outside the magnetosphere and its atmosphere then will interact with the solar wind, a plasma with completely different parameters than the plasma inside the Saturnian magnetosphere. The Cassini spacecraft will perhaps investigate both extreme cases.

Atoms and molecules of hydrogen produced by photochemical reactions in the satellite's thick atmosphere can easily escape from the moon and form a massive doughnut-shaped torus along the orbit of Titan (Eviatar *et al.*, 1990). The material diffuses inward but is prevented from extending much beyond the orbit of Titan

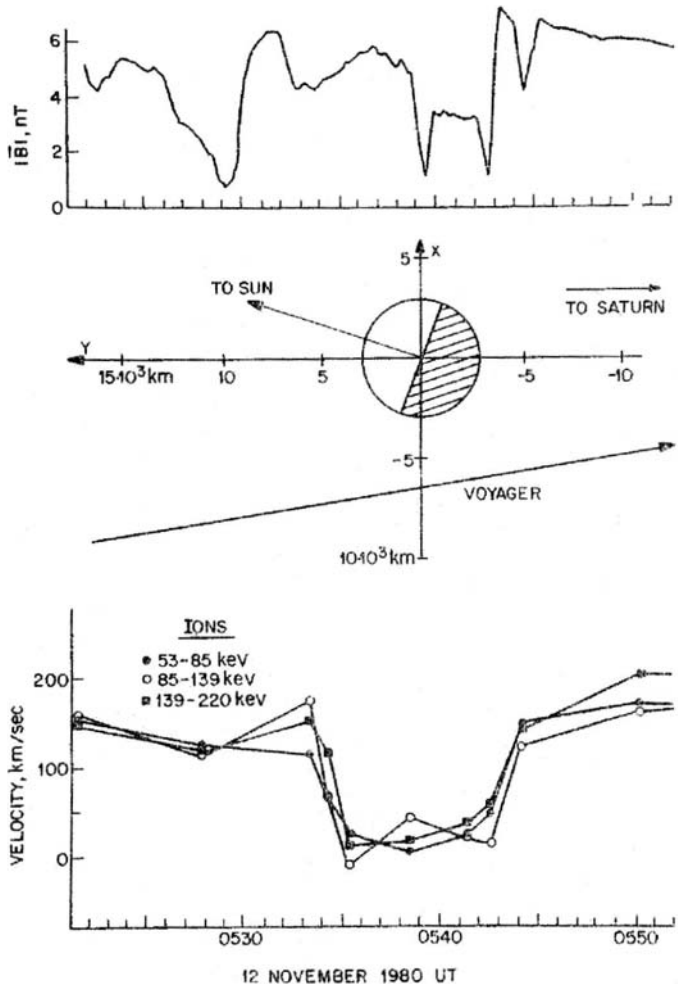

Figure 10. Measurements of magnetic field and energetic particles on board Voyager 1 in the wake of Titan. *From top to bottom:* Measured total magnetic field from Ness *et al.* (1982); trajectory of the spacecraft in the Titan rest frame; velocity of energetic ions as derived from anisotropy measurements (Maclennan *et al.*, 1982).

through the location of the magnetopause. At times Titan is outside the magnetosphere and the question then is whether the torus still exists. Cassini will help to answer this.

Particles from Titan's atmosphere/exosphere interact with energetic particles from the Kronian magnetosphere or with particles from the solar wind if Titan's position is outside the magnetopause. Particle sputtering, ion pick-up, and recombination processes can occur (see Lammer and Bauer, 1993, Neubauer *et al.*, 1984, Cravens *et al.*, 1997, for details).

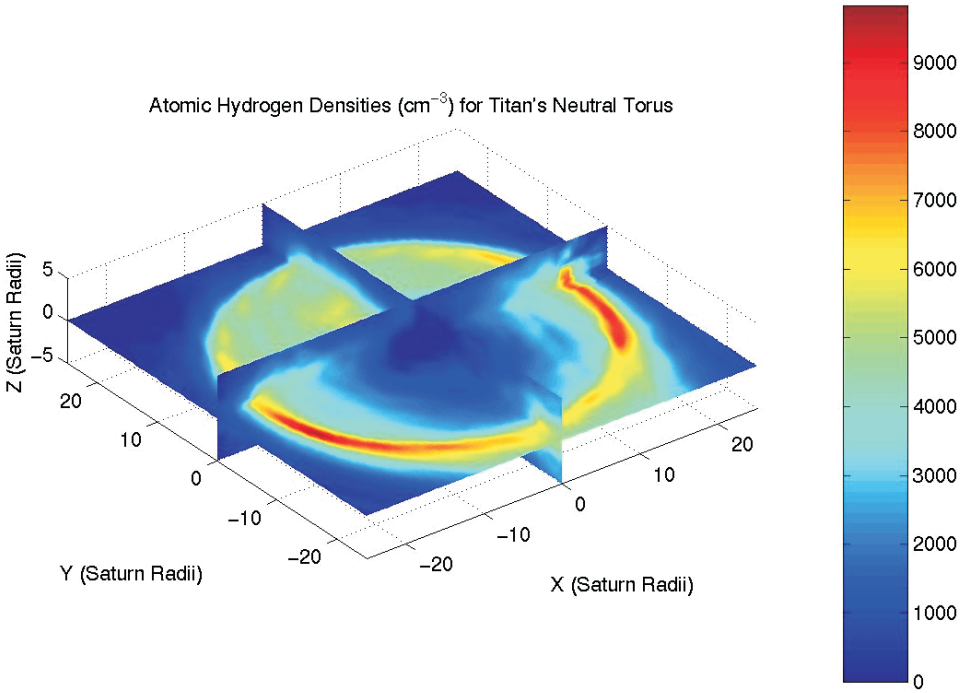

Figure 11. Simulation of the Titan torus.

The interaction of Titan with the surrounding plasma has been extensively modelled by a number of groups (see Nagy *et al.*, 2001; Kabin *et al.*, 1999; Kabin *et al.*, 2000; Brecht *et al.*, 2000; Ledvina *et al.*, 2004b; Ledvina *et al.*, 2004c; Ledvina *et al.*, 2004a; Cravens *et al.*, 1998; and references therein). Those simulations together with the 44 close Titan flybys of the Cassini spacecraft will dramatically enhance the understanding of the interaction between the surrounding plasma and Titan's atmosphere/exosphere.

2.5. Interaction of Magnetospheric Plasma with Icy Satellites

Icy satellites can serve as additional sources of energetic particles in planetary magnetospheres as well as sinks. Energetic particles in the Kronian magnetosphere interact with the atmospheres/exospheres and the surfaces of the icy satellites as shown in Figure 12. Surface sputtering as well as atmospheric sputtering are two of the interaction processes where material from the surface or the atmosphere of the satellite is removed by corotating plasma and energetic particles. However, as shown by Jurac *et al.* (2001), sputtering of the satellite surfaces with heavy ions alone cannot account for the observed OH-cloud in the inner magnetosphere. An additional source in the inner magnetosphere is required.

Neutrals in the vicinity of the moons could also interact with the flowing plasma by charge-exchange reactions or scattering. For completeness, it should be men-

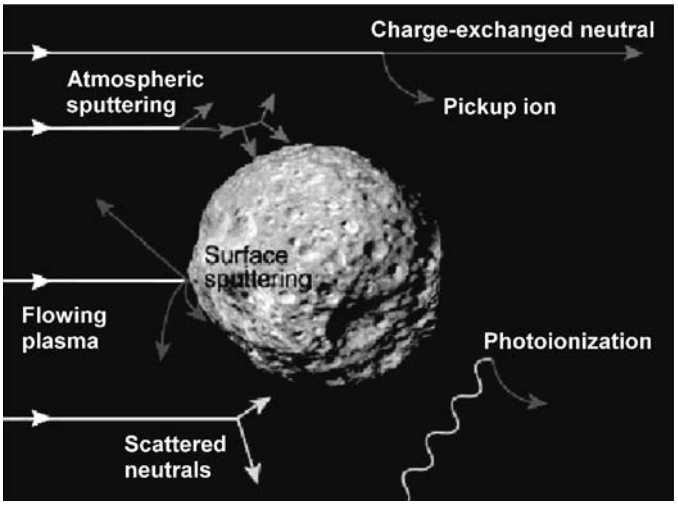

Figure 12. Interaction between magnetospheric particles and the atmosphere/exosphere and the surface of an icy satellite.

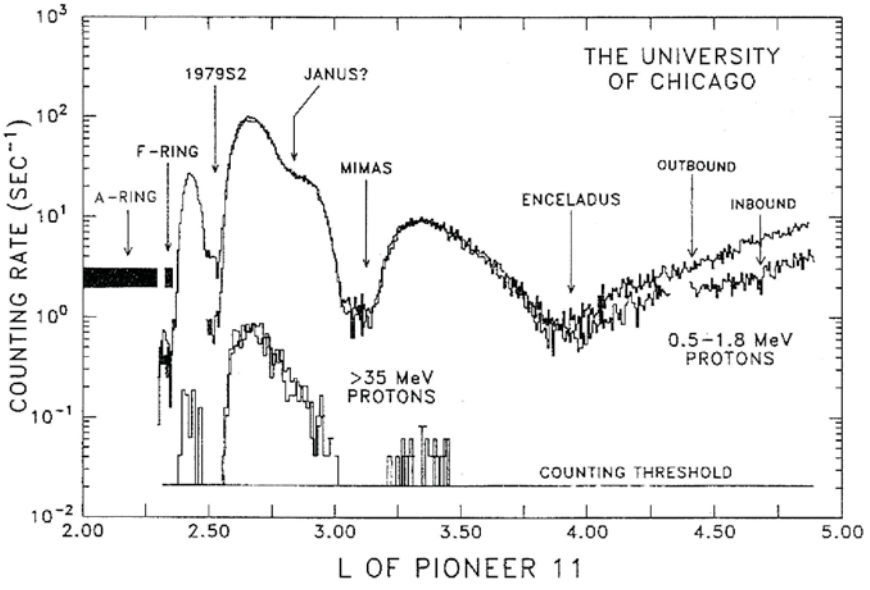

Figure 13. Absorption signatures in the measured counting rates of protons from moons and rings in the Saturnian system (from Simpson *et al.*, 1980.)

tioned that neutrals can also be photoionized by sunlight directly. Cassini will measure the neutral particles directly and will help to determine whether the neutral population is the missing source.

Effects of satellites on the charged particle population are known for a long time. Figure 13 shows the counting rates for protons (0.5-1.8 MeV and $>$ 35 MeV)

measured during the Pioneer 11 encounter at distances between 2 and 5 R_S.

Absorption signatures have been observed during the crossings of the L-shells of Mimas ($3.1R_S$), Enceladus ($4R_S$). For Tethys ($4.8R_S$) and Dione ($6.3R_S$) the signatures are not as obvious as for the other inner moons. Between 4 and $7R_S$ the overall intensity of 1 MeV ions is decreased due to possible absorption of tenuous E-ring material in that region. Changes in the pitch angle distributions of low energy (28-43 keV) protons as Voyager 2 approached the ring plane of the planet at $2.8R_S$ also indicate that processes between the energetic particle population and the ring particles occur. The normal pancake or trapped distribution (maximum intensity at 90 degrees pitch angle) changed into butterfly-type distributions with a significant "bite-out" at 90 degree pitch angle (Carbary *et al.*, 1983a).

At Jupiter, the tilt of the magnetic axis relative to the rotation axis allowed a range of near-equatorial particles to escape absorption. At Saturn these axes are co-aligned with each other and the absorption therefore is much more efficient. Absorption signatures at the smaller satellites closer to the planet are very likely as well.

3. Dynamics of the Kronian Magnetosphere

The dynamics of the Kronian magnetosphere are influenced by processes in the interplanetary vicinity of the planet and by processes inside the magnetosphere. During the Pioneer 11 encounter the Kronian magnetosphere was found in a very disturbed state. One of the largest solar particle events in that solar cycle hit the magnetosphere (Simpson *et al.*, 1980) and compressed it quite extensively. During the Voyager encounters the state of the magnetosphere was more quiescent but also with significant temporal variations between and during the encounters (Krimigis *et al.*, 1983).

Responses of the magnetosphere could be oscillations of the whole magnetosphere or other waves triggered by disturbances from inside or outside the magnetosphere. In addition, similar to the cases at Earth and Jupiter, processes such as reconnection can change the global topology of the magnetosphere on time scales of seconds, hours or even days, especially in the magnetotail.

3.1. Substorms-like Events and Injections

Evidence for Earth-like substorm activity has so far been found in the magnetospheres of Mercury, Uranus and recently at Jupiter. From the Pioneer and Voyager data it was not clear that substorm-like processes also occur at Saturn. However, the time scales within which these large-scale reconfiguration processes might arise are on the order of a few days – very difficult to observe with a flyby mission. At Earth, the solar wind interaction with the magnetosphere provides the energy source for substorms. From the Galileo energetic particle data it could be shown

that substorm-like global reconfiguration processes in the Jovian magnetotail are triggered most probably internally by mass-loading of magnetic field lines (Woch *et al.*, 1999; Krupp *et al.*, 1998; Woch *et al.*, 1998; Kronberg *et al.*, 2004). Periodically every 2-3 days, plasma radially diffuses outward from Io and "load" the magnetic field lines of Jupiter. The result is an arising magnetic instability with a plasmoid release into Jupiter's magnetotail. Since the configuration of Saturn's magnetosphere is believed to be somewhere between Earth and Jupiter it could well be that similar processes happen in Saturn's magnetosphere as well.

The same is true for so-called injection events. Particles suddenly injected into the inner magnetosphere have to drift around the planet in the corotating $\mathbf{E} \times \mathbf{B}$-field. Dependent on their charge and energy they arrive energy-time dispersed at an observer's location. If a spacecraft is at the right time and the right location these injection events can be detected. In the case of Jupiter the orbiting spacecraft Galileo detected injection events in the inner Jovian magnetosphere at nearly all local times and at a whole variety of radial distances (Mauk *et al.*, 1999). Cassini will be in the same position to detect those events in the Saturnian magnetosphere.

3.2. PERIODICITES

Periodicities and oscillations in the Kronian magnetosphere have been detected in plasma and energetic particles as well as in the magnetic field and in plasma wave measurements. The periods detected range from the rotation period of the planet of more than 10 hours to seconds. Some of these observed periodicities are related to the motion of the equatorial plasma sheet, some are caused by wave-particle interaction. Others are believed to originate in a magnetic anomaly inside the planet.

The plasma wave instrument recorded whistler mode waves, hiss and chorus emissions in association with 6 keV electrons (for details see Sittler *et al.*, 1983, and the chapter of P. Zarka, 2005, in this book), and oscillations of 15-20 s in the magnetic field components possibly related to very low energy O^{2+} or O^{+}-ions with resonant energies of 300 eV and 5 eV, respectively, have been observed. Espinosa *et al.* (2003a; 2003b) analysed magnetic field data of Pioneer 11, Voyager 1 and 2 and found a pronounced 10-hour modulation possibly related to an equatorial longitudinal anomaly.

10-hour periodicities have also been observed in energetic charged particles. Looking at count rate ratios of electrons and ions (low energy particles relative to high energy particles) the ratios exhibit a pronounced 10-hour modulation beyond the orbit of Titan (Carbary and Krimigis, 1982). In principle this means a change in the energy spectrum of the particles with the planet's rotation period. The authors could show that this modulation is consistent with the SKR modulation (see Zarka, this book). The charged particle periodicity suggests a basic asymmetry in the Kronian system caused by a magnetic anomaly.

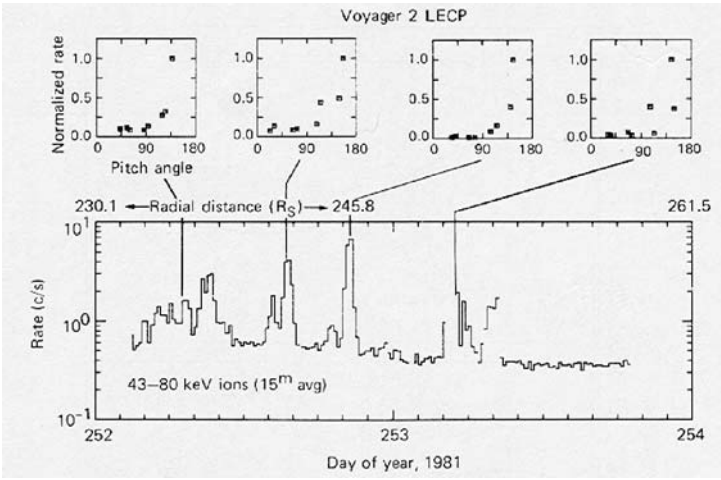

Figure 14. Ion event downstream from Saturn at a distance of $245 R_S$, observed on the outbound path of Voyager 2. Normalized pitch angle distributions (*top*) and count rate (*bottom*) of ions (43-80 keV) measured by the LECP instrument (from Krimigis *et al.*, 1983.)

3.3. Boundary Phenomena/Kronian Particles Outside the Magnetosphere

Outside of about $15 R_S$ detached plasma blobs were observed during two of the three encounters. Both Voyager spacecraft observed these signatures inbound on the dayside magnetosphere whilst the magnetosphere was in a rather quiet state compared to the Pioneer 11 encounter. Regions of these detached plasma blobs are of higher density and colder temperature than the surrounding medium. Sharp dropouts in the north-south of the magnetic field component (null fields) were observed at the same time. It is believed that they are broken off flux tubes from the edge of the equatorial current sheet by the centrifugally driven instability (Goertz, 1983). Lanzerotti *et al.* (1983) could show that the plasma close to the magnetopause at times have high beta plasma conditions which partly could be the consequence of the detached plasma blobs. In this case the internal plasma pressure has to be taken into account and the location of the magnetopause will change tautologically.

The following Table I summarizes the measured distances of bow shock (BS) and magnetopause (MP) crossings as well as the calculated standoff distances for these boundaries.

It is well known from the Earth and from Jupiter that particles originating in the magnetosphere are found outside in interplanetary space. Krimigis *et al.* (1983) reported that upstream and downstream of Saturn at distances of $200 R_S$ and off the dawn bow shock at 400 RS particles with energies of up to 100 keV were released during the Voyager encounters. Figure 14 shows an example of particles observed at $245 R_S$ during the outbound path of Voyager 2.

TABLE I

Measured positions of magnetospheric boundaries at Jupiter and Saturn.

			local time	distance BS (R_p)	standoff BS (R_p)	distance MP (R_p)	standoff MP (R_p)
P 10	1974	Jupiter	1000	108.9	102-130	96.4-50	80-96
		Jupiter	0600	124-189		98-150	
P 11	1974	Jupiter	1000	109.7-79.5	92-100	97-64.5	80-90
		Jupiter	1200	90.8-95		56.6-80	
	1979	Saturn	1000	24-20		17	
		Saturn	1200	49-102		30-40	
VG 1	1979	Jupiter	1000	85.7-55.7	77-103	67.1-46.7	62-85
		Jupiter	0400	199.2-258		158.3-165.4	
	1980	Saturn		26	23	23-24	
		Saturn		78		43-47	
VG 2	1979	Jupiter	1000	98.8-66.5	79-95	71.7-61.9	70-101
		Jupiter	0300	282.3-283.3		169.1-279.4	
	1981	Saturn		32-24	18.5	19	
		Saturn		78-88	50-70		
ULS	1992	Jupiter	1000	113	85-104	110-87	72-104
		Jupiter	1800	109-149		83-124	
GLL	1995	Jupiter	0600	130-214	100-130	120	90
	2000	Jupiter	1750			107-149	84-107
		Jupiter	1920	130-133	82-105	120-150	88-98
	2001	Jupiter	1625	108-125	82-96	102	90
CAS	2001	Jupiter	1900	> 450		204	111
	2004	Saturn	0750 -0800	49.2-40.5		35	
	(SOI)	Saturn	0540				

The count rates of ions with energies between 43 and 80 keV (*bottom panel*) increased by nearly an order of magnitude and the pitch angle distributions (*top panel*) clearly indicate that they travelled along the magnetic field lines connected back to the Saturnian system. In this example the increases of the count rates occurred quasi-periodically at a period of about 5 hours which is half the planet's rotation period. This is another indication of the particles' planetary origin. Two possibilities of explaining these observations are being discussed: (i) leakage out of the magnetosphere or (ii) acceleration of these particles in the vicinity of the planet.

4. Comparison with Jupiter

As mentioned before the Kronian magnetosphere is in some respect Earth-like, in other respects more Jupiter-like. The Jovian and Kronian magnetospheres are both corotation dominated. The driving energy of the system is provided by the planetary rotation. Plasma and energetic particles are (sub)corotating with the planet and are essentially concentrated in a current sheet and an associated plasma sheet around the equator. Modulations with the planets' rotation speed of about 10 hours have been observed in plasma and energetic particle parameters, plasma waves, and magnetic field measurements. At Jupiter this modulation has been explained by the tilt between the dipole axis and the rotation axis of the planet. An observer close to the equator of Jupiter will see the effect of the changing magnetic latitude. Since the particle are closely confined to the magnetic equator the intensities at higher magnetic latitudes drop down with the rotation rate of the planet. At Saturn, however, the rotation and dipole axes are nearly co-aligned with each other. One possibility of explaining a modulation in the data at Saturn would be a magnetic anomaly inside the planet.

In both magnetospheres the sources of plasma and energetic particles are external (solar wind, cosmic rays) and internal. At Jupiter, the most important internal source is given by the moon Io releasing oxygen and sulfur at an enormous rate. At Saturn, the interaction of the moons and the rings provide material through the interaction with magnetospheric ions. In both systems the ionosphere/atmosphere of the planet is an additional source of particles. Tori of particles along the orbits of Io and Europa in the Jovian system and along Titan's orbit at Saturn have been observed. Hydrogen in the recently discovered Europa torus and the reactions of neutrals and charged particles within the torus are also expected in the torus of Titan. However, Europa is very deep in the inner Jovian magnetosphere where the charged particle intensities in the radiation belts are very high. In contrast Titan's orbit is in the outer part of the Kronian magnetosphere close to the magnetopause. It is believed that the neutral particle population is much more important at Saturn than at Jupiter. There is evidence that the Saturnian magnetosphere could be even dominated by neutrals (Krimigis, private communications).

The current understanding of the particle motion at Jupiter (and probably also at Saturn) is a radially outward transport of cold ions followed by a vastly unknown acceleration in the outer magnetosphere. The particles then diffuse radially inward gaining energy by violating the third adiabatic invariant.

5. Expectations from Energetic Particle Measurements onboard Cassini

Onboard Cassini several instruments will measure plasma and energetic particles. As shown in Figure 15 they cover an energy range of almost ten decades in the energy spectrum.

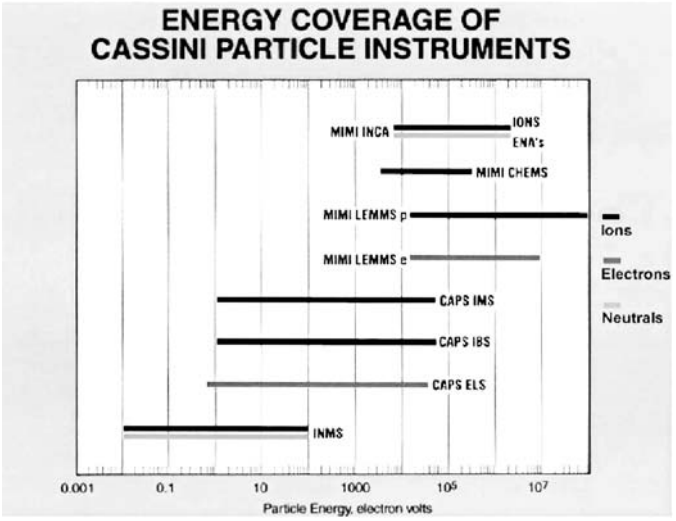

Figure 15. Energy and species coverage of the particle instruments onboard Cassini.

Energetic particles will predominantly be measured by the Magnetospheric Imaging Instrument MIMI which is capable of distinguishing between neutral and charged particles from Saturn's magnetosphere. The Ion Neutral Camera (INCA) which is one out of three detector systems of MIMI will obtain global images of energetic neutral atoms (ENAs) from Saturn's magnetosphere and will determine the composition and energy spectrum of these neutrals with a very high angular resolution. The charged particles in the magnetosphere will be extensively studied by MIMI/CHEMS (Charge and Mass Spectrometer) and MIMI/LEMMS (Low Energy Magnetospheric Measurement System). CHEMS will for the first time measure the charge states of low-energy ions (2-30 keV/q) in the Kronian system and LEMMS will focus on the electron and ion distribution in the keV to MeV range. The suite of detectors of MIMI should be able to distinguish effects of interactions of these particles with the atmosphere, Titan, and the icy moons and rings. A fundamental objective of the energetic particle investigation on Cassini will be to clarify the relative importance of these interactions for the global mass and energy budgets. Cassini and especially the energetic particle measurements together with magnetic field and plasma wave observations will help answer the question about substorms at Saturn as it will study the Kronian system over an extended period of time at various latitudes and local times. Particle instruments on Cassini will also fill the gap in the energy spectrum (4 -50 keV) of ions measured with the plasma instrument PLS and LECP onboard Voyager. The Cassini plasma spectrometer CAPS and the Ion Neutral Mass Spectrometer INMS cover the lower energy ranges.

6. Future Mission Perspectives

The future in the in-situ investigation of outer planets magnetospheres is highly dependent on the advanced technology and the existing power resources on board a spacecraft. Previous missions all relied on the Radioisotope Thermoelectric Generator (RTG). They are used on probes that will travel to a distance from the Sun where solar panels are not practical sources of electricity. As such they are carried on Pioneer 10, Pioneer 11, Voyager 1, Voyager 2, Galileo, Ulysses and Cassini.

Future missions to the outer planets will have nuclear power technology available enabling a new generation of high performance instruments with high power and high data rate capabilities. This technology will provide a new milestone in the exploration of the outer planets. Currently plans exist for:

- The Jupiter Icy Moons Orbiter (JIMO), an ambitious NASA-mission to orbit three planet-sized moons of Jupiter – Callisto, Ganymede and Europa – which may harbor vast oceans beneath their icy surfaces. The mission would orbit each of these moons for extensive investigations of their makeup, their history and their potential for sustaining life.
- The Jupiter Polar Orbiter (JPO) mission, a one-year mission designed to investigate magnetosphere- ionosphere-thermosphere coupling at Jupiter. JPO's prime scientific objectives are (i) characterization of Jupiter's auroral and equatorial emissions through global imaging and identification of the magnetospheric processes responsible for them; (ii) identification of the mechanisms involved in the transport and acceleration of charged particles within the Jovian magnetosphere, particularly in the unexplored high-latitude region, the inner magnetosphere between 6 and 10 jovian radii, and the equatorial magnetosphere at 30 jovian radii; and (iii) characterization of Jupiter's thermospheric winds.
- Titan orbiter and Titan Aerorover NASA mission with an emphasis on both in situ and remote sensing measurements of Titan's surface, atmosphere, ionosphere and magnetospheric interaction. The mission entails a 3 year development phase starting in 2007, launch in 2010 with a 9 year cruise phase to Titan, and about 20 months Titan orbiter-Aerorover phase.
- Europa Orbiter, a proposed follow-on mission to Galileo that would have probed Europa's surface in an attempt to determine the thickness of the ice and locate any ice-water interface is currently on hold.
- A Multi-Disciplinary Investigation of the Jovian System, proposal for a new ESA mission to investigate the Jovian system.

These proposed missions combined with the new results from the Cassini/-Huygens mission at Saturn will help further investigate the gas giants in our solar system in order to better understand the solar system as a whole.

Acknowledgements

This work was in part financed by the German BMBF (Bundesministerium für Bildung und Forschung) through the DLR (Deutsches Zentrum für Luft- und Raumfahrt e.V.) under contract No. 50 OH 0103, and by the Max Planck Gesellschaft.

References

Bastian, T.S., Chenette, D.L., and Simpson, J.A.: 1980, 'Charged particle anisotropics in Saturn's magnetosphere', *J. Geophys. Res.* **85**, 5763–5771.

Blanc, M., *et al.*: 2002, 'Magnetospheric and Plasma Science with Cassini-Huygens', *Space Sci. Rev.* **104**, 253–346.

Brecht, S.H., Luhmann, J.G., and Larson, D.J.: 2000, 'Simulation of the Saturnian magnetospheric interaction with Titan', *J. Geophys. Res.* **105**, 13119–13130.

Bridge, H.S., *et al.*: 1981, 'Plasma observations near Saturn - initial results from Voyager 1', *Science* **212**, 217–224.

Bridge, H.S., *et al.*: 1982, 'Plasma observations near Saturn – initial results from Voyager 2', *Science* **215**, 563–570.

Bunce, E.J., Cowley, S.W.H., and Wild, J.A.: 2003, 'Azimuthal magnetic fields in Saturn's magnetosphere: effects associated with plasma sub-corotation and the magnetopause-tail current system', *Ann. Geophysicae* **21**, 1709–1722.

Carbary, J.F. and Krimigis, S.M.: 1982, 'Charged particle periodicity in the Saturnian magnetosphere', *Geophys. Res. Lett.* **9**, 1073–1076.

Carbary, J.F., Krimigis, S.M., and Ip, W.-H.: 1983a, 'Energetic particle microsignatures of Saturn's satellites', *J. Geophys. Res.* **88**, 8947–8958.

Carbary, J.F., Mauk, B.H., and Krimigis, S.M.: 1983b, 'Corotation anisotropies in Saturn's magnetosphere', *J. Geophys. Res.* **88**, 8937–8946.

Cowley, S.W.H., Bunce, E.J., and O'Rourke, J.M.: 2004, 'A simple quantitative model of plasma flows and currents in Saturn's polar ionosphere', *J. Geophys. Res.* **109**, CiteID A05212.

Cowley, S.W.H. and Bunce, E.J.: 2003, 'Corotation-driven magnetosphere-ionosphere coupling currents in Saturn's magnetosphere and their relation to the auroras', *Ann. Geophysicae* **21**, 1691–1707.

Cravens, T.E., Keller, C.N., and Ray, B.: 1997, 'Photochemical sources of non-thermal neutrals for the exosphere of Titan', *Planet. Space Sci.* **45**, 889–896.

Cravens, T.E., Lindgren, C.J., and Ledvina, S.A.: 1998, 'A two-dimensional multifluid MHD model of Titans plasma environment', *Planet. Space Sci.* **46**, 1193–1205.

Espinosa, S.A., Southwood, D.J., and Dougherty, M.K.: 2003a, 'How can Saturn impose its rotation period in a noncorotating magnetosphere?', *J. Geophys. Res.* **108**, SMP 11–1 – 11–8, 10.1029/2001JA005084.

Espinosa, S.A., Southwood, D.J., and Dougherty, M.K.: 2003b, 'Reanalysis of Saturn's magnetospheric field data view of spin-periodic perturbations', *J. Geophys. Res.* **108**, 10–1 – 10.1029/2001JA005083.

Eviatar, A., Podolak, M., and Richardson, J.D.: 1990, 'Atomic and molecular hydrogen from Titan in the Kronian magnetosphere', *J. Geophys. Res.* **95**, 21007–21016.

Fillius, W. and McIlwain, C.E.: 1980, 'Very energetic protons in Saturn's radiation belt', *J. Geophys. Res.* **85**, 5803–5811.

Frank, L.A., Burek, B.G., Ackerson, K.L., Wolfe, J.H., and Mihalov, J.D.: 1980, 'Plasmas in Saturn's magnetosphere', *J. Geophys. Res.* **85**, 5695–5708.

Gehrels, T. and Matthews, M.S. (eds.): 1984, *Saturn*, The University of Arizona Press, Tucson.
Goertz, C.K.: 1983, 'Detached plasma in Saturn's front side magnetosphere', *Geophys. Res. Lett.* **10**, 455–458.
Hamilton, D.C., Brown, D.C., Gloeckler, G., and Axford, W.I.: 1983, 'Energetic atomic and molecular ions in Saturn's magnetosphere', *J. Geophys. Res.* **88**, 8905–8922.
Hartle, R.E., Sittler, E.C., Ogilvie, K.W., Scudder, J.D., Lazarus, A.J., and Atreya, S.K.: 1982, 'Titan's ion exosphere observed from Voyager 1', *J. Geophys. Res.* **87**, 1383–1394.
Jurac, S., Johnson, R.E., Richardson, J.D., and Paranicas, C.: 2001, 'Satellite sputtering in Saturn's magnetosphere', *Planet. Space Sci.* **49**, 319–326.
Kabin, K., Gombosi, T.I., de Zeeuw, D.L., Powell, K.G., and Israelevich, P.L.: 1999, 'Interaction of the Saturnian magnetosphere with Titan: Results of a three-dimensional MHD simulation', *J. Geophys. Res.* **104**, 2451–2458.
Kabin, K., Israelevich, P.L., Ershkovich, A.I., Neubauer, F.M., Gombosi, T.I., De Zeeuw, D.L., and Powell, K.G.: 2000, 'Titant's magnetic wake: atmospheric or magnetospheric interation', *J. Geophys. Res.* **105**, 10761–10770.
Kennel, C.F.: 1973, 'Magnetospheres of the Planets', *Space Sci. Rev.* **14**, 511–533.
Kivelson, M.G.: 2005, 'The current systems of the Jovian magnetosphere and ionosphere and predictions for Saturn', *Space Sci. Rev.*, this volume.
Krimigis, S.M.: 1982, 'A post-Voyager view of Saturn's environment', *Johns Hopkins APL Technical Digest* **3**(2), 180–188.
Krimigis, S.M. and Armstrong, T.P.: 1982, 'Two-component proton spectra in the inner Saturnian magnetosphere', *Geophys. Res. Lett.* **9**, 1143–1146.
Krimigis, S.M., Carbary, J.F., Keath, E.P., Bostrom, C.O., Axford, W.I., Gloeckler, G., Lanzerotti, L.J., and Armstrong, T.P.: 1981a, 'Characteristics of hot plasma in the Jovian magnetosphere: Results from the Voyager spacecraft', *J. Geophys. Res.* **86**, 8227–8257.
Krimigis, S.M., Armstrong, T.P., Axford, W.I., Bostrom, C.O., Gloekler, G., Keath, E.P., Lanzerotti, L.J., Carbary, L.J., Hamilton, D.C., and Roelof, E.C.: 1981b, 'Low-energy charged particles in Saturn's magnetosphere – results from Voyager 1', *Science* **212**, 225–231.
Krimigis, S.M., Carbary, J.F., Keath, E.P., Armstrong, T.P., Lanzerotti, L.J., and Gloeckler, G.: 1983, 'General characteristics of hot plasma and energetic particles in the Saturnian magnetosphere – results from the Voyager spacecraft', *J. Geophys. Res.* **88**, 8871–8892.
Kronberg, E., Woch, J., Krupp, N., Lagg, A., Khurana, K., and Glassmeier, K.-H.: 2004, 'Mass release at Jupiter-substorm-like processes in the Jovian magnetotail', *J. Geophys. Res.*, in press.
Krupp, N., Woch, J., Lagg, A., Wilken, B., Livi, S., and Williams, D.J.: 1998, 'Energetic particle bursts in the predawn Jovian magnetotail', *Geophys. Res. Lett.* **25**, 1249–1253.
Lammer, H. and Bauer, S.J.: 1993, 'Atmospheric mass loss from Titan by sputtering', *Planet. Space Sci.* **41**, 657–663.
Lanzerotti, L.J., Maclennan, C.G., Lepping, R.P., and Krimigis, S.M.: 1983, 'On the plasma conditions at the dayside magnetopause of Saturn', *Geophys. Res. Lett.* **10**, 1200–1202.
Lazarus, A.J. and McNutt, R.L.: 1983, 'Low-energy plasma ion observations in Saturn's magnetosphere', *J. Geophys. Res.* **88**, 8831–8846.
Ledvina, S.A., Brecht, S.H., and Luhmann, J.G.: 2004a, 'Ion distributions of 14 amu pickup ions associated with Titan's plasma interaction', *Geophys. Res. Lett.* **31**, CiteID L17S10.
Ledvina, S.A., Luhmann, J.G., Brecht, S.H., and Cravens, T.E.: 2004b, 'Titan's induced magnetosphere', *Adv. Space Res.* **33**, 2092–2102.
Ledvina, S.A., Luhmann, J.G., and Cravens, T.E.: 2004c, 'Ambient ion distributions in Saturn's magnetosphere near Titan during a non-Voyager type interaction', *Adv. Space Res.* **33**, 221–226.
Maclennan, C.G., Lanzerotti, L.J., Krimigis, S.M., Lepping, R.P., and Ness, N.F.: 1982, 'Effects of Titan on trapped particles in Saturn's magnetosphere', *J. Geophys. Res.* **87**, 1411–1418.
Mauk, B.H., Williams, D.J., McEntire, R.W., Khurana, K.K., and Roederer, J.G.: 1999, 'Storm-like dynamics of Jupiter's inner and middle magnetosphere', *J. Geophys. Res.* **104**, 22759–22778.

Nagy, A.F., Liu, Y., Hansen, K.C., Kabin, K., Gombosi, T.I., Combi, M.R., Dezeeuw, D.L., Powell, K.G., and Kliore, A.J.: 2001, 'The interaction between the magnetosphere of Saturn and Titan's ionosphere', *J. Geophys. Res.* **106**, 6151–6160.

Ness, N.F., Acuña, M.H., Behannon, K.W., Burlaga, L.F., Connerney, J.E.P., Lepping, R.P., Neubauer, F.M.: 1982, 'Magnetic field studies by Voyager 2 – preliminary results at Saturn', *Science* **215**, 558–563.

Neubauer, F.M., Gurnett, D.A., Scudder, J.D., and Hartle, R.E.: 1984, 'Titan's magnetospheric interaction', in T. Gehrels and M.S. Matthews (eds.), *Saturn*, The University of Arizona Press, Tucson, pp. 760–787.

Northrop, T.G. and Thomsen, M.F.: 1980, 'Theory of scan plane flux anisotropies', *J. Geophys. Res.* **85**, 5719–5724.

Paranicas, C., Decker, R.B., Mauk, B.H., Krimigis, S.M., Armstrong, T.P., and Jurac, S.: 2004, 'Energetic ion composition in Saturn's magnetosphere revisited', *Geophys. Res. Lett.* **31**, CiteID L04810.

Richardson, J.D.: 1986, 'Thermal ions at Saturn – plasma parameters and implications', *J. Geophys. Res.* **91**, 1381–1389.

Santos-Costa, D., Blanc, M., Maurice, S., and Bolton, S.J.: 2003, 'Modeling the electron and proton radiation belts of Saturn', *Geophys. Res. Lett.* **30**, SSC 6–1, 10.1029/2003GL017972.

Saur, J., Mauk, B.H., Kaßner, A., and Neubauer, F.M.: 2004, 'A model for the azimuthal plasma velocity in Saturn's magnetosphere', *J. Geophys. Res.* **109**, CiteID A05217.

Scarf, F.L.: 1973, 'Some comments on the magnetosphere and plasma environment of Saturn', *Cosmic Electrodynamics*.

Schardt, A.W., Behannon, K.W., Lepping, R.P., Carbary, J.F., Eviatar, A., and Siscoe, G.L.: 1984, 'The outer magnetosphere', in T. Gehrels and M.S. Matthews (eds.), *Saturn*, The University of Arizona Press, Tucson, pp. 416–459.

Schardt, A.W.: 1983, 'The magnetosphere of Saturn', *Rev. of Geophys. and Space Phys.* **21**, 390–402.

Simpson, J.A., Bastian, T.S., Chenette, D.L., McKibben, R.B., and Pyle, K.R.: 1980, 'The trapped radiations of Saturn and their absorption by satellites and rings', *J. Geophys. Res.* **85**, 5731–5762.

Sittler, E.C., Ogilvie, K.W., and Scudder, J.D.: 1983, 'Survey of low-energy plasma electrons in Saturn's magnetosphere – Voyagers 1 and 2', *J. Geophys. Res.* **88**, 8847–8870.

Thomsen, M.F., Northrop, T.G., Schardt, A.W., and van Allen, J.A.: 1980, 'Corotation of Saturn's magnetosphere – evidence from energetic proton anisotropies', *J. Geophys. Res.* **85**, 5725–5730.

Van Allen, J.A.: 1984, 'Energetic particles in the inner magnetosphere of Saturn', in T. Gehrels and M.S. Matthews (eds.), *Saturn*, The University of Arizona Press, Tucson, pp. 281–317.

Vasyliūnas, V.M.: 1983, 'Plasma distribution and flow', in A.J. Dessler (ed.), *Physics of the Jovian Magnetosphere*, Cambridge University Press, New York, Chapter 11, pp. 395–453.

Woch, J., Krupp, N., Khurana, K.K., Kivelson, M.G., Roux, A., Perraut, S., Louarn, P., Lagg, A., Williams, D.J., Livi, S., and Wilken, B.: 1999, 'Plasma sheet dynamics in the Jovian magnetotail: signatures for substorm-like processes?', *Geophys. Res. Lett.* **26**, 2137–2140.

Woch, J., Krupp, N., Lagg, A., Wilken, B., Livi, S., and Williams, D.J.: 1998, 'Quasi-periodic modulations of the Jovian magnetotail', *Geophys. Res. Lett.* **25**, 1253–1256.

Zarka, P.: 2005, 'Radio wave emission from the Outer planets before Cassini', *Space Sci. Rev.*, this volume.

RADIO WAVE EMISSION FROM THE OUTER PLANETS BEFORE CASSINI

P. ZARKA[1] and W. S. KURTH[2]
[1] *LESIA, Observatoire de Paris, 92195 Meudon, France*
[2] *Dept. of Physics and Astronomy, The University of Iowa, Iowa City, IA 52242-1479, USA*

Received: 21 June 2004; Accepted in final form: 30 August 2004

Abstract. We review observations and theories of radio wave emissions from the outer planets. These include radio emissions from the auroral regions and from the radiation belts, low-frequency electromagnetic emissions, and atmospheric lightning. For each of these emissions, we present in more details our knowledge of the Saturn counterpart, as well as expectations for Cassini. We summarize the capabilities of the radio instrument onboard Cassini, observations performed during the Jupiter flyby, and first (remote) observations of Saturn. Open questions are listed along with the specific observations that may bring responses to them. The coordinated observations (from the ground and from space) that would be valuable to perform in parallel to Cassini measurements are briefly discussed. Finally, we outline future missions and perspectives.

Keywords: radio wave emission, giant planets

1. Introduction

Study of planetary radio wave emissions started in 1955 with the discovery of the decameter (DAM) emission from Jupiter by Burke and Franklin (1955). Soon interpreted as electron cyclotron emission, it was the first proof of existence of a Jovian magnetic field. DAM is emitted up to 40 MHz, indicating a maximum field intensity above 10 Gauss.

Subsequent observations by the Voyager, Ulysses, and Galileo spacecraft revealed that all magnetized planets (particularly the outer planets) produce intense nonthermal radio emissions. Those are an interesting remote sensing tool of magnetospheric plasmas : they can travel far from their source region, and carry imprints of both their source region characteristics (through their generation mechanism) and of the plasmas they traversed (through various propagation effects). Radio emissions allow us to directly 'see' planetary magnetospheres, but do we understand what we see?

Throughout this paper, we largely refer to previous reviews (and figures) by Zarka (1998, 2000, and 2004a), and by Kurth and Zarka (2001). We cite only those recent papers not covered as well as a few key papers.

'Radio' emissions are electromagnetic free-space modes, either **O**rdinary or e**X**traordinary, that can be propagating to 'infinity', that is in practice far from their source (as illustrated in Figure 1 of Zarka, 2004a). They are polarized circularly

Space Science Reviews 116: 371–397, 2005.
DOI: 10.1007/s11214-005-1962-2

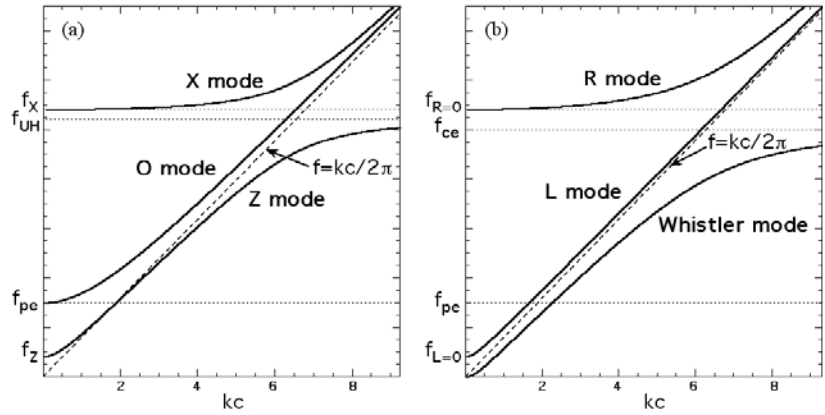

Figure 1. Cold plasma dispersion curves of electromagnetic electronic modes for $f_{pe}/f_{ce} = 0.3$ with ion motions neglected. (a) Quasi-perpendicular propagation. (b) Quasi-parallel propagation.

near their low-frequency (LF) cutoff, respectively in the Left-Hand (LH) and Right-Hand (RH) sense. Figure 1 illustrates the dispersion of electromagnetic modes in a magnetized cold plasma with $f_{pe}/f_{ce} = 0.3$ (with f_{pe} the plasma frequency and f_{ce} the electron cyclotron frequency). When the wave propagation is not strictly parallel to the ambiant magnetic field (so-called quasi-perpendicular), the **O**-mode cutoff is at f_{pe} while that of the **X**-mode is at $f_X \approx \left[1 + (f_{pe}/f_{ce})^2\right] f_{ce}$. In all cases, radio waves can thus propagate in the solar wind only above its local plasma frequency. This frequency lies between $\sim$ 1 and 5 kHz for the outer planets, about 30 kHz at the Earth orbit, and up to $\sim$ 100 kHz around Mercury (see Figure 1 of Zarka, 2000). Planetary radio emissions generated below the local solar wind f_{pe} remain trapped in the magnetospheric cavity. Similarly, ground-based observations are permitted only above $\sim$ 10 MHz, the peak plasma frequency in the Earth's ionosphere. Lower frequency waves are reflected back to space.

An interesting analogy may be done with a metallic mirror: assuming that each atom occupies a typical volume of $(2\text{Å})^3$ and contributes for 1 free electron, we derive an electron density $N_e \sim 10^{29}$ m^{-3} and thus a plasma frequency $f_{pe} \sim 3 \times 10^{15}$ Hz, i.e. a wavelength $\lambda \approx 100$ nm (in the far UV). This explains why a mirror reflects IR and visible light, but is transparent to FUV and X-rays except for grazing incidence $\theta \approx \pi/2$ because the actual LF cutoff is at $f_{pe}/\cos(\theta)$.

The most severe limitation of LF radio observations is the lack of angular resolution, due to the fact that the wavelength-to-instrument size ratio (λ/D) is very large, often $(\lambda/D) \geq 1$. This is dramatically illustrated in Figure 2, which displays two HST images of Saturn's aurora taken in the UV (2a), and a simulation of the corresponding images that would be obtained with Radio eyes (2b): no structure can be distinguished on Saturn's disk and only the time variation of the total emission level, diluted by averaging over the whole image, can be measured.

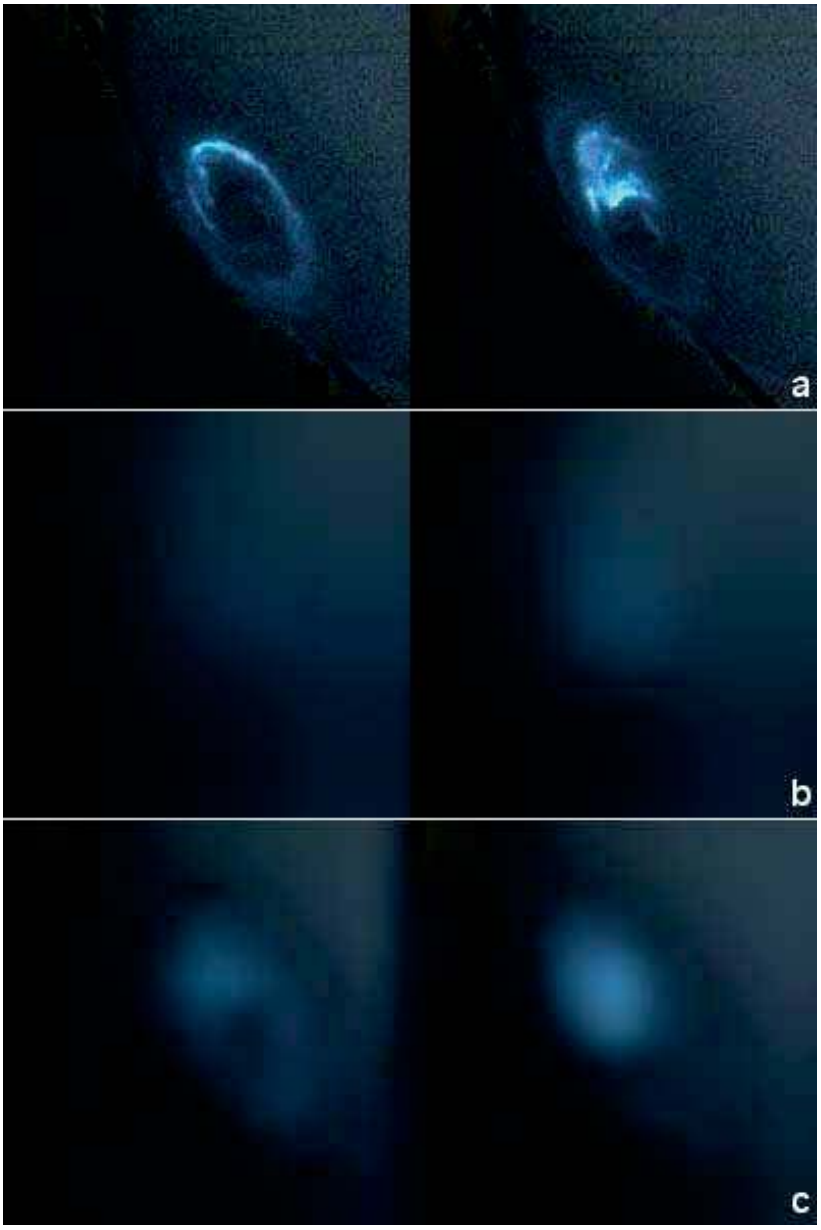

Figure 2. (a) Two HST images of Saturn's southern UV aurora: quiet auroral oval on 18 Jan. 2004, and auroral flare on 26 Jan. 2004. (b) same as (a), degradated to the (absence of) resolution available with LF radio eyes. (c) same as (a), degradated to the resolution ($\sim 1^\circ$) restored by the direction-finding technique. Cassini is assumed to be at $10R_S$ from Saturn.

TABLE I

Planetary radio components characteristics. E=Earth, J=Jupiter, S=Saturn, U=Uranus, N=Neptune, I=Io, G=Ganymede, C=Callisto, NTC=nonthermal continuum, nKOM=narrowband kilometer radiation (from Io's torus). '?' indicates unconfirmed radio detection. f_{UH} is the upper hybrid frequency (see Zarka, 2004a, for definitions of characteristic frequencies of interest).

Radio component	*Planet*	λ (m)	f (kHz)	*Radiation process*
Auroral	E J S U N	$10^1 - 10^3$	10's kHz – 10's MHz	Cyclotron Maser (coherent)
Satellite induced	J-I J-G J-C? S?	$10^1 - 10^2$	$\geq$ MHz	Cyclotron Maser (coherent)
LF e.m. (NTC ...)	E J S U N G	$\sim 10^4$	$\leq$ 10's kHz	Mode conversion e.s. $\rightarrow$ e.m.
Lightning	E J? S U N?	$10^1 - 10^4$	kHz - MHz	Antenna radiation (current discharge)
Radiation belts	J E?	$\sim 10^{-1}$	GHz	Synchrotron (incoherent)
nKOM	J	$\sim 10^3$	$\sim$ 100 kHz	Instabilities $\sim f_{pe}$, f_{UH}?

However, the spectral range of the radio emissions also varies quickly with time (over timescales from well below 1 sec to weeks of months), providing useful information on source locations, generation processes, etc., so that dynamic spectra (such as displayed in Figure 2 of Zarka, 1998) are the primary tool for studying planetary radio emissions. For outer planets radio emissions, such measurements have been performed since more than 4 decades by the RAE 1 and 2 Earth orbiters, the Voyager 1 and 2, Ulysses, Galileo, Wind and Cassini spacecraft, as well as many ground-based radiotelescopes. About 20 more satellites have studied in details the terrestrial radio emissions. The capabilities of the corresponding radio instruments for measuring flux, polarization, **k**-vector (so-called 'direction-finding' – DF) are detailed in Table 2 of Zarka (2000).

Many radiosources are found in planetary magnetospheres, depending on the magnetic field topology, plasma distribution, and magnetospheric dynamics (e.g. the regions of energetic electron precipitations). The main ones are listed in Table I, adapted from Zarka (2000), together with their wavelength/frequency range and their (most probable) radiation process.

Jupiter is the only planet where all components exist (except radio lightning possibly blocked by the ionosphere) (cf. Zarka *et al.*, 2004a). We will focus below on the components relevant to the case of Saturn, i.e. auroral and satellite-induced radio emissions, LF electromagnetic emissions, lightning, and emission from radiation belts.

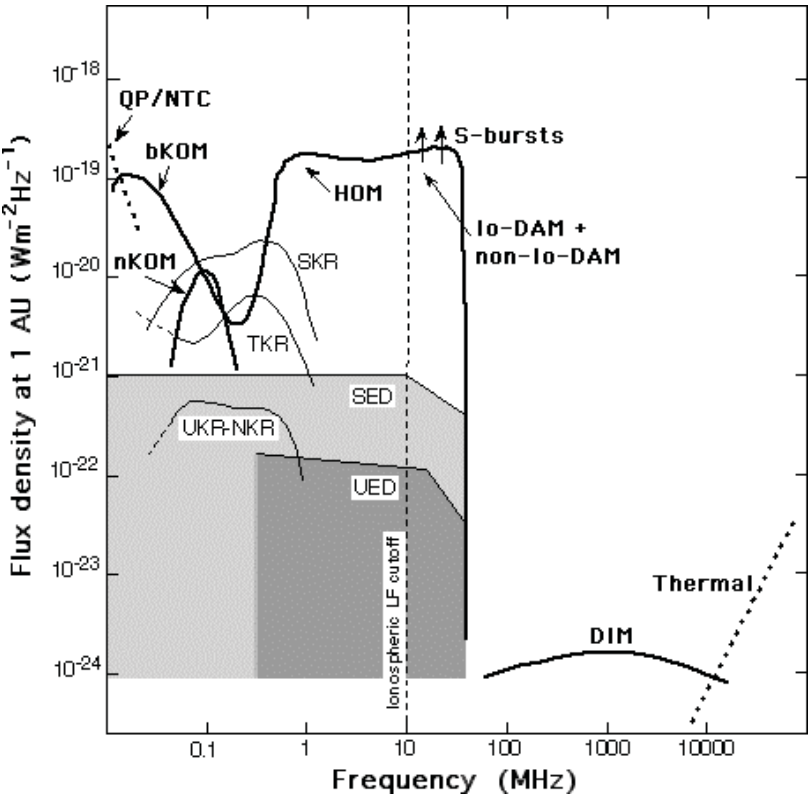

Figure 3. Boldface lines represent average spectra of Jovian radio components normalized for a source-observer distance of 1 AU. Lightface solid lines represent auroral radio emissions spectra for the other radio planets. Grey-shaded regions show ranges of intensities versus frequency for Saturnian and Uranian lightning. Ground-based observations give access to the right of the dashed line (ionospheric cutoff) (after Zarka *et al.*, 2004b). The acronyms denote: bKOM = broadband Kilometer radiation; nKOM = narrowband Kilometer radiation; HOM = Hectometer radiation; SKR/TKR/UKR/NKR = Saturn/Terrestrial/Uranus/Neptune Kilometer radiation; QP = Quasi-Periodic bursts; NTC = Non-Thermal Continuum radiation; DIM/DAM = DecIMeter/DecAMeter radiation; S-bursts = Short bursts; SED/UED = Saturn/Uranus Electrostatic Discharge.

2. Comparative Overview of Outer Planets' Radio Emissions

Figure 3 summarizes the average spectra of most planetary radio components, together with their nomenclature.

2.1. Auroral and Satellite-Induced Radio Emissions

The mid-to-high frequency portion of the planetary radio spectrum (typically between a few kHz and a few MHz) is dominated by emissions believed to be generated via the Cyclotron Maser Instability (CMI), usually relatively close to the

planet on field lines threading the planet's auroras. They are an important part of the physics of planetary auroras.

2.1.1. *Observations*

General properties of auroral radio emissions, as summarized in Zarka (1998) and Zarka (2004a), include:

- Very high intensities: on Figure 3, Jovian hecto-decameter emissions appear 10^5 times stronger than the synchrotron emission from the radiation belts.
- Emission produced along magnetic field lines at the local electron cyclotron frequency ($f \sim f_{ce}$) (Ladreiter *et al.*, 1994b), resulting in a broad total bandwidth over the whole source region ($\Delta f \sim f$).
- Polarization 100% circular (elliptical for the Jovian DAM), with a sense consistent with **X**-mode, i.e. RH from northern magnetic hemispheres, LH from southern ones (Lecacheux, 1988).
- Source regions corresponding to strongly magnetized regions ($f_{pe} \ll f_{ce}$) where unstable keV electron populations exist: these are northern and southern auroral regions. At Earth, plasma cavities exist in these regions (Calvert, 1981), and particles are thought to be accelerated via magnetic reconnection in the magnetotail, so that TKR sources are mainly located in the nightside hemisphere. At Jupiter, field-aligned currents result from corotation breakdown beyond $30-50 R_J$ (Cowley and Bunce, 2001), so that auroral bKOM/HOM/DAM radiosources are found at all local times. At Uranus and Neptune, the large tilt of the planetary magnetic field results in plasma depleted equatorial regions where radio emission generation is also possible (Desch *et al.*, 1991; Zarka *et al.*, 1995).
- Very anisotropic beaming at large angle (generally $\geq 30°$ to 90°) from the magnetic field direction in the source.
- Strong modulation by the planetary rotation at all outer planets, related to the anisotropic beaming, the corotation of the inner/middle magnetosphere, the presence of magnetic anomalies, etc. This modulation is actually used to derive the rotation period of the planetary body (source region of the magnetic field), which cannot be accessed through optical observations due to the superimposed proper motions of the clouds. Analysis of 24 years of ground-based observations of Io-induced decameter emission (Io-DAM) allowed to derive a rotation period of 9h 55m 29.7s $\pm$ 0.1s (Higgins *et al.*, 1997). Analysis of 267 days of Voyager observations of SKR gave a rotation period of 10h 39m 22.4s $\pm$ 7s (Desch and Kaiser, 1981a).
- Modulation by some satellites: the most famous case is of course the strong modulation of part of the Jovian DAM (Bigg, 1964), which induces additional electron precipitation near the magnetic flux tube connecting Io to the planet. Some evidence for radio emissions associated with Ganymede and perhaps Callisto also exists (Hospodarsky *et al.*, 2001). Modulation of SKR by Dione has been suggested by Kurth *et al.* (1981), as discussed below.

- Modulation by solar wind fluctuations, which probably exerts an influence on the external magnetosphere and thus on very high latitude regions. At Earth, Gallagher and D'Angelo (1981) found a strong correlation between the solar wind speed and the TKR output. TKR bursts are also known to be related to inversions of the interplanetary magnetic field (IMF). Other solar wind parameters (density, pressure) intervene at the other planets (see Zarka, 1998, and references therein).
- Modulation by interplanetary shocks compressing the magnetosphere, as recently discovered at Jupiter during the Cassini flyby (Gurnett *et al.*, 2002).
- Strong correlation with UV aurora, as direcly checked at Earth with measurements by DE-1 (Huff *et al.*, 1988) and Viking, and indirectly at Jupiter (Prangé *et al.*, 1993; Gurnett *et al.*, 2002).

Smooth and bursty components often co-exist on the dynamic spectra of auroral and satellite-induced radio emissions (cf. Figure 4 of Zarka, 1998, and Figure 6 of Zarka, 2004a). It is not clear if they must be attributed to different source structures or different generation mechanisms.

2.1.2. *Theory*

The high intensities observed require a highly efficient, coherent generation mechanism, for directly generating free-space **X**-mode, without any conversion step which would reduce the overall efficiency. The CMI proposed by Wu and Lee (1979) is now broadly accepted as the best candidate generation mechanism (Louarn, 1992; Zarka, 1998). We briefly summarize below its main characteristics.

CMI requires $f_{\rm pe} \ll f_{\rm ce}$ in the source region and produces emission at $f \sim f_{\rm X} \approx f_{\rm ce}$ at the expense of electrons perpendicular energy ($\approx m_{\rm e} v_\perp^2/2$), which must be of the order of a few keV. Radio wave amplification requires positive gradients in the electrons distribution relative to perpendicular velocity ($\partial f/\partial v_\perp > 0$) at keV energies. Such gradients do exist in auroral electron distributions (loss-cone or hollow beam, Mizera and Fennel, 1977). CMI then predicts intense emission, beamed at large angle with respect to the source magnetic field. It has an overall efficiency up to 1% at saturation (ratio of wave energy to total electrons energy) consistent with observational estimates (see, e.g., Pritchett, 1986), and may produce fine spectral structures (Baumback and Calvert, 1987).

Direct measurements have been obtained in the Earth's auroral regions by the Viking and FAST satellites. Viking found that TKR sources are laminar cavities (width of the order of 1 km, Hilgers, 1992), dominated by tenuous hot plasma ($1-5$ keV) with quasi-trapped population (Louarn *et al.*, 1990; Zarka, 1998). This implies that wave dispersion should take into account relativistic effects due to hot plasma, and results in emission favored at $\sim 90^\circ$ from the source magnetic field, at frequencies that may be lower than $f_{\rm ce}$ (because then $f_{\rm X} \leq f_{\rm ce}$). FAST measurements brought direct confirmation to these results and extended them via discovery of 'shell' electron distributions, very efficient for wave amplification perpendicular to the magnetic field (Ergun *et al.*, 1998). The wave may be reflected back and

forth several times by the density gradients at the edges of the source cavity, which plays thus the role of a laser cavity and may produce intense fine spectral structures (Calvert, 1982).

2.1.3. *The Case of Saturn*

Saturn Kilometric Radiation is second only to Jupiter in intensity (Figure 3). It extends from a few kHz to 1.3 MHz, with a spectral peak between 100 and 400 kHz. This spectral range reflects Saturn's magnetic dipole moment of 0.215 G R_S^3. Spectral structures such as arcs and bursts are visible in SKR dynamic spectra (cf. Figure 2 of Kurth and Zarka, 2001, and Figure 6c of Zarka, 2004a).

The SKR spectrum was modelled on the basis of the CMI saturated by trapping of the electrons in the wave electric field (Galopeau *et al.*, 1989). The choice of trapping rather than quasilinear diffusion as the main saturation mechanism was justified by the narrow instantaneous bandwidth of SKR fine spectral structures. A good agreement was obtained between computed and observed spectra, the former being generally higher than the latter. This suggests marginal saturation of the SKR emission.

The variations of the measured polarization along the Voyager 1 and 2 flybys allowed Galopeau *et al.* (1995) to constrain the northern and southern SKR source locations. Conjugated high latitude sources fixed in local time were found, with a broad extent towards the morningside at lower latitudes, suggesting a Kelvin-Helmholtz instability at the magnetopause as the source of accelerated electrons responsible for the auroral radio and UV emissions. As an alternative, Cowley *et al.* (2004) gave arguments in favor of upwards currents at the boundary between open and closed field lines. Auroral UV emissions as observed by HST appear to be consistent with the derived SKR source locations (brighter in the morningside) (Trauger *et al.*, 1998).

In spite of the fact that sources are fixed in local time, SKR is strongly modulated at the planetary rotation period about 10h 39.4m. Its variations are also correlated to solar wind fluctuations (especially the ram pressure) (Desch, 1982). Total extinctions of SKR were observed at times when Saturn's magnetosphere was engulfed inside Jupiter's magnetospheric tail. The correlation is so tight that SKR might be used as a proxy for the solar wind pressure during the Cassini tour when the spacecraft will be inside of the magnetosphere. Recent observations (Prangé *et al.*, 2004) suggest that UV aurorae have intensified in response to the arrival at Saturn of the same interplanetary shocks that caused enhanced radio and UV emissions when they passed Jupiter (Gurnett *et al.*, 2002).

The strong SKR modulation at the planetary rotation period is also surprising when one considers that the planetary magnetic field as measured by Pioneer and Voyager spacecraft is nearly axisymmetrical (Connerney *et al.*, 1984). Analysis of the variations of the SKR instantaneous maximum frequency led Galopeau *et al.* (1991; 1992) to derive the existence and estimate the magnitude and position of a magnetic anomaly at high latitudes. An alternate field model, including such

an anomaly while remaining consistent with the available magnetometer measurements, was proposed by Ladreiter *et al.* (1994a). More puzzling are the 1% variations of the SKR period observed at the timescale of months with the Ulysses radio instrument (Galopeau and Lecacheux, 2000). Cecconi and Zarka (2002) proposed an explanation in terms of non-random solar wind variations (e.g. the asymmetrical sawtooth variation of the solar wind flow speed at 10 AU) controlling the local time position of the source, which may broaden or shift the measured radio period through beating of the planetary rotation period ($\sim$ 10h 40m) with the solar wind variations timescale ($13 - 26$ days).

Another puzzling observation by Voyager is the possible control of SKR activity by the satellite Dione (Desch and Kaiser, 1981b; Kurth *et al.*, 1981). Proposed interpretations include occultation of SKR low frequencies by plasma released at a certain orbital phase of the satellite, or an induced radio emission similar to Io-DAM. For such electrodynamic interactions, Zarka *et al.* (2001) derived an empirical law relating the magnetic energy flux of the planetary field intercepted by the obstacle (the satellite's ionosphere or magnetosphere) to the induced radio power. Applied to Dione, this law predicts a negligible effect with a contribution not larger than 0.2% of the average SKR power. In order to reach a few percents, Dione's 'electrodynamic size' should be one order of magnitude larger than its solid body, which implies the existence of either an intrinsic magnetic field or an extended exo-ionosphere.

A control of Saturn's radio emission by Titan is even more unlikely based on the above scaling law: due to Titan's large orbital radius ($\sim 20 R_S$), the power dissipated through an electrodynamic interaction with Saturn's field should be 20 times smaller than for Dione. Titan spends also part of the time outside Saturn's magnetosphere. A zoo of plasma waves is generated in Titan's wake (see review by Neubauer *et al.*, 1984), but as far as radio waves are concerned, the only connection with Titan (apart from lightning – see Section 2.3) involves possible SKR occultations by Titan's ionosphere, that will allow to probe its electron density.

2.2. LF Electromagnetic Emissions

At low frequencies, the radio spectrum can be quite complex if not as powerful as in the above spectral range. Many of the low-frequency radio components are thought to be generated via mode conversion from electrostatic upper hybrid bands in the middle or even outer portion of the planet's magnetosphere such as trapped and escaping continuum radiation reviewed by Kurth (1992). The upper hybrid frequency f_{uh} is related to f_{ce} and f_{pe} by $f_{uh}^2 = f_{ce}^2 + f_{pe}^2$. Further, the upper hybrid band is a special case of the so-called $(n + 1/2) f_{ce}$ or cyclotron harmonic emissions (Kurth *et al.*, 1979) where the frequency of the band is at the upper hybrid resonance frequency. The upper hybrid bands tend to have narrow fractional bandwidths (a few percent or less) and can be quite intense, with electric fields approaching 1 mV/m or more.

The mode conversion mechanism was first proposed to explain low-frequency narrowband emissions at Earth by Jones (1976) based on theory developed by Oya (1971). This is a linear conversion mechanism for which electrostatic waves with the proper polarization at the electron plasma frequency can couple to the left-hand ordinary (**L**-**O**) mode (see review by Jones, 1988). Others have criticized the linear theory, not because it does not result in radio emissions, but because it is thought to be inefficient and incapable of producing the required field strengths (Melrose, 1981; Barbosa, 1982; Rönnmark, 1983). These authors suggest a non-linear mechanism is more likely responsible for most of the observed emissions. Jones' theory has some fairly specific beaming predictions, but the observational evidence for the beaming is mixed (Jones *et al.*, 1987; Morgan and Gurnett, 1991).

Two types of low-frequency radio emissions have been most closely tied to (either) the (linear or non-linear) mode conversion of upper hybrid bands. These are the trapped and escaping non-thermal continuum radiation at Earth first described in detail by Gurnett (1975) and similar emissions observed at other planetary magnetospheres. Trapped continuum radiation is also found in the magnetospheres of Jupiter, Saturn, and Uranus. The lower frequency component is trapped within the planet's magnetosphere because it is generated at frequencies below the electron plasma frequency in the magnetosheath and, therefore, cannot propagate beyond the magnetopause. Eventually the waves can propagate down the magnetotail and escape into the solar wind where the wave frequency exceeds the solar wind plasma frequency. Jupiter's trapped component is perhaps the most spectacular since the very deep density cavities in the magnetospheric lobes are very effective at trapping the electromagnetic waves and the intensities at the lowest frequencies are, subsequently, extremely high. The trapped component of the non-thermal continuum radiation has a much more continuous spectrum than the escaping component but often displays narrowband intensifications. This spectrum is the superposition of emissions from a large number of sources at different frequencies and the effect of Fermi-Compton scattering off the moving walls of the magnetosphere.

The higher frequency escaping component is seen at Earth as well as at Jupiter, Saturn, Uranus, and Neptune. The escaping portion of the continuum radiation is perhaps most clearly related to the upper hybrid conversion mechanism. The escaping continuum radiation is actually a misnomer because it comprises large numbers of very narrowband emissions as in Figure 4. This figure provides some of the best evidence that the upper hybrid bands are intimately tied to the radio emissions as the frequency of the radio emissions closely match those of the upper hybrid bands and the two phenomena appear to be connected at the density gradient on the magnetopause. Other evidence uses the r^{-2} variation in intensity of the radio emissions from the location of upper hybrid bands. The Jovian narrowband emissions often drift to lower frequencies with time. The drifting may indicate that the source plasma is moving outward through the magnetosphere in the range of $15 - 25 R_J$, possibly as a result of the centrifugally-driven interchange instability.

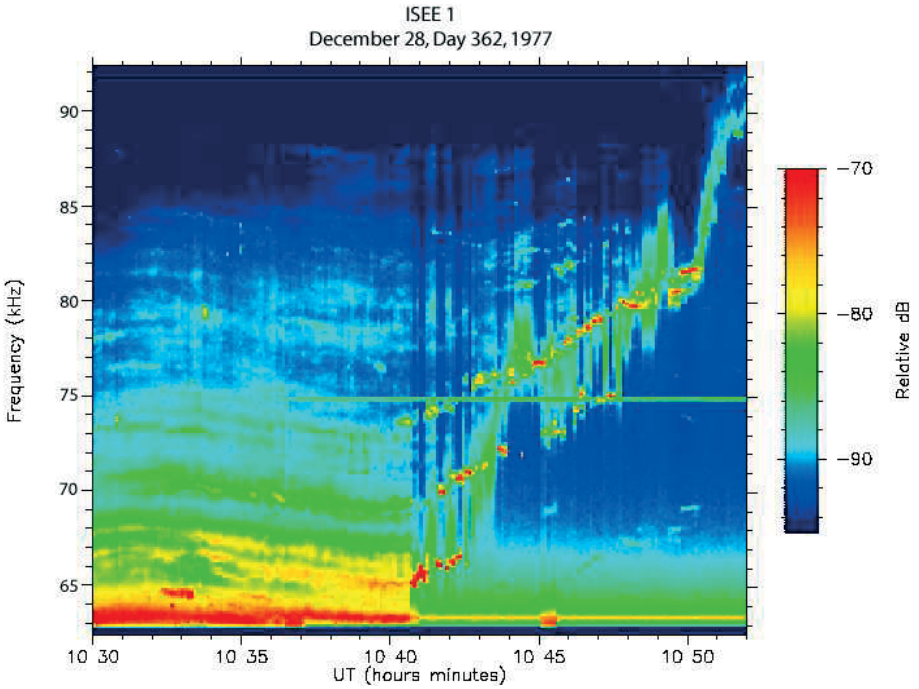

Figure 4. A source of escaping continuum radiation at Earth's plasmapause as observed by ISEE. The narrowband radio emissions are seen being emitted from narrowband electrostatic waves at the upper hybrid resonance frequency (after Kurth, 1982).

Ganymede's magnetosphere is also the source of low frequency ($15 - 50$ kHz) narrowband emissions (Gurnett *et al.*, 1996). Ganymede appears to be the only example of a planetary magnetosphere whose low-frequency (non-CMI) radio emission dominates its spectrum. It is likely that an important criteria for the CMI is not met in Ganymede's magnetosphere, that is that there are no density cavities where $f_{pe}/f_{ce} < 0.3$ as is thought to be the case for other planetary CMI sources.

Other low-frequency planetary radio components evidently not related to the upper hybrid mode conversion mechanism include radio emissions associated with the planet's bow shock (Gurnett, 1975), Jovian type III (also called quasi-periodic or QP) bursts (Kurth *et al.*, 1989; MacDowall *et al.*, 1993), and VLF radio emissions from Jupiter's magnetosheath (Kaiser *et al.*, 1992). The bow shock related emission is quite weak and has not been reported at planets other than Earth although given the ubiquity of bow shocks, it seems surprising that this emission has not been observed at the outer planets.

QP bursts are brief, broadband bursts in the frequency range of a few to 50 kHz which appear quasi-periodically with periods ranging from a couple of minutes to 45 minutes or even longer. Other magnetospheric phenomena reveal periodicities in $\sim 15 - 45$ minute range, including bursts of MeV electrons observed by Ulysses, and high-latitude X-rays associated with auroral features observed by

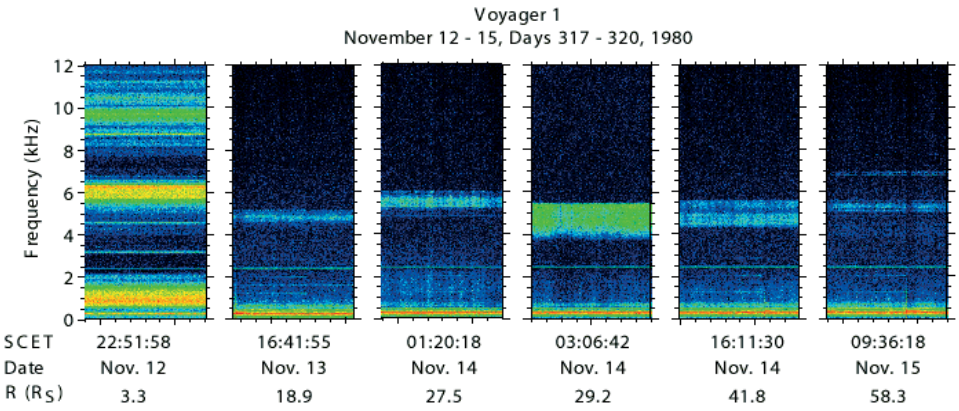

Figure 5. Narrowband radio waves detected at Saturn (Gurnett *et al.*, 1981).

Chandra (Gladstone *et al.*, 2002). QP bursts display evidence of dispersion at the lower frequencies, that may be due to propagation through the relatively dense magnetosheath (Desch, 1994). Terrestrial LF bursts present some similarities with Jovian QP bursts. For those, Steinberg *et al.* (2004) have shown that the dispersion at the lower frequencies is due to propagation through the solar wind.

VLF emissions from Jupiter's magnetosheath have been reported under a variety of terminology over the years including escaping continuum radiation, reradiated emission, and others, demonstrating a lack of a crisp understanding of the source of the emission. These emissions vary in frequency as about twice the solar wind plasma frequency, are strongly modulated at Jupiter's rotation period and appear to be related, in part, to the QP bursts.

Saturn exhibits a complex set of narrowband electromagnetic emissions in the frequency range of 3 to 30 kHz as shown in Figure 5. The spacing of the narrowband radio emissions is in some cases similar to the electron cyclotron frequencies near the orbits of Tethys, Dione, and Rhea, suggesting that the source of the emissions could be related to the magnetospheric interaction with these moons. Two possibilities are that the moons are a source of plasma or that there is a Ganymede-like magnetosphere at one or more of them, although this would seem highly unlikely based on their small masses.

2.3. LIGHTNING

Radio signatures of lightning were discovered by Voyager 1 at Saturn (Warwick *et al.*, 1981). Prior to understanding their atmospheric origin, these spikes were named SED for 'Saturn Electrostatic Discharge'. Similar emissions – accordingly named UED – were observed at a lower rate at Uranus (Zarka and Pedersen, 1986). Only 4 weak events of the same kind were detected by Voyager 2 during the Neptune fly-by (Kaiser *et al.*, 1991).

No radio emission from lightning was detected at Jupiter by any visiting spacecraft (Voyagers, Galileo, and Cassini), although optical flashes (Cook *et al.*, 1979) and LF whistlers (Gurnett *et al.*, 1979) were observed. Zarka (1985b) showed that the low-altitude ionospheric layers discovered by Pioneer 10 and 11 would cause strong absorption (tens of dB) of radio waves generated in the atmosphere. Farrell *et al.* (1999) conversely proposed, on the basis of electric field measurements performed in Jupiter's atmosphere by Galileo's descent probe, that Jovian lightning discharges could have much longer time constants than their Terrestrial or Saturnian counterparts (milliseconds instead of microseconds or less). No reason was provided for the existence of such 'slow' lightning, but it would imply radio emission spectra restricted to very low frequencies, below Jupiter's ionospheric cutoff.

On Venus, the existence of lightning has remained controversial for more than two decades. During the two close-range fly-bys of Venus by Cassini in 1998 and 1999, the sensitive radio receiver onboard the spacecraft detected no statistically significant lightning signal, while it recorded hundreds of lightning radio spikes during the Earth fly-by in 1999, up to 40 dB above the detection threshold (Gurnett *et al.*, 2001). Venus lightning were concluded to be extremely rare ($\ll$ 1 flash/hour) or 100 times weaker than their Terrestrial counterparts. Absence of lightning at Venus could be due to a very low vertical convection, inhibited by the strong horizontal atmospheric circulation.

Figure 6 shows a dynamic spectrum of SED recorded during the Voyager 1 flyby of Saturn. Their occurrence was a few events per minute, variable over the nine month period separating the flybys by Voyager 1 and by Voyager 2. Typical duration was between 30 and 300 msec per event. The broadband spectrum was nearly flat between $\sim$ 20 kHz and 10 MHz, and then decreased with a slope between f^{-1} and f^{-2} towards higher frequencies. Typical instantaneous spectral power was $\sim$ 0.1 to 300 W/Hz (Zarka and Pedersen, 1983), hence a total instantaneous power in the range 10^7 to 10^{10} W. Typical SED and UED spectra are displayed on Figure 3.

The occurrence of SED grouped in recurrent episodes lasting for a few hours led Kaiser *et al.* (1983) to interpret their source as a storm system located in Saturn's equatorial atmosphere. A lower SED occurrence and less well-defined episodes at the time of the Voyager 2 flyby suggested that the storm system spread and weakened in 9 months. The surprising non detection of lightning whistlers or of optical signatures at Saturn was attributed respectively to the fact that field lines threading through the storm system were not sampled by the Voyagers, and to scattered ring light on the nightside of the planet. The presence of a broadband radiosource in Saturn's atmosphere was used to probe by propagation the equatorial ionosphere of the planet (Zarka, 1985a; b). Peak electron densities were found to vary between 6×10^5 cm^{-3} in the dayside and a few 10^3 cm^{-3} in the nightside, and constraints were put on the vertical profile of Ne.

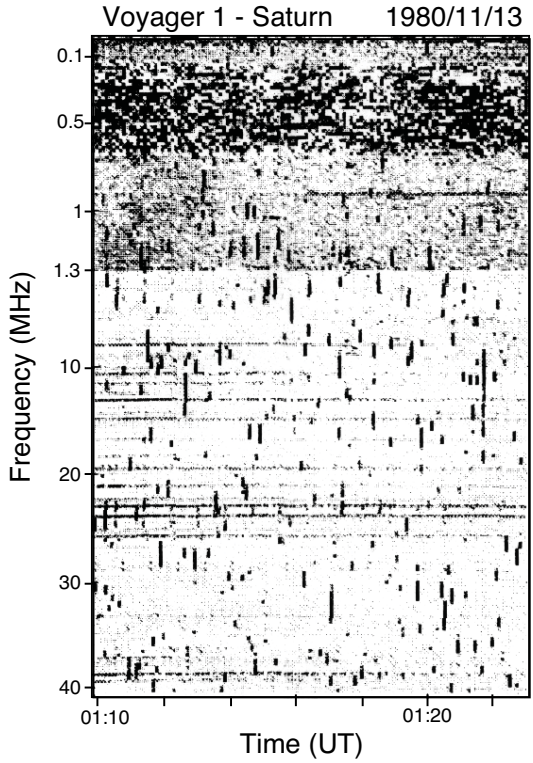

Figure 6. Dynamic spectrum of Saturn's lightning (SED) obtained during Voyager 1 fly-by $\sim$ 1 hour after closest approach, from a range of $\sim$ 5 planetary radii. The radio instrument onboard Voyager sweeps the frequency axis in 6 seconds (198 channels at 30 msec per step, grouped in two linear bands). SED being impulsive broadband phenomena, they appear as short streaks parallel to the frequency axis, randomly distributed over their whole spectrum. Saturn kilometric (auroral) radiation dominates the range $0.1 - 0.7$ MHz.

Evidence for Titan's lightning emissions analogous to SED (i.e. TED) was searched in Voyager radio data during the close flyby of Titan on November 12, 1980 (Desch and Kaiser, 1990). At that time, Voyager 1 was in view of Titan's nightside hemisphere and Saturn's dayside hemisphere, so that SED were blocked by Saturn's ionosphere below a few MHz while TED might have been observable at lower frequencies. No signal was found over a 1.7 hour interval around closest approach to Titan (at 4400 km range).

2.4. Radiation Belts

Jupiter's stable energetic electron belts produce synchrotron emission in the decimeter wavelength range (Carr *et al.*, 1983). The physics of synchrotron radiation is well understood, so that the main challenge of the recent years was to deduce the spatial and spectral distribution of the electrons allowing to best reproduce

the observed 2D and 3D maps of radio radiation. A recent modelling of Jupiter's electron belts through the code 'Salammbô-3D' (energy, radial distance, latitude) originally developed for terrestrial radiation belts, and adapted for the relevant physical processes at Jupiter (radial diffusion, absorption by moons and rings, synchrotron losses ...) provided synthetic 2D radio maps provide in excellent agreement with the observations (cf. Figure 7 of Zarka, 2004a) (Santos-Costa and Bourdarie, 2001). Time-dependence is now studied in order to account for the possible correlation of synchrotron output with solar wind variations (Sicard *et al.*, 2004).

Synchrotron radiation is practically absent at Earth. A tentative answer has been recently proposed by Thorne (2002): the filling of the inner terrestrial electron belts is too low to produce a significant level of synchrotron emission. This low filling could result from the much stronger losses at Earth (as compared to Jupiter) due to interaction with an intense plasma wave background.

The modelling effort developed for Jupiter was tentatively extended to the case of Saturn's radiation belts (Santos-Costa *et al.*, 2003). Absorption by dust (in the inner magnetospheric regions) and interaction with satellites (in the outer regions) were identified as the dominant loss processes, suggesting weak levels of synchrotron emission, and possible strong emission of energetic neutral atoms. Based on relativistic electron measurements in Saturn's magnetosphere by Pioneer 11, Van Allen and Grosskreutz (1989) estimated the intensity and spectral peak of synchrotron radiation: with 8×10^{-23} Wm^{-2} Hz^{-1} around 720 kHz from $20 R_S$, these authors concluded that it would be undetectable against the galactic background and other Saturnian radio emissions.

3. Expectations for Cassini

This section summarizes open questions about Saturn radio emissions, as well as first results from Cassini observations at Jupiter and en-route to Saturn, including a few unpublished results. The aim is to provide a stimulating framework for the analysis of Cassini observations at Saturn.

The Radio and Plasma Wave Science (RPWS) instrument onboard Cassini uses 3 electric monopoles (wires), a 3D magnetic search coil, and a Langmuir probe as sensors. It is connected to several receivers, including a 'radio' or 'High-Frequency' receiver covering the range from 3.5 kHz to 16.1 MHz (Gurnett *et al.*, 2004). This receiver can measure the 4 Stokes parameters (intensity and full polarization) of the incoming waves, as well as their direction of arrival (**k**-vector) with $\sim 1^\circ$ accuracy (Vogl *et al.*, 2004; Cecconi and Zarka, 2004) (see Figure 2c). Its flexibility allows for a number of setups adapted to the study of each Saturnian radio component, and its sensitivity is far better than that of the Voyager and Galileo instruments (Figure 7). Also, the mere fact of being in orbit will enable much more complete surveys than Voyager afforded.

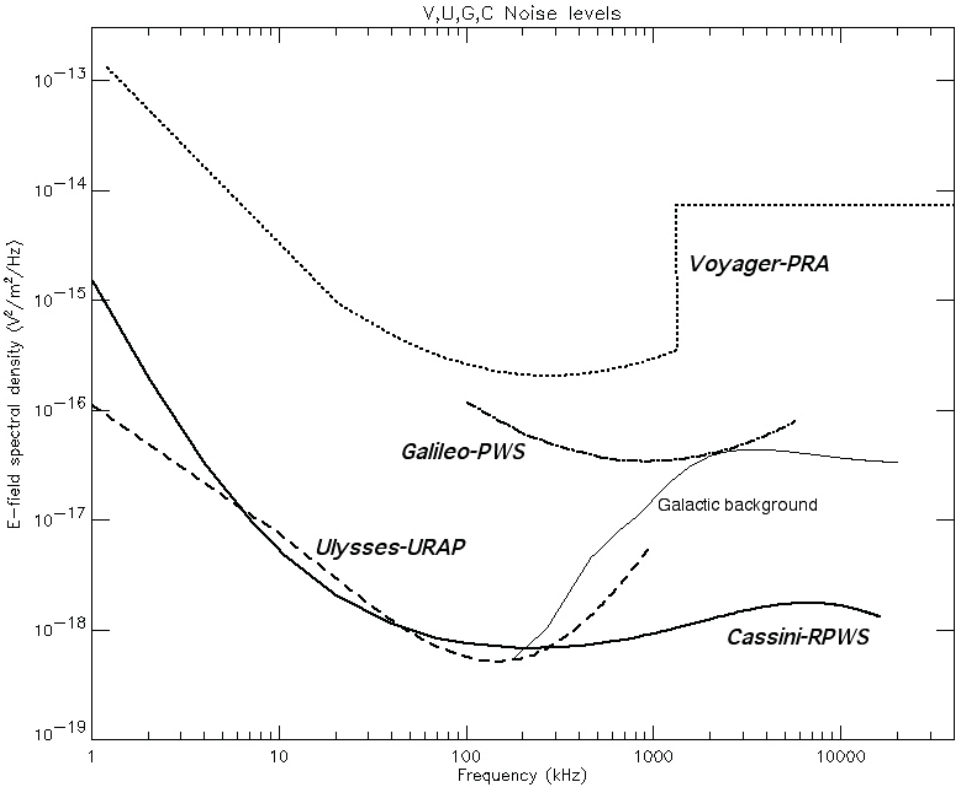

Figure 7. Compared sensitivities of the radio instruments onboard (V)oyager (Planetary Radio Astronomy), (U)lysses (Unified Radio And Plasma waves), (G)alileo (Plasma Wave Science), and (C)assini (Radio and Plasma Wave Science). Galactic background is from Manning and Dulk (2001).

3.1. RPWS Observations at Jupiter

As the steady galactic background is permanently detected by Cassini, it may be use as an absolute reference to calibrate the flux measured by RPWS. Zarka *et al.* (2004a) thus derived updated Jovian LF radio spectra (average and peak) from 6 months of calibrated measurements, and showed that the peak about 10 MHz in the previous reference spectrum by (Carr *et al.*, 1983) was actually due to the poor calibration of the Voyager radio experiment response and the effect of the Earth's ionospheric cutoff on ground-based measurements. They re-derived frequency ranges for each Jovian radio component, as well as new information on their overall beaming (convolution of instantaneous radio beaming by the longitudinal extent of the radiosource), sporadicity, and emitted power. Combining these results to the instantaneous radio beam widths derived by Kaiser *et al.* (2000) from remote observations of HOM and DAM by Cassini and Wind spacecraft, one deduces longitudinal source extents of 10° to 30°.

Gurnett *et al.* (2002) took advantage of the simultaneous presence of Galileo and Cassini near Jupiter to show that interplanetary shocks trigger increases of HOM/DAM emission levels, correlated with fluctuations of auroral UV emission.

Several studies were devoted to the QP bursts from Jupiter, which remain one of the most enigmatic components to date. Kaiser *et al.* (2001) showed that almost any recurrence period between minutes and tens of minutes may be observed. Hospodarsky *et al.* (2004) demonstrated from simultaneous observations by Galileo and Cassini that QP bursts behave in a stroboscopic-like way, not corotating with the planet, and illuminate a broad instantaneous beam ($\sim 2\pi$ sr). Direction-Finding analysis revealed fluctuating sources at very high-latitude, perhaps related to the UV emission from the polar cusp detected with HST (Pallier and Prangé, 2001), or to the pulsed polar X-ray spot observed by Chandra (Gladstone *et al.*, 2002). Zarka *et al.* (2004a) estimated that QP bursts are the most intense Jovian radio component (although $\sim$ 10 times less powerful than HOM due to its smaller bandwidth). At VLF frequencies, Kaiser *et al.* (2004a) suggested that the QP bursts (as well as some of the other low-frequency Jovian radio emissions) enter the magnetosheath and subsequently become dispersed, blended, and/or diffused and 're-radiated' with spectral and temporal characters quite unlike the magnetospheric emissions from which they originate. The resulting band of emission fluctuates with time, possibly in relation with the state of compression of the Jovian magnetosphere (Cecconi, Kivelson *et al.*, in progress).

High time resolution snapshots recorded by Cassini's radio receiver revealed various fine time-frequency structures in Jupiter's radio components. In addition to the well known S-bursts, drifting tones and spectral bands were observed within bKOM (Kurth *et al.*, 2001; Lecacheux *et al.*, 2001). A tentative interpretation of the latter in association with plasma density bubbles in the inner jovian dayside magnetosphere was proposed by Farrell *et al.* (2004a).

Finally, it must be noted that the Jupiter flyby was the first opportunity for an in-flight calibration of the RPWS DF mode, using HOM as a reference radiosource with known position and polarization (Vogl *et al.*, 2004).

3.2. First Observations of Saturn

SKR is detected with RPWS since early 2002, from nearly 3 AU distance. The geometry of Cassini's arrival and insertion in Saturn's orbit is plotted on Figure 8. A campaign of SKR and solar wind measurements by Cassini coordinated with UV images of the aurora by HST took place between Jan. 8 and Feb. 2, 2004. Cassini was then at $\sim$ 0.5 AU from Saturn.

Since its first reobservation back in 2002, SKR is observed with strong circular polarization, either LH or RH (polarization may be mixed at timescales of minutes). This is consistent with Voyager findings (see review by Kaiser *et al.*, 1984) and with generation via the CMI. During the January campaign, SKR polarization was dominantly LH. Cassini was in the southern Kronian (magnetic) hemisphere, at

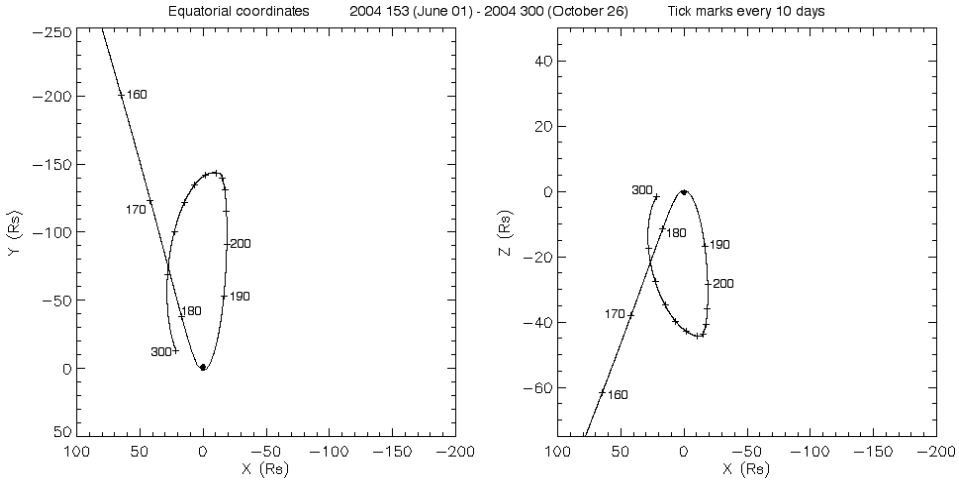

Figure 8. Geometry of Cassini's arrival and insertion in Saturn's orbit.

$-16.3°$ latitude. LH polarization from the southern hemisphere indicates emission on the **X** mode. Figure 9 illustrates the fact that polarization is a very efficient way to automatically isolate SKR from all other emissions (solar, jovian) that may be present on the dynamic spectra, allowing then to derive easily power, frequency range ...

In January, SKR was observed in the range $\sim 10 - 900$ kHz with a power between 10^7 and 5×10^8 W/sr. Correlation of SKR with auroral UV emissions and solar wind fluctuations is under way (Clarke *et al.*, Kurth *et al.*, Crary *et al.*, submitted to Nature, 2004). Impact of interplanetary shocks onto Saturn's magnetosphere also appear, as for Jupiter, to trigger auroral emissions (Prangé *et al.*, submitted to Nature, 2004).

Figure 10 shows one snapshot of SKR waveform captured within a 80 kHz band by the RPWS waveform sub-receiver on 4 Sep. 2002. It reveals that fine time-frequency drifting structures also exist in SKR dynamic spectra (although at longer timescales than Jovian S-bursts).

Groups of sporadic radio signals randomly distributed over the RPWS band and recurring at about Saturn's rotation period were detected in July 2003, at ~ 1 AU from Saturn. Were they SED, these events would then be 10 dB stronger than the most intense SED detected by Voyager 1. However, they disappeared after a few days to reappear only in June 2004, 15 dB weaker than Voyager 1's SED (5 dB weaker than Voyager 2's). If confirmed, these observations would suggest, as Voyager 1 and 2 ones, a great variability of SED occurrence and intensity over timescales of weeks/months, probably reflecting that of the atmospheric storm activity. Conversely, Kaiser *et al.* (2004b) suggest that SED long-term variations could be related to seasonal variations of the atmospheric temperature gradients and turbulence caused by the variable inclination and depth of the ring shadow.

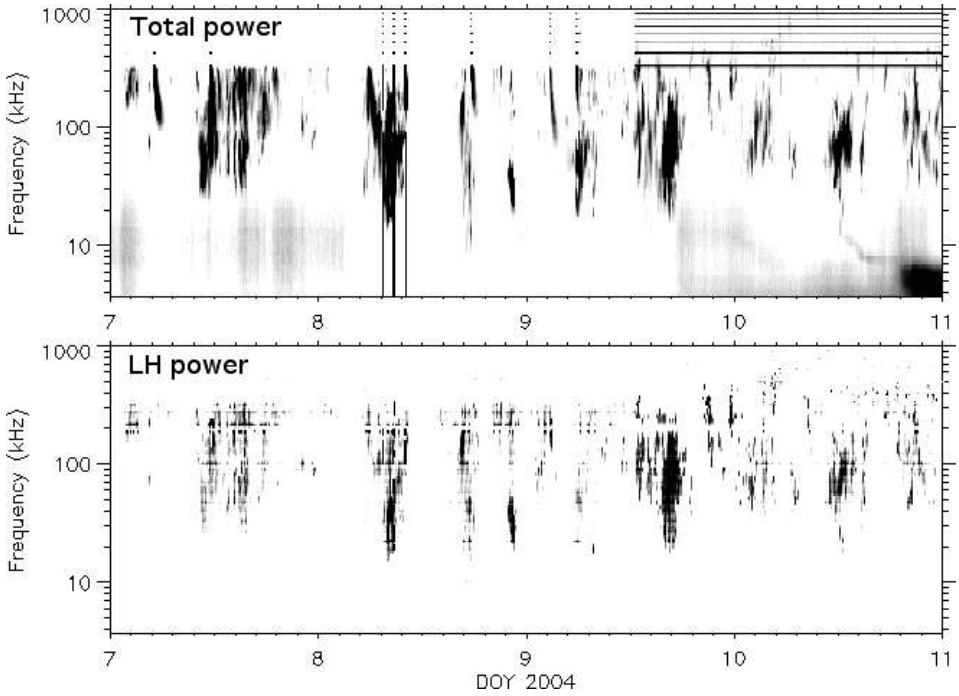

Figure 9. Top: Total power detected by Cassini-RPWS in the range 3.5 – 1000 kHz on 7-10 January 2004. SKR dominates the dynamic spectrum (intensity is proportional to darkness). A solar type III burst is visible at 7.2 d, and intense Jovian VLF emission at the end of DOY 10. Horizontal lines are interference. *Bottom:* Power detected in LH circular polarization. Only SKR remains. Solar and Jovian emissions are automatically 'filtered out'.

This would imply a low level of SED activity until the end of the Cassini tour in 2008-2009.

The ring/Sun geometry might also play a role in the long-term trend revealed by recent Cassini observations in the fluctuations of the SKR period (Lecacheux, RPWS team meeting, University of Iowa, Iowa-City, 3/2004).

The above early radio observations confirm the high quality of Cassini-RPWS measurements, and give a flavour of the many important questions that will be asked – and hopefully answered – during the tour.

3.3. Open Questions about Saturn's Radio Emissions

Cassini offers significant opportunities to improve our understanding of Saturn's radio emissions. The following list of questions, probably not exhaustive, is largely inspired by that of Kurth and Zarka (2001). We also indicate which measurements by Cassini (especially RPWS) will be relevant to answer them:

– Where are the SKR sources? Are they related to a Kelvin-Helmholtz instability at the magnetopause? to upwards currents at the boundary between open

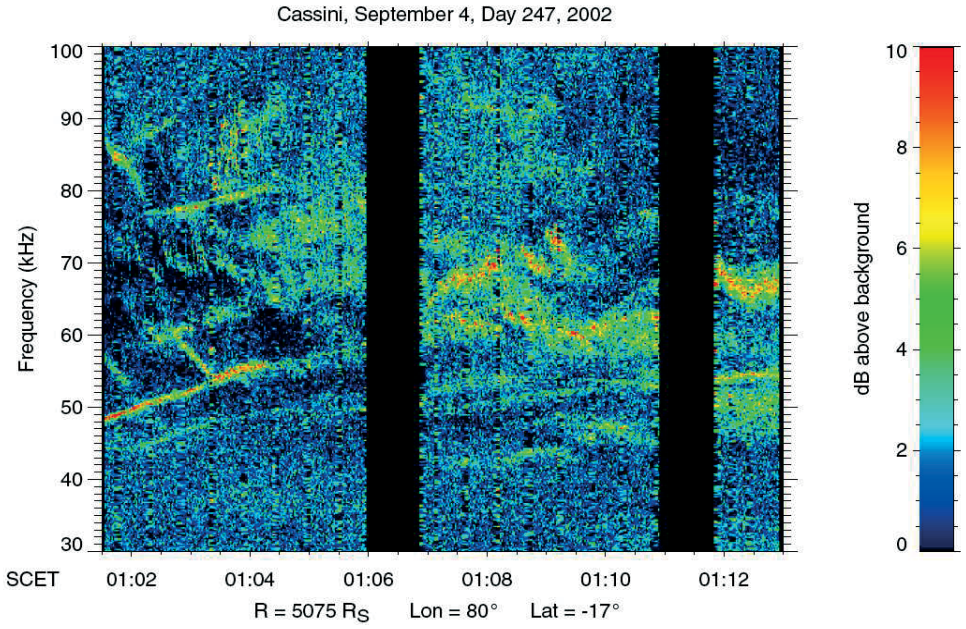

Figure 10. Cassini-RPWS wideband observations of SKR fine structure.

and closed field lines? RPWS Direction-Finding (DF) should provide direct answers.

- What is the shape of electron distributions in SKR sources (loss-cone, hollow beam, shell)? The end of the Cassini mission may give an opportunity for particle measurements at very high latitudes.
- What is the origin of SKR fine time-frequency structures (arcs, bursts ...)? CMI saturated by trapping? resonant cavity? propagation / focussing effects? RPWS polarization and waveform (high-resolution) measurements from various observation points will provide constraints.
- What is the origin of the rotational modulation of SKR? Is it the magnetic anomaly inferred from the SKR high-frequency cutoff Galopeau *et al.* (1991; 1992)? Magnetic field measurements at Cassini's insertion into orbit, at $< 2R_S$ from Saturn's center, will put new constraints on the high order terms of the Kronian field, but we also expect the accumulation of SKR high frequency measurements to provide strong constraints on the near polar field.
- What is the origin of the $\sim 1\%$ variations of the SKR period at timescale of months? Fluctuations of the local time position of the source will be monitored via DF measurements and compared to solar wind variations?
- How well does SKR correlate with solar wind (pressure) variations? Can SKR be used to deduce solar wind conditions when Cassini will be inside of Saturn's magnetosphere? How good does SKR correlates with interplanetary shocks? with UV auroras? Correlation of long time series of radio mea-

surements (incl. source positions derived via DF) with UV and solar wind variations will considerably improve our understanding of the dynamics of Saturn's magnetosphere.
- Is SKR controlled by Dione? by other satellites? Where are the sources of narrowband LF emissions and are they associated with the icy moons? What are the details of the magnetospheric interaction with the moon(s) and how does this result in the generation of radio emissions? This will be studied through localization of radiosources via DF as well as statistics over long series of measurements.
- Are there Kronian analogs of Jovian QP / Terrestrial LF bursts?

DF measurements will allow us to confirm the atmospheric origin of SED, locate individual bursts, and enhance their interest for ionospheric probing: constraints on the electron density will be derived along determined lines of sights. The lower frequency part of RPWS should permit the detection of lightning whistlers, and the waveform sub-receiver to characterize the fine structure of the radio signature. Long series of measurements during the several years tour will improve our understanding of Saturn's meteorology. The sensitivity and DF capabilities of RPWS will be exploited during the $\sim$ 40 close flybys of Titan to try to detect lightning for Titan (TED), whose existence may influence the organic chemistry and production of minor species. The lightning search with RPWS will be very complementary to Huygens probe measurements.

Finally, the sensitivity of RPWS at high-frequencies ($\sim$ 16 MHz), limited only by fluctuations of the galactic radio background, will allow us to search for possible synchrotron radiation (in conjunction with energetic neutral atoms measurements as explained in Section 2.4).

4. Coordinated Observations

Cassini studies may benefit from coordinated observations with several ground-based or space telescopes.

As discussed in Section 3.2, monitoring of UV auroras by HST from a quasi-fixed vantage point in the direction of the Sun, will be compared to Cassini SKR and UV measurements, and to solar wind variations near Saturn (when Cassini will be outside of the magnetosphere), and provide valuable information on the magnetospheric dynamics, which is supposed to be 'intermediate' between the Terrestrial and Jovian cases.

Above the Earth's ionospheric cutoff ($\sim$ 10 MHz) the giant LOw Frequency ARray 'LOFAR' (`www.lofar.org`), which should start operations in 2006, will reach a sensitivity of a few Jansky (1 Jy = 10^{-26} Wm^{-2} Hz^{-1}) with integration over a few MHz $\times$ a few tens of msec. It will thus be able to detect SED down to 10 to 15 dB below their level at the time of the Voyager 1 flyby (Zarka *et al.*, 2004b).

5. Future Missions and Perspectives

Galileo raised at least as many questions as it answered at Jupiter. This exciting situation motivates many projects for the re-exploration of the Jovian system, and especially its poorly explored polar regions. JASSI is a Discovery-class mission which would fly-by Jupiter, and prepare the way for the low-altitude polar obiter JUNO submitted to the NASA 'New Frontiers' programme. These missions will permit very accurate measurements of the planet's gravitational and magnetic fields, as well as direct waves and particles measurements just above the auroral regions. Larger missions like the nuclear-powered JIMO are under study for an exploration of the environment of Jupiter's moons (including their magnetospheric interaction).

Without any doubt, one outcome of the Cassini tour will be a strong motivation for a different, complementary re-exploration of the Saturnian system: JIMO II?

Pertinent studies of Jupiter's and Saturn's magnetospheres could also be performed from the Earth vicinity. The small explorer mission JMEX proposes a monitoring of their UV emissions (from the auroras, the Io torus ...), and radio monitors have been proposed to CNES in France. It has also been shown that ground-based radio observations of Jupiter in the range 10^{-40} MHz with arcsec resolution (e.g. with LOFAR) would provide new information of its high-latitude magnetic field and radio emissions (Zarka, 2004b). At higher frequencies, ground-based decimeter observations form the base of our knowledge of the synchrotron emission from the radiation belts (de Pater, 2004).

A re-exploration of Uranus (or Neptune?) may be considered, in particular 'en-route' to Pluto or the Kuiper belt. But in the near-future ($\sim$ 2012), all space agencies have targeted an in-depth exploration of Mercury and its peculiar, tiny magnetosphere. The search for radio emissions there will certainly provide surprises and new lessons.

6. Concluding Remarks

Why bother with radio 'images' like Figure 2b? In spite of their energetic insignificance ($\sim$ 10^{-6} of the power input in the magnetosphere), auroral radio waves are a remote sensing tool of the magnetospheric structure and dynamics very complementary to UV images or in-situ measurements: high time and frequency resolutions provide insights to the microphysics; Direction-Finding on Cassini restores an angular resolution of $\sim 1^\circ$ (Figure 2c). Radio waves also provide unique information on atmospheric electricity (lightning).

Finally, being produced by a nonthermal coherent mechanism (the CMI), planetary auroral radio waves compete in intensity with solar emissions in the same spectral range. They are thus a promising mean of detecting directly photons from extrasolar planets, which would tell us information about their magnetic field and

greatly expand the field of comparative magnetospheric physics (Zarka *et al.*, 2001; Farrell *et al.*, 2004b).

References

Barbosa, D.D.: 1982, 'Low-level VLF and LF radio emissions observed at Earth and Jupiter', *Rev. Geophys.* **20**, 316–334.

Baumback, M.M. and Calvert, W.: 1987, 'The minimum bandwidth of auroral kilometric radiation', *Geophys. Res. Lett.* **14**, 119–122.

Bigg, E.K.: 1964, 'Influence of the satellite Io on Jupiter's decametric emission', *Nature* **203**, 1008–1010.

Burke, B.F. and Franklin, K.L.: 1955, 'Observations of a variable radio source associated with the planet Jupiter', *J. Geophys. Res.* **60**, 213–217.

Calvert, W.: 1981, 'The auroral plasma cavity', *Geophys. Res. Lett.* **8**, 919–921.

Calvert, W.: 1982, 'A feedback model for the source of auroral kilometric radiation', *J. Geophys. Res.* **87**, 8199–8214.

Carr, T.D., Desch, M.D., and Alexander, J.K.: 1983, 'Phenomenology of magnetospheric radio emissions, in A.J. Dessler (ed.), *Physics of the Jovian Magnetosphere*, Cambridge Univ. Press, New York, pp. 226–284.

Cecconi, B., and Zarka, P.: 2002, 'Origin of a variable apparent radio period for Saturn', *Magnetospheres of the Outer Planets conference*, John Hopkins University, Laurel, MD, USA, 29 July - 2 August, 2002, (abstract).

Cecconi, B., and Zarka, P.: 2004, 'Direction finding and antenna calibration through analytical inversion of radio measurements performed using a system of 2 or 3 electric dipole wire antennas', *Radio Science*, submitted, 2004.

Connerney, J.E.P., Davis, Jr., L., and Chenette, D.L.: 1984, 'Magnetic field models', in T. Gehrels and M.S. Matthews (eds.), *Saturn*, Univ. of Arizona Press, pp. 354–377.

Cook, A.F., II, Duxbury, T.C., and Hunt, G.E.: 1979, 'Firsts results on Jovian lightning', *Nature* **280**, 794.

Cowley, S.H., and Bunce, E.J.: 2001, 'Origin of the main auroral oval in Jupiter's coupled magnetosphere-ionosphere system', *Planet. Space Sci.* **49**, 1067–1088.

Cowley, S.H., Bunce, E.J., and Prangé, R.: 2004, 'Saturn's polar ionospheric flows and their relation to the main auroral oval', *Ann. Geophys. 22*, 1379–1394.

de Pater, I.: 2004, 'LOFAR and Jupiter's Radio (Synchrotron) emissions', *Planet. Space Sci.*, in press.

Desch, M.D.: 1982, 'Evidence for solar wind control of Saturn radio emission', *J. Geophys. Res.* **87**, 4,549–4,554.

Desch, M.D.: 1994, 'Jupiter radio bursts and particle acceleration', *Astrophys. J. Suppl. Ser.* **90**, 541–546.

Desch, M.D. and Kaiser, M.L.: 1981a, 'Voyager measurement of the rotation period of Saturn's magnetic field', *Geophys. Res. Lett.* **8**, 253–256.

Desch, M.D. and Kaiser, M.L.: 1981b, 'Saturn's kilometric radiation – Satellite modulation', *Nature* **292**, 739–741.

Desch, M.D. and Kaiser, M.L.: 1990, 'Upper limit set for level of lightning activity on Titan', *Nature* **343**, 442–444.

Desch, M.D., Kaiser, M.L., Zarka, P., Lecacheux, A., Leblanc, Y., Aubier, M., and Ortega-Molina, A.: 1991, 'Uranus as a Radio Source', in J.T. Bergstralh, E.D. Miner, and M.S. Matthews (eds.), *Uranus*, Univ. Arizona Press, 894–925.

Ergun, R.E., *et al.*, 'FAST satellite wave observations in the AKR source region', *Geophys. Res. Lett.* **25**, 2061–2064.

Farrell, W.M., Kaiser, M.L., and Desch, M.D.: 1999, 'A model of the lightning discharge at Jupiter', *Geophys. Res. Lett.* **26**, 2601–2604, 1999.

Farrell, W.M., Kaiser, M.L., Kurth, W.S., Desch, M.D., Gurnett, D.A., Hospodarsky, G.B., and MacDowall, R.J.: 2004a, 'Remote sensing of possible plasma density bubbles in the inner jovian dayside magnetosphere', *J. Geophys. Res.*, in press.

Farrell, W.M., Lazio, T.J., Zarka, P., Bastian, T., Desch, M.D.: 2004b, 'The radio search for extrasolar planets with LOFAR', *Planet. Space Sci.*, in press.

Gallagher, D.L. and D'Angelo, N.: 1981, 'Correlations between solar wind parameters and auroral kilometric radiation', *Geophys. Res. Lett.* **8**, 1087–1089.

Galopeau, P. and Zarka, P.: 1992, 'Reply to the comment by J. E. P. Connerney and M. D. Desch', *J. Geophys. Res.* **97**, 12,291–12,297.

Galopeau, P. and Lecacheux, A.: 2000, 'Variations of Saturn's radio rotation period measured at kilometer wavelengths', *J. Geophys. Res.* **105**, 13089–13101.

Galopeau, P., Zarka, P., and Le Quéau, D.: 1989, 'Theoretical model of Saturn's kilometric radiation spectrum', *J. Geophys. Res.* **94**, 8739–8755.

Galopeau, P., Ortega-Molina, A., and Zarka, P.: 1991, 'Evidence of Saturn's magnetic field anomaly from SKR high-frequency limit', *J. Geophys. Res.* **96**, 14,129–14,140.

Galopeau, P., Zarka, P., and Le Quéau, D.: 1995, 'Source location of SKR: the Kelvin-Helmholtz instability hypothesis', *J. Geophys. Res.* **100**, 26397–26410.

Gladstone, G.R., *et al.*: 2002, 'A pulsating auroral X-ray hot spot on Jupiter', *Nature* **415**, 1000–1003.

Gurnett, D.A.: 1975, 'The Earth as a radio source: The non-thermal continuum', *J. Geophys. Res.* **80**, 2751–2763.

Gurnett, D.A., Shaw, R.R., Anderson, R.R., Kurth, W.S., and Scarf, F.L.: 1979, 'Whistlers observed by Voyager 1: Detection of lightning on Jupiter', *Geophys. Res. Lett.* **6**, 511–516.

Gurnett, D.A., Kurth, W.S., and Scarf, F.L.: 1981, 'Narrowband electromagnetic emissions from Saturn's magnetosphere', *Nature* **292**, 733–737.

Gurnett, D.A., Kurth, W.S., Roux, A., Bolton, S.J., and Kennel, C.F.: 1996, 'Evidence for a magnetosphere at Ganymede from plasma-wave observations by the Galileo spacecraft', *Nature* **384**, 535–537.

Gurnett, D.A., Zarka, P., Manning, R., Kurth, W.S., Hospodarsky, G.B., Averkamp, T.F., Kaiser, M.L., and Farrell, W.M.: 2001, 'Non-detection at Venus of high-frequency radio signals characteristic of terrestrial lightning', *Nature* **409**, 313–315.

Gurnett, D.A., *et al.*: 2002, 'Control of Jupiter's radio emission and aurorae by the solar wind', *Nature* **415**, 985–987.

Gurnett, D.A., *et al.*: 2004, 'The Cassini Radio and Plasma Wave Investigation', *Space Sci. Rev.*, in press.

Higgins, C.A., Carr, T.D., Reyes, F., Greenman, W.B., and Lebo, G.R.: 1997, 'A redefinition of Jupiter's rotation period', *J. Geophys. Res.* **102**, 22,033–22,041.

Hilgers, A.: 1992, 'The auroral radiating plasma cavities', *Geophys. Res. Lett.* **19**, 237–240.

Hospodarsky, G.B., Christopher, I.W., Menietti, J.D., Kurth, W.S., Gurnett, D.A., Averkamp, T.F., Groene, J.B., and Zarka, P.: 2001, 'Control of Jovian radio emissions by the galilean moons as observed by Cassini and Galileo', in H.O. Rucker, M.L. Kaiser, and Y. Leblanc (eds.), *Planetary Radio Emissions V*, Austrian Acad. Sci. Press, Vienna, pp. 155–164.

Hospodarsky, G.B., Kurth, W.S., Cecconi, B., Gurnett, D.A., Kaiser, M.L., Desch, M.D., and Zarka, P.: 2004, 'Simultaneous observations of jovian quasi-periodic radio emissions by the Galileo and Cassini spacecraft', *J. Geophys. Res.*, in press.

Huff, R.L., Calvert, W., Craven, J.D., Frank, L.A., and Gurnett, D.A.: 1988, 'Mapping of auroral kilometric radiation sources to the aurora', *J. Geophys. Res.* **93**, 11,445–11,454.

Jones, D.: 1976, 'Source of terrestrial non-thermal radiation', *Nature* **260**, 686.

Jones, D.: 1988, 'Planetary radio emissions from low magnetic latitudes: Observations and theories', in H.O. Rucker, S.J. Bauer, and B.M. Pedersen (eds.), *Planetary Radio Emissions II*, Verlag der Österreichischen Akademie der Wissenschaften, Wien, p. 255.

Jones, D., Calvert, W., Gurnett, D.A., and Huff, R.L.: 1987, 'Observed beaming of terrestrial myriametric radiation', *Nature* **328**, 391.

Kaiser, M.L., Connerney, J.E.P., and Desch, M.D.: 1983, 'Atmospheric storm explanation of saturnian electrostatic discharges', *Nature* **303**, 50–53.

Kaiser, M.L., Desch, M.D., Kurth, W.S., Lecacheux, A., Genova, F., Pedersen, B.M., and Evans, D.R.: 1984, 'Saturn as a radio source', in T. Gehrels and M.S. Matthews (eds.), *Saturn*, Univ. of Ariz. Press, Tucson, pp. 378–415.

Kaiser, M.L., Zarka, P., Desch, M.D., and Farrell, W.M.: 'Restrictions on the characteristics of Neptunian lightning', *J. Geophys. Res.* **96**, 19,043–19,047.

Kaiser, M.L., Desch, M.D., Farrell, W.M., MacDowall, R.J., Stone, R.G., Lecacheux, A., Pedersen, B.-M., and Zarka, P.: 1992, 'Ulysses observations of escaping VLF emissions from Jupiter', *Geophys. Res. Lett.* **19**, 649–652.

Kaiser, M.L., Zarka, P., Kurth, W.S., Hospodarsky, G.B., and Gurnett, D.A.: 2000, 'Cassini and Wind stereoscopic observations of jovian nonthermal radio emissions: Measurement of beam widths', *J. Geophys. Res.* **105**, 16,053–16,062.

Kaiser, M.L., Farrell, W.M., Desch, M.D., Hospodarsky, G.B., Kurth, W.S., and Gurnett, D.A.: 2001, 'Ulysses and Cassini at Jupiter: Comparison of the quasi-periodic radio bursts', in H.O. Rucker, M.L. Kaiser, and Y. Leblanc (eds.), *Planetary Radio Emissions V*, Austrian Academy of Sciences Press, Vienna, pp. 41-48.

Kaiser, M.L., Farrell, W.M., Kurth, W.S., Hospodarsky, G.B., and Gurnett, D.A.: 2004a, 'New observations from Cassini and Ulysses of Jovian VLF radio emissions', *J. Geophys. Res.*, in press.

Kaiser, M.L., Farrell, W.M., Desch, M.D., Kurth, W.S., and Zarka, P.: 2004b, 'Saturn's electrostatic discharges: Where are they?', COSPAR, session B0.5/D3.7/C3.4 "Saturn: Cassini/Huygens arrival and system science," Paris.

Kurth, W.S.: 1982, 'Detailed observations of the source of terrestrial narrowband electromagnetic radiation', *Geophys. Res. Lett.* **9**, 1341–1344.

Kurth, W.S.: 1992, 'Continuum radiation in planetary magnetospheres', in H.O. Rucker, S.J. Bauer, and M.L. Kaiser (eds.), *Planetary Radio Emissions III*, Verlag der Österreichischen Akademie der Wissenschaften, Wien, p. 329.

Kurth, W.S. and Zarka, P.: 2001, 'Saturn radio waves', in H.O. Rucker, M.L. Kaiser, and Y. Leblanc (eds.), *Planetary Radio Emissions V*, Austrian Academy of Sciences Press, Vienna, pp. 247–259.

Kurth, W.S., Craven, J.D., Frank, L.A., and Gurnett, D.A.: 1979, 'Intense electrostatic waves near the upper hybrid resonance frequency', *J. Geophys. Res.* **84**, 4,145–4,164.

Kurth, W.S., Gurnett, D.A., and Scarf, F.L.: 1981, 'Control of Saturn's kilometric radiation by Dione', *Nature* **292**, 742–745.

Kurth, W.S., Gurnett, D.A., and Scarf, F.L.: 1989, 'Jovian type III radio bursts', *J. Geophys. Res.* **94**, 6,917–6,924.

Kurth, W.S., Hospodarsky, G.B., Gurnett, D.A., Lecacheux, A., Zarka, P., Desch, M.D., Kaiser, M.L., and Farrell, W.M.: 2001, 'High-resolution observations of low-frequency jovian radio emissions by Cassini', in H.O. Rucker, M.L. Kaiser, and Y. Leblanc (eds.), *Planetary Radio Emissions V*, Austrian Academy of Sciences Press, Vienna, pp. 15–28.

Ladreiter, H.P., Zarka, P., and Lecacheux, A.: 1994a, 'Direction-finding study of Jovian Hectometric and broadband kilometric radio emissions: Evidence for their auroral origin', *Planet. Space Sci.* **42**, 919–931.

Ladreiter, H.P., Galopeau, P., and Zarka, P.: 1994b, 'The magnetic field anomaly of Saturn', International Symposium on *Magnetospheres of Outer Planets*, Graz, Austria (abstract).

Lecacheux, A.: 1988, 'Polarization aspects from planetary radio emissions', in H.O. Rucker *et al.* (eds.), *Planetary Radio Emissions II*, Austrian Acad. Sci. Press, Vienna, pp. 311–326.

Lecacheux, A., Kurth, W.S., and Manning, R.: 2001, 'Sub-second time scales in jovian radio emissions as measured by Cassini/RPWS: Comparison with ground-based observations', in H.O. Rucker, M.L. Kaiser, and Y. Leblanc (eds.), *Planetary Radio Emissions V*, Austrian Academy of Sciences Press, Vienna, pp. 29–39.

Louarn, P.: 1992, 'Auroral planetary radio emissions: Theoretical aspects', *Adv. Space Res.* **12**, (8)121–(8)134.

Louarn, P., Roux, A., De Féraudy, H., Le Quéau, D., André, M., and Matson, L.: 1990, 'Trapped electrons as free energy source for the auroral kilometric radiation', *J. Geophys. Res.* **95**, 5,983–5,995.

MacDowall, R.J., Kaiser, M.L., Desch, M.D., Farrell, W.M., Hess, R.A., and Stone, R.G.: 1993, 'Quasiperiodic jovian radio bursts: observations from the Ulysses radio and plasma wave experiment', *Planet. Space Sci.* **41**, 1059–1072.

Manning, R. and Dulk, G.A.: 2001, 'The Galactic background radiation from 0.2 to 13.8 MHz', *Astron. Astrophys.* **372**, 663–666.

Melrose, D.B.: 1981, 'A theory for the nonthermal radio continua in the terrestrial and Jovian magnetospheres', *J. Geophys. Res.* **86**, 30–36.

Mizera, P.F. and Fennel, J.F.: 1977, 'Signature of electric fields from high and low altitude particle distribution', *Geophys. Res. Lett.* **4**, 311–314.

Morgan, D.D. and Gurnett, D.A.: 1991, 'The source location and beaming of terrestrial continuum radiation', *J. Geophys. Res.* **96**, 9,595–9,613.

Neubauer, F.M., Gurnett, D.A., Scudder, J.D., and Hartle, R.E.: 1984, 'Titan's magnetospheric interaction', in T. Gehrels and M.S. Matthews (eds.), *Saturn*, pp. 760-787, Univ. of Ariz. Press, Tucson, pp. 760–787.

Oya, H.: 1971, 'Conversion of electrostatic plasma waves into electromagnetic waves: Numerical calculation of the dispersion relation for all wavelengths', *Radio Sci.* **6**, 1131.

Pallier, L. and Prangé, R.: 2001, More about the structure of the high latitude Jovian aurorae, *Planet. Space Sci.* **49**, 1159–1173.

Prangé, R., Zarka, P., Ballester, G.E., Livengood, T.A., Denis, L., Carr, T.D., Reyes, F., Bame, S.J., and Moos, H.W.: 1993, 'Correlated variations of UV and Radio emissions during an outstanding jovian auroral event', *J. Geophys. Res.* **98**, 18,779–18,791.

Prangé, R., *et al.*, submitted to *Nature*.

Pritchett, P.L.: 1986, 'Electron-cyclotron Maser instability in relativistic plasmas', *Phys. Fluids* **29**, 2,919–2,930.

Rönnmark, K.: 1983, 'Emission of myriametric radiation by coalescence of upper hybrid waves with low frequency waves', *Ann. Geophys.* **1**, 187.

Santos-Costa, D., and Bourdarie, S.: 2001, 'Modeling the inner Jovian electron radiation belt including non-equatorial particles', *Planet. Space Sci.* **49**, 303–312.

Santos-Costa, D., Blanc, M., Maurice, S., and Bolton, S.J.: 2003, 'Modeling the electron and proton radiation belts of Saturn', *Geophys. Res. Lett.* **30**, SSC 6-1, CiteID 2059, DOI 10.1029/2003GL017972.

Sicard, A., Bourdarie, S., Krupp, N., Lagg, A., Boscher, D., Santos-Costa, D., Gerard, E., Galopeau, P., Bolton, S.J., Sault, R.J., and Williams, D.J.: 2004, 'Long-term dynamics of the inner Jovian electron radiation belts', *Adv. Space Res.* **33**, (11)2039–(11)2044.

Steinberg, J.-L., Lacombe, C., Zarka, P., Hoang, S., and Perche, C.: 2004, 'Terrestrial low-frequency bursts: escape paths of radio waves through the bow shock', *Planet. Space Sci.* **52**, 643–660.

Thorne, R.M.: 2002, 'Why does the Earth not have a significant synchrotron electron belt compared to Jupiter?', 11th International Congress on Plasma Physics, Sydney, Australia, 2002.

Trauger, J.T., *et al.*: 1998, 'Saturn's hydrogen aurora: Wide-field planetary camera 2 imaging from the Hubble Space Telescope', *J. Geophys. Res.* **103**, 20,237–20,244.

Van Allen, J.A. and Grosskreutz, C.L.: 1989, 'Relativistic electrons in Saturn's inner magnetosphere and an estimate of their synchrotron emission', *J. Geophys. Res.* **94**, 8,731–8,738.

Vogl, D.F., *et al.*: 2004, 'In-flight calibration of the Cassini-RPWS antenna system for direction-finding and polarization measurements', *J. Geophys. Res.*, in press.

Warwick, J.W., *et al.*: 1981, 'Planetary radio astronomy observations from Voyager 1 near Saturn', *Science* **212**, 239–243.

Wu, C.S. and Lee, L.C.: 1979, 'A theory of terrestrial kilometric radiation', *Astrophys. J.* **230**, 621–626.

Zarka, P.: 1985a, 'Directivity of Saturn electrostatic discharges and ionospheric implications', *Icarus* **61**, 508–520.

Zarka, P.: 1985b, 'On detection of radio bursts associated with jovian and saturnian lightning', *Astron. Astrophys.* **146**, L15–L18.

Zarka, P.: 1998, 'Auroral radio emissions at the outer planets: observations and theories', *J. Geophys. Res.* **103**, 20,159–20,194.

Zarka, P.: 2000, 'Radio emissions from the planets and their moons', in R.G. Stone, K.W. Weiler, M.L. Goldstein, and J.-L. Bougeret (eds.), *Radio Astronomy at Long Wavelength*, Geophysical Monograph **119**, American Geophysical Union, 167–178.

Zarka, P.: 2004a, 'Radio and plasma waves at the outer planets', *Adv. Space Res.*, in press.

Zarka, P.: 2004b, 'Fast radio imaging of Jupiter's magnetosphere at low frequencies with LOFAR', *Planet. Space Sci.*, in press.

Zarka, P., and Pedersen, B.M.: 1983, 'Statistical study of Saturn electrostatic discharges', *J. Geophys. Res.* **88**, 9,007–9,018.

Zarka, P. and Pedersen, B.M.: 1986, 'Radio detection of Uranian lightning by Voyager 2', *Nature* **323**, 605–608.

Zarka, P., Pedersen, B.M., Lecacheux, A., Kaiser, M.L., Desch, M.D., Farrell, W.M., and Kurth, W.S.: 1995, 'Radio emissions from Neptune, in D. Cruikshank and M.S. Matthews (eds.), *Neptune and Triton*, Univ. Arizona Press, 341–387.

Zarka, P., Treumann, R.A., Ryabov, B.P., and Ryabov, V.B.: 2001, 'Magnetically-driven planetary radio emissions and applications to extrasolar planets', *Astrophys. Space Sci.* **277**, 293–300.

Zarka, P., Cecconi, B., Kurth, W.S.: 2004a, 'Jupiter's low frequency radio spectrum from Cassini/RPWS absolute flux density measurements', *J. Geophys. Res.*, in press.

Zarka, P., Farrell, W.M., Kaiser, M.L., Blanc, E., and Kurth, W.S.: 2004b, 'Study of solar system planetary lightning with LOFAR', *Planet. Space Sci.*, in press.

Address for Offprints: Philippe Zarka, Département de Recherche Spatiale, Observatoire de Paris, Bâtiment 16, 5, place Jules Janssen, F-92195 Meudon Cedex, France; zarka@obspm.fr

IV. SATELLITES AND RINGS

GEOLOGY OF THE ICY SATELLITES

TORRENCE V. JOHNSON
Jet Propulsion Laboratory, California Institute of Technology, Pasadena, CA 91109

Received: 4 September 2004; Accepted in final form: 26 October 2004

Abstract. In the last 25 years, the explorations of the Voyager and Galileo missions have resulted in an entirely new view of the icy worlds orbiting the giant outer planets. These objects show a huge diversity in their characteristics, resulting from their formation histories, internal processes and interactions with their space environments. This paper will review the current state of knowledge about the icy satellites and discuss the exciting prospects for the upcoming Cassini/Huygens mission as it begins a new era of exploration of the Saturn satellite system.

Keywords: Outer planets, icy satellites, cratering, oceans, cryovolcanism, tectonic resurfacing

1. Introduction

The outer reaches of our solar system are realms of ice. Beyond the orbit of Mars current models for the formation of planetary materials from the solar nebula four and a half billion years ago require that much of the solid material be in the form of ice. Furthermore, the decreased solar energy available in this region compared with the inner planets results in low surface temperatures that allow ice to be stable on unprotected planetary surfaces for billions of years. The solar abundance of elements dictates that most of the ice formed in the outer solar system will be water ice, H_2O, with smaller amounts of more volatile condensates, such as NH_3, CH_4 and their hydrated and clathrated (Gautier and Hersant, 2005) forms as well as CO_2 and N_2, also possible, particularly at greater distances.

The 'expected' bulk make-up of a satellite around one of the outer planets is thus a combination of rock (and metals) and water ice, in approximately equal proportions in most chemical models. Observations by Earth and space based telescopes and data from spacecraft have confirmed this picture and most of the outer planet satellites indeed appear to by 'icy satellites', with the major notable exception of rocky, volcanic Io.

One might expect the geology on these frozen worlds to be dominated solely by the continual creation of impact craters from asteroidal and cometary debris over the history of the solar system. Instead, observations by planetary spacecraft, particularly Voyager and Galileo, show a stunning variety in these bodies' current states and their geological histories. The reasons for this geological diversity can be found in the influences of the satellites' compositions, planetary energy sources and their interactions with their environments. The next sections discuss the major

Space Science Reviews 116: 401–420, 2005.
DOI: 10.1007/s11214-005-1963-1

Figure 1. Surfaces of Callisto, Ganymede, Europa (ice rafts), and Io (*from left to right*).

factors that affect the geology of icy satellites and the prospects for the upcoming Cassini/Huygens mission.

2. Major Factors Affecting Icy Satellite Geology

2.1. Cratering

Impact cratering is an important, ubiquitous process throughout the solar system, with every solid body explored to date showing the scars of this bombardment to some degree (again, with the interesting exception of Io, whose volcanic activity is apparently vigorous enough to erase all traces of craters). Our picture of the history of impacts is constrained primarily by studies of the Earth's Moon and by dynamical models of the asteroid and comet populations that supply the flux of bodies that collide with the planets and satellites. The Earth/Moon system is the only place so far where the record of impacts is tied to absolute ages through the precise isotopic dating of rocks, which results in a scenario of very high impact fluxes in the inner solar system in first half to one billion years (the 'late heavy bombardment') followed by a rapid fall off of impacts and relatively constant rates in the last two to three billion years (e.g., Stöffler and Ryder, 2001).

In addition to the primary geological features produced by the cratering process itself – craters, ejecta blankets, scarps, basins and ring formations – the density of craters of various sizes on planetary surfaces provides a major tool for determining the relative ages of geologic features and estimating the absolute age of formations (albeit with considerable uncertainty). Extrapolation of impact derived ages to other parts of the solar system requires extensive theoretical modeling and assumptions concerning the source populations for impactors. In the outer solar system, this creates significant uncertainty due to uncertainties in the relative importance of different populations (e.g. asteroid vs. comet), the distribution of bodies within those populations, and the dynamical processes that produce the impact flux at a given planet.

For the outer planet satellites then (Figure 1), it is easy to estimate a qualitative surface age from the crater statistics if they are either essentially uncratered (like Io – very recent, less than thousands or tens of thousands of years) or very heavily

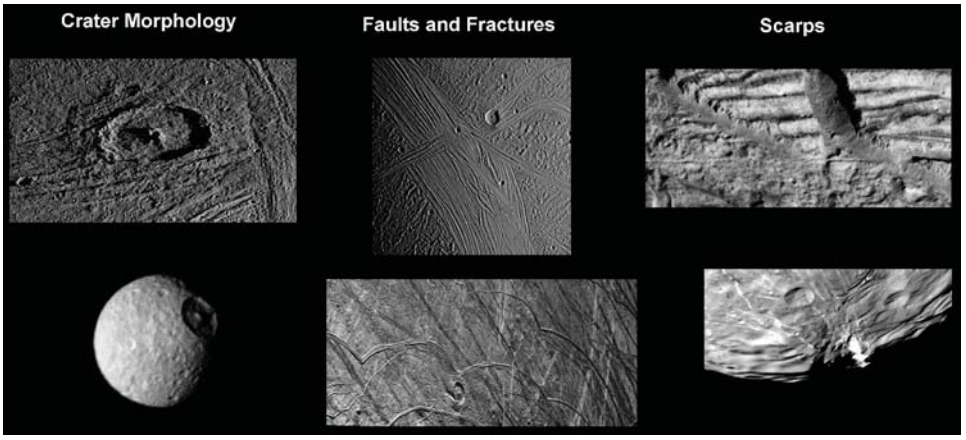

Figure 2. Upper left to right: Ganymede, Ganymede, Europa; *Lower left to right:* Mimas, Europa, Miranda.

cratered (like Callisto – ancient, probably greater than four billion years). The age of surfaces with intermediate (e.g. Ganymede) or low (e.g. Europa) crater densities is more problematical. Current studies of fluxes in the Jupiter system suggest that Jupiter family comets dominate the population and result in uncertainties of about a factor of two in derived ages (at Europa an average age of ∼50 to 100 million years; Zahnle *et al.*, 2004).

2.2. Low Temperatures and Water Ice

The combination of low temperatures (surface T from ∼60 K to ∼140 K) and water ice being a major constituent of the icy satellites has major consequences for their geology. At these temperatures, well below the melting point of water (1 bar, $T_{\rm melt} = 273$ K), ice is a good 'rock'. A surface composed primarily of cold, hard ice can sustain reasonable topographic loads (mountains and craters) and is subject to brittle failure and faulting. Thus the morphology of many features on icy satellites (Figure 2) is remarkably similar to that seen on their rocky counterparts in the inner solar system, the Moon and Mercury, despite large differences in composition and environment.

Although cold ice acts as a brittle rock at satellite surface temperatures, a key factor that leads directly to diverse and active geology on the icy satellites is simply that it is easier to melt ice than to melt rock (Figure 3). The ratio of the melting temperature of the surface material to the surface temperature for icy satellites (∼2-5) is similar to the terrestrial 'rock' bodies (∼2-10). However, the increase in absolute temperature required for melting is much less (∼150 to 250 K compared with ∼700 to 1000 K), making the energy requirements for melting, and therefore viscous behavior or magmatic activity, correspondingly modest. This point was first studied systematically in the context of icy satellites by John Lewis (1971),

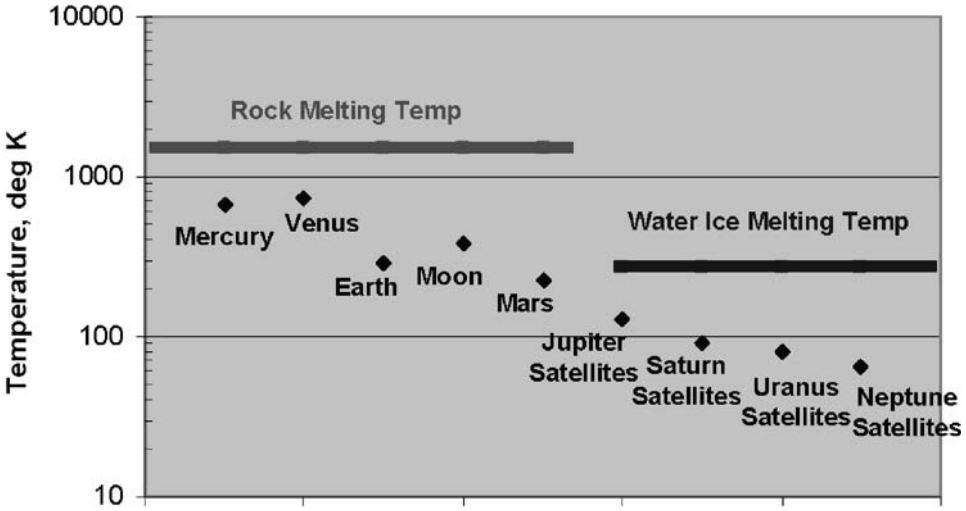

Figure 3. Temperatures of solid surfaces of solar system planetary bodies versus rock and water ice melting temperatures.

prior to the beginning of spacecraft exploration of the outer solar system, and his conclusion that the satellites would prove to be active, geologically interesting worlds was amply confirmed by the results from Voyager and Galileo.

2.3. Energy Sources

In one sense, the geologic features we see on planets are the result of a competition between the endogenic processes that result from internal heat (e.g. volcanism and tectonism) and the exogenic processes which then modify the surface (e.g. cratering, magnetospheric interactions, atmospheric weathering and transport). The primary source of energy for the icy satellites for most of their history is the heat produced by the decay of radioactive elements in their rocky constituents. This heat is often sufficient to raise the internal temperatures of even fairly modest sized satellites to levels close to or above the melting point of ice (see above).

A second major energy source for some satellites is tidal heating, resulting from an orbital configuration where changing solid body tides raised by the primary planet can heat the interior through friction. The role of tidal heating for outer planet satellites was spectacularly demonstrated by the first Voyager observations of Io, where discovery of active volcanism confirmed a theoretical prediction by Peale *et al.* (1979) published only months before the encounter. In the Jupiter system, the orbital resonance responsible for Io's large tidal amplitude also affects Europa and Ganymede and is believed to play a significant role in their geologic histories as well. Tidal heating in one form or another has also been advanced to explain features in the Saturn system (Enceladus) and the Neptune system (Triton).

2.4. Other (Non-water) Volatiles

Although not as plentiful as water, due to the lower solar abundance of their constituent atomic species, other volatiles with lower melting points may be present on icy satellites, particularly on the most distant, colder bodies. The evidence for significant geologic activity even on small, cold satellites certainly argues for some mechanism for lowering the melting point of the icy constituents below that of pure water. Ammonia, NH_3, is of particular interest since a eutectic mixture of water and ammonia has a melting point ($\sim$173 K) significantly below 273 K. Even a relatively small amount of ammonia could thus be capable of significantly affecting geological processes.

Ammonia could be part of the condensed solids from a solar nebula composition, and Lewis (1971; 1972) suggested that this process in equilibrium condensation models might facilitate satellite interior melting. To date, ammonia has not been detected in solid or gaseous form on any of the icy satellites. However, the difficulty of detecting small amounts of ammonia when mixed with water leaves the question of its presence open from an observational perspective.

Carbon bearing volatiles, such as carbon dioxide, CO_2, and hydrocarbons, including methane (CH_4) and more complex molecular species such as ethane, play a role in icy satellite geology under some conditions. Carbon dioxide, of course, plays a major part in the atmosphere and polar ices of Mars and could be stable for at least short times on the surfaces of airless icy moons. In the Jupiter, Saturn and Uranus systems it has been detected only in small quantities on the surfaces of the icy Galilean satellites, Europa, Ganymede and Callisto, apparently as small deposits or inclusions in the surface materials (McCord *et al.*, 1997; 1998a) (Figure 4). Gaseous carbon dioxide, probably released from these surface deposits, has been identified around Callisto, in an extremely tenuous atmosphere (Carlson, 1999). Preliminary Saturn satellite spectral observations from Cassini/Huygens' also show evidence for surface carbon dioxide (Brown *et al.*, 2004). Frozen methane and other hydrocarbons would not be stable for long times icy satellites surfaces inside the orbit of Neptune and have not been detected, but these species do play a major role in Titan's massive atmosphere, where the rain-out of hydrocarbon rich aerosols is believed to produce lakes or seas of liquid hydrocarbons on the surface (Lunine *et al.*, 1983; Lunine, 1993; Courtin, 2005; Coustenis, 2005; Roos-Serote, 2005; Strobel, 2005).

Condensed non-water volatile species become very important geologically at the extremely low temperatures beyond the orbit of Uranus. On Neptune's satellite, Triton, a whole array of frozen volatiles dominates the surface and atmospheric processes. In addition to the water ice 'bedrock', these include frozen nitrogen, methane, carbon dioxide, and carbon monoxide. Based on spectral evidence, Pluto appears to have a similar array of frozen volatiles and may exhibit comparable geologic processes.

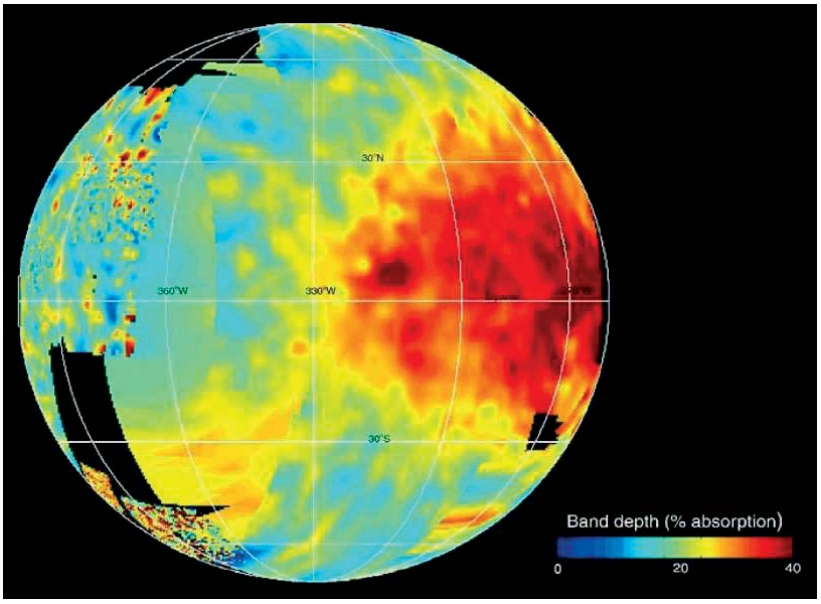

Figure 4. Carbon dioxide absorption at 4.25 μm on Callisto from Gallileo NIMS data (Hibbitts *et al.*, 2000).

2.5. Atmospheric and Magnetospheric Interactions

With the notable exception of Titan, the icy satellites have extremely tenuous atmospheres, the densest only barely 'collisionally thick' (where the mean free path for an atmospheric constituent is less than the scale height). This allows a complex range of interactions between the satellites' surfaces, atmospheric constituents, and the space environment, usually the magnetospheric environment of the primary planet. On the icy satellites of Jupiter, Saturn, and Uranus these effects are primarily chemical modification of the surface (Lane and Domingue, 1997; Lane *et al.*, 1981; McEwen, 1986; Nelson *et al.*, 1986) and long-term loss of volatiles from the satellite. On the Galilean satellites there is evidence for varying amounts of nonvolatile lag deposits produced by volatile loss and thermal segregation (Moore *et al.*, 1999). More extensive volatile/atmospheric modification of the surface geology appears to occur on Triton, as a result of nitrogen and methane volatile exchange between the surface and atmosphere. Titan's massive atmosphere raises the possibility of more extensive modification of geology through direct aeolian erosion, precipitation, and solid/liquid interactions with the putative extensive bodies of liquid hydrocarbons.

2.6. Differentiation

The relative ease of melting the volatile component (mostly water ice) of the icy satellites leads naturally to the expectation that even smaller bodies may be dif-

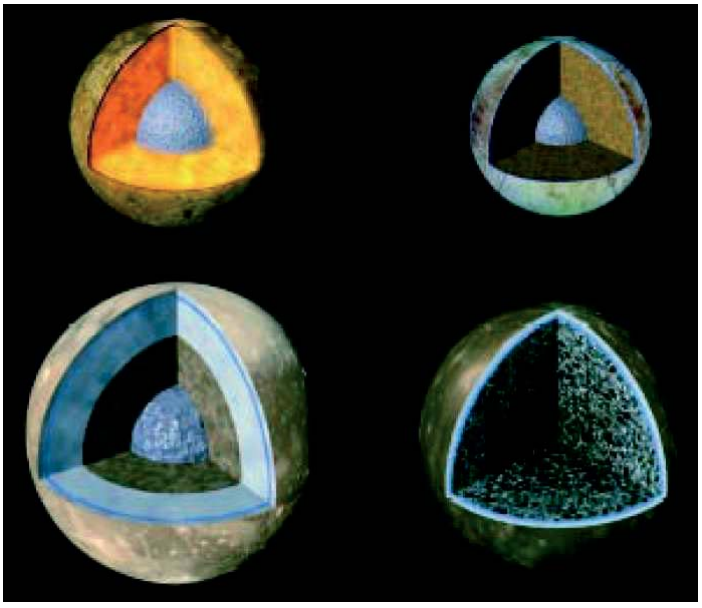

Figure 5. Schematics illustrating the degree of differentiation of the interiors of volcanic Io and the ice-covered satellites Europa, Ganymede, and Callisto.

ferentiated – i.e. the separation of the heavier, rock- and metal-rich, materials from the lighter volatile-rich material and the development of a layered internal structure (Figure 5). Available energy sources to drive differentiation include the initial heat of accretion, decay of both short- and long-lived radionuclides and tides as discussed earlier. Most reviews of satellite thermal history prior to the Galileo mission concluded that complete or nearly complete differentiation of the larger satellites was very likely, although undifferentiated models could not be ruled out. Gravitational measurements from Galileo suggest that at least one large icy satellite, Callisto, is incompletely differentiated (Schubert *et al.*, 2004). Europa and Ganymede on the other hand appear differentiated as expected, at least to the level of separating the heavy constituents from ice, with the gravitational data clearly indicating low density, ice or ice-rich outer layers.

The state of differentiation for other icy satellites is only inferred from models and what we know of their surface geology (evidence of re-surfacing being generally taken to suggest internal heating and a probability of differentiation). Thus, most current models of other icy satellites suggest that Titan, a near twin of Ganymede and Callisto in bulk properties, is likely to be differentiated (although the Galileo results for Callisto raise some doubt about how well we understand even large satellites with significant heat sources) (e.g. Schubert, 1986; Schubert *et al.*, 2004).

Of the other Saturnian satellites, Enceladus shows evidence for large scale resurfacing in Voyager images, and could well be differentiated in spite of its small

size (∼500 km diameter). There is still a large uncertainty concerning the source of energy for Enceladus' geologic activity, however, since its current forced eccentricity is not large enough to produce significant tidal heating (Squyres *et al.*, 1983a; Peale, 1999). Past orbital evolution allowing more heating has been explored, but there is as yet no completely satisfactory scenario for explaining Enceladus' appearance. Many of the other satellites in this system show evidence for lesser degrees of endogenic activity, suggesting that some of them may also prove to be differentiated, although the pre-Cassini evidence is ambiguous. The Uranian satellite system, as with the smaller satellites of Saturn, also exhibits evidence for endogenic processes, including surface faulting and resurfacing, but direct evidence for differentiation is lacking.

The major satellite of Neptune, Triton, may also be a good candidate for a differentiated object. Its surface has been heavily modified by processes ranging from the migration of volatile condensates, geysers, and atmospheric interactions to possible cryovolcanism (Cruikshank, 1996). In addition, its probable origin by capture and subsequent orbital evolution suggests the possibility of strong heating at some point in Triton's past (McKinnon *et al.*, 1996).

2.7. Oceans

Lewis (1971; 1972; 1973) first raised the possibility of satellite oceans in noting that satellites with a significant amount of water ice are capable of melting and significant geological activity at much lower temperatures than primarily silicate terrestrial planets. Thermal models of icy Galilean satellites suggested that radiogenic heating in a differentiated interior could result in principle in a global liquid water ocean at relative shallow depths (Consolmagno and Lewis, 1977; 1978; Fanale *et al.*, 1977). However, the possibility of sub-solidus convection in warm ice layers considerably complicates the problem, and models including convection raised the possibility of freezing satellite oceans on short time scales in many cases (Schubert, 1986). Subsequent modeling has demonstrated the difficulty establishing the presence or absence of oceans on purely theoretical grounds, given the limitations in numerical modeling and uncertainties in the exact composition and rheological properties of the satellites' icy crusts.

The first observational evidence for satellite oceans came from Voyager observations of Europa. Images of the satellite's geologically young, fractured surface provided strong evidence for global re-surfacing. Although not considered definitive proof of a global liquid water layer, these observations were consistent with ocean models (Figure 6). At the same time the demonstration of the importance of tidal heating provided by the discovery of active volcanism on Io led to new models for Europa that suggested that tidal heating could prevent convective freezing of a liquid layer (Squyres *et al.*, 1983b).

Galileo data have now added significantly to the evidence for global oceans under the icy crusts of all three icy Galilean satellites, Europa, Ganymede and

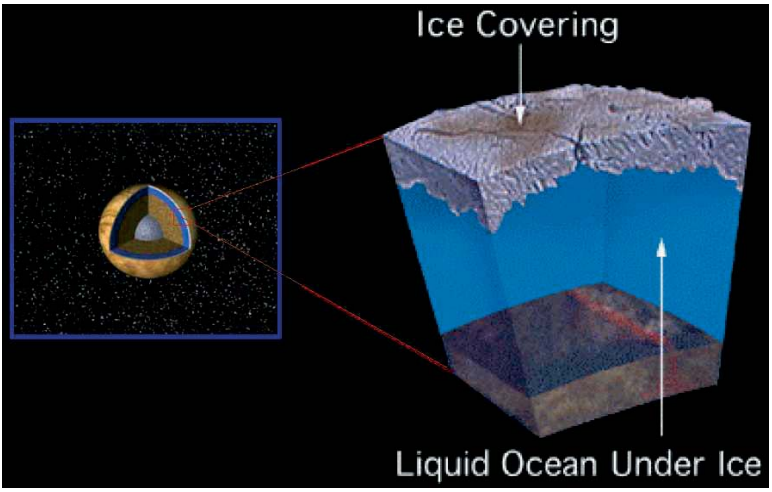

Figure 6. The interior of Europa.

Callisto. High-resolution images of Europa confirm the geologic youthfulness of its surface and show evidence for disruption of the surface in chaos regions where large ice blocks appear to have drifted and rotated (Carr *et al.*, 1998). Spectral evidence also points to sulfate salts materials in many of these young, disrupted regions (McCord *et al.*, 1998b; 1999). Gravitational data, discussed above, indicates that the total thickness of the low-density water and ice crust is between 75 and 150 km thick (Anderson *et al.*, 1997; 1998). All of these data suggest that Europa has a global liquid layer overlain by an ice crust and that the ocean has communicated with the surface over short geologic time scales (∼50-100 Myr; see Pappalardo *et al.*, 1999). A major issue is the thickness of the solid ice crust (brittle plus ductile layers), which is poorly constrained, with estimates ranging from a few kilometers to over twenty or thirty kilometers.

From the point of view of icy satellite geology, the possibilities for what Cassini and Huygens may show us are varied and exciting. Given the possibility of liquid oceans within its sister satellites Ganymede and Callisto, Titan may well have an ocean layer as well. Gravitational and tidal data from tracking Cassini should give strong constraints on its degree of differentiation and the possibility of a global sub-crustal ocean. An upper icy crust similar to Ganymede's, showing the effects of tectonic and impact cratering might be the expected result but for the presence of the moon's massive atmosphere.

Other evidence for oceans comes from magnetic field measurements. When allowance is made for other field perturbations in the satellites' vicinity (from plasma currents, and, in the case of Ganymede, the intrinsic dipole field), each of the icy satellites shows a clear signature of a time dependent induction field produced in response to the changing jovian field in which the satellites are embedded. Electrically conducting layers near the satellites' surfaces are required to

produce the observed response. The conductivity of ice or rock is insufficient and the satellites' ionospheres too tenuous to provide the needed layer. A global layer of water with the conductivity of terrestrial seawater on the other hand would match the observations well (Khurana *et al.*, 1998; Kivelson *et al.*, 1999; 2000).

The magnetic data for Europa are not too surprising in light of the other evidence for a liquid ocean and the role on tidal heating for this satellite. The putative oceans within Ganymede and Callisto may require re-thinking models for thermal history and convection in these satellites. Oceans within the ice/rock shells of Ganymede and Callisto are likely to be at considerable depth ($>\sim 50-100$ km) and 'sandwiched' between a lower layer of a high-density phase of ice (possibly mixed with rock) and an upper low-density layer of ice (see review models by Schubert *et al.*, 2004). Maintaining these oceans in a liquid form in spite of convection in the solid layers, and in the absence of high levels of tidal heating is a challenge for current theoretical models.

2.8. Viscosity and Diapirism

Since the internal temperatures of the icy satellites can approach the melting point of ice even at relatively shallow depths, the effects of low mechanical strength, viscosity and solid state convection all potentially play a role in the geologic processes and the landforms observed on these bodies. An early, pre-Voyager, study of possible viscosity effects for satellites such as Ganymede, even suggested that most large structures such as impact craters and basins might have been effectively erased by viscous relaxation (Johnson and McGetchin, 1973). Although Voyager revealed the satellites to be far more varied than that study suggested, the effects of viscous relaxing are evident in the icy satellites' low overall topography (compared with silicate bodies such as the Moon and Mars), the shallowness of large impact craters and the lack of deep impact basins at the largest scales, displaying instead a new class of low relief impact scar known as palimpsests (see Figure 7). Studies of impacts on icy surfaces now take ice rheology into account at all stages of the process, from the initial transient crater to the subsequent evolution of the structure.

Relatively low viscosity icy crusts are essential to the role of subsolidus convection in transporting heat efficiently and complicating thermal models for the satellites' internal structures. Related viscosity driven processes can also produce distinctive landforms under some circumstances. Small scale ($\sim$10-20 km) domical and pit features on Europa (Figure 7) have been interpreted as evidence of diapirism, a process where thermally and/or compositionally buoyant material rises through a colder, denser layer (salt domes being the archtypical terrestrial example). Calculations supporting these models are one of the strongest arguments for a relatively thick solid ice crust ($\sim$20-30 km) overlying much of Europa's putative ocean. Similar models have been advanced to explain the ubiquitous ridges on Europa's surface (Pappalardo *et al.*, 1998b).

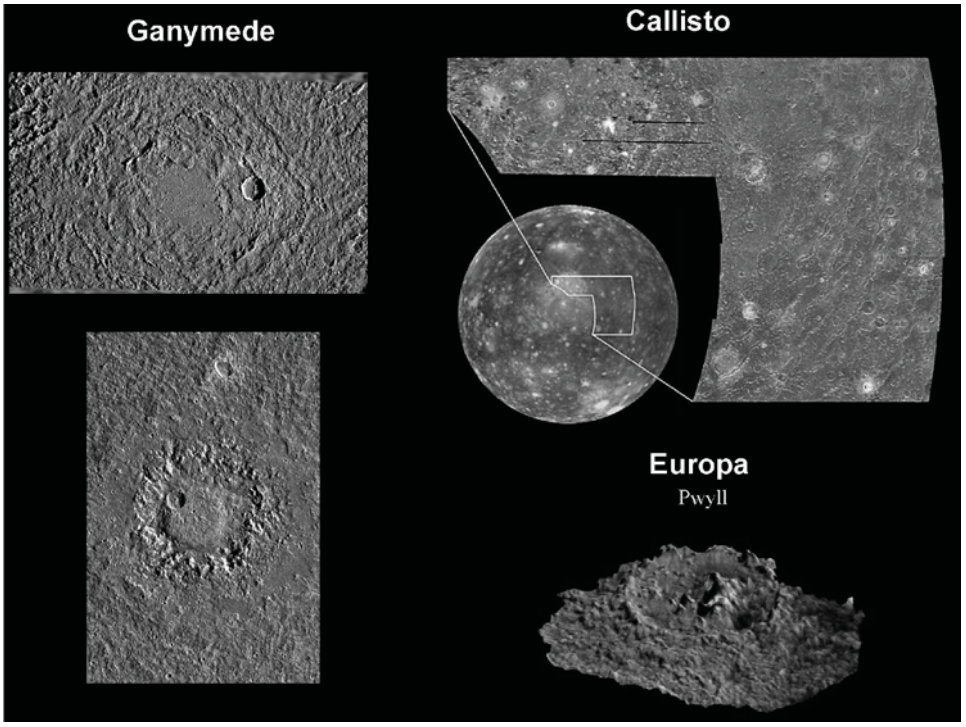

Figure 7. Landforms created by the viscous properties of ice.

2.9. Cryovolcanism vs. Tectonic Resurfacing

Another concept discussed frequently to explain resurfacing of icy satellite surfaces in the post-Voyager literature is that of liquid water volcanism or, more generally, cryovolcanism – volcanic activity at low temperatures. In these scenarios, liquid water (with or without the admixture of 'anti-freeze' contaminants) is seen as playing the role of silicate magma in a crust of solid ice rather than rock. This type of activity in one form or another has been suggested to explain apparently smooth, resurfaced regions on icy satellites, including Europa, Ganymede's (Figure 8) grooved terrain and Enceladus' crater-free terrains. Although appealing intuitively, given the modest energy required to approach the melting point in these bodies, liquid water volcanism as a process faces a number of difficulties. The principle problem is the obvious point that water's unusual phase diagram dictates that the water 'magma' is denser than the solid, making it difficult to bring to the surface from depth. The addition of a dissolved driving gas and/or inclusion of ammonia in the melt has been invoked to mitigate this problem, as well as the possibility that the overlying crust may have denser rock-ice composition (even for terrestrial silicate volcanism such effects can be extremely important). An extensive review of pre-Galileo models for icy tectonics and a discussion of the issues with

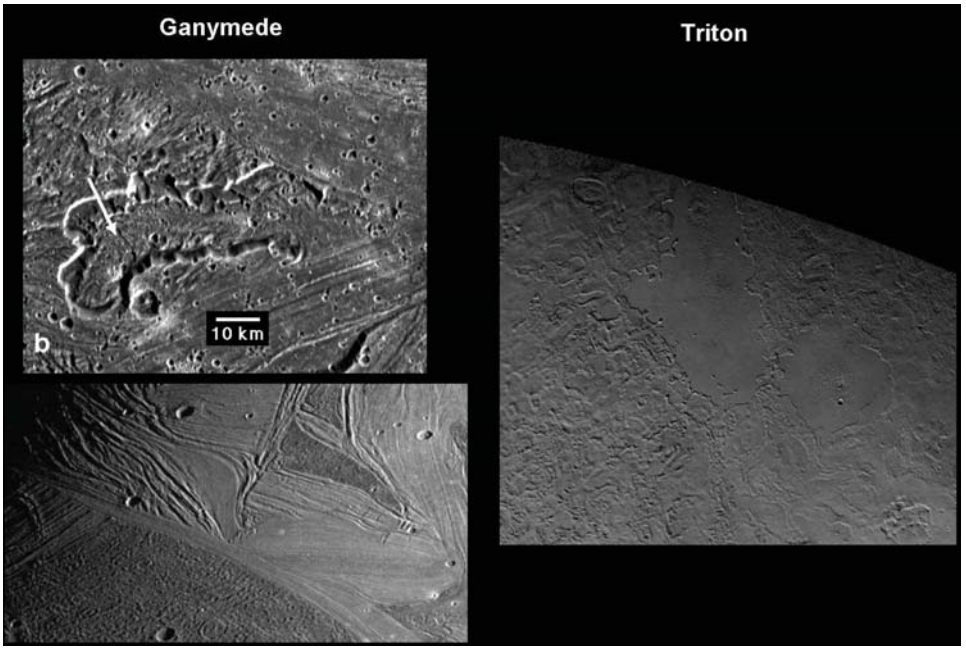

Figure 8. Landforms created by cryovolcanism.

various forms of liquid or partially liquid water volcanism can be found in Squyres and Croft (1986).

Galileo's high-resolution observations of the icy Galilean satellites have cast a new light on the issue of cryovolcanism. Ganymede provides the clearest type example. Many areas that appeared smooth in Voyager's lower resolution images (typically ∼1 km) were interpreted as likely candidates for resurfacing by extensive liquid water volcanism. However, when seen at scales of 100 m or less, most of these regions were revealed as areas where previously existing terrain and structures have been destroyed by extensive fracturing and faulting, showing no evidence for flow-like activity. Absent also were other indications of flooding by magmatic fluids, such as embayed or partially buried craters. Geologic interpretation of Ganymede now attributes most of the destruction and resurfacing of older terrain to a process dubbed 'tectonic resurfacing' (Pappalardo *et al.*, 1998a) (see Figure 9).

Likewise on Europa, although there is abundant evidence for recent, global scale resurfacing, there are few obvious examples of water 'flows' or flooding. Resurfacing appears to have resulted from formation of ridges, faulting, viscous diapiric activity and thermal disruption of chaotic 'ice raft' regions, the latter being the only process that might have resembled the type of activity described earlier as cryovolcanism.

In the Saturnian system, Voyager images show varying degrees of resurfacing of the icy moons, which has been interpreted as the result of liquid water cryovolcanic

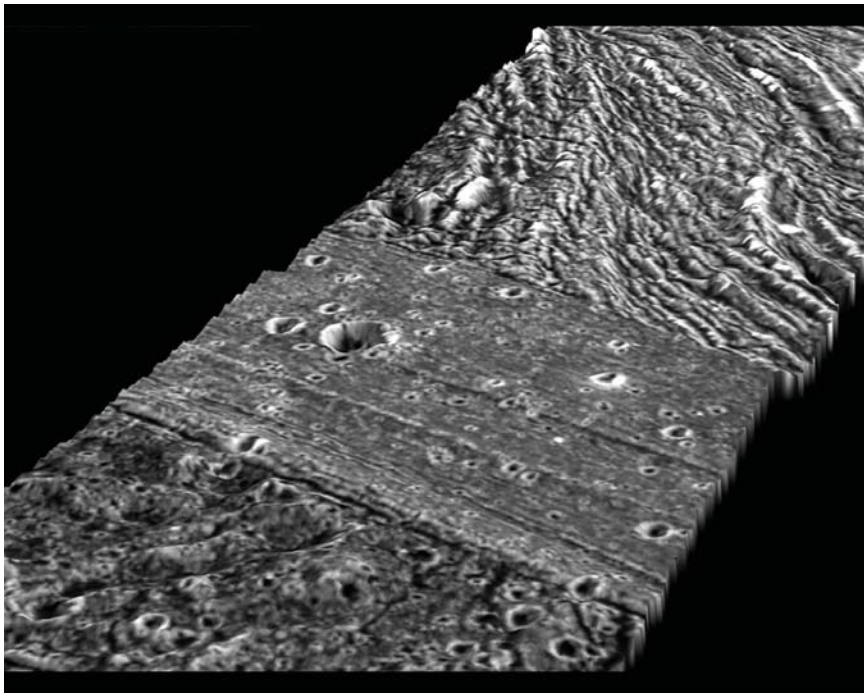

Figure 9. Tectonic resurfacing on Ganymede.

activity. Given the even lower resolution here compared with that for the Galilean satellites, and the results from Galileo's high resolution studies, it is likely that more complex processes may be at work and that Cassini's survey of these bodies may also reveal extensive tectonic resurfacing or suggest other non-volcanic explanations for many of these features.

Perhaps the best case for cryovolcanism can be made for Neptune's strange moon, Triton. Its bulk density suggests a relatively high rock content with associated radiogenic heating and its likely complex dynamical and orbital evolution may have provided a large energy source in the past for heating the interior. Highly volatile condensables including frozen methane, nitrogen and carbon monoxide cover its surface (probably composed primarily of water ice). In Voyagers pictures of Triton's surface two types of cryvolcanism are strongly suggested. First, there are large craters that appear to be extensively flooded by flows of some type. These structures are far more convincing as examples of liquid water or 'slurry' volcanism than features seen on the Jovian or Saturnian moons to date (Smith *et al.*, 1989). Second, Voyager also detected evidence for currently active geyser activity in the southern polar regions. This has been interpreted as volcanism driven by methane or nitrogen and would certainly count as a true form of cryovolcanism (and the only active volcanic activity so far seen outside the Earth and Io). See McKinnon *et al.* (1996), Croft *et al.* (1996), Brown *et al.* (1996), Kirk *et al.* (1996).

3. Prospects for Cassini/Huygens Exploration of Saturn System

In the context of the above brief review of icy satellite geology, what do we expect from satellite observations by the Cassini/Huygens mission? As with Galileo's exploration of the Jupiter system, Cassini/Huygens observations of Saturn's moons will provide orders of magnitude improvements in surface resolution, gravitational studies and the use of a new generation of remote spectral and compositional experiments. In addition, the Huygens Titan probe will provide in situ analyses of the densest satellite atmosphere known, as well as close-up observations of its surface. The following brief sections highlight some of the issues that the mission will address for the moons of Saturn.

3.1. Cratered Icy Satellites

One important component of the Saturn system is a set of medium sized icy worlds, heavily cratered over most of their surface but displaying varying degrees of evidence for tectonic activity, and resurfacing: Mimas, Tethys, Dione, Rhea, and Hyperion. Guided by experience from Galileo's results at Jupiter, it is likely that Cassini will reveal that their surfaces at high resolution are segregated into bright icy areas and dark, non-ice material in topographic lows and as deposits from mass wasting down steep slopes. This material may well be similar to the organic rich hydrated materials on the Galilean satellites, with inclusions of carbon dioxide (preliminary results from Cassini's fly-by of the outer moon, Phoebe, confirm that CO_2 is indeed present in the surface materials of this moon at least (Brown *et al.*, 2004). Resurfaced regions and the 'wispy' terrain on Dione and Rhea might well be the result of tectonic resurfacing, similar to areas seen on Ganymede, rather than the 'classical' cryovolcanism suggested in post-Voyager interpretations.

3.2. Two Strange Satellites: Iapetus and Enceladus

Among the Saturnian moons, Voyager data clearly highlight two for special scrutiny – Iapetus and Enceladus (Figure 10). Iapetus has been recognized since its discovery as a planetary oddity, with one hemisphere (the 'leading hemisphere' with respect to the moon's orbital motion) approximately ten times darker than the other, trailing, hemisphere. Numerous ideas have been advanced to explain this dichotomy, most of them involving the fact that leading hemisphere receives more impacts from debris coming from outside Iapetus' orbit than the trailing side does. Other suggestions invoke 'dirty' cryovolcanic eruptions concentrated on one hemisphere, similar to the situation on the Earth's Moon. Voyager images added to the debate but did not resolve it. Relatively sharp boundaries of the dark region and apparent concentration of dark material in the floors of craters just outside the dark region tend to suggest an endogenic or volcanic origin of the dark material. On the other hand the pattern of the dark unit on the surface of the moon matches the predictions of dynamical impact calculations well. A good review of pre-Cassini

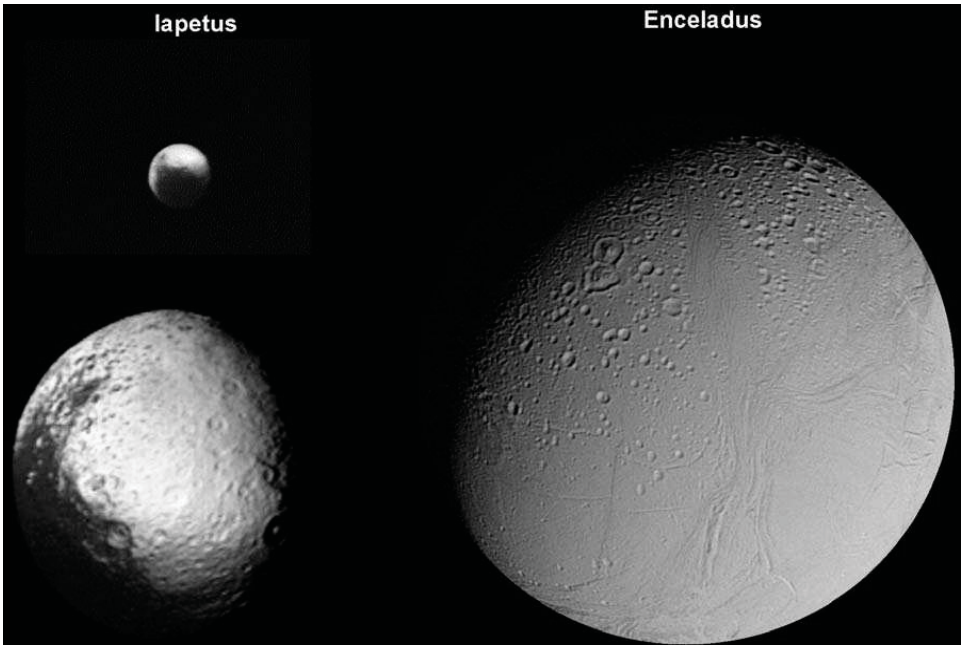

Figure 10. Images by Voyager 2 of Iapetus and Enceladus.

ideas concerning this two-faced satellite can be found in Burns and Matthews (1986). Cassini high-resolution images of the dark unit and the border areas should help resolve the issue. In addition, spectral data should aid in identifying the nature of the dark material and its relationship to other non-ice units on the satellites.

Enceladus is so small (diameter only ∼500 km) that radiogenic heating is expected to be negligible (Schubert, 1986). Nevertheless, Voyager images showed that this moon has the youngest surface geologically of any of the major icy moons. The best Voyager images (resolution about 2 km) show some apparently crater-free regions at high northern latitudes as well as possibly flooded and viscously relaxed craters. The resurfaced region appears relatively smooth with some ridge-like structures. Interpretation of these features has of course included cryovolcanism as a major process, and the association of the main concentration of the tenuous E-ring with the radial distance of Enceladus' orbit also suggests Encecladus as the (possibly volcanic) source of the E-ring material.

A major problem for understanding Enceladus is the lack of an apparent source of energy for its inferred geologic activity. As noted above, radiogenic heating is not believed to be a major factor, unless Enceladus is unusually rich compared with the other satellites in non water components such as ammonia, which could act like an 'anti-freeze' and allow melting at very low temperatures (the ammonia-water eutectic mix is a temperature of ∼173 K). After discovery of Io's volcanism, tidal heating is an obvious candidate. Enceladus does in fact have a forced eccentricity arising from a 2:1 orbital resonance with Dione, but the present value of

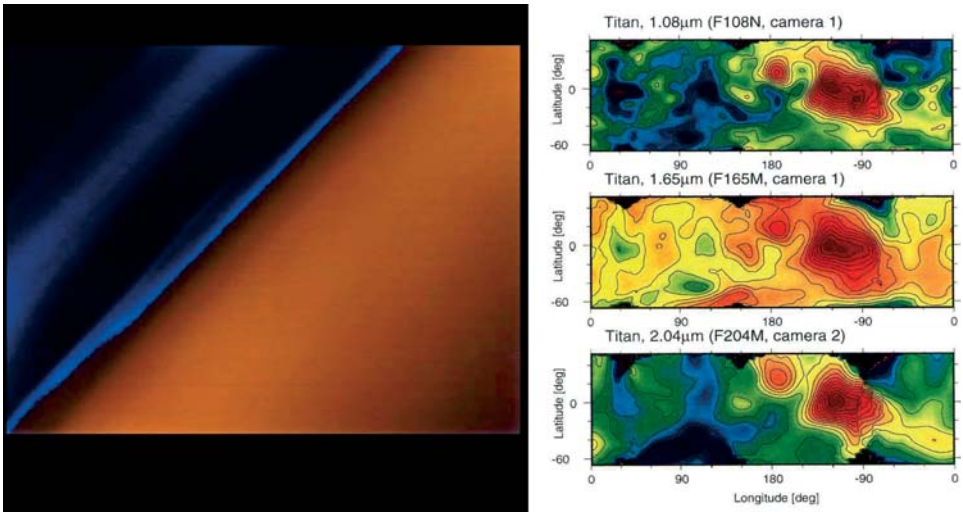

Figure 11. Left: Voyager false color limb haze. *Right:* HST NICMOS images of Titan.

this eccentricity (∼0.0045) is too small to create significant heating at the present time according to most published models. The orbital evolution of Saturn's satellites, however, is quite complicated due to the multiple resonant conditions in the system and the large uncertainties in the detailed calculation of tidal dissipation, and several workers have raised the possibility that Enceladus' orbital eccentricity could have been significantly greater in the past. No completely satisfactory model has yet been offered, however. A recent review of issues related to Enceladus' dynamics and orbital models can be found in Peale (1999).

3.3. TITAN!!

Titan is almost certainly an 'icy' satellite in spite of there being no definitive identification of its surface or crustal composition. It's bulk properties, density and radius, make it the virtual twin of Ganymede and Callisto, with an model ice fraction of about 50%. We knew essentially nothing of its geology prior to the arrival of Cassini/Huygens. Its massive nitrogen atmosphere (Figure 11) and smog-like hydrocarbon aerosols prevented any of Voyager's remote sensing instruments from viewing the surface directly although other investigations obtained detailed atmospheric data including the temperature and pressure profile and upper atmospheric chemistry. Only recently have radar and space and adaptive optics infrared observations started to penetrate Titan's hazes and permit a first look at what lies below. Both radar and infrared techniques show brightness variations across the surface, but the nature of the surface is still unresolved (Campbell *et al.*, 2003; Hartung *et al.*, 2004). The first close up views of Titan from Cassini/Huygens (Figure 12) show an extremely unusual surface (Brown *et al.*, 2004; Porco *et al.*, 2004).

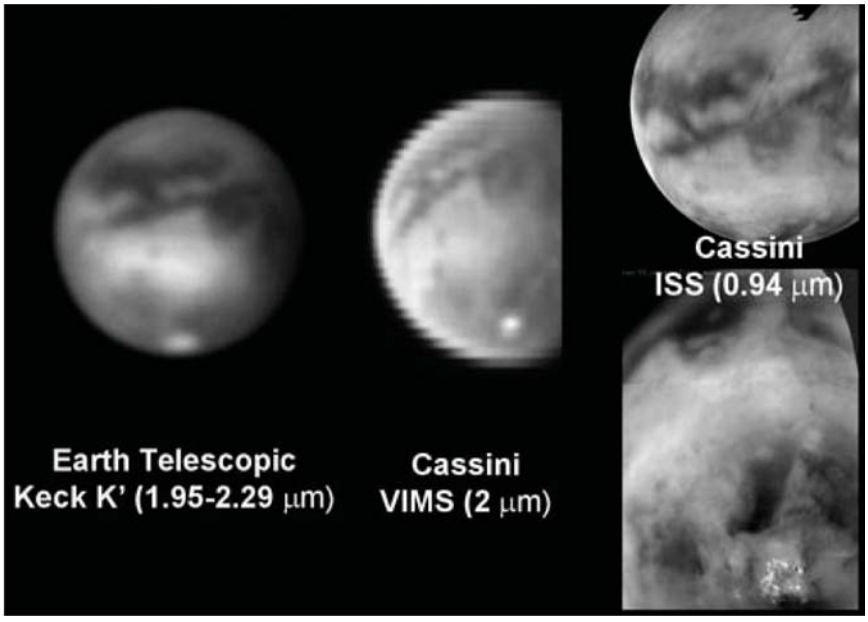

Figure 12. Early surface observations of Titan: Keck adaptive optics image (*left*), Cassini VIMS (*center*), Cassini ISS (*right*).

From the point of view of icy satellite geology, the possibilities for what Cassini and Huygens may show us are varied and exciting. Given the possibility of liquid oceans within its sister satellites Ganymede and Callisto, Titan may well have an ocean layer as well. Gravitational and tidal data from tracking Cassini should give strong constraints on its degree of differentiation and the possibility of a global sub-crustal ocean. An upper icy crust similar to Ganymede's, showing the effects of tectonic and impact cratering might be the expected result but for the presence of the moon's massive atmosphere.

If the atmosphere has persisted for most of Titan's history it should have had at least two major effects on its geology. First, only large impacting bodies would be able to make it through the atmosphere to produce impact craters on the surface. In this case a surface exhibiting only large craters modified by the atmosphere might be the result, as has occurred at Venus. Second, the photochemical processes in the upper atmosphere should have produced large quantities of hydrocarbon aerosols that would precipitate to surface. Calculations of this process have suggested the possibility of extensive bodies of liquid hydrocarbon – lakes or seas – on the surface.

Cassini and Huygens observations will certainly totally revise our now blurry view of this moon. Both the imaging and infrared spectral mapping experiments should be able to view the surface in the same spectral 'windows' used by the Earth and space-based telescopes but with greatly increased resolution, mapping much of the surface at kilometer or even sub-kilometer scales. In addition, Cassini carries

an imaging radar system capable of directly imaging the surface (and sub-surface in some cases). Titan could well be the 'ultimate icy satellite', with a surface affect by both sub-surface and surface oceans, aeolian processes and precipitation.

4. Summary

The icy satellites of the outer solar system display a fascinating variety in their geology. Underlying themes in understanding the history of these moons and the processes which affect them are the presence of water ice a major planetary constituent, the relative ease of raising the interior temperatures of icy moons to a significant fraction of melting temperature by radiogenic and tidal heating, the role of warm ice as viscous medium, tectonic resurfacing and possible cryovolcanism. The start of the Cassini/Huygens orbital and probe mission as this work is being prepared promises to greatly expand our understanding not only of the Saturn satellite system, but icy satellites generally. The next 'brief' reference work of this type will undoubtedly require entire chapters for topics covered here in a paragraph or two.

References

Anderson, J.D., Lau, E.L., Sjogren, W.L., Schubert, G., and Moore, W.B.: 1997, 'Europa's differentiated internal structure: Inferences from two Galileo encounters', *Science* **276**, 1236–1239.

Anderson, J.D., Schubert, G., Jacobson, R.A., Lau, E.L., Moore, W.B., and Sjogren, W.L.: 1998, 'Europa's differentiated internal structure: Inferences from four Galileo encounters', *Science* **281**, 2019–2022.

Brown, R.H., Cruikshank, D.P., Veverka, J., Helfenstein, P., and Eluszkiewicz, J.: 1996, 'Surface composition and photometric properties of Triton', in D.P. Cruikshank (ed.): 1996, *Neptune and Triton*, University of Arizona Press, Tucson, AZ.

Brown, *et al.*: 2004, submitted to *Science*.

Burns, J.A. and Matthews, M.S. (eds.): 1986, *Satellites*, The University of Arizona Press, Tucson, 1021 pp.

Campbell, D.B., Black, G.J., Carter, L.M., Ostro, and Steven, J.: 2003, 'Radar evidence for liquid surfaces on Titan', *Science* **302**, 431–434.

Carlson, R.W.: 1999, 'A tenuous carbon dioxide atmosphere on Jupiter's moon Callisto', *Science* **283**, 820–821.

Carr, M.H., *et al.*: 1998, 'Evidence for a subsurface ocean on Europa', *Nature* **391**, 363–365.

Consolmagno, G.J., and Lewis, J.S.: 1977, 'Preliminary thermal history models of icy satellites', in J.A. Burns (ed.), *Planetary Satellites*, pp. 492–500.

Consolmagno, G.J., and Lewis, J.S.: 1978, 'Evolution of icy satellite interiors and surfaces', *Icarus* **34**, 280–293.

Courtin, R.: 2005, 'Aerosols on the giant planets and Titan', this volume.

Coustenis, A.: 2005, 'Formation and evolution of Titan's atmosphere', this volume.

Croft, S.K., Kargel, J.S., Kirk, R.L., Moore, J.M., Schenk, P.M., and Strom, R.G.: 1996, 'The geology of Triton', in D.P. Cruikshank (ed.): 1996, *Neptune and Triton*, University of Arizona Press, Tucson, AZ.

Cruikshank, D.P. (ed.): 1996, *Neptune and Triton*, University of Arizona Press, Tucson, AZ.
Fanale, F.P., Johnson, T.V., and Matson, D.L.: 1977, 'Io's surface and the histories of the Galilean satellites', in J.A. Burns, *Planetary Satellites*, University of Arizona Press, pp. 379–405.
Gautier, D. and Hersant, F.: 2004, 'Formation and composition of planetesimals – trapping volatiles by clathration', this volume.
Hartung, M., Herbst, T.M., Close, L.M., Lenzen, R., Brandner, W., Marco, O., and Lidman, C.: 2004, 'A new VLT surface map of Titan at 1.575 microns', *Astron. Astrophys.* **421**, L17–L20.
Hibbitts, C.A., McCord, T.B., and Hansen, G.B.: 2000, 'Distributions of CO_2 and SO_2 on the surface of Callisto', *J. Geophys. Res.* **105**, 22541–22557.
Johnson, T.V. and McGetchin, T.R.: 1973, 'Topography on satellite surfaces and the shape of asteroids', *Icarus* **18**, 612–620.
Khurana, K.K., Kivelson, M.G., Stevenson, D.J., Schubert, G., Russell, C.T., Walker, R.J., and Polanskey, C.: 1998, 'Induced magnetic fields as evidence for subsurface oceans in Europa and Callisto', *Nature* **395**, 777–780.
Kirk, R.L., Soderblom, L.A., Brown, R.H., Kieffer, S.W., and Kargel, J.S.: 1986, 'Triton's Plumes: Discovery, Characteristics, and Models', in D.P. Cruikshank (ed.): 1996, *Neptune and Triton*, University of Arizona Press, Tucson, AZ.
Kivelson, M.G., Khurana K.K., Stevenson, D.J., Bennett, L., Joy, S., Russell, C.T., Walker, R.J., Zimmer, C., and Polanskey, C.: 1999, 'Europa and Callisto: Induced or intrinsic fields in a periodically varying plasma environment', *J. Geophys. Res.* **104**, 4609–4625.
Kivelson, M.G., Khurana, K.K., Russell, C.T., Volwerk, M., Walker, R.J., and Zimmer, C.: 2000, 'Galileo magnetometer measurements: A stronger case for a subsurface ocean at Europa', *Science* **289**, 1340–1343.
Lane, A.L. and Domingue, D.L.: 1997, 'IUE's view of Callisto: Detection of an SO_2 absorption correlated to possible torus neutral wind alterations', *Geophys. Res. Lett.* **24**, 1143–1146.
Lane, A.L., Nelson, R.M., and Matson, D.L.: 1981, 'Evidence for sulfur implantation in Europas UV absorption-band', *Nature* **292**, 38–39.
Lewis, J.S.: 1971, 'Satellites of Outer planets – their physical and chemical nature', *Icarus* **15**, 174–185.
Lewis, J.S.: 1972, 'Low-temperature condensation from solar nebula', *Icarus 16*, 241–252.
Lewis, J.S.: 1973, 'Chemistry of the Outer Solar System', *Space Sci. Rev.* **14**, 401–411.
Lunine, J.L.: 1993, 'Does Titan have an ocean? A review of current understanding of Titan's surface', *Rev. Geophys.* **31**, 133–149.
Lunine, J.I., Stevenson, D.J., and Yung, Y.L.: 1983, 'Ethane ocean on Titan', *Science* **222**, 1229–1230.
McCord, T.B., *et al.*: 1997, 'Organics and other molecules in the surfaces of Callisto and Ganymede', *Science* **278**, 271–275.
McCord, T.B., *et al.*: 1998a, 'Non-water-ice constituents in the surface material of the icy Galilean satellites from the Galileo near-infrared mapping spectrometer investigation', *J. Geophys. Res.* **103**, 8603–8626.
McCord, T.B., *et al.*: 1998b, 'Salts an Europa's surface detected by Galileo's near infrared mapping spectrometer', *Science* **280**, 1242–1245.
McCord, T.B., *et al.*: 1999, 'Hydrated salt minerals on Europa's surface from the Galileo near-infrared mapping spectrometer (NIMS) investigation', *J. Geophys. Res.* **104**, 11827–11851.
McEwen, A.S.: 1986, 'Exogenic and endogenic albedo and color patterns on Europa', *J. Geophys. Res.* **91**, 8077–8097.
McKinnon, W.B., Lunine, J.I., and Banfield, D.: 1996, 'Origin and evolution of Triton', in D.P. Cruikshank (ed.), *Neptune and Triton*, University of Arizona Press, pp. 718–763.
Moore, J.M., *et al.*: 1999, 'Mass movement and landform degradation on the icy Galilean satellites: results of the Galileo nominal mission', *Icarus* **140**, 294–312.

Nelson, M.L., McCord, T.B., Clark, R.N., Johnson T.V., Matson D.L., Mosher, J.A., and Soderblom, L.A.: 1986, 'Europa – characterization and interpretation of global spectral surface units', *Icarus* **65**, 129–151.

Pappalardo, R.T., *et al.*: 1998a, 'Grooved terrain on Ganymede: First results from Galileo high-resolution imaging', *Icarus* **135**, 276–302.

Pappalardo, R.T., *et al.*: 1998b, 'Geological evidence for solid-state convection in Europa's ice shell', *Nature* **391**, 365–368.

Pappalardo, R.T., *et al.*: 1999, 'Does Europa have a subsurface ocean? Evaluation of the geological evidence', *J. Geophys. Res.* **104**, 24,015–24,055.

Peale, S.J.: 1999, 'Origin and evolution of the natural satellites', *Ann. Rev. Astron. Astrophys.* **37**, 533–602.

Peale, S.J., Cassen, P., and Reynolds, R.T.: 1979, 'Melting of Io by tidal dissipation', *Science* **203**, 892–894.

Porco, *et al.*: 2004, submitted to *Science*.

Roos-Serote, M.: 2005, 'The changing face of Titan's haze: Is it all dynamics?', this volume.

Schubert, G.: 1986, 'Thermal histories, compositions, and internal structures of the moons of the solar system', in J.A. Burns and M.S. Matthews (eds.), *Satellites*, University of Arizona Press, pp. 224–292.

Schubert, G., Anderson, J.D., Spohn, T., and McKinnon, W.B.: 2004, 'Interior composition, structure and dynamics of the Galilean satellites', in F. Bagenal, T.Dowling, and W. McKinnon (eds.), *Jupiter: The Planet, Satellites and Magnetosphere*, Chapter 13, Cambridge University Press.

Smith, B.A., *et al.*: 1989, 'Voyager-2 at Neptune – imaging science results', *Science* **246**, 1422–1449.

Squyres, S.W. and Croft, S.K.: 1986, 'The tectonics of icy satellites', in J.A. Burns and M.S. Matthews (eds.), *Satellites*, University of Arizona Press, Tucson, AZ, pp. 293–341.

Squyres, S.W., Reynolds, R.T., and Cassen, P.M.: 1983a, 'The evolution of Enceladus', *Icarus* **53**, 319–331.

Squyres, S.W., Reynolds, R.T., Cassen, P.M.: 1983b, 'Liquid water and active resurfacing on Europa', *Nature* **301**, 225–226.

Stöffler, D., and Ryder, G.: 2001, 'Stratigraphy and isotope ages of lunar geologic units: chronological standard for the inner solar system', *Space Sci. Rev.* **96**, 9–54.

Strobel, D.: 2005, 'Photochemistry in outer solar system atmospheres', this volume.

Zahnle, K., Schenk, P.M., Levison, H., and Dones, L.: 2003, 'Cratering rates in the outer solar system', *Icarus* **163**, 263–289.

Zahnle, K., Schenk, P., Dones, L., Levison, H.: 2004, 'Cratering rates in the Jovian system', *Workshop on Europa's Icy Shell: Past, Present, and Future*, February 6-8, 2004, Houston, Texas, abstract # 7052.

Address for Offprints: Torrence V. Johnson, Jet Propulsion Laboratory, California Institute of Technology, Pasadena, CA 91109; `torrence.v.johnson@jpl.nasa.gov`

TRITON, PLUTO, CENTAURS, AND TRANS-NEPTUNIAN BODIES

DALE P. CRUIKSHANK
NASA Ames Research Center, Moffett Field, CA 94035-1000, USA

Received: 7 June 2004; Accepted in final form: 8 October 2004

Abstract. The diverse populations of icy bodies of the outer Solar System (OSS) give critical information on the composition and structure of the solar nebula and the early phases of planet formation. The two principal repositories of icy bodies are the Kuiper belt or disk, and the Oort Cloud, both of which are the source regions of the comets. Nearly 1000 individual Kuiper belt objects have been discovered; their dynamical distribution is a clue to the early outward migration and gravitational scattering power of Neptune. Pluto is perhaps the largest Kuiper belt object. Pluto is distinguished by its large satellite, a variable atmosphere, and a surface composed of several ices and probable organic solid materials that give it color. Triton is probably a former member of the Kuiper belt population, suggested by its retrograde orbit as a satellite of Neptune. Like Pluto, Triton has a variable atmosphere, compositionally diverse icy surface, and an organic atmospheric haze. Centaur objects appear to come from the Kuiper belt and occupy temporary orbits in the planetary zone; the compositional similarity of one well studied Centaur (5145 Pholus) to comets is notable. New discoveries continue apace, as observational surveys reveal new objects and refined observing techniques yield more physical information about specific bodies.

Keywords: Triton; Pluto; Centaurs; Kuiper Belt Objects; ice; infrared spectroscopy

1. Introduction

The sub-planet size bodies in the Solar System beyond Neptune, and including Neptune's large satellite Triton, are sometimes termed *ice dwarfs* because they are composed largely of solid H_2O and other frozen volatile materials. This term stands both in parallel and in contrast to *ice giants*, which characterizes Uranus and Neptune. Triton was found shortly after the discovery of Neptune itself, and because it is fairly bright it was thought from the outset to be relatively large in comparison to other planetary satellites. Pluto was discovered in 1930 as a result of a lengthy search for an external planet that was initiated to find the cause of a perceived gravitational perturbation to Neptune's orbit. It was later found that Neptune's motion was normal, and that Pluto was too small to have caused a noticeable effect in any case. Together with these bodies, we also consider the Centaurs because they formerly were trans-Neptunian objects, although they now have orbits within the planetary region.

The outer Solar System has long been thought to be the repository, and perhaps the place of origin, of the comets. Oort (1950) determined that the long-period ($P \geq 200$ y) and highly inclined comets are derived from a large reservoir of order

Space Science Reviews 116: 421–439, 2005.
DOI: 10.1007/s11214-005-1964-0

50,000 AU from the Sun, while Kuiper (1951) proposed that the comets with periods P≤200 y and lying near the ecliptic plane come from a disk-shaped reservoir that begins just beyond Neptune. Kuiper was led to this possibility by questioning the reality and meaning of an apparent edge to the mass distribution (with heliocentric distance) function of the Solar System that emerges when only the major planets are considered.

Oort's reservoir (the Oort Cloud) of small, icy bodies around the Sun cannot be detected directly, but is known from the slow leakage of individual objects that make their way to the inner Solar System and appear as comets. Similarly, Kuiper's reservoir went undetected, except for the short-period comets coming inward at the rate of a few tens of objects per year, until Jewitt and Luu (1993) discovered the first object beyond Pluto, 1992 QB1.

After some 50 years of study of the concepts proposed by Oort and Kuiper, it is recognized that both the Oort Cloud and the Kuiper belt tell important stories about the origin and evolution of the Solar System, and that similar structures may be common around other stars. With the discovery of nearly 1000 Kuiper belt objects (see below), the concept of a reservoir of short-period comets has advanced well beyond the abstract, and detailed studies of these objects in the aggregate and individually are in progress. This paper is a summary of current knowledge of the origins and physical properties of Triton, Pluto, the bodies in the Kuiper belt, and the Centaurs.

2. Triton

Among the objects discussed here, Triton is the only one for which we have direct knowledge from a close-up, although fleeting, view offered by a spacecraft. In August, 1989, the Voyager 2 spacecraft flew by Neptune, and 5 hours and 14 minutes later passed by Triton at a minimum distance of 39,800 km, conducting a battery of investigations of all aspects of these two bodies and their space environments (Stone and Miner, 1989; Cruikshank, 1995; Miner and Wessen, 2002). Only 40 percent of Triton was imaged, but an astonishing array of surface features was recorded, as well as surface deposits of dark material precipitating from erupting plumes and transported by winds driven by the sublimation of nitrogen from the sunlit south polar region. Three active plumes were seen ejecting material from the surface to a height of 8 km.

Triton's radius is 1352 km and its orbital period is 5.877 days. At a mean distance from Neptune of 14.3 R_N, it is in locked, synchronous rotation and its nearly circular orbit is retrograde. The mean density determined from Voyager observations is 2.06 g cm^{-3}.

Spectroscopy from ground-based telescopes shows the presence of absorption bands of solid N_2, CH_4 , CO_2, CO, and H_2O, all in the region 1.5-2.5 μm (Cruikshank *et al.*, 1998a; Quirico *et al.*, 1999). N_2 is found in the beta phase, which is

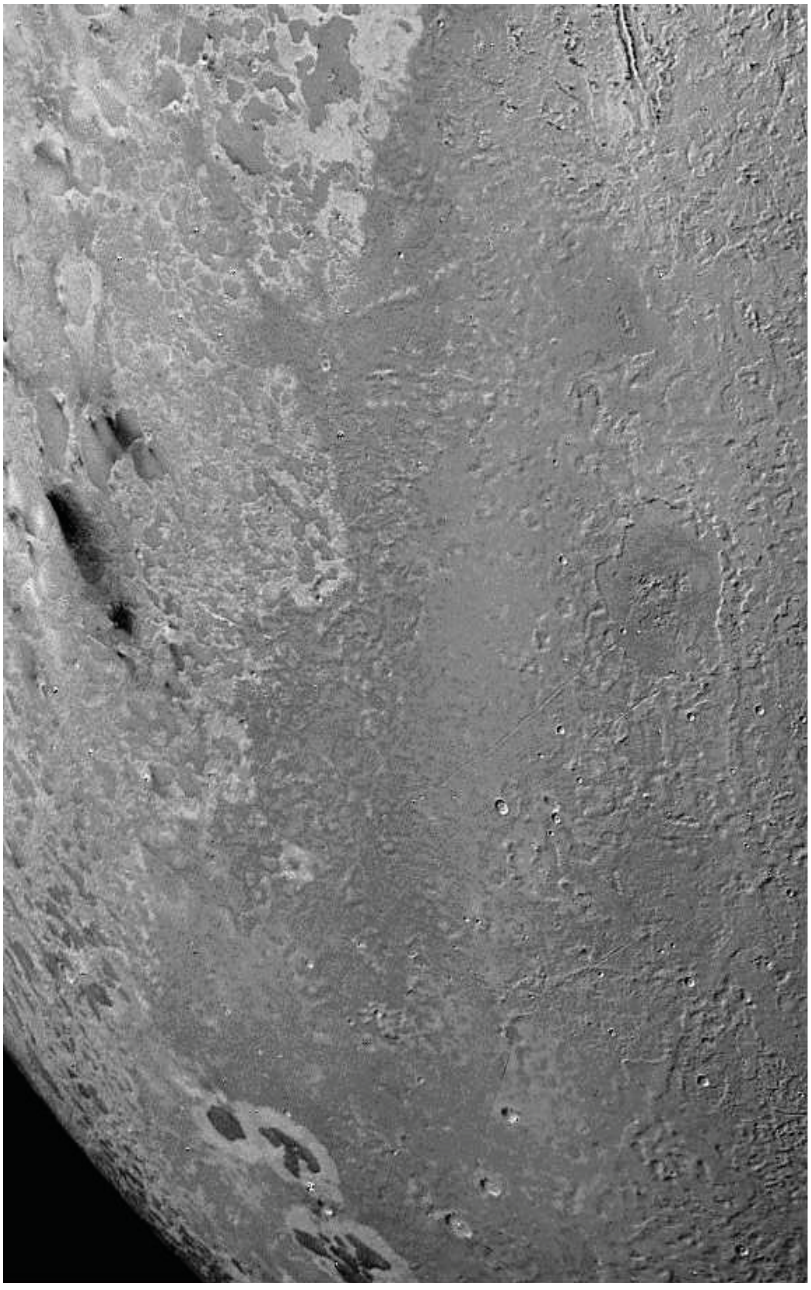

Figure 1. A section of Triton's surface (centered at ~38° E, -15° S). The direction to the S. pole is to the upper left. Left of center is a complex of dark spots (maculae) that appear to be surface deposits deposited by sublimation winds blowing from the S. pole. Right of center is a walled plain (Sipapu Planitia). At the bottom is a complex of flat, dark spots (maculae). At bottom center is the 27-km impact crater Mozamba, the largest seen on Triton. The boundary between the light colored S. polar material and the darker surface runs diagonally from top center toward the lower left side of the picture.

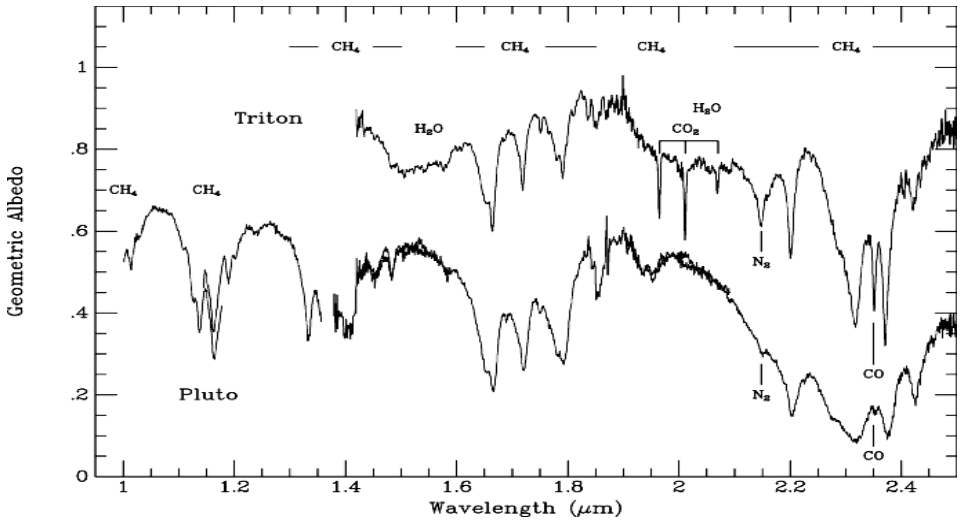

Figure 2. Reflectance spectra of Triton and Pluto from observations by T. C. Owen, D. P. Cruikshank, T. R. Geballe, C. de Bergh, and T. L. Roush with the UKIRT 3.8-m telescope. These and similar data from the same program serve as the basis for the analyses of Triton by Quirico *et al.* (1999) and of Pluto by Douté *et al.* (1999). The absorbing ice species that have been identified are indicated. H_2O has not been reliably identified on Pluto.

stable at $T \geq 36.8$ K. On Triton (and Pluto), solid N_2 occurs as large crystals with dimensions of order centimeters in which the optical pathlength is several centimeters. The CH_4 bands are shifted in wavelength (the matrix shift) by small amounts compared to pure CH_4 because the methane is dissolved in the N_2, appearing as an impurity in the large nitrogen crystals. In the 3-4 μm spectral region, Grundy *et al.* (2002) have found additional CH_4 ice absorption bands with additional unidentified absorption that may arise from nonvolatile solid surface components. Those nonvolatile components include the solid, low-albedo effluent from the plumes, as well as the material giving Triton's surface its overall coloration.

Changes in the color and spectral signature of Triton have been reported in data taken over the time interval 1977-2000 (e.g., Brown *et al.*, 1995). Such changes might arise with the condensation of new deposits of ices on the surface or from the sublimation of ice from large areas as a result of seasonal changes and/or geological activity.

The N_2 surface ice is the principal source of Triton's atmosphere, with the atmospheric pressure apparently in vapor pressure equilibrium at the prevailing temperature. The detection of an atmosphere with surface pressure $p = 16 \pm 3 \mu$bar by the Voyager radio science investigation (Tyler *et al.*, 1989; Yelle *et al.*, 1991) is consistent with the vapor pressure of N_2 at T$\sim$38 K (Broadfoot *et al.*, 1989). Triton's atmospheric gases have not yet been detected spectroscopically, but small amounts of CH_4 and CO are expected on the basis of their vapor pressures. CO_2 and

H_2O are not expected to contribute to the atmosphere because of their exceedingly low vapor pressures at the relevant temperature.

Evidence for change in Triton's surface temperature between the 1989 fly-by of Voyager 2 and 1997 comes from an increase in the pressure in the middle atmosphere ($z = 1400$ km) detected from observations of a stellar occultation (Elliot *et al.*, 1998). The pressure derived from the occultation is 2.3 ± 0.1 μbar, compared to the value of 0.8 ± 0.1 μbar extrapolated from the surface pressure measured by Voyager. The derived middle atmospheric temperature increased from 47 ± 1 K to 50.3 ± 0.5 K. Elliot *et al.* (1998) have calculated on the basis of the vapor pressure of the N_2 surface ice that the surface temperature increased from 37.5 K (in 1989) to 39.3 K in 1997. These changes could be caused by the migration of surface ices or frosts, changes in the optical properties of the surface frost (albedo, scattering efficiency, etc.), and changing heat input (from the Sun and from internal sources) to the ice. In this context, we note that Brown *et al.* (1995) reported a change in the strengths of the CH_4 bands in the spectrum of Triton in the interval 1980–1981. They suggested that a layer of obscuring material (e.g., N_2 frost) had been deposited on portions of Triton's surface in that time interval.

The atmosphere resulting from the sublimation of N_2, CH_4 , and CO ices from Triton's surface is photolyzed by Lyman-alpha photons from the Sun and the interstellar medium (Broadfoot *et al.*, 1989), producing the hydrocarbons C_2H_4, C_2H_6, and C_2H_2. These form haze particles and precipitate to the surface at rates calculated as 135, 28, and 1.3 g/cm^2/Gy, respectively (Krasnopolsky and Cruikshank, 1995). These hydrocarbons and other expected photolytic products (e.g., HCN) have not yet been detected in the spectrum of Triton (Quirico *et al.*, 1999); their concentrations are probably greatly diluted by the cycle of sublimation and condensation of the uppermost surface layers.

The large size of Triton and its circular, retrograde orbit impose special constraints on the origin of this satellite of Neptune. It is thought to have accreted in the region of the solar nebula beyond 30 AU as a member of the very large family of Kuiper belt objects, of which Triton and Pluto are perhaps the largest surviving members. Triton and Pluto share a very similar size and mean density ($\sim$2 g cm^{-3}), suggesting a bulk composition of about 60% silicate rocky material and 40% ice (McKinnon *et al.*, 1995).

In the early Solar System, in the final stages of its accretion, Neptune's orbit expanded, sweeping many Kuiper belt objects into its orbital resonances, thus dynamically stirring the population. Although Neptune's orbit now appears stable, its influence on the bodies in the inner Kuiper belt is still seen, as objects are perturbed both outward and inward to cross the orbits of the major planets. The latter such objects are called Centaurs, and their orbits are stable only for timescales of 10^6 to 10^7 y. Those objects scattered outward that remain in elliptical orbits are called scattered disk objects (see below).

In its late-accretion phase, Neptune's circumplanetary disk served both as a source region for the formation of satellites, and as a medium in which a passing

Kuiper belt object might be slowed sufficiently to permit gravitational capture. It is thought that Triton must have collided with a newly accreted satellite to dissipate enough energy to permit the capture. Subsequent circularization of the orbit resulted from the strong tidal interaction with Neptune as it made close approaches to the planet, at the same time completely disrupting, and perhaps accreting, such regular satellites that might have formed in the disk.

During the few hundred million years of orbital evolution, the dissipation of tidal energy produced a prodigious amount of heat in Triton, far more than needed to completely melt the body. The rate of heating depended on the rate of the evolution of the orbit, which in turn depended on the dissipative qualities of Triton's interior structure; liquid is highly dissipative, solid rock much less so. Thus, once an interior zone, such as a layer of ice, was melted, the heat became concentrated in that region, driving the volatile material toward the surface. Triton must have then had a very massive and vertically extended atmosphere, with temperatures in the range 100-200 K.

3. Pluto and Charon

The Pluto and Charon pair constitutes a binary system in a heliocentric orbit that is eccentric ($e = 0.246$) and inclined ($i = 17.14°$) to the ecliptic plane. Pluto's orbital period is in a 2:3 resonance with the orbital period of Neptune, and although Pluto's orbit crosses that of Neptune, the two planets cannot collide. Pluto was discovered photographically in 1930 in a search for a planet that was thought to perturb the orbit of Neptune, although it was later evident that Pluto is far too small to have such an effect. The satellite Charon was also found photographically, in 1978.

From observations with earth-based telescopes and orbiting observatories the basic physical properties of Pluto and Charon have been established. Their dimensions (Table I) and the orbital parameters of Charon were established through analysis of photometric observations of an extensive series of mutual transits and occultations that occurred in the interval 1985 – 1989 (Binzel and Hubbard, 1997). Fortuitously, these events occurred soon after the discovery of the satellite; if Charon had been discovered just ten years later, the mutual events would have been missed. From the dimensions of the bodies and the orbital parameters of Charon, the bulk densities of both objects have been determined (Table I); the density of Pluto is nearly identical to that of Triton, while Charon is about 15 percent less. At about the time the mutual events were concluding, high-resolution imaging with the Hubble Space Telescope and ground-based telescopes using adaptive optics systems gave the first optical images showing Charon separated from Pluto. Charon's orbital parameters have been refined using such high-definition images (Tholen and Buie, 1997).

Maps of Pluto's surface have been derived from observations of the mutual events (Young *et al.*, 2001) and from images with the Hubble Space Telescope

TABLE I
Physical Properties of Large Objects in the Outer Solar System

Object	Type	Radius (km)	Rotation period (days)	Mean density (g/cm^3)	Surface composition (molecular ices)	Notes
Triton	Neptune's satellite	1352	5.877	2.06	N_2,CH_4, CO, CO_2,H_2O	CH_4 dissolved in N_2 ice
Pluto	Planet	1150*	6.4	2.0±0.06	N_2,CH_4, CO, $(H_2O)^{\dagger}$	Some CH_4 dissolved in N_2, some pure. Locked synchronous rotation with Charon
Charon	Pluto's satellite	600-650	6.4	1.7±0.15	H_2O, NH_3 ‡	Locked synchronous rotation with Pluto
2003 VB_{12} Sedna	Anomalous	650-900	>20			Elliptical orbit perihelion 76 AU, aphelium 480AU
50000 Quaoar	KBO	625				
20000 Varuna	KBO	450				
2004 DW	KBO	~800				
5145 Pholus	Centaur	~100	0.42		Organic solids, H_2O,CH_3OH, minerals	One of the reddest surfaces known
2060 Chiron	Centaur	~90	0.25		H_2O, low-albedo material	Episodic cometary activity
Phoebe	Saturn's Satellite	110	0.39		H_2O, CO_2 other?	Cassini results

* See text for notes on Pluto's radius
† Expected but not detected with certainty
‡ Possibly NH_4OH or some other hydrate of ammonia

(Stern *et al.*, 1997). These images show an uneven distribution of surface units of relatively low albedo on a brighter background, but are insufficient to define basins, craters, or other geological structures. On a large spatial scale, the albedo contrast on Pluto is more pronounced than that for any other solid Solar System body except Saturn's satellite Iapetus. The globally averaged color (0.3-1 μm) and albedo of Pluto can be satisfactorily modeled with a combination of spectrally neutral ices and a small quantity of tholin (Cruikshank *et al.*, 2005). The presence of this complex organic solid material is consistent with the composition of the surface ices and the atmosphere of Pluto, as noted below.

The composition of the surface of Pluto is similar in several respects to that of Triton, with a complex combination of the ices of N_2, CH_4, and CO (Owen *et al.*, 1993; Douté *et al.*, 1999). Methane is present in both a pure form and also dissolved in the solid N_2; the two forms can be distinguished spectroscopically by a small shift in the central wavelengths of the CH_4 bands that occurs when the molecules are incorporated in a matrix as a very dilute component. On Triton, the CH_4 is primarily dissolved in N_2 and a pure component has not been identified. In further contrast with Triton, CO_2 has not been clearly detected on Pluto, and the presence of H_2O ice in the spectrum is ambiguous (Grundy *et al.*, 2002). As with Triton, other condensed hydrocarbons and HCN are expected from photochemical reactions in the N_2 + CH_4 atmosphere (Krasnopolsky and Cruikshank, 1999) but have not yet been reliably detected.

The atmosphere of Pluto expected from the presence of volatile surface ices has been detected by stellar occultations (Elliot *et al.*, 1989), and is also a factor in the interpretation of the mutual transits and occultations with Charon. Methane gas, which is expected to be present in the atmosphere with a partial pressure $\sim 10^{-6}$ relative to N_2 has been weakly detected spectroscopically (Young *et al.*, 1997). A tentative detection at radio wavelengths of the J(2-1) CO line in Pluto's atmosphere has been reported by Bockelée-Morvan *et al.* (2001). Nitrogen, the principal atmospheric component expected on the basis of vapor pressure considerations, remains to be detected in the ultraviolet. The vapor pressure of N_2 is a strong function of temperature, ranging from 1.2 μbar at $T = 34$ K to 590 μbar at $T = 45$ K (Owen *et al.*, 1993). Pluto's surface is not isothermal; measurements with the ISO spacecraft suggest maximum dayside temperatures in the range 54-63 K (Lellouch *et al.*, 2000) and a porous upper few cm of the surface. The atmospheric surface pressure expected from the relatively high temperatures determined from the ISO data is somewhat higher than that inferred from stellar occultations.

The stellar occultation lightcurves, especially at minimum light, can be modeled with either an atmospheric haze (Elliot and Young, 1992) or with a thermal inversion layer in the lower stratosphere that optically masks a troposphere of unknown thickness (Stansberry *et al.*, 1994; Strobel *et al.*, 1996). In fact, a derivation of the exact diameter of Pluto depends upon the correct interpretation of the optical properties of the lower atmosphere. The exact diameter, in turn, is an important factor in establishing Pluto's mean density, the mass being well determined from

the motion of Charon. The Stansberry *et al.* (1994) model suggests a radius of 1190 km, although the unseen troposphere may be some 40 km deep, implying a radius of 1158 km.

The atmosphere of Pluto is variable on a time-scale of years. Observations of a recent (2002) stellar occultation (Elliot *et al.*, 2003; Sicardy *et al.*, 2003) probed Pluto's atmosphere, with the result that the shape of the occultation lightcurve was significantly different from that seen in a stellar occultation in 1988. The difference has been interpreted as an increase by a factor of about two in Pluto's atmospheric pressure; such a difference could arise from the warming of the N_2 surface ice by about 1 K.

Pluto's atmosphere is in a state of rapid hydrodynamic escape, in which light gases escaping by their thermal energy drag along heavier gases. Although this process is not seen on any other planet today, it may have been responsible for the rapid loss of hydrogen from the early atmosphere of the Earth and other terrestrial planets.

The reflectance spectrum of Charon shows the presence of H_2O ice (Dumas *et al.*, 2001) and an additional component that has an absorption band near 2.2 μm for which a hydrate of ammonia has been proposed (Brown and Calvin, 2000). No CH_4 is seen in Charon's spectrum, despite its prominence in the spectrum of Pluto. The H_2O band structure at 1.65 μm in Charon's spectrum indicates that the ice is crystalline, rather than amorphous. Overall, the albedo of Charon is lower than that of Pluto, it is more nearly spectrally neutral than Pluto, and it does not show a large variation in brightness with rotation.

The Pluto-Charon pair is presumed to have originated as a large member of the Kuiper belt (see below).

The *in situ* investigation of the Pluto-Charon pair is a primary science goal of NASA's New Horizons mission, currently intended for launch in 2006. The spacecraft will fly past Pluto and Charon approximately 10 years after launch, and then continue into the Kuiper belt region with the intent to fly by two or more KBOs. A large suite of imaging and spectroscopic investigations will be augmented by radio wavelength measurements of the atmosphere(s) of both bodies by the occultation technique used so successfully in many planetary flyby observations.

4. Centaurs and Trans-Neptunian Bodies

4.1. Centaurs

Centaur objects are small bodies in heliocentric orbits that typically cross the orbits of one or more major planets. Their dynamical lifetimes are of order 10^6 - 10^7 y, and they are presumed to be derived from the Kuiper belt (see below). Some of them (e.g., 2060 Chiron, and P/Schwassmann-Wachmann 1) show episodic cometary activity. By mid-2004, ~60 Centaur objects of various sizes were identified, but

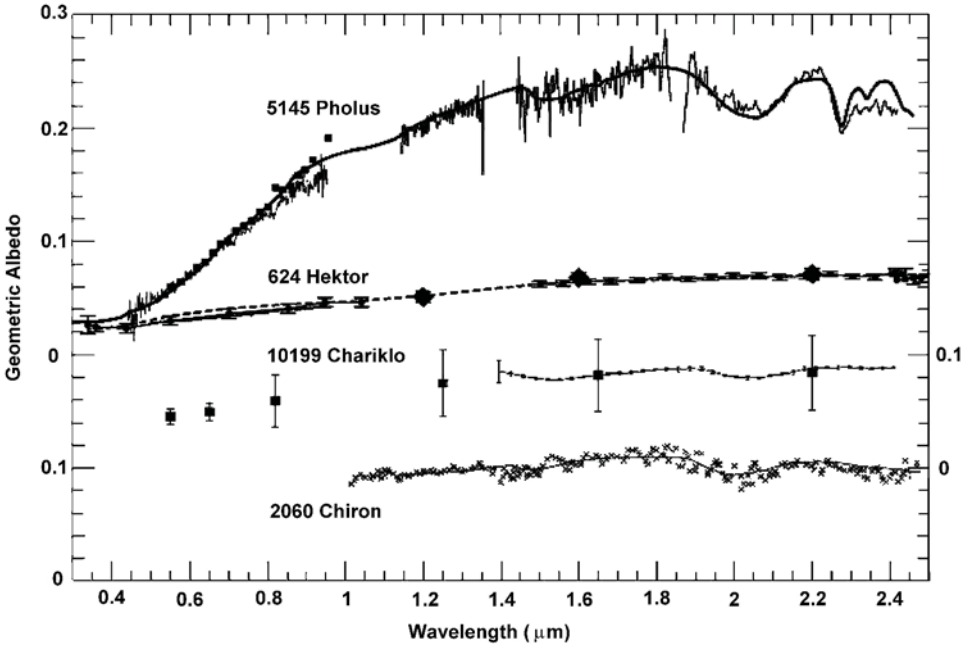

Figure 3. Reflectance spectra of the Centaurs 5145 Pholus, 10199 Chariklo, and 2060 Chiron, as well as the D-type Trojan asteroid 624 Hektor. The solid lines for Pholus and Chiron are models computed with scattering theory and the complex refractive indices of the components identified on each object. All three Centaurs show H_2O ice absorption bands at 1.5 and 2.0 μm, while Pholus shows additional absorption attributed to solid CH_3OH, olivine, and tholin. The spectrum of Hektor, while red in color, is otherwise featureless; the dashed line is a model computed with the mineral pyroxene as the main component.

the statistically projected number is of order 3000 (larger than 100 km diameter). Insofar as the Centaurs are dimensionally and compositionally representative of the Kuiper disk population, their physical properties are of interest, and because they are closer to the Earth, they are more easily observed than the distant and faint Kuiper belt objects. A detailed discussion of Centaur physical properties is given by Barucci *et al.* (2004).

Reflectance spectroscopy (0.4-2.4 μm) of many minerals and ices relevant to the surface compositions of Solar System objects show diagnostic absorption bands (e.g., Gaffey *et al.*, 1993; Brown and Cruikshank, 1993) that can be found in the spectra of asteroids, planetary satellites, and some KBOs and Centaurs. In addition, there is growing recognition of the importance of solid organic macromolecular material as a component of the surfaces of outer Solar System bodies, and the effect on the color and albedo that this material imparts (e.g., Andronico *et al.*, 1987; Hartmann *et al.*, 1987; Cruikshank, 1987; Luu *et al.*, 1994; Cruikshank and Dalle Ore, 2003). Here we show spectra of three Centaurs (Figure 3) that have varying degrees of diagnostic spectral activity.

2060 Chiron has a neutral reflectance at an albedo level of about 0.10, with weak but recognizable H_2O ice bands, notably at 2.0 μm. It shows intermittent cometary behavior in the form of variable brightness of what may be a permanent dust coma, even at its large heliocentric distance (8.45 AU at perihelion) (e.g., Hartmann *et al.*, 1990).

10199 Chariklo has a moderately red reflectance in the photovisual region and is nearly flat in reflectance in the near-infrared (Davies *et al.*, 1993). The photometric points in the near-infrared do not betray the presence of the weak bands of H_2O ice that are clearly seen in the spectrum by Brown *et al.* (1998). They modeled the spectrum 10199 Chariklo with an intimate mixture of H_2O ice, and a red material for which the complex indices were constructed. This computationally derived red component represents a natural material that is analogous to the complex refractory organic solids known as tholins.

5145 Pholus is exceptionally red among the Centaurs and the other small bodies of the outer Solar System observed to date (but see the discussion of Sedna below). The spectrum of 5145 Pholus has been recorded from 0.45 to 2.45 μm (Cruikshank *et al.*, 1998b, and sources quoted therein), as reproduced in Figure 3. The spectrum shows not only the strong red color at short wavelengths, but evidence for the 1.5 and 2.0 μm H_2O ice bands and an absorption complex at 2.27 μm.

The model of Pholus derived by Cruikshank *et al.* (1998b) and shown as the continuous solid line in Figure 3 consists of four spectrally active components, plus grains of amorphous carbon, which is spectrally neutral. Titan tholin (Khare *et al.*, 1984) imparts the steep reflectance between 0.45 and 1.0 μm, H_2O ice is responsible for the broad absorption bands a 1.5 and 2.0 μm, and CH_3OH ice appears to account for the band at 2.27 μm (but see Cruikshank *et al.*, 1998b, for details of this region). An additional component required to bring the model into accord with the data between 1.0-1.4 μm is olivine. This model incorporates the four most abundant materials known to occur in typical comet nuclei: organic solids, the silicate mineral olivine, water ice, and methanol ice, and while the relative abundances and details of the particle sizes and scattering parameters are model-dependent (Poulet *et al.*, 2002), the compositional similarity between this Centaur and comets is notable (Cruikshank *et al.*, 1998c).

4.2. Trans-Neptunian Bodies

Since the pivotal discovery of 1992 QB_1 by Jewitt and Luu (1993), nearly 1000 objects with dimensions 50-600 km have been detected in the trans-Neptunian region. The largest of the bodies detected as of mid-2004 are listed in Table I.

Three distinct dynamical populations have become apparent as the discoveries continue. The first grouping, which includes the majority of the objects discovered to date, is known as the classical Kuiper belt. It consists of objects in near circular orbits with semi-major axes around 45 AU. These orbits are stable against Neptune's perturbations over the age of the Solar System. The second population

consists of objects in orbits with 2 : 3 resonance with Neptune, as in the case of Pluto. These objects are informally called "Plutinos"; the term is etymologically grotesque (an Italian-style diminutive of an anglicized classical Greek proper name), but it has gained widespread usage. Taken together, these two populations are frequently referred to as Kuiper belt objects (KBOs), a term that is used in this paper. The third population consists of objects in highly eccentric orbits with perihelia generally within the classical Kuiper belt (although some are inside Neptune's orbit), but with aphelia far outside. These bodies have been dynamically excited by Neptune; they are called scattered disk objects.

Direct imaging of a number of KBOs has shown that at least 5% of them are binary systems (Noll, 2004); the number of known binaries as of mid-2004 is 14. The angular separations of the two components of a binary are typically 0.25 - 0.5 arcsec. The relative dimensions of the two components vary widely from system to system, and are calculated from their relative brightness and estimates of their surface albedos. In general, the sizes of the two components tend to be very similar, and the barycenter of each of the systems is well outside the body of the primary.

Binary systems may have originated by collision and capture in the presence of a third body at a time when the Kuiper belt was at least 100 times more densely populated that it is now (Weidenschilling, 2002). Other dynamical scenarios have been proposed by Goldreich *et al.* (2002) and Funato *et al.* (2004). The statistical distribution of orbital eccentricities in a large sample of well observed binary KBOs may distinguish among the proposed origin scenarios. Collisions and close encounters among KBOs can disrupt some of the more widely separated and weakly bound binaries, and as noted by Noll (2004) the present population is probably the remnant of a much larger primordial population.

Other lines of evidence also favor a much more dense early Kuiper belt. Accretion models show that the objects could not reach their present sizes unless the Kuiper belt originally contained tens of Earth masses of material, whereas its present mass is of order 0.1 $M_{\oplus}$. Accretion occurred as planetesimals collided at low velocities in an environment of low dynamical excitation. In a recent model by Levison and Morbidelli (2003) the zone of formation of Kuiper belt objects is closer to the Sun than their present positions, and they were subsequently pushed outward as Neptune migrated to larger heliocentric distances. This resulted in a dynamical excitation that increased encounter velocities, leading to collisional disruption and mass depletion. Stern and Kenyon (2003) note that the timescale for collisional disruption of bodies of 100 km size is long and that fewer than 1% of them have been catastrophically disrupted. Smaller bodies of order 1 km in radius are catastrophically disrupted by collisions of timescales 100 to 1000 times shorter, with the result that the great majority of the KBOs of the size of ordinary comets are freshly disrupted.

Multi-color photometry and spectroscopic observations have not kept pace with the discoveries of KBOs and Centaurs because of the need for large-aperture telescopes, but color data and spectra for a number of objects in various categories

and dynamical subclasses are emerging. The most extensive on-going compilation of colors of OSS bodies is that of Hainaut and Delsanti (2002). Efforts to obtain photometric data for a large sample of objects are in progress by Noll *et al.* (2002) and others. Jewitt (2002) compiled and analyzed the colors (treated as a spectral gradient in the region ∼0.4-0.7 μm) of a sample of Kuiper belt objects, Centaurs, Trojan asteroids, comet nuclei, and extinct comets, and concluded that extinct comet colors are distinctly different from those of their progenitor Kuiper belt objects and Centaurs.

A few KBOs have been studied spectroscopically, and ice absorption bands at 1.6, 2.0, and 2.3 μm reveals the presence of H_2O ice in some of them. The bands tend to be weak, as is expected for ice mixed with low-albedo minerals or organic solids. Brown *et al.* (1999) found ice bands on 1996 TO_{66}, and Brown (2003) has found ice bands on 50000 Quaoar. See Dotto *et al.* (2003) and Barucci *et al.* (2004) for more complete reviews.

In the absence of signature spectroscopic features (beyond the H_2O ice seen in a few objects) that might lead to the identification of specific minerals, other ices, or other material, we turn to the indirect analytical technique of modeling the color. Color can be expressed in terms of a spectral gradient, or the normalized slope S (% per 100 nm) of the reflectance after correction for the color of the Sun (e.g., Jewitt, 2002). A positive gradient represents a red color, with the continuum intensity increasing toward longer wavelengths.

Continuum gradients in the spectral reflectance also occur at $\lambda \geq 1$ μm, extending to wavelengths at which the reflected sunlight exceeds the thermal emission from a surface. Thermal emission depends on the temperature of a planetary surface, hence its heliocentric distance and albedo. For objects in the outer Solar System where $T \leq 80$ K, thermal emission becomes significant only at $\lambda \geq 10$ μm. For a few of the small bodies in the OSS there are data extending to 2.5 μm, and color is often defined in terms of the standard JHK photometric bands (1.22, 1.65, and 2.18 μm, respectively).

Barucci *et al.* (2001) made a statistical analysis of BVRIJ colors of 15 KBOs and 7 Centaurs and found a continuous spread of colors from neutral to very red. They defined four groups based on two principal components (eigenvectors of the variance-covariance matrix of the colors) that measure the degree of redness; these groups are shown as geometric albedo in Figure 4.

Cruikshank and Dalle Ore (2003) have modelled the colors of KBOs in the Barucci *et al.* groups to constrain or identify materials that lack signature spectral absorption bands, but can be inferred on the basis of spectral slope, primarily in the region $0.3 \leq \lambda \leq 2.5$ μm, plus the albedo, a measure of the absolute reflectance. Normalized reflectance is insufficient for modeling a planetary surface, and the additional constraint of the absolute level of reflectance at every wavelength is an important discriminating factor in achieving a model with realistic components. The geometric albedo of a surface is a complex, non-linear function of the composition, grain size, and mixing parameters of the surface components. The albedos

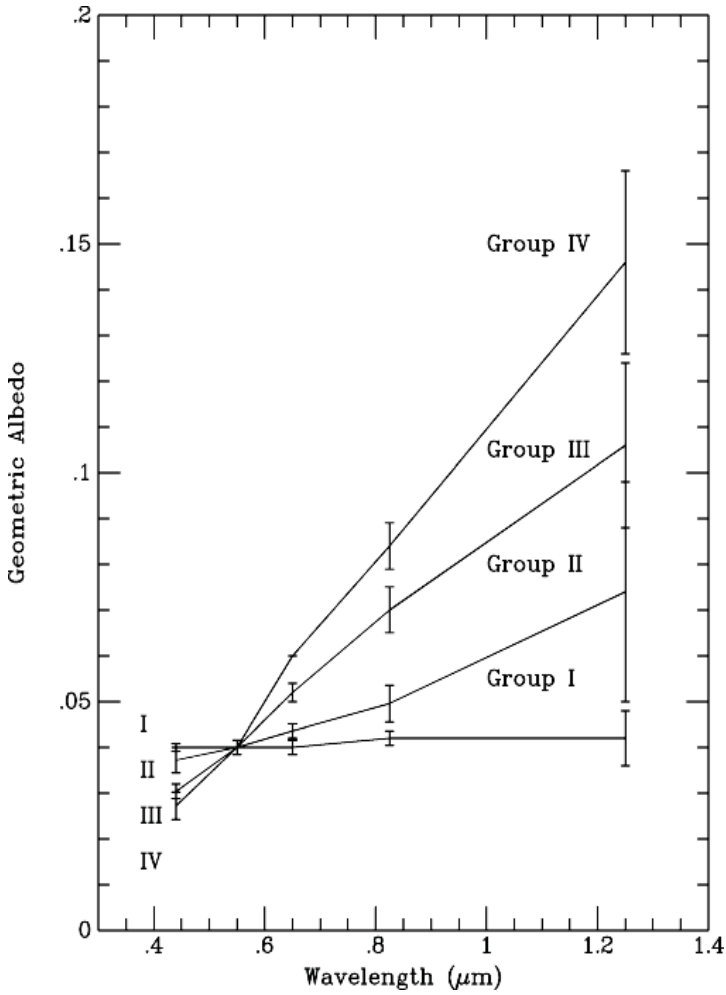

Figure 4. Four groups defined by photometry of Centaurs and Kuiper belt objects by Barucci *et al.* (2001). Representative members of the groups are: Group I (1996 TO_{66}, 2060 Chiron), Group II (10199 Chariklo, 1998 SG35), Group III (1993 SC, 1997 CQ29), Group IV (5145 Pholus, 1994 TB). These curves are normalized to geometric albedo 0.04 at wavelength 0.56 μm.

of Centaurs and Kuiper belt objects are known in only a few cases (e.g., Dotto *et al.*, 2003), and lie in the range 0.04-0.17. Most other OSS objects (small and irregular planetary satellites, Trojan asteroids, and comet nuclei) have albedos in the range 0.02-0.07. Cruikshank and Dalle Ore adopted a geometric albedo of 0.05 at $\lambda = 0.56\ \mu$m; the models will pertain also to higher albedo objects with the same spectral slopes, with a reduction in the contribution of the neutral, low-albedo (amorphous carbon) model component.

Cruikshank and Dalle Ore (2003) matched the geometric albedos and colors of the reddest color groupings of outer Solar System bodies with models computed

with scattering theory and the use of optical properties of synthetic organic solids (tholins), particularly Ice Tholin II and Titan tholin. In their models, elemental amorphous carbon was added to the organic solids to achieve the low geometric albedos observed or assumed for these objects. The presence of elemental carbon can occur in nature by the dehydrogenation of tholins. In the use of tholins to achieve the observed red colors, these model results are consistent with those of several other investigators, including the recent work of Dotto *et al.* (2003) and Doressoundiram *et al.* (2003). The least red objects in the outer Solar System can be modeled with mafic minerals, and do not require the presence of organic solids (Cruikshank *et al.*, 2001), while Emery and Brown (2003) showed that certain large classes of organics are specifically excluded by their mafic mineral models of red Trojan asteroids. For additional discussion of quantitative modeling of KBOs and Centaurs see Cruikshank *et al.* (2003).

The Moon, Mercury, and many asteroids are reddened by a space-weathering process consisting of sputtering of iron from iron-bearing minerals, and the deposition of neutral Fe on grains in the uppermost regolith. When space-weathered minerals found on the lunar surface were incorporated into their models, Cruikshank and Dalle Ore (2003) found that the presence of neutral Fe is not required to achieve the observed albedos and colors, although such space-weathered minerals may occur in modest quantities in the optically accessible surfaces.

4.3. OORT CLOUD

In his classic study of the source region of the long-period comets (P≥200 y) Oort (1950) postulated that about a trillion (10^{12}) icy objects exist in a swarm, or "cloud", centered on the Sun. Each of these objects is in a very large orbit around the Sun, and their periods are longer than about a million years. This swarm is now called the Oort Cloud; its outer extent lies about 1/3 of the way to the next star, or about 100,000 AU (1.5 lightyears) from the Sun. Objects at this great distance are only weakly bound to the Sun, and they are subject to perturbations by the effects of nearby stars and the passage of the Sun and Solar System through a giant molecular cloud in the Galaxy. Such passages occur once every 300-500 million years. In addition, galactic tides (the non-uniform stretching of the Solar System by the gravity field of the center of our Galaxy) can also perturb the orbits of Oort Cloud and cause them to make close passages by the Sun and planets.

Over the course of a million years, about 12 stars pass closely enough to the Solar System to perturb some of the objects in the Oort Cloud. A star is expected to pass within 10,000 AU of the Solar System every 36 million years, and within 3,000 AU every 400 million years, on average. By some estimates, perturbations of the Oort Cloud by such passages can trigger comet showers lasting 2-3 million years, with up to 300 times the normal rate of comets coming in from the Cloud (Weissman, 1998).

The estimated total mass of the icy objects in the Oort Cloud is about 40 $M_\oplus$. The Oort Cloud may be receiving Kuiper belt objects from the scattered disk population. Fernández and Brunini (2000) integrated the orbits of the known scattered disk objects and found that on dynamical half-time of ∼2.5 Gy, about one-third of the objects ended up in the Oort Cloud.

The discovery of a possible member of the inner region of the Oort Cloud (Brown *et al.*, 2004) offers a unique opportunity to study the physical properties of the most distant known object in the Solar System. Brown *et al.* (2004) discovered 2003 VB12 ("Sedna"), which has an inclined (11.9°), highly eccentric (0.84±0.01) orbit with a perihelion distance of 76±4 AU and a semimajor axis of 480±40 AU. Sedna appears to be rotating very slowly (P≥20 days), suggesting the presence of a (so far) unseen satellite. Sedna's thermal flux has remained undetected, suggesting a diameter of ∼1800 km or a bit less. The color of Sedna is very red, comparable to 5145 Pholus (see above), although the spectral features exhibited by Pholus have not yet been detected.

The orbital characteristics have suggested at least three scenarios of origin. Sedna may have been scattered into its present orbit by an unseen planet with mass ∼1 $M_\oplus$ at a heliocentric distance of ∼70 AU; Brown *et al.* (2004) note that none of the known planets in the Solar System can dynamically excite objects from the inner Oort Cloud. Another possibility is that an encounter by a high velocity passing star perturbed Sedna out of the Oort Cloud and into its present orbit. A third scenario, regarded as more likely by Brown *et al.* (2004), has the Sun forming in a star cluster where low-velocity encounters with neighboring stars were frequent. All three possibilities predict the existence of several other objects in orbits comparable to that of Sedna.

Continuing surveys in the trans-Neptunian region, including those anticipated employing powerful new techniques, will produce many new, intriguing, and challenging discoveries. We can hope and expect that such discoveries will further elucidate and clarify the emerging picture of the origin and evolution of the Solar System and the growing number of recognized extrasolar planetary systems.

References

Andronico, G., Baratta, G.A., Spinella, F., and Strazzulla, G.: 1987, 'Optical evolution of laboratory-produced organics – applications to Phoebe, Iapetus, outer belt asteroids and cometary nuclei', *Astron. Astrophys.* **184**, 333–336.

Barucci, M.A., Fulchignoni, M., Birlan, M., Doressoundiram, A., Romon, J., and Boehnhardt, H.: 2001, 'Analysis of Trans-Neptunian and Centaur colours: continuous trend or grouping?', *Astron. Astrophys.* **371**, 1150–1154.

Barucci, M.A., Doressoundiram, A., and Cruikshank, D.P.: 2004, in M.C. Festou, H.U. Keller, and H.A. Weaver (eds.), *Comets II*, The University of Arizona Press, in press.

Binzel, R.P. and Hubbard, W.B.: 1997, 'Mutual events and stellar occultations', in S.A. Stern and D.J. Tholen (eds.), in *Pluto and Charon*, The University of Arizona Press, Tucson, pp. 85-102.

Bockelée-Morvan, D., Lellouch, E., Biver, N., Paubert, G., Bauer, J., Colom, P., and Lis, D.C.: 2001, 'Search for CO gas in Pluto, Centaurs and Kuiper belt objects at radio wavelengths', *Astron. Astrophys.* **377**, 343–353.

Broadfoot, A.L., *et al.*: 1989, 'Ultraviolet spectrometer observations of Neptune and Triton', *Science* **246**, 1459–1466.

Brown, M.E.: 2003, *Bull. Am. Astron. Soc.* **35**, 969 (abstract).

Brown, M.E. and Calvin, W.M.: 2000, 'Evidence for crystalline water and ammonia ices on Pluto's satellite Charon', *Science* **287**, 107–109.

Brown, M.E., Trujillo, C., and Rabinowitz, D.: 2004, *Astrophys. J. Lett.*, in press.

Brown, R.H. and Cruikshank, D.P.: 1993, 'Remote sensing of ices and ice-mineral mixtures in the outer solar system', in C.M. Pieters, and P.A.J. Englert (eds.), *Remote Geochemical Analysis: Elemental and Mineralogical Composition*, The Cambridge University Press, pp. 455–468.

Brown, R.H., Cruikshank, D.P., Veverka, J., Helfenstein, P., and Eluszkiewicz, J.: 1995, 'Surface composition and photometric properties of Triton', in D.P. Cruikshank (ed.), *Neptune and Triton*, The University of Arizona Press, Tucson, pp. 991–1030.

Brown, R.H., Cruikshank, D.P., Pendleton, Y.J., and Veeder G.J.: 1998, 'Identification of water ice on the Centaur 1997 CU26', *Science* **280**, 1430–1432.

Brown, R.H., Cruikshank, D.P., and Pendleton, Y.J.: 1999, 'Water ice on Kuiper belt object 1996 TO_{66}', *Astrophys. J.* **519**, L101–L104.

Calcagno, L., Foti, G., Torrisi, L., and Strazzulla, G.: 1985, 'Fluffy layers obtained by ion bombardment of frozen methane Experiments and applications to Saturnian and Uranian satellites', *Icarus* **63**, 31–38.

Cruikshank, D.P.: 1987, 'Dark matter in the solar system', *Adv. Space Res.* **7**, 109–120.

Cruikshank, D.P. (ed.): 1995, *Neptune and Triton*, The University of Arizona Press, Tucson, 1249 pp.

Cruikshank, D.P. and Dalle Ore, C.M.: 2003, 'Spectral models of Kuiper belt objects and Centaurs', *Earth, Moon, and Planets* **92**, 315–330.

Cruikshank, D. P., Roush, T. L., Owen, T. C., Quirico, E., and de Bergh, C.: 1998a, 'The surface compositions of Triton, Pluto and Charon', in B. Schmitt, C. de Bergh, and M. Festou (eds.), *Ices in the Solar System*, Kluwer Academic Publishers, Dordrecht, pp. 655–684.

Cruikshank, D.P., *et al.*: 1998b, 'The composition of Centaur 5145 Pholus', *Icarus* **135**, 389–407.

Cruikshank, D.P., *et al.*: 1998c, *Bull. Am. Astron. Soc.* **30**, 1094 (abstract).

Cruikshank, D.P., Dalle Ore, C.M., Roush, T.L., Geballe, T.R., Owen, T.C., de Bergh, C., Cash, M.D., and Hartmann, W.K.: 2001, *Icarus* **153**, 348–360.

Cruikshank, D.P., Roush, T.L., and Poulet, F.: 2003, 'Quantitative modeling of the spectral reflectance of Kuiper belt objects and Centaurs', *C. R. Physique* **4**, 783–789.

Cruikshank, D.P., Dalle Ore, C.M., and Imanaka, H.: 2005, *Icarus*, submitted.

Davies, J.K., Sykes, M.V., and Cruikshank, D.P.: 1993, 'Near-infrared photometry and spectroscopy of the unusual minor planet 5145 Pholus (1992AD)', *Icarus* **102**, 166–169.

Doressoundiram, A., Tozzi, G.P., Barucci, M.A., Boehnhardt, H., Fornasier, S., and Romon, J.: 2003, 'ESO Large Programme on Trans-Neptunian Objects and Centaurs: Spectroscopic Investigation of Centaur 2001 BL41 and TNOs (26181) 1996 GQ21 and (26375) 1999 DE9', *Astron. J.* **125**, 2721–2727.

Dotto, E., Barucci, M. A., and de Bergh, C.: 2003, *C. R. Physique* **4**, 775–782.

Douté, S., Schmitt, B., Quirico, E., Owen, T.C., Cruikshank, D.P., de Bergh, C., Geballe, T.R., and Roush, T.L.: 1999, 'Evidence for methane segregation at the surface of Pluto', *Icarus* **142**, 421–444.

Dumas, C., Terrile, R.J., Brown, R.H., Schneider, G., and Smith, B.A.: 2001, 'Hubble Space Telescope NICMOS spectroscopy of Charon's leading and trailing hemispheres', *Astron. J.* **121**, 1163–1170.

Elliot, J.L., Dunham, E.W., Bosh, A.S., Silvan, S.M., Young, L.A., Wasserman, L.H., and Millis, R.L.: 1989, *Icarus* **77**, 148–170.

Elliot, J.L. and Young, L.A.: 1992, *Astron. J.* **103**, 991–1015.
Elliot, J.L., *et al.*: 1998, 'Global warming on Triton', *Nature* **393**, 765–767.
Elliot, J.L., *et al.*: 2003, 'The recent expansion of Pluto's atmosphere', *Nature* **424**, 164–168.
Emery, J.P. and Brown, R.H.: 2003, 'Constraints on the surface composition of Trojan asteroids from near-infrared (0.8-4.0 μm) spectroscopy', *Icarus* **164**, 104–121.
Fernández, J.A. and Brunini, A.: 2000, *Icarus* **145**, 580–590.
Funato, U., Makino, J., Hut, P., Kokubo, E., and Kinoshita, D.: 2004, 'The formation of Kuiper-belt binaries through exchange reactions', *Nature* **427**, 518–520.
Gaffey, S.J., McFadden, L.A., Nash, D., and Pieters, C.M.: 1993, 'Ultraviolet, visible, and near-infrared reflectance spectroscopy: laboratory spectra of geologic materials', in C.M. Pieters and P.A.J. Englert (eds.), *Remote Geochemical Analysis: Elemental and Mineralogical Composition*, Cambridge University Press, New York, pp. 43–77.
Goldreich, P., Lithwick, Y., and Sari, R.: 2002, 'Formation of Kuiper-belt binaries by dynamical friction and three-body encounters', *Nature* **420**, 643–646.
Grundy, W.M., Buie, M.W., and Spencer, J.R.: 2002, 'Spectroscopy of Pluto and Triton at 3–4 microns: possible evidence for wide distribution of nonvolatile solids', *Astron. J.* **124**, 2273–2278.
Hainaut, O.R. and Delsanti, A.C.: 2002, 'Colors of minor bodies in the Outer solar system. A statistical analysis', *Astron. Astrophys.* **389**, 641–664.
Hartmann, W.K., Tholen, D.J., and Cruikshank, D.P.: 1987, 'The relationship of active comets, 'extinct' comets, and dark asteroids', *Icarus* **69**, 33–50.
Hartmann, W.K., Tholen, D.J., Meech, K.J., and Cruikshank, D.P.: 1990, '2060 Chiron – colorimetry and cometary behavior', *Icarus* **83**, 1–15.
Jewett, D.C.: 'From Kuiper belt object to cometary nucleus: The missing ultrared matter', *Astron. J.* **123**, 1039–1049.
Jewitt, D. and Luu, J.: 1993, 'Discovery of the candidate Kuiper belt object 1992 QB1', *Nature* **362**, 730–732.
Khare, B.N., Sagan, C., Arakawa, E.T., Suits, R., Callcot, T.A., and Williams, M.W.: 1984, 'Optical constants of organic tholins produced in a simulated Titanian atmosphere - From soft X-ray to microwave frequencies', *Icarus* **60**, 127–137.
Khare, B.N., Thompson, W. R., Cheng, L., Chyba, C., Sagan, C., Arakawa, E. T., Meisse, C., and Tuminello, P.: 1993, 'Production and optical constraints of ice tholin from charged particle irradiation of (1:6) C_2H_6/H_2O at 77 K', *Icarus* **103**, 290–300, 1993.
Krasnopolsky, V.A. and Cruikshank, D.P.: 1995, 'Photochemistry of Triton's atmosphere and ionosphere', *J. Geohys. Res.* **100**, 21,271–21,286.
Krasnopolsky, V.A. and Cruikshank, D.P.: 1999, 'Photochemistry of Pluto's atmosphere and ionosphere near perihelion', *J. Geophys. Res.* **104**, 21,979–21,996.
Kuiper, G.P.: 1951, 'On the origin of the solar system', in J.A. Hynek (ed.), *Astrophysics*, New York: McGraw-Hill, New York, pp. 357–424.
Lellouch, E., Laureijs, R., Schmitt, B., Quirico, E., de Bergh, C., Crovisier, J., and Coustenis, A.: 2000, 'Pluto's non-isothermal surface', *Icarus* **147**, 220–250.
Levison, H.F. and Morbidelli, A.: 2003, 'The formation of the Kuiper belt by the outward transport of bodies during Neptune's migration', *Nature* **426**, 419–421.
Luu, J., Jewitt, D., and Cloutis, E.: 1994, *Icarus* **109**, 133–144.
McKinnon, W.B., Lunine, J.I., and Banfield, D.: 1995, 'Origin and evolution of Triton', in D.P. Cruikshank (ed.), *Neptune and Triton* , The University of Arizona Press, Tucson, pp. 807–877.
Miner, E.D. and Wessen, R.R.: 2002, *Neptune: The Planet, Rings and Satellites*, Springer Praxis, Chichester, 297 pp.
Noll, K.S.: 2004, *Earth, Moon, and Planets* **92**, 395–407.
Noll, K., Stephens, D., Grundy, W., Millis, R., Buie, M., Spencer, J., Tegler, S., Romanishin, W., and Cruikshank, D.: 2002, *Bull. Am. Astron. Soc.* **34**, 849 (abstract).

Oort, J.: 1950, 'The structure of the cloud of comets surrounding the solar system and a hypothesis concerning its origin', *Bull. Astron. Inst. Neth.* **11**, 91–110.

Owen, T.C., Cruikshank, D.P., Roush, T., de Bergh, C., Brown, R. H., Bartholomew, M. J., Elliot, J., and Young, L. 1993, 'Surface ices and the atmospheric composition of Pluto', *Science* **261**, 745–748.

Poulet, F., Cuzzi, J.N., Cruikshank, D.P., Roush, T., and Dalle Ore, C.M.: 2002, 'Comparison between the Shkuratov and Hapke scattering theories for solid planetary surfaces: Application to the surface composition of two Centaurs', *Icarus* **160**, 313–324.

Quirico, E., Douté, S., Schmitt, B., de Bergh, C., Cruikshank, D.P., Owen, T.C., Geballe, T.R., and Roush, T.L.: 1999, 'Composition, physical state, and distribution of ices at the surface of Triton', *Icarus* **139**, 159–178.

Sicardy, B., *et al.*: 2003, 'Large changes in Pluto's atmosphere as revealed by recent stellar occultations', *Nature* **424**, 168–170.

Stansberry, J.A., Lunine, J.I., Hubbard, W.B., Yelle, R.V., and Hunten, D.M.: 1994, 'Mirages and the nature of Pluto's atmosphere', *Icarus* **111**, 503–513.

Stern, S.A., Buie, M.W., and Trafton, L.: 1997, 'HST high-resolution images and maps of Pluto', *Astron. J.* **113**, 827–843.

Stern, S.A. and Kenyon, S.J.: 2003, 'Collisions, accretion, and erosion in the Kuiper belt', *C. R. Physique* **4**, 803–808.

Stone, E.C. and Miner, E.D: 1989, 'The Voyager 2 encounter with the Neptunian system', *Science* **146**, 1417–1421.

Strobel, D.F., Zhu, X., Summers, M.E., and Stevens, M.H.: 1996, 'On the vertical thermal structure of Pluto's atmosphere', *Icarus* **120**, 266–289.

Tholen, D.J. and Buie, M.W.: 1997, 'The Orbit of Charon', in S.A. Stern and D.J. Tholen (eds.), *Pluto and Charon*, The University of Arizona Press, Tucson, pp. 193–219.

Tyler, G.L., Sweetnam, D.N., Anderson, J.D., Borutzki, S.E., Campbell, J.K., Kursinski, E.R., Levy, G.S., Lindal, G.F., Lyons, J.R., and Wood, G.E.: 1989, 'Voyager radio science observations of Neptune and Triton', *Science* **246**, 1466–1473.

Weidenschilling, S.J.: 2002, 'On the origin of binary transneptunian objects', *Icarus* **160**, 212–215.

Weissman, P.R.: 1998, 'The Oort cloud', *Scientific American* **279**, 84–89.

Yelle, R.V., Lunine, J.L., and Hunten, D.M.: 1991, 'Energy balance and plume dynamics in Triton's lower atmosphere', *Icarus* **89**, 347–358.

Young, L.A., Elliot, J.L., Tokunaga, A., de Bergh, C., and Owen, T.: 1997, 'Detection of gaseous methane on Pluto', *Icarus* **127**, 258–262.

Young, E.F., Binzel, R.P., and Crane, K.: 2001, 'A two-color map of Pluto's sub-Charon hemisphere', *Astron. J.* **121**, 552–561.

Address for Offprints: Dale P. Cruikshank, Astrophysics Branch (Mail Stop 245-6), NASA Ames Research Center, Moffett Field, CA 94035-1000, USA; Dale.P.Cruikshank@nasa.gov

IRREGULAR SATELLITES IN THE CONTEXT OF PLANET FORMATION

DAVID JEWITT and SCOTT SHEPPARD
Institute for Astronomy, University of Hawaii,
2680 Woodlawn Drive, Honolulu, HI 96822

Received: 15 March 2004; Accepted in final form: 20 October 2004

Abstract. All four giant planets in the solar system possess irregular satellites, characterized by large, highly eccentric and/or highly inclined orbits. These bodies were likely captured from heliocentric orbit, probably in association with planet formation itself. Enabled by the use of large-format digital imagers on ground-based telescopes, new observational work has dramatically increased the known populations of irregular satellites, with 74 discoveries in the last few years. A new perspective on the irregular satellite systems is beginning to emerge. We find that the number of irregular satellites measured to a given diameter is approximately constant from planet to planet. This is surprising, given the radically different formation scenarios envisioned for the gas giants Jupiter and Saturn compared to the (much less massive and compositionally distinct) ice giants Uranus and Neptune. We discuss the new results on the irregular satellites and show how these objects might be used to discriminate amongst models of giant planet formation.

Keywords: satellites, Kuiper Belt, gas giant, ice giant, planet formation

1. Introduction

The irregular satellites of the planets are broadly distinguished from their regular counterparts by having large, highly eccentric and/or highly inclined orbits. Satellite accretion in a circumplanetary disk is unable to produce the extreme orbits of the irregular satellites, particularly the numerically dominant objects which follow retrograde trajectories about their parent planets. For this reason, the irregular satellites have long been recognized as likely products of the capture of bodies that were formed elsewhere and were previously in heliocentric orbit (Kuiper, 1956).

As with other definitions in the solar system (e.g., planet vs. Kuiper belt object, asteroid vs. comet) a single definition of the term "irregular satellite" is not agreed upon. The empirical definition as employed here (large, eccentric and/or inclined orbits) is the most simple and probably the most useful. Nesvorny *et al.* (2003) have defined irregulars as those satellites whose orbital planes precess strongly under the influence of solar tides. Fortunately, the two definitions yield essentially identical lists of irregular satellites. The main exception is Neptune's satellite Triton, which is excluded by the Nesvorny definition because it is close to its planet and relatively immune to strong solar perturbations but which meets the empirical definition of an irregular satellite because its motion is retrograde (inclination = 156.8 degrees).

Space Science Reviews 116: 441–455, 2005.
DOI: 10.1007/s11214-005-1965-z

It is clearly a captured object but its small planetocentric distance and its extraordinary size (the diameter of 2700 km is an order of magnitude larger than the next largest irregular) separate it from the other irregulars in important ways. We will not consider it further here.

The number of known irregular satellites of the planets increased slowly through the 20th century, mostly in response to surveys conducted diligently using photographic plates. At Jupiter, for example, the irregular satellite total rose following the initial discovery of J6 Himalia in 1904 to only 9 such objects by the end of the century. Detailed physical observations exist for only one irregular satellite: Saturn's Phoebe was mapped at high resolution by the Cassini spacecraft in June 2004 (Figure 1). While physical observations remain limited, an unprecedented wave of satellite discovery has resulted from the use of wide field charge-coupled device cameras on moderate to large aperture telescopes. Fifty of the 74 recent discoveries have been made by us on Mauna Kea (Sheppard and Jewitt, 2003, see `http://www.ifa.hawaii.edu/~sheppard/satellites/`) with most (46) of these at Jupiter. The number of Jovian irregulars is currently 55 (as of 2004 October 20) while irregular satellites have been identified around all four giant planets (Gladman *et al.*, 1998; 2000; 2001; Holman *et al.*, 2004; Sheppard and Jewitt, 2004). Observational programs to detect irregular satellites are challenging partly because of the faintness of most such objects but also because of the large areas of sky which must be searched. The region in which orbits are potentially stable is of a scale comparable to the Hill radius, defined as

$$r_{\rm H} = a \left(\frac{m_{\rm P}}{3M_{\odot}} \right)^{1/3} \tag{1}$$

where a is the orbital semimajor axis of a planet of mass $m_{\rm P}$, and $M_{\odot}$ is the mass of the sun. Values of $r_{\rm H}$ are given in Table I for each giant planet, in both linear and angular units. At the time of writing, the Hill spheres have been surveyed to near completeness to limiting red magnitude $m_R \sim 23$ at Jupiter, $m_R \sim 24$ at Saturn, and $m_R \sim 26.1$ at Uranus, while Neptune is less complete to $m_R \sim 25.5$.

The purpose of this short paper is to draw attention to the new work and to point out its likely relevance in constraining modes of satellite capture and giant planet formation. Models of gas and ice giant planet formation must be at least consistent with the known properties of the irregular satellite populations. It is not obvious that all proposed models meet this basic requirement. One reason is that the formation models were not specifically constructed to fit the newly-determined properties of the irregular satellite populations of the giant planets. We do not doubt that some of the models can be bent to fit the new irregular satellite data, as discussed below. It is the degree of bending which, we assert, provides an interesting and unexpected way to judge the models.

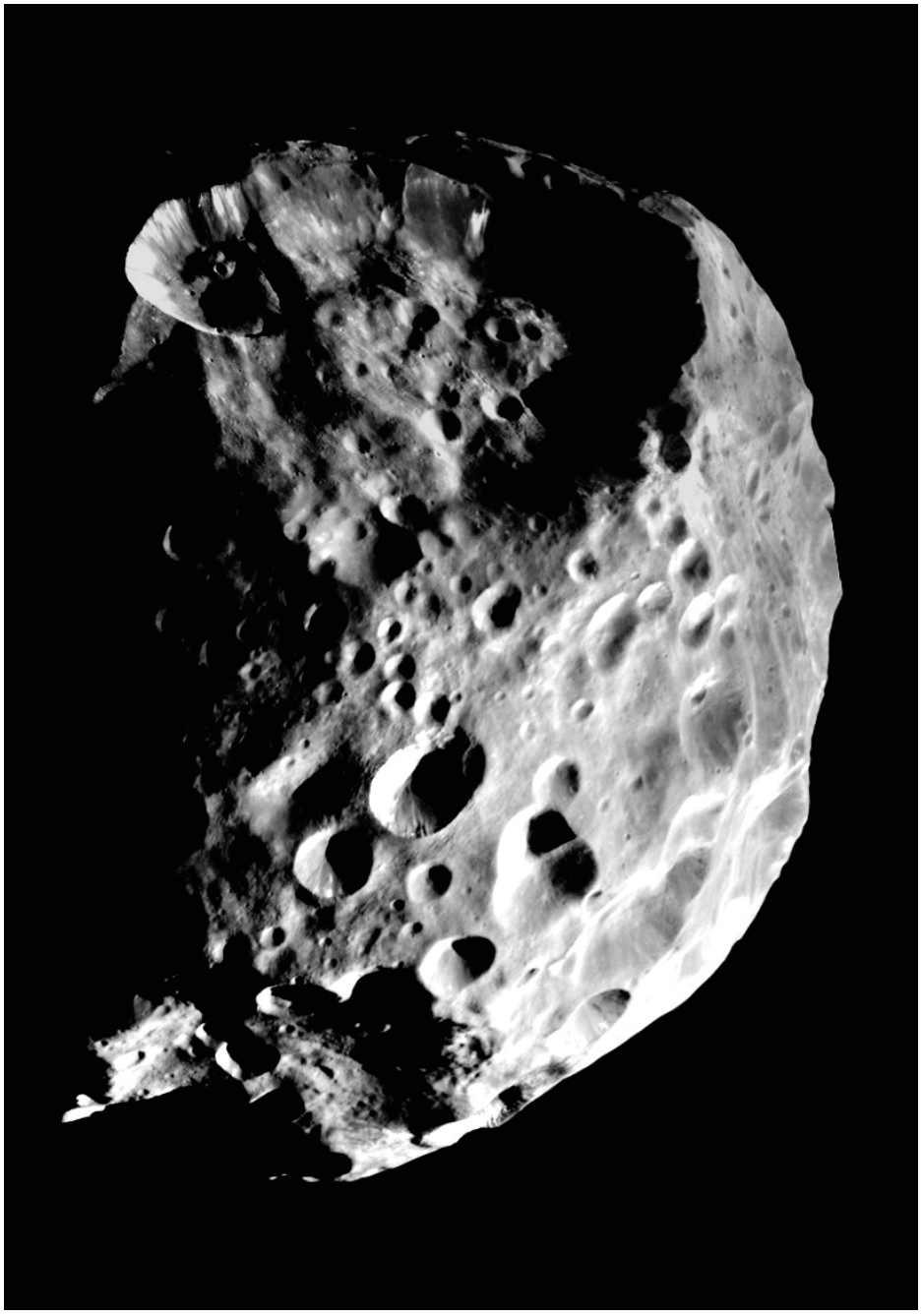

Figure 1. Saturn's ∼200 km diameter irregular satellite Phoebe, as imaged by the Cassini Imaging Science Subsystem in June 2004. This is the only irregular satellite for which highly-resolved physical observations are available. The surface is densely cratered up to sizes approaching the catastrophic disruption limit of the body. Bright ice streaks are visible on some of the steeper slopes (e.g. on the sun-facing wall of the largest visible crater). Image courtesy of NASA and the ISS team.

TABLE I
Numbers of Irregular Satellites

Planet	R [a]	Δm [b]	N_i [c]	N_i^{23} [d]	N_*^{23} [deg] [e]
Jupiter	5	0	55	36	36
Saturn	10	2.6	14	8	10
Uranus	20	5.9	9	4	3
Neptune	30	7.6	7[f]	2[f]	1

[a] Average Planet-Sun distance in AU

[b] Magnitude decrement $\Delta m = 5\log_{10}[R(R-1)/(R_J(R_J\text{-}1)]$, where R_J is the Sun-Jupiter distance

[c] Total number of reported irregular satellites

[d] Number of known irregular satellites with $m_R \leq 23$

[e] Number of irregular satellites with $m_R \leq 23$ expected if each planet holds a satellite population equal to that at Jupiter

[f] If Triton is not counted, $N_i = 6$ and $N_i^{23} = 1$

2. Relation to Planet Formation

A simple chain of reasoning links the capture of the irregular satellites to the epoch of planet formation.

1. The orbits of the irregular satellites, especially the retrograde orbits, cannot be plausibly explained as products of accretion in circumplanetary disks.
2. Such orbits are instead likely to be produced by capture from heliocentric orbits.
3. While temporary capture is easy, permanent capture from heliocentric orbit requires energy dissipation to convert an initially unbound orbit into a bound one.
4. The present-day solar system offers no adequate source of energy dissipation and, therefore, the captures must have occurred at an earlier epoch when dissipation was present.
5. The gross properties of the solar system have changed little since the era of planet formation. Therefore, the irregular satellites were probably captured at very early times, contemporaneous with planet formation.

The relationships between the various small-body populations of the solar system are shown in Figure 2. There, dotted lines emphasize that the irregular satellites, like the Trojan asteroids, have no dynamically plausible source in the modern solar system. By placing satellite capture at very early times, the irregulars open a potentially valuable new window on the planet formation process.

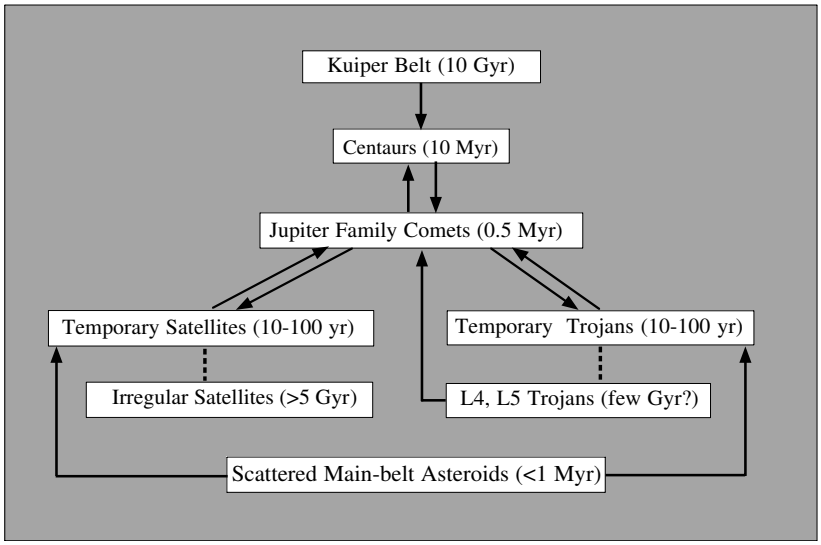

Figure 2. Schematic diagram showing relationships between various small body populations of the solar system. Currently active pathways from the major reservoirs in the Kuiper Belt and main asteroid belts are shown by solid arrows. The approximate dynamical lifetimes of the various populations are indicated. Dotted lines mark currently inactive pathways to the irregular satellites and 1:1 resonators. The dotted pathways may have been active in the early solar system, in the presence of energy dissipation. Figure from Jewitt *et al.* (2004).

2.1. SOURCES OF DISSIPATION

Three potential sources of dissipation in the early solar system have been discussed in the literature in the context of the irregular satellites.

1. Satellite capture could have been aided by dissipation due to gas drag (Pollack *et al.*, 1979). Before reaching their final equilibrium configurations, the gas giants are thought to have sustained transient, bloated gaseous envelopes. Gas drag exerted on solid bodies passing through such envelopes could lead to one of three distinct dynamical outcomes. Small bodies, with a high ratio of cross-sectional area to mass, could be decelerated from heliocentric orbit to spiral into the body of the growing planet. Large bodies, with a small ratio of cross-section to mass, would pass through the envelope with little change in momentum. Intermediate sized bodies could be slowed just enough to avoid the death-spiral into the growing planet but enough to be captured by the planet. The sudden collapse of the envelope would leave some such objects suspended in irregular type orbits (Pollack *et al.*, 1979). One suggested observational signature of capture by gas drag would then be a narrow size distribution corresponding to those objects for which deceleration was “optimal”. (Subsequent collisions, however, might modify the size distribution by breaking-up the captured bodies into smaller fragments, so concealing the tell-tale narrow size range expected from gas drag capture).

2. The sudden mass-growth of the planets leads to a second mechanism of capture, known as "pull-down" capture (Heppenheimer and Porco, 1977). In pull-down capture, a heliocentric body moving at low velocity relative to the parent planet enters the Hill sphere through a Lagrange point. Residence in the Hill sphere would be temporary (with a timescale corresponding typically to tens or hundreds of years) but for the effect of the increasing mass of the growing planet. Provided the planetary mass increases on a timescale that is short compared to the residence time, this mechanism could lead to the permanent capture of any bodies in the vicinity of a giant planet. Very rapid (runaway) mass growth is expected in some models of gas giant formation.
3. Three-body interactions, both collisional and non-collisional, involving two small bodies moving in the vicinity of a massive planet could lead to capture of one of the objects (Colombo and Franklin, 1971; Weidenschilling, 2002). Fragments produced by energetic collisions could also be captured. Collisions between the known irregular satellites are rare (Nesvorny *et al.*, 2003) and the rate of collisions between the known irregular satellites and cometary nuclei is also negligbly small (Nakamura and Yoshikawa, 1995). Therefore, collisional capture could only work efficiently if the initial populations of small bodies were much larger than now observed. This is qualitatively consistent with independent evidence that the solar system underwent an early clearing phase in which the flux of interplanetary bodies was orders of magnitude higher than now (the so called "terminal bombardment"). It is also possible that the irregular satellites are the survivors of a once huge population of temporary satellites, stabilized by 3-body interactions.

3. New Observational Results

The Jovian system, because of its proximity, is observationally the best characterized and serves as a useful reference for comparison with less complete data available for the irregular satellites of the outer planets. This is evident from the inverse square law

$$p_R r^2 = 2.25 \times 10^{22} R^2 \Delta^2 10^{0.4 \Delta m_R}. \tag{2}$$

which connects the radius, r (km), the geometric albedo, p_R, and the heliocentric and geocentric distances, R (AU) and Δ (AU) of the satellite to the apparent brightness. Here, Δm_R is the difference between the R-band magnitude of the Sun and of the satellite. With $R \gg 1$ and substituting $p_R = 0.04$, this relation gives

$$r \sim \left[\frac{R}{5}\right]^2 10^{0.2(24-m_R)}. \tag{3}$$

For example, Equation (3) shows that satellite surveys made to magnitude $m_R = 24$ reach limiting radii $r \sim 1$, 4, 16 and 36 km at Jupiter, Saturn, Uranus and Neptune,

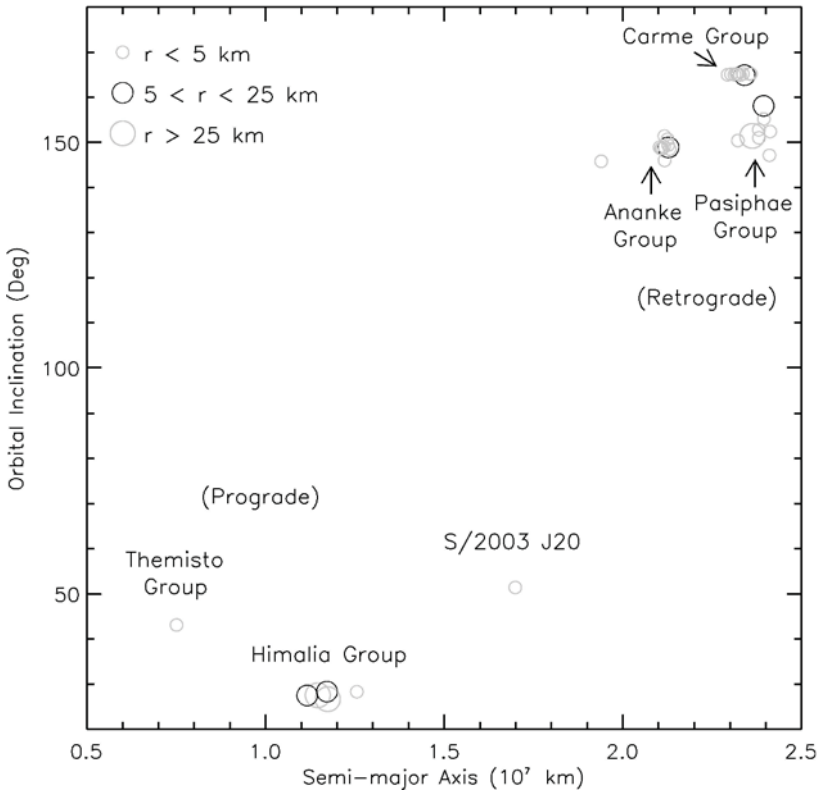

Figure 3. Distribution of the time-averaged orbital semimajor axes and inclinations of the Jovian irregular satellites. The sizes of the satellites are related to the sizes of the symbols, as shown. Only satellites observed on two or more oppositions have been plotted to ensure that the orbital elements are reliable. Note that 2.5×10^7 km corresponds to about 350 Jupiter radii and to about 0.17 AU. Elements were provided by Bob Jacobson of JPL and the figure is from Sheppard and Jewitt (2003).

respectively. For this reason we know of a large number of (mostly small) irregular satellites at Jupiter but only smaller numbers of larger objects at the other giant planets.

The new satellite discoveries, especially those at Jupiter, show evidence for clustering of the orbital properties (Figure 3). The velocity dispersion within each cluster is comparable to the gravitational escape velocity of the largest cluster member (Nesvorny *et al.*, 2003; Sheppard and Jewitt, 2003). This suggests an origin through collisional break-up of precursor bodies after their capture into planetary orbit. If so, Jupiter's irregular satellite clusters point to 6 or 7 precursor objects (3 prograde and 3 or 4 retrograde) with radii in the ∼1 km to ∼85 km range. Consistent with this interpretation are photometric measurements which show color differences between clusters and relative color uniformity within them (Rettig *et al.*, 2001; Grav *et al.*, 2003). Irregular satellites of the other giants are probably also dynamically clustered – Saturn with ∼4 clusters, Uranus with 2 or 3,

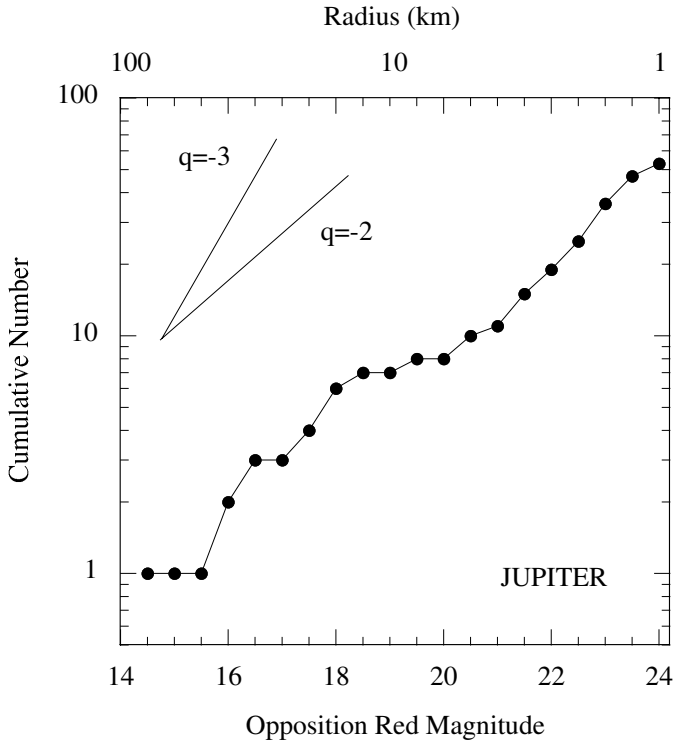

Figure 4. Cumulative number of Jovian irregular satellites as a function of opposition red magnitude, compiled from data available on 2004 February 5. Diagonal lines show the slopes expected if the differential size distribution is a power law with index q = -2 and q = -3. The overall satellite distribution resembles the q = -2 case, but the flattening between m_R = 18 and m_R = 20 shows that the satellite distribution does not follow a simple power law. The upper scale shows the effective circular radius computed on the assumption that the geometric albedo is p_R = 0.04.

Neptune with 3 (or 4 if Triton is counted) – but their known populations are smaller and the cluster parameters less well defined.

Figure 4 shows the cumulative number of Jovian irregular satellites as a function of apparent red magnitude, m_R. The corresponding radii from Equation (3) are shown on the upper x-axis of the figure. The data are believed to be complete to m_R = 23 – the turn-down in the curve in the last point at m_R = 24 may result from objects yet unfound. Note that the satellites are likely to be aspherical and that their magnitudes will vary as a function of rotational phase. This effect, which remains unquantified in the smaller satellites, is not accounted for in Figure 4. Diagonal lines in the Figure mark the brightness distributions that would be expected if the satellite radius distribution obeyed a simple differential power law

$$n(r)dr = \Gamma r^q dr \tag{4}$$

where r is the radius, Γ and q are constants. The satellite distribution is broadly similar to the q = -2 line, but clearly shows deviations from power-law behavior that

are significant. In particular, the flattening of the cumulative distribution between magnitudes $m_R = 18$ and $m_R = 20$ (radii $6 \leq r \leq 16$ km) must reflect a true paucity of such objects in the Jovian irregular satellite population because the current surveys are essentially complete at these high brightness levels (c.f. Sheppard and Jewitt, 2003). The satellite size distribution is flatter than expected for a population in collisional equilibrium (the so-called Dohnanyi, 1969, distribution, for which $q \sim$ -3.5). We lack the statistics to accurately determine the size distribution within the individual dynamical clusters.

We combine the cumulative plot of Figure 4 with information about comparable satellite surveys to compare the irregular satellite populations of the four giant planets. In Table 2 we have listed the total number of irregular satellites for each planet, N_i, regardless of brightness, as well as N_i^{23} (the number having $m_R \leq 23$). (The data were taken from the compilation by the JPL solar system dynamics group at http://ssd.jpl.nasa.gov/. Listed V magnitudes were corrected to R magnitudes using $m_V - m_R = 0.5$). We select $m_R = 23$ as a reference magnitude because each of the giant planets has been surveyed to this level and the populations of brighter satellites can be regarded as well known (certainly to within a factor $\sim$2, probably better). With albedo $p_R = 0.04$, the effective radius would be $r \sim 1.6$ km (Equation 3). The column labelled N_*^{23} is the number of irregular satellites brighter than $m_R = 23$ that are expected if each giant planet possess an intrinsic population identical to that at Jupiter. This number is estimated by scaling the Jovian population for the greater distance of each planet. The magnitude decrement resulting from the greater distance is approximately

$$\Delta m = 5 log_{10} \left[\frac{R(R-1)}{R_{\rm J}(R_{\rm J}-1)} \right] \tag{5}$$

assuming that the planets are observed at opposition. Here, $R_{\rm J} \sim 5$ AU is the average Sun-Jupiter distance. For example, Saturn with $R \sim 10$ AU has $\Delta m =$ 2.6 mag. (Table II) and we read from Figure 4 that the number of irregulars with $m_R \leq$ (23.0 - 2.6) = 10, whereas the actual number is 8. The Table shows the astonishing result that

$$N_*^{23} \sim N_{\rm i}^{23} \ , \tag{6}$$

meaning that the irregular satellite data are consistent with the hypothesis that each of the four giant planets possesses an irregular satellite system like that observed at Jupiter. In other words, the number of irregular satellites per giant planet remains approximately constant (to within a factor of $\sim$2) even as the planetary mass varies by a factor of about 20 from Jupiter to Uranus. (It could be argued that we should count satellite groups rather than individual satellites, since the groups probably represent the true numbers of initially captured bodies. Doing so gives the same result: each giant planet possesses a handful of satellite clusters, the largest members of which have $m_R \leq 23$, consistent with scaling from Jupiter using Equation 5). This result is remarkable, since there are no a-priori reasons why the irregular

TABLE II
Hill spheres of the giant planets

Planet	m_P [a]	a [b] [AU]	r_H [AU] [c]	r_H [deg] [d]
Jupiter	310	5	0.35	5
Saturn	95	10	0.43	2.8
Uranus	15	20	0.47	1.4
Neptune	17	30	0.77	1.5

[a] Planet mass in multiples of Earth's mass (6×10^{24} kg)
[b] Semimajor axis in AU
[c] Radius of Hill sphere in AU
[d] Projected radius of Hill sphere in degrees at opposition

satellite populations of the different planets should be at all similar, even to within order of magnitude.

To drive this core point home, we make it again in a different way in Figures 5 and 6. Figure 5 shows the cumulative number of irregular satellites of each planet brighter than a given apparent red magnitude. (Data for the plot were compiled from the various discovery IAU Circulars and Minor Planet Electronic Circulars, with corrections from V magnitudes to R magnitudes using V - R = 0.4, where necessary). Figure 6 shows the same satellite data as in Figure 5, but with the magnitudes corrected to the opposition heliocentric and geocentric distances of Jupiter using the offsets, Δm, listed in column 3 of Table II. Whereas the curves in Figure 5 are widely separated, those in Figure 6 substantially overlap, showing that the main differences between the statistics of the irregular satellites are artifacts of the different distances of the planets and the finite magnitude limits of the surveys used to study them. If the populations were exactly equal, all four curves in Figure 6 would overlap precisely. That they do not presumably results from real (but small) intrinsic population differences and from photometric corrections for rotation and phase-angle dependent scattering which we have neglected.

We briefly explore some of the consequences of the constancy of the irregular satellite populations.

4. Reconciliation with Giant Planet Formation Models

4.1. Core Accretion

Jupiter and Saturn likely grew by runaway accretion of nebular hydrogen and helium onto a core of higher molecular weight material. Their transient gaseous envelopes are a plausible source of frictional energy dissipation by which the ir-

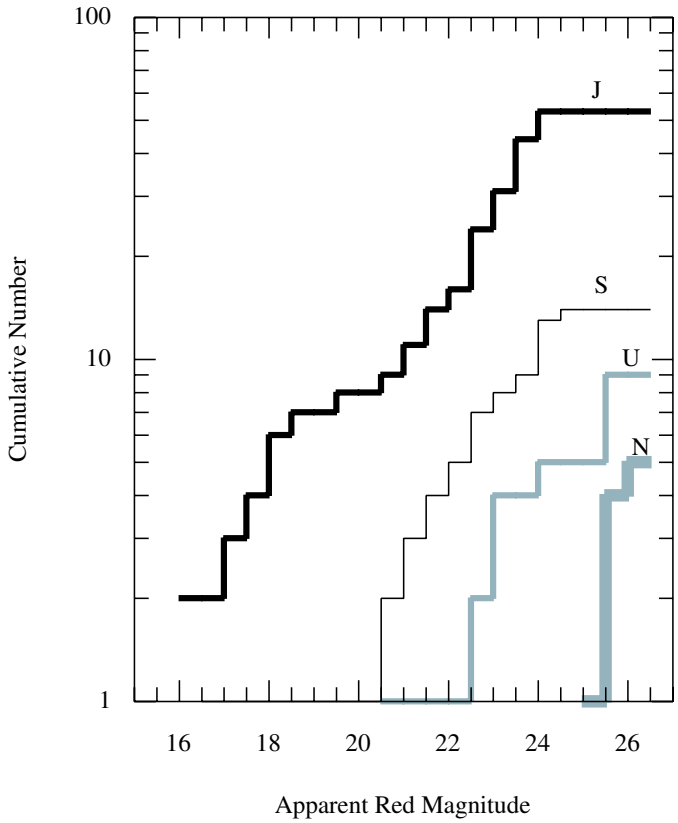

Figure 5. Cumulative numbers of irregular satellites brighter than a given apparent red magnitude (binned in 0.5 mag increments) for each of the four giant planets (J = Jupiter, S = Saturn, U = Uranus, N = Neptune).

regular satellites of these planets might have been captured (Cuk and Burns, 2003). The sudden increase of mass associated with runaway growth could also lead to pull-down capture of the irregular satellites. However, neither gas drag nor pull-down capture can explain the existence of comparable populations of irregular satellites of the ice giants Uranus and Neptune. The latter planets possess little excess hydrogen and helium and are not thought to have undergone dramatic runaway growth as did Jupiter and Saturn. Therefore, gas drag and pull-down capture offer implausible explanations for the existence of irregular satellites of Uranus and Neptune.

4.2. Disk Instabilities

In some models spontaneous collapse of segments of disk (without the need for a high molecular weight core) can occur on extremely short timescales, perhaps as small as a few $\times 10^3$ years (e.g., Boss, 1997). Bodies with the $\sim$100 km size of the

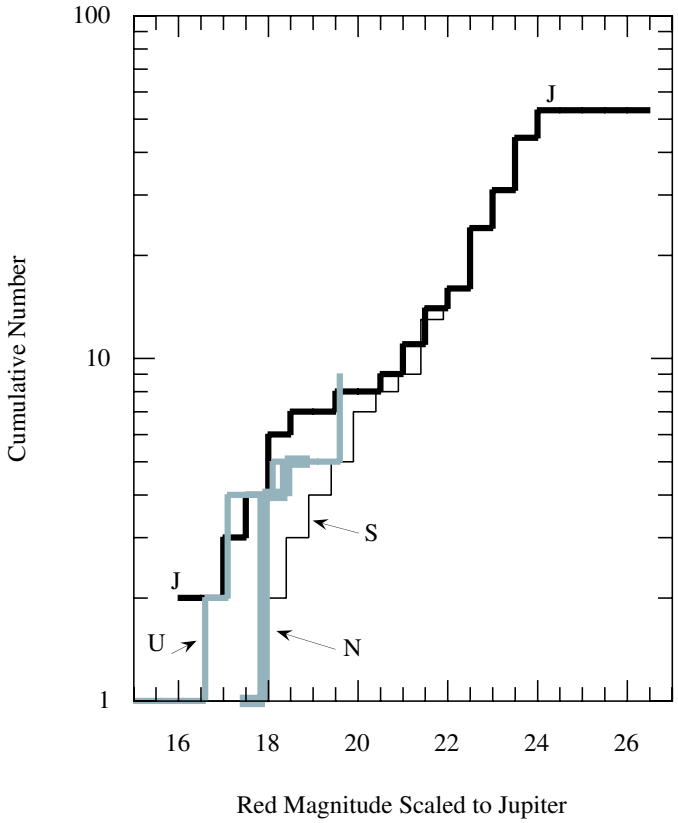

Figure 6. Same as Figure 5 but with the magnitudes of the satellites scaled to the opposition heliocentric and geocentric distances of Jupiter using the inverse square brightness law (see column 3 of Table II). Again, J = Jupiter, S = Saturn, U = Uranus, N = Neptune. The curves in Figure 5 have coalesced.

satellite precursors could not have grown on such short timescales and so would not have been available to be captured. In order to explain the prior existence of the irregular satellites one would need to delay the nebular collapse (i.e., require that the timescale for planetesimal accumulation in an unstable central disk be less than the timescale for gravitational collapse of the nebular gas as a whole). Perhaps this is possible, but it is not a featured result of the disk models of which we are aware. Moreover, disk instabilities cannot account for the highly non-solar (hydrogen and helium depleted) compositions of Uranus and Neptune.

4.3. Ablation Models

To explain the ice giants Uranus and Neptune, Boss (2003) has advocated a model in which these planets are the remnants of $\sim 2\ M_J$ gas giants ablated by a sustained ionizing flux of photons from nearby OB type stars. Essentially, Uranus and Neptune formed like Jupiter and Saturn but, because of their great heliocentric distance

and reduced shielding from ionizing photons by nebular gas, were ablated to their present structures. Decreasing planetary mass poses severe problems for the stability of the irregular satellites (if Jupiter's 310 $M_\oplus$ were whittled away to Uranus' 15 $M_\oplus$ then its irregular satellites would be lost to interplanetary space). One could conjecture that, if the ablation models are correct then the irregular satellites must have been captured at a later time. Even this is problematical, however, because the late stage ice giants would lack the extended gaseous envelopes needed for frictional capture, do not exhibit rapid mass growth needed for pull-down capture, and would not necessarily retain solid body retinues sufficient to guarantee multiple collisions. In short, within the context of the existing models for the origin of the irregular satellites, the satellite data do not appear compatible with the ablation model.

4.4. Rearrangement Models

Thommes *et al.* (1999) suggested that Uranus and Neptune grew alongside the heavy cores of Jupiter and Saturn in the ∼4 to ∼10 AU zone. The ice giants failed to accrete much nebular hydrogen and helium (and therefore never attained gas giant status) as a result of being prematurely scattered out to the gas-poor regions of the outer solar system. Numerical simulations indicate that the irregular satellites of Uranus and Neptune could not survive this violent rearrangement of the solar system (Beauge *et al.*, 2002). Therefore, in the rearrangement models, the irregular satellites must have been captured after the orbits of Uranus and Neptune were circularized near their current locations. The problems then become the same as for the ablation models: there is too little gas to effect capture and too little mass-growth of the planets for capture by the pull-down mechanism. Instead, a plausible collisional origin for the capture of the irregular satellites could perhaps be constructed, given that the circularization of the orbits of the ice giants is due to their tidal interaction with a still massive planetesimal disk. In the simulations of Thommes *et al.* (1999) associated planetary bombardment continues for $\sim 10^7$ yr and this sets the timescale for collisional capture of the irregular satellites.

4.5. Discussion

In stark contrast to Jupiter and Saturn, the ice giants hold only 2 or 3 $M_\oplus$ of hydrogen and helium gas from the nebula, offering greatly reduced opportunity for satellite capture by gas drag. Indeed, the efficacy of gas drag capture around the heavily gas-depleted ice giants has never been demonstrated. Furthermore, in the standard model, the ice giants grew steadily through the accretion of planetesimals with no pronounced mass runaway, so that pull-down capture of the satellites is also inviable. Instead, the existence of the irregular satellites of the ice giants is more compatible with a collisional or 3-body source of dissipation, since such a source requires no assumptions about the gas content or mass growth rate of the planet (Colombo and Franklin, 1971; Nesvorny *et al.*, 2003). The main requirement is a

greatly enhanced density of precursor objects within the Hill spheres of the planets at the time of their formation. Little quantitative work has been done to estimate the capture rate to be expected from this process, although the work of Weidenschilling (2002) concerning the production of Kuiper Belt binaries is clearly relevant.

More puzzling is why the satellite populations of the four giant planets, measured to a given absolute magnitude or size, should be even remotely similar (c.f. Table II). We cannot exclude the possibility that the invariance of the number of irregular satellites, measured with respect to the planetary mass and mode of formation, is simply a coincidence. For example, satellites could have been captured by different processes at different planets (e.g., gas drag and/or pull-down at Jupiter and Saturn, by 3-body interactions within the Hill spheres at Uranus and Neptune) and, by chance, produce similar numbers of satellites. Another possibility is that the irregular satellites of all four giant planets were captured through collisional dissipation, the process which is least tightly coupled to the details of the planet growth mechanism. In this regard we note that the Hill spheres increase in size by a factor of $\sim$2 from Jupiter to Neptune (Table I) and that the associated volumes within which collisions might lead to capture increase by $2^3 \sim 10$. This partially compensates for the decrease in the collision rate expected from the decline in the density of the protoplanetary disk with radius and so could help produce a more shallow variation of satellite number from Jupiter to Neptune than would otherwise be expected.

Capture by gas-drag is the most-discussed model for the origin of the irregular satellites but the reasons for this prominence appear largely historical and are not compelling. Gas drag has not been shown to be effective around the ice giants, where substantial populations of irregular satellites are now known. Worse, the model offers few clear, observationally verifiable predictions for the properties of the irregular satellite systems (other than the strongly violated "prediction" that it should not be effective around planets having little gas, like Uranus and Neptune!). It therefore seems prudent to keep an open mind about the way (or ways) in which the irregular satellites were captured and more theoretical effort on the efficacy of capture by other processes seems warranted. We are especially intrigued by the possibility that 3-body interactions within the planetary Hill spheres could have been responsible for satellite capture and we encourage quantitative investigation of this scenario.

Acknowledgements

We thank Yan Fernández, Jane Luu and Toby Owen for comments. This work was supported by a grant to DJ from the NASA Planetary Astronomy Program.

References

Beauge, C., Roig, F., and Nesvorny, D.: 2002, 'Effects of planetary migration on natural satellites of the outer planets', *Icarus* **158**, 483–498.

Boss, A.: 1997, 'Giant planet formation by gravitational instability', *Science* **276**, 1836–1839.

Boss, A.: 2003, 'Rapid formation of outer giant planets by disk instability', *Astrophys. J.* **599**, 577–581.

Colombo, G. and Franklin, F.: 1971, 'On the formation of the outer satellite groups of Jupiter', *Icarus* **15**, 186–189.

Cuk, M. and Burns, J.: 2003, 'Gas-drag-assisted capture of Himalia's family', *Icarus* **167**, 369–381.

Dohnanyi, J.S.: 1969, 'Collisional model of asteroids and their debris', *J. Geophys. Res.* **74**, 2431–2554.

Gladman, B.J., Nicholson, P.D., Burns, J.A., Kavelaars, J.J., Marsden, B.G., Williams, G.V., and Offutt, W.B.: 1998, 'Discovery of two distant irregular moons of Uranus', *Nature* **392**, 897–899.

Gladman, B., Kavelaars, J.J., Holman, M., Petit, J.-M., Scholl, H., Nicholson, P., and Burns, J.A.: 2000, 'The discovery of Uranus XIX, XX, and XXI. Discovery of 12 satellites of Saturn exhibiting orbital clustering', *Icarus* **147**, 320–324.

Gladman, B., *et al.*: 2001, 'Discovery of 12 satellites of Saturn exhibiting orbital clustering', *Nature* **412**, 163–166.

Grav, T., Holman, M., Gladman, B., and Aksnes, K.: 2003, 'Photometric survey of the irregular satellites', *Icarus* **166**, 33–45.

Heppenheimer,T.A. and Porco,C.: 1977, 'New contributions to the problem of capture', *Icarus* **30**, 385–401.

Holman, M.J., *et al.*: 2004, 'Discovery of five irregular moons of Neptune', *Nature* **430**, 865–867.

Jewitt, D., Sheppard, S., and Porco, C.: 2004, 'Jupiter's outer satellites and Trojans', in F. Bagenal, T. Dowling and W. McKinnon (eds.), *Jupiter*, Cambridge Univ. Press, England.

Kuiper, G.P.: 1956, 'On the origin of the satellites and the Trojans', *Vistas in Astronomy* **2**, 1631–1666.

Nakamura, T. and Yoshikawa, M.: 1995, 'Close encounters and collisions of short-period comets with Jupiter and its satellites', *Icarus* **116**, 113–130.

Nesvorny, D., Alvarellos,J., Dones, L., and Levison, H.: 2003, 'Orbital and collisional evolution of the irregular satellites', *Astron. J.* **126**, 398–429.

Pollack, J.B., Burns, J.A., and Tauber, M.E.: 1979, 'Gas drag in primordial circumplanetary envelopes: a mechanism for satellite capture', *Icarus* **37**, 587–611.

Pollack, J., Hubickyj, O., Bodenheimer, P., Lissauer, J., Podolak, M., and Greenzweig, Y.: 1996, 'Formation of the giant planets by concurrent accretion of solids and gas', *Icarus* **124**, 62–85.

Rettig, T., Walsh, K., and Consolmagno, G.: 2001, 'Implied evolutionary differences of the Jovian irregular satellites from a BVR color survey', *Icarus* **154**, 313–320.

Sheppard, S. and Jewitt, D.: 2003, 'An abundant population of small irregular satellites around Jupiter', *Nature* **423**, 261–263.

Sheppard, S. and Jewitt, D.: 2004, 'Ultradeep survey for irregular satellites of Uranus: limits to completeness', *Astron. J.*, in press.

Thommes, E., Duncan, M., and Levison, H.: 1999, 'The formation of Uranus and Neptune in the Jupiter-Saturn region of the Solar System', *Nature* **402**, 635–638.

Weidenschilling, S.: 2002, 'On the origin of binary Transneptunian objects', *Icarus* **160**, 212–215.

Address for Offprints: David Jewitt and Scott Sheppard, Institute for Astronomy, University of Hawaii, 2680 Woodlawn Drive, Honolulu, HI 96822, USA;
jewitt@ifa.hawaii.edu, sheppard@ifa.hawaii.edu

DYNAMICS AND COMPOSITION OF RINGS

BRUNO SICARDY
Observatoire de Paris and Université Pierre et Marie Curie, Meudon, F-92195, France

Received: 16 April 2004; Accepted in final form: 12 October 2004

Abstract. Planetary rings are found around all four giant planets of our solar system. These collisional and highly flattened disks exhibit a whole wealth of physical processes involving dust grains up to meter-sized boulders. These processes, together with ring composition, can help understand better the formation and evolution of proto-satellite and proto-planetary disks in the early solar system. The present chapter reviews some fundamental aspects of ring dynamics and composition. The forthcoming exploration of the Saturn system by the *Cassini* mission will bring both high resolution and time-dependent information on Saturn's rings.

Keywords: rings, disks, dynamics, planetary formation

1. Planetary Rings

Planetary rings consist in extremely thin disks of innumerable colliding particles revolving around a central planet. They are found around all the four giant planets of our solar system, Jupiter, Saturn, Uranus and Neptune. They exhibit a wide variety of sizes, masses and physical processes. For instance, spiral waves spanning several tens of km, and akin to galactic features, are observed in Saturn's dense rings. At the other end, dust grains submitted to electromagnetic or radiation forces are observed to evolve over a few days only in some tenuous regions of planetary rings.

A complete review of planetary rings clearly remains out of the scope of this chapter. Instead, we would like to address here a few basic issues related to planetary rings, and see how the forthcoming *Cassini* mission to Saturn may help solve some of these issues.

On the long term, one would like to understand better the connections between the rings global parameters (mass, optical depth, etc...) and their local properties (particle size and distribution, velocity dispersion, etc...). Such connections can eventually give clues on the accretion and fragmentation mechanisms which lead to the formation of satellites or planets in the early solar system, or in other proto-planetary disks.

Space Science Reviews 116: 457–470, 2005.
DOI: 10.1007/s11214-005-1966-y

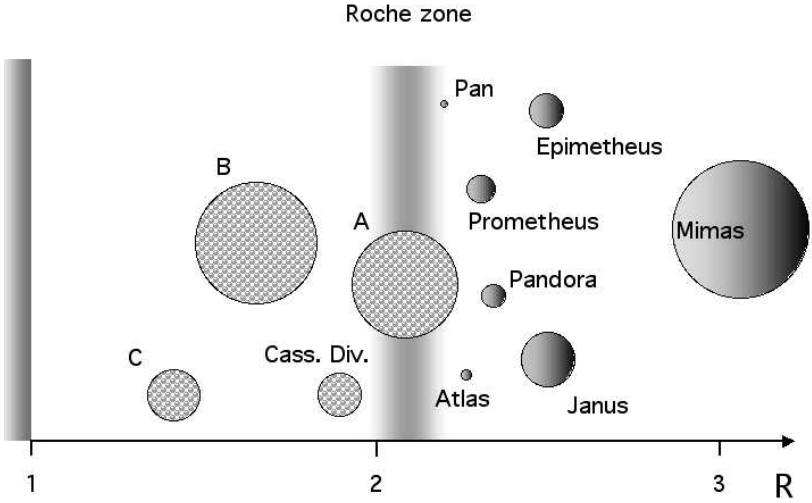

Figure 1. The relative masses of Saturn's inner satellites and rings as a function of their distance to the planet center, in units of the planet radius. The "sizes" of the rings have been calculated by lumping all the material of A, B, C rings and Cassini Division into single bodies (see Esposito, 1993). All the sizes have been plotted so that to respect the relative masses of the various bodies involved. For comparison, Mimas has a diameter of about 500 km. Note the decrease of satellite sizes as one approaches the Roche limit.

2. Rings around Giant Planets

All giant planets are surrounded by rings. Detailed reviews of the dynamical and physical properties of these systems can be found in Borderies *et al.* (1984), Harris (1984), Ward (1984), Nicholson and Dones (1991), Goldreich (1992), Esposito (1993) and Cuzzi (1995). More specific reviews are available for each ring system, see for instance Cuzzi *et al.* (1984) and Esposito *et al.* (1984) for Saturn's rings, Burns *et al.* (2004) for Jupiter's rings, Smith *et al.* (1986), Esposito *et al.* (1991) and French *et al.* (1991) for Uranus' rings, and Smith *et al.* (1989) and Porco *et al.* (1995) for Neptune's rings. Finally, general reviews on rings oriented toward the *Cassini* mission can be found in Cuzzi *et al.* (2002) and Esposito (2002).

All these rings differ in mass by various orders of magnitude. Only Saturn's rings have an integrated mass comparable to those of significant satellites like Mimas or Encelade. For instance, lumping all Saturn's rings into a single body would yield a satellite with a diameter of the order of 500 km, see Figure 1.

We see in this figure that smaller and smaller satellites are encountered as one gets closer to the planet, a natural consequence of tidal stress. Also, these small satellites tend to be underdense, as they have densities in the range 0.4-0.6 g cm^{-3} (Rosen *et al.*, 1991; Nicholson *et al.*, 1992). This indicates that they are probably loose aggregates of icy material, possibly accumulated in the outer regions of the rings, and then driven outward by tidal forces raised by the latters.

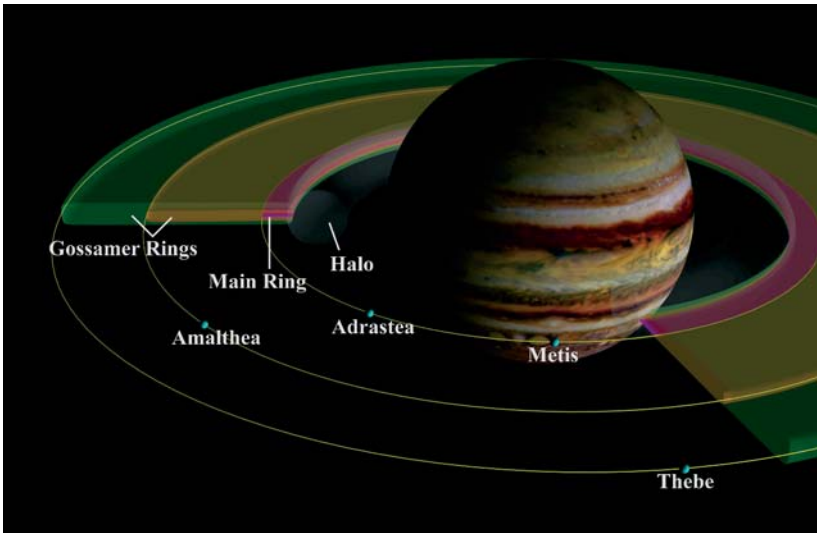

Figure 2. This cartoon depicts schematically the structure of dusty Jupiter rings (taken from `http://photojournal.jpl.nasa.gov`). The inner main ring (*pink*) is associated with the small moons Adrastea and Metis, while the outer gossamer rings (*yellow and green*) are respectively produced by impacts on Amalthea and Thebe (see Burns *et al.*, 2004). The innermost ring (*grey*) is a very tenuous 3D torus produced by dust interacting with Jupiter's magnetic field.

As one gets in the Roche zone of the planet, satellites and rings co-exist, and finally, only collisional rings are found, as tidal forces overcome self-gravity of the satellites.

The other planetary rings exhibit the same general behavior as in Figure 1, i.e. smaller and smaller satellites near the Roche limit, then a mixture of rings and satellites, then only rings (Nicholson and Dones, 1991). However, the cumulated masses of these rings are much smaller than those of Saturn.

For instance, gathering Uranus' observable rings together would amount to a satellite of no more than some tens of km in size, while the same operation would yield a km-sized boby for Neptune's rings, and a lump of some tens of meters at most in the case of Jupiter* (see Esposito, 1993).

Some particularities are associated with each ring system, among which we can quote:

- Jupiter's rings. They are extremely tenuous, as stated above. The dust that we see in these rings is short lived and appears to be associated with small Jovian moons, from which it is excavated, see the discussion below and in Burns *et al.* (2004), as well as Figure 2.
- Uranus' rings. Although some of Uranus' rings are tenuous and wide, several of them are on the contrary very dense (with optical depth up to $\tau > 1$), but

* These mass estimates do *not* take into account possible small satellites or large chunks embedded in those rings, and not discovered yet.

very narrow (1 to 100 km depending on the rings), with extremely sharp edges and solid precession, thus requiring very efficient confinement mechanisms.

- Neptune's rings. Besides some dusty tenuous rings, Neptune possesses ring arc features which span only 40 degrees in longitude, out of the 360 degrees available. Although such a configuration is unstable in a matter of months, it has been maintained for more than 20 years now. Again, this requires very specific confining mechanisms, as explained later.

3. Ring Dynamics

We can divide the physical processes at work in the rings into two main areas.

One area concerns the large (cm-sized or larger) particles which suffer frequent collisions, leading to a continuous chain of accretion/fragmentation phenomena, plus collective behaviors associated with gravitation and collisions. These processes cause among others a viscous spreading of the rings, as well as a secular exchange of angular momentum with nearby satellites. The time scales associated with these processes are relatively long, typically a million years for instance for the viscous spreading of narrow Uranus' rings, to some hundred of millions years for the collapse of Saturn's A ring onto the B ring through the tidal torque from Mimas (Goldreich and Tremaine, 1982; Borderies *et al.*, 1984). These scales could be compared to geological times scales on the Earth. Note, however, that these time scales remain short compared to the age of the solar system.

Another area concerns microscopic particles (mm-sized down to a few micrometers), for which electromagnetic and radiation forces are much more important. The lifetime of these particles is very short (a few hours to a few millenia at most), due to re-accretion, plus radiation and electromagnetic forces (Burns *et al.*, 2004). Consequently, permanent sources must be invoked to explain their presence. Taking again an Earth analog, these processes could be compared to those encountered in meteorology or oceanography, for which time scales of some weeks or months are frequent.

Of course, the two domains described above are not disconnected, as dust can permanently be re-accreted on large particles, while the latters can be disrupted at any moment into small grains due to a collision.

3.1. Large Particles

3.1.1. *Roche Limit*

Loosely speaking, rings are found inside the Roche zone of the central planet, see Figure 1. This can be easily understood as tidal stresses become more important near the planet. Reality is more complex, though, as cohesive forces can allow a satellite to live inside the Roche zone, while collisions can grind a satellite into a ring outside that zone.

The resulting limit between rings and satellites is then a compromise between self-gravity, tensile strength, surface forces, velocity dispersion, particle sizes, etc... In particular it happens that rings and satellites can co-exist in the same region, a feature exhibited in all ring systems.

Even in those regions when only rings are found, the local behavior of the particles can be rather complex, and the very notion of a single particle can become pretty fuzzy. In some cases, there could even be the possibility of liquid and solid phases co-existing in the rings, with narrow regions where colliding particles have large velocity dispersions, and narrow regions where they are stuck together in a rigid manner (Tremaine, 2003).

3.1.2. *Disk Stability*

A detailed discussion and review on disks stability can be found in Binney and Tremaine (1988), from which we extract here some relevant results connected to planetary rings.

Generally, a circumplanetary disk tends to collapse under the influence of collisions, which dissipates energy while conserving angular momentum: the disk is actually the configuration of least energy for a given angular momentum. The collapse, however, does not continue for ever down to an infinitely thin disk of surface density Σ_0, as instabilities then show up. The finite size and masses of the larger particles actually maintain a finite velocity dispersion c_s (i.e. a finite "temperature") in the disk.

This temperature maintains a pressure in the disk, which prevents the gravitational collapse of the smallest scales. A dimensional analysis using the quantities c_s and Σ_0 shows that we can obtain a length by writing $c_s^2/G\Sigma_0$. More precisely, it can be shown disturbances with spatial scales λ smaller than:

$$\lambda_J = \frac{c_s^2}{G\Sigma_0}$$

will be stabilized (i.e. will not gravitationally collapse). It can be shown that λ_J is the 2-D version of a Jeans wavelength.

On the other hand, in a disk rotating at angular velocity Ω, large structures of scale λ display differential velocities of order $\lambda\Omega$. These structures will then spin more and more rapidly as they collapse, reaching a rotational barrier at some point. A new length can be obtained by writing $G\Sigma_0/\Omega^2$. More precisely, disturbances larger than:

$$\lambda_R = \pi^2 \frac{G\Sigma_0}{\Omega^2}$$

are stabilized against gravitational collapse by the disk rotation, which can be seen as a 2-D version of the Roche limit.

The disk is thus stable for disturbances with scales smaller than λ_J and larger than λ_R. The quantity $Q = \sqrt{\lambda_J/\lambda_R}$ is called the *Toomre parameter* (Toomre,

1964). Consequently, the disk is stable at *all* scales if $\lambda_J > \lambda_R$, i.e. if:

$$Q = \frac{c_s \Omega}{\pi G \Sigma_0} > 1.$$

The disk actually adjusts itself so that to be just at the limit $Q \sim 1$, i.e. to be in a state of marginal instability. If for instance Q is smaller than unity (cold disk), then gravitational instabilities build up, the sizes of the largest particles increase, which gravitationally stirs the whole system and eventually increases c_s so that $Q \sim 1$, at which point instabilities disappear. If on the contrary Q is too large (hot disk), then collisions cause fragmentation and dissipation finally damps c_s so that to reach again $Q \sim 1$.

For $Q = 1$, the size of the marginally unstable disturbance is:

$$\lambda_T = 2\pi^2 \frac{G\Sigma_0}{\Omega^2} = 2\frac{c_s^2}{G\Sigma_0} = 2\pi \frac{c_s}{\Omega} = 2\pi h,$$

where $h = c_s/\Omega$ is the thickness of the disk. There are various ways to express h. A physical approach is to note that $m_r = \pi a^2 \Sigma_0$ the total mass available in the ring, where a is the typical radius of that ring. The expressions above then yield:

$$h \sim a \times \frac{m_r}{M},$$

where M is the mass of the central planet.

Typical values of Saturn's rings surface density (in the densest regions) yield $m_r/M \sim 10^{-7}$, while $a \sim 10^5$ km, so that h is of the order of a some tens of meters. This result agrees with independent and indirect measurements of wave propagation in Saturn's rings, and appear as a natural result of marginal stability in a self-gravitating collisional disk.

Furthermore, the marginally instability scale λ_T is of the order some hundreds of meters, and is probably the explanation for the quadrant asymmetries observed in Saturn's A ring (Colombo *et al.*, 1977).

Finally, the thickness of some tens of meters quoted above must be maintained by the gravitational stirring of the largest particles of the rings, of the order of the escape velocity at the surface of those particles, $v_{\rm lib} = \sqrt{2Gm_l/R_l}$, where m_l and R_l are respectively the mass and radius of the largest particles. Equating $v_{\rm lib}$ to $c_s = h\Omega$ yields:

$$R_l \sim \sqrt{\frac{3\Omega^2}{8\pi\rho_l}} h,$$

where ρ_l is the density of the largest particles. Loose agregates of icy particles have typical densities of $\rho_l \sim 100 - 1000$ kg m^{-3}, yielding $R_l \sim$ of a few meters, consistent again with *Voyager* radio experiments (Marouf *et al.*, 1983).

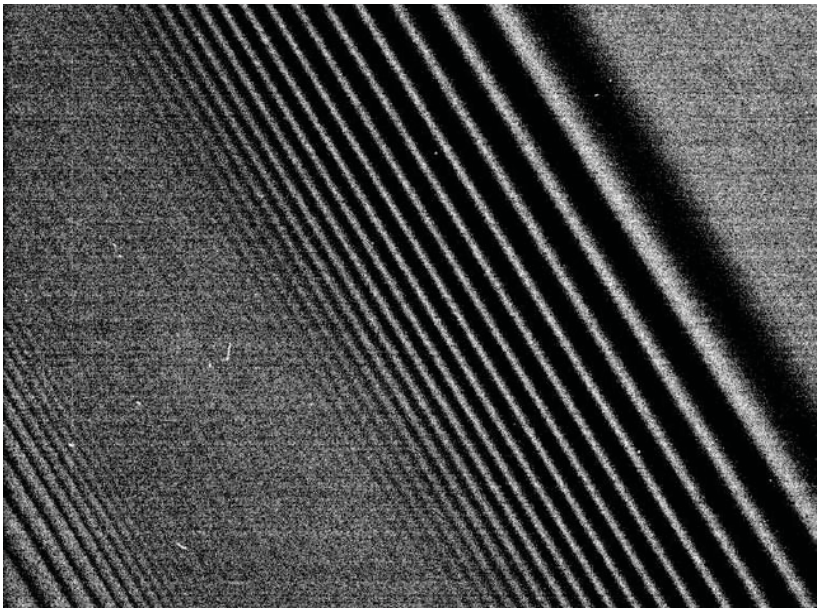

Figure 3. An image of Saturn's dark (unlit) A ring taken by the narrow angle camera on the Cassini spacecraft during its orbit insertion (1st of July 2004, picture taken from `http://antwrp.gsfc.nasa.gov/apod/ap040705.html`). A bending wave excited by the Mimas 5:3 resonance is visible in the upper right, while a density wave associated with the same resonance appears in the lower left corner. Both wave trains yield important clues on the local physical properties of the rings, see text.

3.2. RESONANCES

Many instances of resonances are encountered in planetary rings. They usually involve commensurabilities between the orbital frequencies of ring particle and those of some satellites. Other resonances (the so-called Lorentz resonances) involve commensurabilities between the rotation of the planet magnetic field and the orbital motion of charged particles, see especially the case of Jupiter (Hamilton and Burns, 1993; Burns *et al.*, 2004).

3.2.1. *Spiral Waves*

Resonances amplify the perturbing effect of satellite on the rings. As such, they drive macroscopic effects in the rings. In particular, collective interactions between the particles (due to self gravity of the disk and to collisions) result in spiral wave modes excitation of several tens of km in the radial direction, an easily resolved spatial scale for spacecraft like *Voyager* or *Cassini*.

These features are unique and precious probes of the microscopic properties of the rings, like the kinematic viscosity ν or the local surface density Σ, see the review by Shu (1984) and Figure 3.

For instance, the spacing between consecutive crests in density waves can provide the surface density of the disk, which amounts to $\Sigma \sim 70$ g cm^{-3} in Saturn's A ring (Esposito *et al.*, 1983; Esposito *et al.*, 1984). Similarly, the damping distance of bending waves yields the kinematic viscosity ν, which is in turn connected to the velocity dispersion, and eventually, to the vertical thickness of the rings, yielding $h \sim 10 - 50$ m (Ibid.).

Another important consequence of resonances is that they allow the rings to *secularly* exchange angular momentum and energy with the exciting satellites, see Goldreich and Tremaine (1982). Although complicated in the details, the value of the resonant torque is independent (at least in the linear case) of viscosity, pressure and surface densities over a wide range of values, see Meyer-Vernet and Sicardy (1987). This allows one to give robust estimations of the angular momentum flow between the satellites and the rings.

This flow is much more efficient that tides raised by satellites on the planet. For instance, Saturn's A ring is expected to be pushed towards B ring over typical time scales of some 10^8 years due to resonances with Mimas, a time short compared to the age of the solar system (Goldreich and Tremaine, 1982).

3.2.2. *Sharp Edges*

Another noteworthy effect of resonances between rings and satellites is to truncate in some cases the rings, ensuring the maintenance of very sharp edges of no more that 100 m in the radial direction, while these features should be rapidly destroyed due to the viscous spreading of the particles. Examples of such edges are encountered in the outer part of Saturn's A and B rings, as well as in Uranus' rings.

This sharpness is due to the local inversion of the viscous angular momentum flow for those streamlines in the ring which lie very nearby (a few km) the resonance with the moon (Borderies *et al.*, 1989). This is an interesting example of a very efficient confining mechanism, which may have applications for protoplanetary disk perturbed by already formed planets. Another interesting consequence of highly disturbed streamlines is to potentially ensure the rigid precession of eccentric narrow rings like those of Uranus, see Chiang and Goldreich (2000).

However, most of the sharp features in rings, especially those of Saturn, are *not* associated with resonances. This means that some physics is still missing to explain the abundance of fine scale structures in rings. An interesting possibility in that some of these features in dense rings are caused by phase transitions between solid-like and fluid-like particle organization, see Tremaine (2003).

3.2.3. *Radial Confinement*

The exchange of angular momentum between the rings and the satellites at resonances is such that a satellite always tends to push the ring away from it own orbital location. Thus, two satellites are in principle able to confine a ring between them against viscous spreading, the so-called shepherding mechanism (Borderies *et al.*, 1984).

This is indeed observed in several circumstances, see e.g. the Uranian ϵ ring, whose both edges are confined by the small satellites Ophelia and Cordelia.

Many of the observed narrow rings, however, are not observed to be shepherded by two satellites, either because the latters are too small to be discovered at present, or because some physics is not yet understood. For instance, a single satellite could in some cases confine a narrow ring (Goldreich *et al.*, 1995). In other cases, like Saturn's F ring, two satellites (Prometheus and Pandora) are observed on each side of the ring, but they can hardly confine it in a conventional way as their distances to the ring do not match the expected values predicted by the shepherding mechanism.

3.2.4. *Azimuthal Confinement*

Several examples of arc-like feature are observed in planetary rings, but they are generally short lived. For instance, the features observed in Saturn's F rings during the 1995 ring plane crossing do not survive more than a month or so (Showalter, 2004), and are probably the results of collisions between the members of a so far invisible belt of larger parent bodies (Cuzzi *et al.*, 1984; Poulet *et al.*, 2000).

An exception to that rule is the Neptune's ring arc system. Since their discovery in 1984 (Hubbard *et al.*, 1986), the arcs have been observed again in the following years, either from the ground (Sicardy *et al.*, 1991; Nicholson *et al.*, 1995) or from spacecraft (Smith *et al.*, 1989). Even after ten years, they maintain their basic structure (Dumas *et al.*, 1999; Sicardy *et al.*, 1999), although some changes are detectable. Such time scales are much longer than the time it would take for the Keplerian shear to destroy the arcs, an affair of a few month in the absence of an active azimuthal confinement mechanism.

Among the most promising explanation for this kind of confinement is the action of the so-called corotation resonance sites, akin to the well known Lagrange points L_4 or L_5 of a satellite, but not necessarily sharing the orbit of that satellite (Goldreich *et al.*, 1986). Such a resonance has been identify in the case of Neptune's arcs (Porco, 1991), but more subtle effects, including the mass of the arcs itself, must be taken into account for a satisfying model for these features to be fully consistent (Namouni and Porco, 2002).

3.3. Small Particles

Small particles in rings are submitted to non-gravitational forces which drastically change their dynamics when compared to large particles. While in the latter case collisions and self gravity play an essential role, in the former case the important processes are, among others:

- Electromagnetic forces on charged particles, leading to important effects of the planet magnetic field on the dust particle population (see e.g. Grün *et al.*, 1984), including the so-called Lorentz resonances (Hamilton and Burns, 1993).

- Radiation forces and Poynting-Robertson drag due to the solar photons (and to a lesser extent, the planet radiation), see the detailed review by Burns *et al.* (1979).
- Sticking on and ejection from a so-called regolith layer deposited on larger particles (Poulet *et al.*, 2000).

The time scales associated with these processes are in general much shorter than those exhibited by large particles. Actually, time scales as short as a few days are encountered in the evolution of dust, e.g. in Saturn's F ring (Showalter, 2004). Thus, in order for dust to be observed within planetary rings, permanent sources must be invoked.

These sources are thought to be small satellites, or large particles, which are too faint to be detected by imagery, but large enough to provide the released dust over large time scales. Actually, a stationary state could be reached in some cases, where the dust released during inter-particle collisions or meteoroid bombardment, could be re-accreted by the large particles, thus forming a regolith layer on the latters (Cuzzi and Burns, 1988; Poulet *et al.*, 2000).

In others cases, dust rings are clearly associated with known satellites, see for instance the case of Saturn's E ring with Enceladus (Hamilton and Burns, 1994). An extreme case is offered by Jupiter's rings as observed from the ground and by the *Galileo* spacecraft. While Thebe and Amalthea closely shepherd the main ring, Adrastea or Metis appear to be the main source of particles for the Gossamer ring (de Pater *et al.*, 1998; Burns *et al.*, 2004). In those cases, the dusty rings reach a stationary state where the dust removed by electromagnetic and radiation forces (or satellite sweeping), is replaced by dust produced through meteoroid bombardment of the parent moons, or by collisions between the particles. In such a configuration, the source satellites must be large enough to produce enough dust through bombardment, but not too large for allowing the dust to escape after an impact. This compromise could explain why all satellites are not able to maintain a tenuous dusty ring.

4. Composition

Due to their brightness, Saturn's rings are so far the only ones for which relatively high resolution spectra are available. For other rings, only broad band photometry is presently possible, making the determination of the composition problematical.

Concerning Saturn's rings, the presence of water ice have been detected from several decades (Pilcher *et al.*, 1970). Actually, it is difficult to detect something else than water ice in these rings. Recent works (Poulet and Cuzzi, 2002; Poulet *et al.*, 2003) underline the importance of surface texture and small amount of contaminants for interpreting correctly Saturn's rings spectra, especially in the UV.

An overall fit to Saturn's B ring spectrum by these latter authors (see Figure 4) shows for instance that the observations are well reproduced if the particles are

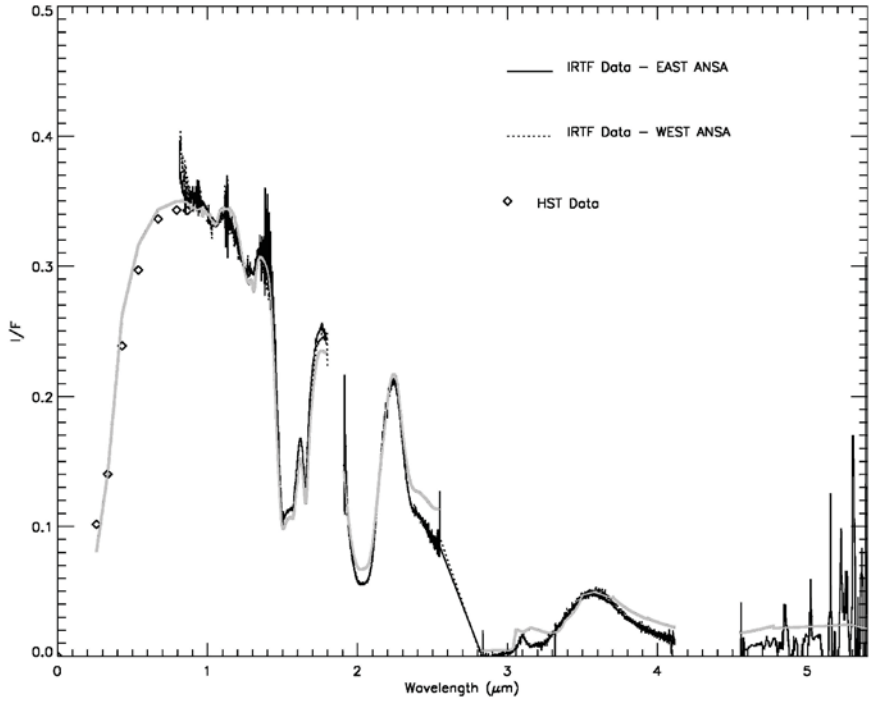

Figure 4. Spectrum of Saturn's B ring taken at 4.7° phase angle, compared with its best-fit model (*grey curve*). The ring particle surface is made of dirty water ice grains of different sizes (typically 10, 100, 1000 micrometers) contaminated by red organic material (taken from Poulet *et al.*, 2003).

covered with an intimate (i.e. 'salt-and-pepper') mixture of grains with different typical sizes, with a discrete size distribution near three different values, namely 10, 100, and 1000 μm. Among them, 95% or so are grains with a few percents of refractory organic solid (tholin) impurities, and 5% are coarse grains of a dark material composed of amorphous carbon.

5. *Cassini* Observations

The present chapter illustrates the variety and complexity of ring dynamics. While the *Voyager* missions brought a huge crop of results during the few weeks of encounters, they nevertheless missed time for a more profound look to rings to be taken. The *Cassini* tour will have several advantages with respect to *Voyager*: first better instruments as technology improved between the 1970's and the 1990's, and second a four year nominal mission, i.e. much more time available for science.

Among some highlighting actions that *Cassini* can take, and without being exhaustive, we can quote:

- Better constrain the particles size distribution using photometry at all wavelengths (from UV to radio) and all phase angles. Other methods (aureole

imaging, stellar and solar occultations, etc...) can also be very useful for this purpose.

- Get the global composition and its "geographical" variations using spectra at all wavelengths (from UV to IR). This may be a challenge, as water ice largely dominates the ring spectrum.
- Follow in real time the evolution of short-lived features like the F ring clumps, the spokes, arc features, or the chaotic behavior of Prometheus and Pandora, etc... This could turn out to be a very important step for understanding better the long term evolution of rings.
- Get the sizes and densities of the small satellites, in particular the underdense small satellites near the rings. By the same token, discover new populations of small satellites near the rings, as the present limit (5 km or so) is fixed by the *Voyager* cameras capabilities, and not by ring dynamics itself.

References

Binney, J. and Tremaine, S.: 1988, *Galactic Dynamics*, Princeton University Press.

Borderies, N., Goldreich, P., and Tremaine, S.: 1984, 'Unsolved problems in planetary ring dynamics', in R. Greenberg and A. Brahic (eds.), *Planetary rings*, The University of Arizona Press, pp. 713–734.

Borderies, N., Goldreich, P., and Tremaine, S.: 1989, 'The formation of sharp edges in planetary rings by nearby satellites', *Icarus* **80**, 344–360.

Burns, J.A., Lamy, P.L., and Soter, S.L.: 1979, 'Radiation forces on small particles in the solar system', *Icarus* **40**, 1–48.

Burns, J.A., Hamilton, D.P., Nicholson, P.D., de Pater, I., Ockert-Bell, M.E., and Thomas, P.C.: 2001, 'The formation of Jupiter's faint ring', *Science* **284**, 1446–1450.

Burns, J.A., Simonelli, D.P., Showalter, M.R., Hamilton, D.P., Porco, C.C., Esposito, L.W., and Throop, H.: 2004, 'Jupiter's Ring-Moon System', in F. Bagenal, T. Dowling, and W. McKinnon (eds.), *Jupiter: Planet, Satellites and Magnetosphere*, Cambridge University Press, in press.

Chiang, E.I, and Goldreich, P: 2000, 'Apse alignment of narrow eccentric planetary rings', *Astron. J.* **540**, 1084–1090.

Colombo, G., Goldreich, P., and Harris, A.W: 1977, 'Spiral structure as an explanation for the asymmetric brightness of Saturn's A ring', *Nature* **264**, 344–345.

Cuzzi, J.N., Lissauer, J.J., Esposito, L.W., Holberg, J.B., Marouf, E.A., Tyler, G.L., and Boischot, A.: 1984, 'Saturn's rings: properties and processes', R. Greenberg and A. Brahic (eds.), *Planetary rings*, The University Of Arizona Press, pp. 73–199.

Cuzzi, J.N. and Burns, J.A.: 1988, 'Charged particle depletion surrounding Saturn's F ring: Evidence for a moonlet belt', *Icarus* **74**, 284–324.

Cuzzi, J.N.: 1995, 'Evolution of planetary ringmon systems', *Earth, Moon, and Planets* **67**, 179–208.

Cuzzi, J.N., *et al.*: 2002, 'Saturn's rings: pre-Cassini status and mission goals', *Space Sci. Rev.* **104**, 209–251.

de Pater, I., Showalter, M.R., Burns, J.A., Nicholson, P.D., Liu, M.C., Hamilton, D.P., Graham, J.R.: 1996, 'Keck infrared observations of Jupiter's ring system near Earth's 1997 ring plane crossing', *Icarus* **138**, 214–223.

Dumas, C., Terrile, R.J., Smith, B.A., Schneider, G., and Becklin, E.E: 1999, 'Stability of Neptune's ring arcs in question', *Nature* **400**, 733–735.

Esposito, L.W., O'Callaghan, M., and West, R.A.: 1983, 'The structure of Saturn's rings: implications from the Voyager stellar occultation', *Icarus* **56**, 439–452.

Esposito, L.W., Cuzzi, J.N., Holberg, J.B., Marouf, E.A., Tyler, G.L., and Porco, C.C.: 1984, 'Saturn's rings: structure, dynamics and particle properties', T. Gehrels and M.S. Matthews (eds.), *Saturn*, The University of Arizona Press, Tucson, pp. 463–545.

Esposito, L.W., Brahic, A., Burns, J.A., and Marouf, E.A.: 1991, 'Particles properties and processes in Uranus' rings', in J.T. Bergstralh, E.D. Miner, and M.S. Matthews (eds.), *Uranus*, The University of Arizona Press, Tucson, pp. 410–465.

Esposito, L.W.: 1993, 'Understanding planetary rings', *Annu. Rev. Earth Planet. Sci.* **21**, 487–523.

Esposito, L.W.: 2002, 'Planetary Rings', *Rep. Prog. Phys.* **65**, 1741–1783.

French, R.G., Nicholson, P.D., Porco, C.C., and Marouf, E.A.: 1991, 'Dynamics and structure of the Uranian rings', in J.T. Bergstralh, E.D. Miner, and M.S. Matthews (eds.), *Uranus*, The University of Arizona Press, Tucson, pp. 327–409.

Goldreich, P.: 1992, 'Puzzles and prospects in planetary ring dynamics', S. Ferraz-Mello (ed.), *Chaos, resonance and collective dynamical phenomena in the solar system*, Kluwer Academic Publishers, Dordrecht Boston London, pp. 65–73.

Goldreich, P., and S. Tremaine, S.: 1982, 'The dynamics of planetary rings', *Ann. Rev. Astron. Astrophys* **20**, 249–283.

Goldreich, P., Tremaine, S., and Borderies, N.: 1986, 'Towards a theory for Neptune's arc rings', *Astron. J.* **92**, 490–494.

Goldreich, P., Rappaport, N., and Sicardy, B.: 1995 'Single-sided shepherding', *Icarus* **118**, 414–417.

Grün, E., Morfill, G.E., and Mendis, D.A.: 1984, 'Dust-magnetosphere interactions', in R. Greenberg and A. Brahic (eds.), *Planetary rings*, The University of Arizona Press, Tucson, pp. 275–332.

Hamilton, D.P. and Burns, J.A.: 1993, 'Lorentz and gravitational resonances on circumplanetary particles', *Adv. Space Res.* **13**, 241–248.

Hamilton, D.P. and Burns, J.A.: 1994, 'The origin of Saturn's E ring: self-sustained, naturally', *Science* **264**, 550–550.

Harris, A.W.: 1984, 'The origin and evolution of planetary rings', in R. Greenberg and A. Brahic (eds.), *Planetary rings*, The University of Arizona Press, pp. 641–659.

Hubbard, W.B., Brahic, A., Sicardy, B., Elicer, L.R., Roques, F., and F. Vilas: 1986, 'Occultation detection of a Neptunian ring-like arc', *Nature* **319**, 636–640.

Marouf, E.A., Tyler, G.L., Zebker, H.A., Simpson, R.A., and Eshleman, V.R.: 1987, 'Particle size distributions in Saturn's rings from Voyager 1 radio occultation', *Icarus* **54**, 189–211.

Meyer-Vernet, N. and Sicardy, B.: 1987, 'On the physics of resonant disk-satellite interaction', *Icarus* **69**, 157–175.

Namouni, F. and Porco, C.: 2002, 'The confinement of Neptune's ring arcs by the moon Galatea', *Nature* **417**, 45–47.

Nicholson, P.D. and Dones, L.: 1991, 'Planetary rings', *Rev. Geophys.* **29**, 313–327.

Nicholson, P.D., Hamilton, D.P., Matthews, K., and Yoder, C.F.: 1992, 'New observations of Saturn's coorbital satellites', *Icarus* **100**, 464–484.

Nicholson, P.D., Mosqueira, I., and Matthews, K.: 1995, 'Stellar occultation observations of Neptune's rings', *Icarus* **113**, 293–330.

Pilcher, C. B., Chapman, C.R., Lebofsky, L.A., and Kieffer, H.H.: 1970, 'Saturn's rings: Identification of water ice', *Science* **167**, 1372–1373.

Porco, C.: 1991, 'An explanation for Neptune's ring arcs', *Science* **400**, 995–1001.

Porco, C.C., Cuzzi, J.N., Esposito, L.W., Lissauer, J.J., and Nicholson, P.D.: 1995, 'Neptune's rings', in D.P. Cruikshank (ed.), *Neptune and Triton*, The University of Arizona Press, Tucson, pp. 703–804.

Poulet, F., Sicardy, B., Nicholson, P.D., Karkoschka, K., and Caldwell, J.: 2000, 'Saturn's ring-plane crossings of August and November 1995: a model for the new F-ring objects', *Icarus*, **144**, 135–148.

Poulet, F. and Cuzzi, J.N.: 2002, 'The Composition of Saturn's Rings', *Icarus* **160**, 350–358.
Poulet, F., Cruikshank, D.P., Cuzzi, J.N., Roush, T.L., and French, R.G.: 2003, 'Compositions of Saturn's rings A, B, and C from high resolution near-infrared spectroscopic observations', *Astron. Astrophys.* **412**, 305–316.
Rosen, P.A., Tyler, G.L., Marouf, E.A., and Jack J. Lissauer, J.J.: 1991, 'Resonance structures in Saturn's rings probed by radio occultation: II. Results and interpretation', *Icarus* **93**, 25–44.
Showalter, M.R.: 2004, 'Disentangling Saturn's F Ring I. Clump Orbits and Lifetimes', *Icarus*, submitted.
Shu, F.H.: 1984, 'Waves in planetary rings', R. Greenberg and A. Brahic (eds.), *Planetary rings*, The University of Arizona Press, pp. 513–561.
Sicardy, B., Roques, F., and A. Brahic: 1991, 'Neptune's rings, 1983–1989: ground-based stellar occultations observations. I. Ring-like detections', *Icarus* **89**, 220–243.
Sicardy, B., Roddier, F., Roddier, C., Perozzi, E., Graves, J.E., Guyon, O., and Northcott, M.J.: 1999, 'Images of Neptune's ring arcs obtained by a ground-based telescope', *Nature* **400**, 731–733.
Smith, B.A., *et al.*: 1986, 'Voyager 2 at Uranus in the Uranian system: Imaging science results', *Science* **233**, 43–64.
Smith, B.A., *et al.*: 1989, 'Voyager 2 at Neptune: Imaging Science results', *Science* **246**, 1422–1449.
Toomre, A.: 1964, 'On the gravitational stability of a disk of stars ' *Astrophys. J.* **139**, 1217–1238.
Tremaine, S.: 2003, 'On the Origin of Irregular Structure in Saturn's Rings', *Astron. J.* **125**, 894–901.
Ward, W.: 1984, 'The solar nebula and the planetesimal disk', in R. Greenberg and A. Brahic (eds.), *Planetary rings*, The University of Arizona Press, Tucson, pp. 660–684.

Address for Offprints: Bruno Sicardy, Observatoire de Paris, LESIA, bâtiment 10, 5, Place Jules Janssen, 92195 Meudon Cédex, France; bruno.sicardy@obspm.fr

EXO-ASTROBIOLOGICAL ASPECTS OF EUROPA AND TITAN: FROM OBSERVATIONS TO SPECULATIONS

FRANÇOIS RAULIN
Laboratoire Interuniversitaire des Systèmes Atmosphériques, LISA-UMR CNRS 7583, Universités Paris 7 et Paris 12, 61 Avenue du Général de Gaulle, F-94000 Créteil, France

Received: 18 May 2004; Accepted in final form: 13 October 2004

Abstract. By extrapolating what we know on the origins of life on Earth, and in particular on the chemical processes which gave rise to the first living system, Europa and Titan appear as two major targets for studies of exo/astrobiology in the outer solar system. With the likely presence of water oceans relatively close to its surface, coupled to possible sources of organics, the emergence and sustaining of life on Europa seems possible. On Titan, it cannot be ruled out. But the main exobiological interest of the largest satellite of Saturn is the presence of a complex organic chemistry which shows many similarities with the prebiotic chemistry which allowed the emergence of life on Earth.

Keywords: Europa, Titan, exobiology, astrobiology, organic chemistry, prebiotic chemistry, biological signatures, life

1. Exobiology in the Outer Solar System

Exobiology, generally speaking, is the study of life in the universe. It includes the study of the origins, distribution and evolution of life and of structures and processes related to life in the universe. Astrobiology covers almost the same fields with the addition of the study of the destiny of life. Thus this wide field which is sometimes also called "Exo-astrobiology" includes the study of the origins of life on Earth and elsewhere, as well as the search for extraterrestrial life, but also the search for organic compounds and the study of organic chemistry and in particular prebiotic-like chemistry in extraterrestrial environments.

One can distinguish two types of planetary bodies of prime interest for exo/astrobiology in the Solar System. These are planetary bodies where (extinct or extant) life may be present and bodies where a complex organic chemistry is taking place. Europa is, with Mars, the most important body of the first type. And Titan, Saturn's largest satellite, is probably, along with comets, one of the most exobiologically interesting bodies of this second kind. Indeed, Europa is often considered as the best planetary target (after Mars) for searching for extraterrestrial life in the solar system. Titan, with an environment very rich in organics, is often considered as one of the best targets to look for prebiotic chemistry at a full planetary scale, and is even considered as a possible habitat for extraterrestrial life.

Now what do we know with certainty about these two outer solar system bodies? How far can we extrapolate our knowledge? How is such an exo/astrobiological

Space Science Reviews 116: 471–487, 2005.
DOI: 10.1007/s11214-005-1967-x

vision of these two bodies supported by observations? This paper will revisit such a vision, on the basis of what (we think) we know about the basic prebiotic processes which were involved in the chemical evolution allowing the emergence of life on Earth. This paper will first very briefly overview our current vision of the Origin of Life on Earth. Then it will try to extrapolate this vision to the case of Europa, then to the case of Titan, and answer the questions: what do we know about these planetary objects from an exo/astrobiological perspective? How far can we speculate? How can we test our hypotheses?

Of course, we must keep in mind that terrestrial life is, so far, the ONLY clear case of life we have ...

2. Chemical Evolution and the Origin of Life on Earth

Although the panspermia hypothesis which assumes that Life on Earth came from extraterrestrial living seeds cannot be fully excluded, it is now widely accepted that the first living systems on our planet are the results of a long chemical evolution which preceded biological evolution. This theory, initially introduced by the soviet biochemist A. Oparin in his 1924 book (see Oparin, 1938) and independently by the British biologist J.B.S. Haldane (1929), assumes that life arose on Earth after a long spontaneous (thermodynamically speaking) evolution of organics from simple molecules to complex organic matter including macromolecules capable of self-replication.

It is also widely accepted that the first successful experimental test of this theory is the now well known and classical Stanley Miller experiment (1953), the 50th anniversary of its first publication having just been celebrated! In this experiment, Miller tried to reproduce some of the initial steps of the chemical evolution of the primitive Earth environment, by subjecting to spark discharges in a closed glass reactor, a gas mixture of methane, ammonia, hydrogen and water vapor in the presence of liquid water. These conditions were assumed to mimic the primitive atmosphere of the Earth and of the oceans. After several days of sparking, he was able to detect the presence of several organics in the reactor, including amino acids. This experiment thus demonstrated the possible formation of organic compounds of biological interest from the chemical evolution of a gas mixture, the model of a planetary atmosphere, under energy flow.

Since 1953, hundreds of similar experiments have been carried out, using various conditions, in particular in terms of energy sources, types of reactor and gas mixture compositions (see Raulin and Frère, 1989, and references therein). With the availability of more and more powerful analytical techniques, detailed molecular, and recently, chiral analysis of the products were performed showing the production of very complex material, including precursors of many compounds of biological interest.

Figure 1 summarizes the nature of the organic products obtained from submit-

Gas Mixture	Products	
	Electric Discharge	UV Light
$CH_4 + NH_3 + H_2O$ (+ H_2)	RH (satur. & unsatur.). RCO_2H HCN & other RCN (mainly satur.) H_2CO, other aldehydes ketones, alcohols Solid --> Amino-acids, N-heterocycles	RH (mainly satur.) RNH_2 HCN & other RCN (mainly satur.) H_2CO, other aldehydes ketones, alcohols Solid --> Amino-acids,
$CH_4 + N_2 + H_2O$	RH (satur. & unsatur.). RCO_2H HCN & other RCN (sat, unsat.) including HC_3N & C_2N_2 H_2CO, other aldehydes Solid --> Amino-acids, N-heterocycles	RH (mainly satur.) RCO_2H H_2CO, other aldehydes at low yield
$CO + NH_3 + H_2O$	HCN Solid --> Amino-acids	
$CO + N_2 + H_2O$ (+ $H^{\#}$) ($^{\#}$: proton irradiation)	RH, CO_2, H_2, NH_3 Solid --> Amino-acids, imidazole	H_2CO, ketones, alcohols Solid --> Amino-acids,
$CO_2 + N_2 + H_2O + H_2$	RH (mainly satur). HCN Other RCN (mainly sat.) H_2CO, other aldehydes Ketones Solid --> Amino-acids	
$CO_2 + N_2 + H_2O$	CO, N_2O Very low organics production	CO, H_2, O_2 Very low organics production

Figure 1. Gas phase organic syntheses from electric discharge or UV irradiation of model atmospheres.

ting gas mixtures of various starting composition to electron or photon irradiation. Three important behaviors can be identified from these experimental data:

1. only reducing mixtures (strongly, such as CH_4-NH_3-H_2-H_2O mixtures or even slightly, such as CO-N_2-H_2O mixtures) allow the production of organic molecules. On the contrary, oxidized mixtures such as CO_2-N_2-H_2O do not give rise to the synthesis of organics at a noticeable level, except if H_2 is present with a H_2/CO_2 ratio close to or higher than 1 (Miller, 1998, and references therein).
2. the gas mixture which gives rise to the widest variety of organics, and in particular to the largest variety of organics of prebiotic (see below) intererest is a N_2-CH_4-H_2O mixture.
3. when organics are produced, the formation occurs in the gas phase but also in the solid phase: the solid products are a prebiotic source of compounds of biological interest, such as amino acids and purine and pyrimidine bases. These solid products are often called "Tholins." This word was invented by Sagan and Khare (1979) (from the Greek word "tholos", meaning muddy) as a generic name for the solid produced during these simulation experiments.

Today, Miller's experiment is not considered anymore as representative of the chemical processes which occurred on the primitive Earth. It required a reduced mixture to allow the production of organic compounds at a detectable concentration and such a mixture does not fit with our current model of the primitive atmosphere of the Earth. However, with his experiment, Miller initiated the development of systematic experimental research on the theory of chemical evolution and the origins of life, and he simultaneously opened a completely new field: prebiotic chemistry. Prebiotic chemistry is organic chemistry in aqueous solution, under plausible conditions of the primitive terrestrial environment, leading to compounds of biological interest.

Miller and many others have studied possible chemical mechanisms involved in the formation of the organic compounds of biological importance in these simulation experiments (see, for instance Miller and Orgel, 1974; Raulin, 1990; Brack, 1998; and references therein). For Miller, the main mechanism of formation of amino acids involves the reaction of HCN with aldehydes in the presence of ammonia in liquid water (so called "Strecker synthesis", well known to organic chemists for more than a century). The corresponding pathways form an aminonitrile the hydrolysis of which produces the corresponding amino acid. Indeed, amino acids are not formed as free amino acids in simulation experiments, but are released from the hydrolysis of a precursor. However, it is not demonstrated that the precursor is the related aminonitrile, because such mechanism would require the (unlikely) formation of a large variety of aldehydes in noticeable concentration, to explain the large variety of amino acids. Another mechanism – although contested – involves HCN polymers or HCN oligomers (Ferris and Hagan, 1984, and references therein). But the most likely mechanism is the formation of even more complex oligomers, complex macromolecular organics of irregular molecular structure –

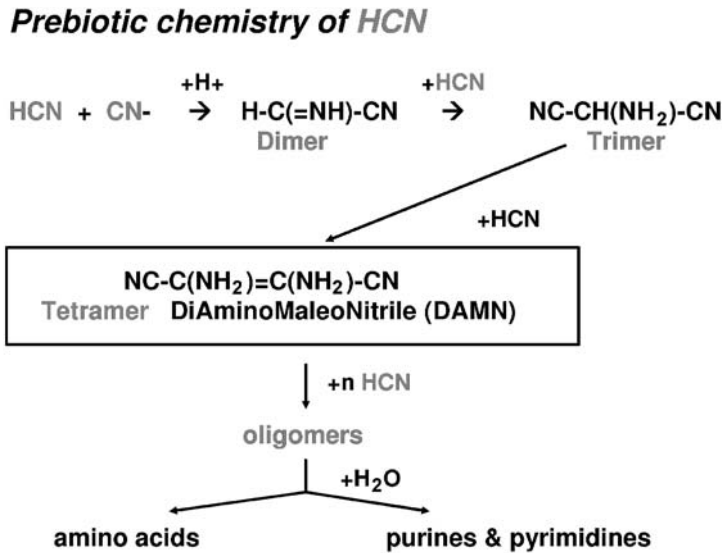

Figure 2. The different pathways of the prebiotic chemistry of hydrogen cyanide.

the tholins, whatever their molecular composition is – followed by their hydrolysis in aqueous solution.

Basic prebiotic chemistry is thus based on the evolution in liquid water of simple and reactive organics like formaldehyde, HCHO, hydrogen cyanide, HCN, cyanoacetylene, HC_3N and other nitriles, and their polymers or oligomers, as well as refractory complex organics, such as tholins. Indeed, the chemistry in aqueous solutions of compounds as simple as HCN, thanks to its molecular structure with a reactive triple bond, or its oligomers, including its tetramer, can produce several molecules of biological interest, including amino acids and heterocyclic bases, as shown in Figure 2.

Of course, in the 50 years of research in this field, the detailed scenario of terrestrial chemical evolution – still very tentative – has drastically evolved!! As mentioned above, the primitive atmosphere of the Earth was probably not the starting point of the prebiotic organic processes, since its main composition (CO_2-N_2-H_2O) was not favorable to the formation of organics.

The main sources of organics are currently believed to be (i.e. Brack, 1998):

- Extraterrestrial influx (comets – nucleus and interplanetary cometary dust, macro- and micro- meteorites.)
- Syntheses of organic matter from inorganic molecules in the vicinity of submarine hydrothermal vents, as well as in shallow basins.

However, the general idea and ingredients involved in the processes of chemical evolution and prebiotic chemistry are still the same, namely Organic matter + Liquid water + Energy. Now, all these ingredients are indeed present on Europa and Titan.

3. Europa

The idea of the possibility of life on Europa is not new: it has developed since the discovery of the possibility of a water ocean below the surface crust of water ice at the time of the Voyager data. Many papers have been published since that time on this question (see for instance, Chyba and Phillips, 2002, for a recent review). The subsurface ocean considered in the recent model published by Melosh *et al.* (2004) implies an ice shell of about 15 km covering a 100 km deep ocean, the temperature of which corresponds to the temperature of water at its maximum density (4 °C). Reynolds *et al.* (1983) reviewed the general requirements for life and examined the possible different sources of energy: thermal, solar and electrical. They estimate a possible biomass density based on solar energy availability of 2×10^{-6} g m^{-2}. This is very small compared to the lower limit of the value of the biomass for the Earth (about 1000 to 10000 g m^{-2}). Nevertheless, this indicates the possible presence of a very limited but not negligible. Furthermore, one must keep in mind that these calculations for Europa are only based on solar energy. Those numbers are only 10^5-10^3 time smaller than the terrestrial biomass. The current value of possible biomass may be higher if the other energy sources present on Europa, in particular heat delivery by radiogenic heat flow, are important. Indeed, more recently, Chyba and Phillips in a very detailed paper (2002), estimate a total steady state biomass for Europa of about 10^{13}-10^{15} g, assuming additional production of hydrogen and oxygen, in the ice and the ocean, through the decay of radioactive ^{40}K, and a biomass turnover time of about 1000 years.

But persistence of life is one aspect, emergence of life is another. Did Europa once include all conditions necessary for chemical evolution to evolve through prebiotic chemistry to self-replicating systems, and biological systems? Water is present but what about organics?

Organics may have been imported to Europa from meteorites, as this probably occurred on Earth. Furthermore, Galilean satellites may be largely made of material from carbonaceous meteorites (Kargel *et al.*, 2000). This fits with the density of CII chondrites (2.5-2.9 relative to water) which is close to that of Europa ($\sim$3). Now CII chondrites include about 2.5% C and 13.5% of H_2O. Since Europa may contain more than 7% of H_2O in mass, if the assumption that it is made of CII chondrites is valid, it may also contain about 1% by mass of carbon atoms (Oro *et al.*, 1992). 50% of this carbon is in the form of a water insoluble complex organic matter. Its chemistry at high temperature (by analogy with the terrestrial deep see vent conditions) may induce the formation of organics of biological interest.

The water soluble organic fraction may represent about 0.05% of the mass of Europa. This includes many organics of biological interest and would correspond to a concentration of dissolved organic carbon in Europa's oceans as high as about 1% (assuming that most of the water is in the liquid phase). A concentration of 1% by mass of organics may be sufficient for an efficient prebiotic evolution, depending on the chemical nature of the organics. For instance, a concentration of 0.1 M of

HCN in aqueous solution (equivalent to 0.3% by mass) allows the polymerization of HCN toward its tetramer and higher oligomers shown on Figure 2. Low temperatures reduce the rate constants of prebiotic chemical reactions, but may increase the concentration of reacting organics by eutectic effect which increases the rate of the reaction. In addition, high pressure conditions such as those present in subsurface oceans, may also induce chemical condensation reactions, essential for the formation of biological macromolecules starting form their monomers, such as polypeptides and polynucleotides from their building blocks (amino acids and nucleotides).

Finally, hydrothermal vents, if they are present on the floor of Europa's oceans, are also favorable locations for increasing chemical complexity, thanks to the heterogeneous processes which can occur at the interface between the hot gases and liquid and solid phases. These processes can be favored by the potential catalytic properties of the mineral phases and by the high thermal gradients, which protect the products from thermal degradation.

Very recent examination of the temperatures of Europa's ocean, suggest that it could have been relatively warm (Melosh *et al.*, 2004). Thus Europa's conditions seem compatible with the emergence and sustaining of life, although a panspermia origin cannot be totally ruled out, but seems very unlikely because of too high energy levels involved during impacts on Europa's surface, due to the absence of dense atmosphere. But what kind of life can we expect? Although a biological evolution to eukaryotic life cannot be excluded (Chela-Flores, 1998, and references therein) a prokaryotic and anaerobic life seems more probable. Archaebacteria-like organisms seems the most likely biota on Europa (Chela-Flores, 1998). Terrestrial archaebacteria are indeed good examples of what can be expected (cf. also D. Prieur, this book). There is a large number of possible examples with different metabolic activities (Oro *et al.*, 1992) as shown on Table I.

How could we detect such life on Europa? The best approach would be a "Hydrobot/cryobot" mission including a cryobot melter probe able to traverse the several kilometers thick ice crust and to release a submersible in the (still hypothetical) Europa oceans. The later could search for hypothetical hydrothermal vents, and, in their vicinity, for hypothetical micro-organisms. However, such a mission raises many crucial problems, in addition to its cost. First it is required to translate terrestrial technology to space; such a translation is far from obvious.

The terrestrial example of lake Vostok in Antarctica (Souchez *et al.*, 2002), is a clear illustration of the problem: after several years of exploration of this subsurface (3 km below the surface) lake, the top of this liquid body has only been reached. Now, scientists are hesitating to go in it. Indeed the problem of biological contamination is crucial in this case, and would be even more crucial in the case of an extraterrestrial liquid water body. Furthermore, the expected density of the biomass in the Europa oceans, as indicated above, may be quite low (about 10 orders of magnitude less than on Earth). Thus, the biological activity in the

TABLE I

Examples of terrestrial organisms of interest for Europa (Oro *et al.*, 1992).

Methanogenic archaebacteria:
Heterotrophic (fermentation): organics + $H_2 \Rightarrow CH_4$ + biosynthetic products
organics = methanol, methylamine, formate, acetate, ...
Autotrophic (CO_2 reduction): $CO_2 + H_2$ or $Fe^o \Rightarrow CH_4$ + biosynthetic products
Thermophilic archaebacteria:
Heterotrophic: (fermentation): yeast extract $\Rightarrow CO_2$ + biosynthetic products
(S respiration): organics + S $\Rightarrow H_2S + CO_2$ + biosynthetic products
Autotrophic: (S reduction): $CO_2 + H_2 + S \Rightarrow H_2S$ + biosynthetic products
organics = alcohols, sugars, formate, acetate, ...
Photosynthetic bacteria:
Photoheterotrophic (anaerobic): organics + light $\Rightarrow$ biosynthetic products
Photoautotrophic (anaerobic): $CO_2 + 2H_2S$ + light $\Rightarrow S_2 + H_2O$ + (HCHO)
Photoautotrophic (oxygenic): $CO_2 + H_2O$ + light $\Rightarrow O_2$ + (HCHO)

hypothetical Europa oceans may be quite limited and difficult to detect, and the importance of potential biological contamination seems much higher.

Consequently, an orbiter mission seems much more reasonable. This will be possible with the NASA-JIMO (Jupiter Icy Moons) mission. It would offer a detailed mapping of Europa and provide data allowing confirmation of the existence of internal oceans. Such mission would also permit a search for traces of biological activity by looking for molecular signatures of metabolic activity such as CH_4, H_2S, HCHO .... It should be emphasized that the presence of organics in an oxidized environment is a clear sign of conditions far from equilibrium, and, consequently a potential sign of life. But such a mission would also need very sensitive techniques (since concentrations may be very low), and isotopic separation capabilities (to measure the $^{13}C/^{12}C$ ratio in particular) to secure the interpretation of the biological origin of these molecules, such as CH_4.

4. Titan

The presence of organics on and in Europa is still speculative, as well as liquid water. On Titan, the presence of liquid water is speculative, but that of organics is not. Only satellite of the solar system having a dense atmosphere. This atmosphere is mainly made of dinitrogen with a few percent of methane, efficient source of organics. Indeed, organic compounds are very abundant in the gas phase and probably in the aerosol phase. In addition to many analogies with the Earth (main chemical composition and vertical profile of the atmosphere, physical and

chemical couplings, energy sources, greenhouse effects, etc. ...) Titan is a planetary body of prime exobiological interest, because of the presence of a complex organic chemistry.

The initial step of this chemistry is relatively well understood. It starts with the dissociation of N_2 and CH_4 through electron and photon impacts. In these processes C_2H_2 and HCN play a key role. These key molecules are formed in the high atmosphere. They then diffuse down to the lower levels where they allow the formation of higher hydrocarbons and nitriles. Additional CH_4 dissociation is supposed to occur in the low stratosphere through a photocatalytic process involving C_2H_2 and polyynes.

Titan's organic chemistry is well mimicked in the laboratory with simulation experiments. Indeed, recent experiments carried out in particular at LISA produce all organic species already detected in the gas phase in Titan's atmosphere, with the right orders of magnitude of relative concentration for most of them. This observation provides an important validation of such experimental simulations. These experiments also produce many other organics. One can extrapolate these results and assume that these additional organics are also present in Titan's atmosphere. Thus, simulation experiments appear as a very useful guide for further searches (both by remote sensing and in situ observations). This, in fact, includes not only the gas phase but also the aerosol phase.

In the gas phase, more than 150 different organic molecules have been detected in the simulation experiments which seem to be the more representative (Coll *et al.*, 1998; 1999a). These global simulations of Titan's atmospheric chemistry use an open reactor flown by a low pressure N_2-CH_4 gas mixture. The energy source is a cold plasma discharge producing mid-energy electrons (around 1-10 eV). The gas phase end products (molecules) are analyzed by IRFTS (Infra Red Fourier Transform Spectroscopy) and GC-MS (Gas Chromatography and Mass Spectrometry) techniques; the transient species (radicals and ions) are determined by on line UV-visible spectroscopy. The evolution of the system is also theoretically described using coupled physical and chemical (ions and neutrals) models. The identified organic products are mainly hydrocarbons and nitriles. The absence of amines at a detectable level, with the exception of ammonia, must be highlighted. These experiments have allowed the detection of all gaseous organic species observed on Titan, including C_4N_2, although unstable at room temperature (Coll *et al.*, 1999b). Among the other organics formed in these experiments and not yet detected in Titan's atmosphere, one should note polyynes (C_4H_2, C_6H_2, C_8H_2) and probably cyanopolyyne HC_4-CN. These compounds are also included in photochemical models of Titan's atmosphere (see Strobel, 2005), where they could play a key role in the chemical schemes allowing the transition from the gas phase products to the aerosols. Also of exobiological interest is the formation of organic compounds with asymmetric carbon such as

CH_3–$C^*H(C_2H_5)$–CH=CH_2 and CH_3–C^*H(CN)–CH=CH_2.

Recent experiments on N_2–CH_4 mixtures including CO at the 100 ppm level (Bernard *et al.*, 2003; Coll *et al.*, 2003) show the incorporation of O atoms in the produced organics, with an increasing diversity of the products (more than 200 were identified). The main O-containing organic compound is neither formaldehyde nor methanol, as expected from theoretical models (both thermodynamic and kinetic), but oxirane (also named ethylene oxide), $(CH_2)_2O$. Oxirane thus appears as a good candidate to search for in Titan's atmosphere. These studies also show the formation of ammonia at noticeable concentration, opening new avenues in the chemical schemes of Titan's atmosphere.

Simulation experiments also produce solid organics, as mentioned above, usually named tholins. These "Titan tholins" are supposed to be laboratory analogues of Titan's aerosols. They have been extensively studied since the first work by Sagan and Khare more than 20 years ago (Khare *et al.*, 1984; 1986; and references therein). These laboratory analogues show very different properties depending on the experimental conditions. For instance, the average C/N ratio of the product varies between less than 1 to more than 11, in the published reports. More recently, dedicated experimental protocols allowing a simulation closer to the real conditions have been developed at LISA using low pressure and low temperature (Coll *et al.*, 1998; 1999a) and recovering the laboratory tholins without oxygen contamination (from the air of the laboratory) in a glove box purged with pure N_2. Representative laboratory analogues of Titan's aerosols have thus been obtained and their complex refractive indices have been determined (Ramirez *et al.*, 2002), with – for the first time – error bars. These data can be seen as a new point of reference to modelers who compute the properties of Titan's aerosols. More recently systematic studies have been carried out on the influence of the pressure of the starting gas mixture on the elemental composition of the tholins. They show that two different chemical-physical regimes are involved in the processes, depending on the pressure, with a transition pressure around 1 mbar (Bernard *et al.*, 2002). This has been confirmed by an independent study very recently (Imanaka *et al.*, 2004).

The molecular composition of these Titan tholins is still very poorly known. Several hypotheses have been published already including HCN polymers or oligomers, HCN-C_2H_2 co-oligomers, HC_3N polymers, HC_3N-HCN co-oligomers (Tran *et al.*, 2003, and references therein). In any case, it seems well established that they are made of macromolecules of relatively low molecular weight (a few thousand Daltons) of largely irregular structure. Indeed, gel filtration chromatography of the water soluble fraction of Titan tholins shows an average molecular mass of about 500 to 1000 Dalton (McDonald *et al.*, 1994). Nevertheless information on the chemical groups included in their structure has been obtained from the determination of their IR and UV spectra and from analysis by pyrolysis-GC-MS techniques (Ehrenfreund *et al.*, 1995; Coll *et al.*, 1998; Imanaka *et al.*, 2004; and references therein). The data shows the presence of aliphatic and benzenic hydrocarbon groups, of CN, NH_2 and C=NH groups. Direct analysis by chemical derivatization techniques before and after hydrolysis allowed the identification

of amino acid or their precursors (Khare *et al.*, 1986). As already mentioned, their optical properties have been determined (Khare *et al.*, 1984; McKay *et al.*, 1996; Ramirez *et al.*, 2002; Tran *et al.*, 2003; Imanaka *et al.*, 2004), because of their importance for retrieving observational data related to Titan. Finally, it is obviously of exo/astrobiological interest to mention that the nutritious properties of Titan tholins for micro-organisms (limited to terrestrial bacteria ...) have also been studied (Stoker *et al.*, 1990) showing that indeed some bacteria do like such nutrients!

Nevertheless, there is a clear need for more systematic studies of these laboratory analogues of Titan aerosols, with new analytical approaches. But there is also a need for a better understanding of the mechanisms involved in the cold plasma for carrying out a more secure extrapolation to Titan. More generally speaking, there is a need for better experimental simulations, where the primary processes are well mimicked including the dissociation of dinitrogen by electron impact with energies close to the case of Titan's atmosphere, and the dissociation of methane through photolysis processes. Such an experiment is currently under development at LISA, with the SETUP (Simulation Expérimerntale et Théorique Utile à la Planétologie) programme which, in a dedicated low temperature flow reactor, couples N_2 dissociation by electron and CH_4 photodissociation by 2 photon (248 nm) laser irradiation, and theoretical studies, in order to improve the chemical schemes. The preliminary results demonstrate the dissociation of methane through the 2 photon process (Gazeau, personal communication).

Titan organic chemistry may be even more complex. It is very likely that Titan's surface is partly covered by liquid bodies, seas or lakes made of liquid methane and ethane including dissolved dinitrogen and other compounds from the atmosphere. The presence of such bodies was expected when considering the evolution of the atmosphere, its current near surface temperature and the need for a methane reservoir (Lunine, 1993, and references therein). Several recent observations of Titan's surface, in particular the latest radar observation from Campbell *et al.* (2003) give strong support to this hypothesis. Titan tholins and most of the organics of prebiotic interest already detected or likely to be present in Titan's atmosphere show a low solubility in such a solvent (Raulin *et al.*, 1995, and references therein), which does not favour an increase of chemical complexity ... However, cosmic rays reaching Titan's surface may induce organic syntheses in the lakes and seas and the additional formation of reactive compounds such as azides as well as the polymerization of HCN (Raulin *et al.*, 1995). Moreover, the interface between the liquid phase and the solid deposits at the surface may include sites of catalytic activity favorable to these additional chemical reactions.

In spite of the surface temperatures, even the presence of liquid water is not excluded. Cometary impacts on Titan may melt surface water ice, offering possible episodes as long as about 1000 years of liquid water (Artemieva and Lunine, 2003). This provides conditions for short terrestrial-like prebiotic syntheses at relatively low temperatures. As mentioned in the case of Europa, the unfavourable effect of

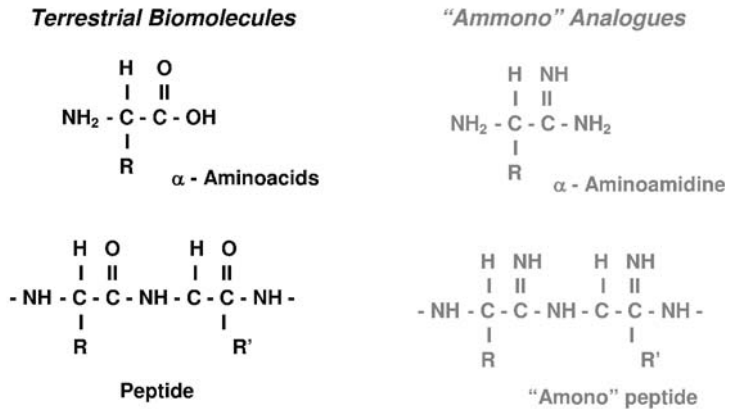

Figure 3. Two examples of "ammono" analogues of biochemical molecules: amino acids and peptides.

low temperatures on the reaction rates can be balanced by the favourable effects of eutectic properties. In addition, the possible presence of a water-ammonia ocean in the depths of Titan, as expected from models of its internal structure (Grasset *et al.*, 2000, and references therein), may also provide an efficient way to convert simple organics into complex molecules, and to reprocess chondritic organic matter into prebiotic compounds. These processes may have very efficiently occurred at the beginning of Titan's history (with even the possibility of the water-ammonia ocean exposed to the surface) allowing a CHNO prebiotic chemistry evolving to compounds of terrestrial biological interest.

Even if these liquid water scenarios are false, the possibility of a pseudo biochemistry, evolving in the absence of a noticeable amount of O atoms cannot be ruled out, with a N-chemistry, based on "ammono" analogues (Figure 3) replacing the O-chemistry (Raulin and Owen, 2002). Such alternatives of terrestrial biochemistry where, in particular the water solvent could be replaced by ammonia or other N-compounds, have also been recently re-examined by Benner (2002) and by Schulze-Makuch and Irwin (2004).

Thus several ways can be envisaged to drive chemistry to prebiotic chemistry and even to biotic systems on Titan. But if life emerged on Titan, are Titan's conditions compatible with the sustaining of life? The surface is too cold and not energetic enough to provide the right conditions. However, the (hypothetical) subsurface oceans may be suitable for life. Fortes (2000) has shown that there are no insurmountable obstacles. With a possible temperature of this ocean as high as about 260 K and the possible occurrence of cryovolcanic hotspots allowing 300 K, the temperature conditions in Titan's subsurface oceans could allow the development of living systems. Even at depth of 200 km, the expected pressure of about 5 kbar is not incompatible with life, as shown by terrestrial examples. The expected pH of an aqueous medium made of 15% by weight of NH_3 is equivalent to a pH of 11.5. Some bacteria can grow on Earth at pH 12. Even the limited

energy resources do not exclude the sustaining of life. Taking into account only the potential radiogenic heat flow ($\sim 5 \times 10^{11}$ W) and assuming that 1% of that is used for volcanic activity and 10% of the later is available for living system metabolism, Fortes (2000) estimates an energy flux available in the subsurface oceans of about 5×10^8 W. Such a flux corresponds to the production of about 4×10^{11} mol of ATP per year and about 2×10^{13} g of biomass per year. If we assume an average turn over for the living systems of the order of a year, the biomass density would be 1 g/m^2. This is higher than on Europa!

Which life can we expect, if any, on Titan? Possible metabolic processes such as nitrate/nitrite reduction or even nitrate/dinitrogen reduction, sulphate reduction and methanogenesis have been considered (Simakov, 2001). It has also been suggested that catalytic hydrogenation of acetylene may be used as a metabolic pathway by Titan's micro-organisms (Abbas and Schulze-Makuch, 2002). If it seems very unlikely that the main constituent of Titan's atmosphere, dinitrogen, is of biological origin (models of the origin and evolution of the atmosphere do not need such a hypothesis, see Owen, 2000), the situation is different for methane. Methanogenic micro-organisms could be one of the potential sources of methane needed to explain the presence of methane in the atmosphere today, in spite of its (relatively) short life time (a few tens million years). But several other sources are possible, including, in addition to the already mentioned surface lakes or seas, cometary impact chemistry (Kress and McKay, 2004) and the presence of methane hydrates in the deep structure of Titan, feeding the atmosphere with the help of surface cryovolcanism. In fact, beyond the exobiological aspects, the origin of methane in Titan's atmosphere is a key question. It shows the whole complexity of Titan's system, which by itself may be almost considered as a living system since it includes many of the characteristics of life: open system, capable of self reproduction (the organics in its environment), and following a long term evolution.

5. Cassini-Huygens Returns

Many of the questions which have been raised above should get answers from the Cassini-Huygens mission which will provide many data of great importance for Exo/astrobiology: We can expect the discovery of many additional atmospheric molecules, including many other organics in particular through the Cassini CIRS (Composite Infra-Red Spectrometer) and the Huygens GC-MS experiments. These instruments will also determine the vertical profiles of many organics, essential to constrain the chemical schemes involved in their formation and, more generally the (photo)chemical models. Cassini-Huygens will allow the first determination of the chemical composition of Titan's aerosols, through the combined ACP (Aerosols Collector and Pyrolyser) and GC-MS experiments. It will allow the determination of the surface states and composition providing essential data on the chemical nature and complexity of the surface. It will allow the confirmation of the presence

of the liquid bodies on Titan's surface and the determination of their composition. Several of the Cassini-Huygens instruments will provide data allowing the quantification of the energy sources in Titan's environment. In particular the possible detection of tropospheric lightning may open new possibilities for organic syntheses in the troposphere. The possible detection of volcanic activity and/or cryovolcanism on Titan' surface will have important consequences for our understanding of the source of methane in the atmosphere and on the origins of the atmosphere. The determination of $^{12}C/^{13}C$ will also provide information on the origin of atmospheric methane, and will indicate if it could be of biological origin (if the observed value is much lower than the solar value) or not. Similar information concerning the origin of N_2 could be obtained from the determination of $^{14}N/^{15}N$ in the atmospheric dinitrogen.

We can expect many other answers to questions of exo/astrobiological interest mentioned above, through the enormous amount of new data expected from this paramount planetary mission, but also many unexpected questions in addition. We thus must also be ready for the unexpected!

Furthermore, several questions will still remain unsolved. This is the case, in particular for the possible presence of enantiomeric excess in the chiral organics present in the gas phase and in the solid phase. Cassini-Huygens will not be able to give detailed data concerning the complexity in the surface organic chemistry, and even less on the complexity in the subsurface organic chemistry. Clear answers to these questions require post Cassini-Huygens in situ exploration of Titan, already considered ... (Lorenz, 2000).

6. Conclusions

Europa is often considered as the best target for searching for extraterrestrial life (after Mars). Indeed the emergence of life on the Galilean satellite cannot be ruled out, nor the possibility of bacterial importation. Moreover, it seems to be a potential harbour for living systems. But direct search for (hypothetical) living systems in the (still hypothetical) Europa subsurface oceans is very speculative and technically difficult. In particular, the problem of potential contamination during such a search for Europa's life is crucial. Indirect search from a detailed spectral mapping of the surface from an orbiter is much easier and within the current technical capabilities.

Titan is a place where a prebiotic-like chemistry is occuring on a planetary scale. But this chemistry is evolving in the quasi-absence of liquid water. The emergence of life although not very likely, because of the low temperatures and energy fluxes, cannot be ruled out. But the level of chemical complexity which can be reached in such an environment is still fully unknown. The Cassini-Huygens mission should be able to provide a fantastic amount of new data of exo/astrobiological importance to Titan, in particular on the complexity of its prebiotic-like chemistry and on the origin of methane, the main source of this chemistry.

Finally, the complementarities of these two planetary bodies for exo/astrobiology should be pointed out. Europa with its likely presence of water may include also organics in its deep structure. Titan, with its organic rich atmosphere and surface, may also include liquid water in its deep structure.

Acknowledgements

Several of the data presented in this paper have been obtained by the following LISA-GPCOS team members: Yves Benilan, Jean-Michel Bernard, Patrice Coll, Marie-Claire Gazeau, Eric Hebrard and Claire Romanzin, and with the help of CNES grants and financial supports from University of Paris 12 and GDR CNRS Exobio. The author also wish to thank John Zarnecki for his help in the preparation of the manuscript, as well as the anonymous referee who reviewed this paper: their comments have been very useful to improve the form and scientific content of the paper.

References

Abbas, O., and Schulze-Makuch, D.: 2002, 'Acetylene-based pathways for prebiotic evolution on Titan', *ESA SP-518*, 345–348.

Artemieva, N. and Lunine, J.: 2003, 'Cratering on Titan: impact melt, ejecta, and the fate of surface organics', *Icarus* **164**, 471–480.

Benner, S.: 2002, 'Weird life: chances versus necessity', Communication at "Weird Life" planning session for NRC Committee on the origins and evolution of life, National Academies of Sciences, USA, `http://www7.nationalacademies.org/ssb/weirdlife.html`

Bernard, J.-M., Coll, P., and Raulin, F.: 2002, 'Variation of C/N and C/H ratios of Titan's aerosols analogues', *Proc. 2d European Workshop on Exo-/Astro-Biology, ESA SP-518*, 623–625.

Bernard, J.-M., Coll, P., Coustenis, A., and Raulin, F.: 2003, 'Experimental simulation of Titan's atmosphere detection of ammonia and ethylene oxide', *Planet. Space Sci.* **51**, 1003–1011.

Brack, A. (ed.): 1998, The Molecular Origins of Life: Assembling Pieces of the Puzzle, Cambridge, New York, Sydney: Cambridge University Press.

Campbell, D.B., Black, G.J., Carter, L.M., and Ostro, S.J.: 2003, 'Radar evidence for liquid surfaces on Titan', *Science* **302**, 431–434.

Chela-Flores, J.: 1998, 'Possible degree of evolution of solar-system microorganisms', in J. Chela-Flores and F. Raulin (eds.), *Exobiology: Matter, Energy and Information in the Origin and Evolution of Life in the Universe*, Kluwer Academic Publishers, pp. 229–234.

Chyba, C.F. and Phillips, C.B.: 2002, 'Europa as an abode of life', *Origins of Life and Evolution of the Biosphere* **32**, 47–68.

Clarke, D.W. and Ferris, J.P.: 1997, 'Titan haze: structure and properties of cyanoacetylene and cyano-acetylene-acetylene photopolymers', *Icarus* **127**, 158–172.

Coll, P., Coscia, D., Gazeau, M.-C., and Raulin, F.: 1998, 'Review and latest results of laboratory investigation of Titan's aerosols', *Origins of Life and Evolution of the Biosphere* **28**, 195–213.

Coll, P., Coscia, D., Smith, N., Gazeau, M.C., Ramirez, S.I., Cernogora, G., Israel, G., and Raulin, F.: 1999a, 'Experimental laboratory simulation of Titan's atmosphere: aerosols and gas phase', *Planet. Space Sci.* **47**, 1331–1340.

Coll, P., Guillemin, J.C., Gazeau, M.C., and Raulin, F.: 1999b, 'Report and implications of the first observation of C_4N_2 in laboratory simulations of Titan's atmosphere', *Planet. Space Sci.* **47**, 1433–1440.

Coll, P., Bernard, J.-M., Navarro-González, R., and Raulin, F.: 2003, 'Oxirane: an exotic oxygenated organic compound in Titan?', *Astrophys. J.* **598**, 700–703.

Ehrenfreund, P., Boon, J.P., Commandeur, J., Sagan, C., Thompson, W.R., and Khare, B.N.: 1995, 'Analytical pyrolysis experiments of Titan aerosol analogues in preparation for the Cassini-Huygens mission', *Adv. Space Res.* **15**, 335–342.

Ferris, J.P. and Hagan, W.J.: 1984, 'HCN and chemical evolution: the possible role of cyano compounds in prebiotic synthesis', *Tetrahedron* **40**, 1093–1120.

Fortes, A.D.: 2000, 'Exobiological implications of a possible ammonia-water ocean inside Titan', *Icarus* **146**, 444–452.

Grasset, O., Sotin, C., and Deschamps, F.: 2000, 'On the internal structure and dynamics of Titan', *Planet. Space Sci.* **48**, 617–636.

Haldane, J.B.S.: 1929, *The Origin of Life*, Rationnalist Annual.

Imanaka, H., Khare, B.N., Elsila, J.E., Bakes, E.L.O., McKay, C.P., Cruikshank, D.P., Sugita, S., Matsui, T., and Zare, R.N.: 2004, 'Laboratory experiments of Titan tholin formed in cold plasma at various pressures: implications for nitrogen-containing polycyclic aromatic compounds in Titan haze', *Icarus* **168**, 344–366.

Kargel, J., Kaye, J., Head, J., Marion, G., Sassen, R., Crowley, J., Ballesteros, O., Grant, S. and Hogenboom, D. : 2000, 'Europa's crust and ocean: origin, composition and the prospect for life', *Icarus* **148**, 226–265.

Khare, B.N., Sagan, C., Arakawa, E.T., Suits, F., Callicott, T.A., and Williams, M.W.: 1984, 'Optical constants of organic tholins produced in a simulated Titanian atmosphere: from soft X-rays to microwave frequencies', *Icarus* **60**, 127–137.

Khare, B.N., Sagan, C., Ogino, H., Nagy, B., Er, C., Schram, K.H., and Arakawa, E.T.: 1986, 'Amino acids derived from Titan tholins', *Icarus* **68**, 176–184.

Kress, M.E. and McKay, C.P.: 2004, 'Formation of methane in comet impacts: implications for Earth, Mars, and Titan', *Icarus* **168**, 475–483.

Lorenz, R: 2000, 'Post-Cassini exploration of Titan: science rational and mission concepts', *J. British Interplan. Soc.* **53**, 218–234.

Lunine, J.I.: 1993, 'Does Titan have an ocean? A review of current understanding of Titan's surface', *Rev. Geophys.* **31**, 133–149.

McDonald, G.D., Thompson, W.R., Heinrich, M., Khare, B.N., and Sagan, C.: 1994, 'Chemical investigation of Titan and Triton tholins', *Icarus* **108**, 137–145.

McKay, C.P.: 1996, 'Elemental composition, solubility, and optical properties of Titan's organic haze', *Planet. Space Sci.* **44**, 741–747.

Melosh, H.J., Ekholm, A.G., Showman, A.P., and Lorenz, R.D.: 2004, 'The temperature of Europa's subsurface water ocean', *Icarus* **168**, 498–502.

Miller, S.L.: 1953, 'A production of aminoacids under possible primitive Earth conditions', *Science* **117**, 528–529.

Miller, S.L.: 1998, 'The endogenous synthesis of organic compounds', in A. Brack (ed.), *The Molecular Origins of Life: Assembling Pieces of the Puzzle*, pp. 59-85, Cambridge University Press, Cambridge, New York, Sydney, pp. 59–85.

Miller, S.L. and Orgel, L.: 1974, *The origins of life on the Earth*, Prentice Hall, N. Jersey.

Oparin, A.I.: 1938, *The Origin of Life*, Macmillan, New York.

Oro, J., Squyres, S. W., Reynolds, R.T., and Mills, T.M.: 1992, 'Europa: prospects for an ocean and exobiological implications', in G. Carle, D. Schwartz, and J. Huntington (eds.), *Exobiology in Solar System Exploration*, *NASA SP-512*, 102–125.

Owen, T.: 2000, 'On the origin of Titan's atmosphere', *Planet. Space Sci.* **48**, 747–752.

Ramirez, S.I., Coll, P., Da Silva, A., Navarro-Gonzalez, R., Lafait, J., and Raulin, F.: 2002, 'Complex refractive index of Titan's aerosol analogues in the 200–900 nm domain', *Icarus* **156**, 515–530.

Raulin, F.: 1990, 'Prebiotic syntheses of biologically interesting monomers in aqueous solutions: facts and constraints', *J. British Interplanet. Soc.* **43**, 39–45.

Raulin, F. and Frère, C.: 1989, 'Gas phase organic syntheses in planetary environments, and the case of Titan', *J. British Interplan. Soc.* **42**, 411–422.

Raulin, F. and Owen, T.: 2002, 'Organic chemistry and exobiology on Titan', *Space Sci. Rev.* **104**, 379–395.

Raulin, F., Bruston, P., Paillous, P., and Sternberg, R.: 1995, 'The low temperature organic chemistry of Titan's geofluid', *Adv. Space Res.* **15**, 321–333.

Reynolds, R., Squyres, S., Colburn, D., and McKay, C.P.: 1983, 'On the habitability of Europa', *Icarus* **56**, 246–254.

Sagan, C. and Khare, B.N.: 1979, 'Tholins : Organic chemistry of interstellar grains and gas', *Nature* **277**, 102–107.

Schulze-Makuch, D. and Irwin, L.N.: 2004, *Life in the Universe, Expectations and Constraints*, Springer.

Simakov, M.B.: 2001, 'The possible sites for exobiological activities on Titan', *ESA SP-496*, 211–214.

Souchez, R., Jean Baptiste, P., Petit, J.R., Lipenkov, V.Y., and Jouzel, J.: 2002, 'What is the deepest part of the Vostok ice core is telling us?', *Earth-Science Reviews* **60**, 131–146.

Stoker, C.R., Boston, P.J., Mancinelli, R.L., Segal, W., Khare, B. N., and Sagan, C.: 1990, 'Microbial metabolism of tholins', *Icarus* **85**, 241–256.

Strobel, D.F.: 2005, 'Photochemistry in outer solar system atmospheres', *Space Sci. Rev.*, this volume.

Tran, B.N., Joseph, J.C., Ferris, J.P., Persans, P.D., and Chera, J.J.: 2003, 'Simulation of Titan haze formation using a photochemical flow reactor: The optical constants of the polymer', *Icarus* **165**, 379–390.

Address for Offprints: Laboratoire Interuniversitaire des Systèmes Atmosphériques, LISA-UMR CNRS 7583, Universités Paris 7 et Paris 12, 61 Avenue du Général de Gaulle, F-94000 Créteil, France; raulin@lisa.univ-paris12.fr

EPILOGUE

LIST OF ACRONYMS

ACE	Advanced Composition Explorer
ACP	Aerosol Collector Pyrolyser experiment on the Huygens probe
bKOM	broadband KilOMeter radiation
BPR	Bright Polar Limb
BS	Bow Shock
CAPS	CAssini Plasma Spectrometer
CFHT	Canada-France-Hawaii Telescope
CHEMS	Charged Energy Mass Spectrometer (subsystem of Cassini/MIMI)
CIRS	Composite InfraRed Spectrometer on board Cassini
CME	Coronal Mass Ejection
CMI	Cyclotron Maser Instability
CRAND	Cosmic Ray Albedo Neutron Decay
DAM	DecAmeter Emission
DF	Direction Finding
DISR	Descent Imager/Spectral Radiometer on board the Huygens probe
DPR	Dark Polar Limb
ECCM	Equilibrium Cloud Coverage Model
ELS	ELectron Spectrometer (subsystem of CAPS)
ENA	Energetic Neutral Atom
EOS	Equation Of State
ESA	European Space Agency
EUV	Extreme Ultraviolet
FOC	Faint Object Camera (HST)
FOS	Faint Object Spectrograph (HST)
FTS	Fourier Transform Spectrometer
GCM	General Circulation Model
GCMS	Gas Chromatograph Mass Spectrometer on the Huygens probe
GHRS	Goddard High Resolution Spectrograph (HST)
GPMS	Galileo Probe Mass Spectrometer
HASI	Huygens Atmospheric Structure Instrument
HOM	HectOMeter radiation
HST	Hubble Space Telescope
IBS	Ion Beam Spectrometer (subsystem of CAPS)
IDP	Interplanetary Dust Particle
IMF	Interplanetary Magnetic Field
IMAGE	NASA mission imaging the Earth's magnetosphere
IMS	Ion Mass Spectrometer (CAPS)
INCA	Ion and Neutral Camera (subsystem of Cassini/MIMI)
INMS	Ion Neutral Mass Spectrometer on board Cassini
IR	InfraRed radiation

IRIS	Infrared RadIometer and Spectrometer on board Voyager
IRTF	InfraRed Telescope Facility of NASA
ISAAC	Infrared Spectrometer And Array Camera
ISM	InterStellar Medium
ISO	Infrared Space Observatory
ISS NA/WA	Imaging Science Subsystem Narrow/Wide Angle camera on board Voyager
IUE	International Ultraviolet Explorer
JASSI	Jupiter Microwave Sounding and Sensing of the Interior
JIM	Jovian Ionospheric Model
JIMO	Jupiter Icy Moon Orbiter
JMEX	Jupiter Magnetospheric EXplorer
JPO	Jupiter Polar Orbiter
JUNO	Jupiter orbiter mission proposed to NASA
KBO	Kuiper Belt Object
LECP	Low Energy Charged Particle Instrument on board Voyager
LEMMS	Low Energy Magnetospheric Measurement System (Cassini/MIMI)
LF	Low-Frequency cutoff
LH	Left-Hand polarization (of plasma waves)
LOFAR	LOw Frequency ARray radio telescope
LTE	Local Thermal Equilibrium
MHD	Magnetohydrodynamics
MIMI	Magnetospheric IMaging Instrument on board Cassini
MP	Magnetopause
NASA	National Aeronautics and Space Administration
NGST	Next Generation Space Telescope
NICMOS	Near Infrared Camera and Multi-Object Spectrometer (HST)
NIMS	Near Infrared Mapping Spectrometer on board Galileo
NIR	Near InfraRed
nKOM	narrowband KilOMeter radiation
NSA	North-South Asymmetry (of Titan hazes)
OGLE	Optical Gravitational Lensing Experiment
PAH	Polycyclic Aromatic Hydrocarbons
PLS	PLasma Spectrometer on board Voyager
POLAR	NASA mission exploring the auroral regions of the Earth's magnetosphere
PPARC	Particle Physics and Astronomy Research Council
PWS	Plasma Wave experiment on board Galileo
RAO	Rising Auroral Oval
RH	Right-Hand polarization (of plasma waves)
RPWS	Radio and Plasma Wave Science experiment on Cassini
RTG	Radioisotope Thermoelectric Generators
SAO	Setting Auroral Oval

SCIPS	Solar Composition Icy PlaneteSimals
SKR	Saturn Kilometric Radiation
SOHO	Solar and Heliospheric Observatory
STIS	Space Telescope Imaging Spectrograph (HST)
SWICS	Solar Wind Ion Composition Spectrometer on board Ulysses
SWS	Short-Wavelength Spectrometer on board Voyager
TEXES	Texas Echelon-cross-Echelle Spectrograph
TKR	Terrestrial Kilometric Radiation
UV	UltraViolet radiation
VIMS	Visible and Infrared Imaging Spectrometer on board Cassini
VLA	Very Large Array radiotelescope (New Mexico)
VLT	Very Large Telescope
WIND	NASA mission exploring Sun-Earth connections

Author Index

Space Science Series of ISSI

1. R. von Steiger, R. Lallement and M.A. Lee (eds.): *The Heliosphere in the Local Insterstellar Medium*. 1996 ISBN 0-7923-4320-4
2. B. Hultqvist and M. Øieroset (eds.): *Transport Across the Boundaries of the Magnetosphere*. 1997 ISBN 0-7923-4788-9
3. L.A. Fisk, J.R. Jokipii, G.M. Simnett, R. von Steiger and K.-P. Wenzel (eds.): *Cosmic Rays in the Heliospehre*. 1998 ISBN 0-7923-5069-3
4. N. Prantzos, M. Tosi and R. von Steiger (eds.): *Primordial Nuclei and Their Galactic Evolution*. 1998 ISBN 0-7923-5114-2
5. C. Fröhlich, M.C.E. Huber, S.K. Solanki and R. von Steiger (eds.): *Solar Composition and its Evolution – From Core to Corona*. 1998 ISBN 0-7923-5496-6
6. B. Hultqvist, M. Øieroset, Goetz Paschmann and R. Treumann (eds.): *Magnetospheric Plasma Sources and Losses*. 1999 ISBN 0-7923-5846-5
7. A. Balogh, J.T. Gosling, J.R. Jokipii, R. Kallenbach and H. Kunow (eds.): *Co-rotating Interaction Regions*. 1999 ISBN 0-7923-6080-X
8. K. Altwegg, P. Ehrenfreund, J. Geiss and W. Huebner (eds.): *Composition and Origin of Cometary Materials*. 1999 ISBN 0-7923-6154-7
9. W. Benz, R. Kallenbach and G.W. Lugmair (eds.): *From Dust to Terrestrial Planets*. 2000 ISBN 0-7923-6467-8
10. J.W. Bieber, E. Eroshenko, P. Evenson, E.O. Flückiger and R. Kallenbach (eds.): *Cosmic Rays and Earth*. 2000 ISBN 0-7923-6712-X
11. E. Friis-Christensen, C. Fröhlich, J.D. Haigh, M. Schüssler and R. von Steiger (eds.): *Solar Variability and Climate*. 2000 ISBN 0-7923-6741-3
12. R. Kallenbach, J. Geiss and W.K. Hartmann (eds.): *Chronology and Evolution of Mars*. 2001 ISBN 0-7923-7051-1
13. R. Diehl, E. Parizot, R. Kallenbach and R. von Steiger (eds.): *The Astrophysics of Galactic Cosmic Rays*. 2001 ISBN 0-7923-7051-1
14. Ph. Jetzer, K. Pretzl and R. von Steiger (eds.): *Matter in the Universe*. 2001 ISBN 1-4020-0666-7
15. G. Paschmann, S. Haaland and R. Treumann (eds.): *Auroral Plasma Physics*. 2002 ISBN 1-4020-0963-1
16. R. Kallenbach, T. Encrenaz, J. Geiss, K. Mauersberger, T.C. Owen and F. Robert (eds.): *Solar System History from Isotopic Signatures of Volatile Elements*. 2003 ISBN 1-4020-1177-6
17. G. Beutler, M.R. Drinkwater, R. Rummel and R. Von Steiger (eds.): *Earth Gravity Field from Space – from Sensors to Earth Sciences*. 2003 ISBN 1-4020-1408-2
18. D. Winterhalter, M. Acuña and A. Zakharov (eds.): *"Mars" Magnetism and its Interaction with the Solar Wind*. 2004 ISBN 1-4020-2048-1
19. T. Encrenaz, R. Kallenbach, T.C. Owen and C. Sotin: *The Outer Planets and their Moons*. ISBN 1-4020-3362-1

Springer – Dordrecht / Boston / London